Origin of Geochemical Heterogeneity in the Mantle: Constraints from Volcanism Associated with Hawaiian and Kerguelen Mantle Plumes

by

Guangping Xu

B.S. Geology
Nanjing University, 1998

M. Eng. Geology
Nanjing University, 2000

SUBMITTED TO THE DEPARTMENT OF EARTH, ATMOSPHERIC AND PLANETARY SCIENCES IN PARTIAL FULFILLMENT OF THE REQUIREMENT FOR THE DEGREE OF

DOCTOR OF PHILOSOPHY IN GEOCHEMISTRY
AT THE
MASSACHUSETTS INSTITUTE OF TECHNOLOGY

AUGUST 2007
[September 2007]

Signature of Author: _____
Department of Earth, Atmospheric and Planetary Sciences
June 15, 2007

Certified by: _____
Frederick A. Frey
Professor of Geochemistry
Thesis Supervisor

Accepted by: _____
Maria Zuber
E.A. Griswold Professor of Geophysics and Planetary Sciences
Department Head

Abstract:

Lavas derived from long-lived mantle plumes provide important information of mantle compositions and the processes that created the geochemical heterogeneity within the mantle. Kerguelen and Hawaii are two long-lived mantle plumes and lavas associated with them have very different geochemical characteristics. In this thesis I studied the geochemical compositions of the lavas associated with Kerguelen plume (Mt. Capitole in Kerguelen Archipelago) and Hawaiian plume (Mauna Kea, East Molokai and West Molokai volcanoes) to understand what processes contributed to the geochemical variations observed in Kerguelen and Hawaiian lavas and the geochemical structure of the mantle beneath them.

Mt. Capitole is in the central part of the Kerguelen Archipelago and is attributed to Cenozoic volcanism arising from the Kerguelen hotspot. Based on the study of Mt. Capitole and previous isotopic data for the Kerguelen Plateau, Kerguelen Archipelago and Heard Island, I propose that two stages of mixing can explain the significant Sr, Nd, Hf and Pb isotopic heterogeneity. The first mixing process, best shown by the submarine lavas from Northern Kerguelen Plateau, is between a depleted component (i.e., relatively low $^{87}Sr/^{86}Sr$ with high $^{143}Nd/^{144}Nd$ and $^{176}Hf/^{177}Hf$), probably related to Southeast Indian Ocean mid-ocean ridge basalt, but possibly intrinsic to the Kerguelen plume, and an enriched Kerguelen plume component. From ~34 Ma to <1 Ma, on average the proportion of the depleted component decreased. Subsequently, a second mixing process involved addition of a component with relatively high $^{87}Sr/^{86}Sr$ (>0.7060) and low $^{143}Nd/^{144}Nd$ (<0.5125) and $^{176}Hf/^{177}Hf$ (<0.2827) and non-radiogenic Pb isotope ratios (<17.9 for $^{206}Pb/^{204}Pb$). I infer that this component was lower continental crust.

At Hawaii there are systematic geochemical differences between the < 3 My Hawaiian shields forming the subparallel spatial trends, known as Loa and Kea. East Molokai (> 1.5 Ma), the oldest volcano on the Kea-trend, maintains the Kea-like geochemical characteristics. As East Molokai and other Kea-trend volcanoes (Mauna Kea, Kohala, Haleakala and West Maui) migrate away from the hotspot and evolve from the shield to postshield stage, isotopic ratios of $^{87}Sr/^{86}Sr$ decrease and $^{143}Nd/^{144}Nd$ and $^{176}Hf/^{177}Hf$ increase in postshield lavas; however, all Kea postshield lavas have similar ratios of Sr, Nd, Hf and Pb showing that the periphery of the hotspot sampled by Kea-trend postshield lavas had long-term geochemical homogeneity (>1.5 My). The temporal changes in Sr, Nd and Hf isotope ratios are attributed to incorporation of a depleted component that dominantly sampled by rejuvenated stage lavas. This depleted component has Kea-trend Pb isotopic characteristics, relatively low $^{208}Pb/^{204}Pb$ at a given $^{206}Pb/^{204}Pb$, and it is probably not related to oceanic lithosphere or the source of mid-ocean ridge basalt.

The Loa-Kea spatial geochemical differences end at West Molokai shield (~ 1.9 Ma) which is the oldest Loa-trend volcano on the double parallel chains. West Molokai shield includes lavas with Loa- and Kea-like geochemical characteristics; a mixed Loa-Kea source is required. In contrast, West Molokai postshield lavas are exclusively Kea-like. This change in source geochemistry can be explained by the observed change in strike of the Pacific plate near Molokai Island so that as West Molokai volcano moved away from a mixed Loa-Kea source it sampled only the Kea side of a bilaterally zoned plume (*Abouchami et al., Nature, v434, 2005*).

Thesis Supervisor: Frederick A. Frey
Title: Professor of Geochemistry

Acknowledgements

I thank my general exam and thesis committee members, Sam Bowring, Fred Frey, Tim Grove, Harry Hemond, Mark Kurz, David Mohrig, Mike Rhodes and Dan Shim for their assistance, encouragement and fruitful discussions over the years. Particularly, I will never be able to express enough gratitude to Fred Frey who gave me tremendous encouragement and made insightful comments on every single sentence I wrote and each idea I came up with. I appreciate the financial support from Sam and Tim by offering to analyze some of my samples (West Molokai isotopes and Mt. Capitole minerals) free of charge and access to their lab resources over the last 6 years. It was a pleasure to have scientific collaboration and numerous discussions with W. Abouchami (MPI), B. Cousens (Carleton Univ.), D. Clague (MBARI), J. Scoates (UBC), J. Blichert-Toft (ENSL), M. Weisler (Univ. Queensland) and D. Weis (UBC). I also benefit discussions with Glenn Gaetani, Eric Hauri, Mike Garcia, Ed Stolper, Terry Plank, M. Lustrino and David R Sherrod.

I benefited from the discussions in two geophysics seminars, "Core-mantle boundary" and "Deep water in the mantle", which were put together by Dan Shim and Stephanie Rondenay.

I thank Shichun Huang for getting me started in the lab, teaching me the ICP-MS analyses and numerous discussions. Frank Dudas is always ready to help me in the clean lab, and I can not get any ICP-MS data without his help. I also thank the following people who helped me in various labs and analytical techniques made possible the research accomplished during this thesis: Ed Boyle, Frank Dudas, Barry Grant, Rick Kayser, Neal Chatterjee, Ila Pillalamarri, Michael Vollinger, Stephanie Ingle, Sonia Doucet, Bruno Kieffer, M. Lo Cascio, Richard Friedman and Jane Barling. The following MIT fellow students and postdocs helped me in various

aspects, Kirsten Nicolaysen, Steve Parman, Lindy Elkins, Steve Singletary, Matt Jackson, Jar Bar, Michael Krawczynski, Christy Till, Etienne Medard, Becky Flowers, Blair Schoene, Noah McLean, Jeremy Boyce, Marc Hesse and Evy Mervely.

It is a pleasure to be TA together with Seth John and Noah McLean for "Analytical Techniques for Studying Environmental and Geologic Samples" and "Petrology", respectively.

I thank the administrative people at 9th floor, Roberta Allard, Vicki McKenna, Carol Sprague and Jacqueline Taylor. Carol Zayotti at 12th floor keeps everything in order and is ready to help whenever I need assistance.

I thank my former advisor, Jiangping Zhai, at Nanjing University for his encouragement and support.

I would never have finished my study at MIT without the support and love of my parents, my brother, my sister, my wife and my two sons!

TABLE OF CONTENTS

Chapter 1 Flood Basalts From Mt. Capitole in the Central Kerguelen Archipelago: Insights Into the Growth of the Archipelago and Source Components Contributing to Plume-related Volcanism

This chapter was published in *Geochemistry, Geophysics and Geosystems*:

Xu, G., F. A. Frey, D. Weis, J. S. Scoates, and A. Giret (2007), Flood basalts from Mt. Capitole in the central Kerguelen Archipelago: Insights into the growth of the archipelago and source components contributing to plume-related volcanism, 39 *Geochem. Geophys. Geosyst.*, 8, doi:10.1029/2007GC001608.

Abstract

The Kerguelen Archipelago, constructed on the submarine Northern Kerguelen Plateau, is attributed to Cenozoic volcanism arising from the Kerguelen hotspot. Geochemical studies of 325 to 1000 m thick lava sections of the ~30 to 25 Ma flood basalt forming the bulk of the archipelago show a temporal change from older tholeiitic basalt to younger slightly alkalic basalt. This compositional transition is expressed in a 630 m lava section at Mt. Capitole where the lava sequence is lowermost tholeiitic basalt overlain by slightly alkalic basalt overlain by plagioclase-rich cumulates that are mixtures of plagioclase-phyric basalt and more evolved magmas. During growth of the flood basalt, magma supply from the hotspot was variable, and at times sufficiently low to enable extensive crystal fractionation, e.g., at Mt. Capitole and nearby Mt. Tourmente only 10 of 120 lava flows have >6 wt% MgO.

Based on this study and previous isotopic data for the ~34 Ma submarine lavas erupted on the Northern Kerguelen Plateau, other flood basalt sections in the Kerguelen Archipelago, and younger lavas erupted in the archipelago and at Heard Island, there is significant Sr, Nd, Hf and Pb isotopic heterogeneity that can be explained by two stages of mixing. The first mixing event, best shown by the submarine lavas, is between components that are related to Indian Ocean mid-ocean ridge basalt (MORB) and the Kerguelen hotspot. From ~34 Ma to <1 Ma, on average the proportion of the MORB-related component decreased. Subsequently, a second mixing process involved addition of a component with relatively high $^{87}Sr/^{86}Sr$ (>0.7060) and low $^{143}Nd/^{144}Nd$ (<0.5125) and $^{176}Hf/^{177}Hf$ (<0.2827) and non-radiogenic Pb isotope ratios (<17.9 for $^{206}Pb/^{204}Pb$). We infer that this component was lower continental crust.

1. Introduction

The Kerguelen hotspot has produced 15 to 24×10^6 km^3 of basaltic magma over ~120 My [*Coffin and Eldholm*, 1994; *Coffin et al.*, 2002]. This long volcanic record includes a large igneous province (Kerguelen Plateau-Broken Ridge), a hotspot track (the >5000 km long ~82–38 Ma Ninetyeast Ridge), and the recently active islands (Kerguelen Archipelago, McDonald and Heard Islands) [e.g., *Wallace et al.*, 2002]. Determination of spatial and temporal variations in geochemical characteristics of the basalt forming the Kerguelen Plateau, Ninetyeast Ridge and Kerguelen Archipelago are essential for understanding the history of the Kerguelen hotspot. The early, dominantly Cretaceous, volcanic activity of the Kerguelen hotspot is recorded in basalt recovered from the Kerguelen Plateau and Broken-Ridge by the Ocean Drilling Program (Legs 119, 120 and 183). Studies of these drill cores show a complex record of varying magma production rates [*Coffin et al.*, 2002] and changes in the relative proportions of magma source components, including mantle plume, mid-ocean ridge basalt (MORB) and continental-related components [e.g., *Mahoney et al.*, 1995; *Frey et al.*, 2002b; *Ingle et al.*, 2002; *Kieffer et al.*, 2002; *Neal et al.*, 2002; *Weis and Frey*, 2002; *Frey et al.*, 2003].

The Cenozoic Kerguelen Archipelago (6500 km^2) formed on the Northern Kerguelen Plateau (Figure 1). The archipelago has a history of volcanism from ~30 to 0.1 Ma that is interpreted as magmatism resulting from the stem of the Kerguelen mantle plume [e.g., *Weis et al.*, 1993; *Nicolaysen et al.*, 2000]. Unlike the submarine Kerguelen Plateau and Ninetyeast Ridge, the Kerguelen Archipelago is currently a subaerial expression of the Kerguelen hotspot that can be studied in detail. The archipelago is largely, 85% of the surface, formed of flood basalt ranging from 28-29 Ma tholeiitic

basalt in the northwest (Mts des Ruches, Fontaine, Bureau and Rabouillère) to 24-26 Ma alkalic basalt in the east (Mt. Crozier and sections at Ravin Jaune & du Charbon) (Figure 1). A transition from tholeiitic to alkalic volcanism occurs in flood basalt sections from the Plateau Central. For example, at Mt. Tourmente (Figure 1), a 597 m section of lava flows ranges from ~ 26 Ma transitional basalt (i.e., near the tholeiitic-alkalic boundary line on a total alkalis vs SiO_2 plot) in the lower 80% of the section to overlying ~ 25.3 Ma alkalic basalt in the upper 20% of the section. In contrast, at Mt. Marion Dufresne, also in the Plateau Central (Figure 1), the lowermost lavas in a 700 m section are alkalic basalt and the lavas become less alkaline upwards in the section [*Annell et al.*, 2007]. If tholeiitic basalt reflects higher magma flux than alkalic basalt, as commonly inferred, the temporal variations in magma flux were different at Mts Tourmente and Marion Dufresne.

With the objective of understanding fluctuations in magma flux arising from the Kerguelen hotspot, we studied a 630 m lava section from Mt. Capitole at an intermediate location on the Plateau Central (Figure 1). We find an upwards, i.e., decreasing age, change from slightly tholeiitic to slightly alkalic basalt in the Mt. Capitole section, but the uppermost plagioclase-phyric lavas reflect a plagioclase accumulation process similar to that forming plagioclase-phyric to -ultraphyric basalt at Mt. Marion Dufresne [*Annell et al.*, 2007]. The accumulation of plagioclase phenocrysts in subgroups of lavas at Mts Capitole and Marion Dufresne provide further evidence for periods of reduced basaltic magma flux from the hotspot.

An important result is that isotopic data for Sr, Nd, Hf and Pb for Mt. Capitole lavas combined with previously published isotopic data for other archipelago lavas can be explained by mixing between three components. First mixing between a component, such

as mid-ocean ridge basalt or its source, with relatively low $^{87}Sr/^{86}Sr$, high $^{143}Nd/^{144}Nd$ and $^{176}Hf/^{177}Hf$ and intermediate $^{206}Pb/^{204}Pb$, with a plume-related component with intermediate $^{87}Sr/^{86}Sr$, $^{143}Nd/^{144}Nd$ and $^{176}Hf/^{177}Hf$ and high $^{206}Pb/^{204}Pb$, ~18.5, followed by addition of a component with high $^{87}Sr/^{86}Sr$, low $^{143}Nd/^{144}Nd$ and $^{176}Hf/^{177}Hf$ and quite low $^{206}Pb/^{204}Pb$ (<18). This last component is isotopically similar to some lower continental crust.

2. Geology

Mt. Capitole in the central part of the Kerguelen Archipelago, near the eastern edge of the Cook ice cap (Figure 1), has a NE-SW orientation and is asymmetric with average slopes of 32° for the western flanks and 18° for the eastern flank. It is cut by basaltic dikes with east-west orientation. In this region of the glaciated plateau, it is not possible to identify distinct volcanic centers.

Fifty-five samples from distinct basalt flows were collected on a westward traverse from the summit (sample 93-459) with an altitude of 860 m to the Vallee des Merveilles, an altitude of 230 m (sample 93-514); intercalated within the basalt flows are sedimentary breccias and conglomerates which indicate temporal breaks in eruption (Figure 2). For example, there is a 4 m thick breccia with angular pebbles of basalt located at 700 m (between samples 93-473 and 93-474), a 0.2 m thick red bed consisting of basaltic pebbles in a red matrix located at 670 m (between samples 93-477 and 93-478), and a 1.5 m thick breccia at 565 m (between samples 93-485 and 93-486). No age information is available but we assume that the Mt. Capitole section formed at ~ 25 Ma, i.e., similar to the age of lavas from Mts Tourmente [*Nicolaysen et al.*, 2000] and Marion Dufresne [*Annell et al.*, 2004].

3. Analytical techniques

Ten samples, mostly plagioclase-phyric, were chosen for analyses of phenocrysts, xenocrysts and amphibole inclusions within plagioclase (Table 1). Olivine, plagioclase, clinopyroxene and amphibole were analyzed with the 4-spectrometer JEOL 733 microprobe at Massachusetts Institute of Technology, using 15 kV accelerating voltage, 10 nA beam current and a beam size of 1 μm (10 μm for plagioclase). The counting time was 40 seconds for all elements except for Ca and Al (30 seconds) and Na (5 seconds) in plagioclase; Na was counted for 15 seconds for pyroxene and amphibole. Analyses of plagioclase, pyroxene, olivine and amphibole are in Table 2.

For whole rock analyses, samples were abraded with sand-paper to remove surficial alteration features and contaminants introduced by sawing. Then they were coarse-crushed in a hydraulic piston crusher and reduced to powder in an agate shatterbox. Major element and some trace element (such as Cr, Ni and V) concentrations were determined by X-ray fluorescence spectrometry at the University of Massachusetts, Amherst (Tables 3 and 4). Major element compositions are reported as the mean of duplicate analyses and loss on ignition (LOI) is the weight loss after heating 10 minutes at 1020°C using Pt-Au crucibles. Estimates of accuracy and precision were discussed by *Rhodes* [1996]. Most trace element abundances (Table 4) were determined at MIT by inductively coupled plasma mass spectrometry using a Fisons VG Plasmaquad 2+S with both internal and external drift monitors. The relative standard deviation for all trace elements determined in BHVO-2 (15 analyses, Table 4) is less than 3% [*Huang and Frey*, 2003]. Scandium was determined by instrumental neutron activation analysis in 21 samples, following the procedures of *Ila and Frey* [2000] (Table 4).

Eighteen relatively fresh samples with minimum alteration were chosen for Sr, Nd, Hf and Pb isotopic analyses at the Pacific Center for Isotopic and Geochemical Research at the University of British Columbia (UBC). Prior to isotopic analysis of Sr, Nd and Pb the samples were leached repeatedly in an ultrasonic bath with 6N HCl following the procedure described by *Weis et al.* [2005]. Analysis of leached and unleached aliquots for sample 93-465 shows that leaching resulted in residues with slightly higher $^{143}Nd/^{144}Nd$ and lower $^{87}Sr/^{86}Sr$ and Pb isotopic ratios (Table 5). At UBC Sr and Nd isotopic ratios were determined using a thermal ionization mass spectrometer (Triton) and Pb isotopic ratios were determined using a multiple-collector ICP-MS (Nu021) [*Weis et al.*, 2005; *Weis et al.*, 2006]. Normalization procedures and data for standards are in the footnotes for Table 5.

About 200 mg of unleached rock powder was dissolved for Hf isotopic analyses, following the procedure of *Blichert-Toft et al.* [1997]. The Hf isotopic compositions were measured on MC-ICP-MS (Nu021) at UBC. The $^{176}Hf/^{177}Hf$ ratios are normalized to the Hf JMC 475 in-house standard value of 0.282160 [*Blichert-Toft et al.*, 1997]. External reproducibility based on three duplicates is within in-run uncertainties, i.e., $< 6\times10^{-6}$ (Table 5).

For Sr and Pb isotopic analyses, plagioclase grains with relatively few inclusions were picked from two samples, 93-459 and 93-471, using a binocular microscope. Leaching procedures followed those of *Housh and Bowring* [1991]: grains were leached using 7N HNO_3 for 30 minutes on a hotplate (~125°C); the residue was rinsed with Milli-Q H_2O, leached by 6N HCl on a hotplate for 30 minutes and rinsed with Milli-Q H_2O; this residue was leached with 5% HF + 0.5N HBr (8:1) for 10 minutes on a hotplate

stirring every 2 minutes followed by rinsing twice with Milli-Q H_2O. This last step was repeated until the sample is white with no visible black inclusions. The final residue was dissolved by concentrated HF and 7N HNO_3. An aliquot was taken for ICP-MS analyses to determine the parent/daughter abundance ratios (Table 6). The remaining aliquots were passed through 120 μL Pb and 50 μL Sr columns and analyzed by a thermal ionization multi-collector mass spectrometer (Micromass Isoprobe-T) at MIT using dynamic mode for Sr and static mode for Pb (Table 5).

4. Results

4.1 Petrography

The textures of Mt. Capitole lavas range from aphyric to moderately phyric (Table 1), typically with a fine-grained groundmass of plagioclase, clinopyroxene, olivine, opaque minerals and devitrified, altered brown glass. Sample 93-472 is an exception; it has an intergranular texture with a coarse-grained groundmass of plagioclase and clinopyroxene and is altered (loss on ignition = 4.4 wt%, Table 3). Most samples (38) contain less than 5 vol% phenocrysts (> 0.7 mm), and 8 samples are aphyric. Most of these aphyric to slightly-phyric lavas are found in the lower part of the section. In contrast, 16 samples contain abundant phenocrysts or xenocrysts (≥ 10 vol% and up to 40 vol%), dominantly plagioclase with sparse clinopyroxene; olivine phenocrysts occur only in sample 93-472; nine of these 16 samples are from the uppermost 170 m (Table 1). Most of these plagioclase grains are 0.7-3 mm in width, but a few laths are up to 7 mm in length; some grains are resorbed (Figure 3a).

The phenocryst assemblages in each of the three studied sections in the Plateau Central (Figure 1) are quite different. Lavas from Mt. Tourmente are largely aphyric; i. e.,

62 of 64 samples have less than 5 vol% phenocrysts [*Frey et al.*, 2002a]. Lavas from the lowermost 300 m of the Mt. Marion Dufresne section are also dominantly aphyric but with decreasing age plagioclase-phyric, up to 60 vol%, lavas are abundant [*Annell et al.*, 2007]. This upwards succession from aphyric to plagioclase-phyric occurs at Mt. Capitole and Mt. Marion Dufresne. However, the latter section is unique in that olivine-phyric, up to 20 vol%, lavas dominate the uppermost 400 m [*Annell et al.*, 2007]. In contrast, only one olivine-phyric (~2 vol%) lava occurs in the Mt. Capitole section (Table 1).

4.2 Mineral Compositions

4.2.1 Plagioclase:

Plagioclase is the most abundant phenocryst/xenocryst in Mt. Capitole basalt, especially in the uppermost 170 m of the section which we refer to as the Upper Transitional Group (Table 1). Within the Upper Transitional Group plagioclase cores range from An_{85} to An_{56} (Table 2a, Figure 4). The plagioclase phenocrysts/xenocrysts in the Upper Transitional Group are texturally distinct from those in the other groups; they are commonly resorbed (Figure 3a) and contain inclusions of olivine, pyroxene, amphibole, Fe-Ti oxides and rare apatite (Figure 3b, c, d, e, f). Rims of large plagioclase grains span a wide compositional range, from sodic-rich compositions (An_{47}) to An_{83} (Table 2). Even more sodic plagioclase ($Ab_{39} - Ab_{70}$) occurs as inclusions (Figures 3c, d, e and 4) and as partial rims surrounding inclusions of olivine, clinopyroxene, amphibole and Fe-Ti oxide (Figure 3c, d, e). The large compositional variation of the plagioclase rims surrounding inclusion minerals (Figure 3d, e), ranging from labradorite to anorthoclase within less than 50 μm, reflects non-equilibrium crystallization. The large plagioclase grains are sieve-textured plagioclase [e.g., *Nelson and Montana*, 1992].

The Mg# (100*molar ratio of Mg/(Mg + Fe^{2+})) of plagioclase is sensitive to the crystallization sequence of plagioclase relative to mafic minerals, i.e., relatively low Mg# is characteristic of plagioclase crystallization after olivine and pyroxene [e.g., *Sisson and Grove*, 1993]. This delayed plagioclase crystallization can result from relatively high H_2O content in the magma [e.g., *Sano and Yamashita*, 2004]. *Annell et al.* [2007] inferred that the relatively lower Mg# (<27) of the high An (80-85%) plagioclase phenocrysts at Mt. Marion Dufresne reflect plagioclase crystallization at 5-6 km under hydrous conditions (>3% H_2O in the magma). In general, plagioclase cores in Mt. Capitole lavas have higher Mg# than those from Mt. Marion Dufresne (Figure 5), and high H_2O contents are not inferred.

4.2.2 Pyroxene

Clinopyroxene is a more common phenocryst in Mt. Capitole lavas than olivine, but it rarely exceeds 3 vol%; sample 93-491 with ~15 vol% clinopyroxene is an exception (Table 1). The Mg# of clinopyroxene phenocrysts ranges from 57 to 81 (Table 2b). Plagioclase phenocrysts in the Upper Transitional Group contain abundant inclusions of clinopyroxene with a similar range in Mg#, but rare pigeonite inclusions with low Mg# (40 to 43) also occur (Figure 3d).

High Al_2O_3 clinopyroxene (5 – 8.6 wt%) occurs in a section of mildly-alkaline lavas from Mt. Crozier in the eastern archipelago (Figure 1). *Damasceno et al.* [2002] concluded that high pressure (up to 12 kbar) fractionation of high-Al_2O_3 clinopyroxene was an important process for these alkalic basalts. Such aluminous clinopyroxene phenocrysts are not present in Mt. Capitole lavas; they range from 1.29-4.71 wt% Al_2O_3,

and crystallization pressures inferred from clinopyroxene/melt thermobarometers are 1 to 2.7 kbar at 1130°C [*Putirka et al.*, 2003].

4.2.3 Olivine

Olivine phenocrysts, ~2 vol%, occur only in sample 93-472 (Table 1) which has the highest MgO content (8.0 wt%) among Mt. Capitole lavas. These olivines are normally zoned, ranging from cores with Fo_{76-82} to rims with Fo_{74-77} (Table 2c). Highly evolved olivine (Fo_{46-63}) also occurs as inclusions in the abundant plagioclase phenocrysts/xenocrysts that characterize the Upper Transitional Group (Tables 1 and 2c and Figure 3d).

4.2.4 Amphibole

Amphibole phenocrysts/microphenocrysts occur in alkaline Kerguelen Archipelago lavas [*Giret et al.*, 1980; *Damasceno et al.*, 2002; *Gagnevin et al.*, 2003]. Amphibole crystals in the Mt. Capitole section are present in the groundmass and as inclusions in plagioclase xenocrysts (Figure 3e and f). They are calcic-amphibole ranging from (titano-) magnesiohornblende to tschermakite according to the classification of *Leake et al.* [1997] (Table 2d). Amphibole inclusions in plagioclase phenocrysts/xenocrysts are commonly enclosed by Na-rich plagioclase rims that vary in compositions along the elongated amphibole inclusion (Figure 3e).

4.3 Whole-rock compositions

4.3.1 Major Elements

Like other sections of flood basalt from the northern and central part of the Kerguelen archipelago, lavas from the Mt. Capitole section are dominantly tholeiitic to

transitional basalt based on a silica-total alkalis diagram (Figure 5). They are evolved basalts with ~46 to 53 wt% SiO_2 and 3.3 to 8 wt% MgO (Table 3). Although there are no simple geochemical variations with relative eruption age, i.e., stratigraphic height in Figure 6, the lava compositions can be divided into three groups that correlate with stratigraphic position. The first group is the uppermost 15 tholeiitic/transitional lavas from above 690 m. These lavas are dominantly plagioclase-phyric (Table 1) and are characterized by relatively high Al_2O_3 coupled with relatively low TiO_2 and Fe_2O_3 (as total iron) (Figure 6). They are designated as the Upper Transitional Group. Sample 93-491, lower in the section at 540 m, is compositionally and petrographically similar to this group (Table 1 and Figure 6). For this group, abundances of SiO_2, Al_2O_3, Na_2O and K_2O are negatively correlated with MgO whereas CaO shows a slight positive correlation (Figure 7). The negative Al_2O_3 – MgO trend of this group contrasts with the positive trend of other Mt. Capitole and Mt. Tourmente lavas (Figure 7). Neither TiO_2 nor P_2O_5 is inversely correlated with MgO in this group (Figure 7).

The second group of Mt. Capitole lavas are samples 93-478 to 93-486 from 660 m to 560 m. They have relatively low SiO_2 contents and $SiO_2/Fe_2O_3^*$ ratios, high TiO_2 and $Fe_2O_3^*$ contents and are alkalic or very close to the tholeiitic-alkalic boundary (Figures 5, 6 and 7). They are designated as the Low-Silica Group. This group does not vary widely in MgO (4.1 to 5.2 wt%); in general its compositional range overlaps with the uppermost group of slightly alkalic lavas in the Mt. Tourmente section (Figure 7).

All other samples from Mt. Capitole, 30 lavas from 680 – 690 m and 230 – 560 m (Figure 6) form the third group designated as Lower Transitional Group. The major

element compositions of this group largely overlap the transitional lavas that occur in the lower 80 % of the Mt. Tourmente section (Figure 7).

In summary, as at Mt. Tourmente, at Mt. Capitole there is a transition from tholeiitic to alkalic basalt with decreasing age; however, plagioclase-rich lavas are abundant in the upper part of the Mt. Capitole section; plagioclase-phyric lavas are absent at Mt. Tourmente [*Frey et al.*, 2002a], but they also occur at Mt. Marion Dufresne [*Annell et al.*, 2007].

4.3.2 Trace Elements

Abundances of Th, Nb, Pb, Zr and Yb are highly correlated in Mt. Captiole lavas; in contrast abundances of K, Rb, Sr and Ba are poorly correlated with Th abundance (Figure 8). The ranges in Rb and K contents (factors of 33 and 8, respectively) are much greater than those for relatively immobile incompatible elements, such as Nb, Zr and Th (factors of 2 to 4). The ranges for Ba and Sr (factors of 3.8 and 3.1, respectively) are comparable to those for immobile incompatible elements. We infer that Mt. Capitole samples experienced post-magmatic alteration and that Rb and K were mobile during the alteration, but that Ba and Sr were less mobile. Despite their relatively low Th content the plagioclase-rich Upper Transitional Group lavas have K, Rb, Sr and Ba contents similar to lavas in the other groups (Figure 8). Note that there is a relative Sr depletion, i.e., relatively low Sr/Ce and Sr/Nd ratios, in the Lower Transitional Group and Low-Silica Group lavas but not in the plagioclase-rich Upper Transitional Group (Figure 9).

All Mt. Capitole samples are enriched in incompatible elements relative to primitive mantle (Figure 9). The highest incompatible element contents are in the low MgO (3.3 to 3.8 wt%) lavas of the Lower Transitional Group; the lowest contents are in

the plagioclase-rich Upper Transitional Group; incompatible element contents in the Low-Silica Group overlap with those of alkalic lavas at Mt. Tourmente (Figure 9). At a given MgO content, incompatible element contents increase in the order: Upper Transitional Group < Lower Transitional Group < Low-Silica Group.

All Mt. Capitole lavas contain relatively low and variable abundances of transition elements (Ni=34-128 ppm; Cr=2-272 ppm, Table 4) that are positively correlated with MgO. Abundance of Sc ranges from 28 to 32 ppm for lavas with MgO greater than 5.5 wt%, but ranges to lower Sc (~24 ppm) with decreasing MgO content (Table 4). Like TiO_2, the Upper Transitional Group samples have the lowest V contents while Low Silica Group lavas have relatively high V abundances (Table 4).

4.4 Sr, Nd, Hf and Pb isotopes

Although there are no long-term systematic temporal variations of Sr, Nd, Hf and Pb isotopic ratios with stratigraphic height, i.e., inferred eruption age, in the Mt. Capitole section, samples of the Upper Transitional and Low-Silica Groups define trends of increasing $^{87}Sr/^{86}Sr$ and decreasing $^{143}Nd/^{144}Nd$, $^{176}Hf/^{177}Hf$ with decreasing height; in contrast the lower Transitional Group lavas show no systematic variations of isotope ratios with height (Figure 10).

Most of the Mt. Capitole lavas define an inverse correlation of $^{87}Sr/^{86}Sr$ and $^{143}Nd^{144}Nd$, but two samples of the Lower Transitional Group are offset to higher $^{87}Sr/^{86}Sr$ (Figure 11a). The lowest $^{87}Sr/^{86}Sr$ ratios are in the lavas of the Low-Silica Group and one of these samples (93-482) has the lowest $^{87}Sr/^{86}Sr$ and highest $^{143}Nd/^{144}Nd$; the Low-Silica Group lavas overlap with the field for Mt. Tourmente but the other two groups include samples that range to higher $^{87}Sr/^{86}Sr$ and lower $^{143}Nd/^{144}Nd$ (Figure 11a).

Mt. Capitole lavas define a positive trend in $^{143}Nd/^{144}Nd$ vs. $^{176}Hf/^{177}Hf$ overlapping with the field of Mt. Tourmente lavas but extend to lower $^{143}Nd/^{144}Nd$ and $^{176}Hf/^{177}Hf$ (Figure 11b); this trend is parallel to the slope of mantle-OIB array [*Vervoort et al.*, 1999].

In plots of $^{208}Pb/^{204}Pb$ and $^{207}Pb/^{204}Pb$ versus $^{206}Pb/^{204}Pb$, there is overlap among the three compositional groups of Mt. Capitole lavas (Figure 12a). Also the two samples of the Lower Transitional Group that are offset to high $^{87}Sr/^{86}Sr$ (Figure 11a) have anomalously high $^{207}Pb/^{204}Pb$ (Figure 12b). One of these samples (93-490) was analyzed in duplicate (Table 5). As with Sr, Nd and Hf isotopic ratios, Pb isotopic ratios in the Low-Silica Group lavas overlap with the field for Mt. Tourmente lavas, but lavas from the Upper and Lower Transitional Group range to higher $^{87}Sr/^{86}Sr$, lower $^{143}Nd/^{144}Nd$ and $^{176}Hf/^{177}Hf$ and higher $^{208}Pb/^{204}Pb$ at a given $^{206}Pb/^{204}Pb$ (Figures 11 and 12).

The Upper Transitional Group lavas from Mt. Capitole show a correlation between $(^{206}Pb/^{204}Pb)_i$ and $(Sr/Nd)_{PM}$ (PM stands for primitive mantle value of *Sun and McDonough* [1989]) (Figure 13). Since high $(Sr/Nd)_{PM}$ is characteristic of plagioclase (Table 6), the plagioclase-rich component is inferred to have relatively high $^{206}Pb/^{204}Pb$. Plagioclase grains from two Upper Transitional Group samples, 93-459 and 93-471, which have the extremes in Sr/Nd ratios among the five samples analyzed for radiogenic isotopes, were analyzed for Sr and Pb isotopes (Table 5). Plagioclase xenocrysts from these two samples have the same Sr and Pb isotope ratios within analytical uncertainties (Figure 12a; Table 5), indicating that these plagioclase xenocrysts were derived from the same source. The plagioclases and whole-rock have similar $^{87}Sr/^{86}Sr$, but as expected from the correlations between Sr/Nd vs $^{206}Pb/^{204}Pb$ (Figure 13), the plagioclase

xenocrysts have more radiogenic Pb isotope ratios than their whole rocks (Figure 12a; Table 5).

5. Discussion

5.1 Origin of Compositional Variations in Mt. Capitole lavas

5.1.1 Role of crystal fractionation and accumulation

Mt. Capitole lavas define two different Al_2O_3 vs. MgO trends, a positive trend, similar to Mt. Tourmente lavas, for the Low-Silica and Lower Transitional Group lavas and a negative trend for the Upper Transitional Group (Figure 14). A negative Al_2O_3 vs. MgO trend defined by Mt. Crozier lavas, in the northeast part of the archipelago (Figure 1), was inferred to reflect fractionation of a clinopyroxene-dominated assemblage at high pressure by *Damasceno et al.* [2002]. They inferred that lithospheric thickness increased as the archipelago evolved from a near-ridge setting at ~40 Ma to its present intraplate location (see inset of Figure 1); therefore younger flood basalts, such as at Mt. Crozier, were likely to stagnate at higher pressure where the fractionating mineral assemblage has a high proportion of clinopyroxene. We favor a different interpretation, i.e., plagioclase accumulation, for the negative Al_2O_3 vs. MgO trend defined by the Upper Transitional Group at Mt. Capitole. The abundant plagioclase (Table 1) is obvious evidence for plagioclase accumulation. In addition, these lavas have the geochemical characteristics of plagioclase, that is, relatively high Al_2O_3 content, relatively low abundance of incompatible elements, $(Sr/Nd)_{PM}$ and $Eu/Eu^* > 1$, relatively high Ba/Th, and positive correlations of Sr/Nd and Eu/Eu^* with Al_2O_3/TiO_2 (Figures 9, 14 and 15). In contrast, the Low-Silica Group and Lower Transitional Group lavas have $(Sr/Nd)_{PM}$ and $Eu/Eu^* < 1$ with $(Sr/Nd)_{PM}$ decreasing as MgO decreases (Figure 15). Such trends are consistent with

co-fractionation of plagioclase and a mafic phase, such as clinopyroxene, which decreased Al_2O_3 and MgO, respectively.

5.1.2 Role of magma mixing

Several characteristics of plagioclase in the Upper Transitional Group group of Mt. Capitole indicate magma mixing: (a) many plagioclase grains are resorbed (Figure 3a); (b) the plagioclase grains have abundant olivine, pyroxene and amphibole inclusions with low Mg# and Na-rich plagioclase rims partly surrounding these inclusions (Figure 3d, e; Table 2), indicating that a plagioclase-rich magma was invaded by a more evolved magma which reacted with the plagioclase crystals via interconnecting channels formed by dissolution; (c) plagioclase is not in isotopic equilibrium with their whole rocks, i.e., plagioclase xenocrysts have more radiogenic Pb isotope ratios (Figure 12a; Table 5).

5.1.3 Role of variable extents of melting

In the lower 500 m of the Mt. Capitole section slightly alkaline lavas (Low-Silica Group) overlie tholeiitic lavas (Lower Transitional Group) (Figures 2 and 5). The nearby Mt. Tourmente section (Figure 1) records a similar compositional change. Moreover the Loa-Silica Group at Mt. Capitole is similar in major and trace element compositions and isotopic ratios (Sr, Nd and Pb) to the upper alkalic lavas in the Mt. Tourmente section (Figures 7, 9, 11 and 14). *Frey et al.* [2002a] inferred that this temporal, tholeiitic to alkalic transition, reflects a decrease in extent of melting with decreasing eruption age.

5.2 Inferences from flood basalt compositions at three locations in the Plateau Central

From northwest to southeast in the Kerguelen Archipelago, the exposed flood basalt changes from older, 29 to 26 Ma, tholeiitic and transitional basalt (Mts de Ruches,

Fontaine, Bureau and Rabouillère; Figure 1) to younger, 25 to 24 Ma, slightly alkalic basalt (Mt. Crozier, Ravin Jaune and Charbon; Figure 1) [*Frey et al.*, 2000; *Damasceno et al.*, 2002]. *Frey et al.* [2000] proposed that this change in composition reflects a decrease in melting extent of the Kerguelen mantle plume as lithosphere thickness increased during the transition from a ridge-centered to intraplate setting in the Northern Kerguelen Plateau (see Figure 1 inset). Also the increasing proportion of highly evolved magmas with decreasing eruption age indicates a decrease in supply of basaltic magma to the crust [*Frey et al.*, 2000]. The flood basalt sections in the Plateau Central are consistent with these interpretations. At Mt. Capitole alkalic basalt overlies tholeiitic basalt; the youngest lavas are plagioclase-phyric lavas that formed by mixing of plagioclase-rich magma with a highly evolved magma. At Mt. Tourmente [*Frey et al.*, 2002a] alkalic basalt overlies tholeiitic to transitional basalt, most lavas are aphyric with low MgO contents (4.05 to 6.38 wt% in 64 lavas). At Mt. Marion Dufresne [*Annell et al.*, 2007] the lower 300 m of alkalic lavas with < 5.2 wt% MgO grades upwards to plagioclase-phyric lavas overlain by 400 m of olvine-phyric, less alkalic lavas with 7 to 11 wt% MgO; within this upper interval there are three quartz-bearing basaltic andesites that reflect mixing of an evolved, quartz-bearing magma with basaltic magma. These characteristics of flood basalt in the Plateau Central show that these sections recorded a complex temporal transition from tholeiitic to alkaline volcanism and that the accompanying decrease in flux of basaltic magma provided time intervals for cooling and fractionation of basaltic magma.

5.3 Origin of Isotopic Variability in Kerguelen Archipelago Lavas

Basalt from the Cenozoic Northern Kerguelen Plateau, the Kerguelen Archipelago, and Heard Island define an inverse trend between $^{87}Sr/^{86}Sr$ and $^{143}Nd/^{144}Nd$ that ranges from the field of Southeast Indian Ridge (SEIR) MORB to $^{87}Sr/^{86}Sr$ of ~0.7060 (Figure 11a). This trend is commonly inferred to reflect mixing of a plume-related component with relatively high $^{87}Sr/^{86}Sr$ and low $^{143}Nd/^{144}Nd$ with a component similar to SEIR MORB [e.g., *Gautier et al.*, 1990]. This conclusion is especially robust for the ~34 Ma submarine Ocean Drilling Program (ODP) Site 1140 basalt recovered from the Northern Kerguelen Plateau, which erupted within 50 km of the SEIR [*Weis and Frey*, 2002]. Among lavas forming the Kerguelen Archipelago, the MORB-like component is minimal in the youngest alkalic lavas (e.g., Mt. Ross and Southeast Province Upper Miocene Series) and some of the oldest tholeiitic lavas (Group P of Mts Bureau and Rabouillère, where P indicates plume-derived, [*Yang et al.*, 1998]) and most abundant in some of the older tholeiitic to transitional basalt (e.g., Group D lavas from Mt. Bureau, where D indicates relatively depleted, [*Yang et al.*, 1998]) (Figure 11a).

In contrast to the well-defined linear trend in Figure 11a, plots of $^{87}Sr/^{86}Sr$, $^{143}Nd/^{144}Nd$, $^{176}Hf/^{177}Hf$ and $^{208}Pb/^{204}Pb$ vs. $^{206}Pb/^{204}Pb$ show more complexity (Figure 16). As in Figure 11a, in Figure 16 Site 1140 basalts from the Northern Kerguelen Plateau extend from the SEIR MORB field toward the Kerguelen plume field ($^{87}Sr/^{86}Sr$ ~0.7052, $^{143}Nd/^{144}Nd$ ~0.5126, $^{176}Hf/^{177}Hf$ ~0.2829 and $^{206}Pb/^{204}Pb$ ~18.53); two-component mixing between Kerguelen plume and MORB-like components is inferred [*Weis and Frey*, 2002]. However, lavas collected from sections of the flood basalt forming the Kerguelen Archipelago define trends that are at high angles to the Site 1140 trend (Figure 16). Some trends, such as the Charbon/Jaune lavas from the Southeast

Province, range from the plume field to higher $^{87}Sr/^{86}Sr$ and lower $^{206}Pb/^{204}Pb$; the Southeast Province UMS field has a similar slope but at higher $^{87}Sr/^{86}Sr$, lower $^{143}Nd/^{144}Nd$ and $^{206}Pb/^{204}Pb$ and higher $^{208}Pb/^{204}Pb$ at a given $^{206}Pb/^{204}Pb$; other groups, such as lavas from Mt. Capitole and Mts des Ruches and Fontaine, define trends subparallel to the trends of the Southeast Province lavas, but they originate from the plume-SEIR MORB mixing trend. Other than Northern Kerguelen Province Site 1140 lavas, the largest proportion of a MORB-related component is in Group D lavas from Mt. Bureau (Figure 16).

We conclude that some lavas, such as Group P of Mt. Bureau and Mt. Rabouillère, Charbon/Jaune and Upper Miocene Series from the Southeast Province, and Heard Island (Big Ben Series) define isotopic fields consistent with mixing of a plume component with a component having higher $^{87}Sr/^{86}Sr$, and lower $^{143}Nd/^{144}Nd$, $^{176}Hf/^{177}Hf$ and $^{206}Pb/^{204}Pb$ and high $^{208}Pb/^{204}Pb$ at a given $^{206}Pb/^{204}Pb$ (Figure 16). However, other groups, such as Group D of Mt. Bureau and Mt. Rabouillère, Mt. des Ruches, Mt. Fontaine, Mt. Tourmente and Mt. Capitole lavas, were created by two distinct mixing processes; the first process involving variable proportions of MORB-like and plume-related components followed by variable addition of a component with high $^{87}Sr/^{86}Sr$, and low $^{143}Nd/^{144}Nd$, $^{176}Hf/^{177}Hf$ and $^{206}Pb/^{204}Pb$ (Figure 16). Evidence that such a component is present in the mantle below the archipelago is a metasomatized, clinopyroxene-bearing dunite xenolith found in a Upper Miocene Series basanite breccia; it has acid-leached whole-rock $^{206}Pb/^{204}Pb$ of 17.72 and $^{87}Sr/^{86}Sr$ of 0.7072 and an acid-leached clinopyroxene separate has $^{87}Sr/^{86}Sr$ of 0.7056 [*Mattielli et al.*, 1999] (see arrow in Figure 16a). The metasomatic component may be derived from the plume, perhaps originating as deeply recycled

continental lithosphere [*Barling et al.*, 1994; *Doucet et al.*, 2005] or deeply recycled oceanic crust containing sediment. Alternatively as concluded by *Mattielli et al.* [1999] and consistent with the two stage mixing model presented here, this component may have been introduced relatively recently during ascent of plume-derived magma, perhaps by interaction with continental components in the underlying Cretaceous Kerguelen Plateau (e.g., ODP Site 747 in Figure 16e).

What is the origin of the component with low $^{143}Nd/^{144}Nd$, $^{176}Hf/^{177}Hf$, $^{206}Pb/^{204}Pb$ and high $^{87}Sr/^{86}Sr$ ratios? Both ancient sediment and subcontinental lithosphere (lower continental crust and mantle) may have these characteristics [e.g., *Huang et al.*, 1995; *Rehkämper and Hofmann*, 1997; *Downes et al.*, 2001; *Liu et al.*, 2004; *Janney et al.*, 2005; *Lustrino*, 2005]. A difficulty with attributing low $^{206}Pb/^{204}Pb$ to recycled sediment is that sediment is likely to be accompanied by a much larger mass of altered igneous crust; this basaltic crust may mask the effects of sediment. For example, altered MORB has very high $^{238}U/^{204}Pb$, and this ratio is further increased by subduction zone processing [*Kelley et al.*, 2005], which counteracts the effect of the low $^{238}U/^{204}Pb$ in sediment. Consequently, models favoring recycled sediments may assume extreme, perhaps unrealistic, values for sediment. As an example, a model for explaining the DUPAL anomaly of Indian Ocean MORB [*Rehkämper and Hofmann*, 1997] used a $^{238}U/^{204}Pb$ ratio of 2, whereas GLOSS (Global subducted sediment) has $^{238}U/^{204}Pb$ of 5.1 [*Plank and Langmuir*, 1998], and a Pb content of 55 ppm whereas GLOSS has 20 ppm Pb [also see *Zhang et al.*, 2005]. In contrast, lower continental crust has relatively low $^{238}U/^{204}Pb$ ratio [~3, *Rudnick and Gao*, 2004], which will lead to relatively low $^{206}Pb/^{204}Pb$ ratio with increasing age.

There is evidence for subcontinental lithospheric mantle beneath the Kerguelen Archipelago; i.e., some harzburgite xenoliths in basanite dikes in the Courbet Peninsula (Figure 1) have the low $^{187}Os/^{188}Os$ characteristic of subcontinental lithospheric mantle [*Hassler and Shimizu*, 1998]. However, basalts from the Kerguelen Archipelago [*Yang et al.*, 1998; *Weis et al.*, 2000]; and Heard Island [*Barling et al.*, 2003] are not characterized by such low Os isotopic ratios. Therefore it is unlikely that subcontinental lithospheric mantle was the major source component that led to the low $^{143}Nd/^{144}Nd$, $^{176}Hf/^{177}Hf$, $^{206}Pb/^{204}Pb$ and high $^{87}Sr/^{86}Sr$ in some archipelago lavas.

Some lower continental crust, especially of Archean age, has very unradiogenic Pb isotopic ratios [e.g., *Dickin*, 1981; *Huang et al.*, 1995]. Moreover, Archean cratons (India, South Africa, Antarctica and Australia) surround the Indian Ocean. Therefore we evaluate evidence for lower continental crust as a component that contributed to Kerguelen Archipelago lavas. Based on oxygen isotopic ratios, the proportion of lower continental crust in Kerguelen Archipelago lavas is small. For example, the few $\delta^{18}O$ measurements of olivine phenocrysts from the Kerguelen and Heard Islands lavas are within the range of upper mantle peridotite and MORB sources [*Eiler et al.*, 1997]. If lower continental crust has $\delta^{18}O$ of ~8.1‰ [*Simon and Lécuyer*, 2005], the absence of anomalous $\delta^{18}O$ in Kerguelen Archipelago and Heard Island basalt limits lower continental crust to less than 14%; i.e., larger amounts of these components would result in $\delta^{18}O$ greater than that found in upper mantle peridotite and MORB sources which range from 5.0 - 5.4‰ [*Eiler et al.*, 1997].

We have previously argued that the absence of relative depletion in Nb and Ta abundance is inconsistent with a continental component contributing to Kerguelen

Archipelago lavas [e.g., *Yang et al.*, 1998; *Doucet et al.*, 2002; *Frey et al.*, 2002a]. Specifically, Kerguelen Archipelago lavas lack the marked relative depletion in Nb, i.e., $(La/Nb)_{PM}$ and $(Th/Nb)_{PM}$ $\geq$1.5 (PM indicates primitive mantle from [*Sun and McDonough*, 1989]), found in Cretaceous basalt forming the Kerguelen Plateau at ODP Sites 738, 747 and 1137 (Figure 17a). Such plateau basalt is interpreted to be plume-derived basalt that assimilated continental crust [*Mahoney et al.*, 1995; *Weis et al.*, 2001; *Ingle et al.*, 2002; *Frey et al.*, 2003]. Mt. Capitole lavas in the Lower Transitional and Low-Silica Groups range from only ~0.75 to ~1 in $(La/Nb)_{PM}$ and $(Th/Nb)_{PM}$, but these ratios are positively correlated (Figure 17a, b). Although low degree of melting (<6%) can change La/Nb and Th/Nb ratios, the melting trend leads to more variable La/Nb than Th/Nb (Figure 17b). Two samples (93-490 and 93-505) from the Lower Transitional Group which are offset to higher $^{87}Sr/^{86}Sr$ at a given $^{143}Nd/^{144}Nd$ and offset to higher $^{207}Pb/^{204}Pb$ at a given $^{206}Pb/^{204}Pb$ have the lowest $^{206}Pb/^{204}Pb$ and relatively high Th/Nb ratios (Figures 11a, 12b and 17b). These characteristics are consistent with the involvement of a continental component. Figure 17b shows mixing trends for two estimates of lower continental crust compositions. We note that these amounts of lower continental crust, 6-20%, are maximum values because the lower continental crust of stable, mature continents (i.e., Archean cratons) may be silicic, e.g., the Lewisian in Scotland [*Rudnick and Gao*, 2004; *Willbold and Stracke*, 2006]. Such lower continental crust is readily partially melted by basaltic magma; consequently lower proportions of incompatible element rich melt would be required.

Compared to oceanic basalt, lower continental crust has distinctive incompatible trace element ratios that involve Nb and Pb. For example, lower continental crust has

Ce/Pb and Nb/U ratios of 5 and 25, respectively [*Rudnick and Gao*, 2004], whereas fresh ocean island basalt (OIB) has Ce/Pb and Nb/U ratio of 25±5 and 47±10, respectively [*Hofmann et al.*, 1986]. Mt Capitole lavas have average Ce/Pb (24±2.7) and Nb/U (45±9.5 for lavas with LOI<2.5%). Although these averages for Mt. Capiotle lavas overlap those of OIB, Mt. Capitole lavas define a weak correlation between Ce/Pb, Nb/U and $(Th/Nb)_{PM}$ (e.g., Figure 17c). Mass balance calculations shows that addition of 18% lower continental crust of *Rudnick and Gao* [2004] or 6% lower continental crust of *Shaw et al.* [1994] decreases Ce/Pb from 23.5 to 18.5 and 21, and Nb/U from 43.5 to 42.3 and 41.3, respectively.

Lavas related to the Kerguelen hotspot that have high $(La/Nb)_{PM}$ also have distinctive radiogenic isotopic ratios. For example, Kerguelen Plateau lavas with high $(La/Nb)_{PM}$ have high $^{208}Pb/^{204}Pb$ at a given $^{206}Pb/^{204}Pb$ [Figure 10 of *Frey et al.*, 2003]. In Figure 17d we show that as in Figure 16, Site 1140 lavas define a mixing line between SEIR MORB and the plume whereas the Big Ben Series of Heard Island and the Upper Miocene Series from Southeast Province in the Kerguelen Archipelago define a trend between the plume and lower continental crust.

6. Summary

Geochemical and petrographic characteristics define three distinct basalt types in the Mt. Capitole section. The Lower Transitional Group, tholeiitic/transitional lavas, is compositionally distinct from the overlying Low Silica Group, transitional to alkalic lavas. This upwards transition from tholeiitic to alkalic composition is also observed at nearby Mt. Tourmente and is analogous to the ~30 to 24 Ma compositional change of the flood basalt forming the bulk of the Kerguelen Archipelago. In contrast the uppermost

lavas, Upper Transitional Group, are distinguished by abundant plagioclase xenocrysts that show evidence for magma mixing.

Mt. Capitole lavas define trends in $^{206}Pb/^{204}Pb$ vs. $^{87}Sr/^{86}Sr$, $^{143}Nd/^{144}Nd$, $^{176}Hf/^{177}Hf$ and $^{208}Pb/^{204}Pb$ that do not extrapolate to the field of SEIR MORB (Figure 16). These trends cannot be explained by plume-MORB mixing. We propose a two-step mixing process for forming the ~29-25 Ma flood basalt of the Kerguelen Archipelago; that is mixing of MORB-like and plume-related components followed by variable addition of a continental-related component with high $^{87}Sr/^{86}Sr$ and low $^{143}Nd/^{144}Nd$, $^{176}Hf/^{177}Hf$ and $^{206}Pb/^{204}Pb$. This temporal sequence of events explains the slopes of arrays for the Mt. Capitole lavas and lavas from Mt. des Ruches and Fontaine (Figure 16). Our mixing scenario schematically illustrated in Figure 16e is similar to that proposed by *Doucet et al.* [2005]. Mixing trend 1 involves the Kerguelen plume- and MORB-like components (thick black curve in Figure 16e). Mixing trend 2 involves addition of a continental component, probably lower continental crust, to a Kerguelen plume derived magma (thick red curve in Figure 16e) or to mixtures of the plume- and MORB-like components (thin red curves in Figure 16e). The first mixing event is best represented by NKP Site 1140 lavas and the second mixing event is consistent with the trend of Mt. Capitole lavas. Since Cretaceous Kerguelen Plateau may underlie the Cenozoic Kerguelen Archipelago, and some basalt forming the plateau has assimilated continental crust [e.g., *Mahoney et al.*, 1995; *Frey et al.*, 2002b], it is possible that the continental crust signature evident in some archipelago lavas was acquired by assimilation of plateau lavas that were contaminated by lower continental crust [*Ingle et al.*, 2003].

Acknowledgements

I thank M. Lo Cascio, Stephanie Ingle and Sonia Doucet for assistance during sample preparation in Brussels, B. Kieffer and J. Barling for help in acquisition of the whole rock isotopic data, F. Dudas and S. Bowring for advice and assistance during plagioclase separation and acquisition of isotopic data, B. Grant and R. Kayser for their assistance with ICP-MS analyses, and P. Ila for her assistance in obtaining INAA data. N. Chatterjee, T.L. Grove, E. Medard and J. Barr are thanked for their assistance in obtaining mineral composition data. Each of these individuals plus M. Lustrino and T. Plank are thanked for helpful discussions. This study was supported by National Science Foundation grants to F.F. and NSERC Discovery grants to D.W. and J. S.. Isotopic data for plagioclase phenocrysts were obtained free of charge with S. Bowring's support. I thank M. Regelous and A. Saunders for their review comments and V. Salters for his comments and suggestions. This chapter was contributed by co-authors (F. Frey, D. Weis, J. Scoates and A. Giret) which lead to the paper published in G^3.

References

Macdonald, G. A., and T. Katsura (1964), Chemical compositional of Hawaiian lavas, *J. Petrol.*, *5*, 82-133.

Giret, A., B. Bonin, and J. M. Léger (1980), Amphibole conpositional trends in oversaturated and undersaturated alkaline plutonic ring complexes, *Canadian Mineralogist*, *18*, 481-495.

Dickin, A. P. (1981), Isotope Geochemistry of Tertiary Igneous Rocks from the Isle of Skye, Nw Scotland, *J. Petrol.*, *22*, 155-189.

Hofmann, A. W., K. P. Jochum, M. Seufert, and W. M. White (1986), Nb and Pb in Oceanic Basalts - New Constraints on Mantle Evolution, *Earth Planet. Sci. Lett.*, *79*, 33-45.

Sun, S.-S., and W. F. McDonough (1989), Chemical and isotopic systematics of oceanic basalts: implications for mantle composition and processes. In: Saunders, A.D., Norry, M.J. (eds.). Magmatism in the Ocean Basins, *Geological Society Special Publication*, *42*, 313-345.

Gautier, I., D. Weis, J. P. Mennessier, P. Vidal, A. Giret, and M. Loubet (1990), Petrology and Geochemistry of the Kerguelen Archipelago Basalts (South Indian-Ocean) - Evolution of the Mantle Sources from Ridge to Intraplate Position, *Earth Planet. Sci. Lett.*, *100*, 59-76.

Housh, T., and S. A. Bowring (1991), Lead Isotopic Heterogeneities within Alkali Feldspars - Implications for the Determination of Initial Lead Isotopic Compositions, *Geochim. Cosmochim. Acta*, *55*, 2309-2316.

Nelson, S. T., and A. Montana (1992), Sieve-Textured Plagioclase in Volcanic-Rocks Produced by Rapid Decompression, *Am. Mineral.*, *77*, 1242-1249.

Sisson, T. W., and T. L. Grove (1993), Experimental Investigations of the Role of H2O in Calc-Alkaline Differentiation and Subduction Zone Magmatism, *Contrib. Mineral. Petrol.*, *113*, 143-166.

Weis, D., F. A. Frey, H. Leyrit, and I. Gautier (1993), Kerguelen Archipelago Revisited - Geochemical and Isotopic Study of the Southeast Province Lavas, *Earth Planet. Sci. Lett.*, *118*, 101-119.

Barling, J., S. L. Goldstein, and I. A. Nicholls (1994), Geochemistry of Heard-Island (Southern Indian-Ocean) - Characterization of an Enriched Mantle Component and Implications for Enrichment of the Sub-Indian Ocean Mantle, *J. Petrol.*, *35*, 1017-1053.

Coffin, M. F., and O. Eldholm (1994), Large Igneous Provinces - Crustal Structure, Dimensions, and External Consequences, *Reviews of Geophysics*, *32*, 1-36.

Shaw, D. M., A. P. Dickin, H. Li, R. H. Mcnutt, H. P. Schwarcz, and M. G. Truscott (1994), Crustal Geochemistry in the Wawa-Foleyet Region, Ontario, *Canadian Journal of Earth Sciences*, *31*, 1104-1121.

Hilton, D. R., J. Barling, and O. E. Wheller (1995), Effect of Shallow-Level Contamination on the Helium Isotope Systematics of Ocean-Island Lavas, *Nature*, *373*, 330-333.

Huang, Y. M., P. Vancalsteren, and C. J. Hawkesworth (1995), The Evolution of the Lithosphere in Southern Africa - a Perspective on the Basic Granulite Xenoliths from Kimberlites in South-Africa, *Geochim. Cosmochim. Acta*, *59*, 4905-4920.

Mahoney, J. J., W. B. Jones, F. A. Frey, V. J. M. Salters, D. G. Pyle, and H. L. Davies (1995), Geochemical Characteristics of Lavas from Broken Ridge, the Naturaliste Plateau and Southernmost Kerguelen Plateau - Cretaceous Plateau Volcanism in the Southeast Indian-Ocean, *Chem. Geol.*, *120*, 315-345.

Rhodes, J. M. (1996), Geochemical stratigraphy of lava flows sampled by the Hawaii Scientific Drilling Project, *J. Geophy. Res.*, *101*, 11729-11746.

Todt, W., R. A. Cliff, A. Hanser, and A. W. Hofmann (1996), Evaluation of a $^{202}Pb/^{205}Pb$ double spike for high-precision lead isotope analysis, *Geophys. Monogr., Am. Geophys. Union*, *95*, 429-437.

Blichert-Toft, J., C. Chauvel, and F. Albarède (1997), Separation of Hf and Lu for high-precision isotope analysis of rock samples by magnetic sector multiple collector ICP-MS, *Contrib. Mineral. Petrol.*, *127*, 248-260.

Eiler, J. M., K. A. Farley, J. W. Valley, E. Hauri, H. Craig, S. R. Hart, and E. M. Stolper (1997), Oxygen isotope variations in ocean island basalt phenocrysts, *Geochim. Cosmochim. Acta*, *61*, 2281-2293.

Leake, B. E., A. R. Woolley, W. D. Birch, M. C. Gilbert, J. D. Grice, F. C. Hawthorne, A. Kato, H. J. Kisch, V. G. Krivovichev, K. Linthout, J. Laird, J. Mandarino, W. V. Maresch, E. H. Nickel, N. M. S. Rock, J. C. Schumacher, D. C. Smith, N. C. N. Stephenson, L. Ungaretti, E. J. W. Whittaker, and G. Youzhi (1997), Nomenclature of amphiboles - Report of the subcommittee on Amphiboles of the International Mineralogical Association Commission on New Minerals and Mineral Names, *European Journal of Mineralogy*, *9*, 623-651.

Rehkämper, M., and A. W. Hofmann (1997), Recycled ocean crust and sediment in Indian Ocean MORB, *Earth Planet. Sci. Lett.*, *147*, 93-106.

Bindeman, I. N., A. M. Davis, and M. J. Drake (1998), Ion microprobe study of plagioclase-basalt partition experiments at natural concentration levels of trace elements, *Geochim. Cosmochim. Acta*, *62*, 1175-1193.

Hassler, D. R., and N. Shimizu (1998), Osmium isotopic evidence for ancient subcontinental lithospheric mantle beneath the Kerguelen Islands, southern Indian Ocean, *Science*, *280*, 418-421.

Plank, T., and C. H. Langmuir (1998), The chemical composition of subducting sediment and its consequences for the crust and mantle, *Chem. Geol.*, *145*, 325-394.

Weis, D., F. A. Frey, A. Giret, and J. M. Cantagrel (1998), Geochemical characteristics of the youngest volcano (Mount Ross) in the Kerguelen Archipelago: Inferences for magma flux, lithosphere assimilation and composition of the Kerguelen plume, *J. Petrol.*, *39*, 973-994.

Yang, H.-J., F. A. Frey, D. Weis, A. Giret, D. Pyle, and G. Michon (1998), Petrogenesis of the flood basalts forming the northern Kerguelen Archipelago: Implications for the Kerguelen Plume, *J. Petrol.*, *39*, 711-748.

Mattielli, N., D. Weis, J. S. Scoates, N. Shimizu, J. P. Mennessier, M. Gregoire, J. Y. Cottin, and A. Giret (1999), Evolution of heterogeneous lithospheric mantle in a plume environment beneath the Kerguelen Archipelago, *J. Petrol.*, *40*, 1721-1744.

Vervoort, J. D., P. J. Patchett, J. Blichert-Toft, and F. Albarede (1999), Relationships between Lu-Hf and Sm-Nd isotopic systems in the global sedimentary system, *Earth Planet. Sci. Lett.*, *168*, 79-99.

Frey, F. A., D. Weis, H. J. Yang, K. Nicolaysen, H. Leyrit, and A. Giret (2000), Temporal geochemical trends in Kerguelen Archipelago basalts: evidence for decreasing magma supply from the Kerguelen Plume, *Chem. Geol.*, *164*, 61-80.

Ila, P., and F. Frey (2000), Trace element analysis of USGS standards AGV2, BCR2, BHVO2, DTS2 and GSP2 by INAA, *Journal of Radioanalysis and Nuclear Chemistry*, *244*, 599-602.

Nicolaysen, K., F. A. Frey, K. V. Hodges, D. Weis, and A. Giret (2000), Ar-40/Ar-39 geochronology of flood basalts from the Kerguelen Archipelago, southern Indian Ocean: implications for Cenozoic eruption rates of the Kerguelen plume, *Earth Planet. Sci. Lett.*, *174*, 313-328.

Weis, D., S. B. Shirey, and F. A. Frey (2000), Re-Os systematics of Kerguelen Plume basalts: Enriched components and lower mantle source, *Eos Trans. AGU*, *81*, Fall Meet. Suppl. Abstract V11C-09.

Chauvel, C., and J. Blichert-Toft (2001), A hafnium isotope and trace element perspective on melting of the depleted mantle, *Earth Planet. Sci. Lett.*, *190*, 137-151.

Downes, H., A. J. W. Markwick, P. D. Kempton, and M. F. Thirlwall (2001), The lower crust beneath cratonic north-east Europe: isotopic constraints from garnet granulite xenoliths, *Terra Nova*, *13*, 395-400.

Weis, D., S. Ingle, D. Damasceno, F. A. Frey, K. Nicolaysen, J. Barling, and L. S. S. Party (2001), Origin of continental components in Indian Ocean basalts: Evidence from Elan Bank (Kerguelen Plateau, ODP Leg 183, Site 1137), *Geology*, *29*, 147-150.

Coffin, M. F., M. S. Pringle, R. A. Duncan, T. P. Gladczenko, M. Storey, R. D. Muller, and L. A. Gahagan (2002), Kerguelen Hotspot Magma Output since 130 Ma, *J. Petrol.*, *43*, 1121-1137.

Damasceno, D., J. S. Scoates, D. Weis, F. A. Frey, and A. Giret (2002), Mineral Chemistry of Mildly Alkalic Basalts from the 25 Ma Mont Crozier Section, Kerguelen Archipelago: Constraints on Phenocryst Crystallization Environments, *J. Petrol.*, *43*, 1389-1413.

Doucet, S., D. Weis, J. S. Scoates, K. Nicolaysen, F. A. Frey, and A. Giret (2002), The Depleted Mantle Component in Kerguelen Archipelago Basalts: Petrogenesis of Tholeiitic-Transitional Basalts From the Loranchet Peninsula, *J. Petrol.*, *43*, 1341-1366.

Eisele, J., M. Sharma, S. J. G. Galer, J. Blichert-Toft, C. W. Devey, and A. W. Hofmann (2002), The role of sediment recycling in EM-1 inferred from Os, Pb, Hf, Nd, Sr isotope and trace element systematics of the Pitcairn hotspot, *Earth Planet. Sci. Lett.*, *196*, 197-212.

Frey, F. A., K. Nicolaysen, B. K. Kubit, D. Weis, and A. Giret (2002a), Flood Basalt from Mont Tourmente in the Central Kerguelen Archipelago: the Change from Transitional to Alkalic Basalt at ~25 Ma, *J. Petrol.*, *43*, 1367-1387.

Frey, F. A., D. Weis, A. Y. Borisova, and G. Xu (2002b), Involvement of Continental Crust in the Formation of the Cretaceous Kerguelen Plateau: New Perspectives from ODP Leg 120 Sites, *J. Petrol.*, *43*, 1207-1239.

Ingle, S., D. Weis, and F. A. Frey (2002), Indian Continental Crust Recovered from Elan Bank, Kerguelen Plateau (ODP Leg 183, Site 1137), *J. Petrol.*, *43*, 1241-1257.

Kieffer, B., N. T. Arndt, and D. Weis (2002), A Bimodal Alkalic Shield Volcano on Skiff Bank: its Place in the Evolution of the Kerguelen Plateau, *J. Petrol.*, *43*, 1259-1286.

Mahoney, J. J., D. W. Graham, D. M. Christie, K. T. M. Johnson, L. S. Hall, and D. L. Vonderhaar (2002), Between a Hotspot and a Cold Spot: Isotopic Variation in the Southeast Indian Ridge Asthenosphere, 86°E-118°E, *J. Petrol.*, *43*, 1155-1176.

Mattielli, N., D. Weis, J. Blichert-Toft, and F. Albarède (2002), Hf Isotope Evidence for a Miocene Change in the Kerguelen Mantle Plume Composition, *J. Petrol.*, *43*, 1327-1339.

Neal, C. R., J. J. Mahoney, and W. J. Chazey, III (2002), Mantle Sources and the Highly Variable Role of Continental Lithosphere in Basalt Petrogenesis of the Kerguelen Plateau and Broken Ridge LIP: Results from ODP Leg 183, *J. Petrol.*, *43*, 1177-1205.

Wallace, P. J., F. A. Frey, D. Weis, and M. F. Coffin (2002), Origin and Evolution of the Kerguelen Plateau, Broken Ridge and Kerguelen Archipelago: Editorial, *J. Petrol.*, *43*, 1105-1108.

Weis, D., and F. A. Frey (2002), Submarine Basalts of the Northern Kerguelen Plateau: Interaction Between the Kerguelen Plume and the Southeast Indian Ridge Revealed at ODP Site 1140, *J. Petrol.*, *43*, 1287-1309.

Barling, J., J. S. McBride, D. D. Lambert, and I. A. Nicholls (2003), Osmium isotope evidence for mantle vs. magma contamination in Heard Island lavas, paper presented at GAC-MAC meeting, Vancouver, BC Canada.

Frey, F. A., M. F. Coffin, P. J. Wallace, and D. Weis (2003), Leg 183 synthesis: Kerguelen Plateau - Broken Ridge - A large igneous province, in *Proc. ODP, Sci. Results*, edited by F. A. Frey, et al., pp. 1-48, College Station, TX.

Gagnevin, D., R. Ethien, B. Bonin, B. Moine, G. Feraud, M. C. Gerbe, J. Y. Cottin, G. Michon, S. Tourpin, G. Mamias, C. Perrache, and A. Giret (2003), Open-system processes in the genesis of silica- oversaturated alkaline rocks of the Rallier-du-Baty Peninsula, Kerguelen Archipelago (Indian Ocean), *J. Volcano. Geoth. Res.*, *123*, 267-300.

Huang, S., and F. A. Frey (2003), Trace element abundances of Mauna Kea basalt from phase 2 of the Hawaii Scientific Drilling Project: Petrogenetic implications of correlations with major element content and isotopic ratios, *Geochem. Geophy. Geosyst.*, *4*, doi:10.1029/2002GC000322.

Ingle, S., D. Weis, S. Doucet, and N. Mattielli (2003), Hf isotope constraints on mantle sources and shallow-level contaminants during Kerguelen hot spot activity since approximate to 120 Ma, *Geochem. Geophy. Geosyst.*, *4*, doi:10.1029/2002GC000482.

Putirka, K. D., H. Mikaelian, F. Ryerson, and H. Shaw (2003), New clinopyroxene-liquid thermobarometers for maric, evolved, and volatile-bearing lava compositions, with applications to lavas from Tibet and the Snake River Plain, Idaho, *Am. Mineral.*, *88*, 1542-1554.

Annell, H., D. Weis, J. Scoates, and A. Giret (2004), Evidence for a Depleted Mantle Component in Mildly Alkalic High-MgO Basalts From Mt. Marion Dufresne, Kerguelen Archipelago, Southern Indian Ocean, *Eos Trans. AGU, 85(47)*, Fall Meet. Suppl., Abstract V31B-1436.

Hanan, B. B., J. Blichert-Toft, D. G. Pyle, and D. M. Christie (2004), Contrasting origins of the upper mantle revealed by hafnium and lead isotopes from the Southeast Indian Ridge, *Nature*, *432*, 91-94.

Liu, Y., S. Gao, H. Yuan, L. Zhou, X. Liu, X. Wang, Z. Hu, and L. Wang (2004), U-Pb zircon ages and Nd, Sr, and Pb isotopes of lower crustal xenoliths from North China Craton: insights on evolution of lower continental crust, *Chem. Geol.*, *211*, 87-109.

Rudnick, R. L., and S. Gao (2004), Composition of the continental crust, in *Treatise on Geochemistry*, edited by H. D. Holland and K. K. Turekian, pp. 1-64, Elsevier-Pergamon, Oxford.

Sano, T., and S. Yamashita (2004), Experimental petrology of basement lavas from Ocean Drilling Program Leg 192: implications for differentiation processes in Ontong Java Plateau magmas, in *Origin and Evolution of the Ontong Java Plateau*, edited by J. G. Fitton, et al., pp. 185-218, Geological Society, London.

Doucet, S., J. S. Scoates, D. Weis, and A. Giret (2005), Constraining the components of the Kerguelen mantle plume: A Hf-Pb-Sr-Nd isotopic study of picrites and high-MgO basalts from the Kerguelen Archipelago, *Geochem. Geophy. Geosyst.*, *6*, doi:10.1029/2004GC000806.

Honda, M., and J. D. Woodhead (2005), A primordial solar-neon enriched component in the source of EM-I-type ocean island basalts from the Pitcairn Seamounts, Polynesia, *Earth Planet. Sci. Lett.*, *236*, 597-612.

Janney, P. E., A. P. Le Roex, and R. W. Carlson (2005), Hafnium Isotope and Trace Element Constraints on the Nature of Mantle Heterogeneity beneath the Central Southwest Indian Ridge (13°E to 47°E), *J. Petrol.*, *46*, 2427 - 2464.

Kelley, K. A., T. Plank, L. Farr, J. Ludden, and H. Staudigel (2005), Subduction cycling of U, Th, and Pb, *Earth Planet. Sci. Lett.*, *234*, 369-383.

Lustrino, M. (2005), How the delamination and detachment of lower crust can influence basaltic magmatism, *Earth Sci. Rev.*, *72*, 21-38.

Simon, L., and C. Lécuyer (2005), Continental recycling: The oxygen isotope point of view, *Geochem. Geophy. Geosyst.*, *6*, doi:10.1029/2005GC000958.

Weis, D., B. Kieffer, C. Maerschalk, W. Pretorius, and J. Barling (2005), High-precision Pb-Sr-Nd-Hf isotopic characterization of USGS BHVO-1 and BHVO-2 reference materials, *Geochem. Geophy. Geosyst.*, *6*, doi:10.1029/2004GC000852.

Zhang, S. Q., J. J. Mahoney, X. X. Mo, A. M. Ghazi, L. Milani, A. J. Crawford, T. Y. Guo, and Z. D. Zhao (2005), Evidence for a Widespread Tethyan Upper Mantle with Indian-Ocean-Type Isotopic Characteristics, *J. Petrol.*, *46*, 829-858.

Graham, D. W., J. Blichert-Toft, C. J. Russo, K. H. Rubin, and F. Albarede (2006), Cryptic striations in the upper mantle revealed by hafnium isotopes in southeast Indian ridge basalts, *Nature*, *440*, 199-202.

Weis, D., B. Kieffer, C. Maerschalk, J. Barling, J. De Jong, G. Williams, D. Hanano, W. Pretorius, N. Mattielli, J. S. Scoates, A. Goolaerts, R. Friedman, and J. B. Mahoney (2006), High precision isotopic characterization of USGS reference materials by TIMS and MC-ICP-MS, *Geochem. Geophy. Geosyst.*, *doi:10.1029/2006001283*.

Willbold, M., and A. Stracke (2006), Trace element composition of mantle end-members: Implications for recycling of oceanic and upper and lower continental crust, *Geochem. Geophy. Geosyst.*, *7*, doi:10.1029/2005GC001005.

Annell, H., S. J. Scoates, D. Weis, and A. Giret (2007), Petrology and phenocryst mineral chemistry in flood basalts from the tholeiitic-alkalic transition, Mt. Marion Dufresne, Kerguelen Archipelago, Southern Indain Ocean, *Canadian Mineralogist*, in press.

Figure Captions

Figure 1. Map of the Kerguelen Archipelago [after *Yang et al.*, 1998] showing the major geologic units, the location of studied stratigraphic sections of flood basalt, and Mt. Ross which is the youngest volcanic edifice in the archipelago. Mt. Capitole (red dot) is in the Plateau Central. Ages for these sections are from [*Weis et al.*, 1993; *Weis et al.*, 1998; *Nicolaysen et al.*, 2000; *Doucet et al.*, 2002; *Annell et al.*, 2004]. Inset is a map showing the Southeast Indian Ocean Ridge (SEIR), the Kerguelen Plateau, a Cretaceous large igneous province, and the Cenozoic Kerguelen Archipelago and Heard Islands located on the Northern and Central Kerguelen Plateau, respectively. Filled stars show Kerguelen Plateau drill sites discussed in the text (Site738, *Mahoney et al.* [1995]; Site 747, *Frey et al.* [2002b]; Site 1137, *Ingle et al.* [2002]; Site 1140, *Weis and Frey* [2002]).

Figure 2. Location of studied samples (black horizons with sample numbers) in the Mt. Capitole section. The base is at 69°17′51"E and 49°19′32"S and the summit is at 69°19′00"E and 49°19′51"S. The vertical exaggeration is a factor of 5. The open regions indicate no outcrop or extremely weathered rocks. Samples with elevation greater than 690 m form the Upper Transitional Group, which is defined on the basis of petrography (Table 1) and lava compositions. Sample 93-491, lower in the section, has the characteristics of this group. The Low-Silica Group lavas from 660 m to 560 m have relatively low $SiO_2/Fe_2O_3^*$ ($Fe_2O_3^*$ is total iron). All other lavas belong to the Lower Transitional Group. Also shown are layers of sedimentary breccias and conglomerates, such as a 4 m-thick breccia with angular

pebbles of basalt at 700 m, a 0.2 m-thick red matrix containing basaltic pebbles at 670 m and a 1.5 m-thick breccia at 565 m.

Figure 3. Backscattered electron images of thin sections of Upper Transitional Group samples. (a) Plagioclase xenocryst from sample 93-471 showing irregular morphology that is interpreted as resorption. (b) Sieve-textured plagioclase xenocryst from 93-465 showing abundant inclusions of clinopyroxene, olivine, amphibole and Fe-Ti oxide. (c) Expanded scale of panel "b" showing Na-rich plagioclase domains. (d) Expanded scale of panel "b" showing olivine, clinopyroxene, pigeonite, amphibole, Fe-Ti oxide and apatite inclusions. The inset with increased contrast shows the Na-rich plagioclase rims around the olivine, clinopyroxene, amphibole and Fe-Ti oxide inclusions. These Na-rich plagioclase rims have variable compositions ranging from An_5 to An_{54}. (e) Expanded scale of panel "c" showing the amphibole inclusion. The inset with increased contrast shows the Na-rich plagioclase rim partly surrounding the amphibole inclusion. Note that the plagioclase An composition decreases systematically along the elongated direction of the amphibole, which indicates non-equilibrium crystallization. (f) Another example of an amphibole inclusion in a plagioclase xenocryst from sample 93-459. Plag – plagioclase; CPX – clinopyroxene; PIG – pigeonite; OL – olivine; AMPH – amphibole; TMT – titanomagnetite.

Figure 4. Mg# (100*molar Mg/(Mg + Fe^{2+})) vs. core An content of plagioclase phenocrysts showing that at a given An content, Mt. Captiole plagioclase has higher Mg# than plagioclase from Mt. Crozier [*Damasceno et al.*, 2002] and Mt. Marion Dufresne [*Annell et al.*, 2007]. The vertical error bar shows one standard

deviation of Mg# measured by electron microprobe. The higher Mg# of Mt. Capitole plagioclase is not a result of analytical bias because the Mt. Captiole and Mt. Crozier data were obtained at MIT. Relatively low Mg# is characteristic of plagioclase crystallization after olivine and pyroxene crystallization. This delayed plagioclase crystallization can result from relatively high magmatic H_2O content. *Annell et al.* [2007] argued that the low Mg# of Mt. Marion Dufresne plagioclase was due to shallow crystallization of a relatively hydrous magma (>3% H_2O).

Figure 5. Na_2O+K_2O vs. SiO_2 classification plot showing that the Mt. Capitole lavas straddle the alkalic-tholeiitic dividing line of Macdonald and Katsura [1964]. The filled squares indicate 15 samples from the uppermost 170 m of the section and 93-491 from the lower section, designated as the "Upper Transitional Group". The 9 filled circles indicate "Low-Silica Group" lavas; they have low $SiO_2/Fe_2O_3^*$ ratios and are from the depth range of 560 m to 660 m. The other 29 samples define the "Lower Transitional Group"; labelled sample 93-510 near the bottom of the section (Figure 2) is the most evolved lava with the lowest MgO and highest SiO_2. Major element data were adjusted to a Fe^{2+}/Fe^{total} ratio of 0.85. In general Mt. Capitole lavas are less alkalic than flood basalts erupted in the Southeast Province [*Frey et al.*, 2000] and at Mt. Crozier in the Courbet Peninsula [*Damasceno et al.*, 2002]. They generally overlap with lavas from Mt. Tourmente [*Frey et al.*, 2002a] and lavas erupted in the north-central (Mt. Bureau and Mt. Rabouillère) and northwest (Mt. des Ruches and Mt. Fontaine) parts of the archipelago [*Yang et al.*, 1998; *Doucet et al.*, 2002].

Figure 6. Abundance of TiO_2, $Fe_2O_3^*$ and Al_2O_3 (wt. %) and $SiO_2/Fe_2O_3^*$ ratio versus stratigraphic height (meters) in the Mt. Capitole section. Fe_2O_3* is total iron as Fe_2O_3. Compared to the Lower Transitional Group, the Upper Transitional Group lavas (elevation greater than 690 m, except for 93-491 at 540 m) have relatively low TiO_2 and $Fe_2O_3^*$ and high Al_2O_3 and $SiO_2/Fe_2O_3^*$, whereas Low-Silica Group lavas (elevation between 560 m and 660 m) have low $SiO_2/Fe_2O_3^*$ and high TiO_2 and $Fe_2O_3^*$.

Figure 7. TiO_2, P_2O_5, CaO, Al_2O_3, K_2O, Na_2O, SiO_2 and $Fe_2O_3^*$ abundance vs. MgO content (all in wt%) for Mt. Capitole samples. The encircled fields shown for comparison are transitional lavas (open field) and alkalic lavas (gray field) from nearby Mt. Tourmente [*Frey et al.*, 2002a]. Note that there is a negative Al_2O_3 – MgO trend for the Upper Transitional Group lavas that contrasts with other Mt. Capitole lavas and the Mt. Tourmente fields. In general, the Low-Silica Group lavas and Lower Transitional Group lavas from Mt. Capitole overlap the alkalic and transitional lavas from Mt. Tourmente, respectively.

Figure 8. Abundance of Rb, K_2O, Sr, Ba, Nb, Pb, Zr, and Yb vs. Th content (all in ppm, except K_2O in weight percent) for Mt. Capitole samples. The 2σ standard deviation indicated in each panel is ±3%. The highest Th and other incompatible element abundances are in two samples (93-510 and 93-511) with the lowest MgO contents (Table 3). Sample 93-483 has higher Pb abundance at a given Th content possibly due to Pb contamination. Abundance of K, Rb, Sr and Ba do not vary systematically with Th content, but Rb and K abundance are much more variable than Sr and Ba abundance.

Figure 9. Incompatible trace element abundance in Mt. Capitole lavas normalized to the primitive mantle estimates of *Sun and McDonough* [1989]. The field for alkalic lavas from Mt. Tourmente overlaps with the Low-Silica Group lavas from Mt. Capitole. Important features are the negative slopes from Nb to Yb with a pronounced relative depletion in Sr for the Low-Silica Group and Lower Transitional Group lavas. The Upper Transitional Group lavas are not depleted in Sr. Mt. Capitole lavas range to high Ba/Rb ratios as a result of Rb depletion.

Figure 10. Initial $^{87}Sr/^{86}Sr$, $^{143}Nd/^{144}Nd$ and $^{176}Hf/^{177}Hf$ vs. stratigraphic height (meters) in the Mt. Capitole section calculated at 25.7 Ma. Although there is no long-term correlation, if grouped together the Upper Transitional and Low Silica Groups define trends of increasing $^{87}Sr/^{86}Sr$ and decreasing $^{143}Nd/^{144}Nd$ and $^{176}Hf/^{177}Hf$ with decreasing eruption age. The 2 sigma errors shown are for analyses of NBS987 (Sr), La Jolla (Nd) and JMC475 (Hf) standard (see Table 5).

Figure 11. (a) Initial $(^{87}Sr/^{86}Sr)_i$ vs. $(^{143}Nd/^{144}Nd)_i$ showing that lavas from the Kerguelen Archipelago and Heard Island define a trend ranging from the field for Southeast Indian mid-ocean-ridge basalt (SEIR N-MORB) to relatively high $^{87}Sr/^{86}Sr$ and low $^{143}Nd/^{144}Nd$. "K. Plume" is the average Kerguelen plume composition from Table 3 of *Weis and Frey* [2002]. Red squares show data for Mt. Capitole lavas. The fields designate data for submarine basalt from ODP Site 1140 on the Northern Kerguelen Plateau [*Weis and Frey*, 2002], several stratigraphic sections from the 29-25 Ma flood basalt forming the Kerguelen Archipelago (i.e., the 28-30 Ma northern sections of Group P (plume) and Group D (relatively depleted) lavas from Mts Bureau and Rabouillère [*Yang, et al.*, 1998], lavas from Mts

Fontaine and des Ruches in the north [*Doucet et al.*, 2002], 25-26 Ma lavas from Mt. Capitole and Mt. Tourmente [*Frey et al.*, 2002a] in the Plateau Central, ~25 Ma lavas from Charbon/Jaune in the Southeast Province [*Frey et al.*, 2000], two groups of younger (<10 Ma) and more alkalic lavas with MgO>3 wt% (i.e., lavas from Mt. Ross [*Weis et al.*, 1998] and basanites of the Upper Miocene Series (UMS) in the Southeast Province [*Weis et al.*, 1993]) and Pleistocene/Holocene lavas (Big Ben Series) from Heard Island [*Barling et al.*, 1994], a recently volcanically active island, 440 km southeast of the archipelago (Figure 1 inset)). A second group of Heard Island lavas, Laurens Peninsula Series, overlaps with the field for Mt. des Ruches and Fontaine. The 2σ uncertainties are less than the size of the symbol. All the data are age-corrected to their eruption ages. Data sources are this study, the above references and *Mahoney et al.* [2002] for SEIR MORB. (b) Expanded scale of panel "a" showing data for the two sections sampling the Plateau Central, i.e., a field for Mt. Tourmente and data points for the 3 Mt. Capitole groups; (c) Initial $(^{143}Nd/^{144}Nd)_i$ vs. $(^{176}Hf/^{177}Hf)_i$ for Kerguelen Archipelago lavas. The fields designate data for submarine basalt from ODP Site 1140 on the Northern Kerguelen Plateau [*Weis and Frey*, 2002], the 30-25 Ma flood basalt forming the Kerguelen Archipelago (lavas from Mts Bureau, Fontaine, Rabouillère, des Ruches and Tourmente), and two groups of younger (<10 Ma) and more alkalic lavas with MgO>3 wt% from the archipelago (Mt. Ross, [*Weis et al.*, 1998] and basanites of the UMS from the Southeast Province, [*Weis et al.*, 1993]). ODP Site 747 lavas, age-corrected to 26 Ma, from the Central Kerguelen Plateau are shown as an example of inferred lower continental crust

contamination in the Cretaceous basalt forming the Kerguelen Plateau [*Frey et al.*, 2002b]. Mantle OIB array is taken from *Vervoort et al.* [1999]; (d) Expanded scale of panel "c" showing data for the two lava sections from the Plateau Central. Data sources are the same as for panel "a" plus *Mattielli et al.* [2002], *Chauvel and Blichert-Toft* [2001], *Hanan et al.* [2004] and *Graham et al.* [2006].

Figure 12. Initial $(^{206}Pb/^{204}Pb)_i$ vs $(^{208}Pb/^{204}P)_i$ and $(^{207}Pb/^{204}Pb)_i$ for Mt. Capitole lavas. (a) They define a linear trend in $^{208}Pb/^{204}Pb$ vs $^{206}Pb/^{204}Pb$, overlapping with one end of the measured field defined by Mt. Tourmente lavas. Plagioclase xenocrysts from Upper Transitional Group lavas have higher initial $^{206}Pb/^{204}Pb$ ratios than the whole rocks. (b) Samples 93-490 and 93-505, which are offset to higher $(^{87}Sr/^{86}Sr)_i$ at a given $(^{143}Nd/^{144}Nd)_i$ (Figure 11) have higher $(^{207}Pb/^{204}Pb)_i$ at a given $(^{206}Pb/^{204}Pb)_i$. Plagioclase data are not shown in panel "b" because of large uncertainties in $^{207}Pb/^{204}Pb$ ratios.

Figure 13. $(Sr/Nd)_{PM}$ vs. initial $(^{206}Pb/^{204}Pb)_i$ for Upper Transitional Group lavas from Mt. Capitole. $(Sr/Nd)_{PM}$ broadly increases with abundance of plagioclase phenocrysts; the exception, sample 93-472, has abundant microphenocrysts of plagioclase. The correlation indicates that plagioclase with high Sr/Nd ratio (Table 6) has radiogenic Pb isotopic ratios. Two sigma errors for $(Sr/Nd)_{PM}$ and $(^{206}Pb/^{204}Pb)_i$ are ±3% and the in-run uncertainties, respectively.

Figure 14. Al_2O_3 vs MgO (wt. %) showing that lavas from the flood basalt sections in the northern Kerguelen Archipelago define broad trends consistent with initial olivine fractionation (negative Al_2O_3 - MgO trend) followed by segregation of a plagioclase-rich assemblage (positive Al_2O_3 - MgO trend). In contrast, the

younger, 24 – 25 Ma, flood basalt from the eastern archipelago (Mt. Crozier and Ravin Jaune and du Charbon) define a steep inverse Al_2O_3 - MgO trend that dominantly reflects high pressure clinopyroxene fractionation [*Damasceno et al.*, 2002]. Mt. Capitole lavas (symbols as in Figure 12) show two trends; the uppermost lavas, Upper Transitional Group, define a negative Al_2O_3 vs. MgO trend, but in this case, the trend reflects plagioclase accumulation. In contrast, the Low-Silica and Lower Transitional Groups define a positive Al_2O_3 vs. MgO trend that is consistent with plagioclase fractionation. Inset shows the fractionation/accumulation trends of different phase assemblages; using the measured plagioclase core and clinopyroxene compositions in Mt. Capitole lavas (Table 2) the vectors for plagioclase addition and clinopyroxene fractionation are similar. Data sources are the same as Figure 5.

Figure 15. Geochemical parameters controlled by plagioclase: (a) $(Sr/Nd)_{PM}$ vs Eu/Eu^*, (b, c) $(Sr/Nd)_{PM}$ and $(Ba/Th)_{PM}$ vs MgO content (wt%), and (d, e) Th abundance and Al_2O_3/TiO_2 versus $(Sr/Nd)_{PM}$. Eu* is Eu abundance interpolated from chondrite-normalized abundances of Sm and Gd and subscript "PM" designates normalized to primitive mantle estimate [*Sun and McDonough*, 1989]. Ten of 16 Upper Transitional Group lavas have more than (or equal to) 10 vol% plagioclase phenocrysts (Table 1), which is consistent with their $(Sr/Nd)_{PM}$ and Eu/Eu^* greater than 1, and relatively high $(Ba/Th)_{PM}$ and Al_2O_3/TiO_2. These are all characteristics of plagioclase accumulation. All other Mt. Capitole lavas define trends of decreasing $(Sr/Nd)_{PM}$ and Eu/Eu* with decreasing MgO and increasing Th. These characteristics reflect plagioclase fractionation. Dashed and solid lines in panel

"d" are plagioclase accumulation/fractionation trends starting from aphyric sample 93-467 (An_{76} (solid line) and An_{52} (dashed line); tick marks are 5% intervals). Partition coefficients (Sr and Nd) for plagioclase are from *Bindeman et al.* [1998] and D_{Th} = 0.05. For Upper Transitional Group, plagioclase accumulation is the major process and for other Mt. Capitole lavas plagioclase fractionation is required, but in detail clinopyroxene (±olivine) fractionation is also required.

Figure 16. Initial $^{87}Sr/^{86}Sr$, $^{143}Nd/^{144}Nd$, $^{176}Hf/^{177}Hf$ and $^{208}Pb/^{204}Pb$ vs $^{206}Pb/^{204}Pb$. All data are age corrected except for Pb data for Mt. Tourmente and SE Charbon/Jaune lavas which lack U and Pb abundance data. Red squares indicate Mt. Capitole data. The 2σ uncertainties are less than the size of the symbol. (a) The field for SEIR N-MORB is at relatively low $^{87}Sr/^{86}Sr$ and $^{206}Pb/^{204}Pb$ whereas the inferred ratios for the Kerguelen mantle plume are at relatively high $^{87}Sr/^{86}Sr$ and $^{206}Pb/^{204}Pb$. The average (K. Plume) and radiogenic (rad. K. Plume in panel "d" and "e") Kerguelen plume compositions are from Table 3 of *Weis and Frey* [2002] for $^{87}Sr/^{86}Sr$, $^{143}Nd/^{144}Nd$ and $^{206}Pb/^{204}Pb$ and from *Mattielli et al.* [2002] for $^{176}Hf/^{177}Hf$. Other data fields are as in Figure 11. Note that samples 41 and 42 from Mt. des Ruches are distinct from other lavas in this section. Lavas from the Northern Kerguelen Plateau, Site 1140, are an example of binary mixing between plume and MORB-like components [*Weis and Frey*, 2002], but the elongated trends defined by the groups of Kerguelen and Heard basalt require components with relatively high $^{87}Sr/^{86}Sr$ and low $^{206}Pb/^{204}Pb$; (b) and (c) $^{143}Nd/^{144}Nd$ and $^{176}Hf/^{177}Hf$ vs $^{206}Pb/^{204}Pb$. In contrast to the trends in (a) the slopes for

archipelago groups are positive because $^{87}Sr/^{86}Sr$ is inversely correlated with $^{143}Nd/^{144}Nd$ and $^{176}Hf/^{177}Hf$. Fields defined by data from the same references as in Figure 11 plus *Chauvel and Blichert-Toft* [2001], *Hanan et al.* [2004] and *Graham et al.* [2006]. (d) $(^{206}Pb/^{204}Pb)_i$ vs $(^{208}Pb/^{204}Pb)_i$ showing Mt. Capitole data and fields for various sections of the Kerguelen Archipelago and Heard Island lavas. Lavas from NKP Site 1140 and Group D lavas from Mt. Bureau and Rabouillère define trends that extrapolate towards the SEIR N-MORB field; these trends were attributed to the mixing of Kerguelen plume and SEIR MORB–like components (thick black lines) [*Yang et al.*, 1998; *Weis and Frey*, 2002], but several sections of lavas from Kerguelen Archipelago (Mt. Capitole, Mt. des Ruches and Fontaine, Mt. Bureau and Rabouillère (Group P) and SE Charbon/Jaune) and Big Ben Series lavas from Heard Island define trends towards higher $^{208}Pb/^{204}Pb$ at a given $^{206}Pb/^{204}Pb$ than the field for SEIR N-MORB. Also shown is a field for continental-related clasts in a conglomerate intercalated with basalt from ODP Site 1137 on the Kerguelen Plateau [*Ingle et al.*, 2002]; none of the Kerguelen Archipelago or Heard Island fields extrapolate toward this field. (e) A schematic diagram showing two mixing events. Triangles are data for Site 1140 lavas. The green field schematically shows that although lower continental crust (LCC) is isotopically heterogeneous, a distinguishing characteristic of many LCC samples is unusually low $^{206}Pb/^{204}Pb$ and variable $^{87}Sr/^{86}Sr$ [e.g., *Huang et al.*, 1995; *Downes et al.*, 2001; *Liu et al.*, 2004; *Lustrino*, 2005]. The field for ODP Site 747 lavas from the Central Kerguelen Plateau (CKP) is an example of

inferred LCC contamination in the Cretaceous basalt forming the Kerguelen Plateau [*Frey et al.*, 2002b].

Note that MORB-plume mixing could be either solid-solid mixing or mixing of melts. The MORB-plume mixing trajectory is for melt mixing whereas the addition of LCC assumes bulk assimilation of LCC, i.e., a maximum estimate (see Table 7 for parameters used for mixing endmembers). Mixing curves between Kerguelen plume and LCC are near linear because Sr/Pb ratios for Kerguelen plume and average LCC are similar. The isotopic variation of Mt. Capitole lavas can be explained by mixing of Kerguelen plume primary melt with 50% SEIR MORB followed by ~6% LCC addition using the modeling parameters in Table 7. The ticks on the red line are proportion of LCC at 1% intervals. The proportions for MORB are indicated next to the black line. Two geographically separate Pleistocene/Holocene lava groups from Heard Island have been studied, Big Ben Series and Laurens Peninsula Series (LPS) [*Barling et al.*, 1994]. Like some lavas from the Kerguelen Archipelago, Big Ben Series lavas (x) extend to low $^{206}Pb/^{204}Pb$ and high $^{87}Sr/^{86}Sr$. In contrast, the LPS lavas (open circle) with high $^{3}He/^{4}He$ (16.2-18.3 R/Ra, *Hilton et al.* [1995]) have lower $^{87}Sr/^{86}Sr$ and higher $^{206}Pb/^{204}Pb$ than proposed for the Kerguelen plume, perhaps reflecting plume heterogeneity.

Figure 17. (a) Abundance ratio of $(Th/Nb)_{PM}$ vs $(La/Nb)_{PM}$ showing the field for Kerguelen Archipelago lavas and Mt. Capitole data for the Low-Silica and Lower Transitional Group (red squares). Subscript PM indicates ratios normalized to primitive mantle ratios [*Sun and McDonough*, 1989]. Also shown is average

lower continent crust (LCC) from *Rudnick and Gao* [2004]. Shown for comparion are data points for oceanic basalt inferred to contain a component derived from continental crust; i.e., Kerguelen Plateau Sites 738, 747 and 1137 [*Mahoney et al.*, 1995; *Frey et al.*, 2002b; *Ingle et al.*, 2002] and Pitcairn Island [*Eisele et al.*, 2002; *Honda and Woodhead*, 2005]. (b) Expanded scale of panel "a" showing the positive trend for Mt. Capitole lavas in the Lower Transitional group (squares) and Low-Silica group (blue circles). Upper Transitional Group lavas from Mt. Capitole which have accumulated plagioclase, not plotted in panel "a", are shown as a field because accumulation of plagioclase creates higher La/Nb ratios at a given Th/Nb [*Bindeman et al.*, 1998]. Lower Transitional Group lavas 93-490 and 93-505 with relatively high $^{87}Sr/^{86}Sr$ and $^{207}Pb/^{204}Pb$ at a given $^{143}Nd/^{144}Nd$ and $^{206}Pb/^{204}Pb$, respectively, have relatively high Th/Nb and La/Nb ratios. These characteristics are consistent with involvement of LCC. Using the average lower continental crust composition of *Rudnick and Gao* [2004], ~20% LCC is needed to explain the maximum variation of Th/Nb and La/Nb ratios in Mt. Captiole lavas. However, if the *Shaw et al.* [1994] estimate of lower continental crust is used, then only 6% LCC is needed. These are maximum values of LCC (see text). Since SEIR N-MORB has low Th/Nb but relatively high La/Nb ratios, the Kerguelen plume composition has to be slightly offset from the trend defined by Mt. Capitole lavas. We note that the average Heard Island LPS (filled large pink triangle) which may represent the extreme Kerguelen plume composition has such La/Nb and Th/Nb ratios.

Trace element compositions for Kerguelen plume, SEIR N-MORB and LCC are in Table 7. The 2σ uncertainties shown in panel "b" are ±3%. (c) Ce/Pb vs $(Th/Nb)_{PM}$ for Mt. Capitole lavas (symbols as in Figure 5). Incorporation of LCC into oceanic basalt creates an inverse correlation. Error bars indicate ±3% 2σ uncertainties. Sample 93-483 and 93-510 are outliers; 93-483 is offset to high Pb in Figure 8, possibly because of Pb contamination, and 93-510 is the most evolved sample (Figures 7 and 8). (d) Initial $^{87}Sr/^{86}Sr$ vs $(La/Nb)_{PM}$ showing that the Kerguelen Plateau Site 1140 data are consistent with mixing of MORB- and Plume-related components whereas the Heard Island Big Ben Series (BBS) and the Upper Miocene Series from the southeast Kerguelen Archipelago (SE UPMS) define a trend between plume and LCC-related components. The Mt. Capitole data define a trend emanating from the MORB-Plume mixing line toward a LCC component.

Table 1 Petrographic characteristics of Mt. Capitole samples

Group	Sample	Height (m)[a]	Phenocryst/xenocryst[b] (volume %)
Upper Transitional Group (UTG)[d]	**93-459**[c]	860	40% plagioclase
	93-460	840	35% plagioclase
	93-461	840	25% plagioclase
	93-462	825	20% plagioclase and < 1% augite
	93-463	815	3% plagioclase
	93-464	810	< 1% plagioclase
	93-465	800	25% plagioclase
	93-467	780	none
	93-468	760	2% plagioclase
	93-469	750	5% plagioclase
	93-470	740	15% plagioclase
	93-471	735	10% plagioclase
	93-472	730	2% olivine, 1% augite and 5% plagioclase
	93-473	715	40% plagioclase
	93-474	690	15% plagioclase
Lower Transitional Group[d]	93-475	690	2% plagioclase
	93-476	685	2% plagioclase
	93-477	680	10% plagioclase
Low-Silica Group[d]	93-478	660	3% plagioclase
	93-479	640	None
	93-480	630	None
	93-481	610	< 1% plagioclase
	93-482	600	< 1% plagioclase
	93-483	590	< 1% plagioclase
	93-484	580	12% plagioclase and 3% augite
	93-485	570	
	93-486	560	18% plagioclase and 2% augite
Lower Transitional Group[d]	93-487	560	< 1% plagioclase
	93-488	550	10% plagioclase
	93-489	540	15% plagioclase
	93-490	540	< 1% plagioclase and augite
UTG[d]	**93-491**	540	25% plagioclase and 15% augite
Lower Transitional Group[d]	93-492	540	15% plagioclase
	93-493	530	< 1% plagioclase and augite
	93-494	520	< 1% plagioclase and augite
	93-495	510	< 1% plagioclase
	93-496	505	< 1% plagioclase
	93-497	490	< 1% plagioclase
	93-498	480	< 1% plagioclase
	93-499	470	< 1% plagioclase and augite
	93-500	465	< 1% plagioclase and augite
	93-501	455	< 1% plagioclase
	93-502	440	none
	93-503	435	< 1% plagioclase
	93-504	430	< 1% plagioclase
	93-505	420	< 1% plagioclase
	93-506	410	< 1% plagioclase
	93-507	400	< 1% plagioclase
	93-508	390	none
	93-509	380	none
	93-510	350	< 1% plagioclase and augite
	93-511	310	< 1% plagioclase
	93-512	270	none
	93-513	250	none
	93-514	230	< 1% plagioclase

[a] Meters above sea level. [b] Phenocrysts/xenocrysts are crystals with size ≥ 0.7mm. Volume proportions estimated from observation of thin sections using polarizing microscope. [c] Names in bold indicate samples with analyses by electron microprobe. [d] Based on petrography and whole rock composition, the Mt. Capitole lavas are divided into three groups that correlate with their stratigraphic positions. See the text for details.

Table 2a Plagioclase compositions (wt%) of Mt. Capitole lavas (determined by electron microprobe at MIT)

		SiO_2	Al_2O_3	FeO	MgO	CaO	Na_2O	K_2O	Total	An	Ab	Or
Upper Transitional Group												
93-459 plag1	core	50.66	31.12	0.59	0.18	14.30	3.32	0.13	100.3	69.9	29.4	0.8
93-459 plag1	rim	49.36	32.03	0.66	0.15	15.03	2.57	0.11	99.9	75.9	23.5	0.7
93-459 plag2	core	49.65	31.65	0.57	0.14	14.88	2.78	0.10	99.8	74.3	25.1	0.6
93-459 plag2	rim	52.05	30.13	0.76	0.09	12.84	3.85	0.22	99.9	64.0	34.7	1.3
93-459 plag3	core	49.22	32.36	0.57	0.15	15.36	2.68	0.09	100.4	75.6	23.9	0.5
93-459 plag3	rim	48.90	32.50	0.69	0.08	15.55	2.35	0.09	100.2	78.1	21.4	0.6
93-459 plag4	core	48.04	33.02	0.56	0.13	15.18	2.34	0.09	99.3	77.8	21.7	0.5
93-459 plag4	rim	48.66	31.58	0.63	0.14	14.87	2.87	0.09	98.9	73.7	25.8	0.5
93-459 plag5	core	51.16	30.56	0.59	0.13	13.69	3.64	0.17	100.0	66.8	32.1	1.0
93-459 plag5	mid-core	49.35	32.03	0.59	0.15	14.98	2.63	0.11	99.8	75.4	24.0	0.7
93-459 plag5	rim	49.21	32.23	0.59	0.11	15.16	2.56	0.11	100.0	76.1	23.3	0.6
93-459 plag5	rim	49.28	31.93	0.57	0.13	15.07	2.66	0.13	99.8	75.2	24.0	0.8
93-459 plag6	core	49.31	31.87	0.54	0.15	14.84	2.82	0.12	99.7	73.9	25.4	0.7
93-459 plag6	rim	49.02	31.67	0.58	0.14	15.09	2.83	0.12	99.5	74.1	25.2	0.7
93-459 plag7	core	48.89	31.90	0.56	0.16	15.13	2.90	0.11	99.7	73.8	25.6	0.7
93-459 plag7	core	48.81	32.45	0.59	0.17	15.52	2.57	0.09	100.2	76.5	23.0	0.5
93-459 plag7	core	48.22	32.62	0.53	0.16	15.97	2.37	0.08	99.9	78.5	21.1	0.5
93-459 plag7	rim	48.86	32.35	0.59	0.13	15.26	2.48	0.13	99.8	76.7	22.6	0.8
93-459 plag7	rim	48.66	32.22	0.60	0.10	15.37	2.66	0.11	99.7	75.6	23.7	0.7
93-459 plag8	core	48.60	32.55	0.52	0.15	15.65	2.61	0.11	100.2	76.4	23.0	0.6
93-459 plag8	rim	54.91	27.88	0.96	0.09	10.34	5.52	0.43	100.1	49.6	47.9	2.5
93-459 plag8	rim	48.28	32.94	0.62	0.13	15.61	2.46	0.08	100.1	77.5	22.1	0.5
93-459 plag9	core	48.87	32.61	0.56	0.16	15.78	2.67	0.09	100.7	76.1	23.3	0.5
93-459 plag9	rim	49.31	32.02	0.82	0.15	15.03	3.08	0.12	100.5	72.5	26.8	0.7
93-459 plag10	core	49.10	31.79	0.52	0.15	15.62	2.58	0.08	99.8	76.6	22.9	0.5
93-459 plag11	core	48.81	32.51	0.57	0.13	15.46	2.64	0.09	100.2	76.0	23.5	0.5
93-459 plag11	rim	49.01	32.06	0.68	0.11	15.16	2.85	0.11	100.0	74.2	25.2	0.6
93-459 plag12	groundmass	55.52	27.84	0.84	0.05	10.22	5.53	0.48	100.5	49.1	48.1	2.8
93-459 plag13	groundmass	52.69	29.70	1.09	0.16	12.40	4.14	0.25	100.4	61.4	37.1	1.5
93-460 plag1	core	48.00	33.22	0.58	0.13	16.37	2.03	0.08	100.4	81.3	18.2	0.5
93-460 plag1	core	49.08	32.88	0.63	0.17	15.86	2.42	0.09	101.1	77.9	21.5	0.6
93-460 plag1	mid-core	47.93	33.58	0.54	0.14	16.64	1.67	0.07	100.6	84.2	15.3	0.4
93-460 plag1	rim	52.52	30.08	0.61	0.15	13.10	3.75	0.20	100.4	65.1	33.7	1.2
93-460 plag1	rim	48.52	33.00	0.52	0.13	15.92	2.37	0.07	100.5	78.4	21.1	0.4
93-460 plag1	rim	48.00	33.62	0.53	0.14	16.50	2.07	0.08	100.9	81.1	18.4	0.5
93-460 plag1	rim	52.10	30.51	0.67	0.14	13.34	3.64	0.18	100.6	66.3	32.7	1.0
93-460 plag1	rim	47.50	33.66	0.51	0.14	16.61	2.15	0.06	100.6	80.7	18.9	0.4
93-460 plag2	core	50.77	31.55	0.53	0.16	14.42	3.26	0.11	100.8	70.5	28.8	0.7
93-460 plag2	core	48.67	32.99	0.58	0.14	16.24	2.08	0.08	100.8	80.8	18.7	0.5
93-460 plag2	core	49.38	32.50	0.60	0.14	15.45	2.57	0.09	100.8	76.4	23.0	0.6
93-460 plag2	core	48.92	32.68	0.61	0.15	15.66	2.45	0.09	100.6	77.5	21.9	0.5
93-460 plag2	rim	53.07	30.02	0.66	0.13	12.74	3.92	0.22	100.8	63.4	35.3	1.3
93-460 plag2	rim	49.13	32.71	0.59	0.11	15.69	2.56	0.09	100.9	76.8	22.7	0.5
93-460 plag3	core	50.58	31.41	0.61	0.13	14.35	3.46	0.13	100.7	69.1	30.1	0.7
93-460 plag3	core	49.37	32.68	0.60	0.14	15.36	2.99	0.10	101.2	73.5	25.9	0.6
93-460 plag3	rim	52.39	30.36	0.62	0.16	13.38	3.82	0.17	100.9	65.3	33.8	1.0
93-460 plag4	core	50.05	32.20	0.58	0.17	15.00	3.02	0.11	101.1	72.8	26.5	0.7
93-460 plag4	core	49.28	32.80	0.61	0.15	15.55	2.52	0.10	101.0	76.9	22.5	0.6
93-460 plag4	rim	49.56	32.69	0.64	0.12	15.69	2.49	0.09	101.3	77.3	22.2	0.5
93-460 plag4	rim	52.72	29.98	0.74	0.13	12.75	3.91	0.23	100.5	63.4	35.2	1.4
93-460 plag5	core	50.60	31.85	0.65	0.14	14.46	3.23	0.14	101.1	70.6	28.6	0.8
93-460 plag5	core	50.24	31.85	0.55	0.15	14.64	2.89	0.12	100.4	73.1	26.2	0.7
93-460 plag5	rim	48.92	32.90	0.67	0.15	15.94	2.42	0.10	101.1	78.0	21.4	0.6
93-460 plag5	rim	49.60	32.32	0.55	0.13	15.23	2.67	0.12	100.6	75.3	23.9	0.7
93-460 plag6	core	50.24	31.44	0.55	0.23	14.83	3.00	0.14	100.4	72.6	26.6	0.8

93-460 plag6	rim	48.19	33.54	0.63	0.14	16.50	2.01	0.08	101.1	81.5	18.0	0.5
93-460 plag6	rim	49.31	32.53	0.60	0.18	15.28	2.72	0.10	100.7	75.2	24.2	0.6
93-460 plag7	core	48.99	32.59	0.61	0.17	15.75	2.27	0.11	100.5	78.8	20.6	0.6
93-460 plag7	rim	49.14	32.75	0.53	0.17	15.90	2.30	0.11	100.9	78.8	20.6	0.7
93-460 plag8	core	47.44	33.96	0.48	0.14	17.44	1.72	0.06	101.3	84.5	15.1	0.4
93-460 plag8	rim	49.07	33.04	0.52	0.14	15.99	2.17	0.10	101.0	79.8	19.6	0.6
93-460 plag8	rim	52.73	29.78	0.68	0.15	12.63	3.78	0.26	100.0	63.9	34.6	1.6
93-460 plag9	groundmass	52.65	30.08	0.77	0.16	12.85	3.97	0.21	100.7	63.3	35.4	1.2
93-462 plag1	core	49.14	32.01	0.59	0.15	15.28	2.67	0.08	99.9	75.6	23.9	0.5
93-462 plag1	rim	48.27	32.54	0.64	0.13	16.02	2.55	0.05	100.2	77.4	22.3	0.3
93-462 plag2	core	49.10	32.14	0.60	0.13	15.42	2.73	0.08	100.2	75.4	24.1	0.5
93-462 plag2	rim	49.07	33.10	0.60	0.13	15.79	2.35	0.08	101.1	78.4	21.1	0.5
93-462 plag2	rim	54.70	28.25	0.64	0.10	11.05	4.99	0.34	100.1	53.9	44.1	2.0
93-462 plag3	core	49.12	32.37	0.53	0.14	15.53	2.44	0.10	100.2	77.4	22.0	0.6
93-462 plag3	rim	53.73	29.06	0.76	0.09	11.82	5.18	0.30	100.9	54.8	43.5	1.7
93-462 plag4	core	48.26	32.90	0.62	0.13	16.05	2.08	0.08	100.1	80.6	18.9	0.5
93-462 plag4	rim	55.69	27.01	1.56	0.33	9.64	5.54	0.47	100.2	47.7	49.5	2.8
93-462 plag5	core	48.67	32.45	0.58	0.14	15.53	2.60	0.10	100.1	76.3	23.1	0.6
93-462 plag5	rim	49.83	31.75	0.63	0.17	15.25	2.89	0.12	100.6	74.0	25.4	0.7
93-462 plag6	core	50.59	31.78	0.63	0.15	14.65	3.12	0.11	101.0	71.7	27.6	0.6
93-462 plag6	rim	58.41	26.02	0.79	0.03	7.96	7.13	0.66	101.0	36.8	59.6	3.6
93-462 plag7	core	53.10	29.65	0.96	0.16	12.46	4.29	0.23	100.9	60.8	37.9	1.3
93-462 plag7	rim	62.35	22.62	1.34	0.29	4.09	7.76	1.74	100.2	20.2	69.5	10.3
93-465 plag1	core	47.65	33.00	0.55	0.17	16.41	2.17	0.07	100.0	80.4	19.2	0.4
93-465 plag1	rim	48.77	32.14	0.71	0.12	15.40	2.82	0.13	100.1	74.6	24.7	0.7
93-465 plag1	rim	48.71	32.11	0.75	0.11	15.49	2.75	0.14	100.1	75.1	24.1	0.8
93-465 plag2	core	48.45	32.56	0.58	0.15	15.99	2.16	0.07	100.0	80.0	19.6	0.4
93-465 plag2	rim	48.78	32.28	0.62	0.13	15.50	2.41	0.09	99.8	77.6	21.9	0.5
93-465 plag2	rim	48.62	32.60	0.65	0.14	15.95	2.20	0.06	100.2	79.7	19.9	0.4
93-465 plag3	core	48.32	33.00	0.59	0.14	16.19	2.16	0.06	100.5	80.3	19.4	0.4
93-465 plag3	rim	48.35	32.61	0.65	0.13	16.12	2.31	0.06	100.2	79.1	20.5	0.3
93-465 plag4	core	48.99	31.64	0.58	0.17	15.09	2.73	0.09	99.3	74.9	24.6	0.5
93-465 plag4	rim	47.98	32.92	0.62	0.12	15.94	2.34	0.06	100.0	78.7	20.9	0.4
93-465 plag4	rim	48.58	32.48	0.62	0.12	15.68	2.43	0.09	100.0	77.7	21.8	0.5
93-465 plag5	core	48.46	32.49	0.62	0.16	15.63	2.88	0.08	100.3	74.7	24.9	0.4
93-465 plag5	rim	48.32	32.38	0.59	0.17	15.79	2.34	0.05	99.6	78.6	21.1	0.3
93-465 plag5	rim	48.71	32.29	0.66	0.12	15.57	2.78	0.09	100.2	75.2	24.3	0.5
93-465 plag6	core	47.66	32.72	0.51	0.13	16.16	2.27	0.05	99.5	79.5	20.2	0.3
93-465 plag6	rim	53.13	29.25	0.73	0.11	12.19	4.40	0.23	100.0	59.7	39.0	1.4
93-465 plag6	rim	47.57	32.64	0.70	0.12	16.01	2.37	0.06	99.5	78.6	21.1	0.4
93-465 plag7	core	48.13	32.48	0.59	0.16	15.85	2.58	0.07	99.9	77.0	22.6	0.4
93-465 plag7	core	48.33	33.22	0.72	0.08	16.18	2.16	0.08	100.8	80.2	19.3	0.5
93-465 plag7	rim around olivine inclusion	54.43	28.64	1.00	0.12	11.37	5.12	0.29	101.0	54.2	44.1	1.7
93-465 plag7	core	48.50	32.93	0.74	0.06	15.90	2.13	0.08	100.3	80.1	19.4	0.5
93-465 plag7	core	65.53	20.90	0.46	0.02	2.10	8.25	3.62	100.9	9.8	70.0	20.2
93-465 plag7	core	58.76	25.91	0.49	0.04	7.93	6.96	0.64	100.7	37.3	59.2	3.6
93-465 plag7	core	49.41	32.15	0.70	0.11	15.12	2.65	0.12	100.3	75.3	23.9	0.7
93-465 plag7	core	49.50	32.73	0.54	0.16	15.66	2.38	0.13	101.1	77.8	21.4	0.7
93-465 plag7	core	48.91	33.33	0.64	0.15	16.22	2.03	0.11	101.4	81.0	18.3	0.6
93-465 plag7	rim	47.86	32.90	0.58	0.16	16.29	2.23	0.06	100.1	79.9	19.8	0.3
93-465 plag7	rim	49.11	31.78	0.60	0.16	15.18	2.69	0.08	99.6	75.4	24.1	0.5
93-465 plag7	rim around amphibole inclusion	53.91	29.04	0.96	0.28	12.01	4.34	0.29	100.8	59.5	38.8	1.7
93-465 plag7	rim around amphibole inclusion	56.49	27.42	0.55	0.15	9.95	5.60	0.45	100.6	48.2	49.1	2.6
93-465 plag7	rim around amphibole inclusion	57.53	26.68	0.39	0.17	9.16	5.93	0.69	100.6	44.2	51.8	4.0
93-465 plag7	rim around amphibole inclusion	57.06	27.45	0.46	0.07	9.66	6.03	0.56	101.3	45.5	51.4	3.2
93-465 plag7	rim around amphibole inclusion	52.80	30.07	0.64	0.22	13.23	4.11	0.29	101.4	62.9	35.4	1.7
93-465 plag7	rim around amphibole inclusion	56.15	27.69	0.45	0.16	10.22	5.58	0.50	100.8	48.9	48.3	2.9
93-465 plag7	rim around olivine inclusion	56.23	27.82	0.83	0.14	10.25	5.17	0.37	100.8	51.1	46.7	2.2
93-465 plag7	rim around pyroxene inclusion	66.95	20.16	0.47	0.03	1.08	7.58	4.76	101.1	5.3	67.0	27.7

93-465 plag7	rim around pyroxene inclusion	59.19	26.03	0.60	0.09	7.48	6.80	0.73	100.9	36.2	59.6	4.2
93-465 plag7	rim around pyroxene inclusion	54.70	28.18	1.14	0.24	10.47	5.00	0.38	100.1	52.4	45.3	2.2
93-465 plag7	rim around pyroxene inclusion	56.89	27.70	0.69	0.11	9.56	5.44	0.49	100.9	47.8	49.3	2.9
93-465 plag7	rim around pyroxene inclusion	58.11	27.00	0.61	0.10	8.92	5.97	0.55	101.3	43.8	53.0	3.2
93-465 plag8	core	48.62	33.14	0.62	0.20	15.80	2.51	0.14	101.0	77.0	22.2	0.8
93-465 plag8	rim	53.10	29.38	0.98	0.13	12.37	4.65	0.29	100.9	58.5	39.8	1.7
93-465 plag9	core	49.85	31.39	0.57	0.17	14.61	3.24	0.08	99.9	71.1	28.5	0.4
93-465 plag9	rim	48.54	32.35	0.56	0.16	15.56	2.58	0.08	99.8	76.6	23.0	0.5
93-465 plag9	rim	47.90	32.43	0.57	0.15	15.75	2.58	0.06	99.5	76.9	22.8	0.4
93-465 plag9	rim	48.00	32.75	0.62	0.12	15.97	2.37	0.07	99.9	78.5	21.1	0.4
93-465 plag10	core	47.91	33.04	0.54	0.16	16.05	2.27	0.05	100.0	79.4	20.3	0.3
93-465 plag10	rim	47.60	32.62	0.52	0.13	16.00	2.55	0.07	99.5	77.3	22.3	0.4
93-465 plag11	core	47.88	32.87	0.52	0.15	16.02	2.32	0.05	99.8	79.0	20.7	0.3
93-465 plag11	rim	48.02	32.66	0.74	0.11	16.04	2.25	0.07	99.9	79.4	20.2	0.4
93-465 plag12	core	48.72	32.71	0.54	0.15	15.96	2.73	0.08	100.9	76.0	23.5	0.4
93-465 plag12	rim	48.38	32.68	0.52	0.13	16.06	2.23	0.08	100.1	79.6	20.0	0.5
93-465 plag12	rim	53.51	29.40	0.69	0.12	12.07	4.52	0.25	100.6	58.7	39.8	1.4
93-465 plag12	rim	47.79	33.03	0.54	0.01	16.22	1.97	0.03	99.6	81.8	18.0	0.2
93-465 plag12	rim	54.97	28.86	0.65	0.00	11.30	4.96	0.31	101.1	54.7	43.5	1.8
93-465 plag13	core	48.77	33.06	0.52	0.00	16.29	2.39	0.05	101.1	78.8	20.9	0.3
93-465 plag13	rim	48.90	33.33	0.53	0.03	16.11	2.19	0.05	101.1	80.0	19.7	0.3
93-465 plag14	groundmass	59.49	24.67	0.79	0.13	7.02	6.92	1.06	100.1	33.7	60.2	6.1
93-471 plag1	core	50.62	31.65	0.58	0.18	14.96	2.80	0.10	100.9	74.2	25.2	0.6
93-471 plag1	core	50.02	32.10	0.62	0.18	15.06	2.83	0.10	100.9	74.2	25.2	0.6
93-471 plag1	core	49.89	32.09	0.57	0.17	15.24	2.56	0.09	100.6	76.2	23.2	0.5
93-471 plag1	core	50.49	31.66	0.56	0.18	14.68	2.96	0.10	100.6	72.9	26.6	0.6
93-471 plag1	core	48.34	33.14	0.48	0.16	16.42	1.84	0.08	100.4	82.8	16.8	0.5
93-471 plag1	core	49.72	32.20	0.60	0.22	15.30	2.76	0.08	100.9	75.0	24.5	0.4
93-471 plag1	core	48.83	32.71	0.54	0.19	15.92	2.49	0.08	100.8	77.6	22.0	0.4
93-471 plag1	rim	48.86	32.77	0.53	0.12	15.76	2.37	0.07	100.5	78.3	21.3	0.4
93-471 plag1	rim	49.27	32.52	0.50	0.17	15.79	2.54	0.07	100.9	77.1	22.5	0.4
93-471 plag1	rim	48.45	33.26	0.55	0.17	16.26	2.26	0.06	101.0	79.6	20.1	0.4
93-471 plag1	rim	48.43	33.14	0.56	0.15	16.15	2.10	0.07	100.6	80.6	19.0	0.4
93-471 plag1	rim	48.41	33.22	0.57	0.16	16.47	2.06	0.07	101.0	81.2	18.4	0.4
93-471 plag1	rim	48.67	32.86	0.60	0.15	16.02	2.34	0.07	100.7	78.8	20.8	0.4
93-471 plag1	rim	48.82	32.93	0.59	0.17	15.82	2.33	0.07	100.7	78.6	21.0	0.4
93-471 plag1	rim	49.20	32.91	0.58	0.18	15.82	2.51	0.08	101.3	77.3	22.2	0.5
93-471 plag2	core	48.14	33.36	0.53	0.17	16.50	1.94	0.06	100.7	82.2	17.5	0.4
93-471 plag3	core	49.30	32.32	0.56	0.17	15.58	2.58	0.08	100.6	76.6	22.9	0.5
93-471 plag3	rim	47.98	33.28	0.59	0.12	16.37	1.78	0.05	100.2	83.3	16.4	0.3
93-471 plag4	core	48.34	33.44	0.58	0.14	16.27	1.92	0.05	100.7	82.1	17.6	0.3
93-471 plag5	core	48.63	32.78	0.54	0.16	16.02	2.15	0.06	100.4	80.2	19.4	0.4
93-471 plag5	rim	48.72	32.96	0.61	0.14	15.86	2.15	0.07	100.5	80.0	19.6	0.4
93-471 plag6	rim	54.43	29.09	0.54	0.11	11.58	4.66	0.22	100.6	57.1	41.6	1.3
93-471 plag7	core	49.41	32.38	0.61	0.21	15.61	2.49	0.09	100.8	77.2	22.3	0.5
93-471 plag7	core	49.10	32.57	0.53	0.20	15.46	2.63	0.07	100.6	76.1	23.5	0.4
93-471 plag7	core	48.51	33.20	0.54	0.21	16.22	2.27	0.06	101.0	79.5	20.1	0.3
93-471 plag7	rim	48.53	33.09	0.52	0.23	15.91	2.23	0.08	100.6	79.4	20.1	0.5
93-471 plag7	rim	50.94	31.42	0.55	0.23	14.40	3.22	0.11	100.9	70.7	28.6	0.6
93-471 plag7	rim	49.17	32.80	0.58	0.21	15.54	2.44	0.09	100.8	77.4	22.0	0.5
93-471 plag8	core	49.12	32.72	0.58	0.24	15.49	2.61	0.08	100.8	76.3	23.2	0.5
93-471 plag9	core	49.49	32.78	0.49	0.20	15.58	2.54	0.07	101.2	76.9	22.7	0.4
93-471 plag10	groundmass	53.07	29.20	0.90	0.07	12.15	4.14	0.27	99.8	60.9	37.5	1.6
93-472 plag1	core	50.25	31.38	0.45	0.17	14.32	3.23	0.09	99.9	70.6	28.8	0.5
93-472 plag1	rim	50.78	31.25	0.50	0.14	14.26	3.34	0.10	100.4	69.8	29.6	0.6
93-472 plag2	groundmass	51.10	30.67	0.47	0.20	13.82	3.53	0.12	99.9	67.9	31.4	0.7
93-473 plag1	core	50.37	31.83	0.51	0.16	14.86	2.94	0.12	100.8	73.1	26.2	0.7
93-473 plag1	rim	50.85	31.42	0.54	0.16	14.19	3.59	0.13	100.9	68.1	31.2	0.8

93-473 plag2	core	50.18	31.70	0.52	0.17	14.63	2.97	0.11	100.3	72.6	26.7	0.7
93-473 plag2	rim	48.84	32.62	0.53	0.17	15.75	2.73	0.09	100.7	75.7	23.7	0.5
93-473 plag3	core	51.01	30.97	0.52	0.19	14.07	3.66	0.13	100.5	67.5	31.8	0.7
93-473 plag4	core	48.44	32.91	0.46	0.13	16.05	2.39	0.07	100.5	78.5	21.1	0.4
93-473 plag4	rim	49.80	31.82	0.55	0.14	14.88	3.17	0.10	100.5	71.7	27.7	0.6
93-474 plag1	core	51.13	31.08	0.62	0.20	13.87	3.46	0.16	100.5	68.3	30.8	0.9
93-474 plag1	rim	51.83	30.55	0.74	0.16	13.65	3.98	0.22	101.1	64.7	34.1	1.2
93-474 plag2	core	53.92	28.91	0.62	0.19	11.98	4.60	0.26	100.5	58.1	40.4	1.5
93-491 plag1	core	50.19	31.17	0.67	0.19	14.29	2.94	0.11	99.6	72.4	27.0	0.6
93-491 plag1	rim	54.69	28.20	0.73	0.11	10.92	4.98	0.32	100.0	53.8	44.4	1.9
93-491 plag1	rim	52.85	29.51	0.58	0.17	12.62	4.20	0.18	100.1	61.8	37.2	1.0
93-491 plag2	core	51.68	30.42	0.62	0.20	13.44	3.72	0.15	100.2	66.1	33.0	0.9
93-491 plag2	rim	53.23	29.34	0.58	0.14	12.14	4.19	0.22	99.8	60.7	38.0	1.3
93-491 plag3	core	50.54	31.07	0.66	0.17	14.19	3.16	0.15	99.9	70.7	28.5	0.9
93-491 plag3	rim	54.12	28.81	0.66	0.12	11.47	4.84	0.28	100.3	55.8	42.6	1.6
93-491 plag4	core	50.54	31.33	0.64	0.16	14.36	3.16	0.10	100.3	71.1	28.3	0.6
93-491 plag4	rim	52.52	30.07	0.66	0.16	12.90	4.21	0.16	100.7	62.3	36.8	0.9
93-491 plag4	rim	53.18	29.46	0.62	0.16	12.27	4.27	0.21	100.2	60.6	38.2	1.2
93-491 plag5	core	54.15	28.83	0.58	0.14	11.56	4.76	0.25	100.3	56.5	42.1	1.4
93-491 plag5	rim	53.86	28.69	0.86	0.31	11.53	4.59	0.24	100.1	57.3	41.3	1.4
93-491 plag6	rim	52.66	29.60	0.63	0.16	12.53	4.26	0.21	100.0	61.1	37.7	1.2
93-491 plag6	core	53.07	29.42	0.58	0.17	12.34	4.14	0.20	99.9	61.5	37.3	1.2
93-491 plag7	core	51.13	30.92	0.64	0.16	13.88	3.33	0.13	100.2	69.2	30.0	0.8
93-491 plag7	rim	51.19	30.53	0.70	0.18	13.75	3.60	0.14	100.1	67.3	31.9	0.8
93-491 plag8	core	50.44	31.14	0.67	0.16	14.38	3.04	0.10	99.9	71.9	27.5	0.6
93-491 plag8	rim	53.34	29.62	0.55	0.16	12.27	4.46	0.21	100.6	59.6	39.2	1.2
93-491 plag9	core	53.34	29.41	0.61	0.14	12.32	4.51	0.19	100.5	59.5	39.4	1.1
93-491 plag10	core	53.07	29.77	0.63	0.16	12.49	4.46	0.20	100.8	60.0	38.8	1.1
93-491 plag11	plag inclusion in plag11	52.94	29.94	0.71	0.14	12.75	3.98	0.20	100.7	63.2	35.7	1.2

Table 2b Pyroxene compositions (wt%) of Mt. Capitole lavas (determined by electron microprobe at MIT)

	SiO_2	TiO_2	Al_2O_3	Cr_2O_3	FeO	MnO	MgO	CaO	Na_2O	Total	mg#
93-459 cpx inclusion in plag5	50.08	1.19	2.00	0.02	10.75	0.23	14.34	20.61	0.34	99.6	70.4
93-459 cpx in groundmass	49.07	1.95	4.14	0.04	10.93	0.20	13.73	19.85	0.33	100.2	69.1
93-459 cpx in groundmass	48.07	2.36	5.05	0.06	10.65	0.20	13.49	20.06	0.37	100.3	69.3
93-459 cpx in groundmass	48.48	2.19	3.79	0.00	12.60	0.30	12.80	19.23	0.49	99.9	64.4
93-459 cpx in groundmass	48.88	2.01	4.79	0.31	8.47	0.16	14.18	20.96	0.37	100.1	74.9
93-459 cpx in groundmass	50.98	1.20	2.17	0.00	10.84	0.26	14.10	19.94	0.43	99.9	69.9
93-460 cpx1 core	49.92	1.69	3.84	0.09	9.24	0.20	14.15	21.21	0.30	100.6	73.2
93-460 cpx1 rim	51.12	1.36	1.72	0.00	12.19	0.27	13.11	20.02	0.28	100.1	65.7
93-460 cpx1 rim	52.16	1.14	1.85	0.00	10.20	0.27	14.56	20.67	0.32	101.2	71.8
93-460 cpx2 core	51.97	1.00	2.56	0.06	9.08	0.21	15.80	19.82	0.28	100.8	75.6
93-460 cpx2 core	50.43	1.31	3.99	0.20	8.05	0.19	14.76	21.22	0.36	100.5	76.6
93-460 cpx2 rim	51.57	1.11	2.06	0.02	9.69	0.24	14.40	20.68	0.33	100.1	72.6
93-460 cpx3 core	52.29	0.82	2.17	0.08	8.17	0.23	16.05	20.24	0.27	100.3	77.8
93-462 cpx in groundmass	52.00	1.02	1.76	0.00	11.35	0.16	14.32	19.72	0.20	100.5	69.2
93-465 pigeonite inclusion1 in plag7	51.25	0.32	0.10	0.02	33.31	0.72	12.99	3.08	0.12	101.9	41.0
93-465 pigeonite inclusion2 in plag7	50.59	0.48	0.50	0.02	32.67	0.63	12.41	3.16	0.12	100.6	40.4
93-465 pigeonite inclusion3 in plag7	49.85	0.47	0.16	0.12	33.16	0.62	14.13	2.89	0.00	101.4	43.2
93-465 cpx inclusion1 core in plag7	51.43	1.13	2.32	0.04	8.84	0.21	14.62	20.82	0.38	99.8	74.7
93-465 cpx inclusion1 rim in plag7	50.47	1.46	3.22	0.25	9.33	0.17	14.51	20.37	0.36	100.1	73.5
93-465 cpx inclusion2 core in plag7	51.42	1.17	1.70	0.00	10.47	0.17	14.24	20.35	0.40	99.9	70.8
93-465 cpx inclusion2 rim1 in plag7	52.43	1.22	1.62	0.00	12.07	0.26	14.12	20.18	0.31	102.2	67.6
93-465 cpx inclusion2 rim2 in plag7	51.16	1.47	2.14	0.00	11.54	0.24	13.66	20.51	0.44	101.2	67.9
93-465 cpx inclusion3 in plag7	52.40	1.28	0.97	0.00	15.83	0.40	12.77	18.33	0.39	102.4	59.0
93-465 cpx inclusion4 in plag7	51.33	1.10	1.18	0.00	14.25	0.40	13.05	18.66	0.30	100.3	62.0
93-465 cpx inclusion5 in plag7	51.19	1.43	1.82	0.00	14.39	0.38	11.72	18.56	0.31	99.8	59.2
93-465 cpx inclusion6 in plag7	51.04	1.45	2.22	0.00	10.68	0.20	13.62	20.73	0.38	100.3	69.5
93-465 cpx inclusion in plag12	51.05	1.51	2.64	0.00	13.21	0.12	14.15	18.61	0.46	101.8	65.6
93-465 cpx in groundmass	48.07	1.27	4.86	0.26	12.45	0.29	12.97	17.60	0.52	98.3	65.0
93-465 cpx in groundmass	49.17	1.67	4.47	0.38	10.54	0.26	13.86	19.99	0.42	100.8	70.1
93-465 cpx in groundmass	52.16	0.82	1.94	0.21	8.54	0.24	16.84	18.63	0.39	99.8	77.9
93-465 cpx in groundmass	51.55	1.06	2.14	0.08	9.90	0.26	15.18	19.64	0.37	100.2	73.2
93-465 cpx in groundmass	49.69	1.49	4.16	0.30	9.00	0.23	14.84	20.34	0.35	100.4	74.6
93-471 cpx inclusion1 in plag1	50.66	1.39	3.19	0.07	9.23	0.17	15.24	20.50	0.32	100.8	74.6
93-471 cpx inclusion2 in plag1	50.63	1.53	2.78	0.04	10.66	0.23	14.33	20.56	0.37	101.2	70.5
93-471 cpx inclusion3 in plag1	52.38	0.73	1.17	0.01	14.78	0.33	14.97	16.40	0.31	101.1	64.4
93-471 cpx inclusion1 in plag5	52.26	0.94	2.10	0.06	9.58	0.20	16.18	19.05	0.32	100.7	75.1
93-471 cpx inclusion2 in plag5	51.07	1.31	2.75	0.05	14.18	0.33	17.01	13.91	0.17	100.8	68.1
93-471 cpx in groundmass	50.73	1.21	2.49	0.09	10.93	0.24	14.43	20.18	0.34	100.6	70.2
93-472 cpx1 core	50.07	1.79	3.70	0.17	9.31	0.19	14.28	20.00	0.28	99.8	73.2
93-472 cpx1 rim	49.32	2.08	3.58	0.03	11.02	0.21	13.43	19.77	0.35	99.8	68.5
93-472 cpx2 core	50.48	1.10	1.42	0.04	15.09	0.29	12.44	18.36	0.22	99.5	59.5
93-472 cpx3 core	52.13	1.03	1.94	0.20	8.50	0.19	15.76	20.15	0.26	100.2	76.8
93-472 cpx3 rim	50.64	1.00	1.29	0.06	16.19	0.38	12.24	17.67	0.23	99.7	57.4
93-473 cpx inclusion core in plag2	49.00	2.15	3.81	0.11	11.56	0.23	13.36	19.88	0.29	100.4	67.3
93-473 cpx inclusion rim in plag2	50.15	1.86	2.27	0.00	14.32	0.36	13.35	18.04	0.26	100.6	62.4
93-486 cpx1 core	51.54	1.21	2.49	0.19	9.79	0.23	15.31	19.92	0.31	101.0	73.6
93-486 cpx1 rim	51.35	1.18	2.50	0.15	9.47	0.23	15.43	19.86	0.29	100.5	74.4
93-486 cpx2 core	51.04	1.13	2.91	0.23	8.66	0.22	15.52	20.05	0.21	100.0	76.2
93-486 cpx2 rim	51.15	1.09	1.55	0.01	14.80	0.37	13.10	17.81	0.27	100.2	61.2
93-486 cpx2 rim	51.61	1.20	2.29	0.08	9.20	0.20	15.60	19.79	0.27	100.2	75.1

93-486 cpx3 core	52.28	0.90	2.35	0.12	8.28	0.17	15.92	20.36	0.26	100.6	77.4
93-486 cpx3 core	51.66	1.10	2.03	0.08	9.35	0.25	15.39	19.40	0.32	99.6	74.6
93-486 cpx3 rim	51.40	1.03	1.47	0.01	12.64	0.35	14.42	18.38	0.31	100.0	67.0
93-486 cpx3 rim	51.39	1.07	1.73	0.02	13.14	0.30	14.47	17.96	0.26	100.3	66.3
93-486 cpx3 rim	52.03	0.98	2.35	0.14	8.90	0.23	15.72	20.09	0.26	100.7	75.9
93-491 cpx1 core	51.68	0.93	2.76	0.34	7.57	0.17	16.23	20.21	0.26	100.2	79.3
93-491 cpx1 rim	51.38	0.95	2.56	0.28	7.94	0.21	16.19	20.47	0.33	100.3	78.4
93-491 cpx2 core	51.41	0.81	2.63	0.40	7.55	0.18	16.03	20.39	0.25	99.6	79.1
93-491 cpx2 rim	51.63	0.80	2.46	0.52	6.98	0.15	16.28	20.43	0.27	99.5	80.6
93-491 cpx2 rim	51.56	1.20	1.44	0.08	11.65	0.23	14.98	18.58	0.24	100.0	69.6
93-491 cpx3 core	51.48	0.86	2.27	0.24	7.75	0.17	16.07	20.27	0.25	99.4	78.7
93-491 cpx3 rim	51.82	0.93	2.51	0.26	7.77	0.21	15.95	20.31	0.23	100.0	78.5
93-491 cpx4 core	51.75	0.96	2.53	0.23	8.08	0.17	15.92	20.58	0.22	100.5	77.8
93-491 cpx4 rim	52.08	0.81	2.20	0.30	7.23	0.20	16.40	20.44	0.26	99.9	80.2
93-491 cpx4 rim	51.43	0.82	1.14	0.05	15.95	0.46	14.08	16.39	0.18	100.5	61.1
93-491 cpx4 rim	52.22	0.88	1.83	0.30	9.29	0.21	16.22	18.90	0.27	100.1	75.7
93-491 cpx5 core	52.11	0.86	1.92	0.22	8.40	0.23	16.30	19.96	0.24	100.2	77.6
93-491 cpx5 rim	51.78	0.91	2.38	0.23	8.35	0.22	16.02	19.79	0.28	100.0	77.4
93-491 cpx6 core	49.34	1.46	4.71	0.51	9.42	0.25	16.29	16.74	0.35	99.1	75.5
93-491 cpx6 rim	52.37	0.83	1.61	0.40	8.74	0.27	17.05	18.38	0.22	99.9	77.7
93-491 cpx7 core	50.54	1.17	3.58	0.39	8.78	0.21	15.50	19.78	0.30	100.3	75.9
93-491 cpx7 rim	52.21	0.97	1.39	0.15	11.26	0.23	16.51	17.19	0.21	100.1	72.3
93-491 cpx8 core	50.30	1.31	3.93	0.27	9.32	0.14	15.97	18.31	0.32	99.9	75.3
93-491 cpx8 rim	51.43	1.28	2.18	0.12	11.52	0.23	15.27	18.21	0.23	100.5	70.3
93-491 cpx9 core	51.42	1.10	2.82	0.25	8.13	0.16	16.06	20.49	0.30	100.7	77.9
93-491 cpx inclusion1 in plag11	49.00	1.57	3.19	0.00	17.13	0.29	13.26	14.72	0.15	99.3	58.0
93-491 cpx inclusion2 in plag11	49.94	1.62	2.11	0.03	17.66	0.37	11.20	18.39	0.26	101.6	53.1

Table 2c Olivine compositions (wt%) of Mt. Capitole lavas (determined by electron microprobe at MIT)

	SiO_2	Cr_2O_3	FeO	MnO	MgO	CaO	NiO	Total	mg#
93-465 olivine inclusion1 core in plag7	35.07	0.01	37.12	0.55	26.16	0.38	0.06	99.4	55.7
93-465 olivine inclusion1 rim in plag7	34.67	0.06	42.64	0.61	20.29	0.27	0.07	99.0	45.9
93-465 olivine inclusion2 in plag7	35.72	0.02	32.04	0.40	30.98	0.34	0.08	99.6	63.3
93-465 olivine in groundmass near plag7	34.65	0.07	43.39	0.64	23.39	0.36		102.6	49.0
93-472 olivine1 core	39.38	0.01	17.06	0.24	41.94	0.30	0.18	99.1	81.4
93-472 olivine1 rim	38.27	0.03	20.86	0.27	39.45	0.30	0.12	99.3	77.1
93-472 olivine1 rim	38.84	0.03	22.43	0.25	37.60	0.35	0.15	99.7	74.9
93-472 olivine2 core	38.41	0.02	19.18	0.26	40.44	0.31	0.17	98.8	79.0
93-472 olivine2 rim	38.65	0.04	21.57	0.32	38.42	0.36	0.22	99.6	76.0
93-472 olivine3 core	38.89	0.05	19.36	0.31	40.85	0.28	0.24	100.0	79.0
93-472 olivine4 core	38.24	0.03	22.27	0.32	38.42	0.40	0.12	99.8	75.5
93-472 olivine5 core	38.26	0.03	21.21	0.31	39.26	0.38	0.10	99.6	76.7
93-472 olivine6 core	39.43	0.01	16.99	0.18	42.61	0.27	0.11	99.7	81.7
93-472 olivine6 rim	38.23	0.02	22.72	0.27	37.48	0.35	0.13	99.3	74.6
93-472 olivine7 core	38.35	0.01	20.47	0.29	39.52	0.36	0.11	99.2	77.5
93-472 olivine7 rim	38.06	0.01	23.06	0.31	37.62	0.38	0.09	99.6	74.4

Table 2d Composition (wt%) of amphibole inclusion in plagioclase phenocrysts/xenocrysts in Mt. Capiotle lavas

	SiO_2	TiO_2	Al_2O_3	Cr_2O_3	FeO	MnO	MgO	CaO	Na_2O	Total	mg#
93-459 amph inclusion in plag4	43.82	4.91	3.12	0.04	21.90	0.42	11.93	12.67	0.50	99.3	49.3
93-459 amph inclusion in plag4	43.27	4.66	2.77	0.04	22.34	0.47	11.61	12.22	0.53	97.9	48.1
93-459 amph inclusion in plag7	42.61	5.41	2.35	0.05	23.49	0.36	12.05	13.19	0.38	99.9	47.8
93-459 amph inclusion in plag7	43.83	5.09	3.11	0.01	23.78	0.31	11.49	11.89	0.55	100.1	46.3
93-459 amph inclusion in plag7	43.98	5.37	3.22	0.08	22.99	0.33	11.17	12.14	0.59	99.9	46.4
93-459 amph inclusion in plag8	44.55	4.25	5.47	0.04	22.65	0.29	12.08	11.56	1.13	102.0	48.7
93-459 amph inclusion in plag8	43.82	4.79	2.90	0.10	21.08	0.38	12.83	12.72	0.84	99.5	52.0
93-460 amph inclusion in plag3	44.26	5.05	2.70	0.02	17.15	0.25	13.21	16.07	0.80	99.5	57.9
93-462 amph inclusion in plag2	43.91	4.79	3.95	0.05	18.38	0.46	12.19	13.15	0.64	97.5	54.2
93-465 amph inclusion1 rim1 in plag7	48.42	2.15	2.02	0.03	20.86	0.43	14.06	10.93	0.28	99.2	54.6
93-465 amph inclusion1 core in plag7	45.14	5.07	3.08	0.00	20.55	0.29	15.91	8.86	0.26	99.2	58.0
93-465 amph inclusion1 rim2 in plag7	44.62	4.64	4.66	0.05	23.89	0.48	10.86	10.02	0.62	99.8	44.8
93-465 amph inclusion1 rim3 in plag7	45.35	4.80	3.92	0.08	22.47	0.39	12.84	9.85	0.66	100.4	50.4
93-465 amph inclusion1 rim4 in plag7	43.70	4.69	2.89	0.04	22.56	0.36	12.81	10.70	0.39	98.1	50.3
93-465 amph inclusion1 rim5 in plag7	44.30	4.14	2.47	0.05	22.56	0.40	13.91	9.96	0.58	98.4	52.4
93-465 amph inclusion9 in plag7	45.64	5.10	2.97	0.07	18.54	0.34	15.35	11.52	0.51	100.0	59.6
93-465 amph inclusion11 in plag8	42.65	4.52	3.24	0.01	21.29	0.37	12.71	12.81	0.36	98.0	51.6
93-465 amph inclusion12 in plag9	45.87	4.16	4.28	0.07	19.17	0.48	12.82	11.21	0.46	98.5	54.4
93-471 amph inclusion in plag7	45.00	4.35	3.37	0.06	21.41	0.43	13.36	12.05	0.57	100.6	52.6
93-491 amph inclusion in plag7	41.16	5.32	4.20	0.09	24.62	0.64	9.82	10.79	0.40	97.0	41.5
93-491 amph inclusion3 in plag11	43.32	5.26	2.64	0.05	23.81	0.60	10.71	11.17	0.31	97.9	44.5

Table 3 Major element compositions (wt %) in basalt from Mt. Capitole

Sample	Height(m)	SiO_2	TiO_2	Al_2O_3	$Fe_2O_3^*$	MnO	MgO	CaO	Na_2O	K_2O	P_2O_5	TOTAL	LOI
Upper Transitional Group lavas													
93-459	860	48.71	2.04	18.05	10.97	0.17	4.78	11.57	2.74	0.67	0.26	99.96	1.36
93-460	840	48.69	2.39	16.80	12.44	0.19	4.67	10.52	2.91	0.88	0.34	99.83	2.99
93-461	840	48.77	2.60	15.35	13.35	0.20	4.93	10.56	3.01	0.78	0.34	99.89	0.57
93-462	825	48.49	2.33	16.22	12.41	0.19	5.46	11.00	2.65	0.64	0.29	99.68	5.20
93-463	815	48.13	2.33	15.71	12.92	0.19	6.47	10.76	2.43	0.66	0.28	99.88	1.62
93-464	810	48.18	2.76	14.55	13.89	0.20	5.81	10.44	2.88	0.70	0.32	99.73	2.20
93-465	800	48.50	2.27	16.20	12.17	0.18	6.00	11.10	2.55	0.69	0.26	99.92	2.29
93-467	780	48.50	2.61	14.29	13.39	0.21	6.54	10.91	2.66	0.48	0.32	99.91	1.94
93-468	760	48.45	2.53	14.94	13.19	0.18	6.42	11.00	2.04	0.51	0.30	99.56	4.42
93-469	750	48.89	2.49	14.54	13.05	0.19	6.27	10.90	2.46	0.56	0.30	99.65	1.91
93-470	740	47.95	2.35	15.92	12.25	0.18	6.30	10.75	2.93	0.54	0.27	99.44	2.47
93-471	735	48.52	2.38	15.91	12.50	0.19	6.24	11.13	2.46	0.59	0.28	100.20	2.94
93-472	730	47.24	2.27	15.10	12.90	0.19	8.00	11.15	2.27	0.46	0.29	99.87	4.39
93-473	715	47.89	2.50	15.89	13.30	0.20	5.93	10.37	2.88	0.55	0.31	99.82	4.23
93-474	690	48.57	2.73	15.00	13.08	0.19	5.48	10.80	2.79	0.57	0.37	99.58	1.18
93-491	540	48.58	2.52	14.49	12.96	0.19	7.12	11.01	2.12	0.20	0.29	99.48	3.07
Lower Transitional Group lavas													
93-475	690	49.51	3.26	13.31	14.65	0.20	4.55	10.19	2.86	0.77	0.45	99.75	1.95
93-476	685	49.12	3.23	13.20	14.80	0.20	5.06	9.74	2.90	1.00	0.45	99.70	2.20
93-477	680	48.50	3.17	14.25	14.31	0.18	5.22	10.08	2.85	0.76	0.41	99.73	1.49
Low Silica Group lavas													
93-478	660	47.88	3.87	12.95	16.39	0.26	4.62	9.76	2.73	0.47	0.50	99.43	1.66
93-479	640	49.33	3.74	13.18	15.84	0.20	4.19	9.42	2.85	0.97	0.50	100.22	2.04
93-480	630	48.55	3.89	12.59	16.42	0.24	4.58	9.38	2.76	0.80	0.48	99.69	0.77
93-481	610	47.12	4.20	13.27	16.47	0.24	4.82	9.83	2.95	0.71	0.52	100.13	1.40
93-482	600	46.17	4.47	13.30	17.31	0.26	4.59	9.13	2.72	0.98	0.55	99.48	1.17
93-483	590	47.69	4.02	13.34	15.72	0.27	4.65	10.32	2.60	0.75	0.47	99.83	2.18

93-484	580	47.46	3.78	13.52	15.98	0.24	4.93	10.47	2.40	0.41	0.43	99.62	1.91
93-485	570	47.76	3.75	13.38	15.85	0.22	5.18	10.21	2.39	0.60	0.44	99.78	1.14
93-486	560	47.33	3.83	14.18	16.01	0.22	4.61	10.11	2.92	0.42	0.45	100.08	1.68
Lower Transitional Group lavas													
93-487	560	48.75	3.56	12.93	15.70	0.22	4.95	9.75	2.36	0.47	0.45	99.14	0.92
93-488	550	49.25	3.48	13.16	15.12	0.23	5.05	10.08	2.34	0.44	0.42	99.57	0.89
93-489	540	48.58	3.29	13.60	14.74	0.22	5.39	10.40	2.53	0.35	0.40	99.50	1.53
93-490	540	51.66	3.82	12.87	14.51	0.18	3.77	8.60	2.80	1.02	0.48	99.71	0.94
93-492	540	47.84	3.33	13.70	15.00	0.25	5.82	10.31	2.53	0.40	0.41	99.59	1.54
93-493	530	47.57	3.35	13.84	15.31	0.19	5.84	10.41	2.29	0.23	0.37	99.40	2.98
93-494	520	49.66	3.34	12.97	15.01	0.22	5.01	9.53	2.78	0.74	0.40	99.66	0.33
93-495	510	49.88	3.32	13.20	14.44	0.19	4.94	9.42	2.80	0.83	0.40	99.42	0.40
93-496	505	50.29	3.50	13.39	14.41	0.24	4.56	8.66	2.95	1.02	0.44	99.46	0.75
93-497	490	49.10	3.55	13.32	15.30	0.25	5.10	9.25	2.80	0.57	0.44	99.68	0.93
93-498	480	49.86	3.63	13.30	15.36	0.20	4.69	9.28	2.74	0.50	0.44	100.00	1.61
93-499	470	49.48	3.23	13.23	14.31	0.23	5.43	10.08	2.74	0.45	0.39	99.57	1.21
93-500	465	49.73	3.57	13.24	14.74	0.26	5.34	9.55	2.86	0.63	0.43	100.35	1.04
93-501	455	49.39	3.14	13.93	14.35	0.22	5.17	10.26	2.98	0.49	0.37	100.30	1.20
93-502	440	48.52	3.00	14.26	13.60	0.22	5.96	10.72	2.66	0.51	0.33	99.78	1.31
93-503	435	48.53	3.31	13.62	14.82	0.21	5.58	10.49	2.38	0.33	0.39	99.66	1.29
93-504	430	48.25	3.90	13.33	15.86	0.30	5.05	9.19	2.17	0.90	0.47	99.42	6.31
93-505	420	51.43	3.93	13.31	14.15	0.18	3.95	8.54	2.69	0.98	0.50	99.66	2.26
93-506	410	49.76	3.46	13.80	14.67	0.27	4.73	8.69	2.97	0.89	0.49	99.73	1.84
93-507	400	50.18	3.44	13.71	14.95	0.21	4.37	8.63	3.00	1.08	0.49	100.06	1.27
93-508	390	50.22	3.72	12.91	15.17	0.20	4.37	8.34	2.97	1.19	0.48	99.57	1.16
93-509	380	50.54	3.51	13.15	14.38	0.21	4.39	8.67	3.23	0.99	0.47	99.54	0.61
93-510	350	52.88	3.50	13.41	13.48	0.18	3.29	7.14	3.30	1.62	0.69	99.49	0.57
93-511	310	51.39	3.68	13.60	14.37	0.23	3.78	8.37	2.81	1.01	0.60	99.84	1.93
93-512	270	50.93	2.90	13.50	13.71	0.20	5.12	9.53	2.83	0.65	0.37	99.74	0.43
93-513	250	50.68	2.83	13.88	13.62	0.21	5.35	9.76	2.48	0.48	0.36	99.65	0.88
93-514	230	50.14	3.30	13.42	14.45	0.19	4.74	9.04	3.13	0.71	0.41	99.53	1.24

1) Major oxide abundances (wt. %) were determined by X-ray fluorescence (XRF) at the University of Massachusetts following the procedures of *Rhodes* [1996].

2) $Fe_2O_3^*$ indicates all iron reported as Fe_2O_3.

3) LOI (Loss on ignition) indicates weight loss after heating to 1020°C for 30 minutes.

Table 4 Trace element abundances (ppm) in basalt from Mt. Capitole

	Rb	Ba	Th	U	Nb	Ta	La	Ce	Pb	Pr	Nd	Sr	Zr	Hf	Sm	Eu	Gd	Tb	Dy	Ho	Y	Er	Tm	Yb	Lu	Ni (XRF)	Cr (XRF)	V (XRF)	Sc (INAA)
Upper Transitional Group lavas																													
93-459	7.97	168	1.83	0.321	16.0	1.00	14.3	35.1	1.43	4.31	18.2	410	124	2.98	4.20	1.53	4.35	0.685	3.88	0.75	22.2	1.96	0.293	1.68	0.242	40	60	222	25.9
93-460	14.4	231	2.31	0.360	20.4	1.24	18.9	41.0	1.73	5.44	22.8	379	163	3.77	5.21	1.74	5.23	0.830	4.68	0.92	26.7	2.39	0.353	2.08	0.300	31	27	237	31.6
93-461	15.2	186	2.00	0.444	20.0	1.26	18.1	41.3	1.83	5.75	24.0	367	171	4.00	5.62	1.89	5.79	0.919	5.19	1.02	28.9	2.62	0.376	2.25	0.325	36	51	301	
93-462	8.04	152	1.74	0.322	15.9	1.01	14.7	34.5	1.38	4.45	19.6	362	137	3.29	4.62	1.59	4.76	0.753	4.28	0.85	24.2	2.17	0.318	1.89	0.271	42	86	243	
93-463	8.47	150	1.59	0.298	16.1	1.00	14.4	32.2	1.35	4.39	18.6	331	132	3.09	4.44	1.49	4.51	0.717	4.08	0.79	23.2	2.05	0.293	1.75	0.256	72	108	250	
93-464	7.57	188	2.14	0.381	19.2	1.23	18.1	41.5	1.70	5.33	23.3	361	159	3.89	5.45	1.88	5.55	0.880	4.98	0.99	28.0	2.53	0.371	2.19	0.314	41	85	269	
93-465	9.85	170	1.53	0.315	14.1	0.91	13.1	31.5	1.26	3.93	17.2	349	118	2.89	4.12	1.45	4.17	0.673	3.80	0.75	21.3	1.92	0.276	1.64	0.236	47	126	240	
93-467	3.05	182	1.92	0.389	18.2	1.13	16.2	40.7	1.71	5.22	22.4	329	155	3.84	5.40	1.89	5.57	0.879	4.93	0.98	27.7	2.52	0.372	2.13	0.304	51	100	300	
93-468	6.02	235	1.75	0.229	16.6	1.02	14.7	36.8	1.54	4.64	20.3	298	139	3.40	4.86	1.69	4.98	0.793	4.40	0.86	24.6	2.22	0.330	1.91	0.267	52	106	253	
93-469	5.13	159	1.76	0.353	16.9	1.03	14.9	36.5	1.53	4.63	20.1	317	143	3.43	4.86	1.69	5.03	0.806	4.48	0.88	25.9	2.26	0.336	1.95	0.278	52	106	271	
93-470	6.65	176	1.69	0.275	16.7	1.04	14.4	36.2	1.52	4.61	19.8	349	137	3.37	4.77	1.69	4.95	0.779	4.39	0.86	24.4	2.23	0.331	1.88	0.267	64	96	269	
93-471	8.60	164	1.55	0.284	16.8	1.03	14.9	34.2	1.36	4.66	20.1	331	143	3.29	4.71	1.64	4.82	0.768	4.34	0.85	24.4	2.22	0.307	1.83	0.273	67	91	241	
93-472	6.17	114	1.34	0.171	14.2	0.89	12.8	30.9	1.11	4.01	17.6	389	127	2.83	4.23	1.46	4.37	0.698	3.88	0.77	21.6	1.97	0.284	1.67	0.237	109	281	212	27.5
93-473	7.23	147	1.83	0.222	16.1	1.01	15.2	33.5	1.46	4.56	19.7	291	145	3.38	4.70	1.59	4.75	0.755	4.23	0.83	24.1	2.11	0.305	1.83	0.259	54	118	258	
93-474	3.56	198	2.58	0.500	22.0	1.33	20.5	42.8	2.10	6.01	26.0	349	195	4.54	6.13	1.98	6.19	0.976	5.52	1.08	31.5	2.82	0.412	2.41	0.346	51	120	281	
93-491	1.17	96	1.89	0.340	17.0	1.08	14.7	35.1	1.49	4.75	21.0	301	160	3.94	5.17	1.74	5.35	0.850	4.84	0.94	26.9	2.43	0.352	2.08	0.296	150	240	235	28.7
Lower Transitional Group lavas																													
93-475	6.33	232	3.02	0.648	26.6	1.60	24.0	51.8	2.23	7.08	30.1	323	233	5.35	7.09	2.23	7.14	1.138	6.42	1.27	37.2	3.30	0.482	2.86	0.409	36	54	289	
93-476	17.1	224	2.93	0.620	25.9	1.56	22.8	51.3	2.25	6.81	29.5	300	225	5.24	6.94	2.18	7.16	1.136	6.35	1.25	36.8	3.26	0.484	2.79	0.402	36	56	294	
93-477	7.05	201	2.52	0.441	22.6	1.38	21.2	47.2	2.02	6.24	26.7	343	203	4.67	6.35	2.10	6.33	1.003	5.61	1.09	32.5	2.82	0.404	2.39	0.342	43	73	330	
Low-Silica Group lavas																													
93-478	8.86	210	2.97	0.555	29.1	1.72	24.4	54.5	2.28	7.64	33.0	323	262	5.97	7.96	2.57	8.34	1.329	7.38	1.46	43.5	3.76	0.558	3.22	0.462	29	69	337	
93-479	21.8	214	2.92	0.654	29.1	1.71	23.7	53.9	2.27	7.55	32.0	298	249	5.76	7.63	2.42	8.00	1.278	7.11	1.41	40.2	3.69	0.548	3.14	0.461	27	30	326	
93-480	7.79	218	2.97	0.637	28.5	1.73	24.5	56.2	2.29	7.55	32.2	306	258	5.95	7.84	2.46	7.94	1.277	7.17	1.41	40.8	3.65	0.532	3.11	0.450	27	42	355	
93-481	5.35	202	2.83	0.526	29.4	1.74	23.2	52.9	2.21	7.38	31.8	297	251	5.85	7.80	2.49	8.00	1.280	7.14	1.41	40.3	3.67	0.544	3.12	0.446	30	48	383	
93-482	14.1	219	3.27	0.661	34.0	2.08	26.5	60.9	2.42	8.55	37.2	347	298	6.82	8.99	2.90	9.29	1.485	8.35	1.64	47.6	4.30	0.639	3.66	0.523	27	38	412	31.6
93-483	21.1	177	2.56	0.564	27.5	1.69	23.3	53.8	2.56	7.34	32.3	330	244	5.72	7.85	2.57	8.30	1.302	7.39	1.43	43.1	3.72	0.552	3.15	0.449	43	70	372	
93-484	3.15	166	2.51	0.516	24.9	1.53	21.4	48.4	1.86	6.61	29.2	329	226	5.30	7.22	2.31	7.34	1.183	6.64	1.30	38.7	3.39	0.491	2.86	0.405	40	72	315	
93-485	9.70	164	2.67	0.607	25.0	1.53	22.2	49.3	2.12	6.86	29.8	327	236	5.53	7.27	2.31	7.44	1.187	6.75	1.31	38.8	3.34	0.486	2.89	0.408	49	53	309	
93-486	1.97	200	3.00	0.531	29.0	1.83	23.6	56.7	2.36	7.60	33.3	355	259	6.21	8.22	2.71	8.54	1.358	7.69	1.51	43.6	3.95	0.573	3.32	0.471	28	40	358	
Lower Transitional Group lavas																													
93-487	8.84	185	2.71	0.588	25.6	1.59	21.8	51.8	2.16	6.89	30.0	306	233	5.60	7.30	2.37	7.57	1.197	6.72	1.32	38.6	3.42	0.508	2.89	0.409	34	55	320	
93-488	9.59	158	2.54	0.558	25.5	1.60	21.6	49.8	2.11	6.79	29.7	302	231	5.46	7.35	2.35	7.61	1.205	6.65	1.31	37.7	3.38	0.486	2.91	0.409	45	89	320	

93-489	4.58	159	2.70	0.518	24.9	1.58	21.9	52.5	2.03	6.69	29.4	344	232	5.45	7.15	2.33	7.30	1.181	6.58	1.29	38.3	3.34	0.475	2.84	0.403	47	66	301	
93-490	18.3	227	3.25	0.737	28.1	1.78	25.7	57.9	2.57	7.67	33.6	333	268	6.34	8.06	2.56	8.15	1.295	7.30	1.42	41.8	3.64	0.523	3.08	0.435	27	34	307	
93-492	3.95	158	2.54	0.503	25.1	1.49	20.2	48.7	1.98	6.37	27.8	318	227	5.19	6.76	2.19	7.05	1.129	6.30	1.25	37.7	3.21	0.474	2.71	0.389	51	63	331	
93-493	2.00	192	2.27	0.424	23.8	1.52	19.1	46.5	1.97	6.32	26.9	304	216	4.96	6.69	2.14	6.84	1.098	6.11	1.20	35.2	3.08	0.458	2.64	0.382	39	38	327	
93-494	9.52	184	2.51	0.591	25.5	1.59	21.9	51.0	2.07	6.95	30.7	316	233	5.42	7.42	2.35	7.46	1.226	6.72	1.31	38.1	3.47	0.481	2.84	0.419	39	83	347	
93-495	12.7	172	2.61	0.603	24.2	1.48	21.1	46.1	1.94	6.47	28.5	340	227	5.29	6.92	2.21	7.09	1.148	6.40	1.24	37.3	3.19	0.465	2.80	0.396	38	45	333	
93-496	21.0	206	3.05	0.690	26.9	1.66	24.2	48.5	2.38	7.22	30.9	313	252	5.88	7.42	2.36	7.48	1.207	6.76	1.34	38.7	3.42	0.505	2.99	0.426	28	56	341	
93-497	5.09	210	3.10	0.635	26.0	1.62	24.6	51.9	2.33	7.36	31.7	324	247	5.75	7.65	2.44	7.68	1.238	6.87	1.37	40.2	3.56	0.518	3.03	0.437	28	44	351	
93-498	14.1	182	3.02	0.607	29.0	1.85	25.6	58.1	2.49	7.86	33.3	323	265	6.19	8.02	2.50	8.06	1.296	7.13	1.41	41.9	3.70	0.538	3.16	0.445	25	30	319	
93-499	8.80	182	2.64	0.578	25.3	1.54	21.3	50.8	2.05	6.68	29.3	337	228	5.39	7.11	2.35	7.42	1.174	6.61	1.28	38.6	3.33	0.496	2.86	0.402	49	79	305	
93-500	13.1	211	3.01	0.650	27.0	1.69	24.5	54.3	2.33	7.28	31.2	317	249	5.85	7.47	2.35	7.62	1.221	6.84	1.35	38.9	3.49	0.507	2.96	0.429	49	136	313	
93-501	4.00	156	2.18	0.441	19.8	1.24	17.6	40.1	1.75	5.43	23.7	317	184	4.33	5.77	1.89	5.94	0.946	5.36	1.05	30.9	2.71	0.392	2.33	0.334	36	40	313	
93-502	3.13	149	1.96	0.389	19.1	1.20	16.0	37.1	1.59	5.09	22.2	306	171	4.11	5.57	1.88	5.76	0.924	5.16	1.03	29.5	2.66	0.398	2.27	0.322	58	123	326	
93-503	1.61	157	2.54	0.579	24.1	1.44	20.3	47.1	1.97	6.40	27.2	309	219	5.09	6.63	2.13	6.76	1.083	6.11	1.21	34.7	3.12	0.450	2.65	0.378	52	76	314	
93-504	12.6	187	2.84	0.653	25.2	1.67	20.4	52.7	2.23	7.17	29.6	290	226	5.53	7.10	2.29	7.18	1.152	6.37	1.23	33.1	3.20	0.459	2.70	0.383	50	78	327	
93-505	18.9	215	3.22	0.732	28.2	1.76	24.5	56.2	2.56	7.45	32.6	336	271	6.23	7.98	2.54	7.83	1.245	6.93	1.33	39.0	3.38	0.498	2.92	0.416	29	43	334	
93-506	9.89	245	3.54	0.737	31.6	1.87	26.9	60.8	2.49	8.38	35.7	344	291	6.60	8.55	2.66	8.61	1.362	7.69	1.51	43.9	3.93	0.575	3.41	0.487	24	34	327	
93-507	19.6	232	3.35	0.789	31.3	1.95	26.3	61.0	2.75	8.26	35.0	322	289	6.61	8.37	2.63	8.27	1.316	7.40	1.44	41.6	3.73	0.535	3.23	0.460	24	29	329	
93-508	26.6	241	3.40	0.790	32.2	2.02	28.2	65.2	2.73	8.72	38.0	313	292	6.76	8.87	2.70	8.82	1.414	7.89	1.53	44.2	4.08	0.554	3.33	0.495	23	32	329	
93-509	12.5	317	3.39	0.770	32.3	1.97	28.0	63.8	2.71	8.46	36.5	332	286	6.82	8.72	2.76	8.82	1.405	7.82	1.52	43.8	3.97	0.570	3.38	0.485	31	37	327	
93-510	38.1	321	4.87	1.144	41.9	2.35	36.1	83.8	3.11	11.65	46.8	332	392	8.61	10.85	3.25	10.64	1.687	9.42	1.85	53.7	4.79	0.700	4.10	0.592	11	5	333	24.9
93-511	12.9	284	4.59	0.910	41.0	2.46	35.7	81.9	3.45	10.78	45.9	334	373	8.73	10.85	3.29	10.95	1.745	9.56	1.86	54.6	4.89	0.699	4.09	0.579	18	3	334	
93-512	8.98	187	2.75	0.583	23.3	1.45	21.7	46.9	2.10	6.39	27.9	327	215	5.09	6.68	2.13	6.80	1.076	6.06	1.19	34.7	3.05	0.442	2.58	0.367	26	53	284	
93-513	5.92	174	2.63	0.572	23.8	1.51	20.8	46.2	2.08	6.45	27.5	316	220	5.14	6.67	2.05	6.64	1.079	5.95	1.16	34.0	3.00	0.438	2.57	0.360	32	34	267	
93-514	6.71	223	3.19	0.608	26.8	1.66	24.3	55.4	2.39	7.38	32.1	354	260	6.04	7.70	2.52	7.88	1.233	7.00	1.36	39.8	3.46	0.504	2.96	0.420	27	34	325	
BHVO-	9.48	135	1.30	0.446	19.0	1.22	15.2	38.4	1.53	5.57	24.9	399	178	4.42	6.16	2.03	6.13	0.963	5.30	1.01	28.3	2.50	0.350	2.05	0.286				

Ni, Cr and V were determined by XRF at Univ. of Mass. following the procedures of *Rhodes* [1996]. Sc was determined by INAA at MIT following the procedures of *Ila and Frey* [2000]. All others were determined by ICP-MS at MIT. The abundances for BHVO-2 are the average values of 15 analyses, with relative stand deviation of ≤3% [*Huang and Frey* , 2003].

Table 5. Sr, Nd, Hf and Pb isotope compositions for Mt. Capitole whole rock lavas and plagioclase phenocrysts

Sample number	$^{87}Sr/^{86}Sr$	2σ	$(^{87}Sr/^{86}Sr)_i$	$^{143}Nd/^{144}Nd$	2σ	$(^{143}Nd/^{144}Nd)_i$	$^{176}Hf/^{177}Hf$	2σ	$(^{176}Hf/^{177}Hf)_i$	$^{206}Pb/^{204}Pb$	2σ	$(^{206}Pb/^{204}Pb)_i$	$^{207}Pb/^{204}Pb$	2σ	$(^{207}Pb/^{204}Pb)_i$	$^{208}Pb/^{204}Pb$	2σ	$(^{208}Pb/^{204}Pb)_i$
Upper Transitional Group																		
93-459	0.704835	10	0.70481	0.512685	8	0.51266	0.282863	4	0.28286	18.4418	13	18.384	15.5512	15	15.548	38.9699	36	38.861
93-459			0.70482			0.51265						18.387			15.549			38.926
93-459 plag	0.704740	10	0.70474							18.465	23	18.45	15.584	19	15.58	38.894	52	38.88
93-463	0.704832	9	0.70481	0.512697	6	0.51267	0.282876	4	0.28287	18.3973	11	18.341	15.5398	9	15.537	38.8821	22	38.783
93-465	0.704828	9	0.70480	0.512693	7	0.51267	0.282886	4	0.28288	18.4193	8	18.356	15.5426	7	15.540	38.8937	20	38.792
93-465	0.704808	7	0.70478	0.512697	3	0.51267	0.282882	5	0.28288	18.4191	11	18.355	15.5424	9	15.539	38.8915	21	38.789
93-465UL	0.704875	7		0.512680	5					18.4236	8	18.360	15.5459	8	15.543	38.9124	21	38.810
93-471	0.704802	7	0.70477	0.512705	6	0.51268	0.282884	4	0.28288	18.4037	8	18.351	15.5421	7	15.540	38.8658	20	38.770
93-471			0.70478			0.51267						18.337			15.539			38.814
93-471 plag	0.704761	8	0.70476							18.462	35	18.45	15.640	29	15.640	38.910	70	38.90
93-472	0.704772	6	0.70476	0.512704	5	0.51268	0.282885	4	0.28288	18.4718	26	18.391	15.5536	24	15.550	38.9414	57	38.840
Low Silica Group																		
93-479	0.704783	7	0.70471	0.512717	5	0.51269	0.282905	4	0.28290	18.4721	8	18.399	15.5505	7	15.547	38.9155	19	38.807
93-482	0.704716	8	0.70467	0.512728	5	0.51270	0.282897	4	0.28289	18.4562	13	18.386	15.5488	12	15.546	38.8762	28	38.762
93-483	0.704776	9	0.70471	0.512714	5	0.51269				18.4386	10	18.382	15.5520	9	15.549	38.8991	26	38.814
Lower Transitional Group																		
93-476	0.704913	6	0.70485	0.512686	7	0.51266	0.282884	5	0.28288	18.3954	8	18.325	15.5449	8	15.542	38.8748	22	38.765
93-490	0.705046	6	0.70499	0.512694	6	0.51267	0.282871	4	0.28287	18.3769	10	18.304	15.5514	9	15.548	38.8102	26	38.704
93-490	0.705039	7	0.70498	0.512690	6	0.51267	0.282869	3	0.28286	18.3906	14	18.318	15.5520	13	15.549	38.8299	32	38.724
93-495	0.704770	6	0.70473	0.512722	6	0.51270	0.282897	5	0.28289	18.4618	13	18.382	15.5553	12	15.552	38.8682	34	38.754
93-505	0.705060	9	0.70500	0.512689	5	0.51266	0.282869	4	0.28286	18.3938	7	18.321	15.5494	7	15.546	38.8425	18	38.736
93-507	0.704841	8	0.70478	0.512706	5	0.51268	0.282891	5	0.28289	18.4200	5	18.347	15.5407	6	15.537	38.8488	15	38.746
93-510	0.704935	6	0.70482	0.512704	5	0.51268	0.282894	5	0.28289	18.4243	9	18.331	15.5405	7	15.536	38.8534	19	38.721
93-512	0.704790	7	0.70476	0.512717	6	0.51269	0.282887	5	0.28288	18.4382	15	18.367	15.5421	13	15.545	38.8800	35	38.770
93-512	0.704803	7	0.70477	0.512706	5	0.51268	0.282881	6	0.28288	18.4451	14	18.374	15.5487	13	15.539	38.9004	33	38.790

1. Within each group samples are in stratigraphic order.

2. Prior to isotopic analyses, all samples were acid-leached following the procedures of *Weis et al.* [2005]. The effects of acid leaching are shown by data for leached and unleached (UL) aliquots of sample 93-465.

3. Measured Sr isotopic ratios were normalized to $^{86}Sr/^{88}Sr$=0.1194 and Nd ratios were normalized to $^{146}Nd/^{144}Nd$=0.7219. Mean measured $^{87}Sr/^{86}Sr$ for NBS 987 at UBC during the course of study was 0.710260 ± 13 (2σ, n=42) and $^{143}Nd/^{144}Nd$ for La Jolla standard was 0.511858 ± 7 (2σ, n=18). $^{176}Hf/^{177}Hf$ ratios reported were normalized to JMC475 Hf standard of 0.282160. Pb isotopic ratios were measured using Tl spiking (with a $^{205}Tl/^{203}Tl$ = 2.3885) for fractionation correction *Weis et al.* [2005]. Mean measured $^{206}Pb/^{204}Pb$, $^{207}Pb/^{204}Pb$ and $^{208}Pb/^{204}Pb$ for NBS 981 Pb standard at UBC were 16.9418 ± 22 (2σ, n=94), 15.4979 ± 26 (2σ, n=94) and 36.7184 ± 63 (2σ, n=94), respectively. The Pb isotopic ratios of plagioclase were analyzed by TIMS at MIT using a fractionation correction of 0.12 ± 0.03 %/amu, based on the values of *Todt et al.* [1996].

4. Two sigma (2σ) errors apply to last decimal place. The external reproducibility for $^{87}Sr/^{86}Sr$ and $^{143}Nd/^{144}Nd$ based on three duplicates (93-465, 93-490 and 93-512) are better than 20×10^{-6} and 11×10^{-6}, respectively, that is within or slightly larger than the machine in-run uncertainties. The external reproducibility at UBC for $^{206}Pb/^{204}Pb$, $^{207}Pb/^{204}Pb$ and $^{208}Pb/^{204}Pb$ are better than 744 ppm, 428 ppm and 525 ppm, respectively.

5. Subscript "*i*" (initial) measured ratios corrected to 25.7 Ma, the age of lavas from nearby Mt. Tourmente. Parent/daughter abundance ratios used for age corrections are data for unleached samples (Table 4) except for sample 472 which has a very high Nb/U ratio indicating U loss; therefore Nb/U=40 was used to calculate U content which was used to calculate the initial Pb isotope ratios. For samples 93-471 and 93-459 parent/daughter ratios are also available for leached samples; the calculated initial ratios for the two sets of parent/daughter ratios are within analytical uncertainties.

Table 6 Selected trace element ratios for whole rocks and plagioclase phenocrysts

	$(Sr/Nd)_{PM}$	$^{87}Rb/^{86}Sr$	$^{147}Sm/^{144}Nd$	$^{238}U/^{204}Pb$	$^{235}U/^{204}Pb$	$^{232}Th/^{204}Pb$
93-459 plagioclase	28.5	0.00157	0.138	3.19	0.0232	9.6
93-459 whole rock leached[a]	2.74	0.054	0.196	12.6	0.091	34
93-459 whole rock unleached[b]	1.45	0.056	0.140	14.4	0.104	86
93-471 plagioclase	22.1	0.00193	0.127	1.81	0.0132	7.5
93-471 whole rock leached	2.44	0.067	0.207	15.2	0.111	41
93-471 whole rock unleached	1.05	0.075	0.141	13.3	0.097	76

[a] whole rock was leached repeatedly in 6 N HCl following the same procedures used in Sr, Nd and Pb isotope analyses before dissolving for ICP-MS analyses; [b] results from Table 4

Table 7 Trace element contents and isotopic ratios for modelling

	$^{87}Sr/^{86}Sr$	$^{206}Pb/^{204}Pb$	$^{208}Pb/^{204}Pb$	Sr	Pb	Th	Nb	La
Kerguelen plume (av.)	0.70523	18.533	39.2	300	3	1.05	10.5	7.7
Kerguelen plume (rad.)		18.642	39.38					
SEIR N-MORB	0.703	17.98	37.8	100	0.25	0.05	1	1.4
LCC (Huang et al., 1995)	0.707	16.44	36.85					
LCC (Rudnick and Gao, 2004)				348	4	1.2	5	8
LCC (Shaw et al., 1994)				447	6	2.6	5.6	21

Isotopic compositions of average (av.) and radiogenic (rad.) Kerguelen plume are from *Weis and Frey* [2002]. SEIR N-MORB isotopic compositions are the averages of N-MORB data from *Mahoney et al.* [2002] and *Kempton et al.* [2002]. We estimated the trace element compositions of SEIR N-MORB using *Mahoney et al.* [2002] data based on mg# - X plots. Lower continental crust isotopic compositions are from a xenolith composition from *Huang et al.* [1995]. The trace element compositions of lower continental crust are from *Rudnick and Gao* [2002] for average LCC and *Shaw et al.* [1994] for stable and mature LCC.

We estimated Sr, TH, Nb and La contents for the Kerguelen plume melt using MgO-X plots for the flood basalts. The slopes of such plots change abruptly at ~6.5 wt% MgO, reflecting the onset of cotectic crystallization and fractionation of plagioclase and clinopyroxene. Lavas with >6.5 wt% define a nearly horizontal trend due to olivine fractionation and we averaged the abundances of Sr, Th, Nb and La of samples with > 6.5 wt% MgO. Due to scarcity of Pb data for Kerguelen Archipelago lavas, we calculated a Pb content for Kerguelen plume melt based the most primitive melt composition of Mt. Capitole lavas and the proportion of MORB which can be constrained by Sr contents and isotopic ratios.

There are large uncertainties in estimating of trace element contents of primary melts for Kerguelen plume and SEIR N-MORB as well as choosing isotopic ratios and concentrations in LCC, therefore, the modeling is schematic and qualitative rather than quantitative.

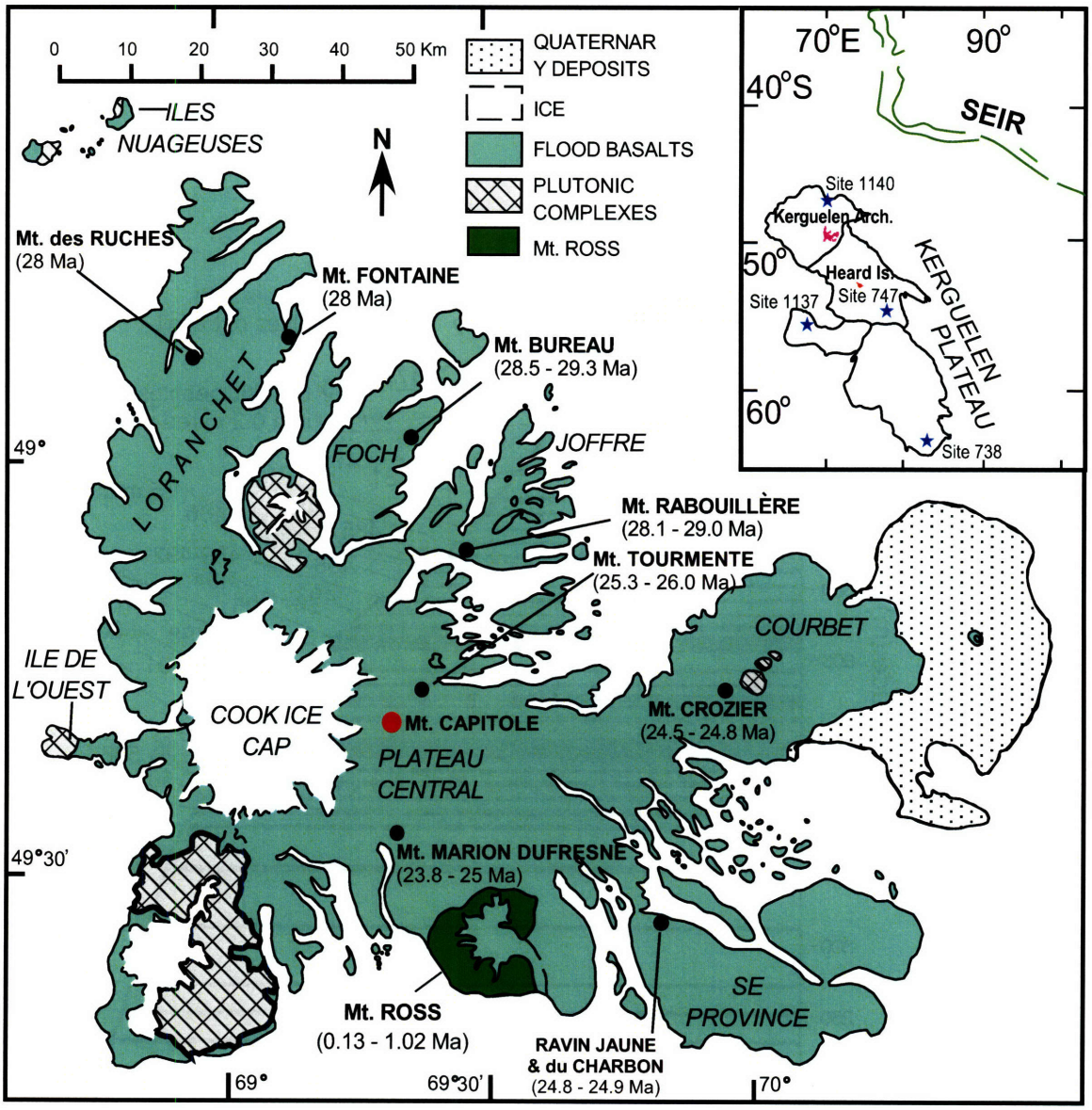
0 10 20 30 40 50 Km
QUATERNARY DEPOSITS
ICE
FLOOD BASALTS
PLUTONIC COMPLEXES
Mt. ROSS
N
ILES NUAGEUSES
Mt. des RUCHES
(28 Ma)
Mt. FONTAINE
(28 Ma)
Mt. BUREAU
(28.5 - 29.3 Ma)
LORANCHET
FOCH
JOFFRE
Mt. RABOUILLÈRE
(28.1 - 29.0 Ma)
Mt. TOURMENTE
(25.3 - 26.0 Ma)
COURBET
ILE DE L'OUEST
COOK ICE CAP
Mt. CAPITOLE
PLATEAU CENTRAL
Mt. CROZIER
(24.5 - 24.8 Ma)
Mt. MARION DUFRESNE
(23.8 - 25 Ma)
Mt. ROSS
(0.13 - 1.02 Ma)
RAVIN JAUNE & du CHARBON
(24.8 - 24.9 Ma)
SE PROVINCE
49°
49°30'
69°
69°30'
70°
70°E
90°
40°S
SEIR
Site 1140
Kerguelen Arch.
50°
Heard Is.
Site 1137
Site 747
KERGUELEN PLATEAU
60°
Site 738

Fig. 1

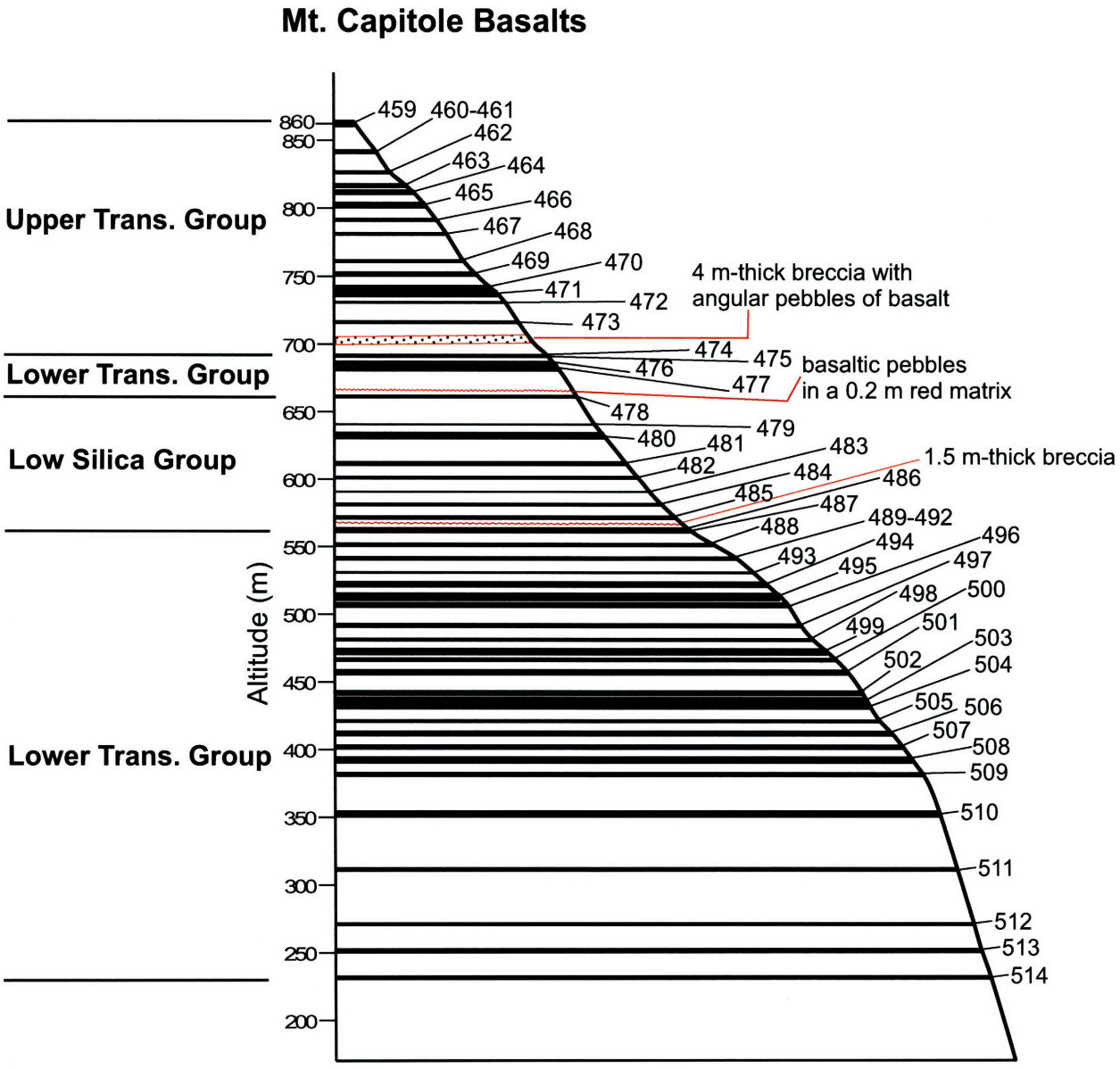
Mt. Capitole Basalts
Upper Trans. Group
Lower Trans. Group
Low Silica Group
Lower Trans. Group
Altitude (m)
860
850
800
750
700
650
600
550
500
450
400
350
300
250
200
459
460-461
462
463
464
465
466
467
468
469
470
471
472
473
474
475
476
477
478
479
480
481
482
483
484
485
486
487
488
489-492
493
494
495
496
497
498
499
500
501
502
503
504
505
506
507
508
509
510
511
512
513
514
4 m-thick breccia with angular pebbles of basalt
basaltic pebbles in a 0.2 m red matrix
1.5 m-thick breccia

Fig. 2

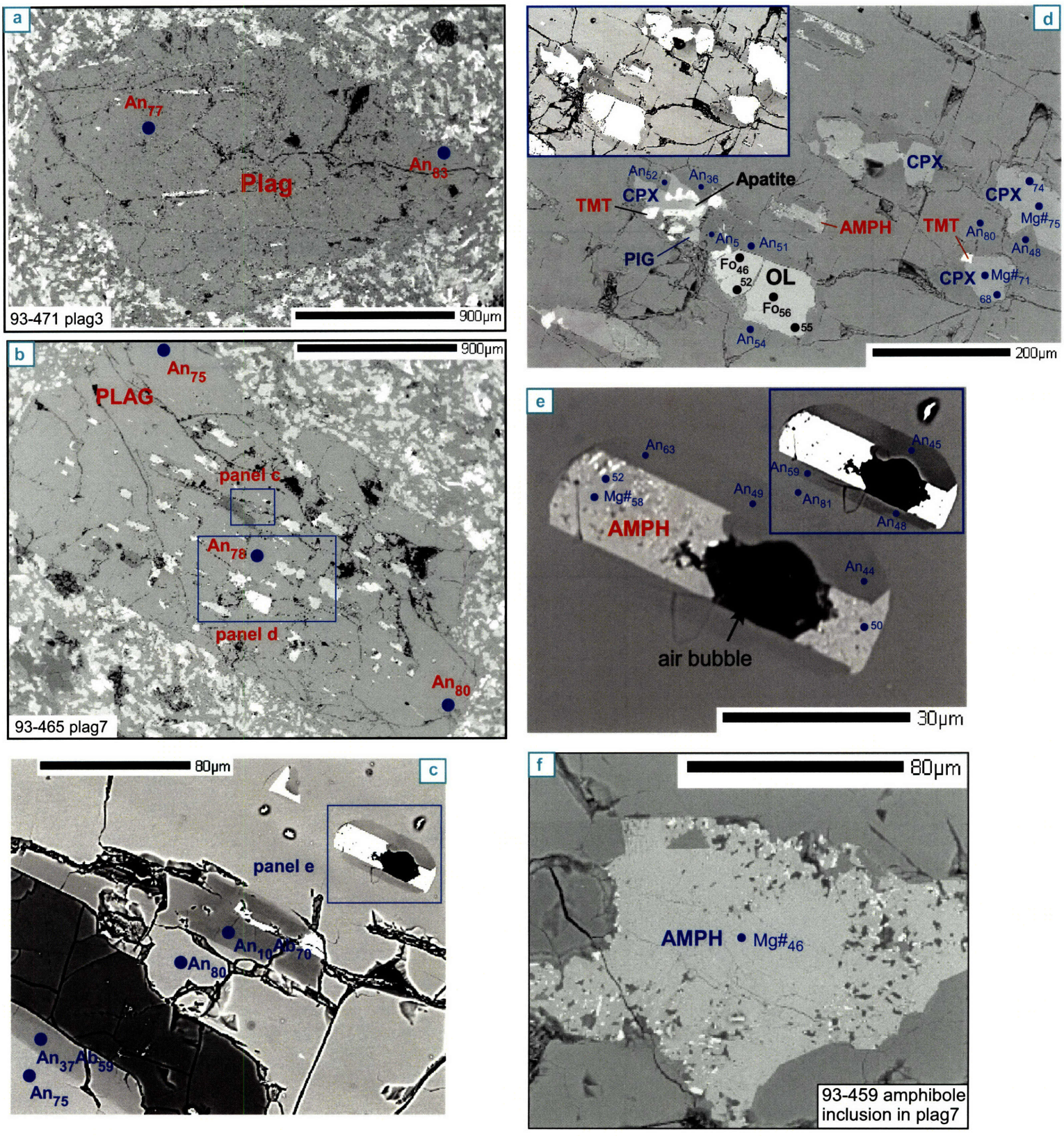
a
An77
Plag
An83
93-471 plag3
900µm
b
900µm
An75
PLAG
panel c
An78
panel d
An80
93-465 plag7
c
80µm
panel e
An10
An70
An80
An37
An59
An75
d
An52
An36
Apatite
CPX
TMT
AMPH
An5
An51
PIG
Fo46
52
OL
Fo56
55
An54
CPX
74
Mg#75
TMT
An80
An48
CPX
Mg#71
68
200µm
e
An63
52
Mg#58
AMPH
An49
An59
An81
An45
An48
An44
50
air bubble
30µm
f
80µm
AMPH
Mg#46
93-459 amphibole inclusion in plag7

Fig. 3

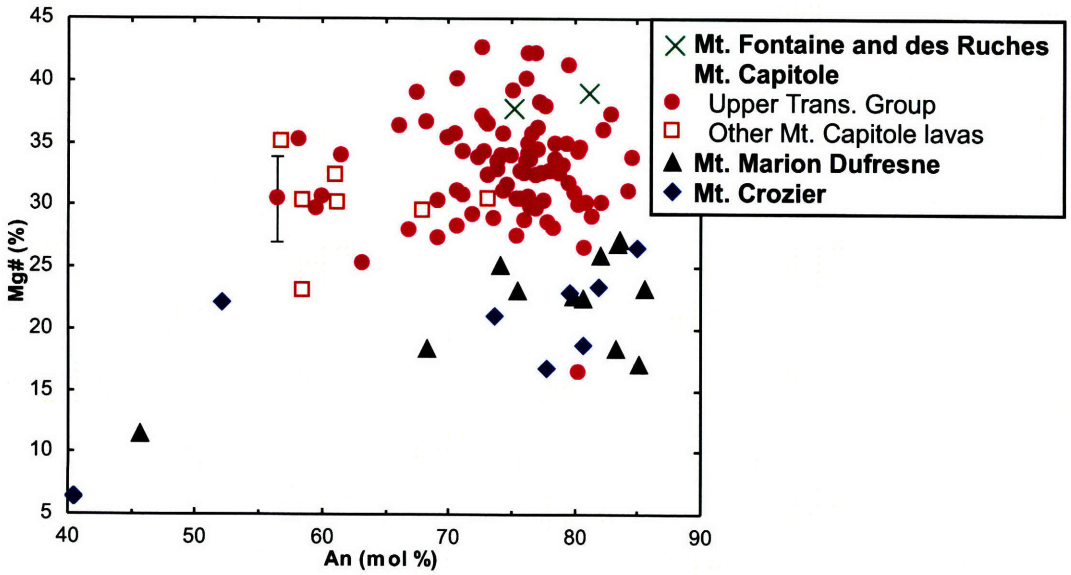
Mg# (%)
An (mol %)
Mt. Fontaine and des Ruches
Mt. Capitole
Upper Trans. Group
Other Mt. Capitole lavas
Mt. Marion Dufresne
Mt. Crozier

Fig. 4

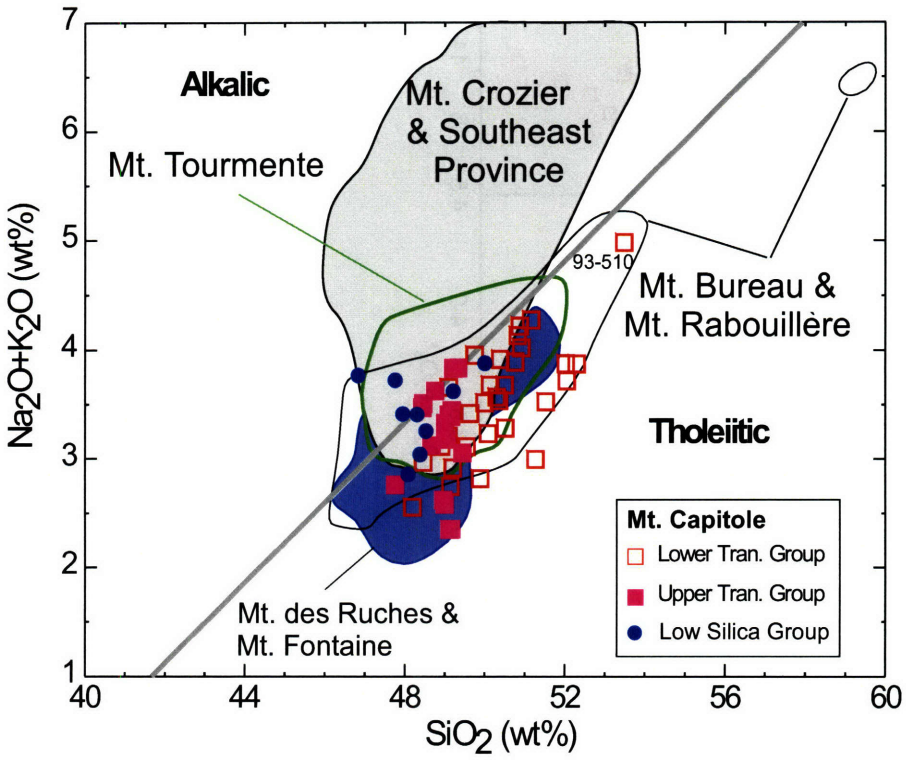
Alkalic
Mt. Crozier
& Southeast
Province
Mt. Tourmente
93-510
Mt. Bureau &
Mt. Rabouillère
Tholeiitic
Mt. Capitole
Lower Tran. Group
Upper Tran. Group
Low Silica Group
Mt. des Ruches &
Mt. Fontaine
Na2O+K2O (wt%)
SiO2 (wt%)
1
2
3
4
5
6
7
40
44
48
52
56
60

Fig. 5

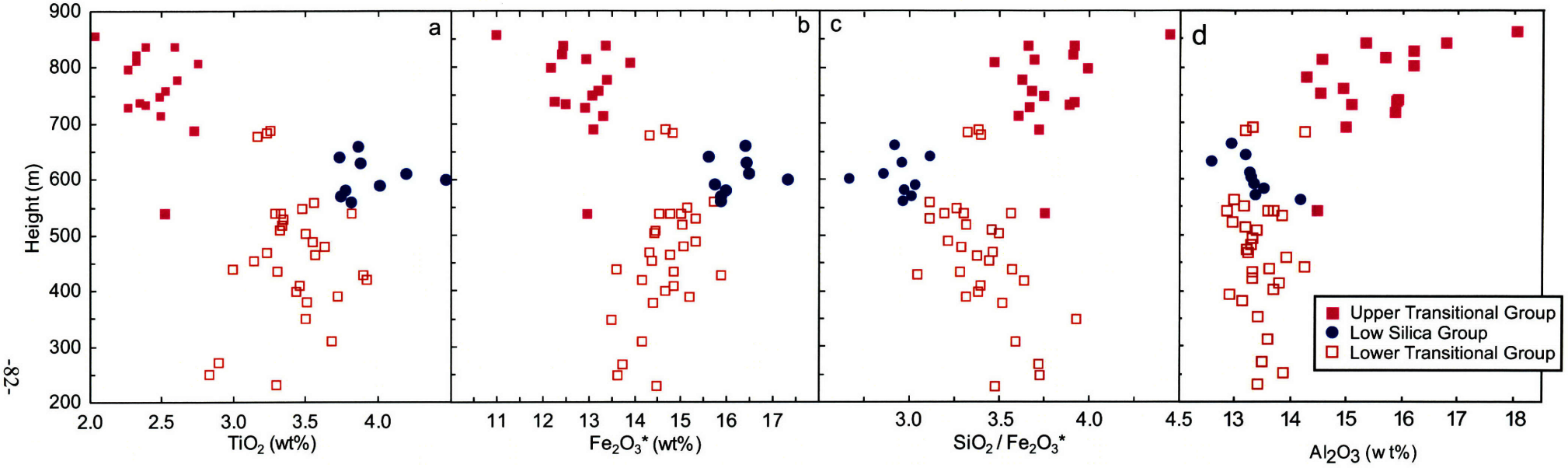
a
b
c
d
Height (m)
900
800
700
600
500
400
300
200
2.0
2.5
3.0
3.5
4.0
TiO2 (wt%)
11
12
13
14
15
16
17
Fe2O3* (wt%)
3.0
3.5
4.0
4.5
SiO2 / Fe2O3*
13
14
15
16
17
18
Al2O3 (wt%)
Upper Transitional Group
Low Silica Group
Lower Transitional Group

Fig. 6

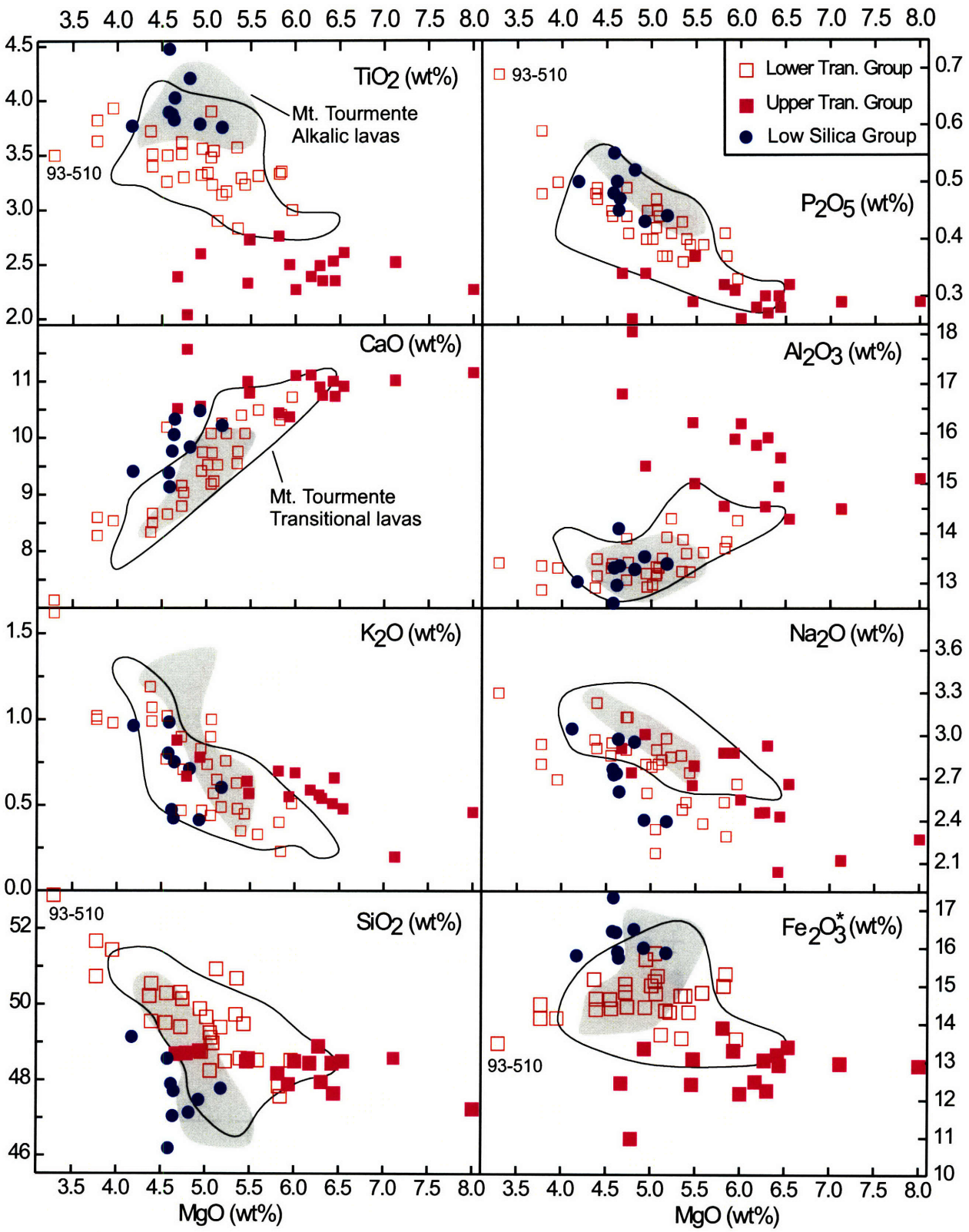
TiO2 (wt%)
Mt. Tourmente
Alkalic lavas
93-510
93-510
Lower Tran. Group
Upper Tran. Group
Low Silica Group
P2O5 (wt%)
CaO (wt%)
Mt. Tourmente
Transitional lavas
Al2O3 (wt%)
K2O (wt%)
Na2O (wt%)
93-510
SiO2 (wt%)
Fe2O3* (wt%)
93-510
MgO (wt%)
MgO (wt%)

Fig. 7

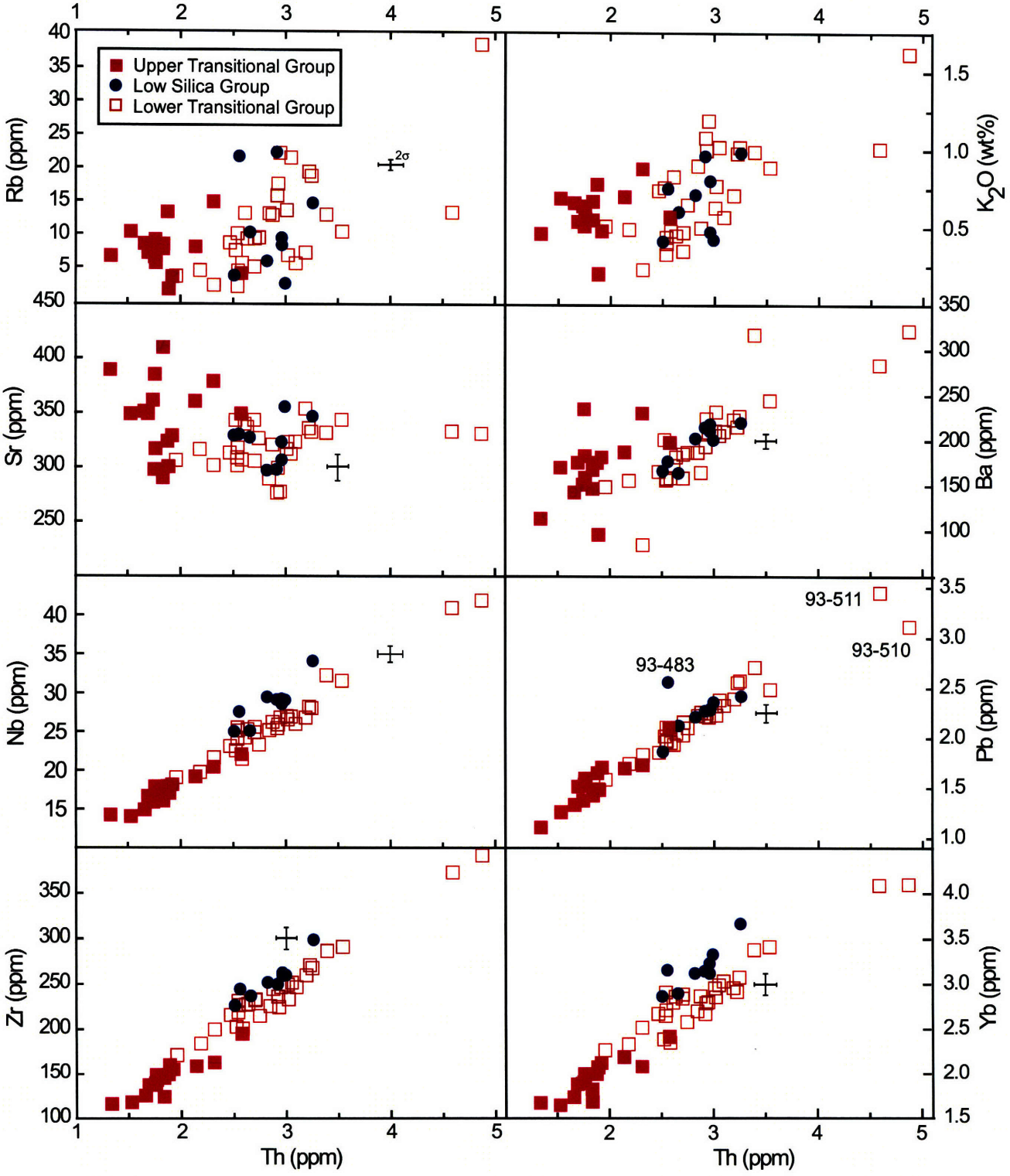
Upper Transitional Group
Low Silica Group
Lower Transitional Group
2σ
Rb (ppm)
K2O (wt%)
Sr (ppm)
Ba (ppm)
Nb (ppm)
Pb (ppm)
Zr (ppm)
Yb (ppm)
93-511
93-510
93-483
Th (ppm)
Th (ppm)

Fig. 8

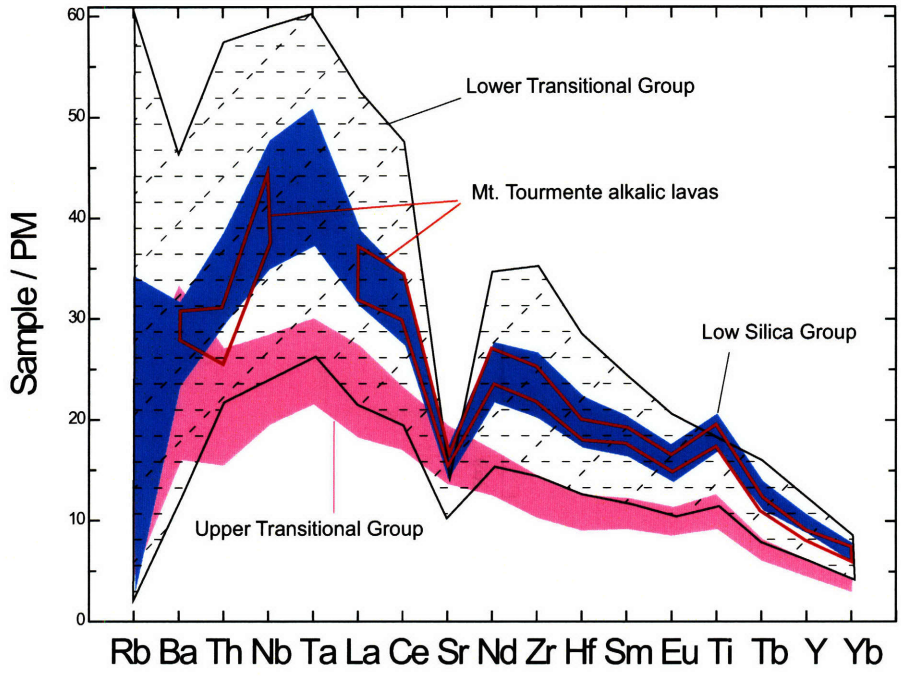
Sample / PM
60
50
40
30
20
10
0
Lower Transitional Group
Mt. Tourmente alkalic lavas
Low Silica Group
Upper Transitional Group
Rb Ba Th Nb Ta La Ce Sr Nd Zr Hf Sm Eu Ti Tb Y Yb

Fig. 9

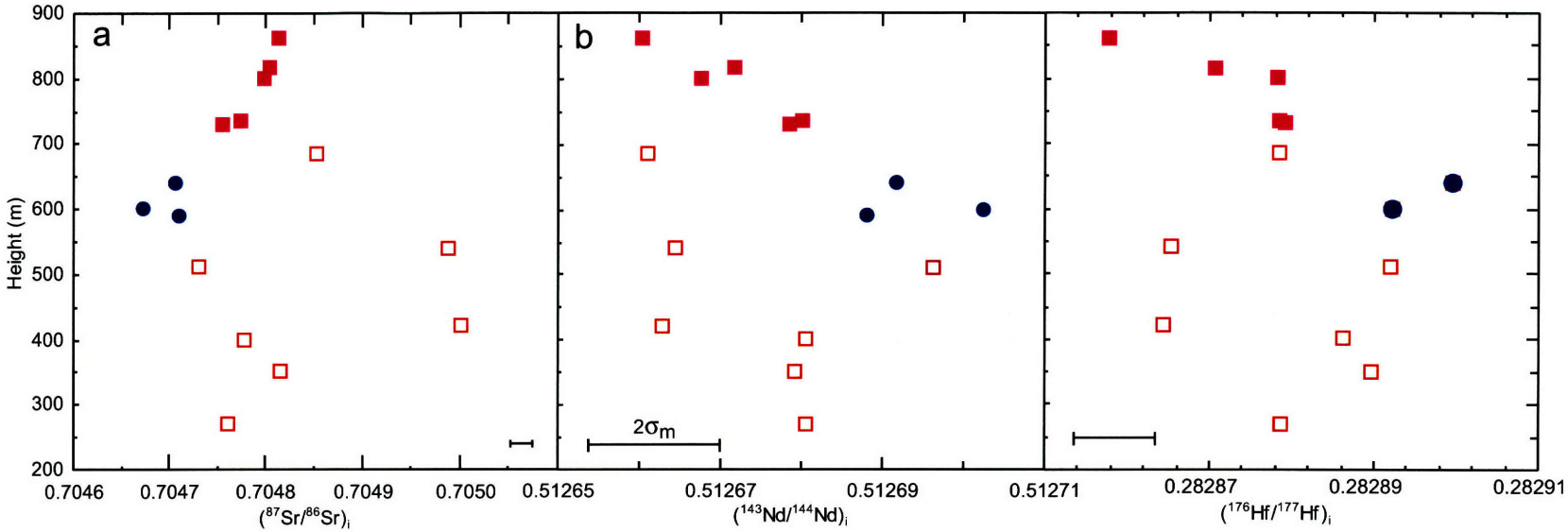
a
b
Height (m)
900
800
700
600
500
400
300
200
0.7046
0.7047
0.7048
0.7049
0.7050
$(^{87}Sr/^{86}Sr)_i$
0.51265
0.51267
0.51269
0.51271
$2\sigma_m$
$(^{143}Nd/^{144}Nd)_i$
0.28287
0.28289
0.28291
$(^{176}Hf/^{177}Hf)_i$

Fig. 10

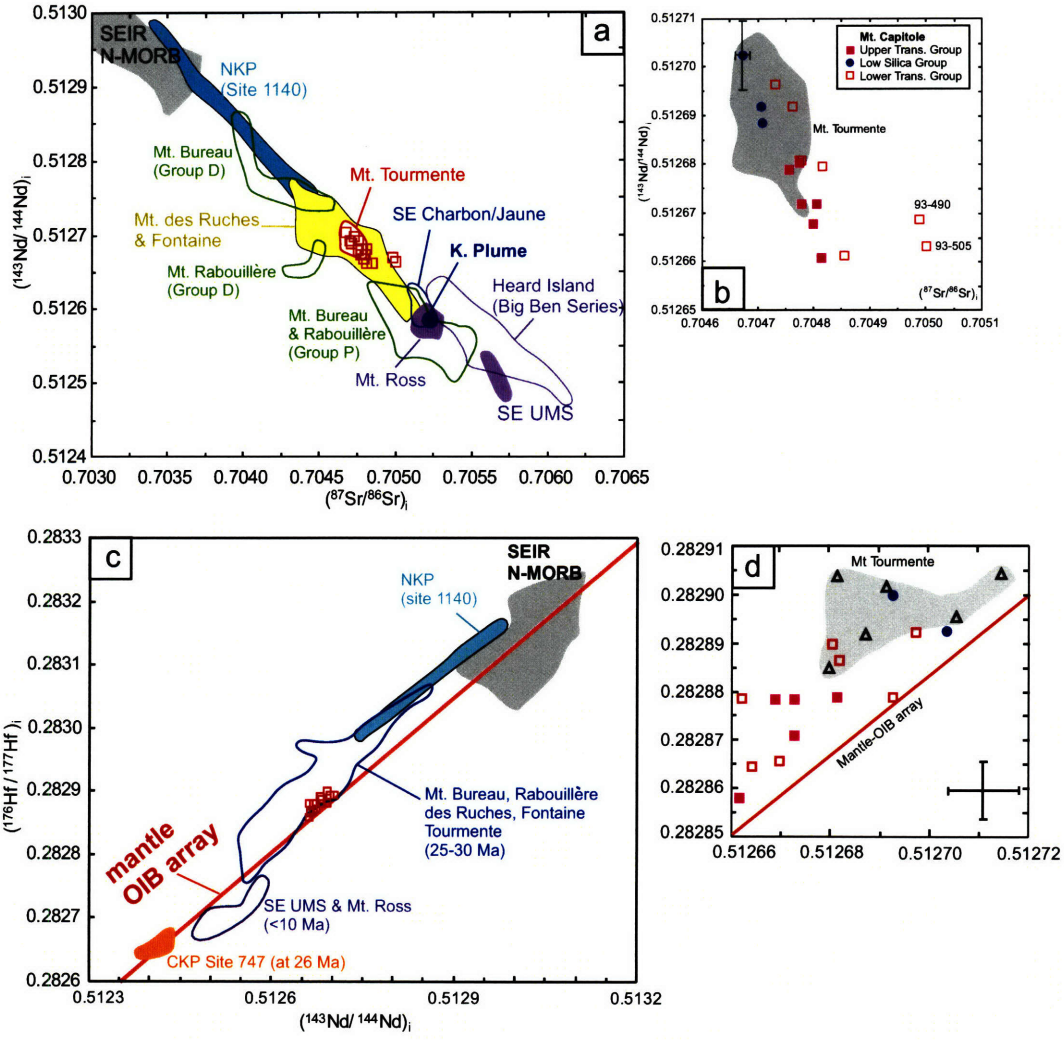
a
SEIR
N-MORB
NKP
(Site 1140)
Mt. Bureau
(Group D)
Mt. Tourmente
Mt. des Ruches
& Fontaine
SE Charbon/Jaune
K. Plume
Mt. Rabouillère
(Group D)
Heard Island
(Big Ben Series)
Mt. Bureau
& Rabouillère
(Group P)
Mt. Ross
SE UMS
$(^{143}Nd/^{144}Nd)_i$
$(^{87}Sr/^{86}Sr)_i$
b
Mt. Capitole
Upper Trans. Group
Low Silica Group
Lower Trans. Group
Mt. Tourmente
93-490
93-505
c
SEIR
N-MORB
NKP
(site 1140)
Mt. Bureau, Rabouillère
des Ruches, Fontaine
Tourmente
(25-30 Ma)
mantle
OIB array
SE UMS & Mt. Ross
(<10 Ma)
CKP Site 747 (at 26 Ma)
$(^{176}Hf/^{177}Hf)_i$
$(^{143}Nd/^{144}Nd)_i$
d
Mt Tourmente
Mantle-OIB array

Fig. 11

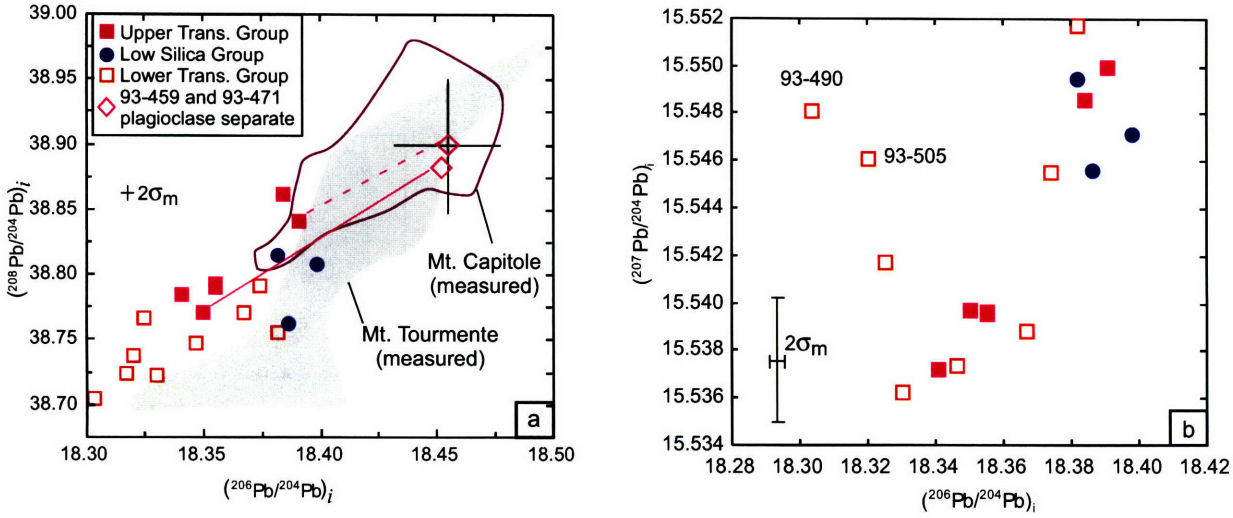
Upper Trans. Group
Low Silica Group
Lower Trans. Group
93-459 and 93-471
plagioclase separate
+2σm
Mt. Capitole
(measured)
Mt. Tourmente
(measured)
a
b
93-490
93-505
2σm
(208Pb/204Pb)i
(206Pb/204Pb)i
(207Pb/204Pb)i
(206Pb/204Pb)i

Fig. 12

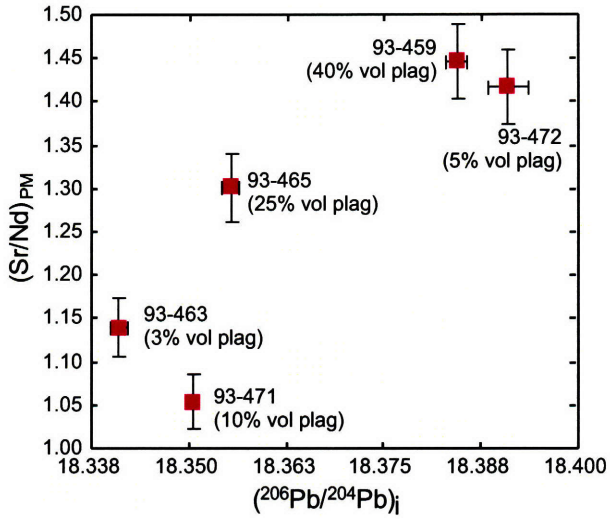
1.50
1.45
1.40
1.35
1.30
1.25
1.20
1.15
1.10
1.05
1.00
(Sr/Nd)PM
18.338
18.350
18.363
18.375
18.388
18.400
(206Pb/204Pb)i
93-459
(40% vol plag)
93-472
(5% vol plag)
93-465
(25% vol plag)
93-463
(3% vol plag)
93-471
(10% vol plag)

Fig. 13

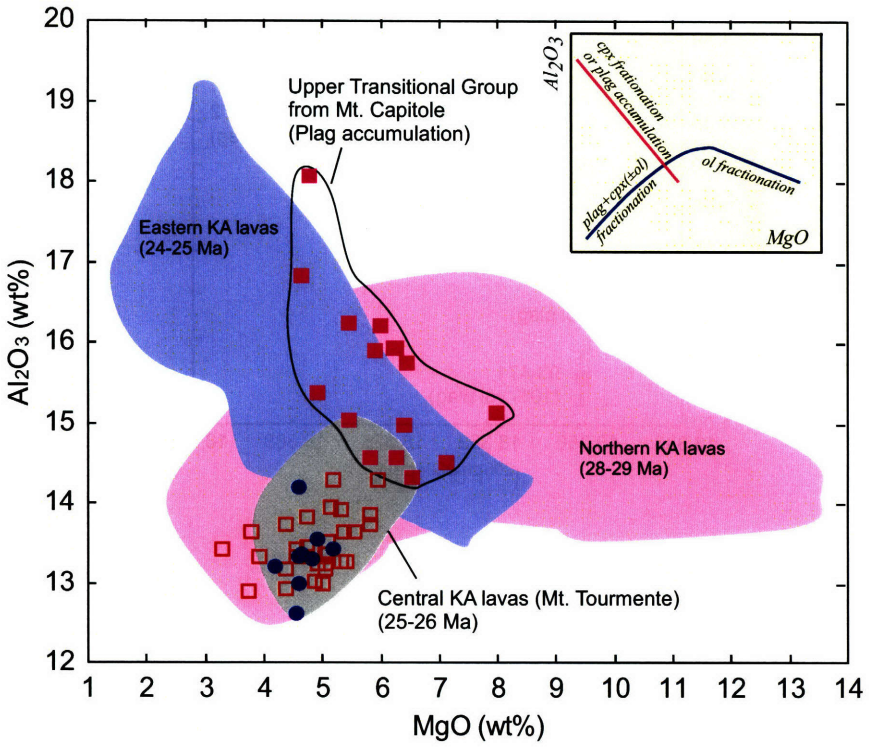
Upper Transitional Group
from Mt. Capitole
(Plag accumulation)
Eastern KA lavas
(24-25 Ma)
Northern KA lavas
(28-29 Ma)
Central KA lavas (Mt. Tourmente)
(25-26 Ma)
Al2O3 (wt%)
MgO (wt%)
Al2O3
cpx fractionation
or plag accumulation
plag+cpx(±ol)
fractionation
ol fractionation
MgO

Fig. 14

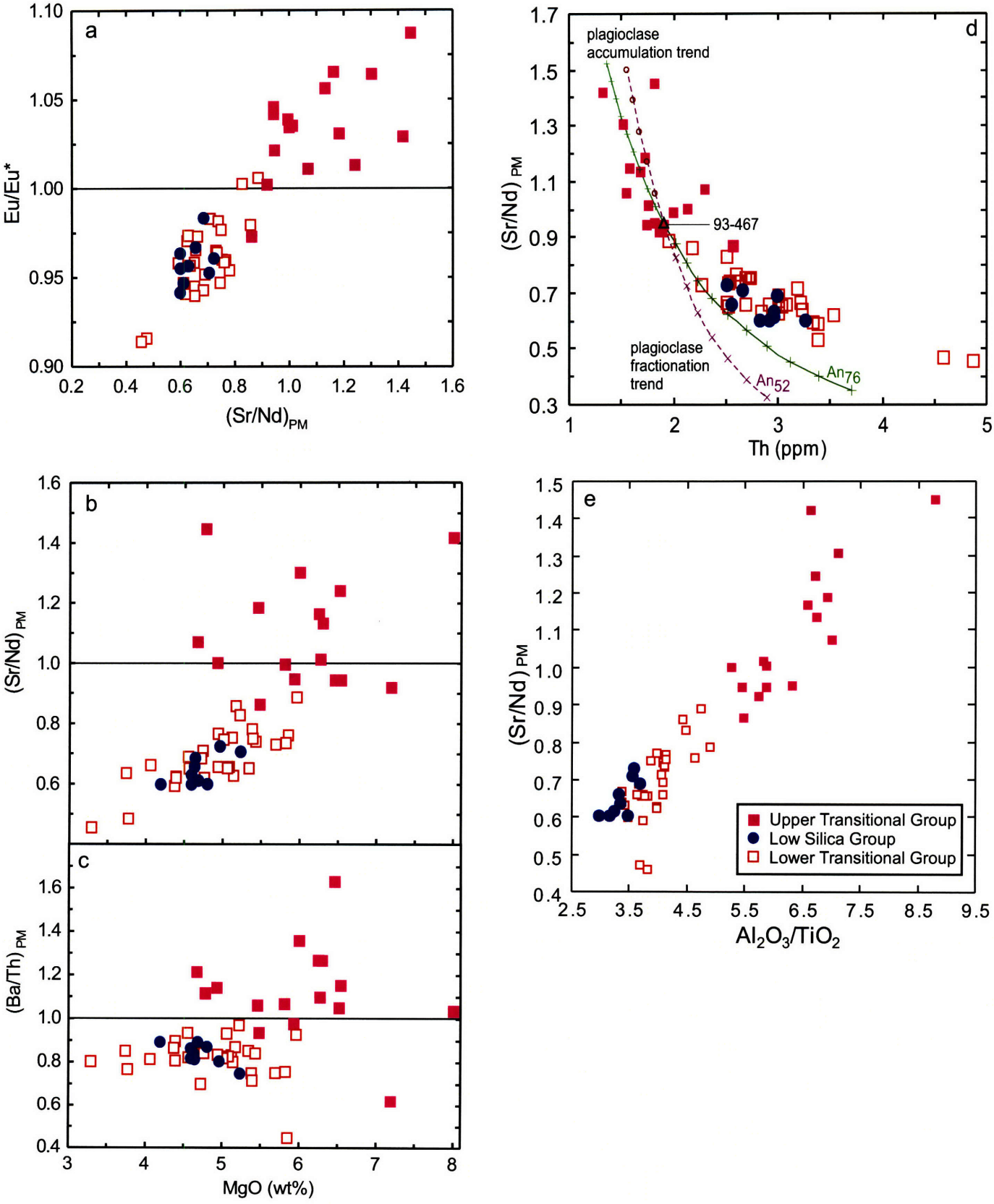
a
Eu/Eu*
(Sr/Nd)PM
b
(Sr/Nd)PM
c
(Ba/Th)PM
MgO (wt%)
d
plagioclase
accumulation trend
93-467
plagioclase
fractionation
trend
An52
An76
(Sr/Nd)PM
Th (ppm)
e
(Sr/Nd)PM
Upper Transitional Group
Low Silica Group
Lower Transitional Group
Al2O3/TiO2

Fig. 15

Fig. 16

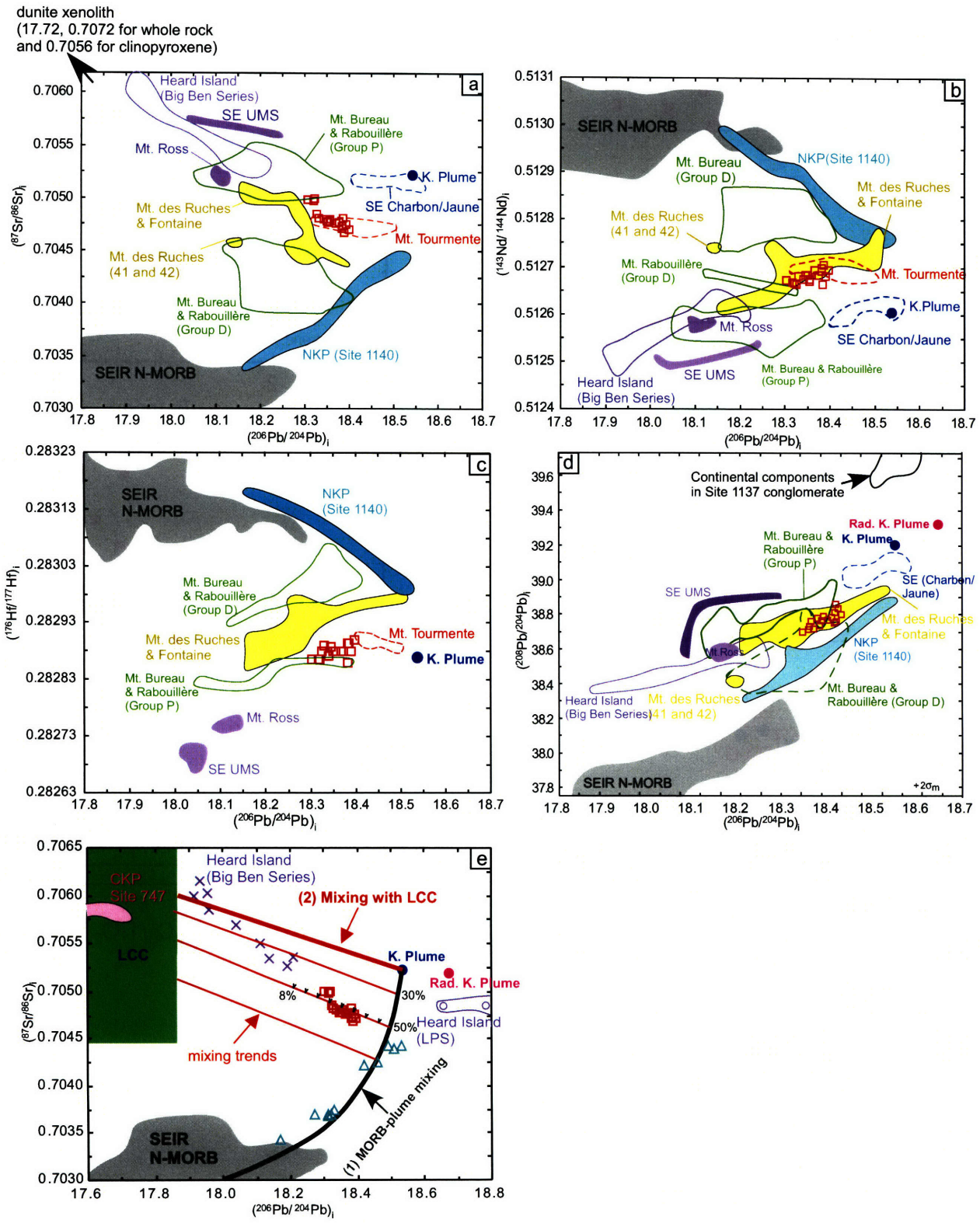
dunite xenolith
(17.72, 0.7072 for whole rock
and 0.7056 for clinopyroxene)
a
Heard Island
(Big Ben Series)
SE UMS
Mt. Ross
Mt. Bureau
& Rabouillère
(Group P)
K. Plume
SE Charbon/Jaune
Mt. Tourmente
Mt. des Ruches
& Fontaine
Mt. des Ruches
(41 and 42)
Mt. Bureau
& Rabouillère
(Group D)
NKP (Site 1140)
SEIR N-MORB
$(^{87}Sr/^{86}Sr)_i$
$(^{206}Pb/^{204}Pb)_i$
b
SEIR N-MORB
NKP(Site 1140)
Mt. Bureau
(Group D)
Mt. des Ruches
& Fontaine
Mt. des Ruches
(41 and 42)
Mt. Rabouillère
(Group D)
Mt. Tourmente
K.Plume
Mt. Ross
SE Charbon/Jaune
Heard Island
(Big Ben Series)
SE UMS
Mt. Bureau & Rabouillère
(Group P)
$(^{143}Nd/^{144}Nd)_i$
$(^{206}Pb/^{204}Pb)_i$
c
SEIR
N-MORB
NKP
(Site 1140)
Mt. Bureau
& Rabouillère
(Group D)
Mt. Tourmente
Mt. des Ruches
& Fontaine
K. Plume
Mt. Bureau
& Rabouillère
(Group P)
Mt. Ross
SE UMS
$(^{176}Hf/^{177}Hf)_i$
$(^{206}Pb/^{204}Pb)_i$
d
Continental components
in Site 1137 conglomerate
Rad. K. Plume
Mt. Bureau &
Rabouillère
(Group P)
K. Plume
SE (Charbon/
Jaune)
SE UMS
Mt. des Ruches
& Fontaine
NKP
(Site 1140)
Mt. Ross
Heard Island
(Big Ben Series)
Mt. des Ruches
(41 and 42)
Mt. Bureau &
Rabouillère (Group D)
SEIR N-MORB
$+2\sigma_m$
$(^{208}Pb/^{204}Pb)_i$
$(^{206}Pb/^{204}Pb)_i$
e
CKP
Site 747
LCC
Heard Island
(Big Ben Series)
(2) Mixing with LCC
K. Plume
Rad. K. Plume
8%
30%
50%
Heard Island
(LPS)
mixing trends
(1) MORB-plume mixing
SEIR
N-MORB
$(^{87}Sr/^{86}Sr)_i$
$(^{206}Pb/^{204}Pb)_i$

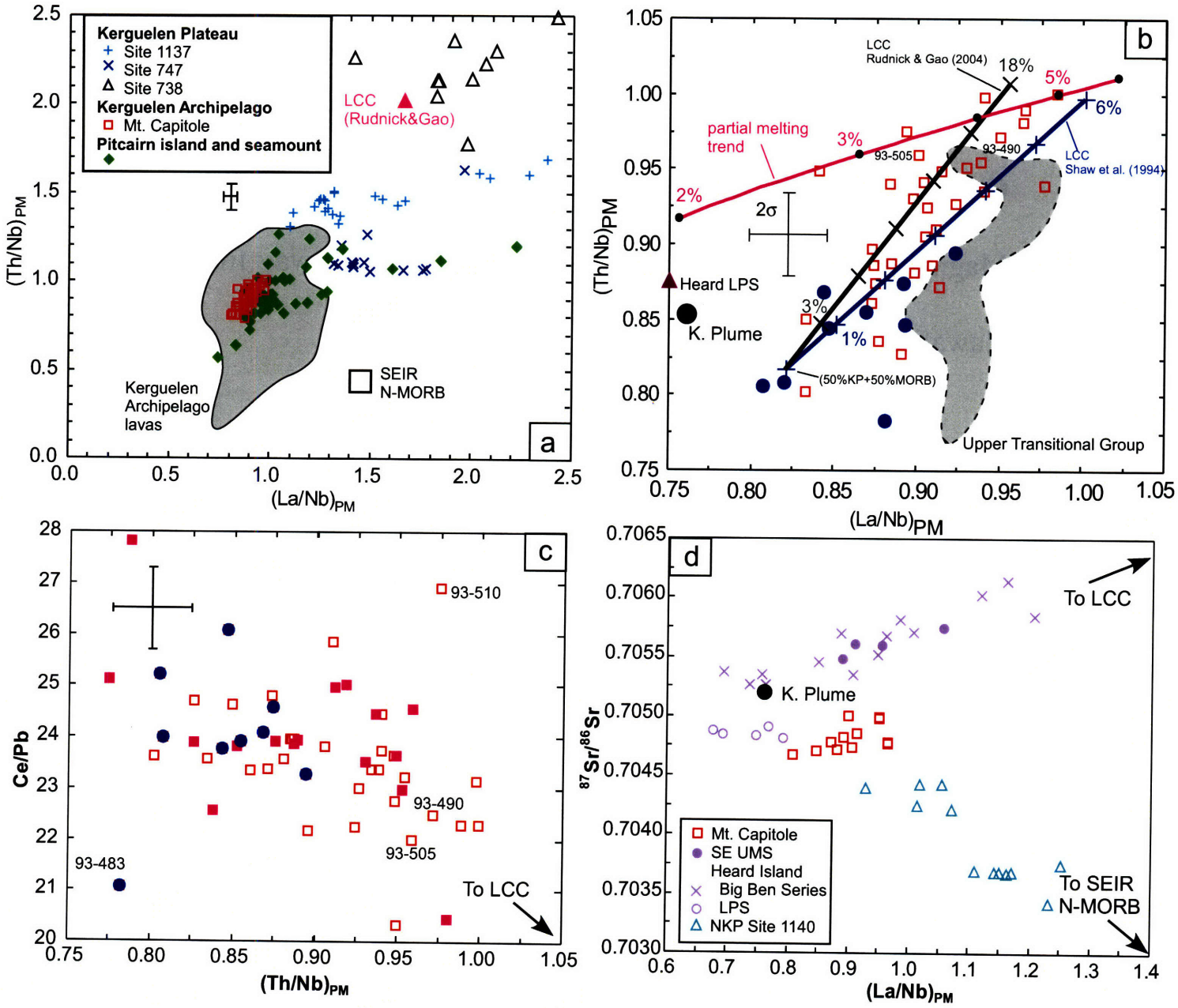
Kerguelen Plateau
Site 1137
Site 747
Site 738
Kerguelen Archipelago
Mt. Capitole
Pitcairn island and seamount
LCC
(Rudnick&Gao)
Kerguelen
Archipelago
lavas
SEIR
N-MORB
a
(Th/Nb)PM
(La/Nb)PM
LCC
Rudnick & Gao (2004)
18%
5%
6%
partial melting
trend
3%
2%
93-505
93-490
LCC
Shaw et al. (1994)
2σ
Heard LPS
K. Plume
3%
1%
(50%KP+50%MORB)
Upper Transitional Group
b
c
93-510
93-490
93-505
93-483
To LCC
Ce/Pb
d
To LCC
K. Plume
87Sr/86Sr
Mt. Capitole
SE UMS
Heard Island
Big Ben Series
LPS
NKP Site 1140
To SEIR
N-MORB

Fig. 17

Chapter 2 East Molokai and other Kea Trend Volcanoes: Magmatic Processes and Sources as they Migrate Away from the Hawaiian Hotspot

This chapter was published in *Geochemistry, Geophysics and Geosystems*:

Xu, G., F. A. Frey, D. A. Clague, D. Weis, and M. H. Beeson (2005), East Molokai and other Kea-trend volcanoes: Magmatic processes and sources as they migrate away from the Hawaiian hot spot, *Geochem. Geophys. Geosyst.*, 6, Q05008, doi: 10.1029 / 2004GC000830.

Abstract

There are geochemical differences between shield lavas from the two parallel trends, Kea and Loa, defined by young Hawaiian volcanoes. The shield of East Molokai volcano, at greater than 1.5 My, is the oldest volcano on the Kea-trend. Sequences of older tholeiitic to younger alkalic basalt that erupted as this volcano evolved from the shield to postshield stage of volcanism are well exposed. Much younger, ~0.34 -0.57 My, alkalic basalt and basanite erupted during rejuvenated-stage volcanism. Like rejuvenated-stage lavas erupted at other Hawaiian volcanoes, rejuvenated-stage East Molokai lavas have relatively low $^{87}Sr/^{86}Sr$ and high $^{143}Nd/^{144}Nd$. Such ratios reflect a source component with a long-term depletion in abundance of incompatible elements. Based on positive correlations of $^{87}Sr/^{86}Sr$ versus $^{206}Pb/^{204}Pb$ and negative correlations of these isotopic ratios with Nb/Zr, a smaller proportion of this depleted component also contributed to the late shield/postshield lavas erupted at East Molokai and the other Kea-trend volcanoes, Haleakala and Mauna Kea. At each of these Kea-trend volcanoes, as the volcano moved away from the hotspot, the extent of melting and magma supply from the mantle decreased, the depth of melt segregation increased and there was an increasing role for a component with long-term relative depletion in incompatible elements. This depleted component has Kea-trend Pb isotopic characteristics, relatively low $^{208}Pb/^{204}Pb$ at a given $^{206}Pb/^{204}Pb$, and it is probably not related to oceanic lithosphere or the source of mid-ocean ridge basalt.

The overlap in Sr, Nd and Pb isotope ratios of recent Kilauea shield lavas and 550 ka Mauna Kea shield lavas has been used to argue that Kea-trend shield volcanism samples a vertically continuous, geochemically distinct stripe which persisted in the hotspot source for 550 ka (*Eisele et al.*, 2003; *Abouchami et al.*, 2005). As Kea-trend volcanoes migrate away from the hotspot and evolve from the shield to postshield stage there are systematic changes in Sr, Nd and Pb isotope ratios. However, the overlap of Sr, Nd and Pb isotope ratios in late shield/postshield lavas from Mauna Kea (<350 ky) and East Molokai (~1.5 My) show that the periphery of the hotspot sampled by Kea-trend postshield lavas also had long-term geochemical homogeneity.

1. Introduction

The geochemical characteristics of lavas forming Hawaiian volcanoes reflect the source components associated with the Hawaiian plume, the melting processes and the post-melting processes that occur during magma ascent. Two major observations are: (1) The geochemistry of erupted lavas systematically change as individual volcanoes evolve through a series of growth stages (i.e., preshield, shield, postshield and rejuvenated) that are associated with volcano growth as the lithosphere approaches, overrides and recedes from the hot spot [e.g., *Chen and Frey*, 1985]; (2) Recent Hawaiian volcanoes define two sub-parallel echelon trends, the Kea and Loa trends [Figure 1, *Jackson et al.*, 1972; *Clague and Dalrymple*, 1987], whose lavas are generally geochemically distinct [e. g., *Tatsumoto*, 1978; *Lassiter et al.*, 1996; *Abouchami et al.*, 2005] thereby indicating a large-scale spatial arrangement of different source components.

There are good exposures of the shield to post-shield transition at the recent (<1.5 My) Kea volcanoes, Mauna Kea, Kohala, Haleakala and West Maui. In this paper we characterize the shield to post-shield transition on the oldest Kea trend volcano, East Molokai (>1.5 My; McDougall, 1964; Naughton et al., 1980) (Figure 1). We use major and trace element abundances and Sr, Nd and Pb isotopic ratios for lavas erupted at the end of shield building, i.e., during the transition from tholeiitic to alkalic volcanism, and for younger rejuvenated-stage basalt, including submarine lavas, to understand the final growth stages of East Molokai volcano. We compare the temporal changes in isotopic ratios and correlated trace element abundance ratios in these East Molokai lavas with analogous lava sequences at Mauna Kea, Kohala, Haleakala and West Maui. Our overall objective is to understand the processes, such as partial melting and fractionation

crystallization, and magma sources that are important as a Kea volcano moves away from the hotspot.

2. Geological setting

The island of Molokai consists of two coalesced volcanoes. West Molokai Volcano rises only 421 m above sea level and has not been deeply eroded [*Stearns and Macdonald*, 1947]. East Molokai Volcano, which rises 1515 m above sea level, forms the eastern two-thirds of the island (Figure 1). The north coast of East Molokai is a series of spectacular sea cliffs, locally more than 915 m high. The sea cliffs, and the large deep valleys of the north coast, provide excellent exposure of subaerially erupted lava flows. *Beeson* [1976] and *Clague and Beeson* [1980] studied the Kalaupapa section; this thick sequence of interbedded tholeiitic, transitional and alkalic lavas is dominated by alkalic lavas near the top of the section which range in age from ~1.50 My to ~1.75 My [*McDougall*, 1964; *Naughton et al.*, 1980]. Rejuvenated-stage lavas at East Molokai are exposed at Kalaupapa Peninsula on the north coast where alkalic olivine basalt erupted from a small lava shield surmounted by a deep summit crater (Figure 1). These lavas with an eruption age of about 0.34~0.57 My [*Clague et al.*, 1982] and a lack of significant marine erosion, indicate that the origin of the East Molokai sea cliffs was by landsliding rather than erosion [*Holcomb*, 1985]. The Wailau landslide deposits are a result (Figure 1). Submarine erupted rejuvenated-stage lavas have also been recovered by submersible dives from a terrace on the north slope [Figure 1; *Clague and Moore*, 2002].

3. Samples Studied

In addition to 28 samples from the Kalaupapa section (including 26 samples from *Beeson*, 1976), samples from the Halawa Valley (22), Pelekunu Valley (7), Waikolu

Valley (7), a water tunnel section (16) and two alkalic lavas (one from east coast near Mokuhooniki and the other from near a gaging station) were studied (Table 1, Figure 1). In the more intensely sampled sections of Kalaupapa and Halawa Valley the lava compositions range from tholeiitic to transitional basalt for the oldest samples to alkalic basalt, and hawaiite/mugearite for the youngest samples (Figure 2a, b). Transitional lavas are defined by their proximity to the tholeiitic basalt-alkalic basalt boundary in a SiO_2 versus total alkalis classification plot (Figure 3). These East Molokai lavas erupted during the evolution from late shield growth to the post-shield stage. Most of the samples from the other sections (Pelekuna Valley, Waikolu Valley and water tunnel) are tholeiitic to transitional basalt; therefore they may be slightly older sections than those from Kalaupapa section and Halawa Valley. Although we cannot rigorously assign our samples to the shield or postshield stages, the important point is that intercalated tholeiitic and alkalic basalt is characteristic of late shield and early postshield growth of Hawaiian volcanoes [e.g., *Clague and Dalrymple*, 1987]. In contrast, there is no ambiguity in assigning eleven submarine and subaerial samples to the rejuvenated-stage [*Clague et al.*, 1982; *Clague and Moore*, 2002] (Table 1).

4. Petrography

Most of the lavas collected from the Kalaupapa section are porphyritic except for a few in the upper part of the section. The porphyritic lavas commonly contain 20 to 30 vol% phenocrysts of olivine, clinopyroxene and plagioclase. Olivine phenocrysts are the most abundant in the lower part of the Kalaupapa section. Augite phenocrysts are usually only about a third as abundant as olivine phenocrysts. The plagioclase phenocryst content is less than 10 vol% except for two lavas (69KLPA-28 and 69KLPA-29) from the upper section that have abundant plagioclase phenocrysts (~20 vol%) [*Beeson*, 1976]. Lavas

from the Halawa Valley section have a lower olivine/plagioclase ratio and are like the upper part of Kalaupapa section in that respect. Tholeiitic basalt from Waikolu Valley contains almost no olivine, either as phenocrysts or in the groundmass. Lavas from Pelekunu Valley and water tunnel section are aphyric except that 71PELE-37 and M4.6+150F have olivine as the dominant phenocryst and clinopyroxene is more abundant than plagioclase.

Five rejuvenated-stage lavas from the Kalaupapa Peninsula contain abundant olivine phenocrysts (up to 16 vol%) with lesser amounts of plagioclase and clinopyroxene phenocrysts and microphenocrysts [*Clague et al.*, 1982]. Submarine rejuvenated-stage lavas recovered by Pisces V are olivine phyric with up to 20 vol% olivine phenocrysts [*Clague and Moore*, 2002].

5. Analytical techniques

Major element contents were analyzed over several years by different methods in four laboratories (See Table 2). Trace element abundances (Table 3) were determined at MIT by inductively coupled plasma mass spectrometry (ICP-MS) using a Fisons VG Plasmaquad 2+S with both internal and external drift monitors. Trace element results are reported as the mean of duplicate analyses (usually within ±5%). The chemical procedures and estimates of accuracy and precision were discussed by *Huang and Frey* [2003]. The submarine rejuvenated stage lavas were previously analyzed for trace elements [*Clague and Moore*, 2002], but were reanalyzed at MIT for internal consistency. A subset of samples had abundances of Sc, Co and Cr determined by instrumental neutron activation analysis (INAA) following the procedures of *Ila and Frey* [1984, 2000]. Because only a subset of samples were analyzed by INAA, we use the ICP-MS

data for Sc in figures. Sc values determined by the two techniques generally agree within ±5%.

Samples for Sr, Nd and Pb isotopic analyses were selected to encompass the entire range of compositions (Table 4). The chemical procedures used are similar to those described by *Weis and Frey* [1996]. Powder, 150-200 mg, was weighed into a 15 ml Telfon beaker and leached repeatedly with 6.0 N HCl in an ultrasonic bath for approximately 15-minute intervals. The leachate and any suspended solids were pipetted off and discarded, and this process was repeated until the resultant leachate was clear (typically four to five washes). The leached powder was rinsed twice with Mill-Q H_2O before drying on a hot plate. Samples were then digested for a minimum of 48 hours using concentrated HF and a few drops of 6.0 N HNO_3. After verification of complete dissolution, samples were evaporated and the residual cake was dissolved for 12 hours in 6.0 N HCl. Sr and Nd were run on thermal ionization mass spectrometer (Triton) on single Ta filament and triple Re-Ta filaments, respectively, and Pb was run on an MC-ICP-MS (Nu021) at University of British Columbia. See Table 4 footnotes for normalization procedures, precision estimates and data for standards.

6. Results

6. 1 Major elements

Whole-rock compositions are given in Table 2. Volatile free compositions were determined by recalculation of total iron as Fe_2O_3, subtracting H_2O and CO_2, and then normalizing to 100 percent. These compositions are used in all diagrams involving major elements.

The East Molokai lavas range widely in major element compositions (e.g, SiO_2: 43 - 55 wt% and MgO: 2 - 18 wt%); they are dominantly alkalic and tholeiitic basalt, but some of the youngest lavas in the sections include hawaiite, mugearite and benmoreite (Figures 2 and 3). Lavas from the Kalaupapa section and Halawa Valley are dominantly alkalic and lavas from Pelekuna Valley, Waikolu Valley and Water Tunnel are interbedded tholeiitic and alkalic basalt (Figure 3). Rejuvenated-stage lavas range from alkalic basalt to basanite and picro-basalt (Figure 3).

With decreasing MgO content, the SiO_2, Al_2O_3, Na_2O and P_2O_5 contents of the late shield/postshield lavas systematically increase with steeper slopes for MgO less than ~6.5 wt% (Figure 4). In contrast, the CaO and TiO_2 versus MgO trends show marked inflections with their abundance decreasing significantly as MgO content decreases to less than 6 wt% (CaO) or 4 wt% (TiO_2) (Figure 4). Qualitatively, such trends are consistent with established liquid lines of descent for Hawaiian shield lavas; i.e., dominantly olivine fractionation at $\geq$ 7 wt% MgO with clinopyroxene becoming a fractionating phase at $\leq$ 7 wt% MgO and Fe-Ti oxides at $\leq$ 4 wt% MgO [e.g., *Wright and Fiske*, 1971; *Clague et al.*, 1995].

Relative to the late shield/postshield stage lavas, the rejuvenated-stage lavas at a given MgO content have distinctly high CaO and low TiO_2 and P_2O_5, except for two samples (71KAUH-1 and MOE2) from Kauhako crater. These two crater samples have higher TiO_2 and P_2O_5 and lower SiO_2 than the other rejuvenated-stage lavas (Figure 4). Also rejuvenated-stage lavas from East Molokai have relatively higher Na_2O and most also have higher Na_2O/K_2O ratios at a given MgO than late shield/post-shield lavas when the latter are adjusted for K loss (Figure 4e, g). The wide range of Na_2O/K_2O ratios

shown by the rejuvenated-stage lavas is likely a magmatic feature since unaltered rejuvenated stage glasses, occurring as silt-size grains in a turbidite collected as Piston Core 4, 40 km north of Molokai [*Sherman and Garcia*, 2002], range widely in Na_2O/K_2O at ~6.3 wt% MgO (Figure 4g). As with Na_2O/K_2O, the TiO_2 and P_2O_5 of rejuvenated stage glass grains in turbidite cores show a large range in TiO_2 and P_2O_5 (Figure 4d, f).

6.2 Trace elements

Like P_2O_5, the abundance of highly incompatible trace elements, such as Nb, define a broad inverse trend with MgO content (Figure 5a). In order to define the behavior of incompatible trace elements during the petrogenesis of the shield/postshield and rejuvenated-stage East Molokai lavas, we plot abundance of various incompatible elements versus Th which is highly incompatible in the phenocryst phases, insensitive to minor alteration, and has a large abundance variation, factor of 8. The best correlations are for the relatively immobile, highly incompatible elements Ba, Nb and Ta (not shown) (Figure 6). Correlation coefficients of Rb (0.92) and U (0.91, not shown) with Th content are not as strong. In particular, the wide range in Rb abundance (0.5 to 47.3 ppm), a factor of ~100, compared to less than 10 for other incompatible trace elements shows the well established result that Rb, like K (factor of 17 in abundance range, Table 2), was mobile during postmagmatic alteration processes [e.g., *Feigenson et al.*, 1983; *Fodor et al.*, 1987; *Frey et al.*, 1990, 1994; *Jackson et al.*, 1999].

As expected, evolved alkalic lavas have the highest abundance of Rb, Ba, Nb and Pb and the tholeiitic lavas generally have the lowest abundance (Figure 6). For these elements the rejuvenated-stage lavas largely overlap with the field defined by the late shield/postshield basalt (Figure 6). As elements plotted on the vertical axis in Figure 6

become less incompatible (e.g., Zr, Sr, Y and Yb), their trends become increasingly convex upwards. In fact, the late shield/postshield alkalic lavas with relatively high Th contents have relatively uniform Y and Yb contents (abundance range of 2.7 and 2.5, respectively); sample 69KLPA-33, a mugearite, is an exception. In addition, for these elements rejuvenated-stage lavas are clearly offset from the late shield/postshield lavas to low X/Th ratios (Figure 6e-h).

A relative depletion of Th for all East Molokai lavas is apparent in primitive mantle (PM) normalized plots (Figure 7). For example, all East Molokai lavas have $(Ba/Th)_{PM}$ significantly greater than unity and this is a characteristic of all Hawaiian lavas [*Hofmann and Jochum*, 1996; *Huang and Frey*, 2003; *Yang et al.*, 2003). The most extreme enriched patterns (e.g., high La/Yb) are for mugearite (69KLPA-33) that is relatively depleted in Sr, Hf and Ti and the benmoreite (M4.9+300D) that has a relative depletion in Ti (Figure 7). An important feature in the primitive mantle normalized plots is the negative slope from Ta to Yb (Figure 7). Most late shield/postshield lavas have sub-parallel patterns for highly and moderately incompatible elements (from Rb to Ti), but from tholeiitic to alkalic basalt there is a progressive increase in abundance of highly incompatible elements. The lowest abundances are in tholeiitic basalt, presumably main shield lavas, from the Wailau landslide. From Rb to Sr the alkalic rejuvenated-stage lavas overlap with the field for basaltic late shield/postshield lavas, but they range to lower abundances for the more compatible elements from Nd to Yb (Figure 7).

6.3 Isotopes (Sr, Nd, Pb)

Late shield/postshield lavas As Hawaiian volcanoes evolve from the shield building to the postshield-stage there is a temporal trend to lower $^{87}Sr/^{86}Sr$ and higher $^{143}Nd/^{144}Nd$.

This trend was first recognized for lavas from Haleakala (East Maui) [*Chen and Frey*, 1985] and Kohala [*Hofmann et al.*, 1987; *Lanphere and Frey*, 1987] and more recent studies of the Hawaii Scientific Drilling Project (HSDP) cores from Mauna Kea show a similar trend [*Lassiter et al.*, 1996; *Abouchami et al.*, 2000; *Bryce et al.*, manuscript in revision, 2005]. Late shield/postshield lavas from Kalaupapa section of East Molokai show a similar temporal trend (Figure 2c, d). The range of Sr and Nd isotopic variation is relatively large for Haleakala, i.e., the range from Honomanu (late shield) to Kula and Hana (postshield) in Figure 8a. Note that the Hana Volcanics were reclassified as postshield lavas by *Sherrod et al.* [2003]. In contrast, late shield/postshield lavas from the other four Kea trend volcanoes (Mauna Kea, Kohala, West Maui and East Molokai) are less variable in $^{87}Sr/^{86}Sr$ and $^{143}Nd/^{144}Nd$ and most importantly their fields in Figure 8a overlap.

When lavas from several Hawaiian volcanoes are considered there is a well-defined inverse correlation between $^{143}Nd/^{144}Nd$ and $^{87}Sr/^{86}Sr$, but this correlation is not well defined by East Molokai and West Maui late shield/postshield lavas (Figure 8a). For example, East Molokai alkalic and tholeiitic lavas span a similar limited range in $^{143}Nd/^{144}Nd$ ratios, but the tholeiitic lavas are offset to higher $^{87}Sr/^{86}Sr$ ratios (Figure 8b). Nine acid-leached East Molokai lavas analyzed by *Basu and Faggart* [1996] also range more widely in $^{87}Sr/^{86}Sr$ than $^{143}Nd/^{144}Nd$ (Figure 8b).

In $^{206}Pb/^{204}Pb$ versus $^{207}Pb/^{204}Pb$ and $^{208}Pb/^{204}Pb$ plots the late shield/postshield lavas from the 5 Kea-trend volcanoes define two groups: Mauna Kea, West Maui, East Molokai, and Kohala (Hawi Volcanics) compared to Kohala (Pololu Volcanics) and Haleakala (Figure 9a, c). Both groups have relatively low $^{208}Pb/^{204}Pb$ ratio at a given

$^{206}Pb/^{204}Pb$, a characteristic of Kea -type lavas [*Abouchami et al.*, 2005]; however, lavas from the first group range to higher $^{206}Pb/^{204}Pb$ than lavas from the second group (Figure 9a).

Shield-stage lavas define a negative $^{87}Sr/^{86}Sr$ vs $^{206}Pb/^{204}Pb$ correlation, but as first clearly demonstrated by postshield lavas from Haleakala, the Kula and Hana Volcanics, a positive correlation is characteristic of postshield lavas [*West and Leeman*, 1987] (Figure 9d). This reversal of slope reflects a marked temporal change in source components contributing to growth of Hawaiian volcanoes. Figure 9d shows that 4 Kea volcanoes define a positive $^{87}Sr/^{86}Sr$ versus $^{206}Pb/^{204}Pb$ trend during late-shield and postshield growth. A trend for postshield lavas from Kohala (Hawi Volcanics) is not shown because there are insufficient data.

Rejuvenated stage lavas The East Molokai rejuvenated-stage lavas are relatively homogenous in Sr and Nd isotopes with higher $^{143}Nd/^{144}Nd$ and lower $^{87}Sr/^{86}Sr$ ratios than late shield/postshield lavas (Figure 8a). Relative to the fields for other rejuvenated stage lavas they overlap with the Koloa Volcanics from Kauai and Lahaina Volcanics from West Maui, and are offset to lower $^{87}Sr/^{86}Sr$ than the Honolulu Volcanics from Oahu (Figure 8c). East Molokai rejuvenated-stage lavas define the same positive trend as East Molokai late shield/postshield lavas on $^{206}Pb/^{204}Pb$ versus $^{208}Pb/^{204}Pb$, but they have lower $^{206}Pb/^{204}Pb$ ratios (Figure 9a). The trend defined by East Molokai rejuvenated-stage lavas overlaps with North Arch lavas in $^{206}Pb/^{204}Pb$-$^{208}Pb/^{204}Pb$ space but is distinct from Honolulu Volcanics and Koloa Volcanics which are offset to higher $^{208}Pb/^{204}Pb$ at given $^{206}Pb/^{204}Pb$ (Figure 9b). In the $^{87}Sr/^{86}Sr$ versus $^{206}Pb/^{204}Pb$ plot rejuvenated stage lavas from East Molokai overlap with the fields for North Arch lavas and Lahaina Volcanics

(Figure 9d). In general the positive correlations defined by late-shield/postshield lavas trend towards the fields of rejuvenated stage / North Arch lavas (Figure 9d).

East Molokai lavas recovered from the Wailau landslide The submarine landslide deposits north of Molokai Island are inferred to be derived from East Molokai volcano [see Figure 1 and also Figures 13 and 15 of *Moore and Clague*, 2002]. Since it is likely that basalt exposed in these landslide deposits is older than our subaerially collected samples, the landslide samples provide information about the temporal variation of geochemical characteristics during growth of the East Molokai shield. Glass-rich volcaniclastic rocks are abundant in the landslide deposits. The glasses are tholeiitic basalt and document the diversity of lava compositions erupted during shield growth [*Clague et al.*, 2002; *Shinozaki et al.*, 2002]. Five whole-rocks from landslide blocks have been analyzed for major and trace element abundance and isotopic ratios of Sr, Nd and Pb [*Tanaka et al.*, 2002]. Compared to the late shield/postshield lavas, these samples are not as enriched in highly incompatible elements (Figure 7). They define two distinct groups in isotopic ratios (Figures 8a and 9a, c, d). In subsequent discussion of trace element and isotopic characteristics we compare these submarine landslide samples with our data for subaerial late shield/postshield lavas.

7. Discussion

Our broad objectives are to define the changes in magma sources, melting process and crustal evolution of magmas as Kea-trend volcanoes migrate away from the hotspot. We compare the transition from late shield to postshield volcanism at five Kea-trend volcanoes and also the subsequent transition to rejuvenated-stage volcanism at East

Molokai and West Maui volcanoes. We first focus on lavas from East Molokai by considering the effects of crustal processes on their geochemical characteristics.

7.1 Crustal Processes: Compositional effects of post-magmatic alteration

Late shield/postshield lavas *Clague and Beeson* [1980] noted that lavas from the Kalaupapa section of East Molokai can be divided into two groups based on K/Ba, i.e., groups with average K/Ba of ~16 and ~26 (see Figure 10b); they inferred that K/Ba differences reflected magmatic characteristics and a role for residual phlogopite during melting. Since publication of this paper there has been recognition that K abundance in Hawaiian lavas is commonly affected by post-magmatic alteration [e.g., *Feigenson et al.*, 1983; *Fodor et al.*, 1987; *Frey et al.*, 1990, 1994; *Jackson et al.*, 1999]. Typically loss of K results in bulk rock K_2O/P_2O_5 ratios less than unity which contrast with ratios of 1.5-2 in unaltered Hawaiian lavas (e.g., historical Mauna Loa lavas have K_2O/P_2O_5 of about 1.6, *Rhodes*, 1995; Puu Oo Kilauea lavas, ~1.84, *Garcia et al.*, 2000]. Also Rb is more severely affected than K so that lavas with low K_2O/P_2O_5 typically have anomalously high K/Rb [e.g., *Frey et al.*, 1994]. Five samples from the Kalaupapa section (69KLPA-2, 69KLPA-5A, 69KLPA-8B, 69KLPA-9A and 69KLPA-14A) have low K_2O/P_2O_5 ($\leq$1.0), extremely high K/Rb (>1600) and low K/Ba (<20) (Figure 10). Consequently we conclude that the K/Ba differences among East Molokai lavas emphasized by *Clague and Beeson* [1980] reflect post-magmatic alteration rather than magmatic processes.

Rejuvenated stage lavas Except for one sample, 74KAL-1, East Molokai rejuvenated stage lavas have high K_2O/P_2O_5 (>1.5) and low K/Rb (385-565) (Figure 10a). In contrast, sample 74KAL-1 has the lowest K_2O/P_2O_5 (1.35) and K/Ba (12.8) and the

highest K/Rb (840) (Figure 10); among the rejuvenated-stage lavas it was the most significantly affected by post-magmatic alteration.

7. 2 Crustal processes: Role of crystal fractionation

Late shield/postshield lavas The importance of crystal fractionation, depends in part on magma supply rates from the mantle. For example, the transition from shield to postshield volcanism occurs as a Hawaiian volcano moves away from the hotspot. Initially this transition is a change from tholeiitic to alkalic volcanism, commonly interpreted as reflecting a decrease in extent of melting [e.g., *Chen and Frey*, 1985]. The resulting decrease in magma supply leads to magma stagnation, cooling and crystal fractionation. Consequently, evolved alkalic lavas, e.g., hawaiites, are important in postshield-stage volcanism. Also there is evidence that the depth of fractionation increases with decreasing age [e.g., *Clague*, 1987; *Frey et al.*, 1990]. In this section, we discuss the role of crystal fractionation during the late evolution of East Molokai volcano and then compare the late-stage evolution of several Kea-trend volcanoes.

For East Molokai lavas with greater than ~8 wt% MgO the major control on compositions was fractionation and accumulation of olivine phenocrysts and chromite which occurs as inclusions in olivine phenocrysts and as microphenocrysts in the groundmass. This inference is based on: (1) the strong positive correlation between modal olivine abundance and MgO content in the Kalaupapa section (Figure 5c); (2) the positive MgO-Cr correlation (Figure 5b); (3) the uniform CaO/Al_2O_3 ratios (0.74-0.88) with varying MgO content, except for two lavas with abundant augite phenocrysts (71PELE-37 and M4.6+150F) and higher CaO/Al_2O_3 ratios (0.98 and 1.08, respectively)

(Figures 11a); and (4) the slight increase in Sc content with decreasing MgO from ~18 to 8 wt% (Figure 11b).

For lavas with less than 6.5 wt% MgO, an important role for clinopyroxene fractionation is inferred from the positive trends for CaO and Sc abundance, and CaO/Al_2O_3 ratios versus MgO content (Figures 4c and 11). Three evolved (hawaiite/mugearite/benmoreite) postshield lavas (69KLPA-33, 70KAWE-1C and dike M4.9+300D) with low abundances of MgO and Sc, low CaO/Al_2O_3 ratios (Figure 11) and negative Ti anomalies (Figure 7) are offset to higher Nb/Zr ratios than other late shield/postshield lavas (Figure 12a). These evolved lavas reflect fractionation of clinopyroxene and Fe-Ti oxides (e.g., titanomagnetite and ilmenite). Since fractionation of Fe-Ti oxides cannot increase the Nb/Zr ratios [*Nielsen et al.*, 1994; *Nielsen and Beard*, 2000; *Jang and Naslund*, 2003], the high Nb/Zr ratios require extensive fractionation of clinopyroxene (Figure 12a).

Although not obvious from the negative Al_2O_3 versus MgO trend (Figure 4b) the broad positive correlation of Sr/Ce vesus Eu/Eu* (Figure 13), and decreasing Sr/Ce with increasing abundance of a highly incompatible element, such as Nb (Figure 12b), indicate that plagioclase fractionation also occurred.

Within the postshield stages at Mauna Kea, Kohala and West Maui there is an abrupt transition both in eruption age and composition from older, dominantly basalt to younger, solely hawaiite to trachyte lavas with an obvious gap in major element composition [*Stearns and Macdonald*, 1942; *Spengler and Garcia*, 1988; *Frey et al.*, 1990]. This gap is also apparent in Figure 12b; specifically the relatively young evolved lavas, hawaiites and mugearites, forming the Laupahoehoe and Hawi Volcanics at Mauna Kea and Kohala,

respectively, define a distinct trend offset to high Nb at a given Sr/Ce (Figure 12b). Also at East Molokai, 3 samples are offset to high Nb/Zr at a given Tb/Yb and high Nb at a given Sr/Ce (Figure 12). These may be relatively young lavas; sample M4.9+300D is a dike, 69KLPA-33 is the youngest sample in the Kalaupapa section (Figure 2a), and 70KAWE-1C is a surface flow. *Frey et al.* [1990] inferred that offset to high Nb at a given Sr/Ce reflects dominantly clinopyroxene fractionation and derivation of hawaiite from basalt at moderate pressure, perhaps at a depth of 20 km. Therefore a general characteristic of the postshield evolution of Kea-trend volcanoes is that as the volcano enters the postshield stage, fractionation of a plagioclase-bearing assemblage occurs at low pressure but as the volcano migrates further away from the hotspot there is a diminishing supply of basaltic magma from the plume and basaltic magma stagnates deep within the crust or at the crust/mantle boundary where the fractionating mineral assemblage is initially dominated by clinopyroxene [*Feigenson e al.*, 1983; also see Figure 4 of *Clague*, 1987 and Figure 15 of *Frey et al.*, 1990]. Plagioclase fractionation does not occur at these depths until high Al_2O_3 contents of 17-18% are attained (Figure 4b).

Rejuvenated stage lavas Rejuvenated stage lavas have MgO ranging from 6.3 wt% to 16 wt% (Figure 4). Consistent with the abundance of olivine phenocrysts, liquid line of descent calculations using MELTS [*Ghiorso and Sack*, 1995] show that olivine fractionation is the dominant process in the evolution of rejuvenated-stage lavas. The negative trends for MgO-CaO and MgO-Sc and uniform CaO/Al_2O_3 ratios (0.79-0.84) show that clinopyroxene fractionation was not an important process for these lavas (Figures 4c and 11). Also the negative trend on $MgO-Al_2O_3$ imply that fractionation of

plagioclase was not important during evolution of rejuvenated-stage East Molokai lavas (Figure 4b). In summary, like other rejuvenated stage lavas (Honolulu Volcanics and Koloa Volcanics) the olivine-dominated crustal evolution of East Molokai rejuvenated stage lavas differs substantially from that of the alkalic postshield lavas.

7.3 Constraints on the Melting Process: Mineralogy of Residual Phases and Extents of Melting

7.3.1 Late shield/postshield stage lavas

East Molokai lavas define three sub-parallel trends for Nb/Zr versus Tb/Yb (Figure 12a). Nb is more incompatible than Zr in clinopyroxene and garnet and both phases can control Nb/Zr; in contrast because heavy rare earth elements are compatible in garnet, Tb/Yb is much more sensitive to garnet than clinopyroxene [e.g., Figure 10c of *Frey et al.*, 2000; *Pertermann et al.*, 2004]. Therefore, the positive Nb/Zr vs Tb/Yb trends for East Molokai lavas (Figure 12a) reflect residual garnet. In detail, the relatively older East Molokai tholeiitic (and transitional) lavas have lower Tb/Yb ratios than alkalic lavas, and the lowest Tb/Yb ratios are in the presumably older tholeiitic basalt from the Wailau landslide (Figure 12a). A similar temporal trend characterizes Mauna Kea volcano where the late shield to post-shield, subaerially erupted lavas have relatively higher Tb/Yb and show a clear trend of garnet control, whereas older submarine lavas have lower Tb/Yb and a poor Tb/Yb-Nb/Zr trend (Figure 12a). We infer that as Kea volcanoes age and pass from the tholeiitic shield to alkalic late shield/postshield magmatism there is an increasing role for residual garnet. An enhanced role for garnet is inconsistent with the change to a more depleted source composition; i.e., lower $^{87}Sr/^{86}Sr$ and higher $^{143}Nd/^{144}Nd$ (Figure 2) and presumably less garnet because of lower Al_2O_3 and CaO

contents. This contradiction can be alleviated if the alkalic basalt was generated at lower extents of melting and segregated at higher pressure.

7.3.2 Rejuvenated stage lavas

Hawaiian rejuvenated stage lavas are alkalic and the well-studied Honolulu Volcanics and Koloa Volcanics are highly enriched in incompatible elements [*Clague and Frey*, 1982; *Feigenson*, 1984]. Such enrichments are attributed to derivation by low extents of melting of an incompatible-element enriched, garnet-bearing source [e.g., *Clague and Frey*, 1982; *Clague and Dalrymple*, 1988; *Yang et al.*, 2003]. Samples with the highest abundance of incompatible elements also have anomalous ratios of incompatible elements such as Zr/Sm, Nb/La, Ti/Eu, K/Ce, that are typically uniform in oceanic basalt. These variations are attributed to the effects of minor residual phlogopite, amphibole, and Ti-rich phases [e.g., *Clague and Frey*, 1982; *Feigenson*, 1984; *Class and Goldstein*, 1997; *Yang et al.*, 2003].

The abundance ratios Nb/La, Zr/Sm, Ti/Eu and K/Ce are highly correlated in lavas from the Honolulu Volcanics, North Arch and rejuvenated-stage East Molokai lavas (Figure 14). Honolulu Volcanics with the lowest SiO_2 contents have the most extreme ratios (Figure 15), i.e., very different from primitive mantle ratios in Figure 14. These samples are inferred to have formed by the lowest extent of melting, and they were most affected by residual phlogopite and Ti-rich phases [*Clague and Frey*, 1982; *Yang et al.*, 2003]. In contrast, rejuvenated-stage East Molokai lavas have relatively high SiO_2 content and particularly the submarine samples have near primitive mantle ratios of Zr/Sm and Ti/Eu (Figure 14). Compared to these submarine samples, the subaerial East Molokai samples range to lower K/Ce, Zr/Sm and Nb/La (Figure 14). Given the isotopic

similarity of submarine and subaerial rejuvenated-stage lavas we infer a range in extent of melting. Finally, compared to the lavas that we studied, an even larger range in relative extent of melting is indicated by the wide range of TiO_2, P_2O_5 and Na_2O/K_2O at a given MgO (Figure 4d, f, g) of submarine glass grains derived from rejuvenated-stage East Molokai lavas [*Sherman and Garcia*, 2002]; no trace element data are available for these glasses.

7.4 Constraints on source components

7.4.1 Comparison of late shield/postshield East Molokai lavas with East Molokai shield lavas from Wailau landslide

Three of five lavas recovered from the Wailau landslide [*Tanaka et al.*, 2002] have Sr and Nd isotope ratios within the field of late shield/postshield East Molokai lavas (Figure 8a) and two of these have high $^{206}Pb/^{204}Pb$ and $^{208}Pb/^{204}Pb$ that are on an extrapolation of the East Molokai trend; i.e., they are on the Kea trend (Figure 9a). Two other samples have Sr, Nd and Pb isotopic ratios unlike those of other East Molokai lavas; they are most similar to the late shield lavas from Haleakala (Honomanu Volcanics in Figure 8a). Their Loa-trend Pb isotopic character (Figure 9a) may be another example of a Kea volcano with a subset of lavas having the Pb isotopic ratios characteristic of Loa-trend volcanoes. Other examples are Mauna Kea [*Eisele et al.*, 2003] and Haleakala [*Ren et al.*, 2005].

7.4.2 Source components in late shield/postshield East Molokai lavas

The isotopic ratios $^{87}Sr/^{86}Sr$ and $^{206}Pb/^{204}Pb$ of East Molokai late shield/postshield lavas are correlated with their compositions; e.g., these isotopic ratios are positively correlated with SiO_2 and negatively correlated with Nb/Zr (Figure 16). Such trends require two geochemically distinct source components. One component lies within the

field of Hawaiian shield lavas (Figure 16b). In regard to the other component the important result is that the negative Nb/Zr vs $^{206}Pb/^{204}Pb$ trend defined by late shield/post-shield East Molokai lavas contrasts markedly with the positive trend defined by Hawaiian shield lavas (Figure 16b). A similar contrast was noted in $^{87}Sr/^{86}Sr$ versus $^{206}Pb/^{204}Pb$ (Figure 9d). In each case (Figures 9d and 16b), the trend of late shield/postshield East Molokai lavas extrapolates toward the field for rejuvenated-stage lavas from East Molokai. It is apparent that the low $^{87}Sr/^{86}Sr$, low $^{206}Pb/^{204}Pb$ and high Nb/Zr source component that dominates the East Molokai rejuvenated-stage lavas also contributed to the late shield/post-shield lavas. As an aside, the strong correlation of Nb/Zr with $^{87}Sr/^{86}Sr$ for East Molokai late shield/postshield lavas also suggests that the poor correlation of $^{87}Sr/^{86}Sr$ versus $^{143}Nd/^{144}Nd$ (Figure 8b) is not a result of alteration effects on $^{87}Sr/^{86}Sr$.

7.4.3 Comparison of late shield/postshield lavas from Kea trend volcanoes

Shield-stage lavas from the geographically defined Kea and Loa trend volcanoes (Figure 1) have little overlap in Pb isotope space [e.g., *Tatsumoto*, 1978; *Stille et al.*, 1986; *Abouchami et al.*, 2005]. In detail, Pb isotopic analyses of lavas recovered by HSDP from Mauna Kea, a Kea-trend volcano, show that the lavas define three distinct Pb isotope arrays labeled as "Kea-lo8", "Kea-mid8" and "Kea-hi8" [*Eisele et al.*, 2003]. Most of the shield lavas belong to the Kea-mid8 group. *Eisele et al.* [2003] and *Abouchami et al.* [2005] found that modern Kilauea and 350 - 550 ky Mauna Kea shield lavas, forming the Kea-mid8 array, have the same Pb isotopic signature. Because at these respective times the locations of the Kilauea and Mauna Kea shields were similar relative to plume center, they argued for a long-lived, spatially constrained source for Kea lavas.

Based on Sr-Nd-Hf-Pb similarities of lavas from the uppermost West Maui shield with Mauna Kea and Kilauea lavas, *Gaffney et al.* [2003] also argued that the Kea end-member has maintained its distinctive geochemical character for ~1.5 My.

Assuming that Kea volcanoes evolve from the shield- to postshield-stage at a uniform distance from the plume, i.e., constant relative migration rate of Pacific plate over the plume, another test of the long-term uniformity of the sources and processes generating Hawaiian magmas is to compare the isotopic characteristics of late shield/postshield stage lavas from Kea trend volcanoes. Indeed there is a first order similarity in temporal variation of isotopic ratios. *Chen and Frey* [1985] and *Chen et al.* [1991] showed that as Haleakala volcano evolved from late shield to post-shield volcanism isotopic ratios of $^{87}Sr/^{86}Sr$ and $^{206}Pb/^{204}Pb$ decrease. We find the same result for East Molokai (Figure 2c). Recent studies of late shield and post-shield lavas at Mauna Kea [*Lassiter et al.*, 1996; *Blichert-Toft et al.*, 2003] show the same temporal trend.

In both the $^{87}Sr/^{86}Sr$ vs $^{206}Pb/^{204}Pb$ and Nb/Zr vs $^{206}Pb/^{204}Pb$ plots late shield/postshield lavas from East Molokai, Mauna Kea, Haleakala and West Maui lavas lie on the same trend (Figures 9d and 16b). Clearly the late shield/postshield lavas at these four Kea volcanoes show the influence of the low $^{206}Pb/^{204}Pb$, low $^{87}Sr/^{86}Sr$ and high Nb/Zr component that was important in creating rejuvenated-stage lavas.

East Molokai compared to Mauna Kea and West Maui *Huang and Frey* [2003] defined the basaltic post-shield group of Mauna Kea lavas as including the oldest (~75 to 250 ky) subaerially exposed Hamakua Volcanics and the uppermost subaerially erupted part of the HSDP cores. The shield to post-shield transition is gradual and with decreasing age, alkalic basalt is intercalated with tholeiitic basalt, SiO_2 content decreases

and ratios such as La/Yb and Nb/Zr increase. This post-shield group defines the Kea-lo8 Pb-Pb array of *Eisele et al.* [2003]. Mauna Kea post-shield group lavas are the comparable evolutionary stage to East Molokai late shield/postshield lavas. Late shield/postshield lavas from East Molokai, Mauna Kea and West Maui lavas overlap in Sr-Nd-Pb space (Figures 8a and 9a, c, d), thereby indicating a long-term similarity in the source components and processes contributing to this phase of Kea volcano growth.

East Molokai compared to Kohala and Haleakala Two other Kea trend volcanoes, Kohala and Haleakala, have also evolved to the postshield stage. Late shield/postshield lavas from Haleakala and Kohala lavas overlap with East Molokai and Mauna Kea late shield/postshield lavas in Sr-Nd space (Figure 8a). For Pb isotopic ratios the evolved alkalic lavas of the postshield Hawi Volcanics (Kohala) overlap with the field for East Molokai late shield/postshield lavas, but the late shield Pololu Volcanics (Kohala) have less radiogenic ratios (Figure 9a). Also postshield Haleakala lavas (Kula & Hana Volcanics) range to low Pb ratios that overlap with East Molokai rejuvenated stage lavas.

7.4.4 Source components in East Molokai rejuvenated stage lavas

Compared to shield and postshield lavas, the relatively low $^{87}Sr/^{86}Sr$ and high $^{143}Nd/^{144}Nd$ of rejuvenated stage lavas (Figure 8a, c) require a larger role for a depleted component, i.e., with long-term low Rb/Sr and high Sm/Nd in the source of rejuvenated-stage lavas. An important result is that the East Molokai rejuvenated-stage lavas lie on the same $^{206}Pb/^{204}Pb$ vs $^{208}Pb/^{204}Pb$ and Nb/Zr vs $^{206}Pb/^{204}Pb$ and $^{87}Sr/^{86}Sr$ trends defined by the late shield/postshield lavas (Figures 9b and 16b, c). These linear trends indicate that East Molokai late shield/postshield lavas and rejuvenated stage lavas sampled a common depleted component with low $^{206}Pb/^{204}Pb$ and $^{87}Sr/^{86}Sr$. The rejuvenated-stage

East Molokai lavas contain a larger proportion of this depleted component. Hence a relatively unradiogenic Pb component with relatively low $^{87}Sr/^{86}Sr$ and high $^{143}Nd/^{144}Nd$ was available for ~ 1 My, i.e, rejuvenated stage lavas are ~ 0.34 - 0.57 My [*Clague et al.*, 1982] and postshield-stage lavas are 1.35-1.49 My [*McDougall*, 1964]. This component lies on the upper boundary of the EPR (East Pacific Rise) MORB field in a Pb-Pb isotopic ratio plot, but it is distinct from the MORB field in a $^{87}Sr/^{86}Sr$ versus $^{206}Pb/^{204}Pb$ (Figure 9b, d). *Frey et al.* [2005] have argued that this depleted component is intrinsic to the Hawaiian hot spot and not related to MORB-related lithosphere or asthenosphere.

8. Summary and implications

Rejuvenated-stage lavas from East Molokai are alkalic lavas with Sr and Nd isotope ratios that overlap with fields for rejuvenated-stage lavas from other Hawaiian volcanoes (e.g., Koloa Volcanics from Kauai). These lavas were derived by variable extents of melting of a depleted source, i.e. a source with $^{143}Nd/^{144}Nd$ greater than and $^{87}Sr/^{86}Sr$ less than primitive mantle, with garnet as a residual phase. Rejuvenated-stage lavas from Hawaiian volcanoes define linear trends of Zr/Sm, Ti/Eu and K/Ce versus Nb/La (Figure 14), and these ratios are correlated with SiO_2 content (Figure 15). These trends reflect variable extents of melting, relatively low for the Honolulu Volcanics with low SiO_2 and $(Zr/Sm)_{PM} < 1$ and relatively high for submarine rejuvenated-stage lavas from East Molokai which have higher SiO_2 content and $(Zr/Sm)_{PM} \sim 1$.

Late shield/postshield lavas from East Molokai volcano include intercalated tholeiitic and alkalic basalt with a few highly evolved alkalic lavas, hawaiite to benmoreite. Where stratigraphic control is available, with decreasing eruption age alkalinity increases, $^{87}Sr/^{86}Sr$ decreases and there is an increasing role for residual garnet. East Molokai shares

these geochemical features with three other Kea-trend volcanoes (Mauna Kea, Kohala and Haleakala); the temporal trend of $^{87}Sr/^{86}Sr$ at West Maui is more complex [e.g., *Tatsumoto et al.*, 1987; *Gaffney et al.*, 2004]. The change from tholeiitic to alkalic volcanism reflects a decreasing extent of melting as the volcano overrides the cooler outer parts of the plume. The increase in depth of melt segregation implied by an increasing role for residual garnet is not inferred from dynamical model of *Ribe and Christensen* [1999] for plume melting, but it is consistent with the prism shaped plume proposed by *Lassiter et al.* [1996, see their Figure 9] which shows that the depth of melt segregation is restricted to greater depths near the edge of the plume.

Late shield/postshield lavas from five Kea-trend volcanoes (Mauna Kea, Hawi Volcanics of Kohala, Kula and Hana Volcanics of Haleakala, West Maui and East Molokai) are variable in isotopic ratios of Sr, Nd and Pb, but they define overlapping fields in $^{87}Sr/^{86}Sr$ vs $^{143}Nd/^{144}Nd$ and have the low $^{208}Pb/^{204}Pb$ ratio at a given $^{206}Pb/^{204}Pb$ that is typical of Kea-trend volcanoes (Figures 8a and 9a). $^{87}Sr/^{86}Sr$ and $^{206}Pb/^{204}Pb$ in these lavas are inversely correlated with Nb/Zr (Figure 16). This trend can be explained by mixing of the Kea shield component (i.e., the relatively low $^{87}Sr/^{86}Sr$, high $^{143}Nd/^{144}Nd$, high $^{206}Pb/^{204}Pb$ end of range defined by Hawaiian shield lavas) with a depleted component that dominates rejuvenated stage lavas. Compared to the Kea shield component, this component has lower $^{87}Sr/^{86}Sr$, higher $^{143}Nd/^{144}Nd$ and lower $^{206}Pb/^{204}Pb$, and is not MORB-related lithosphere or asthenosphere [Figure 9d; *Frey et al.*, 2005]. Rejuvenated-stage and late shield/postshield lavas from East Molokai contain variable amounts of the same depleted component as previously inferred on the basis of relative magma volumes [*Clague*, 1987, p246].

The similar temporal variations of radiogenic isotopic ratios in late shield/postshield lavas from the four Kea volcanoes (Mauna Kea, Kohala, Haleakala and East Molokai) are consistent with horizontal heterogeneity in the plume, i.e., as the volcano moves off the hotspot a common depleted source component was sampled by each volcano. Moreover, the complete overlap in Sr-Nd-Pb isotopic ratios of the relatively young postshield Mauna Kea lavas (<350 ky) and older (~1.5 My) shield/postshield East Molokai lavas are consistent with long-term vertical continuity of geochemically distinct stripes at the edge of the plume, as well as in the interior (See Figure 13f of *Eisele et al.*, 2003). An interesting question is – do Kea and Loa trend volcanoes sample the same depleted component as they move off the hotspot? Isotopic data are sparse for postshield lavas from Loa volcanoes, but postshield lavas from Hualalai retain their distinctive Loa Pb isotopic signature (Figure 9a). Apparently, the edge of the plume is not concentrically zoned, i.e, the distinctive Loa and Kea-trend signatures extend to the plume edges.

Acknowledgements

This chapter benefited from the review comments of M. Feigenson, Z.-Y. Ren, Y. Tatsumi and W. White. I thank the efforts of co-authors (F. Frey, D. Clague, D. Weis and M. Beeson) which led to publish this chapter in G^3. I am indebted to J. G. Moore (U.S. Geological Survey) who, with M.H. Beeson, collected nearly all the samples used in this study. The trace element and isotopic study would not have been possible without their joint effort. I thank Bruno Kieffer, Jane Barling and Claude Maerschalk for helping with the Sr, Nd and Pb analyses and their advice when I was visiting in the Pacific Centre for Isotopic and Geochemical Research chemistry lab. Rick Kayser and Sean Higgins are thanked for their assistance in ICP-MS analysis and P. Ila for her supervision of the MIT neutron activation facility. A.R. Basu is thanked for sharing his unpublished East Molokai Pb data. This research was supported by National Science Foundation Grant EAR-0105557 and a grant from the David and Lucile Packard Foundation to MBARI.

References

Abouchami, W., S. J. G. Galer, and A. W. Hofmann (2000), High precision lead isotope systematics of lavas from the Hawaiian Scientific Drilling Project, *Chem. Geol.*, *169*, 187-209.

Abouchami, W., A. W. Hofmann, S. J. G. Galer, F. A. Frey, J. Eisele, and M. Feigenson (2005), Long-lived heterogeneities and lateral dichotomy of the Hawaiian Plume, *Nature*, in press.

Basu, A. R., and B. E. Faggart (1996), Temporal isotopic variations in the Hawaiian mantle plume: the Lanai anomaly, the Molokai fracture zone and a seawater-altered lithospheric component in Hawaiian volcanism. In: Earth Processes: Reading the Isotopic Code, *Am. Geophys. Union Monogr.*, *95*, 149-159.

Beeson, M. H. (1976), Petrology, mineralogy, and geochemistry of the East Molokai volcanic series, *U.S. Geol. Surv. Prof. Pap.*, *961*, 1-53.

Blichert-Toft, J., D. Weis, C. Maerschalk, A. Agranier, and F. Albarède (2003), Hawaiian hot spot dynamics as inferred from the Hf and Pb isotope evolution of Mauna Kea volcano, *Geochem. Geophys. Geosyst.*, *4(2)*, 8704, doi: 10.1029/2002GC000340.

Bryce, J. G., D. J. DePaolo, and J. C. Lassiter (2005), Sr, Nd and Os isotopes in a 2.84 km section of Mauna Kea volcano: Implications for the geochemical structure of the Hawaii plume, *in revision for Geochem. Geophys. Geosyst.*

Castillo, P. R., E. Klein, J. Bender, C. Langmuir, S. Shirey, R. Batiza, and W. White (2000), Petrology and Sr, Nd, and Pb isotope geochemistry of mid-ocean basalt glasses from the 11°45'N to 15°00'N segment of the East Pacific Rise, *Geochem. Geophys. Geosyst.*, *1*, 1999GC000024.

Chen, C.-Y., and F. A. Frey (1985), Trace element and isotopic geochemistry of lavas from Haleakala volcano, East Maui, Hawaii: implications for the origin of Hawaiian basalts, *J. Geophys. Res.*, *90*, 8,743-8,768.

Chen, C.-Y., F. A. Frey, and M. O. Garcia (1990), Evolution of alkalic lavas at Haleakala Volcano, East Maui, Hawaii: major, trace element and isotopic constraints, *Contrib. Mineral. Petrol.*, *105*, 197-218.

Chen, C.-Y., F. A. Frey, M. O. Garcia, G. B. Dalrymple, and S. R. Hart (1991), The tholeiitic to alkalic basalt transition at Haleakala volcano, Maui, Hawaii, *Contrib. Mineral. Petrol.*, *106*, 183–200.

Chen, C.-Y., F. A. Frey, J. M. Rhodes, and R. M. Easton (1996), Temporal geochemical evolution of Kilauea volcano: Comparison of Hilina and Puna basalt, in Earth Processes: Reading the Isotopic Code, *Geophys. Monogr. Ser.*, vol. *95*, edited by A. Basu and S. R. Hart, pp. 161–181, AGU, Washington, D.C.

Clague, D. A., and M. H. Beeson (1980), Trace element geochemistry of the East Molokai Volcanics Series, Hawaii, *Am. J. Sci.*, *280A*, 820-844.

Clague, D. A., D.-G. Chen, R. Murnane, M. H. Beeson, M. A. Lanphere, G. B. Dalrymple, W. Friesen, and R. T. Holcomb (1982), Age and petrology of the Kalaupapa basalt, Molokai, Hawaii, *Pac. Sci.*, *36*, 411-420.

Clague, D. A., and F. A. Frey (1982), Petrology and trace-element geochemistry of the Honolulu Volcanics, Oahu: Implications for the oceanic mantle below Hawaii. *J. Petrol.*, *23*, 447-504.

Clague, D. A., and G. B. Dalrymple (1987), The Hawaiian-Emperor volcanic chain; Part I: Geologic evolution, *U.S. Geol. Surv. Prof. Pap.*, *1350*, 5-54.

Clague, D. A. (1987), Hawaiian alkaline volcanism, Fitton, J. G. and B. G. J. Upton (eds), Alkaline igneous rocks, *Geol. Soc. Spec. Pub.*, *30*, 227-252.

Clague, D. A., and G. B. Dalrymple (1988), Age and petrology of alkalic postshield and rejuvenated-stage lava from Kauai, Hawaii, *Contrib. Mineral. Petrol.*, 99 (2), 202-218.

Clague, D. A., J. G. Moore, J. E. Dixon, and W. B. Friesen (1995), Petrology of submarine lavas from Kilauea's Puna Ridge, Hawaii, *J. Petrol.*, 36 (2), 299-349.

Clague, D. A., J. G. Moore, and A. S. Davis (2002), Volcanic breccia and hyaloclastite in blocks from the Nuuanu and Wailau Landslides, Hawaii, In: Hawaiian Volcanoes: Deep Underwater Perspectives, *AGU Monogr., 128*, 297-310.

Clague, D. A., and J. G. Moore (2002), The proximal part of the giant submarine Wailau landslide, Molokai, Hawaii, *J. Volc. Geotherm. Res.*, *113*, 259-287.

Class, C., and S. L. Goldstein (1997), Plume-lithosphere interactions in the ocean basins; constraints from the source mineralogy, *Earth Planet. Sci. Lett.*, *150*, 245-260.

Cousens, B. L., D. A. Clague, and W. D. Sharp (2003), Chronology, chemistry, and origin of trachytes from Hualalai volcano, Hawaii, *Geochem. Geophys. Geosyst.*, *4* (9), 1078, dio:10.1029/2003GC000560.

Dixon, J. E., D. A. Clague, P. Wallance, and R. Poreda (1997), Volatiles in Alkalic Basalts from the North Arch Volcanic Field, Hawaii: Extensive Degassing of Deep Submarine-erupted Alkalic Series Lavas, *J. Petrol.*, 38, 911-939.

Eisele, J., W. Abouchami, S. J. Galer, and A. W. Hofmann (2003), The 320 kyr Pb isotope evolution of Mauna Kea lavas recorded in the HSDP-2 drill core. *Geochem. Geophys. Geosyst.*, *4(5)*, 8710, doi:10.1029/2002GC000339.

Feigenson, M. D., A. W. Hofmann, and F. J. Spera (1983), Case studies on the origin of basalt II, The transition from tholeiitic to alkalic volcanism on Kohala Volcano, Hawaii, *Contrib. Mineral. Petrol.*, *84*, 390-405.

Feigenson, M. D. (1984), Geochemistry of Kauai volcanics and a mixing model for the origin of Hawaiian alkali basalts, *Contrib. Mineral. Petrol.,* 87 (2), 109-119.

Fekiacova, Z., and W. Abouchami (2003), Pb isotope evolution of Koolau (Oahu, Hawaii), *EOS Trans. AGU Fall Meet. Suppl. Abstract,* V32A-0991, F1557.

Fodor, R. V., G. R. Bauer, R. S. Jacobs, and T. J. Bornhorst (1987), Kahoolawe Island, Hawaii: tholeiitic, alkalic, and unusual hydrothermal (?) "enrichment" characteristics, *J. Volc. Geotherm. Res.*, *31*, 171-176.

Frey, F. A., W. S. Wise, H. West, S. T. Kwon, and A. Kennedy (1990), Evolution of Mauna Kea volcano, Hawaii: Petrologic and geochemical constraints on postshield volcanism, *J. Geophys. Res.*, *95*, 1271–1300.

Frey, F. A., M. O. Garcia, W. S. Wise, A. Kennedy, P. Gurriet, and F. Albarède (1991), The evolution of Mauna Kea volcano, Hawaii: Petrogenesis of tholeiitic and alkalic basalts, *J. Geophys. Res.*, *96*, 14,347–14,375.

Frey, F. A., M. O. Garcia, and M. F. Roden (1994), Geochemical characteristics of Koolau Volcano: Implications of intershield geochemical differences among Hawaiian volcanoes, *Geochim. Cosmochim. Acta*, *58*, 1441-1462.

Frey, F. A., D. A. Clague, J. J. Mahoney, and J. M. Sinton (2000), Volcanism at the edge of the Hawaiian plume: Petrogenesis of submarine alkalic lavas from the North Arch volcanic field, *J. Petrol.*, *41*, 667-691.

Frey, F. A., S. Huang, J. Blichert-Toft, M. Regelous, and M. Boyet (2005), Origin of depleted components in basalt related to the Hawaiian Hotspot: Evidence from isotopic and incompatible element ratios, *Geochem. Geophys. Geosyst.*, *6*, Q02L07, doi:10.1029/2004GC000757.

Gaffney, A. M., B. K. Nelson, and J. Blichert-Toft (2004), Geochemical constraints on the role of oceanic lithosphere in intra-volcano heterogeneity of West Maui, Hawaii, *J. Petrol.*, *45*, 1663-1687.

Galer, S. J. G., and W. Abouchami (1998), Practical application of lead triple spiking for correction of instrumental mass discrimination. *Mineral. Mag.*, *62A*, 491-492.

Galer, S. J. G., W. Abouchami, and J. D. Macdougall (1999), East Pacific Rise MORB through the Pb isotope looking-glass. *EOS Trans. AGU*, 80, F1086.

Garcia, M. O., B. A. Jorgenson, J. J. Mahoney, E. Ito, and A. J. Irving (1993), An evaluation of temporal geochemical evolution of Loihi summit lavas: Results from Alvin submersible dives, J. Geophys. Res., *98*, 535–550.

Garcia, M. O., D. J. P. Foss, H. B. West, and J. J. Mahoney (1995), Geochemical and isotopic evolution of Loihi volcano, Hawaii, *J. Petrol.*, *36*, 1644–1647.

Garcia, M. O., K. H. Rubin, M. D. Norman, J. M. Rhodes, D. W. Graham, D. W. Muenow, and K. Spencer (1998), Petrology and geochronology of basalt breccia from the 1996 earthquake swarm of Loihi Seamount, Hawaii; magmatic history of its 1996 eruption, *Bull. Volc.*, *59 (8)*, 577-592.

Garcia, M. O., A. J. Pietruszka, J. M. Rhodes, and K. Swanson (2000), Magmatic processes during the prolonged Pu'u 'O'o eruption of Kilauea Volcano, Hawaii Anonymous, In commemoration of Keith Gordon Cox, 1933-1998, *J. Petrol.*, *41* (7), 967-990.

Ghiorso, M. S., and R. O. Sack (1995), Chemical mass transfer in magmatic processes. IV. A revised and internally consistent thermodynamic model for the interpolation and internally consistent thermodynamic model for the interpolation and extrapolation of liquid-solid equilibria in magmatic systems at elevated and pressures, *Contrib. Mineral. Petrol.*, 119, 197-212.

Hart, S. R., and T. Dunn (1993), Experimental cpx/melt partitioning of 24 trace elements, *Contrib. Mineral. Petrol.*, *113(1)*, 1-8.

Hegner, E., D. Unruh, and M. Tatsumoto (1986), Nd-Sr-Pb isotope constraints on the source of West Maui volcano, Hawaii, *Nature*, *319*, 478-480.

Hofmann, A. W., and W. M. White (1983), Ba, Rb and Cs in the Earth's mantle, *Z. Naturforssch*, *38a*, 258–266.

Hofmann, A. W., M. D. Feigenson, and I. Raczek (1987), Kohala revisited, *Contrib. Mineral. Petrol.*, *95*, 114-122.

Hofmann, A. W., and K. P. Jochum (1996), Source characteristics derived from very incompatible trace elements in Mauna Loa and Mauna Kea basalts (Hawaiian Scientific Drilling Project). *J. Geophys. Res.*, *101*, 11,831-11,839.

Holcomb, R. T. (1985), The caldera of East Molokai volcano, Hawaiian Islands, *Nat. Geogr. Soc. Res. Reports*, *21*, 81-87.

Holcomb, R, T., B. K. Nelson, P. W. Reiners, and N. Sawyer (2000), Overlapping volcanoes: The origin of Hilo Ridge, Hawaii, *Geology*, *28*, 547-550.

Huang, S., and F. A. Frey (2003), Trace element abundaces of Mauna Kea basalt from phase 2 of the Hawaii Scientific Drilling Project: Petrogenetic implications of correlations with major element content and isotopic ratios, *Geochem. Geophys. Geosyst.*, *4(6)*, 8711, doi: 10.1029/2002GC000322.

Ila, P., and F. A. Frey (1984), Utilization of neutron activation analysis in the study of geologic materials. In Harling, O. K., Clark, L., von der Hardt, P. (eds) Use and Development of Low and Medium Flux Research Reactors, *Atomkernenergie Kerntechnik, suppl.* to vol. *44*, 710-716.

Ila, P., and F. A. Frey (2000), Trace element analysis of USGS standards AGV2, BCR2, BHVO2, DTS2 and GSP2 by INAA, *J. Radioanalysis Nuclear Chem.*, *244*, 599-602.

Jackson, E. D., E. A. Silver, and G. B. Dalrymple (1972), Hawaiian-Emperor chain and its relation to Cenozoic circumpacific tectonics, *Geol. Soc. Am. Bull.*, *83*, 601-618.

Jackson, M. C., R. A. Wilmoth, and F. A. Frey (1999), Geology and petrology of basaltic lavas and dikes of the Koolau Volcano in the Trans-Koolau exploratory tunnels, Oahu, Hawaii, *Bull. Volc.*, *60*, 381–401.

Jang, Y.-D., and H. R. Naslund (2003), Major and trace element variation in ilmenite in the Skaergaard Intrusion: petrologic implications, *Chem. Geol.*, *193*, 109-125.

Kennedy, A. K., S. T. Kwon, F. A. Frey, and H. B. West (1991), The isotopic composition of postshield lavas from Mauna Kea Volcano Hawaii, *Earth Planet. Sci. Lett.*, *103*, 339–353.

Lanphere, M. A., and F. A. Frey (1987), Geochemical evolution of Kohala Volcano, Hawaii, *Contrib. Mineral. Petrol.*, 95 (1), 100-113.

Lassiter, J. C., D. J. Depaolo, and M. Tatsumoto (1996), Isotopic evolution of Mauna Kea volcano: Result from the initial phase of the Hawaii Scientific Drilling Project, *J. Geophys. Res.*, *101*, 11,769-11,780.

Lassiter, J. C., E. H. Hauri, P. W. Reiners, and M. O. Garcia (2000), Generation of Hawaiian post-erosional lavas by melting of a mixed lherzolite/pyroxenite source, *Earth Planet. Sci. Lett.*, *178*, 269-284.

LeMaitre, R. W. (1991), A classification of igneous rocks and glossary of terms, *Blackwell Scientific Publications*, Oxford, 193 pp.

Macdonald, G. A., and T. Katsura (1964), Chemical composition of Hawaiian lavas. *J. Petrol.*, *5*, 82-133.

McDougall, I. (1964), Potassium-argon ages from lavas of the Hawaiian Islands, *Geol. Soc. Am. Bull.*, *75*, 107-128.

Moore, J. G., and D. A. Clague (2002), Mapping of the Nuuanu and Wailau Landslides in Hawaii, In: Hawaiian Volcanoes: Deep Underwater Perspectives, *AGU Monogr.*, *128*, 223-244.

Naughton, J. J., G. A Macdonald, and V. A. Greeberg (1980), Some additional potassium-argon ages of Hawaiian rocks: the Maui volcanic complex of Molokai, Lanai, and Maui, *J. Volc. Geotherm. Res.*, *7*, 339-355.

Nielsen, R. L., L. M. Forsythe, W. E. Gallahan, and M. R. Fisk (1994), Major- and trace-element magnetite-melt equilibria In: Foley, S. F. and S. R., der Laan (eds), Trace-element partitioning with application to magmatic processes, *Chem. Geol.*, *117*, 167-191.

Nielsen, R. L. and J. S. Beard (2000), Magnetite-melt HFSE partitioning, *Chem. Geol.*, *164*, 21-34.

Niu, Y., K. D. Collerson, R. Batiza, I. J. Wendt, and M. Regelous (1999), Origin of enriched-type mid-ocean ridge basalt at ridges far from mantle plumes: The East Pacific Rise at 11°20'N, *J. Geophys. Res.*, *104*, 7,067-7,087.

Norman, M. D., and M. O. Garcia (1999), Primitive magmas and source characteristics of the Hawaiian Plume; Petrology and geochemistry of shield picrites, *Earth Planet. Sci. Lett.*, *168*, 27–44.

Pertermann, M., M. M. Hirschmann, K. Hametner, D. Gu¨nther, and M. W. Schmidt (2004), Experimental determination of trace element partitioning between garnet and silica-rich liquid during anhydrous partial melting of MORB-like eclogite, *Geochem. Geophys. Geosyst.*, 5, Q05A01, doi:10.1029/2003GC000638.

Pietruszka, A. J., and M. O. Garcia (1999), A rapid fluctuation in the mantle source and melting history of Kilauea Volcano inferred from the geochemistry of its historical summit lavas (1790–1982), *J. Petrol.*, *40*, 1321–1342.

Regelous, M., Y. Niu, J. I. Wendt, R. Batiza, A. Greig, and K. D. Collerson (1999), Variations in the geochemistry of magmatism on the East Pacific Rise at 10°30'N since 800 ka, *Earth Planet. Sci. Lett.*, *168*, 45-63.

Reiners, P. W., and B. K. Nelson (1998), Temporal-compositional-isotopic trends in rejuvenated-stage magmas of Kauai, Hawaii, and implications for mantle melting processes, *Geochim. Cosochim. Acta*, *62*, 2,347-2,368.

Ren, Z.-Y., T. Shibata, M. Yoshikawa, K. T. M. Johnson, and E. Takahashi (2005), Isotope compositions of the submarine Hana Ridge lavas, Haleakala volcano, Hawaii: implications for source compositions, melting process and the structure of Hawaiian plume, *J. Petrol.,* in press.

Rhodes, J. M. (1995), The 1852 and 1868 Mauna Loa picrite eruptions: Clues to parental magma compositions and the magmatic plumbing system, in Mauna Loa Revealed, *Geophys. Monogr. Ser.*, vol. *92*, edited by J. M. Rhodes and J. P. Lockwood, pp. 241–262, AGU, Washington, D.C..

Rhodes, J. M. (1996), Geochemical stratigraphy of lava flows sampled by the Hawai'i Scientific Drilling Project, *J. Geophys. Res.*, *101*, 11,729-11,746.

Ribe, N. M., and U. R. Christensen (1999), The dynamical origin of Hawaiian volcanism, *Earth Planet. Sci. Lett.*, *171*, 517-531.

Roden, M. F., T. Trull, S. R. Hart, and F. A. Frey (1994), New He, Sr, Nd and Pb isotopic constraints on the constitution of the Hawaiian plume: Results from Koolau Volcano, Oahu, Hawaii, *Geochim. Cosmochim. Acta*, *58*, 1,431–1,440.

Sherrod, D. R., Y. Nishimitsu, and T. Tagami (2003), New K-Ar ages and the geologic evidence against rejuvenated-stage volcanism at Haleakala, East Maui, a postshield-stage volcano of the Hawaiian island chain, *Geol. Soc. Am. Bull.*, *115*, 683-694.

Shinozaki, K., Z.-Y. Ren, and E. Takahashi (2002), Geochemical and Petrological characteristics of Nuuanu and Wailau landslide blocks, In: Hawaiian Volcanoes: Deep Underwater Perspectives, *Am. Geophys. Union Monogr.*, *128*, 297-310.

Spengler, S. R., and M. O. Garcia (1988), Geochemistry of the Hawi lavas, Kohala Volcano, Hawaii, *Contrib. Mineral. Petrol.*, *99*, 90-104.

Stearns, H. T., and G. A. Macdonald (1942), Geology and ground-water resources of the island of Maui, Hawaii, pp. 321, U.S. Geol. Surv., Hawaii.

Stearns, H. T., and G. A. Macdonald (1947), Geology and ground-water resources of the island of Molokai, Hawaii, *Hawaii Div. Hydrogr. Bull.*, *11*, pp. 113.

Stille, P., D. M. Unruh, and M. Tatsumoto (1983), Pb, Sr, Nd and Hf isotopic evidence of multiple sources for Oahu, Hawaii basalts, *Nature*, *304*, 25-29.

Stille, P., D. M. Unruh, and M. Tatsumoto (1986), Pb, Sr, Nd, and Hf isotopic constraints on the origin of Hawaiian basalts and evidence for a unique mantle source, *Geochim. Cosmochim. Acta*, *50*, 2,303-2,319.

Sun, S.-S., and W. F. McDonough (1989), Chemical and isotopic systematics of oceanic basalts: Implications for mantle composition and processes, in Magmatism in the Ocean Basins, edited by A. D. Saunders and M. J. Norry, *Geol. Soc. Spec. Publ.*, *42*, 313–345.

Tanaka, R., E. Nakamura, and E. Takahashi (2002), Geochemical Evolution of Koolau Volcano, Hawaii. In: Hawaiian Volcanoes: Deep Underwater Perspectives, *AGU Monogr.*, *128*, 311-332

Tatsumoto, M. (1978), Isotopic composition of lead in oceanic basalt and implication to mantle evolution, *Earth Planet. Sci. Lett.*, *38*, 63-87.

Tatsumoto, M., E. Hegner, and D.M. Unruh (1987), Origin of the West Maui volcanic rocks inferred from Pb, Sr, and Nd isotopes and a multicomponent model for oceanic basalt, *U.S. Geol. Survey Prof. Pap.*, *1350*, 723-744.

Weis, D., and F. A. Frey (1996), Role of the Kerguelen Plume in generating the eastern Indian Ocean seafloor, *J. Geophys. Res., 101 (6)*, 13,831-13,849.

West, H. B., and W. P. Leeman (1987), Isotopic evolution of lavas from Haleakala Crater, Hawaii, *Earth Planet. Sci. Lett., 84*, 211-225.

West, H. B., M. O. Garcia, F. A. Frey, and A. Kennedy (1988), Nature and cause of compositional variation among the Alkalic Cap lavas of Mauna Kea volcano, Hawaii, *Contrib. Mineral. Petrol., 100*, 383-397.

West, H. B., and W. P. Leeman (1994), The open-system geochemical evolution of alkalic cap lavas from Haleakala Crater, Hawaii, USA, *Geochim. Cosmochim. Acta, 58*, 773-796.

Wright, T. L., and R. S. Fiske (1971), Origin of the differentiated and hybrid lavas of Kilauea volcano, Hawaii, *J. Petrol.*, 12(1), 1-65.

Yang, H.-J., F. A. Frey, and D. A. Clague (2003), Constraints on the source components of lavas forming the Hawaiian North Arch and Honolulu Volcanics, *J. Petrol., 44*, 603-627.

Figure captions

Figure 1 Map of Molokai Island showing locations of studied sections (after *Beeson*, 1976), and location of East Molokai Volcano on the Kea trend of recent Hawaiian volcanoes. The locations for submarine rejuvenated stage lavas, ~15 km northeast of Kalaupapa Peninsula [*Clague and Moore*, 2002], and Wailau landslide lavas, ~50 km north of Kalaupapa Peninsula [*Tanaka et al.*, 2002] are not to scale.

Figure 2 Alkalinity versus stratigraphic position for (a) Kalaupapa section and (b) 71HALW section showing the temporal variation of composition ranging from tholeiitic for the oldest samples to alkalic lavas for the youngest samples. Alkalinity is defined as the vertical deviation from the alkalic-tholeiitic dividing line of *Macdonald and Katsura* [1964]; see Figure 3. Open symbols are for hawaiite and mugearite using the classification scheme of Figure 3; (c) $^{87}Sr/^{86}Sr$ and (d) $^{143}Nd/^{144}Nd$ versus stratigraphic position for Kalaupapa section. From the bottom to the top $^{87}Sr/^{86}Sr$ decreases and $^{143}Nd/^{144}Nd$ increases. The error bars are the 2σ calculated from the mean of 42 analyses of NBS 987 Sr standard and 18 analyses of La Jolla Nd standard

Figure 3 Na_2O+K_2O versus SiO_2 classification plot showing that the East Molokai late shield/postshield lavas range from tholeiitic (open symbols) to alkalic basalt (filled symbols) and hawaiite, mugearite and benmoreite (labeled). Classification fields are from *LeMaitre* [1991]; the alkalic-tholeiitic dividing line is from *Macdonald and Katsura* [1964]. Major element data were adjusted to a $Fe^{3+}/(Fe^{2+} + Fe^{3+})$ molar ratio of 0.10. Due to K_2O mobility the K_2O/P_2O_5 ratio ranges widely (0.36 to 2.0, except for a benmoreite dike with 2.8) in these late shield/postshield lavas. Therefore, the K_2O contents of late shield/postshield lavas are corrected to a K_2O/P_2O_5 ratio of 1.71, a typical ratio for fresh Hawaiian lavas [*Rhodes*, 1995; *Garcia et al.*, 2000]. Benmoreite dike (M4.9+300D) has high K_2O/P_2O_5 ratio (2.8) and was not adjusted for potassium loss. Rejuvenated stage lavas did not experience significant potassium loss ($K_2O/P_2O_5>1.3$) and were not adjusted for possible K_2O loss. Wailau landslide samples (Figure 1) are tholeiitic basalts derived from the East Molokai shield that were analyzed for Sr, Nd and Pb isotope ratios

by *Tanaka et al.* [2002]. These samples are not corrected for potassium loss (K_2O/P_2O_5>1.1).

Figure 4 MgO vs SiO_2, Al_2O_3, CaO, TiO_2, Na_2O, P_2O_5 and Na_2O/K_2O. Open symbols indicate tholeiitic lavas and solid symbols indicate alkalic lavas. In the SiO_2 panel the most evolved postshield lavas and two rejuvenated-stage lavas with lower SiO_2 contents are labeled. Two lavas with abundant clinopyroxene phenocrysts (M4.6+150F and 71PELE-37) are labeled in Al_2O_3 and CaO panels. In the Na_2O/K_2O panel late shield/postshield lavas were adjusted to a constant K_2O/P_2O_5 ratio for potassium loss as in Figure 3. The benmoreite dike and rejuvenated stage lavas were not adjusted. The thick line is a liquid line of descent calculation for fractional crystallization using MELTS [*Ghiorso and Sack*, 1995] at pressure=1 kbar, fO_2 = FMQ-2, and 1.0 wt% H_2O and rejuvenated lava P253-11B as a starting composition. The choice of fO_2 and water content are based on data for North Arch lavas [*Dixon et al.*, 1997]. This choice of pressure yields only olivine as a fractionating phase in the interval from 16 to 6.5 wt% MgO. The dashed rectangles in panels d, f and g show the range for East Molokai rejuvenated stage glasses from *Clague and Moore* [2002] (square) and *Sherman and Garcia* [2002] (triangle). The green fields in the inserts in panels d, f and g are enlargements of the dashed rectangles. These glass data show that rejuvenated-stage magmas are compositionally more diverse than the whole-rock data.

Figure 5 Abundance of Nb and Cr and abundance of olivine phenocryst versus MgO content. Open symbols indicate tholeiitic lavas and solid symbols indicate alkalic lavas as defined in Figure 3. Abundance of the highly incompatible trace element, Nb, is negatively correlated with MgO content whereas the compatible element Cr is positively correlated. The strong correlation between modal olivine abundance and MgO content for lavas from Kalaupapa section reflects the important role of olivine fractionation and accumulation during the evolution of lavas with MgO contents greater than ~6 wt%. Modes of olivine phenocryst for Kalaupapa section are from *Beeson* [1976].

Figure 6 Th versus Rb, Ba, Nb, Pb, Zr, Sr, Y and Yb. Open symbols indicate tholeiitic lavas and solid symbols indicate alkalic lavas as defined in Figure 3. Although Th abundance in East Molokai late shield/postshield lavas is strongly correlated with these elements, the correlation coefficient decreases as the element on the vertical axis increases in compatibility. In panel "a" the highly evolved lavas are labeled.
The trend for rejuvenated-stage lavas overlaps those for late shield/postshield lavas in panels a to d, but in panels e to h the rejuvenated-stge lavas are offset to high Th/X ratios (X=Zr, Sr, Y or Yb) which exceed those of primitive mantle. Dashed line has slope equal to primitive mantle ratio [*Sun and McDonough*, 1989]. The fields in panels c, e, f, g and h for Honolulu Volcanics and North Arch lavas designated by blue lines [*Yang et al.*, 2003] show that offsets to high Th/X are characteristic of rejuvenated-stage lavas. Rejuvenated-stage lava 74KAL-1 is labelled in panel "a" because it has lost Rb during alteration (see text). Among East Molokai rejuvenated-stage lavas labelled sample 74KAUH-1 in panel "a" has the highest abundances of incompatible elements.

Figure 7 Incompatible trace element abundances normalized to the primitive mantle (PM) estimates of *Sun and McDonough* [1989]. Important features of the fields are the negative slopes from Ta to Yb, the high Ba/Th ratios, and the relatively low abundances in rejuvenated-stage lavas. Individual patterns are shown for 3 highly evolved lavas and 71HALW-9 which has a pattern different from other last shield/postshield lavas. Three evolved lavas have prominent depletions in Ti. Main shield samples occurring in the Wailau landslide deposits are tholeiitic basalt with relatively low abundances [*Tanaka et al.*, 2000]. The gray shaded field is for all the other late shield/postshield lavas except the four marked with sample names.

Figure 8 (a) $^{87}Sr/^{86}Sr$ - εNd fields for late shield/postshield lavas from the five Kea-trend Volcanoes and East Molokai rejuvenated stage lavas. The Sr-Nd isotopic ratios of late shield/postshield lavas from East Molokai broadly overlap the fields for West Maui, Haleakala, Kohala and Mauna Kea late shield/postshield lavas. Three of the five East Molokai samples from the Wailau landslide overlap with the field for East Molokai late shield/postshield samples. Mauna Kea late shield/postshield lavas include on-land

sections, and subaerially erupted lavas cored by the Hawaiian Scientific Drilling Project (HSDP). εNd is calculated from $10^4 \times [(^{143}Nd/^{144}Nd)_{sample}/(^{143}Nd/^{144}Nd)_{CHUR}-1]$ where $(^{143}Nd/^{144}Nd)_{CHUR} = 0.512638$.

(b) Note that tholeiitic lavas (open circles) from East Molokai have higher $^{87}Sr/^{86}Sr$ ratio than most alkalic lavas (solid circles). Plus symbol denotes acid-leached samples analyzed by *Basu and Faggart* [1996] and collected from the same Kalaupapa section which is predominantly alkalic lavas. The error bars are the 2σ calculated from the mean of 42 analyses of NBS 987 Sr standard and 18 analyses of La Jolla Nd standard.

(c) $^{87}Sr/^{86}Sr$- εNd for Hawaiian rejuvenated stage / North Arch lavas. Rejuvenated stage lavas from East Molokai overlap with fields for Lahaina Volcanics and Koloa Volcanics, and are offset to lower $^{87}Sr/^{86}Sr$ relative to the Honolulu Volcanics. The error bars are the 2σ calculated for the mean of 42 analyses of NBS 987 Sr standard and 18 analyses of La Jolla Nd standard.

Data sources: Mauna Kea-*Kennedy et al.* [1991], Lassiter et al. [1996], Bryce et al. [manuscript in revision, 2005]; Kohala-*Stille et al.* [1986], *Hofmann et al.* [1987]; Haleakala- *West and Leeman* [1987], *Chen et al.* [1990, 1991]; West Maui - *Hegner et al.* [1986], *Tatsumoto et al.* (1987), *Gaffney et al.* [2004]; East Molokai- *Basu and Faggart* [1996], *Tanaka et al.* [2002] for Wailau landslide and this study; Lahaina Volcanics - *Hegner et al.* [1986], *Tatsumoto et al.* [1987], *Gaffney et al.* [2004]; Honolulu Volcanics - *Stille et al.*, [1983], *Lassiter et al.* [2000]; Koloa Volcanics - *Reiners and Nelson* [1998]; North Arch lavas- *Frey et al.* [2000]; EPR MORB- *Niu et al.* [1999], *Regelous et al.* [1999], *Castillo et al.* [2000].

Figure 9 (a) $^{206}Pb/^{204}Pb$-$^{208}Pb/^{204}Pb$ for late shield/post-shield lavas from the five Kea-trend Volcanoes. The Loa-Kea boundary is defined by *Abouchami et al.* [2005]. Most lavas from Kea-trend volcanoes lie to the right side of this trend. Data points shown for East Molokai have maximum 2σ less than the size of the symbol. East Molokai late shield/post-shield lavas have relatively higher $^{206}Pb/^{204}Pb$ ratios than lavas from Haleakala volcano but overlap with field of Mauna Kea and West Maui late shield/postshield lavas. Pb isotopic data for West Maui shield/postshield lavas from *Hegner et al.* [1986] and *Tatsumoto et al.* [1987] are not plotted due to their large

uncertainty. Postshield stage lavas from Hualalai, a Loa trend volcano, are shown for comparison; (b) $^{206}Pb/^{204}Pb$-$^{208}Pb/^{204}Pb$ for four suites of Hawaiian rejuvenated stage and North Arch lavas compared with fields for late shield/postshield lavas from 5 Kea-trend volcanoes and EPR MORB triple-spike data from *Galer et al.* [1999]. The black line is the regression line for East Molokai late shield/postshield lavas (solid circles) and rejuvenated stage lavas (open circles). (c) $^{206}Pb/^{204}Pb$-$^{207}Pb/^{204}Pb$ for East Molokai lavas and fields for late shield/postshield lavas from 4 Kea trend volcanoes. Also shown are rejuvenated-stage and North Arch lavas. (d) $^{87}Sr/^{86}Sr$ -$^{206}Pb/^{204}Pb$ isotope fields for five Kea-trend volcanoes and rejuvenated stage/North Arch lavas. Hawaiian shield lavas define an inverse trend whereas postshield (e.g., Haleakala) define a positive trend. East Molokai late shield/postshield-stage lavas define a broadly positive trend overlapping the field of Mauna Kea late shield/postshield lavas and trend toward the fields of Hawaiian rejuvenated stage/North Arch lavas.

Data sources: Kilauea – *Abouchami et al.* [2005]; Mauna Kea - *Abouchami et al.* [2000], *Eisele et al.* [2003], *Abouchami et al.* [2005]; Mauna Loa – *Abouchami et al.* [2000], *Abouchami et al.* [2005]; Hualalai – *Cousens et al.* [2003]; Kohala-*Holcomb et al.* [2000], *Abouchami et al.* [2005]; Haleakala - *West* [1987], *Chen et al.* [1990, 1991], *Ren et al.* [2005]; West Maui - *Gaffney et al.* [2004]; East Molokai – A. Basu [unpublished data], *Tanaka et al.* [2002] and this study; Koolau- *Roden et al.* [1994]; Lahaina Volcanics - *Hegner et al.* [1986], *Tatsumoto et al.* [1987], *Gaffney et al.* [2004]; Honolulu Volcanics- *Lassiter et al.* [2000], *Fekiacova and Abouchami* [2003]; Koloa Volcanics – *Lassiter et al.* [2000]; North Arch lavas-*Frey et al.* [2000]; EPR MORB – *Galer et al.* [1999], *Niu et al.* [1999], *Regelous et al.* [1999], *Castillo et al.* [2000].

Figure 10. K/Rb and K/Ba versus K_2O/P_2O_5 for East Molokai lavas. Five lavas (69KLPA-2, 69KLPA-5A, 69KLPA-8B, 69KLPA-9A and 69KLPA-14A) from the Kalaupapa section with relatively low K_2O/P_2O_5 ratios have high K/Rb ratios indicating loss of K and Rb during post-magmatic alteration. Five other labeled late shield/postshield lavas have $K_2O/P_2O_5<1$ and "normal" K/Rb. The only rejuvenated stage lava showing evidence for alteration is subaerial sample 74KAL-1 which has lower K_2O/P_2O_5 (1.35) and higher K/Rb (840) ratios than other rejuvenated stage East Molokai

lavas. Based on K/Ba ratios lavas from the Kalaupapa section of East Molokai can be divided into the two circled groups [*Clague and Beeson*, 1980]; lavas with low K/Ba ratios have low K_2O/P_2O_5 and high K/Rb ratios thereby indicating loss of K and Rb. PM denotes value for primitive mantle from *Sun and McDonough* [1989].

Figure 11 (a) MgO-CaO/Al_2O_3 and (b) MgO-Sc for East Molokai lavas. For the late shield/postshield lavas the positive trend between MgO vs CaO/Al_2O_3 at low MgO contents reflects the control of clinopyroxene fractionation. Sc defines a complex trend reflecting a change from olivine (negative slope) to clinopyroxene dominated fractionation (positive slope). The rejuvenated stage lavas show no evidence for clinopyroxene fractionation. Evolved late shield/postshield lavas and two rejuvenated stage lavas from Kauhako crater are labeled in panel a. Two lavas (M4.6+150F and 71PELE-37) with abundant clinopyroxene phenocrysts and high CaO/Al_2O_3 ratios are also labeled.

Figure 12 (a) Tb/Yb versus Nb/Zr for the East Molokai lavas. East Molokai late shield/postshield stage lavas display a positive trend overlapping with Mauna Kea subaerial (late shield/postshield) lavas. Three evolved lavas with relative Ti depletion and low Sc abundances are offset to higher Nb/Zr. Clinopyroxene fractionation is the only likely process to cause such an increase in Nb/Zr. The clinopyroxene fractional crystallization trend, with 10% increments shown as green plus symbols, used the partition coefficients for clinopyroxene/alkalic basalt from *Hart and Dunn* [1993]. These intervals are maximum estimates because the partition coefficients will increase as the melt evolves from basalt to hawaiite. Such extensive amounts of clinopyroxene fractionation are qualitatively consistent with the low CaO/Al_2O_3 and Sc of these samples (Figure 11). The rejuvenated stage lavas define a positive trend offset from late shield/postshield lavas to higher Nb/Zr ratios, presumably because of a source with high Nb/Zr. PM denotes value for primitive mantle from *Sun and McDonough* [1989]. Symbols as in Figure 3; (b) Nb (ppm) versus Sr/Ce for East Molokai late shield/postshield lavas. Three highly evolved East Molokai lavas are labeled. For comparison, fields are shown for Mauna Kea and Kohala. The inset shows the

fractionation trends of the mineral assemblages listed in parentheses. Cpx, plag and oliv are the abbreviations of clinopyroxene, plagioclase and olivine, respectively. The basalt to hawaiite transition at Mauna Kea and Kohala reflect fractionation of a plagioclase-poor and clinopyroxene-rich assemblage at moderate pressure. Data sources: East Molokai – this study, Wailau landslide – *Tanaka et al.* [2002]; Kohala – Spengler and Garcia [1988]; Mauna Kea – *West et al.* [1988], *Frey et al.* [1990, 1991], *Huang and Frey* [2003].

Figure 13 Sr/Ce vs Eu/Eu* for East Molokai lavas. All the East Molokai lavas (except Wailau landslide samples) define a positive trend indicating plagioclase control. Symbols as in Figure 3. PM denotes value for primitive mantle from *Sun and McDonough* [1989].

Figure 14 Na/La vs (a) Zr/Sm, (b) Ti/Eu and (c) K/Ce for Hawaiian rejuvenated stage and North Arch lavas. These lavas define strong positive trends. The large filled square is the primitive mantle value from *Sun and McDonough* [1989]. Error bars (±5%, 2σ) for Nb/La, Zr/Sm, Ti/Eu and K/Ce are shown for East Molokai rejuvenated stage lavas. The pink field designates the submarine rejuvenated-stage lavas from East Molokai.

Figure 15 SiO_2 contents vs Zr/Sm, Ti/Eu, Zr/Hf and Nb/Zr for Hawaiian rejuvenated stage and North Arch lavas. SiO_2 contents are corrected for olivine fractionation and accumulation by adding or subtracting equilibrium olivine until the whole rock composition is in equilibrium with olivine with Fo=90. Error bars shown for Zr/Sm, Ti/Eu Zr/Hf, and Nb/Zr are ±5% (2σ) for East Molokai rejuvenated stage lavas. The pink field designates the submarine rejuvenated-stage lavas from East Molokai.

Figure 16 $^{206}Pb/^{204}Pb$ versus SiO_2 contents and Nb/Zr vs $^{206}Pb/^{204}Pb$ and $^{87}Sr/^{86}Sr$ for East Molokai lavas. (a) $^{206}Pb/^{204}Pb$ ratios are positively correlated with SiO_2 contents for late shield/postshield lavas. Despite the sensitivity of SiO_2 content to crystal fractionation, late shield/postshield alkalic lavas have lower SiO_2 contents and $^{206}Pb/^{204}Pb$ ratios than tholeiitic lavas except the highly altered sample 69KLPA-5A. Regression lines for East Molokai late shield/postshield lavas in SiO_2 - $^{206}Pb/^{204}Pb$ panel and all East Molokai lavas in Nb/Zr vs $^{206}Pb/^{204}Pb$ and $^{87}Sr/^{86}Sr$ panels are also shown. (b and c) East Molokai

lavas, late shield/postshield and rejuvenated stage, define a negative trend in Nb/Zr vs $^{206}Pb/^{204}Pb$ and $^{87}Sr/^{86}Sr$. Late shield/postshield lavas from West Maui and Mauna Kea overlap with late shield/postshield East Molokai lava. The postshield Kula and Hana Volcanics from Haleakala span the gap between late shield/postshield and rejuvenated-stage East Molokai lavas. Note that the negative trend for Nb/Zr and $^{206}Pb/^{204}Pb$ defined by late shield/postshield lavas contrasts markedly with the positive trend for Hawaiian shield stage lavas. Data sources for shield fields are the same as Figure 9d plus *Chen et al.* [1996], *Garcia et al.* [1993, 1995, 1998], *Rhodes* [1996], *Norman and Garcia* [1999], *Pietruszka and Garcia* [1999]. Kohala lavas are not shown because there are no Nb/Zr data for samples analyzed for isotopic ratios.

Table 1. Locations of East Molokai late shield/postshield and rejuvenated stage lavas

Sample name	# of samples	Location	Alkalinity	Eruption environment	Reference
Late shield to Postshield lavas					
71PELE-	7	Pelekunu Valley	tholeiitic to alkalic	Subaerial	This study
70WAIK- and 71WAIK-	7	Waikolu Valley			This study
*M- and NE Portal	16	Water Tunnel			This study
71KPA-	2	Kalaupapa			This study
69KLPA-	26				Beeson (1976)
70HALW- and 71HALW-	22	Halawa Valley			This study
70MOL-1C	1	East coast near Mokuhooniki	alkalic		This study
70KAWE-1C	1	Near Gaging station			This study
Rejuvenated stage lavas					
74KAL-1	1	Kalaupapa Peninsula	alkalic	Subaerial	Clague et al. (1982)
80KAL-1	1	Kauhako Crater in Kalaupapa Peninsula			
71KAUH-1	1	500 m to the north of Kauhako Crater			
71KAUH-2	1				
MOE2	1	Kauhako Crater in Kalaupapa Peninsula			Naughton et al. (1980)
P252-2	1	North flank of Kalaupapa Peninsula		Submarine	Clague & Moore (2002)
P253-	4	North submarine slope of Molokai Island			

* Detailed locations for Water Tunnel sample are listed in Appendix Table A1.

Table 2 Major element contents (wt%) for East Molokai lavas

	Pelekunu Valley (Late shield/postshield)							Waikolu Valley (Late shield/postshield)					
	71PELE-77	71PELE-78	71PELE-37	71PELE-42F	71PELE-19	71PELE-20	71PELE-21	71WAIK-14F	71WAIK-10F	71WAIK-1	70WAIK-7	70WAIK-6	70WAIK-5
	PB	B	B	B	B	B	B	B	B	B	B	B	B
SiO_2	45.60	47.10	45.60	50.50	49.70	49.60	49.60	48.90	49.90	47.20	48.30	49.50	46.90
TiO_2	2.68	4.09	1.88	3.10	3.00	2.83	3.09	2.93	2.92	3.25	3.48	2.89	2.97
Al_2O_3	14.80	15.10	9.26	13.20	13.70	13.90	13.80	14.20	13.50	13.50	16.20	14.00	12.30
Fe_2O_3	7.41	5.46	2.96	3.08	3.70	3.59	4.82	3.09	4.35	4.74	3.50	2.96	2.49
FeO	5.80	7.77	10.20	8.66	8.91	8.74	8.26	9.37	8.41	8.51	8.19	9.21	10.00
MnO	0.16	0.19	0.18	0.21	0.18	0.20	0.20	0.18	0.19	0.18	0.16	0.18	0.18
MgO	8.81	4.96	17.30	5.80	6.43	6.49	6.18	6.72	6.01	7.21	4.57	6.69	10.30
CaO	10.70	9.83	9.97	10.60	10.80	10.80	10.50	11.30	10.40	10.40	10.40	11.10	10.80
Na_2O	2.55	3.53	1.65	2.30	2.38	2.20	2.43	2.27	2.54	2.61	3.30	2.31	2.53
K_2O	0.60	1.17	0.36	0.55	0.25	0.24	0.17	0.27	0.37	0.34	0.93	0.37	0.69
P_2O_5	0.36	0.64	0.23	0.33	0.31	0.30	0.34	0.33	0.30	0.44	0.54	0.32	0.42
H_2O+	0.52	0.23	0.31	0.77	0.40	0.66	0.46	0.48	0.42	0.68	0.29	0.47	0.28
H_2O-	0.31	0.06	0.19	0.69	0.38	0.64	0.42	0.27	0.67	0.65	0.10	0.29	0.04
CO_2	0.12	0.06	0.05	0.81	0.14	0.17	0.07	0.11	0.06	0.34	0.07	0.06	0.12
LOI	0.54	<0.01	<0.01	1.15	0.56	0.97	0.46	0.24	0.90	0.80	0.01	0.25	<0.01
Total	100.5	100.2	100.1	100.6	100.3	100.4	100.3	100.4	100.0	100.1	100.0	100.4	100.0

Bas - Basanite, PB - Picro-basalt, B - Basalt, H - Hawaiite, M - Mugearite, Ben - Benmoreite. The samples from the three valleys were collected by M. H. Beeson in 1970 and 1971 and those from inside the water tunnel were collected by J. G. Moore in 1966. Samples are ordered by increasing stratigraphic depth within Pelekunu Valley, Waikolu Valley, Water tunnel, Kalaupapa section, 71HALW section and submarine rejuvenated stage lavas. Major element contents for lavas from Kalaupapa section except 71KPA-1 and 71KPA-2 were taken from Beeson (1976). Major element contents for subaerial and submarine rejuvenated stage lavas were taken from Clague et al. (1982) and Clague and Moore (2002). All the other major element data are from this study

Table 2 (continued)

	Water Tunnel (Late shield/postshield)													
70WAIK-1	NE PORTAL	M5.4+50F	M5.3+375F	M5.3+40F	M5.1+10F	M4.9+300D	M4.6+150F	M4.6F	M4.3F	M4.1F	M4.3+1F	M3.9F	M3.3F	M2.5F
B	B	B	B	B	B	dike / Ben	B	B	B	B	B	B	B	B
47.10	49.70	47.10	49.50	47.90	49.90	55.40	47.60	49.70	49.00	46.90	48.60	50.10	47.60	46.40
3.94	3.35	3.82	2.89	2.37	3.22	1.56	1.85	3.70	3.63	3.21	3.71	3.92	2.43	2.11
14.00	14.20	14.10	14.00	11.40	14.10	17.50	11.30	13.40	13.80	15.00	13.70	13.10	13.30	11.60
3.54	3.29	4.08	3.72	2.84	4.13	3.01	3.29	2.82	2.78	3.65	2.89	4.15	1.72	2.66
10.40	8.92	10.01	8.53	9.41	8.25	4.90	7.75	10.51	10.28	9.13	10.36	10.30	9.52	9.84
0.20	0.17	0.20	0.18	0.18	0.17	0.23	0.16	0.19	0.19	0.17	0.19	0.21	0.16	0.18
5.66	5.64	5.80	6.52	13.70	5.53	2.33	14.80	5.40	5.91	7.43	5.99	4.78	11.20	14.60
9.99	10.60	10.60	11.10	9.33	10.20	4.69	11.10	9.99	10.00	10.60	10.10	8.92	10.90	9.48
2.91	2.82	2.58	2.33	1.88	2.62	5.99	1.62	2.63	2.85	2.96	2.85	2.97	2.29	2.15
0.60	0.61	0.17	0.40	0.39	0.67	2.39	0.32	0.81	0.82	0.66	0.81	0.91	0.51	0.45
0.55	0.45	0.47	0.34	0.30	0.43	0.85	0.21	0.47	0.51	0.44	0.51	0.57	0.33	0.28
0.63	0.27	0.71	0.34	0.24	0.42	0.25	0.19	0.32	0.16	0.13	0.15	0.34	0.11	0.11
0.31	0.29	0.57	0.20	0.13	0.38	0.23	0.07	0.08	0.06	0.04	0.04	0.16	<0.01	0.04
0.09	0.05	0.29	0.12	0.08	0.08	0.17	0.08	0.08	0.09	0.10	0.09	0.12	0.10	0.08
0.43	<0.01	0.73	0.26	<0.01	0.41	0.24	<0.01	<0.01	<0.01	<0.01	<0.01	<0.01	<0.01	<0.01
99.9	100.4	100.5	100.2	100.2	100.1	99.5	100.3	100.1	100.1	100.4	100.0	100.6	100.2	100.0

Table 2 (continued)

		Kalaupapa section (Late shield/postshield)											
M1.5F	M1.3F	71KPA-2	71KPA-1	69KLPA-1	69KLPA-2	69KLPA-3	69KLPA-4	69KLPA-5A	69KLPA-7A	69KLPA-8B	69KLPA-9A	69KLPA-11	69KLPA-14A
B	B	B	B	B	PB	B	B	B	B	B	B	B	B
47.90	47.20	47.30	49.00	47.38	45.14	46.92	49.04	45.66	46.48	45.99	45.36	45.77	46.47
4.09	3.77	3.51	4.03	2.81	2.61	2.55	3.20	1.87	3.00	2.09	2.08	3.25	3.06
14.30	15.40	14.60	13.10	13.50	13.28	14.24	14.33	11.32	15.57	13.14	13.07	14.87	14.31
3.55	3.24	7.05	5.04	3.18	5.65	4.09	5.94	4.49	4.25	4.59	6.64	4.56	3.21
9.58	9.68	6.34	8.96	9.74	7.67	8.64	7.14	7.57	8.64	7.84	6.30	9.13	10.08
0.19	0.18	0.18	0.20	0.19	0.18	0.19	0.19	0.18	0.18	0.17	0.18	0.20	0.19
5.02	5.77	5.35	5.98	9.24	12.42	9.18	5.66	16.98	7.19	12.87	13.07	7.45	8.33
9.43	9.27	10.00	9.57	9.92	10.14	9.92	10.26	9.44	9.75	9.90	9.63	9.59	10.00
3.72	3.50	3.02	2.81	2.58	1.94	2.10	2.59	1.47	3.02	2.02	1.96	2.48	2.68
1.18	1.16	0.85	0.62	0.54	0.19	0.17	0.64	0.14	0.68	0.26	0.23	0.40	0.43
0.72	0.58	0.51	0.51	0.40	0.26	0.32	0.41	0.21	0.42	0.26	0.26	0.44	0.42
0.09	0.21	0.55	0.31	0.21	0.36	0.83	0.34	0.26	0.41	0.42	0.58	1.20	0.37
<0.01	0.13	0.49	0.13	0.18	0.32	0.71	0.12	0.25	0.32	0.39	0.43	0.54	0.29
0.10	0.13	0.43	0.10										
<0.01	<0.01	0.59	<0.01										
99.9	100.2	100.2	100.4	99.9	100.2	99.9	99.9	99.8	99.9	99.9	99.8	99.9	99.8

Table 2 (continued)

69KLPA-15A H	69KLPA-16A B	69KLPA-16B B	69KLPA-17A B	69KLPA-19B B	69KLPA-19D B	69KLPA-20A B	69KLPA-23B B	69KLPA-25A B	69KLPA-27 B	69KLPA-28 Bas	69KLPA-29 B
48.48	46.05	45.42	45.54	47.34	47.98	45.77	47.18	46.69	45.52	45.64	48.15
3.38	2.68	2.70	2.72	3.78	3.76	3.56	3.39	3.39	2.76	3.30	3.40
15.42	12.12	12.53	12.50	15.72	15.41	15.50	15.20	15.65	13.95	14.04	17.20
2.32	2.58	7.04	6.71	7.90	4.57	7.86	5.36	4.85	8.48	4.09	4.52
10.08	10.36	6.57	6.79	5.49	8.29	5.85	7.83	8.59	5.37	10.16	7.20
0.19	0.19	0.20	0.19	0.20	0.20	0.18	0.19	0.19	0.20	0.20	0.19
5.09	12.34	11.43	11.29	4.00	4.31	6.46	5.90	5.91	8.91	8.11	3.78
10.12	10.06	9.60	9.65	8.34	8.81	9.16	9.56	8.67	10.01	9.17	9.36
3.16	2.30	2.26	2.31	3.54	3.62	3.00	3.05	2.88	2.16	2.96	3.66
0.79	0.69	0.68	0.68	1.20	1.20	0.88	0.85	0.89	0.45	0.98	1.12
0.51	0.35	0.40	0.36	0.67	0.68	0.51	0.48	0.48	0.36	0.59	0.62
		0.50	0.10	0.33	0.16	0.48	0.29	0.81	0.84	0.36	0.20
0.11	0.04	0.52	0.60	0.89	0.52	0.50	0.43	0.81	0.79	0.26	0.28
99.7	99.8	99.9	99.4	99.4	99.5	99.7	99.7	99.8	99.8	99.9	99.7

Table 2 (continued)

				Halawa Valley (Late shield/postshield)								
69KLPA-30	69KLPA-31	69KLPA-32	69KLPA-33	71HALW-7	71HALW-6	71HALW-5	71HALW-4	70HALW-1	70HALW-3	70HALW-4	70HALW-5	70HALW-6
B	B	B	M	B	B	B	B	B	M	B	B	B
47.76	46.30	45.82	51.40	48.60	46.40	46.20	49.90	48.80	50.70	48.90	48.70	48.40
3.29	3.47	2.61	2.34	3.21	3.25	3.71	2.97	3.00	3.50	3.70	4.19	3.78
17.88	16.58	12.68	17.67	14.90	14.80	14.80	14.70	14.20	14.90	14.90	13.90	15.10
7.13	3.32	6.08	5.11	3.30	5.54	4.33	2.33	2.40	7.01	3.50	3.89	4.58
4.69	9.54	7.35	4.95	9.81	7.79	9.60	9.69	9.90	5.39	8.91	9.55	8.12
0.19	0.20	0.20	0.21	0.19	0.18	0.20	0.17	0.18	0.22	0.18	0.20	0.18
3.53	5.55	11.24	2.97	4.94	7.29	5.77	5.63	6.40	2.59	4.65	4.29	4.47
8.93	8.73	9.64	6.04	10.30	10.10	10.90	10.90	11.20	6.06	9.65	8.79	9.34
3.49	3.17	2.27	5.08	2.86	3.07	2.55	2.57	2.67	4.47	3.60	3.72	3.45
1.06	1.10	0.63	2.00	0.60	0.70	0.21	0.58	0.51	1.81	1.06	1.17	1.00
0.59	0.62	0.32	1.09	0.46	0.46	0.48	0.38	0.40	1.03	0.65	0.74	0.63
0.58	0.85	0.56	0.38	0.43	0.37	0.97	0.36	0.22	0.77	0.22	0.47	0.59
0.61	0.38	0.56	0.41	0.25	0.30	0.62	0.16	0.20	1.41	0.24	0.41	0.56
				0.11	0.09	0.15	0.07	0.08	0.09	0.04	0.04	0.11
				0.40	0.18	0.89	0.03	<0.01	1.93	<0.01	0.37	0.77
99.7	99.8	100.0	99.7	100.0	100.3	100.5	100.4	100.2	100.0	100.2	100.1	100.3

Table 2 (continued)

70HALW-9 B	70HALW-11 B	71HALW-8 B	71HALW-9 B	71HALW-11 B	71HALW-12 B	71HALW-13 B	71HALW-16 B	71HALW-17 B	71HALW-20 B	71HALW-22 B	71HALW-23 B	71HALW-24 H
47.40	47.70	48.40	48.60	47.00	47.60	47.80	48.40	48.60	48.40	47.30	48.50	48.60
4.56	4.04	3.33	3.41	3.28	3.29	3.78	3.94	3.44	4.19	3.70	3.53	3.65
13.50	13.70	14.60	14.70	15.60	16.80	14.10	14.00	15.70	14.00	14.20	16.50	16.60
4.96	4.93	5.20	3.71	3.80	5.99	3.31	5.13	3.54	4.10	4.91	5.98	6.82
9.48	8.88	7.11	8.72	8.64	5.59	9.71	8.43	8.42	9.45	8.54	5.96	5.47
0.20	0.18	0.16	0.18	0.17	0.15	0.19	0.20	0.16	0.21	0.19	0.17	0.17
4.56	5.33	5.20	5.32	5.85	4.38	5.80	4.50	4.59	4.31	6.08	3.84	3.25
9.11	9.69	9.99	10.20	10.60	9.56	10.50	9.45	10.40	8.51	9.63	8.70	7.98
3.35	3.29	3.01	3.09	2.81	3.06	3.08	3.31	3.17	3.58	3.37	3.78	3.99
1.14	1.04	0.80	0.79	0.45	0.92	0.72	0.95	0.82	1.18	1.04	1.30	1.37
0.71	0.60	0.49	0.50	0.45	0.49	0.55	0.62	0.52	0.71	0.64	0.68	0.71
0.42	0.38	0.53	0.47	0.73	1.21	0.32	0.46	0.48	0.72	0.36	0.74	0.76
0.48	0.45	0.74	0.54	0.62	0.81	0.24	0.67	0.47	0.68	0.16	0.30	0.70
0.11	0.04	0.07	0.06	0.18	0.08	0.09	0.05	0.13	0.09	0.15	0.07	0.08
0.33	0.44	1.25	0.58	0.95	1.77	0.14	0.50	0.53	0.94	0.12	0.84	1.31
100.0	100.3	99.6	100.3	100.2	99.9	100.2	100.1	100.4	100.1	100.3	100.1	100.2

Table 2 (continued)

Late shield/postshield		Rejuvenated stage lavas (Subaerial)						Rejuvenated stage lavas (Submarine)			
70MOL-1C	70KHWE-1c	P252-2	74KAL-1	71KAUH-2	71KAUH-1	MOE2	80KAL-1	P253-12	P253-11B	P253-10A	P253-9
H	H	B	B	PB	Bas	Bas	B	B	PB	B	B
49.10	48.10	46.1	45.8	45.59	43.7	43.02	45.4	45.9	44.0	46.1	46.1
3.68	3.05	1.42	1.59	1.73	2.43	2.17	1.97	1.97	1.67	2.01	1.96
15.60	16.80	12.5	13.7	12.86	12.2	11.82	13.4	14.8	11.5	15.5	14.9
6.54	3.09	1.82	3.68	1.92	14.9	5.26	13.6	4.40	3.10	4.78	3.99
6.44	8.29	10.6	9.11	10.73	-	9.19	-	7.38	9.63	7.04	7.48
0.17	0.21	0.18	0.19	0.18	0.18	0.16	0.18	0.15	0.17	0.25	0.15
2.86	4.24	13.7	10.4	13.06	11.9	13.76	10.3	7.89	15.7	6.29	8.29
7.07	7.30	9.84	10.9	10.32	10.8	10.37	11.2	12.0	9.48	12.5	12.0
4.24	4.20	2.35	2.29	2.41	2.57	2.74	2.77	2.92	2.30	3.01	2.90
1.57	1.52	0.33	0.27	0.42	0.74	0.74	0.55	0.66	0.57	0.64	0.62
0.91	1.20	0.20	0.20	0.21	0.35	0.33	0.26	0.25	0.24	0.25	0.22
0.69	0.90	0.43	0.57	0.24		0.88		0.69	0.67	0.70	0.49
1.08	0.45	0.20	0.61	0.20		0.21		0.22	0.20	0.26	0.23
0.08	0.18	0.04	0.19	0.02							
1.43	1.54										
100.0	99.5	99.7	99.5	99.9	99.8	100.7	99.6	99.9	99.9	100.0	100.0

Table 3 Trace element contents (ppm) for East Molokai lavas

	Pelekunu Valley (Late shield/postshield)			Waikolu Valley (Late shield/postshield)			Water tunnel (Late shield/postshield)						
	71PELE-37	71PELE-19	71PELE-21	71WAIK-14F	71WAIK-10F	71WAIK-1	NE PORTAL	M5.3+375F	M5.3+40F	M5.1+10F	M4.9+300D	M4.6+150F	M4.6F
	PB	B	B	B	B	B	B	B	B	B	dike/Ben	B	B
Sc	30.0	32.1	31.5	30.3	33.0	28.6	28.7	30.7	24.7	26.1	4.18	27.6	29.1
Rb	7.45	3.20	2.10	3.47	5.58	3.88	9.79	5.83	6.95	13.3	48.7	5.57	14.6
Sr	319	358	349	396	311	498	475	419	353	469	1251	351	498
Y	29.1	33.5	35.3	32.6	36.2	34.6	37.3	33.3	27.8	37.1	46.4	18.9	37.4
Zr	118	187	191	190	170	227	244	187	162	231	546	120	257
Nb	12.4	14.8	14.4	15.1	12.7	21.2	19.5	14.5	12.9	20.0	85.2	10.5	23.8
Ba	112	80.8	89.1	85.9	72.4	181	150	110	102	165	784	96.5	196
La	15.0	12.8	12.5	13.1	11.3	18.2	17.9	13.2	11.8	18.2	67.1	9.63	20.5
Ce	27.0	31.8	32.0	34.0	29.0	45.2	45.4	34.7	29.5	45.4	146	23.9	51.7
Pr	4.82	5.01	5.13	5.21	4.54	6.72	6.67	5.31	4.47	6.71	18.2	3.56	7.54
Nd	22.2	23.8	24.2	24.4	21.8	30.5	31.5	25.0	21.2	30.2	72.5	16.6	34.4
Sm	5.38	6.41	6.71	6.47	6.05	7.59	8.11	6.84	5.58	7.90	14.2	4.21	8.42
Eu	1.91	2.20	2.31	2.21	2.07	2.50	2.63	2.27	1.85	2.57	4.31	1.44	2.71
Tb	0.860	1.10	1.17	1.08	1.13	1.17	1.28	1.12	0.92	1.23	1.66	0.65	1.28
Gd	5.78	6.82	7.10	6.79	6.70	7.61	8.06	7.05	5.74	7.92	11.55	4.23	8.35
Dy	4.66	6.11	6.44	5.83	6.33	6.34	6.97	6.11	5.04	6.73	8.56	3.58	6.85
Ho	0.872	1.16	1.23	1.11	1.23	1.17	1.32	1.16	0.96	1.26	1.54	0.65	1.28
Er	2.12	2.97	3.09	2.76	3.18	2.92	3.29	2.95	2.40	3.23	3.84	1.66	3.16
Tm	0.292	0.428	0.449	0.408	0.482	0.408	0.469	0.417	0.343	0.443	0.537	0.234	0.434
Yb	1.58	2.40	2.56	2.29	2.76	2.33	2.59	2.31	1.91	2.55	3.12	1.25	2.50
Lu	0.223	0.334	0.351	0.317	0.387	0.319	0.365	0.328	0.262	0.347	0.430	0.175	0.358
Hf	2.89	4.55	4.66	4.57	4.22	5.39	5.74	4.60	3.89	5.51	11.44	2.93	5.97
Ta	0.739	0.910	0.895	0.934	0.774	1.29	1.21	0.927	0.773	1.24	4.88	0.635	1.45
Pb	0.786	1.13	0.975	0.932	1.15	1.44	1.26	1.06	0.844	1.34	4.66	0.747	1.48
Th	0.805	0.880	0.913	0.946	0.770	1.35	1.23	0.931	0.770	1.30	5.92	0.670	1.56
U	0.295	0.264	0.283	0.251	0.242	0.273	0.399	0.269	0.957	0.990	0.982	0.204	0.496
Sc*	30.3	31.3	31.6	31.6		27.8	28.6	30.2	25.4	26.5	4.1	27.8	28.3
Cr*	1168	125	80	134		248	114	103	621	145	8.0	1072	63
Co*	83.8	43.8	44.1	45.2		46.7	38.3	42.8	63.7	39.7	6.1	65.4	42.4

* analyzed by INAA at MIT and all the other trace element data were obtained by ICP-MS at MIT following the procedure of *Huang and Frey* [2003]

Table 3 (continued)

Kalaupapa section											
(Late shield/postshield)											
69KLPA-1	69KLPA-2	69KLPA-5A	69KLPA-8B	69KLPA-9A	69KLPA-14A	69KLPA-16A	69KLPA-17A	69KLPA-27	69KLPA-30	69KLPA-32	69KLPA-33
B	PB	B	B	B	B	B	B	B	B	B	M
27.9	28.4	26.0	26.9	25.4	27.9	26.1	27.0	27.5	19.7	26.8	9.6
7.88	0.78	0.50	1.24	0.93	2.09	11.6	11.3	6.08	16.7	10.4	41.7
460	421	320	403	388	492	499	426	487	731	396	971
33.0	23.8	20.1	31.8	29.4	36.8	26.5	32.3	34.5	39.5	32.7	100.2
214	154	126	146	145	229	203	184	190	297	182	527
19.4	15.4	10.4	14.2	14.0	22.1	23.0	21.7	19.6	33.5	19.8	66.5
163	121	81.4	119	115	185	218	192	197	315	177	669
17.0	11.5	9.84	13.3	12.5	24.2	19.7	23.8	21.5	31.8	18.8	66.9
41.4	28.7	23.9	29.2	29.0	48.5	47.1	40.4	42.1	68.4	39.9	127
6.26	4.32	3.80	4.68	4.66	7.98	6.69	7.29	6.98	10.1	6.21	19.6
28.6	20.3	17.7	22.6	21.7	35.3	29.2	32.2	31.3	44.3	27.9	85.5
7.21	5.20	4.55	5.64	5.50	8.28	6.81	7.21	7.36	10.0	6.45	17.8
2.33	1.78	1.51	1.91	1.87	2.67	2.18	2.34	2.41	3.21	2.05	5.56
1.12	0.835	0.714	0.906	0.862	1.26	0.966	1.03	1.07	1.39	0.946	2.39
7.20	5.29	4.57	6.06	5.78	8.22	6.40	7.06	7.21	9.30	6.34	17.10
6.03	4.50	3.84	4.77	4.76	6.68	5.08	5.50	5.80	7.22	4.90	12.64
1.15	0.85	0.72	0.93	0.92	1.24	0.93	1.00	1.10	1.36	0.93	2.58
2.77	2.07	1.76	2.34	2.24	3.12	2.22	2.36	2.69	3.25	2.28	6.72
0.383	0.292	0.233	0.317	0.307	0.411	0.296	0.317	0.348	0.427	0.313	0.948
2.24	1.62	1.39	1.82	1.78	2.36	1.71	1.79	2.04	2.53	1.72	5.35
0.311	0.228	0.192	0.261	0.257	0.340	0.234	0.246	0.283	0.347	0.239	0.846
5.02	3.67	3.11	3.48	3.44	5.36	4.70	4.34	4.48	6.71	4.23	10.85
1.17	0.958	0.662	0.860	0.854	1.35	1.44	1.32	1.22	2.05	1.20	3.89
1.41	0.861	0.731	0.881	0.913	1.35	1.34	1.10	1.28	1.90	1.10	3.96
1.23	0.857	0.672	0.888	0.872	1.48	1.54	1.36	1.29	2.24	1.20	4.94
0.399	0.169	0.162	0.192	0.192	0.257	0.331	0.428	0.419	0.370	0.401	1.54
27.8	29.3	26.3	27.7	27.2	25.56	27.2	27.3	28.6	21.4	28.9	9.2
388	678	1031	827	804	320	696	731	553	67	743	19.9
57	66	79	72	74.2	56.5	67.6	69.6	64	33	69	18.5

Table 3 (continued)

Halawa Valley (Late shield/postshield)								(Late shield /postshield)	Rejuvenated stage lavas (Subaerial)			
71HALW-6	71HALW-4	70HALW-1	70HALW-4	71HALW-9	71HALW-13	71HALW-17	71HALW-22	70KAWE-1c	P252-2	74KAL-1	71KAUH-2	71KAUH-1
B	B	B	B	B	B	B	B	H	B	B	PB	Bas
25.5	28.2	28.1	23.3	25.3	26.6	23.4	25.5	10.8	24.7	26.7	25.5	23.5
11.7	8.82	6.63	18.1	11.5	7.07	9.17	19.3	29.7	6.76	2.68	9.00	15.6
540	481	483	618	549	539	610	641	1283	274	322	331	533
36.2	31.0	31.7	43.0	50.5	43.9	45.4	47.8	47.0	19.8	20.2	21.2	21.9
227	198	201	326	260	280	269	308	362	70.6	69.5	94.0	140
19.6	17.7	19.5	31.4	24.8	27.3	27.7	32.8	56.4	13.3	13.8	18.5	31.0
173	141	164	269	230	239	239	290	546	159	176	220	433
18.1	15.8	17.1	27.4	36.6	25.7	28.4	28.6	48.6	11.0	12.7	14.1	22.9
42.9	39.1	41.0	67.2	58.6	59.2	61.0	68.0	103	23.6	25.9	29.7	47.7
6.59	5.85	6.23	9.63	10.7	8.85	9.82	9.72	14.9	3.09	3.51	3.95	6.22
30.5	26.5	28.5	42.7	47.5	39.7	44.1	42.9	63.7	13.4	15.0	17.0	26.2
7.61	6.63	7.00	10.1	10.8	9.56	10.2	10.1	13.5	3.35	3.71	4.11	5.89
2.52	2.18	2.33	3.21	3.46	3.05	3.29	3.17	4.34	1.17	1.30	1.42	1.96
1.20	1.04	1.08	1.49	1.64	1.43	1.50	1.46	1.73	0.610	0.650	0.683	0.834
7.73	6.59	6.90	9.68	11.00	9.47	10.07	9.75	11.91	3.73	4.04	4.30	5.65
6.50	5.65	5.84	7.88	8.76	7.64	7.95	7.75	8.85	3.52	3.68	3.80	4.29
1.21	1.08	1.11	1.48	1.63	1.45	1.48	1.51	1.58	0.692	0.725	0.727	0.768
3.06	2.68	2.75	3.62	3.82	3.47	3.50	3.75	3.82	1.77	1.86	1.82	1.86
0.410	0.359	0.371	0.488	0.541	0.510	0.507	0.498	0.501	0.264	0.267	0.266	0.255
2.39	2.10	2.19	2.87	2.96	2.78	2.78	2.86	2.95	1.46	1.50	1.48	1.37
0.339	0.297	0.305	0.408	0.410	0.389	0.382	0.412	0.414	0.211	0.214	0.212	0.191
5.37	4.72	4.91	7.37	5.94	6.49	6.10	7.11	7.83	1.89	1.87	2.36	3.53
1.21	1.09	1.21	1.90	1.47	1.64	1.63	1.99	3.28	0.764	0.725	0.991	1.70
1.40	1.12	1.24	1.72	2.31	1.64	1.63	1.86	2.83	0.812	0.850	0.991	1.49
1.26	1.14	1.28	2.11	1.56	1.77	1.77	2.27	3.82	1.12	1.23	1.39	2.44
0.457	0.355	0.347	0.674	0.480	0.505	0.538	0.515	1.16	0.395	0.209	0.324	0.663
23.7	27.3	28.9	22.7	25.5	27.4	23.7				27.4	27.8	
107	93	172	52	116	140	96				537	578	
53.1	40	44.9	34.6	41.5	41.6	36.2				54	63	

Table 3 (continued)

Rejuvenated stage lavas (Submarine)			
P253-12 B	P253-11B PB	P253-10A B	P253-9 B
29.2	23.7	30.0	28.9
11.1	8.95	11.2	10.5
352	305	373	345
23.4	18.7	24.2	23.5
102	88.6	105	101
19.7	17.5	20.1	19.5
231	205	225	234
13.6	12.2	14.0	13.6
29.6	26.3	30.4	29.3
3.97	3.48	4.06	3.94
17.3	15.2	17.7	17.4
4.26	3.69	4.36	4.27
1.48	1.26	1.52	1.48
0.749	0.615	0.766	0.752
4.67	3.90	4.74	4.62
4.22	3.43	4.31	4.27
0.816	0.661	0.839	0.820
2.10	1.68	2.13	2.10
0.305	0.245	0.315	0.309
1.71	1.36	1.72	1.72
0.240	0.194	0.240	0.243
2.68	2.33	2.76	2.66
1.14	1.06	1.16	1.14
1.00	0.891	1.13	1.02
1.40	1.29	1.42	1.41
0.656	0.578	0.517	0.498

Table 4. Sr, Nd and Pb isotopic compositions for East Molokai lavas

Sample	$^{87}Sr/^{86}Sr$	2σ	$^{143}Nd/^{144}Nd$	2σ	$^{206}Pb/^{204}Pb$	2σ	$^{207}Pb/^{204}Pb$	2σ	$^{208}Pb/^{204}Pb$	2σ
Late shield/postshield lavas										
71PELE-19	0.703548	7	0.513017	5	18.5320	63	15.4782	43	38.0378	131
71PELE-19*					18.5566	14	15.4834	13	38.0475	32
71PELE-21	0.703524	7	0.513029	10	18.5325	9	15.4815	8	38.0418	20
71PELE-21*					18.5300	15	15.4792	12	38.0300	37
71WAIK-14F	0.703527	9	0.513015	11	18.5412	43	15.4965	39	38.0761	107
71WAIK-10F	0.703542	8	0.513039	5	18.5316	10	15.4816	9	38.0559	22
NE Portal	0.703564	8			18.5106	11	15.5027	9	38.0541	22
MT 5.3+375F	0.703572	7	0.513021	6	18.4945	11	15.4942	9	38.0259	24
MT 4.6F	0.703521	8	0.513006	6	18.4897	9	15.4929	8	38.0386	28
69KLPA-1	0.703558	7	0.512997	5						
69KLPA-2	0.703498	7	0.513019	5	18.4232	11	15.4822	9	37.9557	26
69KLPA-5A	0.703582	7	0.512974	8	18.4339	9	15.4948	8	37.9680	21
69KLPA-5A*	0.703576	6	0.512991	6						
69KLPA-5A UL	0.703626	8	0.512992	5						
69KLPA-8B	0.703496	7	0.513008	5	18.4196	18	15.4860	15	37.9567	41
69KLPA-8B*	0.703506	7	0.513022	5						
69KLPA-9A	0.703499	8	0.513016	5	18.4262	15	15.4874	13	37.9662	32
69KLPA-14A	0.703501	8	0.513023	6	18.4357	14	15.4868	11	37.9651	29
69KLPA-16A	0.703346	6	0.513021	7	18.3867	10	15.4812	7	37.9377	19
69KLPA-27	0.703456	7	0.513019	5						
69KLPA-30	0.703437	8	0.513022	5						
69KLPA-32	0.703472	8	0.513003	10						
69KLPA-33	0.703393	7	0.513018	6						
71HALW-4	0.703498	7	0.513012	6	18.4568	13	15.4840	12	37.9827	30
71HALW-13	0.703528	7			18.4631	12	15.4880	11	38.0045	28
Rejuvenated stage lavas										
P252-2	0.703146	7	0.513063	7	18.1974	15	15.4502	14	37.7777	42
P252-2*					18.1984	15	15.4452	14	37.7595	34
P252-2 UL					18.2380	13	15.4604	10	37.8132	30
74KAL-1	0.703154	8	0.513068	7	18.1742	130	15.4411	110	37.7357	274
P253-12	0.703172	7	0.513072	6	18.1737	19	15.4496	16	37.7601	39
P253-11B	0.703164	7	0.513064	5	18.1572	31	15.4501	25	37.7486	69
P253-9	0.703181	7	0.513057	6	18.1955	57	15.4601	58	37.7846	134

* Duplicate analysis of separate aliquot. Figures show data with the lowest uncertainty.

UL All samples were acid-leached (see text) except for two analyses with UL suffix. For these samples acid-leaching lowered Sr and Pb isotopic ratios but did not change the Nd ratios

2σ applies to last decimal place (s).

Sr data were normalized to $^{86}Sr/^{88}Sr=0.1194$ and Nd were normalized to $^{146}Nd/^{144}Nd=0.7219$. Mean measured $^{87}Sr/^{86}Sr$ for NBS 987 standard during the course of study was 0.710260 ± 13 (2σ, n=42) and $^{143}Nd/^{144}Nd$ for La Jolla standard was 0.511858 ± 7 (2σ, n=18). The external reproducibility for $^{87}Sr/^{86}Sr$ and $^{143}Nd/^{144}Nd$ based on two duplicates are better than 10×10^{-6} and 17×10^{-6}, respectively, i.e., within or slightly larger than the machine in-run uncertainties. Pb isotopic ratios were corrected for instrumental mass fractionation by adding a Tl spike and using a $^{205}Tl/^{203}Tl$ of 2.3885. Mean measured $^{206}Pb/^{204}Pb$, $^{207}Pb/^{204}Pb$ and $^{208}Pb/^{204}Pb$ for NBS 981 Pb standard were 16.9418 ± 21 (2σ, n=105), 15.4979 ± 25 (2σ, n=105) and 36.7184 ± 61 (2σ, n=105), respectively. These numbers are in agreement, within errors, with TIMS triple-spike values [*Galer and Abouchami*, 1998]. The external reproducibility for $^{206}Pb/^{204}Pb$, $^{207}Pb/^{204}Pb$ and $^{208}Pb/^{204}Pb$ are better than 0.01%, 0.03% and 0.05%, respectively.

Table A1 Location for Water Tunnel samples

Sample	distance from SW Portal (km)
M1.3F	1.96
M1.5F	2.26
M2.5F	3.76
M3.3F	4.96
M3.9F	5.87
M4.1F	6.17
M4.3F	6.47
M4.3+1F	6.47
M4.6F	6.92
M4.6+150F	6.97
M4.9+300D (dike)	7.46
M5.1+10F	7.68
M5.3+40F	7.99
M5.3+375F	8.09
M5.4+50F	8.14
NE Portal	8.17

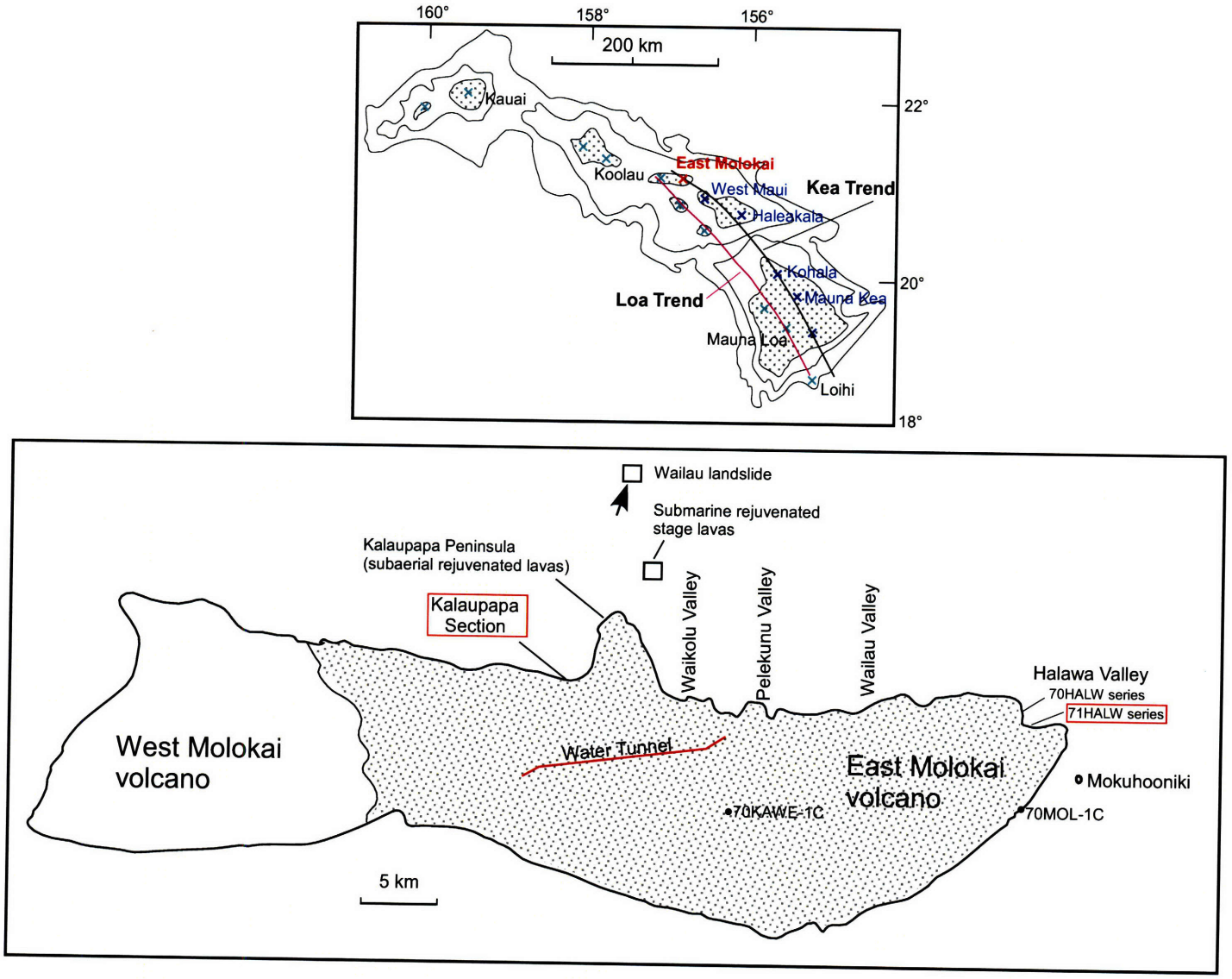
160°
158°
156°
200 km
22°
20°
18°
Kauai
Koolau
East Molokai
West Maui
Kea Trend
Haleakala
Kohala
Mauna Kea
Loa Trend
Mauna Loa
Loihi
Wailau landslide
Submarine rejuvenated stage lavas
Kalaupapa Peninsula (subaerial rejuvenated lavas)
Kalaupapa Section
Waikolu Valley
Pelekunu Valley
Wailau Valley
Halawa Valley
70HALW series
71HALW series
West Molokai volcano
Water Tunnel
East Molokai volcano
Mokuhooniki
70KAWE-1C
70MOL-1C
5 km

Fig. 1

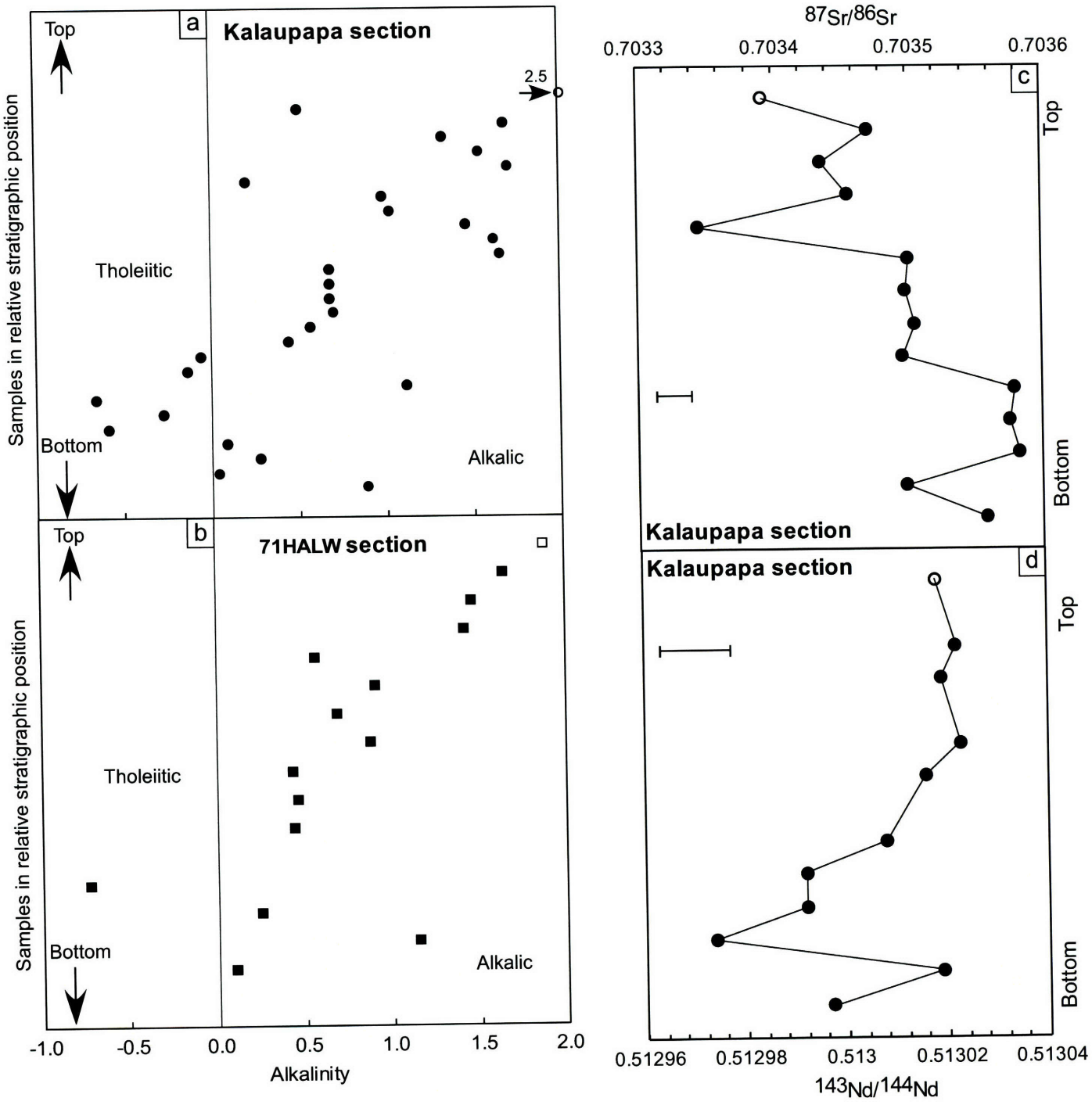
a
Kalaupapa section
Top
Bottom
Tholeiitic
Alkalic
2.5
Samples in relative stratigraphic position
b
71HALW section
Top
Bottom
Tholeiitic
Alkalic
Samples in relative stratigraphic position
-1.0
-0.5
0.0
0.5
1.0
1.5
2.0
Alkalinity
87Sr/86Sr
0.7033
0.7034
0.7035
0.7036
c
Top
Bottom
Kalaupapa section
d
Kalaupapa section
Top
Bottom
0.51296
0.51298
0.513
0.51302
0.51304
143Nd/144Nd

Fig. 2

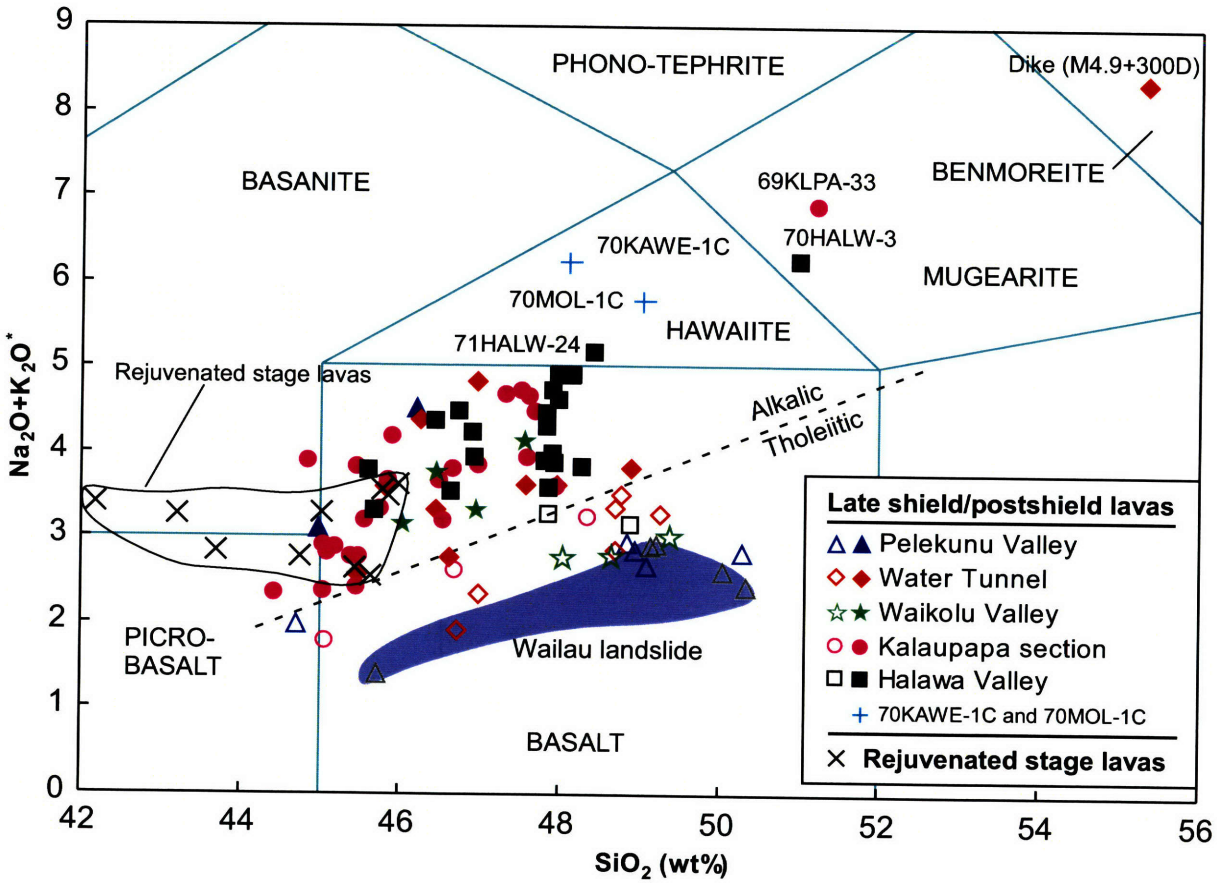
PHONO-TEPHRITE
Dike (M4.9+300D)
BASANITE
69KLPA-33
BENMOREITE
70KAWE-1C
70HALW-3
MUGEARITE
70MOL-1C
HAWAIITE
71HALW-24
Rejuvenated stage lavas
Alkalic
Tholeiitic
PICRO-
BASALT
Wailau landslide
BASALT
Late shield/postshield lavas
Pelekunu Valley
Water Tunnel
Waikolu Valley
Kalaupapa section
Halawa Valley
70KAWE-1C and 70MOL-1C
Rejuvenated stage lavas
$Na_2O+K_2O^*$
SiO_2 (wt%)
0
1
2
3
4
5
6
7
8
9
42
44
46
48
50
52
54
56

Fig. 3

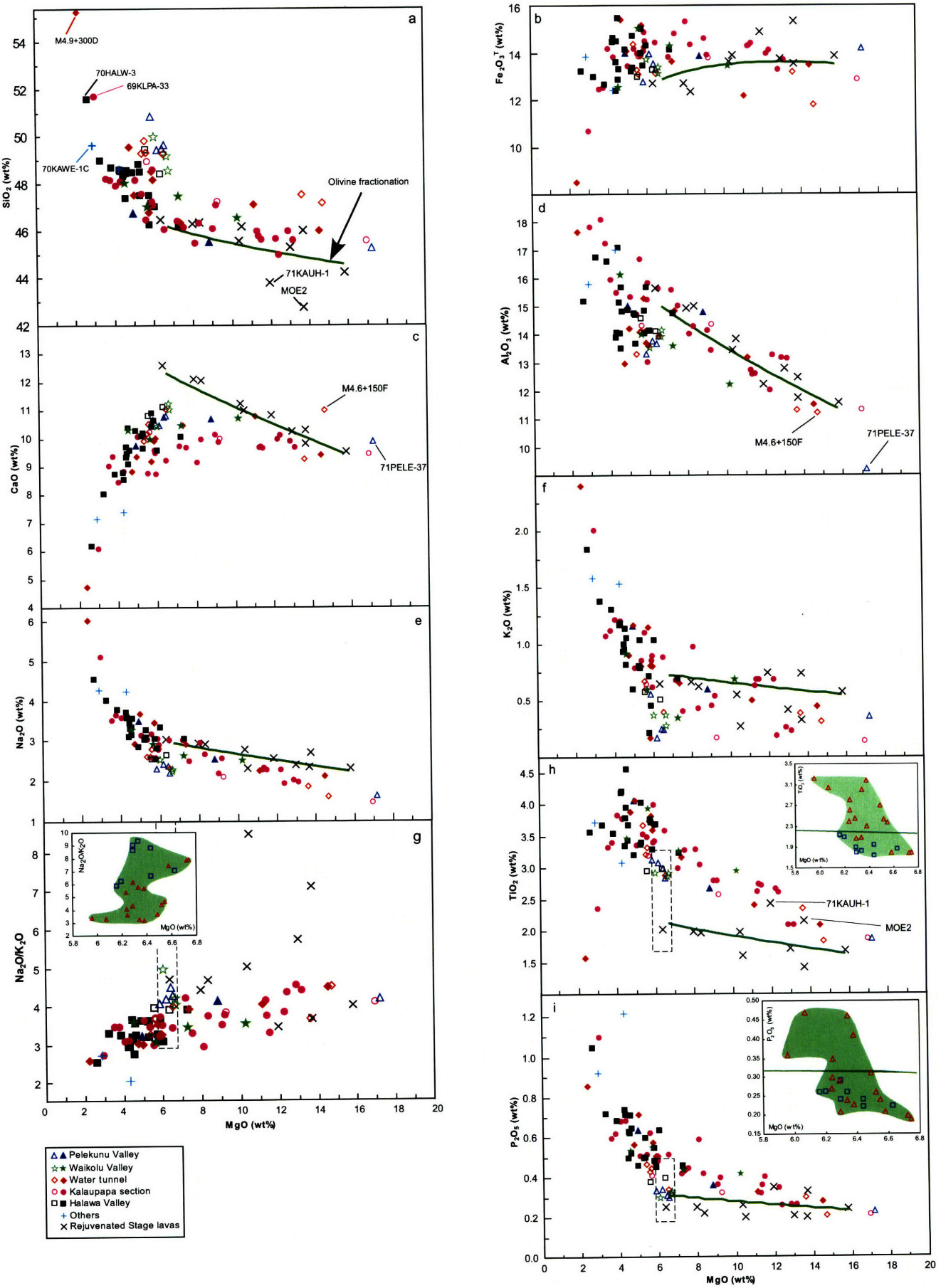
a
M4.9+300D
70HALW-3
69KLPA-33
70KAWE-1C
Olivine fractionation
71KAUH-1
MOE2
SiO2 (wt%)
b
Fe2O3T (wt%)
c
M4.6+150F
71PELE-37
CaO (wt%)
d
Al2O3 (wt%)
e
Na2O (wt%)
f
K2O (wt%)
g
Na2O/K2O
h
TiO2 (wt%)
i
P2O5 (wt%)
MgO (wt%)
Pelekunu Valley
Waikolu Valley
Water tunnel
Kalaupapa section
Halawa Valley
Others
Rejuvenated Stage lavas

Fig. 4

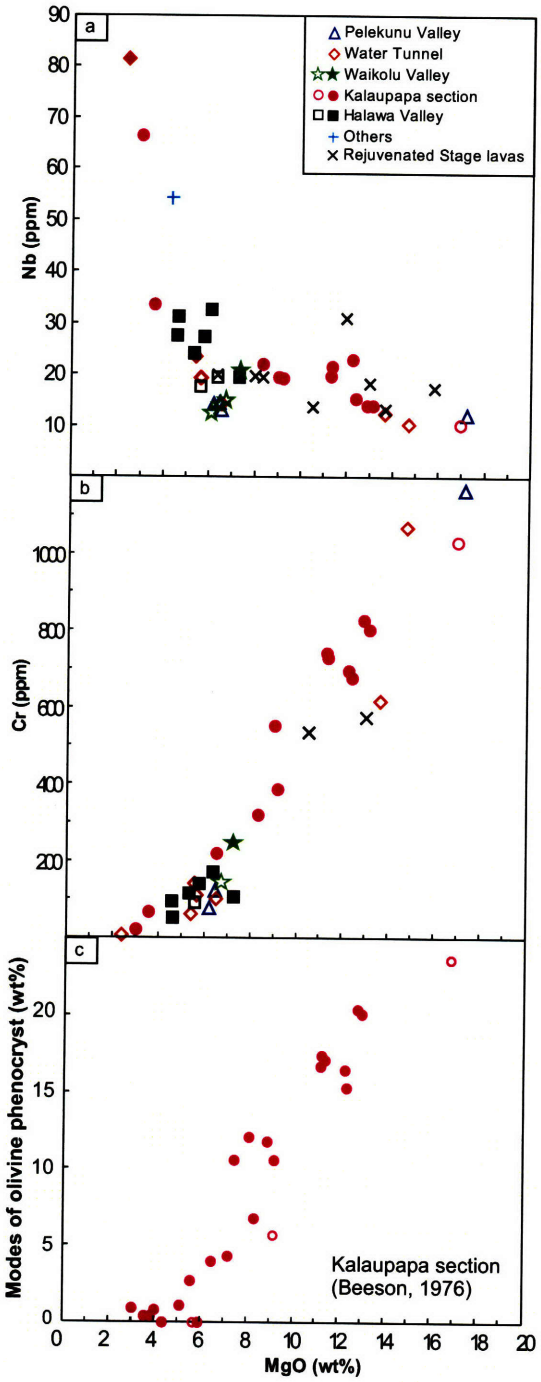
a
b
c
Pelekunu Valley
Water Tunnel
Waikolu Valley
Kalaupapa section
Halawa Valley
Others
Rejuvenated Stage lavas
Nb (ppm)
Cr (ppm)
Modes of olivine phenocryst (wt%)
MgO (wt%)
Kalaupapa section
(Beeson, 1976)

Fig 5

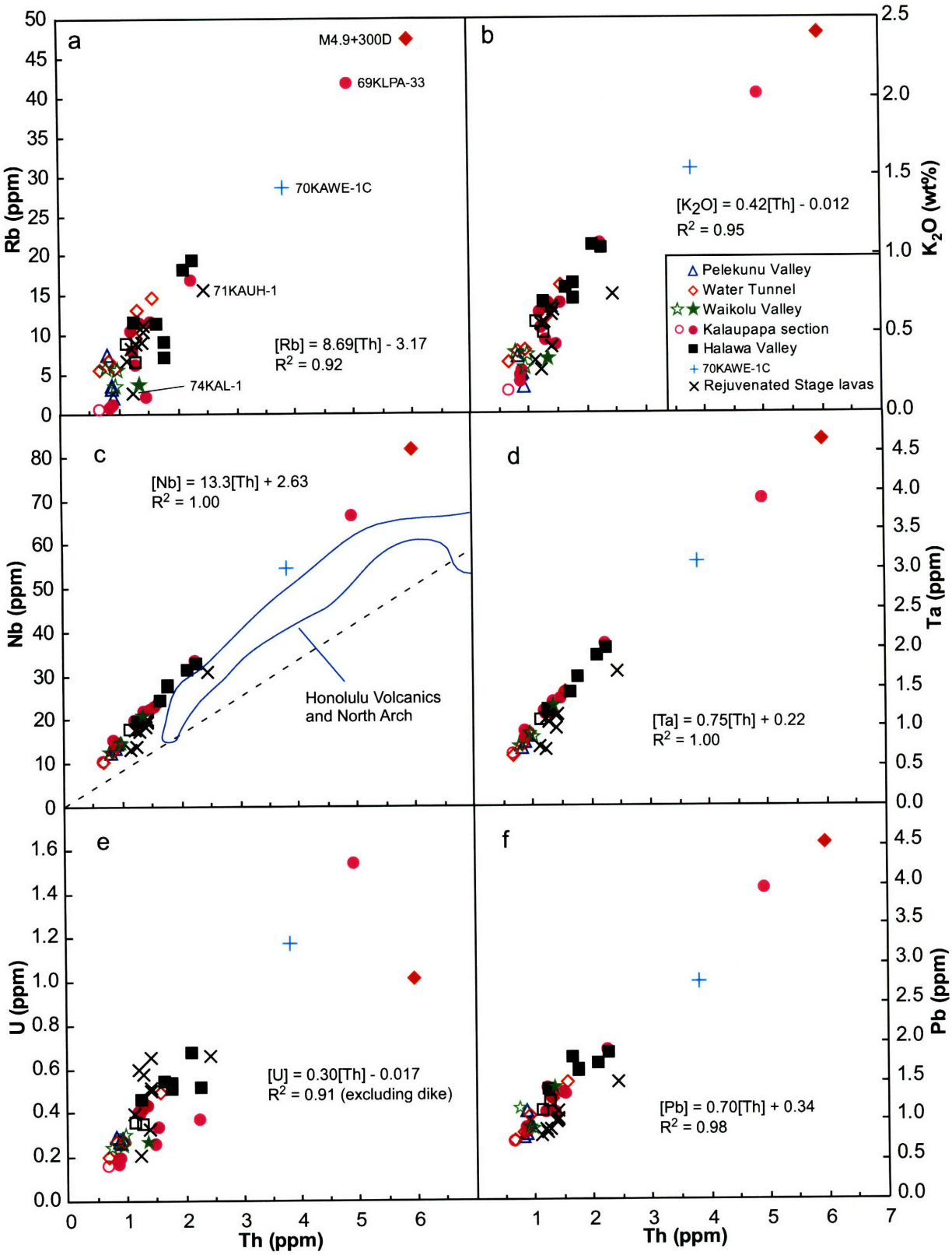
a
M4.9+300D
69KLPA-33
70KAWE-1C
71KAUH-1
74KAL-1
[Rb] = 8.69[Th] - 3.17
R2 = 0.92
Rb (ppm)
b
[K2O] = 0.42[Th] - 0.012
R2 = 0.95
Pelekunu Valley
Water Tunnel
Waikolu Valley
Kalaupapa section
Halawa Valley
70KAWE-1C
Rejuvenated Stage lavas
K2O (wt%)
c
[Nb] = 13.3[Th] + 2.63
R2 = 1.00
Honolulu Volcanics
and North Arch
Nb (ppm)
d
[Ta] = 0.75[Th] + 0.22
R2 = 1.00
Ta (ppm)
e
[U] = 0.30[Th] - 0.017
R2 = 0.91 (excluding dike)
U (ppm)
f
[Pb] = 0.70[Th] + 0.34
R2 = 0.98
Pb (ppm)
Th (ppm)
Th (ppm)

Fig. 6

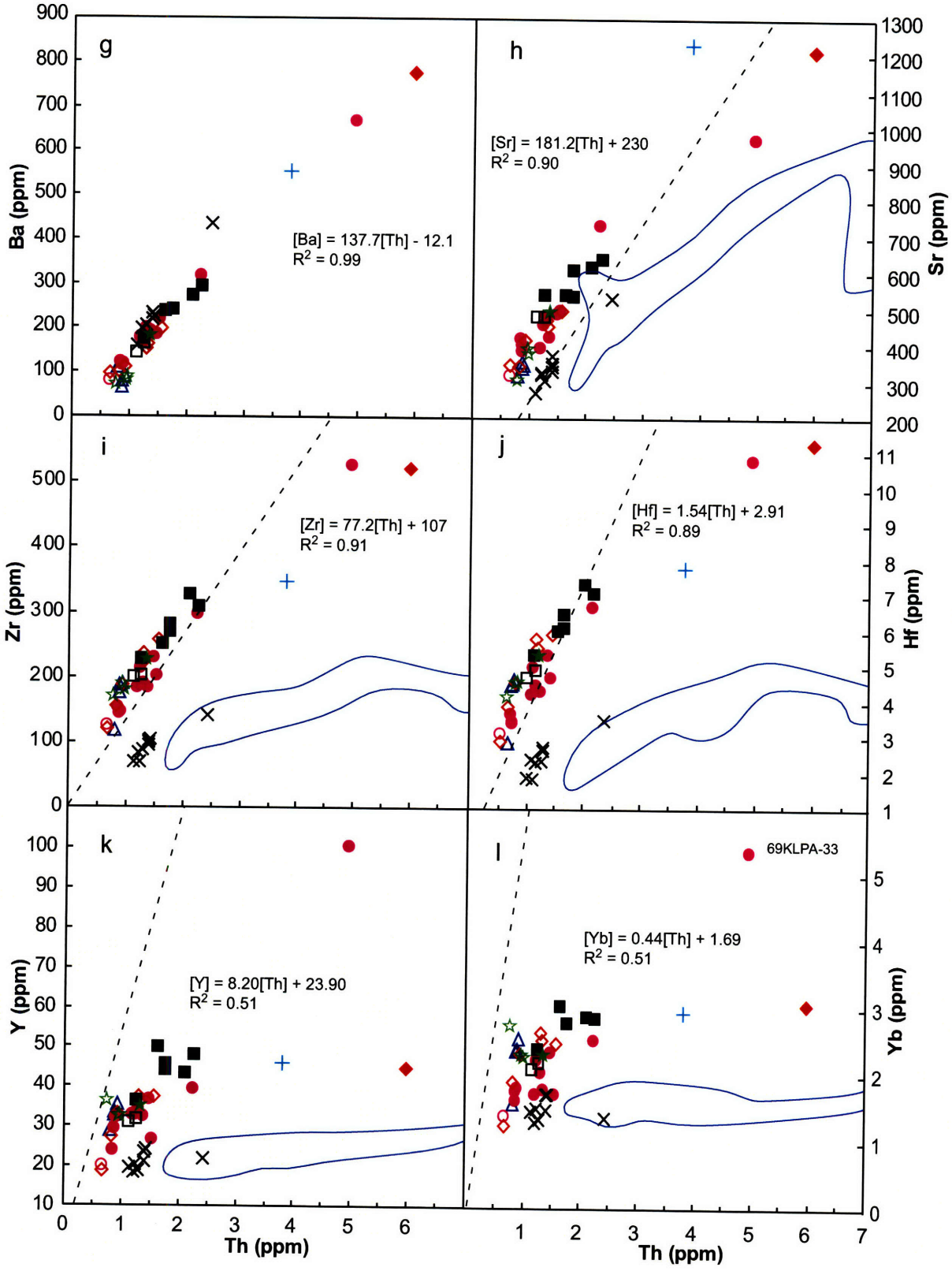

Fig. 6 (continued)

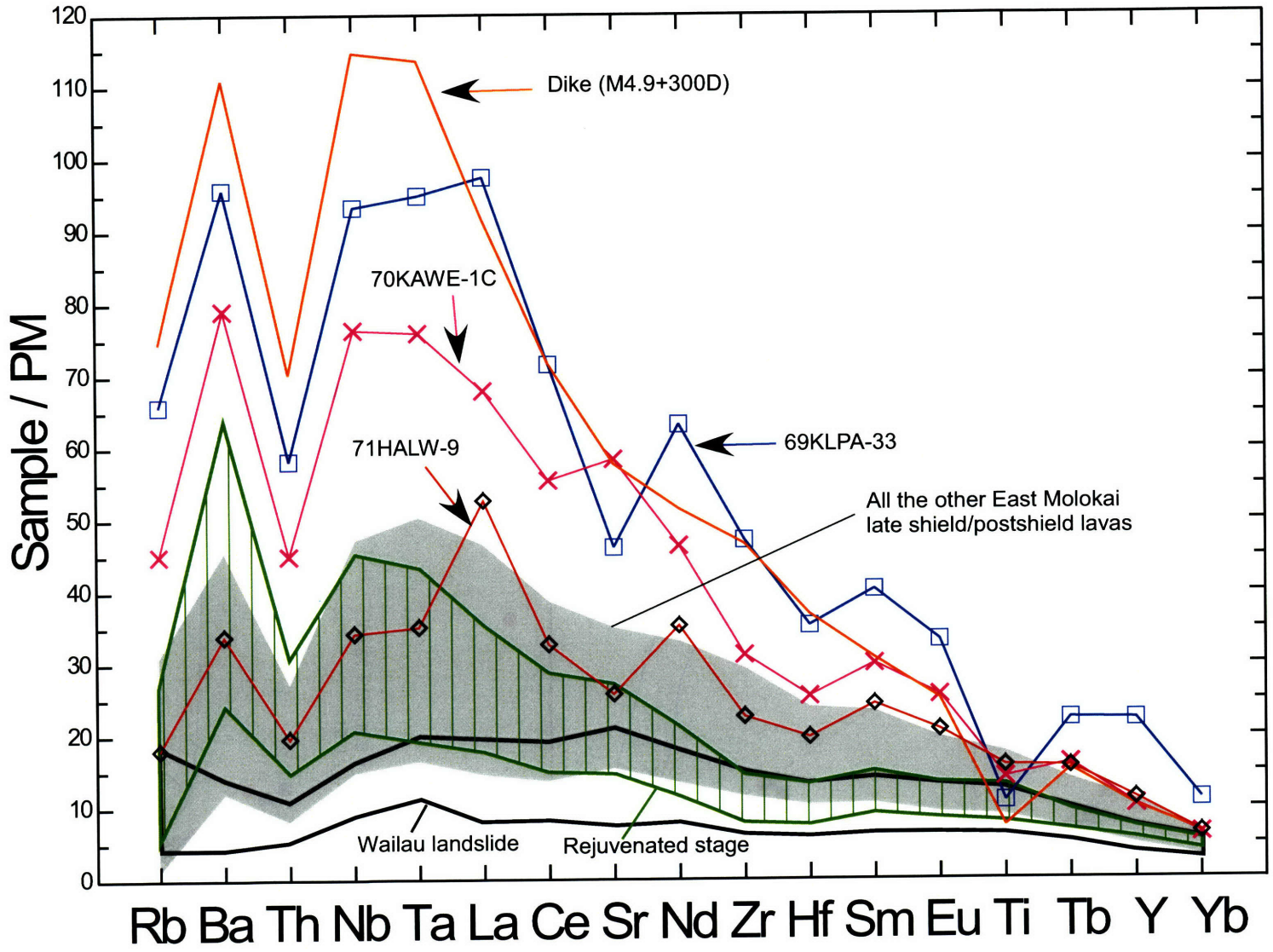
Sample / PM
120
110
100
90
80
70
60
50
40
30
20
10
0
Dike (M4.9+300D)
70KAWE-1C
71HALW-9
69KLPA-33
All the other East Molokai
late shield/postshield lavas
Wailau landslide
Rejuvenated stage
Rb Ba Th Nb Ta La Ce Sr Nd Zr Hf Sm Eu Ti Tb Y Yb

Fig. 7

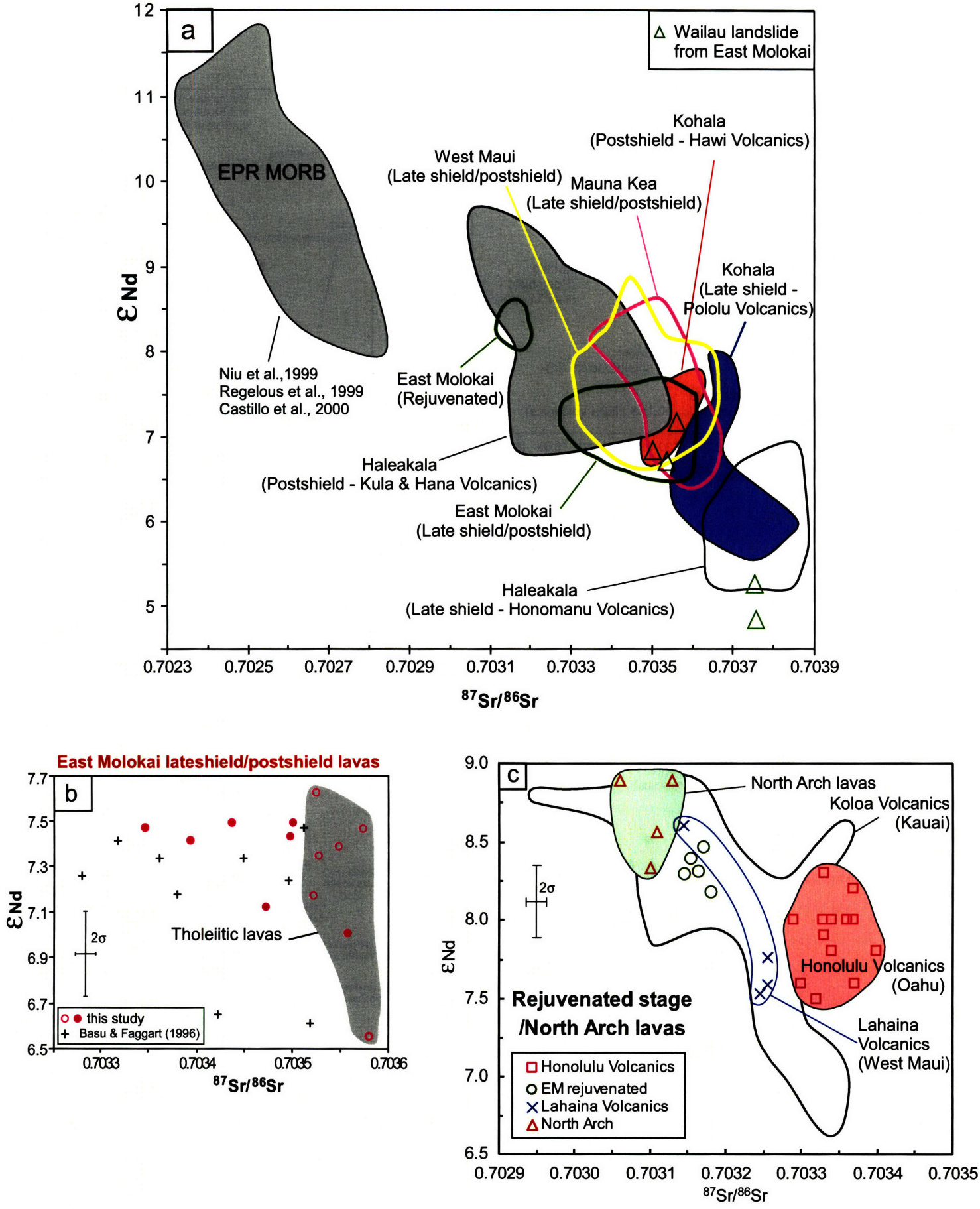
a
Wailau landslide from East Molokai
EPR MORB
Niu et al.,1999
Regelous et al., 1999
Castillo et al., 2000
West Maui
(Late shield/postshield)
Mauna Kea
(Late shield/postshield)
Kohala
(Postshield - Hawi Volcanics)
Kohala
(Late shield - Pololu Volcanics)
East Molokai
(Rejuvenated)
Haleakala
(Postshield - Kula & Hana Volcanics)
East Molokai
(Late shield/postshield)
Haleakala
(Late shield - Honomanu Volcanics)
εNd
87Sr/86Sr
East Molokai lateshield/postshield lavas
b
Tholeiitic lavas
2σ
this study
Basu & Faggart (1996)
c
North Arch lavas
Koloa Volcanics
(Kauai)
Honolulu Volcanics
(Oahu)
Lahaina
Volcanics
(West Maui)
Rejuvenated stage
/North Arch lavas
Honolulu Volcanics
EM rejuvenated
Lahaina Volcanics
North Arch

Fig. 8

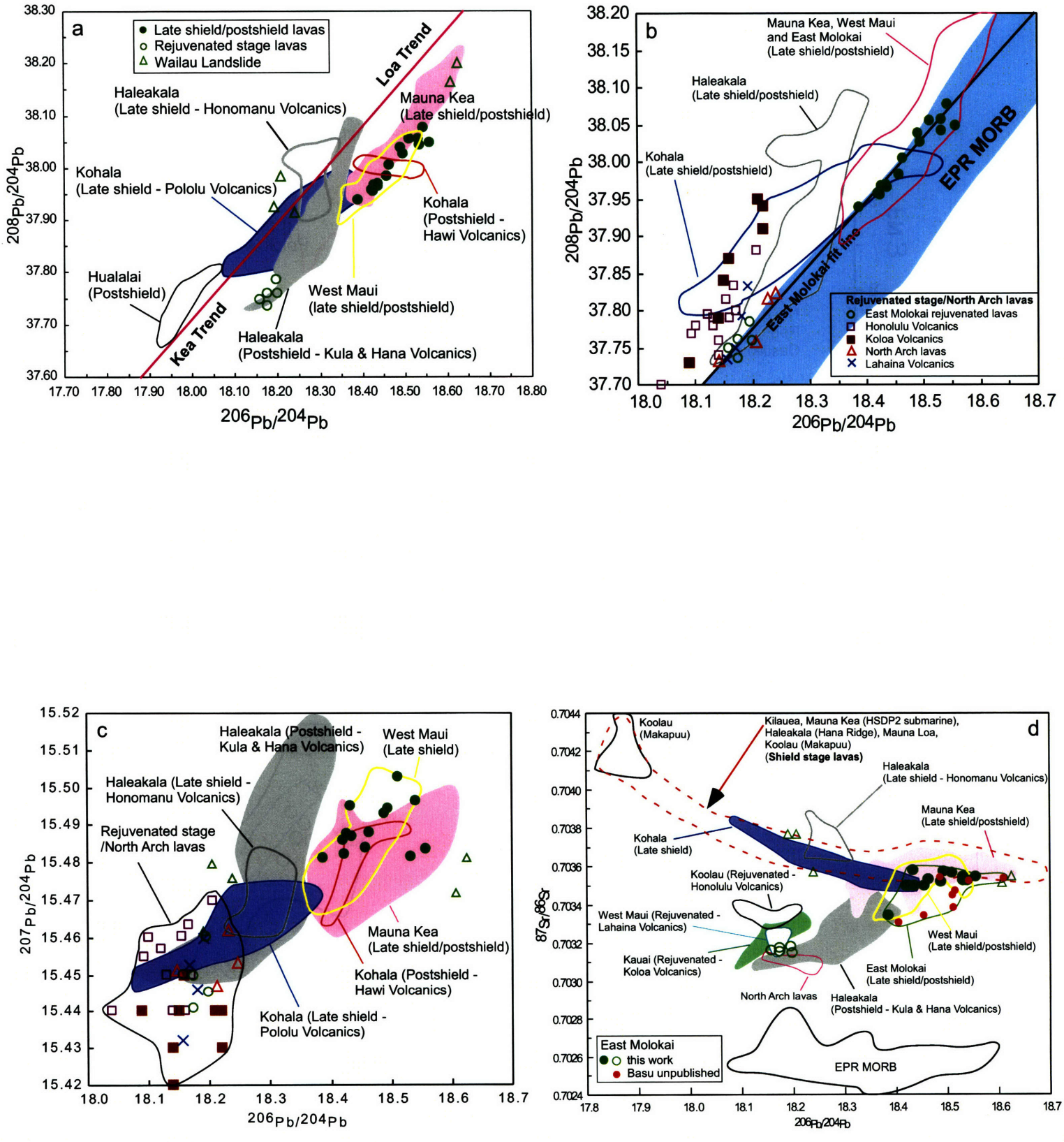
a
Late shield/postshield lavas
Rejuvenated stage lavas
Wailau Landslide
Loa Trend
Kea Trend
Haleakala
(Late shield - Honomanu Volcanics)
Mauna Kea
(Late shield/postshield)
Kohala
(Late shield - Pololu Volcanics)
Kohala
(Postshield -
Hawi Volcanics)
Hualalai
(Postshield)
West Maui
(late shield/postshield)
Haleakala
(Postshield - Kula & Hana Volcanics)
208Pb/204Pb
206Pb/204Pb
b
Mauna Kea, West Maui
and East Molokai
(Late shield/postshield)
Haleakala
(Late shield/postshield)
Kohala
(Late shield/postshield)
EPR MORB
East Molokai fit line
Rejuvenated stage/North Arch lavas
East Molokai rejuvenated lavas
Honolulu Volcanics
Koloa Volcanics
North Arch lavas
Lahaina Volcanics
208Pb/204Pb
206Pb/204Pb
c
Haleakala (Postshield -
Kula & Hana Volcanics)
West Maui
(Late shield)
Haleakala (Late shield -
Honomanu Volcanics)
Rejuvenated stage
/North Arch lavas
Mauna Kea
(Late shield/postshield)
Kohala (Postshield -
Hawi Volcanics)
Kohala (Late shield -
Pololu Volcanics)
207Pb/204Pb
206Pb/204Pb
d
Koolau
(Makapuu)
Kilauea, Mauna Kea (HSDP2 submarine),
Haleakala (Hana Ridge), Mauna Loa,
Koolau (Makapuu)
(Shield stage lavas)
Haleakala
(Late shield - Honomanu Volcanics)
Mauna Kea
(Late shield/postshield)
Kohala
(Late shield)
Koolau (Rejuvenated -
Honolulu Volcanics)
West Maui (Rejuvenated -
Lahaina Volcanics)
Kauai (Rejuvenated -
Koloa Volcanics)
West Maui
(Late shield/postshield)
East Molokai
(Late shield/postshield)
North Arch lavas
Haleakala
(Postshield - Kula & Hana Volcanics)
East Molokai
this work
Basu unpublished
EPR MORB
87Sr/86Sr
206Pb/204Pb

Fig. 9

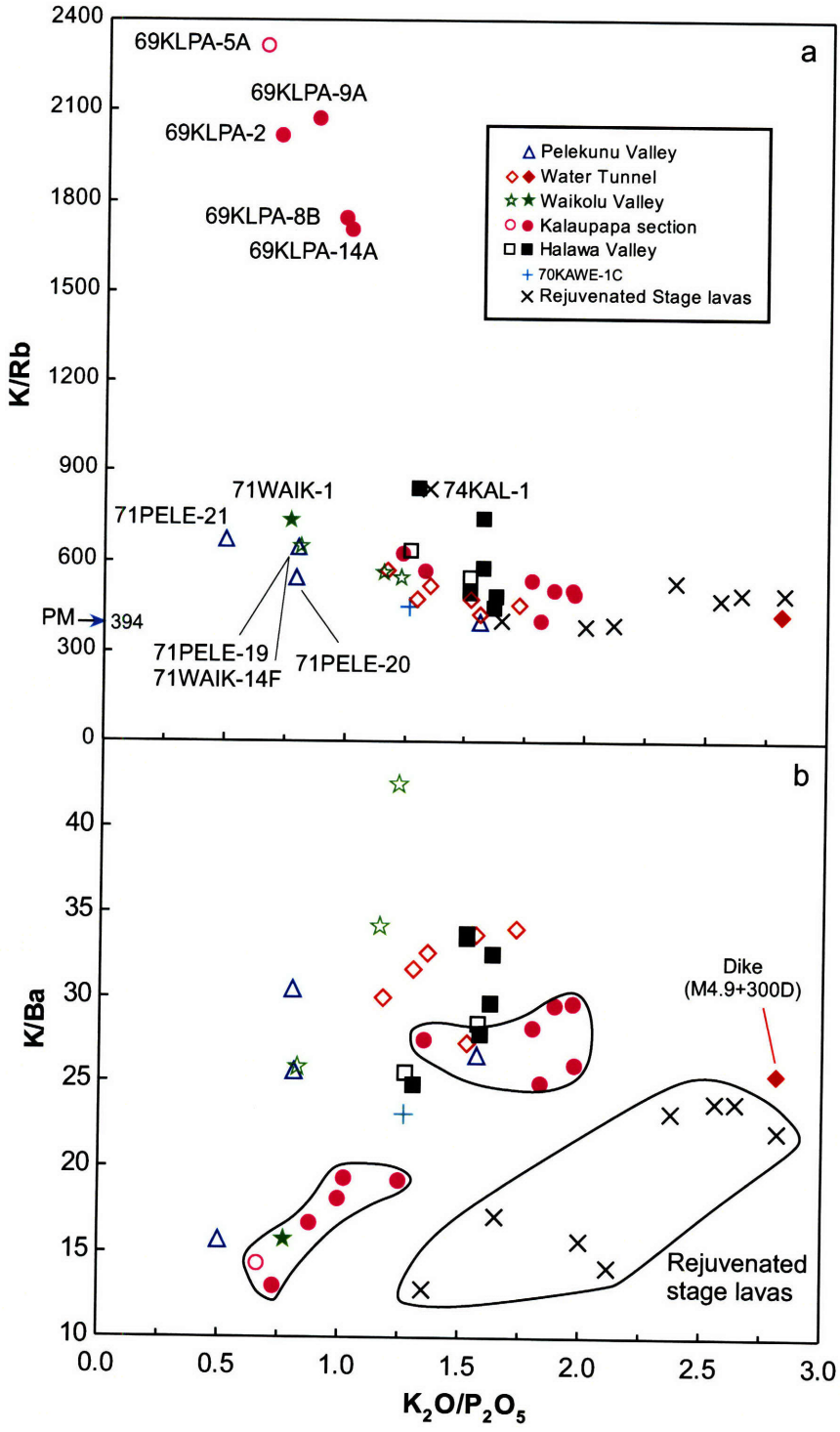
a
b
69KLPA-5A
69KLPA-9A
69KLPA-2
69KLPA-8B
69KLPA-14A
71WAIK-1
74KAL-1
71PELE-21
71PELE-19
71WAIK-14F
71PELE-20
PM
394
Pelekunu Valley
Water Tunnel
Waikolu Valley
Kalaupapa section
Halawa Valley
70KAWE-1C
Rejuvenated Stage lavas
Dike
(M4.9+300D)
Rejuvenated
stage lavas
K/Rb
K/Ba
K_2O/P_2O_5
2400
2100
1800
1500
1200
900
600
300
0
40
35
30
25
20
15
10
0.0
0.5
1.0
1.5
2.0
2.5
3.0

Fig. 10

Fig. 11

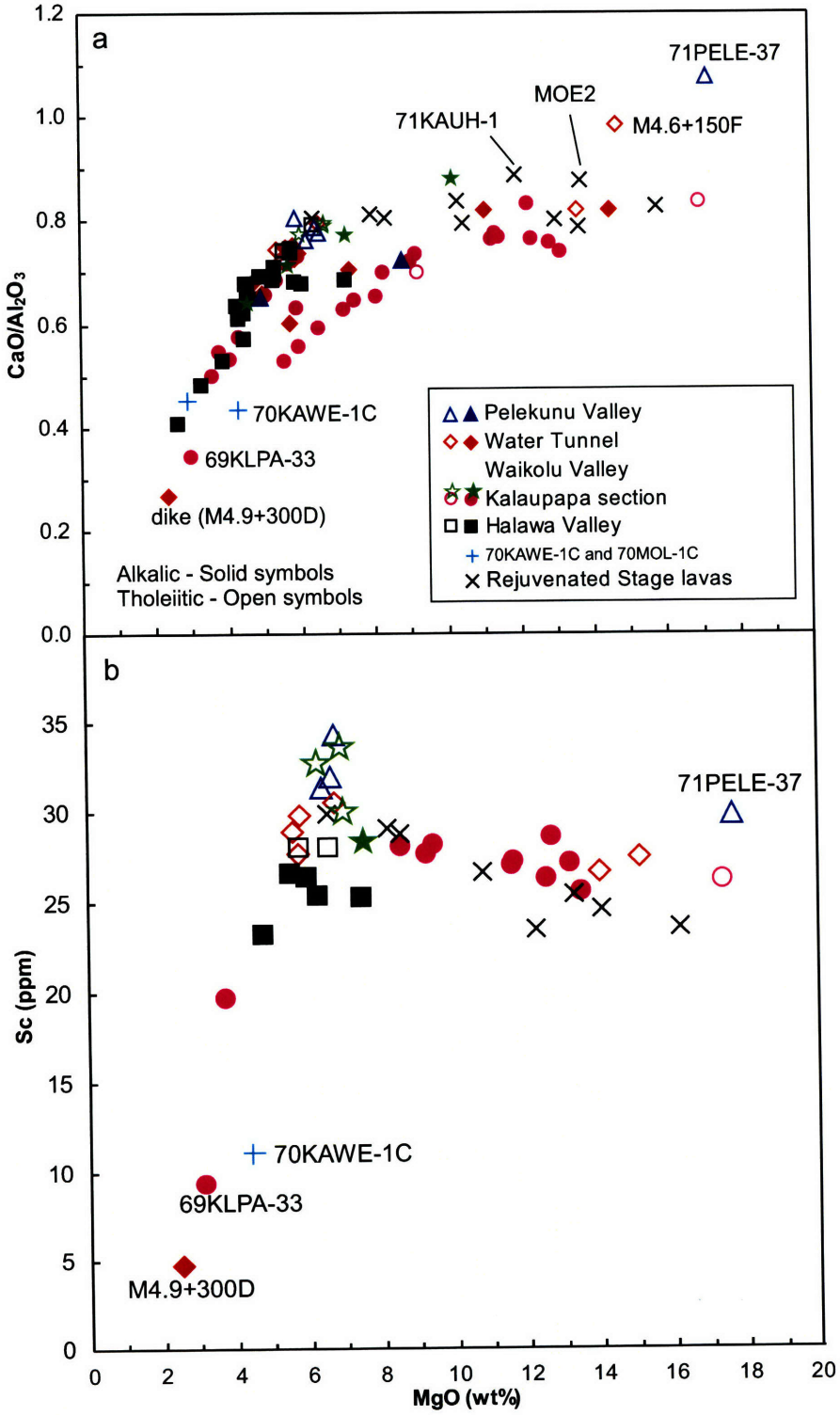
a
b
71PELE-37
MOE2
71KAUH-1
M4.6+150F
70KAWE-1C
69KLPA-33
dike (M4.9+300D)
Alkalic - Solid symbols
Tholeiitic - Open symbols
Pelekunu Valley
Water Tunnel
Waikolu Valley
Kalaupapa section
Halawa Valley
70KAWE-1C and 70MOL-1C
Rejuvenated Stage lavas
CaO/Al2O3
Sc (ppm)
MgO (wt%)
M4.9+300D

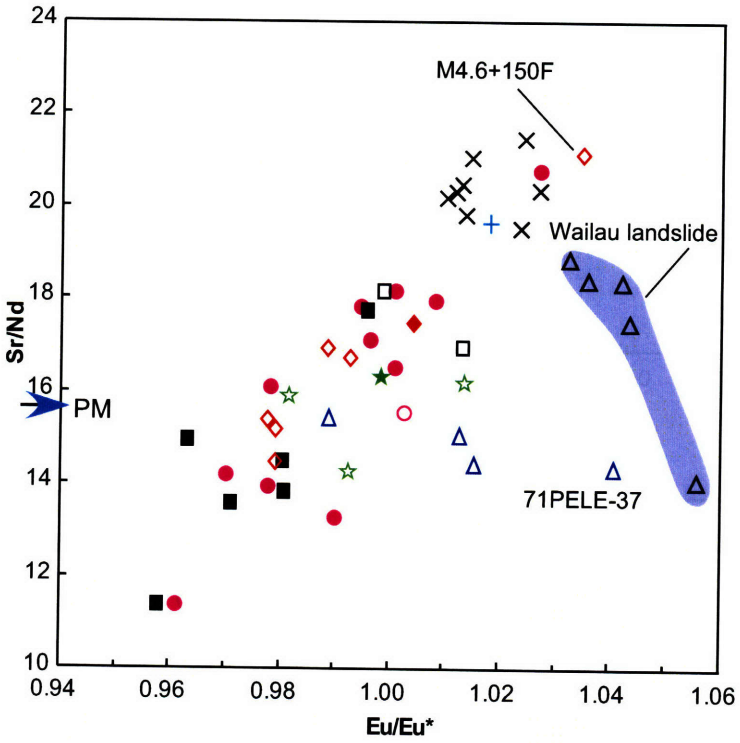
M4.6+150F
Wailau landslide
PM
71PELE-37
Sr/Nd
Eu/Eu*
24
22
20
18
16
14
12
10
0.94
0.96
0.98
1.00
1.02
1.04
1.06

Fig. 12

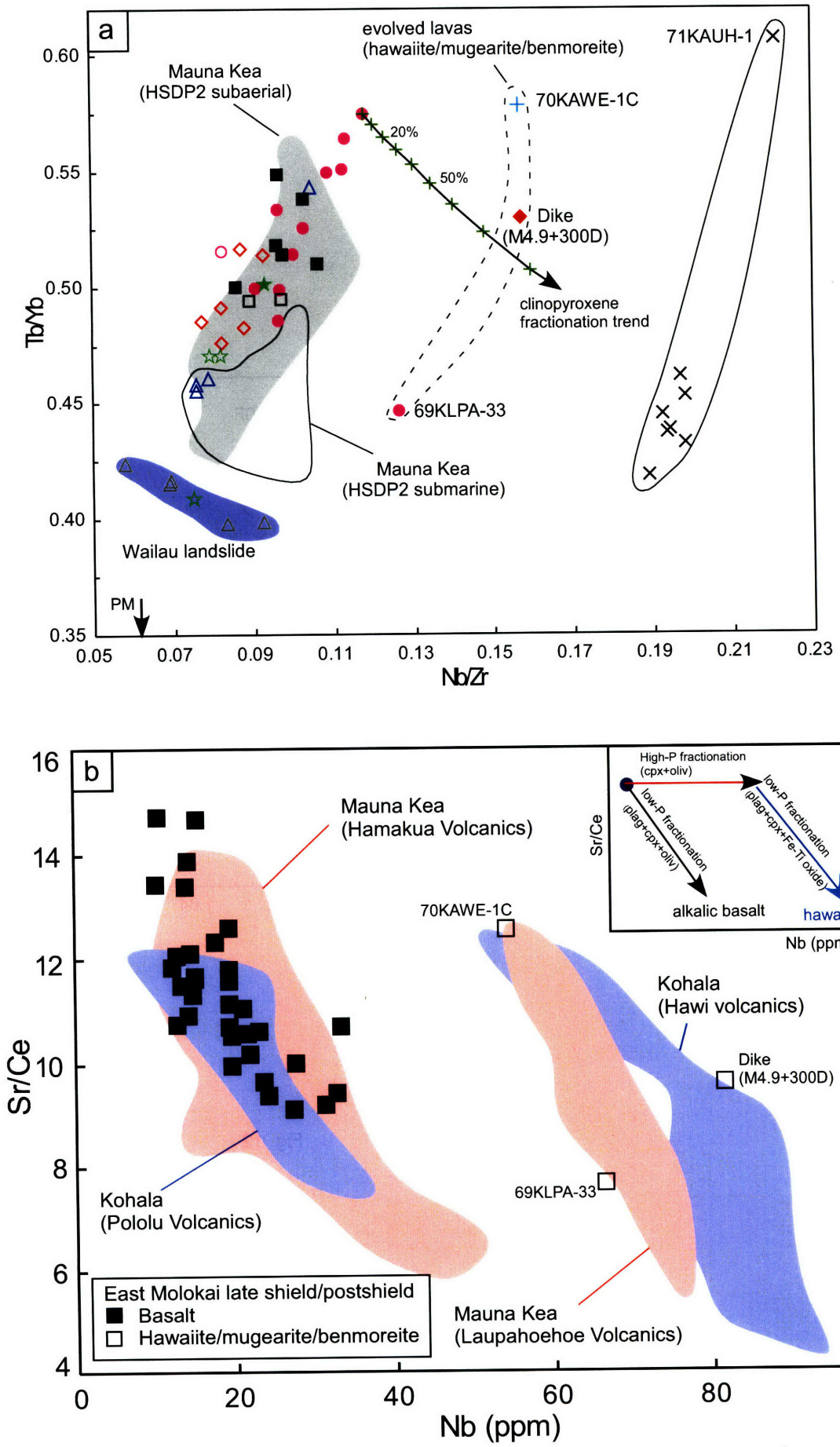
a
evolved lavas
(hawaiite/mugearite/benmoreite)
71KAUH-1
Mauna Kea
(HSDP2 subaerial)
70KAWE-1C
20%
50%
Dike
(M4.9+300D)
clinopyroxene
fractionation trend
69KLPA-33
Mauna Kea
(HSDP2 submarine)
Wailau landslide
PM
TbYb
NbZr
0.60
0.55
0.50
0.45
0.40
0.35
0.05
0.07
0.09
0.11
0.13
0.15
0.17
0.19
0.21
0.23
b
Mauna Kea
(Hamakua Volcanics)
High-P fractionation
(cpx+oliv)
low-P fractionation
(plag+cpx+oliv)
low-P fractionation
(plag+cpx+Fe-Ti oxide)
alkalic basalt
hawaiite
Sr/Ce
Nb (ppm)
70KAWE-1C
Kohala
(Hawi volcanics)
Dike
(M4.9+300D)
69KLPA-33
Kohala
(Pololu Volcanics)
Mauna Kea
(Laupahoehoe Volcanics)
East Molokai late shield/postshield
Basalt
Hawaiite/mugearite/benmoreite
Sr/Ce
Nb (ppm)
16
14
12
10
8
6
4
0
20
40
60
80
100

Fig. 13

Fig. 14

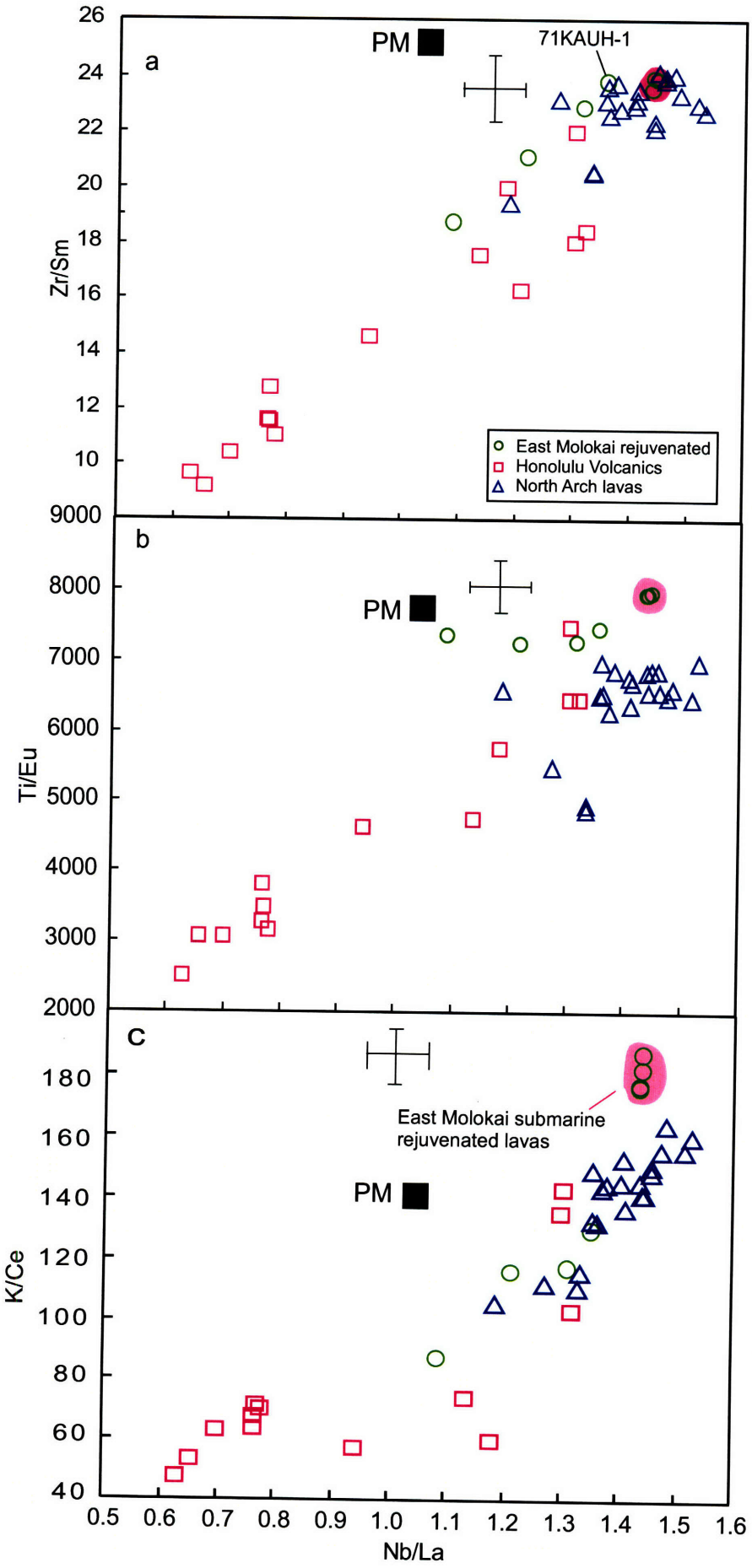
a
PM
71KAUH-1
Zr/Sm
East Molokai rejuvenated
Honolulu Volcanics
North Arch lavas
b
PM
Ti/Eu
c
East Molokai submarine
rejuvenated lavas
PM
K/Ce
Nb/La

Fig. 15

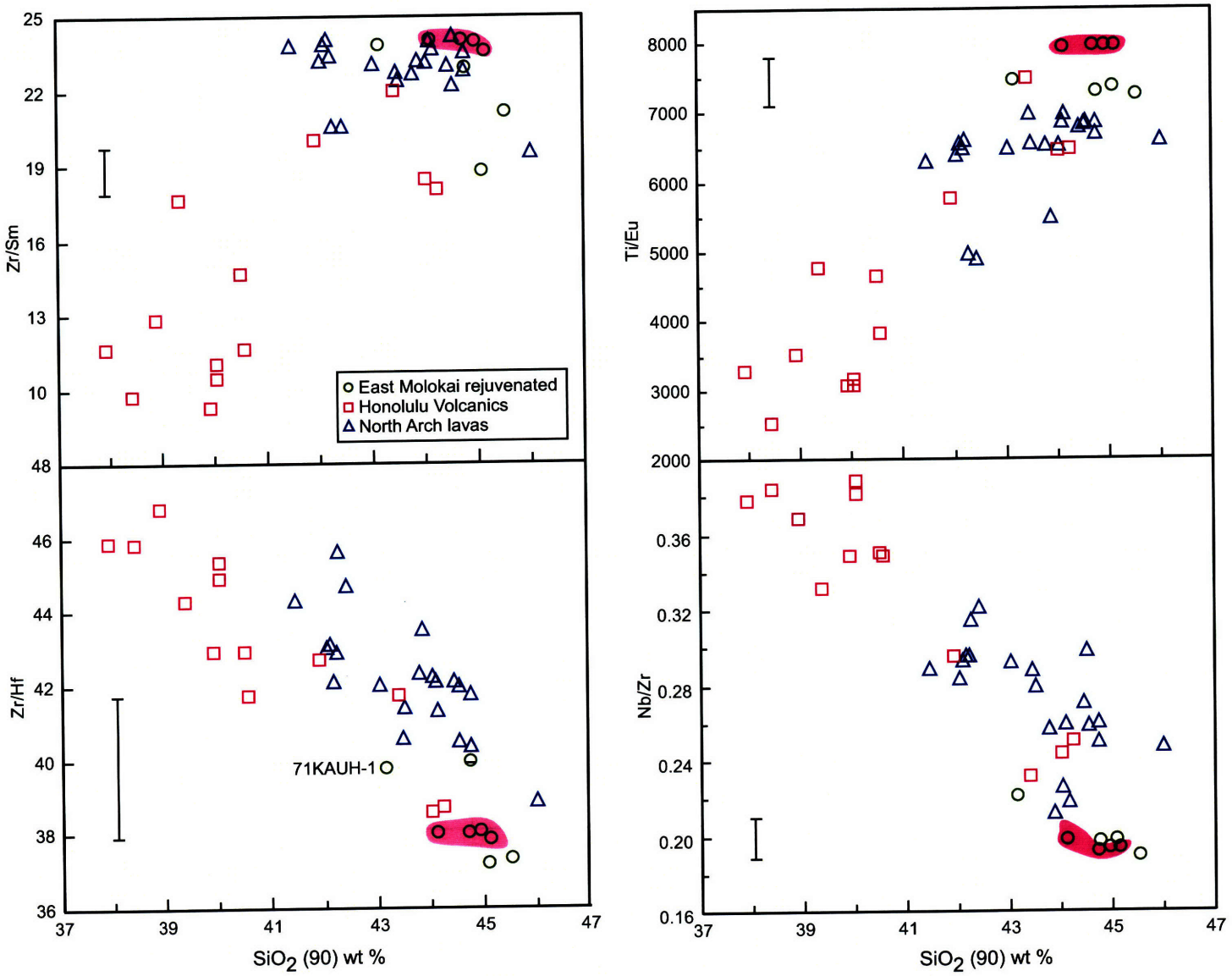
Zr/Sm
Zr/Hf
Ti/Eu
Nb/Zr
SiO2 (90) wt %
SiO2 (90) wt %
East Molokai rejuvenated
Honolulu Volcanics
North Arch lavas
71KAUH-1

Fig. 16

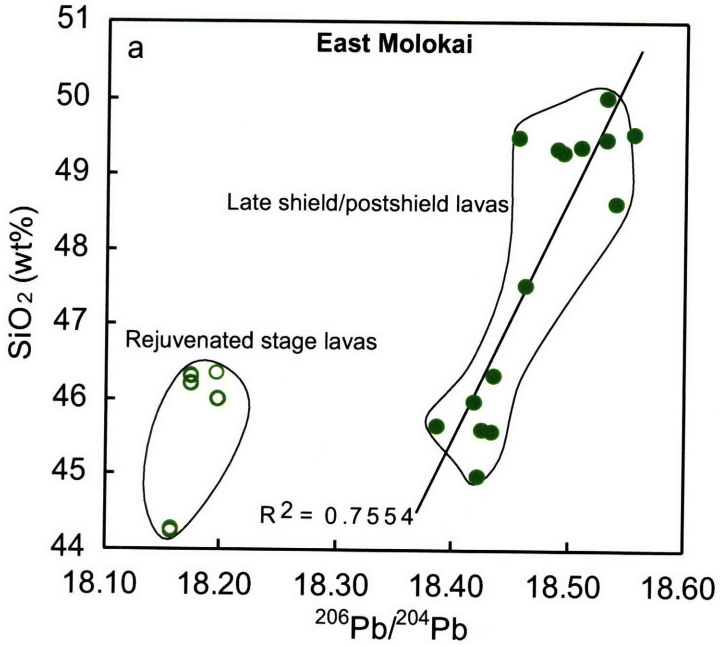
a
East Molokai
Late shield/postshield lavas
Rejuvenated stage lavas
R2 = 0.7554
SiO2 (wt%)
206Pb/204Pb

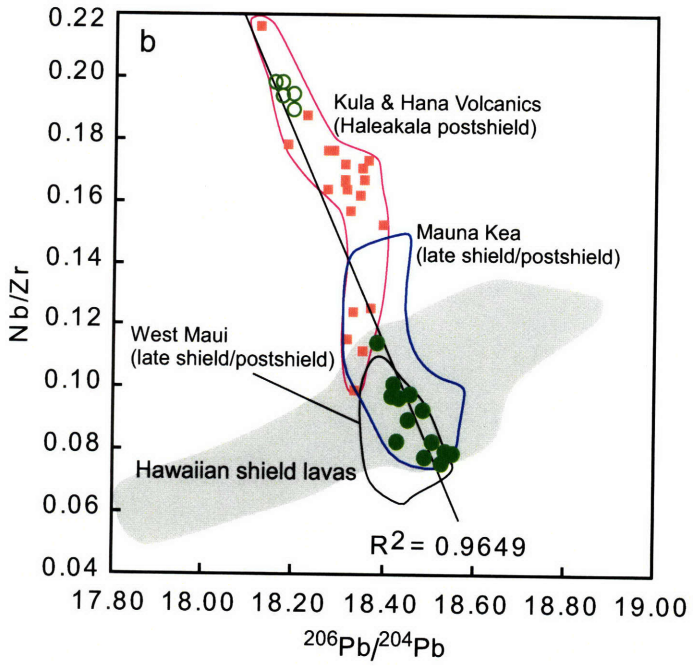
b
Kula & Hana Volcanics
(Haleakala postshield)
Mauna Kea
(late shield/postshield)
West Maui
(late shield/postshield)
Hawaiian shield lavas
R2 = 0.9649
Nb/Zr
206Pb/204Pb

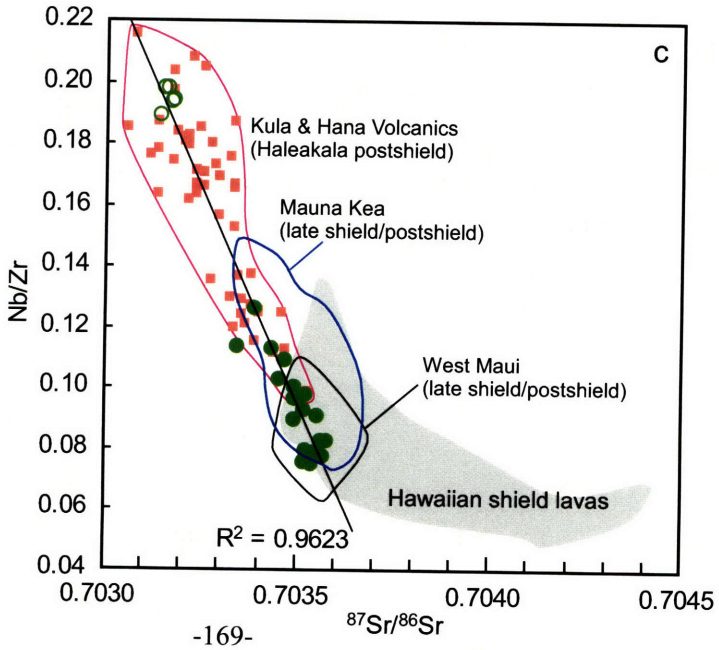
c
Kula & Hana Volcanics
(Haleakala postshield)
Mauna Kea
(late shield/postshield)
West Maui
(late shield/postshield)
Hawaiian shield lavas
R2 = 0.9623
Nb/Zr
87Sr/86Sr

Chapter 3 Geochemical Characteristics of West Molokai Shield- and Postshield-stage Lavas: Constraints on Hawaiian Plume Models

This chapter is in press in *Geochemistry, Geophysics and Geosystems*:

Xu, G., F. A. Frey, D. A. Clague, W. Abouchami, J. Blichert-Toft, B. Cousens, and M. Weisler (2007), Geochemical characteristics of West Molokai shield- and postshield-stage lavas: Constraints on Hawaiian plume models, 39 *Geochem. Geophys. Geosyst.*, 8, doi:10.1029/2006GC001554 (in press).

Abstract

There are systematic geochemical differences between the < 3 Myr Hawaiian shields forming the subparallel spatial trends, known as Loa and Kea. These spatial and temporal geochemical changes provide insight into the spatial distribution of geochemical heterogeneities within the source of Hawaiian lavas, and the processes that create the Hawaiian plume. Lavas forming the ~ 1.9 Ma West Molokai volcano are important for evaluating alternative models proposed for the spatial distribution of geochemical heterogeneities because: (1) the geochemical distinction between Loa and Kea trends may end at the Molokai Fracture Zone [*Abouchami et al.*, Nature, 435:851-856, 2005] and (2) West Molokai is a Loa-trend volcano that has exposures of shield and postshield lavas. This geochemical study (major and trace element abundances and isotopic ratios of Sr, Nd, Hf and Pb) shows that the West Molokai shield includes lavas with Loa- and Kea-like geochemical characteristics; a mixed Loa-Kea source is required. In contrast, West Molokai postshield lavas are exclusively Kea-like. This change in source geochemistry can be explained by the observed change in strike of the Pacific plate near Molokai Island so that as West Molokai volcano moved away from a mixed Loa-Kea source it sampled only the Kea side of a bilaterally zoned plume (*Abouchami et al., 2005*).

1. Introduction

The processes that create long-lived sources of hotspot-derived magma, i.e., a mantle plume, are reflected in the geochemical characteristics of the magmas. First order results are the well known geochemical differences between ocean island and mid-ocean ridge basalts and the geochemical diversity of ocean island basalts [e.g., *Hofmann*, 2004]. Most recently the recognition of systematic spatial and temporal geochemical variations in Hawaiian basalts have provided constraints on the processes that create the Hawaii plume [*Abouchami et al.*, 2005; *Bryce et al.*, 2005; *Ito and Mahoney*, 2005; *Ren et al.*, 2005b].

Recent Hawaiian volcanoes define two parallel trends, Kea and Loa, and according to *Jackson et al.* [1972], East Molokai is on the Kea trend while West Molokai is a Loa trend volcano (Figure 1a). *Hieronymus and Bercovici* [2001] evaluated the physical parameters that lead to sub-parallel chains of volcanoes and the spacing of volcanoes along these chains. They argued that a double chain of volcanoes, the Kea and Loa trends, can form during periods of high plume flux, i.e., a wide plume stress region. Alternatively, a double chain of volcanoes can arise from an off axis volcanic load created by a change in relative motion of the hotspot and overriding plate [*DePaolo et al.*, 2001; *Hieronymus and Bercovici*, 2001].

Lavas forming Loa- and Kea-trend volcanoes differ in major and trace element abundances and isotopic ratios of Sr, Nd, Hf and Pb [e.g., *Lassiter et al.*, 1996]; one of the most reliable discriminants is higher $^{208}Pb/^{204}Pb$ at a given $^{206}Pb/^{204}Pb$ for Loa volcanoes compared with Kea volcanoes [e.g., *Tatsumoto*, 1978; *Abouchami et al.*,

2005]. A popular hypothesis is that Loa and Kea volcanoes sample different parts of a plume that is geochemically zoned in cross-section [e.g., *Lassiter et al.*, 1996; *Abouchami et al.*, 2005; *Bryce et al.*, 2005] (Figure 2), but *Blichert-Toft et al.* [2003] emphasized that vertical heterogeneities within the plume are also important. A complication to the zoned models (Figure 2) is that Loa-like lavas occur in at least two Kea volcanoes: Mauna Kea [e.g., *Eisele et al.*, 2003] and Haleakala [*Ren et al.*, 2005a]. To explain this complexity, *Ren et al.* [2005b] and *Herzberg* [2005], proposed that on a < 1 km scale, both Loa and Kea sources are present but that on ~ 20 km scale, depending upon location, either Loa or Kea sources dominate (Figure 2d).

Previously, we showed that lavas erupted at East Molokai volcano have Kea-like geochemical characteristics [*Xu et al.*, 2005]. Based on Kea-like Pb isotopic ratios of a dredged sample inferred to be from West Molokai (sample D8-1 in Figure 1b), *Abouchami et al.* [2005] concluded that West Molokai volcano is also Kea-like and that the isotopic differences between Loa and Kea trend lavas do not extend to Molokai Island (Figure 1a). However, *Tanaka et al.* [2002] noted that Sr-Nd-Pb isotopic ratios of three subaerially-erupted shield lavas from West Molokai [*Stille et al.*, 1986; *West et al.*, 1987] overlap with the field for Mauna Loa lavas, and concluded that the West Molokai shield includes lavas with both Kea- and Loa-like geochemical characteristics. However, these data for subaerial shield lavas, obtained more than 20 years ago, have large uncertainties compared to modern techniques, especially for determination of Pb isotopic ratios, and no Hf isotope data exist. In this study we focused on West Molokai lavas and find that this shield includes basalt with

diverse geochemical characteristics, ranging from lavas similar to the extreme Loa endmember (i.e., Koolau (Makapuu stage); *Huang and Frey* [2005b]) to Kea-like samples. The presence of Kea- and Loa-like lavas in West Molokai is consistent with small-scale Kea and Loa heterogeneities in the source (Figure 2d).

An important aspect of understanding Hawaiian magmatism is that a typical Hawaiian volcano evolves through four petrologically defined stages [e.g., *Clague and Dalrymple*, 1987]: alkalic preshield stage (~ 3% of volcano volume, observed at Loihi seamount [*Moore et al.*, 1982], Kilauea [*Sisson and Lipman*, 2002], and Hualalai [*Coombs et al.*, 2006; *Hammer et al.*, 2006] and assumed to be present at all Hawaiian volcanoes); main tholeiitic shield stage (~95-98% of the volume, present in all volcanoes); alkalic postshield (~1% of the volume, present at some volcanoes); alkalic rejuvenated stage (<1% of the volume, present at some volcanoes). Postshield stage and rejuvenated stage lavas are geochemically distinct from associated shield lavas [e.g., *Chen and Frey*, 1985]; therefore, they are important in documenting changes in magmatic processes and sources as a Hawaiian volcano matures. Previous studies [*Gaffney et al.*, 2004; *Xu et al.*, 2005] used the overlap of Sr, Nd, and Pb isotope ratios in late shield/postshield lavas from Mauna Kea (<350 ka), West Maui and East Molokai (~1.5 Ma) to show that the portion of the hotspot sampled by Kea-trend late shield/postshield lavas had long-term geochemical continuity (Figure 1a). Do Loa-trend volcanoes also maintain their distinct isotopic characteristics as they transit from shield-stage to postshield-stage volcanism? Among Loa-trend volcanoes Hualalai, Kahoolawe and West Molokai have postshield lavas. Hualalai

postshield lavas have a Loa-trend Pb isotopic signature [*Cousens et al.*, 2003; *Xu et al.*, 2005], while Kahoolawe postshield and shield lavas overlap in Sr and Nd isotopic ratios [*Huang et al.*, 2006]. Another objective of this study is to compare the isotopic characteristics of shield and postshield stage lavas from West Molokai. In contrast to Hualalai and Kahoolawe, we find that postshield lavas at West Molokai are Kea-like in their isotopic signature.

2. Geology

Molokai was part of Maui Nui, a single large island at about 1.2 Ma that included the present-day islands of Maui, Kahoolawe, Molokai and Lanai, an area 50% larger than the Big Island of Hawaii today (Figure 1a) [*Price and Elliott-Fisk*, 2004]. West Molokai, the older of the two volcanoes on the island of Molokai, has a peak height of only 421 m. East Molokai volcano, which rises 1515 m above sea level, forms the eastern two-thirds of the island and overlies lavas of West Molokai volcano. West Molokai has received little attention owing to its poorly dissected condition and extensive soil cover. Shield stage lava flows dip 2 to 10 degrees away from the principal southwest and subordinate northwest rift zones, which join near the summit (Figure 3). Some dikes are exposed where coastal erosion has cut into the rift zones. Unlike East Molokai or most other Hawaiian volcanoes, there is no evidence of a summit caldera. About 16 small spatter and cinder cones are preserved on the surface of West Molokai, particularly in the northwest quadrant of the volcano; those that have been sampled (Figure 3) range in composition from alkalic basalt to hawaiite. These cones and the flows erupted from them constitute the alkalic postshield stage.

No rejuvenated stage lava is known at West Molokai. Beneath the sea, West Molokai extends west-southwest to Penguin Bank, which has a flat surface at a depth of 55 m below sea level. Penguin Bank may be a subsided portion of the southwest rift zone of West Molokai volcano but is more likely to be a separate shield volcano (Figure 1a).

Three samples of postshield-stage alkalic basalt and hawaiite were dated using K-Ar techniques in the U.S. Geological Survey laboratory at Menlo Park by G. B. Dalrymple. The samples are from the western flank (Figure 3). The results, presented in Table 1 show that the postshield lavas erupted between 1.72±0.06 and 1.81±0.06 Ma; they are statistically indistinguishable and could all have erupted at 1.76±0.05 Ma, which we take as the age of the postshield stage. *Clague* [1987] previously reported this age, but the analytical data were not published. This age postdates by about 0.13 Ma the end of the shield stage, represented by a highly fractionated tholeiitic flow exposed near the summit (our samples 71WMOL-1, 74WMOL-3, and 74WMOL-5 are from the same unit; see Figure 3) that McDougall [1964] dated at 1.89±0.06 Ma (corrected to modern decay constants). The time period between the shield tholeiitic and postshield alkalic stages is therefore inferred to be on the order of several hundred thousand years, but could be much shorter.

3. **Sample location**

Fifty-four whole-rock samples collected from West Molokai were studied including 14 samples which experienced post-magmatic REE-Y enrichment [*Clague*, 1987] similar to that documented at Kahoolawe volcano [*Fodor et al.*, 1992]. Samples with REE-Y enrichment were not chosen for isotopic studies.

Forty-seven whole-rock samples were collected from the subaerial surface of West Molokai volcano; locations are shown in Figure 3. Many of the tholeiitic lavas (20) were collected along highway 460 northwest of Puu Nana. Most of the alkalic lavas (15 of the 18 alkalic basalts and hawaiites) are from the northwest part of West Molokai (Figure 3).

Glasses were collected from the margins of two tholeiitic dikes southeast (<500 m) of Puu Nana and an alkalic dike from near the north coast at Kaa Gulch (Figure 3).

Seven breccia samples were collected by the remotely operated vehicle (Tiburon) ~20 km from the submarine north coast of West Molokai (T307 in Figure 1b). Based on their location, these samples originated from the West Molokai shield. They were collected while traversing upwards along a sediment-covered slope with outcrops of thin breccia units. Samples R1 and R2 are from a lower breccia unit with R1 below R2, samples R3 and R4 are loose blocks, samples R6 and R7 are from the same outcrop of an overlying unit and sample R8 is from an upper breccia unit. Probably, but not certainly, the sequence R1 to R8 is a chronologic sequence of decreasing age.

In addition to basaltic clasts, glasses from the submarine breccia slope were also analyzed; they include glass grains in sediment cores, glass from rinds on basalt clasts in samples R4 and R8, glass from the breccia matrix of samples R2 and R7, glass in crack-filling hyaloclastite in sample R8, and glass inclusions in olivine from sample R8. Several of these glasses, including rinds on basalt clasts in R4 and R8 are relatively undegassed, i.e., S contents > 0.056 wt% (Table 2), indicating that they were derived from submarine flows [*Dixon et al.*, 1991]. However, melt inclusions in

olivine from the uppermost sample, R8, include degassed and undegassed glass (Table 2). Mixing of subaerially- and submarine-erupted magmas is implied; a likely scenario is that subaerially-erupted, hence degassed, magma retreated into a magma reservoir [the 1959 Kilauea Iki eruption is an example, *Dixon et al.*, 1991], was incorporated into olivine and subsequently included in a submarine-erupted magma. An important implication is that West Molokai existed as a subaerial shield when this submarine breccia formed.

4. Sample preparation

The subaerial whole-rock samples were coarse crushed and pieces were hand-picked using a binocular microscope in order to avoid highly altered portions and sawed surfaces. The freshest pieces (~ 4-6 gram) were washed in an ultrasonic bath three times (5 minutes each) using MQ-H_2O; they were dried on a hotplate and crushed into fine powder in an agate shatterbox. These powders were used for trace element analyses by inductively coupled plasma mass spectrometry (ICP-MS) and after acid leaching, isotopic analyses were determined by thermal ionization mass spectrometry (TIMS) and multicollector ICP-MS (See Appendix for analytical methods).

Glass from the three dikes was removed using a mini-saw before coarsely crushing to less than 2 mm pieces. Fresh glass was picked from the greater than 0.5 mm but less than 2 mm fraction. This glass was coarsely crushed in agate and fresh pieces were selected using a binocular microscope before crushing to fine powders for trace element analysis by ICP-MS.

Basaltic clasts from the submarine breccia slope were crushed in an agate mortar for trace element and isotopic analyses and in steel for major element analysis. Major and trace element abundances were determined at the Geoanalytical Laboratory at Washington State University, and Sr, Nd, Hf and Pb isotopic ratios were determined at Carleton University, Ecole Normale Supérieure in Lyon and Max-Planck-Institut fur Chemie (See Appendix for analytical methods).

5. Petrography

Many of the West Molokai shield stage tholeiitic lava flows are less than 50 cm thick. The subaerial lavas have 3% to 25% vesicles and are sparsely porphyritic (<2%) with olivine, plagioclase, clinopyroxene and orthopyroxene phenocrysts, but lavas from the submarine breccia slope have abundant olivine phenocrysts (>10%) except T307-R2 with less than 2%. The postshield stage alkalic lavas, dominantly hawaiite with subordinate alkalic basalt, are typically aphyric.

6. Geochemical results

6.1 Major element compositions

Lavas from West Molokai range from older, tholeiitic basalt and basaltic andesite (hereafter referred to as highly fractionated tholeiite) forming the shield to younger alkalic basalt and hawaiite forming the postshield (Figure 4).

Glasses: Glass from West Molokai has been used to infer a local origin of artifacts from the Moomomi region on the north flank of the shield (Figure 3). Specifically *Weisler and Clague* [1998] showed that these artifacts are compositionally similar, either to glass margins on tholeiitic dikes found near the summit or on the north shore

dike of alkalic basalt (Figure 5 and Appendix Table 1).

A new result is that glasses from the submarine breccia slope (T307 in Figure 1b) are tholeiitic basalt (Table 2), but they are compositionally distinct from glass margins on the dikes and artifact glasses; specifically, at a given MgO content submarine glasses are offset to higher CaO and lower Na_2O and P_2O_5, but they have similar SiO_2 contents (Figure 5a, b, c); also in a Al_2O_3/CaO vs TiO_2/Na_2O plot the artifact and dike glasses overlap the Mauna Loa field whereas the submarine glasses overlap the Mauna Kea field (Figure 5d). Relative to tholeiitic glasses, the alkalic glasses have lower CaO and SiO_2 and higher Na_2O contents (Figure 5a, b, c).

Whole rock: The tholeiitic whole-rock compositions (Table 3) overlap the tholeiitic glass compositions (Figure 6). For lavas with MgO > 7% (basaltic clasts from the submarine breccia slope, see Table 3) the contents of CaO, SiO_2, TiO_2, Al_2O_3, Fe_2O_3* and P_2O_5 increase with decreasing MgO which is consistent with olivine fractionation and accumulation (Figure 6). For the basaltic lavas with MgO < 7%, CaO content is positively correlated with MgO thereby indicating the important role of clinopyroxene fractionation (Figure 6a). Some highly fractionated tholeiitic samples range to high SiO_2 (>53%) at low MgO contents (4-5%); these samples have higher SiO_2, P_2O_5, and lower CaO, Al_2O_3, Fe_2O_3* and TiO_2 at a given MgO than other tholeiitic samples (Figure 6), indicating fractionation of clinopyroxene + plagioclase + Fe-Ti oxides. Such highly evolved tholeiitic lavas have previously been described from distant parts of rift zones where isolated magma chambers cooled and fractionated [*Helz and Wright*, 1992; *Clague et al.*, 1995; *Yang et al.*, 1999]. However, at West Molokai and

Waianae [*Sinton*, 1987] these fractionated tholeiitic lavas erupted near the summit, perhaps produced as the sub-caldera reservoir filled with tholeiitic melt cooled and crystallized as magma supply rate waned at the end of shield stage.

Compared to tholeiitic lavas, at a given MgO content, alkalic basalt lavas have lower CaO and SiO_2 and higher TiO_2, Fe_2O_3* and P_2O_5 (Table 3, Figure 6). These differences are consistent with the commonly inferred decrease in extent of melting that accompanies the transition from shield to postshield stages [e.g., *Yang et al.*, 1996].

Relative to basalt, hawaiites from the Kea volcanoes (such as Mauna Kea and East Molokai) are characterized by relatively high SiO_2 (> 49%), low Fe_2O_3* (< 12%) and low TiO_2 (< 3%) (Table 3 and gray shaded fields in Figure 6b, c and e). These features can be explained by Fe-Ti oxide segregation [*West et al.*, 1988; *Frey et al.*, 1990]. In contrast, West Molokai hawaiites trend to relatively low SiO_2 and high Fe_2O_3 and TiO_2 contents showing that Fe-Ti oxide fractionation was less important in the formation of West Molokai hawaiite (Figure 6).

6.2 Trace element abundances

Trace element data are reported in Table 4. Thorium content is positively correlated with abundances of other immobile, incompatible elements (e.g., Nb and Zr) in tholeiitic lavas (Figure 7). Three of the four fractionated tholeiitic lavas with relatively low CaO, Fe_2O_3* and TiO_2 are offset to lower Nb/Th, Sr/Nb and Eu/Th ratios (Figure 7), which is consistent with Fe-Ti oxides and plagioclase in the fractionating mineral assemblage that led to these tholeiitic lavas; i.e., Nb is

compatible in Fe-Ti oxides [*Jang and Naslund*, 2003] and Sr and Eu are compatible in plagioclase relative to clinopyroxene and olivine [e.g., *Bindeman et al.*, 1998; *Blundy and Dalton*, 2000; *Bedard*, 2005].

Relative to tholeiitic lavas, at a given MgO content, alkalic basalts have higher contents of incompatible elements such as Th (Figure 7f), but they have similar contents of heavy rare earth elements (e.g., Lu in Figure 7e). These differences are consistent with the interpretation that the parental magmas of alkalic basalt were derived by lower extents of melting with significant residual garnet [e.g., *Yang et al.*, 1996]. Hawaiites have the highest abundances of Th, Nb, Zr, Sr and Eu (Figure 7) and relatively low Sc and Ni contents (Table 4). These characteristics are expected of low MgO lavas derived from an alkalic parental magma by extensive fractionation of a clinopyroxene-rich and plagioclase-poor assemblage. This scenario, plagioclase and olivine-dominated fractionation of shield stage tholeiitic basalt followed by higher pressure clinopyroxene-dominated fractionation of postshield alkalic lavas is evident at Mauna Kea volcano [*Frey et al.*, 1990].

6.3 Sr, Nd, Hf and Pb isotopic ratios

Isotopic data, Sr, Nd, Hf and Pb for West Molokai lavas are given in Table 5; in addition, Hf isotopic data for previously studied East Molokai lavas [*Xu et al.*, 2005] are listed in Table 6. West Molokai tholeiitic and alkalic lavas define inverse trends in $^{87}Sr/^{86}Sr$ versus $^{143}Nd/^{144}Nd$ and $^{176}Hf/^{177}Hf$ plots (Figure 8). At the low $^{87}Sr/^{86}Sr$ and high $^{143}Nd/^{144}Nd$ and $^{176}Hf/^{177}Hf$ end, West Molokai tholeiitic lavas overlap with the field for Kea shield lavas, but other West Molokai tholeiitic lavas extend to higher

$^{87}Sr/^{86}Sr$ and lower $^{143}Nd/^{144}Nd$ and $^{176}Hf/^{177}Hf$ overlapping with Loa shield lavas; the extreme is sample T307R2, which is similar to the Hawaiian endmember defined by Koolau (Makapuu stage) lavas (Figure 8). Two postshield West Molokai alkalic basalts and five hawaiites, are nearly homogenous in terms of Sr, Nd and Hf isotopic ratios (Figure 8). Two tholeiitic basalts, 89KAA-2 and T307R4, have isotopic ratios of Sr and Nd similar to these postshield lavas (Figure 8). Sample 89KAA-2 is from Kaa Gulch where alkalic basalt and hawaiite were also sampled (Figure 3); sample T307R4 is from a loose block on a submarine slope of sediment-covered thin breccia units (see section 3); therefore, it is possible that these tholeiitic basalts were intercalated with alkalic basalts erupted in the postshield stage as observed at Mauna Kea [*Frey et al.*, 1991].

On an εNd-εHf plot, West Molokai lavas define a linear trend (Figure 9). Alkalic postshield and some shield tholeiitic lavas overlap with the field for Kea shield lavas; most of the West Molokai shield lavas overlap with the field for Mauna Loa lavas. The two most extreme West Molokai lavas (84WMOL-1D(N) and T307R2) are close to or overlap the field defined by lavas forming the Lanai and Koolau (Makapuu-stage) shields.

In εNd vs. εHf plot, East Molokai late shield/postshield lavas overlap with the field for other Kea shields, such as Mauna Kea (Figure 9). Like other rejuvenated-stage lavas, East Molokai rejuvenated-stage lavas are offset form the shield trend to higher εHf at a given εNd; this offset has been interpreted as evidence for a non-MORB (mid-ocean ridge basalt) related, depleted component in the plume

source [e.g., *Frey et al.*, 2005; *Fekiacova et al.*, 2007].

West Molokai lavas range widely in $^{206}Pb/^{204}Pb$ ratios (17.84-18.44) and define elongated trends in $^{206}Pb/^{204}Pb$ vs $^{208}Pb/^{204}Pb$ and $^{207}Pb/^{204}Pb$ space (Figure 10). The West Molokai alkalic lavas have relatively high Pb isotopic ratios and overlap with the field for late shield and postshield lavas from East Molokai; in contrast, most West Molokai tholeiitic shield lavas have low ratios (except for submarine samples T307R4, R6, R7 and R8), and their trend extends to the fields for Koolau (Makapuu-stage) and Lanai shield lavas with sample T307R2 at the low $^{206}Pb/^{204}Pb$ extreme (Figure 10). Relative to other West Molokai tholeiitic lavas, samples 84WMOL-1D(N) and especially T307R2, which have distinctly high $^{87}Sr/^{86}Sr$, and low $^{143}Nd/^{144}Nd$ and $^{176}Hf/^{177}Hf$ (Figures 8 and 9), are offset to higher $^{208}Pb/^{204}Pb$ at a given $^{206}Pb/^{204}Pb$; i.e., they have the highest $^{208}Pb^*/^{206}Pb^*$ (defined as ($^{208}Pb/^{204}Pb$-29.475) / ($^{206}Pb/^{204}Pb$-9.307)), which is a characteristic of Loa-trend lavas [*Abouchami et al.*, 2005].

7. Discussion

A major objective of this study is to determine if West Molokai lavas have dominantly Loa- or Kea-trend geochemical characteristics, and in particular, to determine if the geochemical distinction between Loa- and Kea-trend lavas terminated at Molokai Island as proposed by *Abouchami et al.* [2005]. Although a minority of lavas at some volcanoes are exceptions, most shield-forming lavas of Kea- and Loa-trend volcanoes can be distinguished by differences in major and trace element abundances and isotopic ratios [e.g., *Frey and Rhodes*, 1993; *Frey et al.*, 1994;

Lassiter et al., 1996; *Abouchami et al.*, 2005]. In the following discussion, we use each of these data sets to determine whether West Molokai shield lavas are Kea- or Loa-like. Because the magmatic characteristics of West Molokai lavas have been variably affected by post-magmatic alteration, we first determined the geochemical effects of such alteration (see Appendix 2). Based on Appendix 2 our discussion of magmatic characteristics uses the major element composition of glasses, the trace element ratios Zr/Nb, Sr/Nb and La/Nb (screened for La/Nb<1.25) and isotopic ratios of Sr, Nd, Hf and Pb.

7.1 Loa or Kea? Constraints from the major element contents of West Molokai tholeiitic glass

Glasses are useful in showing major element differences between Loa- and Kea-trend volcanoes because they represent unaltered, quenched melt. A difficulty with using the major element composition of glasses is that, like West Molokai glasses, they typically have relatively low MgO contents (<7%) (Figure 5). Consequently, they have been affected by fractionation of clinopyroxene and plagioclase; for example, West Molokai glasses with <6.5 % MgO clearly show the effects of clinopyroxene fractionation, i.e. a positive CaO-MgO trend (Figure 5a). Therefore it is necessary to use an MgO filter, > 6.5 %, to show the differences between Loa- and Kea-trend volcanoes. For example, the large data sets for glasses from Mauna Kea [HSDP core, *Garcia*, 1996; *Stolper et al.*, 2004] and Mauna Loa [*Moore and Clague*, 1987; *Garcia et al.*, 1989; *Moore and Clague*, 1992; *Garcia et al.*, 1995; *Moore et al.*, 1995; *Garcia*, 1996] show that, relative to Mauna Kea glasses, Mauna Loa glasses range to higher

Al_2O_3/CaO and lower TiO_2/Na_2O (Figure 5d). The West Molokai glasses collected during dive T307 and glass collected subaerially (i.e., artifacts and dikes) differ significantly in that the submarine glasses have higher CaO at a given MgO and higher Al_2O_3/CaO (Figure 5a, d). Therefore, the submarine glasses are Kea-like whereas subaerial glasses (i.e., artifacts and glasses on dike margins) are Loa-like (Figure 5d).

7.2 Loa or Kea? Constraints from trace element ratios in West Molokai whole rocks and glasses

Shield and postshield lavas from Mauna Kea have Sr/Nb < 28 (224 of 226 analyses) and Zr/Nb < 13 (218 of 226 analyses) whereas lavas from Mauna Loa have Sr/Nb > 28 and Zr/Nb > 13 (79 of 87 analyses) (Figure 11). Although these incompatible trace element ratios can be affected by crystal fractionation of plagioclase and clinopyroxene, they are correlated with isotopic ratios in Hawaiian shield lavas (Figure 12); therefore, these Loa-Kea differences are interpreted to reflect source characteristics for Loa- and Kea-trend volcanoes [e.g., *Frey and Rhodes*, 1993; *Huang and Frey*, 2003; *Ren et al.*, 2005b].

Shield tholeiitic lavas from West Molokai range from 11.6 to 15.3 in Zr/Nb. Subaerial tholeiitic whole rocks and glasses with MgO > 6.5% have Zr/Nb > 14 and plot within the field for Mauna Loa lavas (Figure 11). Submarine breccia clast samples (T307R1, R2 and R3, all with MgO > 7.4 %) from the lower part of the north slope also have high, Mauna Loa-like, Sr/Nb and Zr/Nb ratios whereas samples collected farther upslope (T307R4, R6, R7 and R8) have low, Mauna Kea-like ratios (Figure 11). If eruption age decreases upward on this submarine breccia slope a Loa-

to Kea-like temporal trend is inferred from the breccia clasts. However, glasses from this submarine breccia slope with diverse origins, such as glass rinds on basaltic clasts and glass grains in sediment (Table 2), have Kea-like major element characteristics (Figure 5). Consequently, the robust result is that major and trace element compositions of the West Molokai shield lavas show that both Loa- and Kea-like compositions are present.

7.3 Loa or Kea? Constraints from Sr-Nd-Hf-Pb isotopic ratios of West Molokai lavas

Sr, Nd and Hf isotopic ratios for the West Molokai shield lavas range widely (Figures 8 and 9). At one extreme, samples are close to (84WMOL-1D(N)) or within (T307R2) the field for the Loa endmember defined by Makapuu-stage lavas of the Koolau shield. *Abouchami et al.* [2005] proposed that Pb isotopic ratios are the best geochemical discriminant between Loa and Kea lavas. In particular, Loa lavas have high $^{208}Pb/^{204}Pb$ at a given $^{206}Pb/^{204}Pb$, as measured by $^{208}Pb^*/^{206}Pb^*$. Consistent with their Loa-like Sr, Nd and Hf isotopic ratios, samples 84WMOL-1D(N) and T307R2 have relatively low $^{206}Pb/^{204}Pb$ and the highest $^{208}Pb^*/^{206}Pb^*$ (Figures 10 and 13). At the other extreme, samples 89KAA-2 and T307R4, R6, R7 and R8 have Kea-like isotopic ratios very similar to those of the West Molokai alkalic postshield lavas.

In summary, West Molokai lavas shifted from a shield containing both Loa- and Kea-like lavas to a postshield with only Kea-like geochemical characteristics. However, among the studied subaerial- and submarine-erupted West Molokai shield lavas, age constraints are not sufficient to assess if there was a systematic temporal

trend, such as Loa to Kea, during growth of the West Molokai shield. Based on existing data we infer a temporally random sampling of Loa- and Kea-like sources. In support of this inference a sample (MAH-35) studied by *Shinozaki et al.* [2002] collected from close to the summit of West Molokai has a major element composition very similar to T307R2, notably relatively low CaO and Fe_2O_3 and high SiO_2 at a given MgO (Figure 6). Consequently, Loa-like samples occur low in the submarine breccia section and near the summit.

Also sample D8-1, dredged approximately 40 km from the West Molokai coastline (see Figure 1b and *Tanaka et al.* [2002]), has considerably lower $^{87}Sr/^{86}Sr$, higher $^{143}Nd/^{144}Nd$ and more radiogenic Pb isotopic ratios than any West Molokai lava in this study (Figures 8a, and 9); it overlaps in these ratios with the field of Nuuanu landslide samples that are inferred to be early, Kea-like lavas of the Koolau shield (Kalihi-stage) [*Tanaka et al.*, 2002]. In this case the West Molokai and Koolau shields have sampled the full isotopic range expressed by younger Loa- and Kea-trend volcanoes. Alternatively, we note that the dredge location of sample D8-1 is within or close to the proposed boundary of the Nuuanu landslide which is inferred to originate from Koolau volcano (Figure 1c) [*Moore and Clague*, 2002; *Shinozaki et al.*, 2002]. Hence, it is possible that this dredge sample erupted at Koolau volcano rather than at West Molokai.

7.4 Effects of the Molokai Fracture Zone on Hawaiian volcanism

Previous geochemical studies suggested that the Molokai Fracture Zone (MFZ) had an important influence on Hawaiian volcanism [e.g., *Basu and Faggart*, 1996;

Abouchami et al., 2005]. The MFZ, a large-offset fracture zone in the northeast Pacific Ocean, was named from its intersection with the Hawaiian island chain in the vicinity of Molokai Island [*Menard*, 1962]. It is considerably more complex than a simple offset of oceanic crust with different ages because it consists of several ENE-WSW tectonic lineaments forming two major bands, the Oahu and Maui strands, which cross the Hawaiian island chain (Figure 1a) [*Searle et al.*, 1993]. Oceanic lithosphere on opposite sides of the strands has different ages and thicknesses [*ten Brink and Brocher*, 1988; *Searle et al.*, 1993]. For example, the Pacific crust south of Oahu is older by ~15 My. *Hieronymus and Bercovici* [2001] noted that such differences should be evident in the volcanism on opposite sides of the fracture zone, but the small inferred difference in lithospheric thickness, only a few kilometers, is an unlikely explanation for the dramatic increase in volume at ~2 Ma at Maui Nui. More likely explanations are temporal variation in plume flux [*Robinson and Eakins*, 2006].

Basu and Faggart [1996] argued that the MFZ enabled influx of a lower mantle plume component represented by the Hawaiian geochemical endmember defined by the Koolau (Makupuu stage), Lanai and Kahoolawe shields. If the MFZ influenced sampling of the plume source, this component should be abundant in the West Molokai shield which is located between the Lanai and Koolau shields (Figure 1a). Although we do not know the volumetric proportion, the occurrence of two West Molokai shield lavas at disparate locations that have the geochemical signature of Koolau (Makapuu-stage) lavas (i.e., high $^{87}Sr/^{86}Sr$, low $^{143}Nd/^{144}Nd$, $^{176}Hf/^{177}Hf$ and $^{206}Pb/^{204}Pb$ and high $^{208}Pb^*/^{206}Pb^*$) is consistent with the MFZ facilitating sampling

of this Loa endmember.

7.5 Spatial Distribution of Geochemical Heterogeneities in the Hawaiian Plume

Geochemical heterogeneities in Hawaiian lavas provide constraints on the origin of the plume and the processes that lead to plume-related volcanism. For example, geochemical differences between shield lavas erupted on the spatial Kea- and Loa-trends have been used to propose alternative models for the spatial distribution of geochemical heterogeneities within the plume. These alternatives include: (1) concentric zonation created during plume ascent (Figure 2a), perhaps distorted by physical interaction between the plume and migrating oceanic lithosphere (Figure 2b); (2) bilateral asymmetry in the form of geochemically distinct, <50 km wide, streaks that are vertically continuous for possibly hundreds of kilometers (Figure 2c); these streaks were created as a plume ascends after sampling geochemical heterogeneities in the lower mantle; (3) a random distribution of geochemical heterogeneities with different solidi that are sampled in different proportions in the core to margin temperature gradient within the plume (Figure 2e).

7.5.1 Constraints from geochemical changes during shield stage volcanism

The geochemically zoned plume hypotheses for the Hawaiian plume (Figure 2) arose to explain the geochemical differences between shields dominated by Loa- and Kea-like volcanoes, but some shields are composed of both Loa- and Kea-like lavas, e.g., West Molokai (this paper), Koolau [*Tanaka et al.*, 2002; *Haskins and Garcia*, 2004; *Huang and Frey*, 2005b], Haleakala [*Ren et al.*, 2005a; *Abouchami and Frey*, 2006] and Mauna Kea [e.g., *Blichert-Toft et al.*, 2003; *Eisele et al.*, 2003; *Huang and*

Frey, 2003; *Kurz et al.*, 2004; *Rhodes and Vollinger*, 2004].

A new constraint on the distribution of Loa- and Kea-like heterogeneities in the plume arises from studies of Molokai Island; all subaerially erupted samples from East Molokai volcano are Kea-like [*Xu et al.*, 2005]. In contrast, ~20 km to the west, West Molokai lavas, both subaerially and submarine erupted, require localized Loa- and Kea-like heterogeneities in the source. The extreme model for explaining such short-term isotopic variability is a locally heterogeneous source [e.g., *Zindler et al.*, 1984]. These local heterogeneities may vary in proportion with location (Figure 2d), in particular, dominantly Kea-like in the source of East Molokai lavas to both Kea- and Loa-like sources in the source of West Molokai shield lavas to dominantly Loa-like in the source of Penguin Bank lavas, erupted west of the West Molokai shield (Figure 1a) [*Clague et al., in preparation, 2007*]. This spatial zonation can be explained if East Molokai and Penguin Bank sampled the Kea and Loa sides, respectively, of a bilaterally zoned plume, whereas the West Molokai shield sampled a transition zone where Kea- and Loa-like sources were both abundant (Figure 14a).

7.5.2 Constraints from geochemical changes accompanying the shield to postshield transition

The models in Figure 2 lead to different predictions for the temporal geochemical variation during the transition from the shield to postshield stage (Table 7a). Specifically, a concentrically zoned model predicts that a Loa-like shield should change to a Kea-like postshield as the Loa volcano migrates from the core to margin of the plume, whereas a Kea shield formed at the plume margin is expected to retain a

Kea-signature as it enters the postshield stage. However, if a radially zoned plume is distorted by physical interaction with the lithosphere (e.g., Figure 2b, Figure 17 of *Bryce et al.* [2005]), the postshield stage of a Loa volcano may not sample the presumed Kea-like margin. The temporal evolution, Kea-like shield and postshield and Loa-like shield and postshield, is expected for the asymmetrically zoned models (Figure 2c, d) providing that the Loa-Kea compositional boundary is aligned with the direction of plate motion (see Figure 3 of *Abouchami et al.* [2005]). In contrast, the randomly distributed heterogeneity model (Figure 2e) predicts that different proportions of components in magma arise because the components have different solidus temperatures; for example, lavas derived from the hotter plume core should have a higher proportion of the component with a high solidus temperature than lavas derived from the plume margin, such as postshield lavas.

An important question is - which component, Loa or Kea has the lower solidus? *Huang et al.* [2005a] proposed that the Loa component has the lowest solidus because the extreme Loa end-member, represented by Koolau shield (Makapuu stage) originated from recycled oceanic crust and sediment [*Huang and Frey*, 2005b]. This inference is consistent with the relatively high Ni and SiO_2 contents of Makapuu lavas that led *Sobolev et al.* [2005] to propose a dominantly pyroxenite source for Makapuu lavas; a hypothesis supported by the recent Pb isotope study on Koolau Volcano [*Fekiacova et al.*, 2007]. However, if the Loa component has a relatively low solidus temperature it should be the dominant contributor to all postshield magmas.

Postshield lavas have been studied at the Kea-trend volcanoes, Mauna Kea,

Kohala, Haleakala and East Molokai. In each case the decreasing magma flux is accompanied by a change from tholeiitic to alkalic lavas, consistent with a decrease in extent of melting as the volcano migrated to the lower temperature plume margin. Generally, relative to shield lavas, Kea postshield lavas have lower $^{87}Sr/^{86}Sr$ and higher $^{143}Nd/^{144}Nd$, and postshield lavas from the different Kea volcanoes define overlapping fields in Sr-Nd isotopic space [*Xu et al.*, 2005]. Therefore, a depleted (i.e., lower $^{87}Sr/^{86}Sr$ and higher $^{143}Nd/^{144}Nd$) component becomes important as a Kea volcano samples the plume margin [*Xu et al.*, 2005]. In contrast, relative to shield lavas, the associated postshield lavas may have higher (Kohala) or lower (Mauna Kea) $^{206}Pb/^{204}Pb$. Regardless, the Kea-like $^{208}Pb^*/^{206}Pb^*$ (< 0.95) occurs in Kea shield and postshield lavas. This Pb isotopic similarity of Kea shield and postshield lavas has been used to argue that the Kea component has persisted for 1.5 Ma [*Gaffney et al.*, 2004; *Abouchami et al.*, 2005; *Xu et al.*, 2005]. The persistence of the Kea signature from shield to postshield lavas is consistent with models 1 to 4 (Table 7a and Figures 2a, b, c, d) but inconsistent with model 5 in Table 7 and Figure 2e if the Loa component has a lower solidus temperature.

At the Loa-trend volcanoes, Hualalai and Kahoolawe, the postshield lavas retain the Loa-like Pb isotopic signature ($^{208}Pb^*/^{206}Pb^* > 0.95$) [*West et al.*, 1987; *Cousens et al.*, 2003 and references therein; *Hanano et al.*, 2005; *Xu et al.*, 2005; *Huang et al.*, 2006]. This observation is inconsistent with the concentrically zoned model (Figure 2a and model 1 in Table 7a), but consistent with the distorted radial zonation [*Bryce et al.*, 2005] and bilaterally zoned [*Abouchami et al.*, 2005] models, i.e., Figure 2b, c, d

and models 2, 3, 4 in Table 7a.

In summary, models 2, 3, and 4 (Table 7a) are consistent with existing data for the shield to postshield evolution of Loa and Kea trend volcanoes. None of these models, however, explains the trend to lower $^{87}Sr/^{86}Sr$ and higher $^{143}Nd/^{144}Nd$ during the shield to postshield transition of Kea-trend volcanoes. Nevertheless, we ask – can the West Molokai data distinguish between radially and bilaterally zoned models? We suggest that the change at West Molokai volcano from a shield composed of Loa- and Kea-like lavas to a Kea-like postshield can be best explained by a bilaterally zoned model if the direction of Pacific plate motion changed relative to the strike of the bilateral zonation axis (e.g., Figure 3 of *Abouchami et al.* [2005]). Specifically, the Pacific plate motion changed at 2-3 Ma, between Oahu and Molokai Islands in the vicinity of the Molokai Fracture Zone (Figure 1) and subsequent volcanism created the distinct Loa and Kea trends [*Wessel and Kroenke*, 1997; *Hieronymus and Bercovici*, 2001]. This change in plate motion from N65°W at Oahu to N30°W at Maui [*DePaolo et al.*, 2001] would affect the sampling of a bilaterally zoned plume. That is, the West Molokai shield sampled a central region of the plume core comprised of significant amounts of Loa and Kea components, but because the strike of the Pacific plate changed from N65°W to N30°W the postshield stage of West Molokai sampled the Kea half of the zoned plume (Figure 14).

8. Conclusions

At West Molokai, a Hawaiian volcano on the Loa spatial trend, both shield tholeiitic basalt and postshield alkalic lavas are exposed. Geochemical data for these

lavas and associated glasses lead to the following conclusions:

(1) Compared to postshield hawaiite from Kea-trend volcanoes (Mauna Kea, Kohala, Haleakala), hawaiites from West Molokai have lower SiO_2 and higher Fe_2O_3* and TiO_2 contents. Fractionation of Fe-Ti oxides was more important in the fractionation process that led to hawaiites at these Kea-trend volcanoes than at West Molokai.

(2) Tholeiitic glasses associated with West Molokai shield stage lavas range widely in major element compositions; artifact glasses and their presumed sources, glassy dike margins, are Loa-like (e.g., low CaO at a given MgO content); in contrast submarine glasses collected from a sediment-covered breccia slope have Kea-like compositions.

(3) Most West Molokai tholeiitic shield basalts have high Zr/Nb (>13) and Sr/Nb (>32) ratios overlapping the Mauna Loa field, but some shield and all postshield lavas have lower Zr/Nb and Sr/Nb ratios that overlap the Mauna Kea field.

(4) Most West Molokai shield stage lavas have higher $^{87}Sr/^{86}Sr$ and $^{208}Pb^*/^{206}Pb^*$, lower $^{143}Nd/^{144}Nd$, $^{176}Hf/^{177}Hf$ and $^{206}Pb/^{204}Pb$ than postshield lavas; they overlap the field defined by Mauna Loa lavas and one sample is like the extreme Hawaiian geochemical endmember represented by Koolau (Makapuu-stage) lavas. In contrast, four shield and all postshield lavas plot in the field of Kea-trend lavas.

(5) We infer that the West Molokai shield was derived from a bilaterally zoned plume source, Kea in the northeast, Loa in the southwest, with a central zone composed of Loa- and Kea-like components. The change to exclusively Kea-like

characteristics in the West Molokai postshield reflects the change in strike of the Pacific plate in the vicinity of Molokai Island.

Acknowledgement

I thank Frank Dudas for his help and guidance for the Sr, Nd and Pb isotope analyses and column separations. Sam Bowring is thanked for providing financial support for the isotopic analyses at MIT. Rick Kayser is thanked for his assistance in ICP-MS analysis. F. Albarède, S. Galer, M. Garcia and S. Huang are thanked for their comments and discussion. M. Bizimis, an anonymous reviewer, and V. Salters are thanked for their constructive reviews. I thank the co-authors (F.A. Frey, D.A. Clauge, W. Abouchami, J. Blichert-Toft, B. Cousens and M. Weisler) for their contributions which lead to publication of this chapter at G^3. This research was supported by NSF Grant EAR-0607895 to F.A. Frey, the David and Lucile Packard Foundation to MBARI to D.A. Clague and financial support from INSU to J. Blichert-Toft.

References

Abouchami, W., and F. A. Frey (2006), Temporal Evolution of Pb Isotopes in Shield Lavas from Haleakala Volcano, *Geophysical Research Abstracts*, *8*.

Abouchami, W., S. J. G. Galer, and A. W. Hofmann (2000), High precision lead isotope systematics of lavas from the Hawaiian Scientific Drilling Project, *Chem. Geol.*, *169*, 187-209.

Abouchami, W., A. W. Hofmann, S. J. G. Galer, F. A. Frey, J. Eisele, and M. Feigenson (2005), Lead isotopes reveal bilateral asymmetry and vertical continuity in the Hawaiian mantle plume, *Nature*, *434*, 851-856.

Basu, A. R., and B. E. Faggart (1996), Temporal isotopic variations in the Hawaiian mantle plume: the Lanai anomaly, the Molokai Fracture Zone and a seawater-altered lithospheric component in Hawaiian volcanism, in *Earth Processes: Reading the isotopic code*, edited by A. R. Basu and S. R. Hart, pp. 149-159, Geophysical Monograph, AGU, Washington, D. C.

Bedard, J. H. (2005), Partitioning coefficients between olivine and silicate melts, *Lithos*, *83*, 394-419.

Bindeman, I. N., A. M. Davis, and M. J. Drake (1998), Ion microprobe study of plagioclase-basalt partition experiments at natural concentration levels of trace elements, *Geochim. Cosmochim. Acta*, *62*, 1175-1193.

Blichert-Toft, J., and F. Albarède (1999), Hf isotopic compositions of the Hawaii Scientific Drilling Project core and the source mineralogy of Hawaiian basalts, *Geophy. Res. Lett.*, *26*, 935-938.

Blichert-Toft, J., F. A. Frey, and F. Albarède (1999), Hf isotope evidence for pelagic sediments in the source of Hawaiian basalts, *Science*, *285*, 879-882.

Blichert-Toft, J., D. Weis, C. Maerschalk, A. Agranier, and F. Albarède (2003), Hawaiian hot spot dynamics as inferred from the Hf and Pb isotope evolution of Mauna Kea volcano, *Geochem. Geophy. Geosyst.*, *4*, doi:10.1029/2002GC000340.

Blundy, J., and J. Dalton (2000), Experimental comparison of trace element partitioning between clinopyroxene and melt in carbonate and silicate systems, and implications for mantle metasomatism, *Contrib. Mineral. Petrol.*, *139*, 356-371.

Bryce, J. G., D. J. DePaolo, and J. C. Lassiter (2005), Geochemical structure of the Hawaiian plume: Sr, Nd, and Os isotopes in the 2.8 km HSDP-2 section of Mauna Kea volcano, *Geochem. Geophy. Geosyst.*, *6*, doi:10.1029/2004GC000809.

Chen, C. Y., F. Frey, J. M. Rhodes, and R. M. Easton (1996), Temporal geochemical evolution of Kilauea volcano: Comparison of Hilina and Puna basalt, in *Earth Processes: Reading the isotopic code*, edited by A. Basu and S. R. Hart, pp. 161-181, Geophysical Monograph, AGU, Washington, D.C.

Chen, C. Y., and F. A. Frey (1985), Trace-Element and Isotopic Geochemistry of Lavas from Haleakala Volcano, East Maui, Hawaii - Implications for the Origin of Hawaiian Basalts, *Journal of Geophysical*

Research-Solid Earth and Planets, *90*, 8743-8768.

Clague, D. A. (1987), Petrology of West Molokai Volcano, *Geol. Soc. Am. Abs.*, *19*, 366.

Clague, D. A., and G. B. Dalrymple (1987), The Hawaiian-Emperor volcanic chain: Part I: Geologic evolution, *U.S. Geol. Sury. Prof. Pap.*, *1350*, 5-54.

Clague, D. A., J. G. Moore, J. E. Dixon, and W. B. Friesen (1995), Petrology of Submarine Lavas from Kilaueas Puna Ridge, Hawaii, *J. Petrol.*, *36*, 299-349.

Cohen, A. S., R. K. ONions, and M. D. Kurz (1996), Chemical and isotopic variations in Mauna Loa tholeiites, *Earth Planet. Sci. Lett.*, *143*, 111-124.

Coombs, M. L., T. W. Sisson, and P. W. Lipman (2006), Growth history of Kilauea inferred from volatile concentrations in submarine-collected basalts, *J. Volcano. Geoth. Res.*, *151*, 19-49.

Cousens, B. L., D. A. Clague, and W. D. Sharp (2003), Chronology, chemistry, and origin of trachytes from Hualalai Volcano, Hawaii, *Geochem. Geophy. Geosyst.*, *4*, doi:10.1029/2003GC000560.

DePaolo, D. J., J. G. Bryce, A. Dodson, D. L. Shuster, and B. M. Kennedy (2001), Isotopic evolution of Mauna Loa and the chemical structure of the Hawaiian plume, *Geochem. Geophy. Geosyst.*, *2*, doi:10.1029/2000GC000139.

Dixon, J. E., D. A. Clague, and E. M. Stolper (1991), Degassing History of Water, Sulfur, and Carbon in Submarine Lavas from Kilauea Volcano, Hawaii, *J. Geol.*, *99*, 371-394.

Eisele, J., W. Abouchami, S. J. G. Galer, and A. W. Hofmann (2003), The 320 kyr Pb isotope evolution of Mauna Kea lavas recorded in the HSDP-2 drill core, *Geochem. Geophy. Geosyst.*, *4*, doi:10.1029/2002GC000339.

Fekiacova, Z., W. Abouchami, S. J. G. Galer, M. Garcia, and A. W. Hofmann (2007), Temproal evolution of Koolau volcano: inferences from isotope results on the Koolau Scientific Drilling Project (KSDP) and Honolulu Volcanics, *Earth Planet. Sci. Lett., in press.*

Fodor, R. V., F. A. Frey, G. R. Bauer, and D. A. Clague (1992), Ages, Rare-Earth Element Enrichment, and Petrogenesis of Tholeiitic and Alkalic Basalts from Kahoolawe Island, Hawaii, *Contrib. Mineral. Petrol.*, *110*, 442-462.

Frey, F. A., M. O. Garcia, and M. F. Roden (1994), Geochemical Characteristics of Koolau Volcano - Implications of Intershield Geochemical Differences among Hawaiian Volcanos, *Geochim. Cosmochim. Acta*, *58*, 1441-1462.

Frey, F. A., M. O. Garcia, W. S. Wise, A. Kennedy, P. Gurriet, and F. Albarède (1991), The Evolution of Mauna-Kea Volcano, Hawaii - Petrogenesis of Tholeiitic and Alkalic Basalts, *Journal of Geophysical Research-Solid Earth and Planets*, *96*, 14347-14375.

Frey, F. A., S. Huang, J. Blichert-Toft, M. Regelous, and M. Boyet (2005), Origin of depleted components in basalt related to the Hawaiian hot spot: Evidence from isotopic and incompatible

element ratios, *Geochem. Geophy. Geosyst.*, *6*, doi:10.1029/2004GC000757.

Frey, F. A., and J. M. Rhodes (1993), Intershield geochemical differences among Hawaiian volcanoes: implications for source compositions, melting process and magma ascent paths, *Phil. Trans. R. Soc. Lond. A*, *342*, 121-136.

Frey, F. A., W. S. Wise, M. O. Garcia, H. West, S. T. Kwon, and A. Kennedy (1990), Evolution of Mauna-Kea Volcano, Hawaii - Petrologic and Geochemical Constraints on Postshield Volcanism, *Journal of Geophysical Research-Solid Earth and Planets*, *95*, 1271-1300.

Gaffney, A. M., B. K. Nelson, and J. Blichert-Toft (2004), Geochemical constraints on the role of oceanic lithosphere in intra-volcano heterogeneity at West Maui, Hawaii, *J. Petrol.*, *45*, 1663-1687.

Gaffney, A. M., B. K. Nelson, and J. Blichert-Toft (2005), Melting in the Hawaiian plume at 1-2 Ma as recorded at Maui Nui: The role of eclogite, peridotite, and source mixing, *Geochem. Geophy. Geosyst.*, *6*, doi:10.1029/2005GC000927.

Garcia, M. O. (1996), Petrography and olivine and glass chemistry of lavas from the Hawaii Scientific Drilling Project, *J. Geophy. Res.*, *101*, 11701-11713.

Garcia, M. O., T. P. Hulsebosch, and J. M. Rhodes (1995), *Olivine-rich submarine basalts from the Southwest rift zone of Mauna Loa volcano: implications for magmatic processes and geochemical evolution*, 219-239 pp., Geophysical Monograph, AGU, Washington, D.C.

Garcia, M. O., D. W. Muenow, K. E. Aggrey, and J. R. Oneil (1989), Major Element, Volatile, and Stable Isotope Geochemistry of Hawaiian Submarine Tholeiitic Glasses, *Journal of Geophysical Research-Solid Earth and Planets*, *94*, 10525-10538.

Hammer, J. E., M. L. Coombs, P. J. Shamberger, and J.-I. Kimura (2006), Submarine sliver in North Kona: A window into the early magmatic and growth history of Hualalai Volcano, Hawaii, *J. Volcano. Geoth. Res.*, *151*, 157-188.

Hanano, D., D. Weis, S. Aciego, J. Scoates, and D. DePaolo (2005), Geochemical systematics of Hawaiian postshield lavas: Implications for the chemical structure of the Hawaiian mantle plume, *Eos Trans. AGU, 86 (52), Fall Meet. Suppl., Abstract V41D-1497.*

Haskins, E. H., and M. O. Garcia (2004), Scientific drilling reveals geochemical heterogeneity within the Ko'olau shield, Hawai'i, *Contrib. Mineral. Petrol.*, *147*, 162-188.

Hauri, E. H., J. C. Lassiter, and D. J. DePaolo (1996), Osmium isotope systematics of drilled lavas from Mauna Loa, Hawaii, *J. Geophy. Res.*, *101*, 11793-11806.

Helz, R. T., and T. L. Wright (1992), Differentiation and Magma Mixing on Kilauea East Rift-Zone - a Further Look at the Eruptions of 1955 and 1960 .1. The Late 1955 Lavas, *Bull. Volcano.*, *54*, 361-384.

Herzberg, C. (2005), Mantle geochemistry: Big lessons from little droplets, *Nature*, *436*, 789-790.

Hieronymus, C. F., and D. Bercovici (2001), A theoretical model of hotspot volcanism: Control on

volcanic spacing and patterns via magma dynamics and lithospheric stresses, *J. Geophy. Res.*, *106*, 683-702.

Hofmann, A. W. (2004), Sampling Mantle Heterogeneity through Oceanic Basalts: Isotopes and Trace Elements, in *Treatise on Geochemistry*, edited by H. D. Holland and K. K. Turekian, pp. 61-101, Elsevier-Pergamon, Oxford.

Huang, S., M. Bizimis, R. V. Fodor, and G. R. Bauer (2006), Geochemical Structure of the Hawaiian Plume: Constraints from the shield to postshield transition, *Eos Trans. AGU, 87(52), Fall Meet. Suppl.* , Abstract V13B-0665.

Huang, S., and F. A. Frey (2003), Trace element abundances of Mauna Kea basalt from phase 2 of the Hawaii Scientific Drilling Project: Petrogenetic implications of correlations with major element content and isotopic ratios, *Geochem. Geophy. Geosyst.*, *4*, doi:10.1029/2002GC000322.

Huang, S., and F. A. Frey (2005a), The Geochemical Structure of the Hawaiian Plume, *Eos Trans. AGU, 86(52), Fall Meet. Suppl.* , Abstract V51A-1466.

Huang, S. C., F. Frey, J. Blichert-Toft, R. V. Fodor, and G. P. Xu (2005a), Depleted rejuvenated-stage source component in Hawaiian shield-stage lavas, *Geochim. Cosmochim. Acta*, *69*, A104-a104.

Huang, S. C., and F. A. Frey (2005b), Recycled oceanic crust in the Hawaiian Plume: evidence from temporal geochemical variations within the Koolau Shield, *Contrib. Mineral. Petrol.*, *149*, 556-575.

Huang, S. C., F. A. Frey, J. Blichert-Toft, R. V. Fodor, G. R. Bauer, and G. P. Xu (2005b), Enriched components in the Hawaiian plume: Evidence from Kahoolawe Volcano, Hawaii, *Geochem. Geophy. Geosyst.*, *6*, doi:10.1029/2005GC001012.

Ito, G., and J. J. Mahoney (2005), Flow and melting of a heterogeneous mantle: 1. Method and importance to the geochemistry of ocean island and mid-ocean ridge basalts, *Earth Planet. Sci. Lett.*, *230*, 29-46.

Jackson, D. E., E. A. Silver, and G. B. Dalrymple (1972), Hawaiian-Emperor chain and its relation to Cenozoic circumpacific tectonics, *Geol. Soc. Am. Bull.*, *83*, 601-618.

Jang, Y. D., and H. R. Naslund (2003), Major and trace element variation in ilmenite in the Skaergaard Intrusion: petrologic implications, *Chem. Geol.*, *193*, 109-125.

Kennedy, A. K., S. T. Kwon, F. A. Frey, and H. B. West (1991), The Isotopic Composition of Postshield Lavas from Mauna-Kea Volcano, Hawaii, *Earth Planet. Sci. Lett.*, *103*, 339-353.

Kurz, M. D., J. Curtice, D. E. Lott, and A. Solow (2004), Rapid helium isotopic variability in Mauna Kea shield lavas from the Hawaiian Scientific Drilling Project, *Geochem. Geophy. Geosyst.*, *5*, doi:10.1029/2002GC000439.

Kurz, M. D., T. C. Kenna, D. P. Kammer, J. M. Rhodes, and M. O. Garcia (1995), Isotopic evolution of Mauna Loa volcano: a view from the submarine Southwest Rift Zone, in *Mauna Loa Revealed:*

Structure, Composition, History, and Hazards, edited by J. M. Rhodes and J. P. Lockwood, pp. 289-306, Geophysical Monograph, AGU, Washington, D. C.

Lassiter, J. C., D. J. DePaolo, and M. Tatsumoto (1996), Isotopic evolution of Mauna Kea volcano: Results from the initial phase of the Hawaii Scientific Drilling Project, *J. Geophy. Res.*, *101*, 11769-11780.

Macdonald, G. A., and T. Katsura (1964), Chemical compositional of Hawaiian lavas, *J. Petrol.*, *5*, 82-133.

McDougall, I. (1964), Potassium-argon ages from lavas of the Hawaiian Islands, *Geol. Soc. Am. Bull.*, *75*, 107-128.

Menard, H. W. (1962), Correlation between length and offset on very large wrench faults, *J. Geophys. Res. Solid Earth*, *67*, 4096-4098.

Moore, J. G., W. B. Bryan, M. H. Beeson, and W. R. Normark (1995), Giant Blocks in the South Kona Landslide, Hawaii, *Geology*, *23*, 125-128.

Moore, J. G., and D. A. Clague (1987), Coastal lava flows from Mauna Loa and Hualalai volcanoes, Kona, Hawaii, *Bull. Volcano.*, *49*, 752-764.

Moore, J. G., and D. A. Clague (1992), Volcano Growth and Evolution of the Island of Hawaii, *Geol. Soc. Am. Bull.*, *104*, 1471-1484.

Moore, J. G., and D. A. Clague (2002), Mapping the Nuuanu and Wailau landslides in Hawaii, in *Hawaiian Volcanoes: Deep Underwater Perspectives*, edited by E. Takahashi, et al., pp. 223-244, Geophysical Monograph, AGU, Washington, D. C.

Moore, J. G., D. A. Clague, and W. R. Normark (1982), Diverse Basalt Types from Loihi Seamount, Hawaii, *Geology*, *10*, 88-92.

Pietruszka, A. J., and M. O. Garcia (1999), The size and shape of Kilauea Volcano's summit magma storage reservoir: a geochemical probe, *Earth Planet. Sci. Lett.*, *167*, 311-320.

Price, J. P., and D. Elliott-Fisk (2004), Topographic History of the Maui Nui Complex, Hawaii, and Its Implications for Biogeography, *Pacific Science*, *58*, 27-45.

Ren, Z.-Y., T. Shibata, M. Yoshikawa, K. T. M. Johnson, and E. Takahashi (2005a), Isotope Compositions of Submarine Hana Ridge Lavas, Haleakala Volcano, Hawaii: Implications for Source Compositions, Melting Process and the Structure of the Hawaiian Plume, *J. Petrol.*, *doi:10.1093/petrology/egi074*.

Ren, Z. Y., S. Ingle, E. Takahashi, N. Hirano, and T. Hirata (2005b), The chemical structure of the Hawaiian mantle plume, *Nature*, *436*, 837-840.

Rhodes, J. M. (1995), The 1852 and 1868 Mauna Loa picrite eruptions: clues to parental magma compositions and the magmatic plumbing system, in *Mauna Loa Revealed: Structure, Composition,*

History, and Hazards, edited by J. M. Rhodes and J. P. Lockwood, pp. 241-262, Geophysical Monograph, AGU, Washington, D. C.

Rhodes, J. M. (1996), Geochemical stratigraphy of lava flows sampled by the Hawaii Scientific Drilling Project, *J. Geophy. Res.*, *101*, 11729-11746.

Rhodes, J. M., and S. R. Hart (1995), Episodic trace element and isotopic variations in historical Mauna Loa lavas: implications for Magma and plume dynamics, in *Mauna Loa Revealed: Structure, Composition, History, and Hazards*, edited by J. M. Rhodes and J. P. Lockwood, pp. 263-288, Geophysical Monograph, AGU, Washington, D. C.

Rhodes, J. M., and M. J. Vollinger (2004), Composition of basaltic lavas sampled by phase-2 of the Hawaii Scientific Drilling Project: Geochemical stratigraphy and magma types, *Geochem. Geophy. Geosyst.*, *5*, doi:10.1029/2002GC000434.

Robinson, J. E., and B. W. Eakins (2006), Calculated volumes of individual shield volcanoes at the young end of the Hawaiian Ridge, *J. Volcano. Geoth. Res.*, *151*, 309-317.

Roden, M. F., T. Trull, S. R. Hart, and F. A. Frey (1994), New He, Nd, Pb, and Sr Isotopic Constraints on the Constitution of the Hawaiian Plume - Results from Koolau Volcano, Oahu, Hawaii, USA, *Geochim. Cosmochim. Acta*, *58*, 1431-1440.

Searle, R. C., R. T. Holcomb, J. B. Wilson, M. L. Holmes, R. J. Whittington, E. S. Kappel, B. A. McGregor, and A. N. Shor (1993), The Molokai Fracture Zone near Hawaii, and the Late Cretaceous change in Pacific/Farallon spreading Direction, in *The Mesozoic Pacific: Geology, Tectonics, and Volcanism*, edited by M. S. Pringle, et al., pp. 155-169, Geophysical Monograph, AGU, Washington, D. C.

Shinozaki, K., Z.-Y. Ren, and E. Takahashi (2002), Geochemical and Petrological characteristics of Nuuanu and Wailau landslides blocks, in *Hawaiian Volcanoes: Deep Underwater Perspectives*, edited by E. Takahashi, et al., pp. 297-310, Geophysical Monograph, AGU, Washington, D.C.

Sims, K. W. W., D. J. DePaolo, M. T. Murrell, W. S. Baldridge, S. Goldstein, D. Clague, and M. Jull (1999), Porosity of the melting zone and variations in the solid mantle upwelling rate beneath Hawaii: Inferences from U-238-Th-230-Ra-226 and U-235-Pa-231 disequilibria, *Geochim. Cosmochim. Acta*, *63*, 4119-4138.

Sinton, J. M. (1987), Revision of stratigraphic nomenclature of Waianae Volcano, Oahu, Hawaii, *U.S. Geological Survey Bulleton*, *1775A*, A9-A15.

Sisson, T. W., and P. W. Lipman (2002), Submarine alkalic through tholeiitic shield-stage development of Kilauea Volcanoe, Hawaii, in *Hawaiian Volcanoes: Deep Underwater Perspectives*, edited by E. Takahashi, et al., pp. 193-219, Geophysical Monograph, AGU, Washington, D.C.

Sobolev, A. V., A. W. Hofmann, S. V. Sobolev, and I. K. Nikogosian (2005), An olivine-free mantle source of Hawaiian shield basalts, *Nature*, *434*, 590-597.

Steiger, R. H., and E. Jager (1977), Subcommission on Geochronology - Convention on Use of Decay Constants in Geochronology and Cosmochronology, *Earth Planet. Sci. Lett.*, *36*, 359-362.

Stille, P., D. M. Unruh, and M. Tatsumoto (1986), Pb, Sr, Nd, and Hf Isotopic Constraints on the Origin of Hawaiian Basalts and Evidence for a Unique Mantle Source, *Geochim. Cosmochim. Acta*, *50*, 2303-2319.

Stolper, E., S. Sherman, M. Garcia, M. Baker, and C. Seaman (2004), Glass in the submarine section of the HSDP2 drill core, Hilo, Hawaii, *Geochem. Geophy. Geosyst.*, *5*, doi:10.1029/2003GC000553.

Stracke, A., V. J. M. Salters, and K. W. W. Sims (1999), Assessing the presence of garnet-pyroxenite in the mantle sources of basalts through combined hafnium-neodymium-thorium isotope systematics, *Geochem. Geophy. Geosyst.*, *1*, doi:10.1029/1999GC000013.

Tanaka, R., E. Nakamura, and E. Takahashi (2002), Geochemical evolution of Koolau Volcano, Hawaii, in *Hawaiian Volcanoes: Deep Underwater Perspectives*, edited by E. Takahashi, et al., pp. 311-332, Geophysical Monograph, AGU, Washington, D.C.

Tatsumoto, M. (1978), Isotopic Composition of Lead in Oceanic Basalt and Its Implication to Mantle Evolution, *Earth Planet. Sci. Lett.*, *38*, 63-87.

ten Brink, U. S., and T. M. Brocher (1988), Multichannel Seismic Evidence for Variations in Crustal Thickness across the Molokai Fracture-Zone in the Mid-Pacific, *Journal of Geophysical Research-Solid Earth and Planets*, *93*, 1119-1130.

Wanless, V. D., M. O. Garcia, J. Michael Rhodes, D. Weis, and M. D. Norman (2006), Shield-stage alkalic volcanism on Mauna Loa Volcano, Hawaii, *J. Volcano. Geoth. Res.*, *151*, 141-155.

Weisler, M. I., and D. A. Clague (1998), Characterization of archaeological volcanic glass from Oceania: The utility of three techniques, in *Archaeological Obsidian Studies: Methods and theory*, edited by M. S. Shackley, pp. 103-128, Plenum Press, New York and London.

Wessel, P., and L. Kroenke (1997), A geometric technique for relocating hotspots and refining absolute plate motions, *Nature*, *387*, 365-369.

West, H. B., M. O. Garcia, F. A. Frey, and A. Kennedy (1988), Nature and Cause of Compositional Variation among the Alkalic Cap Lavas of Mauna-Kea Volcano, Hawaii, *Contrib. Mineral. Petrol.*, *100*, 383-397.

West, H. B., D. C. Gerlach, W. P. Leeman, and M. O. Garcia (1987), Isotopic Constraints on the Origin of Hawaiian Lavas from the Maui Volcanic Complex, Hawaii, *Nature*, *330*, 216-220.

Xu, G., F. A. Frey, D. A. Clague, D. Weis, and M. H. Beeson (2005), East Molokai and other Kea-trend volcanoes: Magmatic processes and sources as they migrate away from the Hawaiian hot spot, *Geochem. Geophy. Geosyst.*, *6*, doi:10.1029/2004GC000830.

Yang, H. J., F. A. Frey, D. A. Clague, and M. O. Garcia (1999), Mineral chemistry of submarine lavas

from Hilo Ridge, Hawaii: implications for magmatic processes within Hawaiian rift zones, *Contrib. Mineral. Petrol., 135*, 355-372.

Yang, H. J., F. A. Frey, J. M. Rhodes, and M. O. Garcia (1996), Evolution of Mauna Kea volcano: Inferences from lava compositions recovered in the Hawaii Scientific Drilling Project, *J. Geophy. Res., 101*, 11747-11767.

Zindler, A., H. Staudigel, and R. Batiza (1984), Isotope and trace element geochemistry of young Pacific seamounts: implications for the scale of upper mantle heterogeneity, *Earth Planet. Sci. Lett., 70*, 175-195.

Figure Caption

Figure 1 (a) Young, ≤ 2 Ma Hawaiian volcanoes, i.e., from Molokai Island to Loihi seamount, define the subparallel spatial trends, known as Loa and Kea. Although *Jackson et al.* [1972] included Koolau volcano on the Loa-trend, West Molokai is the oldest Loa-trend volcano on the subparallel portion of the Loa- and Kea-trends. The Molokai Fracture Zone cross-cuts the Hawaiian Ridge in the vicinity of Molokai Island but is a complex feature consisting of two separate bands [*Searle et al.*, 1993]. (b) Map showing the location of dredged sample D8-1 which was interpreted to be from West Molokai [*Tanaka et al.*, 2002] and dive T307 samples relative to the boundaries of the Nuuanu and Wailau landslides derived from the Koolau and East Molokai shield, respectively [after *Moore and Clague*, 2002].

Figure 2 Five different plume models proposed to explain the geochemical differences between Loa and Kea shields. (a) The concentrically zoned model assumes that Loa-trend volcanoes sample the core of the plume whereas Kea-trend volcanoes sample the margin of the plume [e.g., *Lassiter et al.*, 1996]; (b) The radially zoned plume model is a variant of the concentrically zoned plume model [*Bryce et al.*, 2005], which includes downstream distortion of the plume by interaction with the Pacific lithosphere. In this model, Loa volcanoes never sample the margin of the plume; (c) The bilaterally zoned plume model [*Abouchami et al.*, 2005] assumes that the southwest side of the plume is geochemically distinct from the northeast side of the plume; (d) The partly ordered zonation model [e.g., *Herzberg*, 2005] has the proportion of randomly distributed heterogeneities (in red) varying systematically from the Loa to Kea parts of the plume; (e) The randomly distributed heterogeneity model has no systematic zonation [*Huang and Frey*,

2005a; *Ren et al.*, 2005b]. As drawn, Loa volcanoes sample a higher proportion of heterogeneities with low solidii, perhaps recycled oceanic crust and sediment (red color) whereas Kea volcanoes which are at the plume center sample a higher proportion of components (blue background) with high solidii. Note that all of these models emphasize the lateral zonation of the plume (i. e., horizontal heterogeneity) and do not consider vertical heterogeneities; *Blichert-Toft et al.* [2003] argued that because of the inferred high upwelling velocity of the plume vertical heterogeneities are also important and should not be neglected.

Figure 3 Map of western Molokai Island showing locations of the studied samples. The thick dashed lines represent the southwest and northwest rift zones. The dive samples (T307) were collected from ~10 km north of the West Molokai coast (Figure 1b). Most of the tholeiitic lavas were collected along highway 460 northwest of Puu Nana. Samples 84WMOL-1C and 84WMOL-1D were collected along highway 460 between the two arrows. Three tholeiitic glass samples (WM-11, 89FDD-1 and 89FDD-2) were collected from two dikes southeast (<500 m) of Puu Nana. An alkalic glass from a dike (89KAA-1) was collected near the north coast at Kaa Gulch. All the other glass samples are artifacts from settlement sites near Moomomi on the north coast. Most alkalic basalt and hawaiite were sampled from the northwest West Molokai, i.e., beach cobbles, near western coastal outcrops from Kawakiuiki to Puu o Kaiaka, and cones, Okoli, Puu Apalu and Nau Puu Kulua, close to the 100 m contour. Three alkalic samples (in red) were analyzed for K-Ar ages (Table 1).

Figure 4 Na_2O+K_2O versus SiO_2 classification plot showing that the West Molokai whole rocks

and glass range from tholeiitic to alkalic basalt and hawaiite. The alkalic-tholeiitic dividing line is from *Macdonald and Katsura* [1964]. Major element data were adjusted to a $Fe^{3+}/(Fe^{2+} + Fe^{3+})$ molar ratio of 0.10. Whole rock samples with K_2O/P_2O_5 less than 1.21 were corrected for K_2O loss during alteration (see Appendix Figure 2). Most whole-rock (54 samples) and glass data are from this paper but also plotted are literature data from *Macdonald and Katsura* [1964] (2 samples) and *Shinozaki et al.* [2002] (36 samples).

Figure 5 MgO vs CaO, SiO_2 and Na_2O and TiO_2/Na_2O vs Al_2O_3/CaO for West Molokai glasses. The alkalic glasses of artifacts are identical to that of the alkalic dike, and they are distinguished from tholeiitic glasses by lower CaO and SiO_2 but higher Na_2O at a given MgO content. Note that at a given MgO content tholeiitic glasses from the submarine breccia slope have higher CaO and lower Na_2O than tholeiitic glasses from the artifacts and dikes. To avoid the effects of clinopyroxene and plagioclase fractionation panel "d" shows data only for glasses with MgO > 6.5%. Fields for a typical Loa volcano (Mauna Loa) and a typical Kea volcano (Mauna Kea) are distinct; submarine West Molokai glasses overlap with the Mauna Kea field and the West Molokai artifacts and dike glasses overlap with the Mauna Loa field. Data sources: West Molokai – this study; Mauna Kea – *Garcia et al.* [1996], *Stolper et al.* [2004]; Mauna Loa – *Garcia et al.* [1989], *Garcia et al.* [1995], *Garcia et al.* [1996], *Moore and Clague* [1987; 1992], *Moore et al.* [1995].

Figure 6 MgO vs CaO, SiO_2, TiO_2, Al_2O_3, Fe_2O_3* and P_2O_5 for West Molokai whole rocks. For comparison tholeiitic glass data in which the total iron was converted to $Fe_2O_3^*$ are shown as green fields. Also shown for comparison are dark gray fields for Mauna Kea hawaiite. The arrows

in panels "a", "b" and "d" show the effect of olivine, plagioclase, clinopyroxene and Fe-Ti oxide fractionation. Two West Molokai samples, MAH-35 [*Shinozaki et al.*, 2002] and T307R2 (this paper, Table 3), which have Koolau (Makapuu-stage)-like major element compositions (i.e., high SiO_2, low CaO, TiO_2 and Fe_2O_3* at a given MgO content) are labeled. Five samples with high SiO_2 contents (>53%) (designated as highly fractionated tholeiites (HFT)) which have experienced fractionation of clinopyroxene, plagioclase and Fe-Ti are grouped. In panel "b" lavas with K_2O/P_2O_5 <1.3 which have lost K are labeled as a field. The whole rock data from this study and literature data (2 samples from *Macdonald and Katsura* [1964] and 36 samples from *Shinozaki et al.* [2002]) were plotted using the same symbols for clarity.

Figure 7 Th abundance vs Nb, Zr, Sr, Eu, Lu and MgO abundances for West Molokai lavas. Tholeiitic basalts with REE-Y enrichment are not shown in the Th-Eu and Th-Lu panels. The 2 sigma uncertainties for the trace elements analyzed by ICP-MS are ±3%.

Figure 8 $^{87}Sr/^{86}Sr$ vs. (a) $^{143}Nd/^{144}Nd$ and (b) $^{176}Hf/^{177}Hf$ for West Molokai and East Molokai lavas. For comparison the fields are shield stage lavas from Kea and Loa volcanoes in panel "a" and Mauna Kea shield and postshield lavas and Loa shield lavas in panel "b". Only acid-leached Sr and Nd isotopic data were used to define fields for Kea and Loa volcanoes. The error bars are 2σ calculated for the means of 27 analyses of the NBS 987 Sr standard, 12 analyses of the JNdi-1 Nd standard and 28 analyses of the JMC-475 Hf standard. Data sources are East Molokai – this study, *Xu et al.* [2005] and *Basu and Faggart* [1996]; West Molokai – this study; note that sample D8-1 (panel a) is a dredged sample inferred to be erupted at West Molokai [*Tanaka et al.*, 2002] but it

has Sr and Nd isotopic ratios distinct from all of our data for West Molokai samples; Hualalai postshield – *Cousens et al.* [2003], *Sims et al.* [1999], *Stracke et al.* [1999], *Stille et al.* [1986]; Mauna Loa – *Abouchami et al.* [2000], *Blichert-Toft and Albarède* [1999], *Cohen et al.* [1996], *DePaolo et al.* [2001], *Hauri et al.* [1996], *Kurz et al.* [1995], *Rhodes and Hart* [1995], *Stracke et al.* [1999]; Mauna Kea – *Abouchami et al.* [2000], *Blichert-Toft and Albarède* [1999], *Blichert-Toft et al.* [2003], *Bryce et al.* [2005], *Kennedy et al.* [1991], *Lassiter et al.* [1996]; Kilauea – *Chen et al.* [1996], *Pietruszka and Garcia* [1999]; Kahoolawe – *West et al.* [1987], *Huang et al.* [2005b]; Haleakala – *Ren et al.* [2005a]; West Maui – *Gaffney et al.* [2004]; Lanai – *Gaffney et al.* [2005]; Koolau – *Roden et al.* [1994], *Blichert-Toft et al.* [1999].

Figure 9 εNd (defined as $10000*(^{143}Nd/^{144}Nd/0.512638-1)$) vs εHf (defined as $10000*(^{176}Hf/^{177}Hf/0.282772-1)$) for East Molokai and West Molokai lavas. Also shown are fields for late shield/postshield lavas from Kea volcanoes (Mauna Kea, West Maui) and fields for shield lavas from Mauna Loa, Lanai and Koolau (Makapuu stage). Tholeiitic basalts 89KAA-2, T307R1, R4, R6, R7 and R8 that have Nd and Hf isotopic ratios overlapping with the Kea field are labeled on the figure. Tholeiitic basalt 84WMOL-1D(N) and T307R2 with the most unradiogenic Nd and Hf isotopic ratios are also labeled. Data sources are the same as for Figure 8.

Figure 10 $^{206}Pb/^{204}Pb$ vs $^{208}Pb/^{204}Pb$ and $^{207}Pb/^{204}Pb$ for West Molokai lavas and sample D8-1 (see Figure 8 caption). Fields for East Molokai, Mauna Loa, Lanai, and Koolau (Makapuu stage and KSDP) are shown. Filled symbols are for triple-spike data and open symbols are for traditional TIMS data. West Molokai lavas straddle the Loa-Kea boundary line defined by *Abouchami et al.*

(2005). Data sources: this study as well as *Abouchami et al.* [2000], *Abouchami et al.* [2005], *Fekiacova et. al.* [2007], *Wanless et al.* [2006], *Tanaka et al.* [2002], *Xu et al.* [2005]. The 2 sigma errors shown are the maximum in-run uncertainties for triple-spike data and conventional TIMS (Table 5).

Figure 11 Sr/Nb vs Zr/Nb for West Molokai lavas. Fields for Mauna Kea and Mauna Loa are shown for comparison. Only lavas with major element data and with MgO >6.5% are included to minimize the effect of clinopyroxene, plagioclase and Fe-Ti oxide fractionation on Sr/Nb and Zr/Nb ratios. The 2 sigma uncertainties are 3%. Subaerially exposed West Molokai shield lavas overlap the Mauna Loa field but postshield lavas overlap the Mauna Kea field. Samples (Rx) from the north breccia slope range from Loa-like at the bottom (R2) to Kea-like at the top (R4, R6, R7, R8). A complication to the distinct fields shown for Mauna Loa and Mauna Kea is that submarine lavas from the Southwest rift zone of Mauna Loa define a trend extending into the field for Mauna Kea. These submarine rift zone lavas are Loihi-like in their Sr/Nb and Zr/Nb, $^{3}He/^{4}He$ and Pb isotopic ratios and they are the oldest, estimated as 100 - 300 ka, Mauna Loa lavas studied [*Kurz et al.*, 1995]. Data sources: Mauna Kea – *Frey et al.* [1990; 1991], *Yang et al.* [1996], *Huang and Frey* [2003]; Mauna Loa – *Rhodes* [1995], *Rhodes* [1996], *Rhodes and Hart* [1995], *Rhodes and Vollinger* [2004].

Figure 12 La/Nb and Sr/Nb vs $^{208}Pb^{*}/^{206}Pb^{*}$ and La/Nb vs $^{143}Nd/^{144}Nd$ for West Molokai lavas. Fields for Mauna Kea and Kilauea, and Lanai and Koolau (Makapuu stage) are shown for comparison. Filled symbols are for triple-spike Pb data and open symbols are for traditional TIMS

Pb data. Samples which experienced fractionation of plagioclase and Fe-Ti oxide are not plotted. These trace element ratios in West Molokai shield lavas are correlated with radiogenic isotopic ratios and trend from the Loa to Kea fields. Therefore, we infer that La/Nb, Sr/Nb and Zr/Nb (not shown) are source related. La/Nb is shown because this ratio is less sensitive than Zr/Nb and Sr/Nb to processes such as partial melting and crystallization. Data sources: *Abouchami et al.* [2005], *Eisele et al.* [2003], *Gaffney et al.* [2005], *Huang and Frey* [2003; 2005b], *Pietruszka et al.* [1999].

Figure 13 (a) $^{208}Pb^*/^{206}Pb^*$ vs $^{176}Hf/^{177}Hf$ for West Molokai and East Molokai lavas and (b) $^{208}Pb^*/^{206}Pb^*$ vs $^{87}Sr/^{86}Sr$ for West Molokai lavas. Fields for lavas from Kea and Loa volcanoes are shown for comparison. Filled symbols are for triple-spike Pb data and open symbols are for traditional TIMS Pb data. Only literature data with Pb isotopes analyzed by triple-spike and MC-ICP-MS are used in defining the fields for Loa and Kea lavas. Using this filter, the fields for lavas from Loa and Kea volcanoes overlap only slightly; the region of overlap is defined by lavas from Loihi and the low SiO_2 group of shield lavas at Mauna Kea. West Molokai shield lavas include Loa- and Kea-like lavas whereas postshield alkalic basalt and hawaiite are Kea-like. Data sources are the same as Figure 8.

Figure 14. Sampling of a bilateral asymmetrically zoned plume which is dominantly Kea component in the northeast (red) and dominantly Loa component in the southwest (blue); but a few Kea-like heterogeneities are in the Loa region and vice versa. These two portions are separated by a central zone that has similar amounts of Loa and Kea components. The latter zone

was sampled by the West Molokai shield which includes both Loa- and Kea-like lavas. The black arrow in each panel indicates the direction of the Pacific plate movement, ~ N65°W in panel a gradually changing to ~N30°W in panel d. Figure modified from [*Abouchami et al.*, 2005; *Herzberg*, 2005; *Ren et al.*, 2005b].

(a) At ~3 Ma the Pacific Plate is striking N65°W over the hotspot; East and West Molokai and Penguin Bank are in the pre-shield or early shield stages.

(b) At 2 to 3 Ma, the strike of the Pacific plate is more northerly and starting to change from N65°W (the strike from Oahu to Midway Island) to N30°W (the strike from Maui Island to Loihi seamount). West Molokai volcano is centered over the hotspot and sampling a central region where Loa- and Kea-like heterogeneities are both abundant.

(c) At ~2 Ma, the strike of the Pacific Plate is further to the north as West Molokai volcano enters the late-shield stage.

(d) At 1.8 Ma, the strike of the Pacific plate is now N30°W, as defined by volcanoes from Maui to Loihi. West Molokai volcano has entered the postshield stage and is now sampling the dominantly Kea part of the plume.

Table 1 K-Ar Age data for West Molokai alkalic lavas

Sample	K_2O (wt %)	weight (g)	$^{40}Ar^*$ (mol/g)	$^{40}Ar^*$ %	Age (My)	σ
84WMOL-5	1.030 ± 0.005	12.389	2.73×10^{-12}	21.8	1.838	0.092
(Puu Apalu)		11.392	2.46×10^{-12}	15.8	1.658	0.083
			Weighted Mean Age		**1.74**	**0.13**
71WMOL-4	1.489 ± 0.012	9.761	3.59×10^{-12}	19.4	1.673	0.084
(Na Puu Kulua)		9.883	3.80×10^{-12}	28.0	1.771	0.089
			Weighted Mean Age		**1.72**	**0.08**
84WMOL-3	1.361 ± 0.010	9.776	3.62×10^{-12}	12.0	1.847	0.093
(Puu o Kaiaka)		9.570	3.48×10^{-12}	22.2	1.776	0.089
			Weighted Mean Age		**1.81**	**0.06**

Isotopic abundance and decay constants for ^{40}K are $\lambda_\beta=4.962\times10^{-10}$/yr, $\lambda_\varepsilon=0.581\times10^{-10}$/yr, and $^{40}K/K=1.167\times10^{-4}$ [*Steiger and Jager*, 1977]. Errors are estimates of analytical precision at 68% confidence level. Means are weighted by the inverse of the variances. Analyses done at the U.S. Geological Survey in 1985-1986 by G.B. Dalrymple.

Table 2. Glass compositions (wt%) for rinds and sand grains

Sample	analysis #	type	SiO_2	TiO_2	Al_2O_3	FeO	MnO	MgO	CaO	Na_2O	K_2O	P_2O_5	S	Cl	Total
T307-R2	1, 3-5	glass in breccia matrix	51.65	2.45	13.90	10.99	0.16	6.79	11.04	2.28	0.30	0.22	**0.076**	0.012	99.88
T307-R4	1-6	glass rinds on basltic clast in breccia	51.31	2.45	13.96	10.55	0.17	7.17	11.11	2.22	0.30	0.22	**0.093**	0.011	99.56
T307-R7	1-2		51.17	2.29	13.21	11.07	0.13	9.14	10.67	2.10	0.27	0.21	**0.096**	0.026	100.51
T307-R7	3-4		51.71	2.52	14.07	11.45	0.18	6.55	10.98	2.27	0.32	0.24	**0.102**	0.013	100.55
T307-R7	5	sand grains in hyaloclastite	52.09	2.57	13.87	11.81	0.15	6.54	11.24	2.21	0.29	0.26	0.017	0.008	101.06
T307-R7	6		52.23	2.20	13.96	10.93	0.11	7.01	11.62	2.17	0.23	0.19	0.014	0.007	100.70
T307-R7	7		51.97	2.34	14.23	11.02	0.18	6.89	11.41	2.24	0.27	0.23	0.006	0.013	100.80
T307-R8	12		51.07	2.50	13.57	11.83	0.11	7.42	11.06	2.04	0.28	0.23	0.034	0.007	100.14
T307-R8	13	glass inclusion in olivine	50.82	2.48	13.20	12.46	0.16	7.14	11.01	1.98	0.27	0.25	0.013	0.015	99.80
T307-R8	5		51.46	2.26	13.75	11.10	0.11	7.45	10.94	2.09	0.28	0.20	**0.067**	0.006	99.71
T307-R8	1-2, 4, 11	glass rinds	51.48	2.31	13.74	11.00	0.14	7.51	10.98	2.10	0.27	0.22	**0.056**	0.012	99.81
T307-R8	6-10	sand grains in hyaloclastite filling lava crack	51.67	2.60	13.74	11.92	0.15	6.38	10.97	2.20	0.30	0.25	0.004	0.009	100.18
T307-PC65	1		51.41	2.57	14.31	10.85	0.20	6.57	11.13	2.27	0.30	0.25	**0.104**	0.014	100.13
T307-PC65	2		51.34	2.98	13.35	12.70	0.22	5.83	10.47	2.43	0.52	0.35	0.017	0.015	100.25
T307-PC65	3		51.13	2.72	13.86	11.67	0.18	6.24	10.65	2.30	0.33	0.27	**0.122**	0.014	99.67
T307-PC65	4		51.72	2.97	13.32	12.61	0.22	5.86	10.63	2.48	0.51	0.34	0.017	0.009	100.70
T307-PC65	5		51.58	2.93	13.34	12.48	0.20	5.81	10.46	2.43	0.50	0.37	0.013	0.008	100.13
T307-PC65	6		51.30	2.91	13.27	12.72	0.15	5.77	10.40	2.44	0.51	0.32	0.024	0.014	99.86
T307-PC65	7		51.37	2.57	14.27	10.90	0.17	6.59	11.07	2.32	0.29	0.25	**0.110**	0.010	100.07
T307-PC65	8	glass in push core (PC) sediment, collected from the bottom of the dive at 3451 mbsl	51.78	2.33	14.13	10.64	0.15	7.15	11.11	2.28	0.33	0.22	0.014	0.014	100.18
T307-PC65	9		50.75	2.37	13.73	10.83	0.16	8.00	10.98	2.12	0.28	0.24	**0.083**	0.012	99.67
T307-PC65	10		51.23	2.98	13.35	12.75	0.15	5.84	10.41	2.37	0.51	0.33	0.008	0.010	99.96
T307-PC65	11		51.33	2.83	13.96	12.07	0.16	6.18	10.82	2.28	0.32	0.26	**0.107**	0.014	100.50
T307-PC65	12		51.46	2.77	13.96	11.94	0.14	6.21	10.80	2.38	0.35	0.29	**0.110**	0.016	100.57
T307-PC65	13		51.38	2.98	13.35	12.87	0.24	5.75	10.58	2.28	0.51	0.36	0.014	0.007	100.33
T307-PC65	14		51.73	2.42	14.31	10.64	0.19	6.93	11.09	2.30	0.34	0.22	0.010	0.008	100.19
T307-PC65	15		51.40	3.03	13.20	12.96	0.20	5.68	10.37	2.51	0.51	0.34	0.010	0.007	100.22
T307-PC65	16		51.48	3.00	13.38	12.69	0.18	5.83	10.42	2.51	0.49	0.36	0.016	0.005	100.39
T307-PC76	1		51.73	2.92	13.35	12.69	0.18	6.73	10.55	2.39	0.50	0.35	0.012	0.005	101.43
T307-PC76	2		51.73	2.90	13.28	12.63	0.17	5.80	10.55	2.36	0.50	0.34	0.011	0.006	100.29
T307-PC76	3		51.70	2.94	13.35	12.82	0.20	5.89	10.48	2.39	0.48	0.34	0.017	0.012	100.65
T307-PC76	4	glass grains in sediment, collected from the top of the dive at 3337 mbsl	51.62	2.88	13.45	12.58	0.17	5.89	10.67	2.37	0.52	0.36	0.016	0.018	100.58
T307-PC76	5		51.94	2.95	13.37	12.60	0.20	5.82	10.52	2.43	0.51	0.35	0.014	0.013	100.74
T307-PC76	6		51.77	2.94	13.41	12.71	0.18	5.89	10.52	2.36	0.50	0.34	0.012	0.011	100.64
T307-PC76	7		51.77	2.96	13.18	12.85	0.22	5.85	10.44	2.43	0.53	0.37	0.011	0.006	100.63

Glass with S contents > 0.05 wt% (in bold) are submarine erupted and the others are degassed and erupted subaerially [Dixon et al., 1991]

Table 3 Major element compositons of West Molokai lavas(wt%)

	Lab	SiO_2	TiO_2	Al_2O_3	Fe_2O_3	FeO	Fe_2O_3*	MnO	MgO	CaO	Na_2O	K_2O	P_2O_5	LOI	H_2O+	H_2O^-	CO_2	Total
Postshield stage lavas																		
Hawaiite																		
71WMOL-4	USGS	47.30	3.66	16.00				0.30	4.73	7.52	4.03	1.45	0.95					98.14
71WMOL-4	UMASS	47.49	3.66	16.08			13.48	0.26	4.83	7.49	4.16	1.49	0.94	0.24				99.88
84WMOL-2	USGS	46.10	4.52	16.00				0.16	3.30	7.41	4.22	1.20	0.78					97.89
84WMOL-3	USGS	47.60	3.71	15.40				0.19	4.99	7.72	4.01	1.32	0.88					98.52
84WMOL-4	USGS	46.10	4.10	15.50				0.18	4.50	7.95	3.93	1.20	0.79					97.65
74PH-2	UMASS	47.35	4.07	16.55			14.85	0.17	3.52	6.72	4.35	1.35	0.90	1.46				99.83
74PH-3	USGS	46.40	4.15	15.50				0.15	3.81	6.73	4.10	1.31	0.79					96.24
74PH-4	UMASS	46.45	4.50	17.61			15.99	0.82	2.16	5.45	4.32	1.41	0.94	3.74				99.65
806-GEO-1	USGS	47.50	3.76	15.80	5.94	7.07		0.19	4.95	7.75	4.30	1.42	0.91		0.37	0.15	0.08	98.99
WMO-15B	USGS	47.30	3.77	15.70	6.99	6.49		0.18	4.12	7.74	4.07	1.34	0.89		0.75	0.54	0.02	97.89
WMO-13	USGS	46.70	4.15	15.30	7.51	6.65		0.18	5.06	7.91	3.98	1.26	0.81		0.41	0.35	0.01	98.76
86GEO-1	UMASS	47.30	3.73	15.83			13.63	0.20	4.92	7.55	4.53	1.42	0.89	0				100.00
Alkalic basalt																		
84WMOL-5	USGS	45.50	4.63	15.00				0.19	5.69	8.50	3.64	1.03	0.68					99.06
29-GEO-2	USGS	44.60	4.35	15.60	3.87	11.10		0.19	6.41	8.57	3.38	0.87	0.67		0.62	0.12	0.03	99.22
29-GEO-3	USGS	46.53	4.16	16.12				0.18	5.98	8.44	3.37	0.92	0.64					100.69
Shield stage lavas																		
Tholeiite																		
71WMOL-1	USGS	53.61	2.93	14.05	2.31	9.06		0.16	3.92	7.90	3.10	1.13	0.70		0.89	0.22	0.01	98.64
74WMOL-4	USGS	53.10	2.94	13.70	3.00	8.30		0.16	4.17	7.81	3.14	1.04	0.71		1.20	0.47	0.01	97.77
74WMOL-5	USGS	53.50	2.90	13.40	2.65	8.60		0.16	4.03	7.53	3.13	1.18	0.72		1.30	0.42	0.01	97.53
804-GEO-1	USGS	52.80	3.43	13.10	3.46	8.32		0.17	4.63	8.65	2.62	1.01	0.56		1.03	0.28	0.01	98.40
89KAA-2	UMASS	50.13	2.89	13.94			12.77	0.17	6.14	10.34	2.60	0.53	0.38	0.01				
71WMOL-3	USGS	51.15	2.63	13.98	1.79	9.72		0.17	6.58	10.35	2.36	0.54	0.31		0.31	0.12	0.01	99.40
74KAN-1	USGS	48.30	2.39	13.60	4.20	7.20		0.17	7.04	10.60	2.45	0.12	0.30		1.30	0.66	0.08	95.95
74KAN-2	USGS	46.90	3.29	14.10	4.72	8.98		0.20	6.20	10.50	2.24	0.14	0.48		0.99	0.90	0.16	97.28
74PH-1	USGS	48.00	2.74	14.30	6.99	5.50		0.18	6.04	10.20	2.08	0.15	0.31		1.23	1.59	0.15	95.79
74WMOL-1	USGS	46.90	3.44	15.50	4.80	9.00		0.18	5.60	8.75	2.30	0.12	0.51		1.30	0.82	0.01	96.62
74WMOL-2	USGS	47.90	2.77	14.90	6.95	5.00		0.29	5.69	9.51	2.00	0.10	0.34		3.00	2.20	0.01	94.75
74WMOL-3	USGS	48.80	2.48	14.30	3.50	8.10		0.26	6.68	9.99	2.19	0.10	0.31		1.20	0.77	0.01	96.36
74WMOL-6	USGS	47.30	2.62	14.60	7.49	5.23		0.25	5.81	9.72	1.97	0.08	0.26		1.78	1.97	0.20	94.58
74WMOL-7	USGS	47.20	3.19	14.60	4.19	9.10		0.19	5.96	10.40	2.21	0.13	0.38		0.93	0.68	0.30	97.13
74WMOL-8	USGS	49.60	2.51	13.80	5.15	6.90		0.16	6.41	9.31	2.32	0.30	0.28		1.50	0.95	0.01	96.22
74WMOL-9	USGS	48.20	3.35	14.00	3.35	9.50		0.18	5.72	9.70	2.93	0.15	0.45		1.40	0.45	0.01	97.19
74WMOL-10	USGS	49.00	3.35	14.30	5.20	8.30		0.16	5.23	9.27	2.62	0.13	0.46		1.00	0.97	0.01	97.50
74WMOL-11	USGS	47.30	3.39	14.10	4.85	8.60		0.18	5.83	9.79	2.54	0.20	0.50		1.50	0.59	0.01	96.79
74WMOL-12	USGS	47.30	2.66	14.30	4.80	7.50		0.17	6.55	10.30	2.50	0.09	0.29		1.40	0.79	0.01	95.98
74WMOL-13	USGS	50.30	2.45	13.90	3.00	8.64		0.17	6.55	10.50	2.15	0.34	0.28		0.35	0.88	0.08	97.98
84WMOL-1C (S)	UMASS	48.95	3.11	14.26			13.84	0.19	5.96	10.19	2.52	0.25	0.38	0.74				99.65
84WMOL-1D (S)	UMASS	48.21	3.38	15.53			14.83	0.18	5.20	9.36	2.67	0.14	0.41	2.38				99.91
84WMOL-1C (NW)	UMASS	48.41	3.35	15.10			14.65	0.18	5.57	9.75	2.54	0.14	0.31	1.66				100.00

84WMOL-1C (NE)	UMASS	48.33	3.27	15.23			14.49	0.18	5.51	9.75	2.62	0.14	0.29	1.78				99.81
84WMOL-1D (N)	UMASS	50.55	2.63	13.81			13.14	0.19	6.21	10.29	2.36	0.36	0.31	0.75				99.85
32-GEO-1	USGS	50.60	3.13	13.90	5.12	7.45		0.15	5.26	9.78	2.70	0.65	0.42		0.78	0.39	0.01	98.65
805-GEO-1	USGS	49.80	2.44	13.90	5.41	6.20		0.15	6.76	10.60	2.25	0.12	0.30		0.69	1.58	0.01	97.39
808-GEO-1	USGS	50.80	2.95	13.80	5.23	7.17		0.15	5.54	9.82	2.57	0.63	0.39		0.60	0.66	0.01	98.53
813-GEO-1	USGS	51.30	2.41	14.10	3.26	8.23		0.16	6.31	9.91	2.32	0.48	0.31		0.85	0.46	0.01	98.46
815-GEO-1	USGS	51.30	3.24	13.20	4.21	8.72		0.17	5.42	9.49	2.68	0.66	0.43		0.43	0.24	0.01	99.10
895-GEO-1	USGS	51.40	2.76	13.70	3.66	8.50		0.16	6.15	9.86	2.34	0.53	0.35		0.70	0.28	0.01	99.04
91-GEO-1	USGS	51.90	2.54	13.80	3.00	8.64		0.17	6.61	10.30	2.28	0.44	0.30		0.53	0.10	0.02	99.68
WMO-16	USGS	49.10	2.78	14.20	4.66	8.23		0.17	6.46	10.60	2.53	0.14	0.34		0.60	0.57	0.01	98.74
Tholeiitic basalt clasts from submarine breccia slope																		
T307R1	WSU	49.6	2.086	12		11.36		0.166	12.66	9.66	1.99	0.32	0.283					100.13
T307R2	WSU	52.59	2.122	13.87		10.26		0.15	7.46	9.17	2.85	0.61	0.304					99.39
T307R3	WSU	49.05	1.888	11.09		11.3		0.166	14.38	8.9	1.9	0.4	0.221					99.30
T307R4	WSU	49.48	2.124	11.79		10.82		0.166	13.06	9.62	1.92	0.27	0.195					99.45
T307R6	WSU	48.76	1.812	10.52		10.42		0.164	16.74	8.52	1.77	0.22	0.167					99.09
T307R7	WSU	49.16	1.853	10.84		10.26		0.162	15.5	8.89	1.84	0.24	0.172					98.92
T307R8	WSU	47.45	1.693	9.57		10.99		0.166	19.68	7.86	1.6	0.24	0.152					99.40

Notes for Table 3

(1) Samples with prefix of "71WMOL" were collected by D. Jackson and M. Beeson in 1971; "GEO" samples were collected by M. Weisler; all the other samples were collected by D.Clague.
(2) N, NW, NE and S after the sample names for 84WMOL-1 indicate the relative direction of the road outcrop.
(3) Lab indicates analytical facility: United States Geological Survey (USGS); University of Massachusetts of Amherst (UMASS).
(4) Volatile free compositions were used in all diagrams involving major elements. They were determined by recalculation of total iron as Fe_2O_3, subtracting H_2O and CO_2, and then normalizing to 100 percent.

Table 4 Trace element compositions of West Molokai lavas (ppm)

	Cs	Rb	U	Ba	Th	Nb	Ta	Zr	Hf	Sr	Pb	La	Ce	Pr	Nd	Sm	Eu	Gd	Tb	Dy	Ho	Er	Tm	Yb	Lu	Y	Sc	Ni*
Postshield stage lavas																												
Hawaiite																												
74Ph-3	0.13	21.8	0.74	357	2.35	35.8	2.21	350	8.15	805	2.23	38.4	74.1	12.8	59.7	14.6	4.71	14.72	2.14	11.43	2.18	5.28	0.73	3.99	0.55	67.5	15.6	12
74PH-4	0.15	23.0	0.91	436	2.60	37.3	2.34	372	8.95	758	2.17	34.2	77.7	12.0	56.5	13.8	4.54	13.56	1.96	10.49	2.07	5.27	0.76	4.54	0.67	65.3	16.2	
WMO-13	0.55	26.1	0.78	346	2.29	35.0	2.27	339	8.12	824	2.17	32.4	71.4	11.8	55.7	13.7	4.48	13.82	2.04	10.81	2.00	4.84	0.66	3.65	0.50	56.4	15.7	
WMO-15B	0.31	24.9	0.76	386	2.72	37.8	2.35	378	8.88	789	2.53	36.3	81.1	12.7	57.4	13.7	4.36	13.04	1.93	10.20	1.83	4.39	0.59	3.31	0.45	52.7	15.3	
86GEO-1	0.26	24.8	0.87	378	2.59	39.0	2.40	389	9.10	793	2.48	36.2	75.5	12.4	56.1	13.2	4.15	12.50	1.86	9.73	1.81	4.37	0.59	3.32	0.45	54.1	14.6	
806GEO-1	0.26	25.2	0.90	389	2.64	39.2	2.46	393	9.22	827	2.50	36.2	79.1	12.4	56.0	13.3	4.19	12.48	1.86	9.74	1.80	4.30	0.59	3.33	0.45	53.3	14.9	1
74PH-2	0.25	23.6	0.85	419	2.62	38.3	2.36	376	8.87	823	2.39	39.7	83.6	13.1	58.9	14.0	4.40	13.69	2.01	10.53	1.93	4.59	0.62	3.42	0.46	55.2	15.6	
71WMOL-4	0.27	26.1	0.99	486	2.83	42.8	2.63	429	9.81	912	2.35	40.6	91.4	13.8	61.9	14.3	4.47	13.53	2.00	10.57	1.92	4.66	0.63	3.60	0.49	57.1	14.8	28
84WMOL-2	0.20	20.8	0.81	360	2.22	31.5	1.94	321	7.60	797	2.11	30.9	69.5	10.8	49.5	12.2	3.91	11.86	1.77	9.34	1.72	4.23	0.57	3.17	0.44	48.7	17.1	45
84WMOL-3	0.21	24.1	0.84	460	2.60	38.4	2.34	378	8.75	799	2.48	34.6	79.3	11.7	52.6	12.8	4.02	11.99	1.79	9.35	1.74	4.10	0.56	3.17	0.42	50.6	15.4	40
84WMOL-4	0.12	19.8	0.77	354	2.29	35.8	2.24	343	8.16	828	2.03	31.5	74.5	11.1	50.5	12.3	3.87	11.58	1.76	9.33	1.72	4.22	0.58	3.29	0.45	48.7	15.7	32
Alkalic basalt																												
29-GEO-2	0.21	14.8	0.61	238	1.68	26.1	1.68	296	7.07	730	1.77	24.1	60.4	9.1	41.5	10.4	3.21	9.97	1.50	8.06	1.49	3.62	0.50	2.80	0.38	41.5	18.4	67
29-GEO-3*																												64
84WMOL-5	0.43	21.9	0.68	304	2.04	31.8	1.96	308	7.34	772	1.92	27.4	65.0	9.5	42.9	10.4	3.35	10.01	1.53	8.02	1.48	3.59	0.48	2.77	0.37	42.5	17.8	53
89KAA-1 (glass)	0.25	16.4	0.58	227	1.70	22.8	1.44	268	6.47	584	2.38	21.8	54.3	7.9	36.3	9.3	2.88	8.76	1.32	7.10	1.29	3.15	0.44	2.39	0.33	36.2	24.6	
Shield stage lavas																												
Tholeiite																												
71WMOL-1	0.22	18.2	0.60	206	1.98	23.4	1.48	360	8.80	392	2.58	26.3	65.3	9.9	45.9	11.6	3.38	11.59	1.80	10.01	1.93	4.86	0.70	3.97	0.56	55.4	23.7	47
74WMOL-4	0.24	16.0	0.57	192	2.04	23.9	1.52	368	9.16	399	2.26	27.6	65.2	10.3	48.0	12.1	3.58	12.29	1.90	10.71	2.06	5.23	0.75	4.22	0.59	58.8	23.8	19
74WMOL-5	0.22	19.3	0.61	210	2.04	24.4	1.52	376	9.15	399	2.34	27.7	68.0	10.4	48.0	12.0	3.54	12.04	1.89	10.27	1.98	5.03	0.73	4.11	0.58	57.5	23.8	22
804GEO-1	0.19	18.3	0.51	235	1.52	20.2	1.28	303	7.33	411	1.83	22.6	57.7	8.8	41.8	11.2	3.51	11.63	1.83	10.38	1.98	5.13	0.73	4.05	0.58	58.7	29.4	170
74KAN-1	0.02	0.5	0.14	54	0.73	11.0	0.72	163	4.10	392	1.05	11.6	28.8	4.6	22.0	6.0	2.00	6.42	1.01	5.77	1.13	2.88	0.40	2.32	0.33	34.3	31.9	85
74KAN-2	0.03	1.2	0.26	60	1.05	15.9	1.01	227	5.67	401	1.42	15.8	41.3	6.3	30.0	8.1	2.64	8.35	1.32	7.46	1.43	3.64	0.51	2.92	0.41	40.7	33.1	70
74PH-1	0.02	0.4	0.17	101	0.84	11.9	0.77	175	4.41	375	1.06	12.4	30.7	4.9	23.5	6.4	2.12	6.73	1.08	6.13	1.18	3.02	0.43	2.48	0.34	34.1	32.8	75
74WMOL-9	0.03	0.2	0.17	103	1.21	17.8	1.15	246	6.05	427	1.60	18.3	42.0	6.9	33.3	8.8	2.90	9.22	1.44	8.13	1.60	4.02	0.59	3.31	0.47	46.8	32.8	98
74WMOL-11	0.04	0.5	0.27	90	1.29	18.5	1.21	269	6.75	415	3.41	18.9	48.8	7.5	36.3	9.6	3.10	9.81	1.56	8.74	1.66	4.26	0.61	3.47	0.49	47.4	32.5	68
74WMOL-13	0.07	5.5	0.22	84	0.71	10.6	0.70	162	3.99	370	1.05	11.2	29.4	4.5	21.7	5.9	1.96	6.19	0.98	5.61	1.07	2.76	0.39	2.22	0.32	30.9	31.7	93
808GEO-1	0.13	10.6	0.34	142	1.02	15.4	0.98	200	5.01	437	1.22	14.5	35.6	5.6	26.2	6.9	2.29	6.96	1.10	6.11	1.15	2.87	0.41	2.35	0.32	32.9	31.7	67
815GEO-1	0.20	11.5	0.37	144	1.08	15.9	1.01	220	5.42	387	1.42	16.2	37.8	6.4	30.9	8.4	2.81	8.89	1.40	7.93	1.53	3.93	0.55	3.16	0.45	44.1	30.3	58
84WMOL-1c (S)	0.06	1.3	0.26	99	1.08	15.9	1.01	225	5.58	404	1.40	14.8	37.1	6.0	29.0	7.9	2.60	8.32	1.32	7.46	1.44	3.68	0.53	2.99	0.42	40.9	33.8	
84WMOL-1d (S)	0.09	0.4	0.23	92	1.35	18.5	1.20	269	6.68	414	1.71	18.1	44.7	7.3	34.7	9.1	2.98	9.38	1.47	8.13	1.53	3.95	0.57	3.19	0.44	45.1	32.1	
84WMOL-1c (NW)	0.12	0.5	0.25	68	1.11	16.0	1.05	226	5.83	394	1.41	15.8	36.3	6.1	28.8	7.9	2.56	8.30	1.31	7.46	1.46	3.75	0.55	3.07	0.43	43.5	32.7	
84WMOL-1C (NE)	0.05	0.5	0.21	83	1.29	18.1	1.15	259	6.47	407	1.59	13.8	36.9	6.0	28.8	8.2	2.77	8.45	1.35	7.54	1.47	3.80	0.56	3.17	0.46	41.1	31.9	
84WMOL-1d (N)	0.09	4.5	0.23	95	0.83	12.5	0.80	177	4.37	378	1.10	14.1	34.0	5.4	25.2	6.7	2.24	7.16	1.12	6.37	1.25	3.32	0.47	2.58	0.37	39.7	32.2	
89KAA-2	0.14	7.6	0.30	151	1.01	15.6	1.00	193	4.81	438	1.28	14.2	36.1	5.4	25.6	6.9	2.24	7.00	1.09	6.09	1.17	2.91	0.42	2.36	0.33	33.1	30.8	
89FDD-1 (glass)	0.12	8.4	0.27	109	0.80	11.9	0.77	167	4.21	394	2.07	12.1	31.2	4.7	22.2	6.0	2.01	6.21	0.99	5.58	1.06	2.71	0.38	2.21	0.31	29.9	31.4	
89FDD-2 (glass)	0.11	7.4	0.25	96	0.73	11.0	0.73	159	4.06	366	1.81	11.0	29.1	4.4	21.0	5.8	1.92	6.00	0.96	5.43	1.03	2.67	0.38	2.20	0.31	29.5	30.6	
Tholeiitic basalt clasts from submarine breccia slope																												
T307R1	0.05	3.8	0.66	43	0.42	8.0	0.51	116	3.13	278	0.63	7.8	19.6	3.0	15.0	4.4	1.53	4.86	0.77	4.39	0.83	2.14	0.29	1.77	0.26	24.4	29.0	442
T307R2	0.10	7.5	0.57	97	0.58	9.7	0.60	140	3.67	420	1.21	11.9	27.9	4.1	19.4	5.4	1.76	5.43	0.81	4.49	0.82	2.06	0.28	1.69	0.25	24.1	25.4	167
T307R3	0.11	5.7	0.14	65	0.47	8.6	0.54	110	2.99	294	0.74	8.6	20.8	3.1	14.8	4.3	1.47	4.65	0.72	4.08	0.76	1.96	0.27	1.63	0.24	22.1	27.4	543

T307R4	0.05	4.2	0.15	53	0.47	9.8	0.63	114	3.10	240	0.54	8.2	20.2	3.1	14.8	4.4	1.50	4.92	0.78	4.50	0.86	2.13	0.30	1.83	0.28	24.7	29.8	500
T307R6	0.05	3.3	0.11	35	0.38	8.2	0.52	98	2.66	208	0.47	6.8	16.9	2.6	12.5	3.8	1.35	4.39	0.68	3.99	0.76	1.97	0.28	1.66	0.25	22.4	27.3	786
T307R7	0.10	3.4	0.23	38	0.38	8.1	0.51	97	2.62	232	0.47	6.8	16.8	2.6	12.4	3.8	1.33	4.33	0.69	3.98	0.75	1.96	0.28	1.67	0.25	22.4	27.5	743
T307R8	0.10	3.3	0.11	27	0.35	7.4	0.48	87	2.39	181	0.50	6.3	15.4	2.3	11.4	3.4	1.16	3.75	0.60	3.49	0.65	1.66	0.23	1.42	0.21	19.2	24.6	840
REE-Y enriched tholeiite																												
74WMOL-12	0.04	0.2	0.19	55	0.79	12.1	0.78	178	4.48	386	1.09	15.4	30.4	5.5	26.7	7.2	2.48	8.51	1.31	7.56	1.53	3.97	0.55	2.94	0.42	56.0	33.3	92
91GEO-1	0.12	7.5	0.23	96	0.69	10.3	0.66	156	3.90	355	1.04	12.8	32.0	5.2	25.9	7.3	2.71	8.80	1.35	7.79	1.60	4.16	0.55	2.94	0.43	57.8	31.2	73
WMO-16	0.03	0.6	0.19	88	0.84	11.6	0.81	172	4.49	400	1.15	20.7	30.1	7.2	36.0	9.8	3.49	12.64	1.98	11.74	2.52	6.70	0.93	4.88	0.76	85.0	31.9	
74WMOL-6	0.29	0.5	0.17	100	0.71	11.7	1.51	160	4.82	359	1.06	40.2	83.9	23.4	151	54.0	21.2	93.4	15.4	96.1	20.9	56.4	8.02	42.8	6.60	662	32.1	139
32GEO-1*		12		161		18		200		452		45.0	89.0													132	31	59
805GEO-1*		3		41		12		152		381		21.0	33.0													122	36	92
813GEO-1*		11		89		12		156		377		26.0	54.0													68	33	74
895GEO-1*		10		95		14		170		369		80.0	175.0													172	35	75
74WMOL-1*		4		110	1.45	15		249	6.80	340		42.0	61.0		88.5	27.6	9.74	30.3	3.69				1.85	9.05	1.13	108	32	79
74WMOL-2*		4		284	0.90	10		164	4.30	368		51.0	35.0		41.0	9.8	3.48	19.3	1.66				1.07	4.75	0.74	150	31	118
74WMOL-3*		4		140	0.90	8		154	4.10	388		48.0	116.0		79.5	22.8	7.79	29.0	3.01				1.46	8.00	1.02	88	31	120
74WMOL-7*		2		73	1.10	17		204	5.20	382		43.0	45.0		62.0	15.9	5.25	21.4	3.81				1.68	8.90	1.28	204	30	99
74WMOL-8*		7		91	0.90	16		158	3.95	364		24.5	30.0		39.5	10.9	3.68	14.9	1.56				0.86	4.45	0.59	56	31	135
74WMOL-10*		7		86	1.30	14		227	6.25	432		48.5	47.0		56.0	14.3	5.08	20.6	2.11				1.09	6.60	0.96	118	31	84

All data determined by ICP-MS at MIT and Washington State University (T307- samples) except that Ni data for all samples were determined by XRF, and REE and Sc in 10 REE-Y enriched tholeiitic basalt (designated by *) were determined by INAA.

Table 5. Sr, Nd, Hf and Pb isotope data for West Molokai samples

	$^{87}Sr/^{86}Sr$	2σ	$^{143}Nd/^{144}Nd$	2σ	$^{176}Hf/^{177}Hf$	2σ	$^{206}Pb/^{204}Pb$	2σ	$^{207}Pb/^{204}Pb$	2σ	$^{208}Pb/^{204}Pb$	2σ
Postshield stage lavas												
Hawaiite												
86 GEO-1	0.703662	10	0.513000	8	0.283105	4	18.423	2	15.492	2	37.983	4
74 PH-2	0.703635	10	0.512998	9	0.283113	5	18.402	3	15.503	2	37.986	5
71 WMOL-4	0.703662	10	0.512985	6	0.283109	4	18.419	1	15.489	1	37.985	3
84 WMOL-4	0.703636	13	0.513001	8	0.283108	4	18.409	2	15.510	2	38.012	5
84 WMOL-4 Rep	0.703648	7										
84 WMOL-4 TS							18.3962	23	15.4914	29	37.9642	93
84 WMOL-3	0.703638	8	0.512992	6	0.283116	5	18.378	2	15.474	2	37.897	4
Alkalic basalt												
29 GEO-2	0.703622	14	0.513005	6	0.283113	4	18.426	3	15.487	2	37.957	5
84 WMOL-5	0.703631	8	0.512984	8	0.283115	5	18.371	2	15.469	2	37.878	5
84 WMOL-5 TS							18.3911	21	15.4878	26	37.9482	84
Shield stage lavas												
Tholeiite												
84 WMOL-D(N)	0.703968	8	0.512867	7	0.283030	4	18.105	2	15.470	2	37.912	5
84 WMOL-D(N) Rep	0.703973	8										
84 WMOL-D(N) Dup	0.703972	8					18.085	2	15.444	2	37.831	4
84 WMOL-D(N) TS							18.0952	32	15.4575	40	37.8874	131
74 WMOL-13	0.703815	10	0.512933	18	0.283072	4	18.080	2	15.469	2	37.849	4
74 WMOL-13 Rep	0.703816	10										
74 WMOL-13 Dup							18.071	2	15.458	2	37.810	6
74 WMOL-13 TS							18.0688	19	15.4560	24	37.8153	78
815 GEO-1	0.703733	10	0.512949	6	0.283084	4	18.123	2	15.465	2	37.816	4
808 GEO 1	0.703720	8	0.512958	7	0.283086	4	18.237	2	15.487	2	37.921	5
808 GEO 1 Rep	0.703725	8										
808 GEO 1 TS							18.2316	19	15.4736	25	37.8886	80
74 KAN-1	0.703777	7					18.094	4	15.453	3	37.793	8
74 PH-1	0.703705	8					18.170	4	15.442	3	37.788	8
74 PH-1 TS							18.1783	23	15.4578	29	37.8490	93
89 KAA-2	0.703592	8	0.512996	7	0.283110	4	18.234	3	15.485	3	37.874	8
89 KAA-2 Dup	0.703593	10										
74 WMOL-5	0.703762	10	0.512932	7	0.283082	5	18.092	1	15.447	1	37.777	2
74 WMOL-5 Rep	0.703772	8										
74 WMOL-5 TS							18.1020	25	15.4588	31	37.8221	102
804 GEO-1	0.703757	10	0.512949	6	0.283082	5	18.118	2	15.464	2	37.834	5
71WMOL-1*	0.70378	5	0.512930	28			18.133	17	15.455	18	37.751	59

71WMOL-3*	0.70376	5	0.512940	22			18.167	18	15.460	19	37.754	58
Tholeiitic basalt clasts from submarine breccia slope												
T307R1	0.703697[C]	13	0.512954[C]	4	0.283110	4	18.225[C]	5	15.459[C]	4	37.850[C]	10
T307R1 TS			0.512976	6	0.283119[L]	3	18.2285	22	15.4651	22	37.8985	64
T307R2	0.704098	8	0.512706	5	0.282956[L]	4	17.8427	24	15.4349	29	37.7415	91
T307R4	0.703666[C]	12	0.513003[C]	4	0.283141	4	18.438[C]	18	15.470[C]	15	38.003[C]	37
T307R4			0.513009	4	0.283143[L]	3						
T307R6			0.513002	5	0.283138[L]	3	18.3740	23	15.4623	27	38.0107	85
T307R7			0.512997	7	0.283144[L]	5	18.3774	35	15.4646	43	38.0209	140
T307R8			0.513005	6	0.283136[L]	4	18.4358	47	15.4731	47	38.0996	134

Table 5 notes

1. Most Sr, Nd and Pb isotopic data were obtained at MIT, exceptions are:
   (a) 71WMOL-1 and -3 Sr, Nd and Pb data from Stille et al. [1986];
   (b) T307R1 and R4 Sr, Nd and Pb data obtained at Carleton University by B. Cousens;
   (c) Nd data for T307 samples obtained at Ecole Normale Supérieure in Lyon (ENSL) by J. Blichert-Toft;
   (d) Pb data by the triple spike technique (TS) obtained at Max-Planck-Institut fur Chemie (MPI) by W. Abouchami.
2. Sr data were normalized to $^{86}Sr/^{88}Sr=0.1194$ and Nd were normalized to $^{146}Nd/^{144}Nd=0.7219$. Mean measured $^{87}Sr/^{86}Sr$ for NBS987 during the course of study at MIT was 0.710240 ± 13 (2σ, n=27) and $^{143}Nd/^{144}Nd$ for JNdi-1 in house standard was 0.512103 ± 8 (2s, n=12). This standard value is generally lower by 0.000013 compared with JNdi-1 value of 0.512115 [Tanaka et al., 2000]. Therefore, all the Nd reported were corrected for inter-lab bias to JNdi-1 of 0.512115. Two samples, T307R1 and R4, analyzed at Carleton University (superscript C) were also corrected based on measured Sr standard NBS987 of 0.710251 and Nd La Jolla standard of 0.511846.

   The Pb analyses are corrected for fractionation using the NBS-981 standard. The average ratios measured for NBS-981 by conventional TIMS at MIT are $^{206}Pb/^{204}Pb$ = 16.896 ± 0.016, $^{207}Pb/^{204}Pb$ = 15.437 ± 0.022 and $^{208}Pb/^{204}Pb$ = 36.527 ± 0.070 (2 sigma) on the basis of 61 runs during the course of this study. The fractionation correction is 0.12 ± 0.03 %/amu. The average ratios measured for NBS-981 by conventional TIMS at Carleton are $^{206}Pb/^{204}Pb$ = 16.890 ± 0.012, $^{207}Pb/^{204}Pb$ = 15.429 ± 0.014 and $^{208}Pb/^{204}Pb$ = 36.502 ± 0.048 (2 sigma) on the basis of 73 runs during the course of the study. The fractionation correction is 0.13 %/amu. The average ratios measured for NBS-981 by triple spike method are $^{206}Pb/^{204}Pb$ = 16.9447 ± 0.0015, $^{207}Pb/^{204}Pb$ = 15.5024 ± 0.0015 and $^{208}Pb/^{204}Pb$ = 36.7350 ± 0.0034 (2 sigma) on the basis of 12 runs during the course of this study. The reported Pb data, conventional TIMS and triple-spike are normalized to the value of Galer and Abouchami [1998] for NBS-981 which requires fractionation correction of 0.135%/amu for conventional TIMS.
3. All the Hf isotopic ratios were analyzed at Ecole Normale Supérieure in Lyon. Most samples were not acid-leached; analyses of leached (superscript "L") and unleached aliquots for T307R1 and R4 are not significantly different in $^{176}Hf/^{177}Hf$. The Hf data are reported relative to JMC-475 Hf standard of 0.282160.
4. Samples with postfix "Dup" are full procedural duplicates, i.e., separate aliquot of powder. Samples with postfix "Rep" are duplicate runs on TIMS. Samples with postfix "TS" designate Pb data obtained by triple-spike technique.
5. In figures the Sr result with smaller error, and the Nd data from Ecole Normale Supérieure in Lyon were used when there are duplicates and the average of duplicates for Pb are plotted. The leached Hf data were used when both leached and unleached data exist.
6. * for 71WMOL-1 and 71WMOL-3 indicates data from Stille et al. [1986]; the Sr and Nd isotopic data are plotted in the figures but Pb isotopic data are not used due to large uncertainties.
7. Indicated 2σ are in-run uncertainties and apply to the last decimal places.

Table 6. Hf and Nd isotopic data for East Molokai

Sample name	$^{176}Hf/^{177}Hf$	2σ	$^{143}Nd/^{144}Nd$
Late shield/postshield lavas			
71PELE-19	0.283120	5	0.513017
71PELE-21	0.283137	4	0.513029
71WAIK-14F	0.283133	4	0.513015
71WAIK-10F	0.283137	5	0.513039
MT 5.3+375F	0.283121	5	0.513021
MT 4.6F	0.283107	4	0.513006
71HALW-4	0.283113	4	0.513012
Rejuvenated stage lavas			
74KAL-1	0.283175	5	0.513068
P5-252-2	0.283182	5	0.513063
P5-253-9	0.283172	3	0.513057
P5-253-11B	0.283174	4	0.513064
P5-253-12	0.283180	4	0.513072

Reported 2σ applies to the last decimal place. Nd data are from *Xu et al.* [2005].

Table 7a Predicted shield to postshield geochemical changes based on simple models for the spatial distribution of geochemical heterogeneities in Hawaiian plume

	Model	Predicted Geochemical Characteristics	
		shield	postshield
1	Concentrically zoned (Figure 2a)	Kea	Kea
		Loa	Kea
2	Radially zoned with distortion arising from lithosphere interaction (Figure 2b)	Kea	Kea
		Loa	Loa
3, 4	Bilaterally zoned (Figure 2c, d)	Kea	Kea
		Loa	Loa
5	Random heterogeneity (Figure 2e) sampled differently at different temperatures with the Kea component having a higher solidus than the Loa component (see text)	Kea	Loa
		Loa	Loa

Table 7b Observed geochemical characteristics in Loa volcanoes

West Molokai	Loa	Kea
Kahoolawe	Loa	Loa
Hualalai	Loa	Loa

Fig. 1

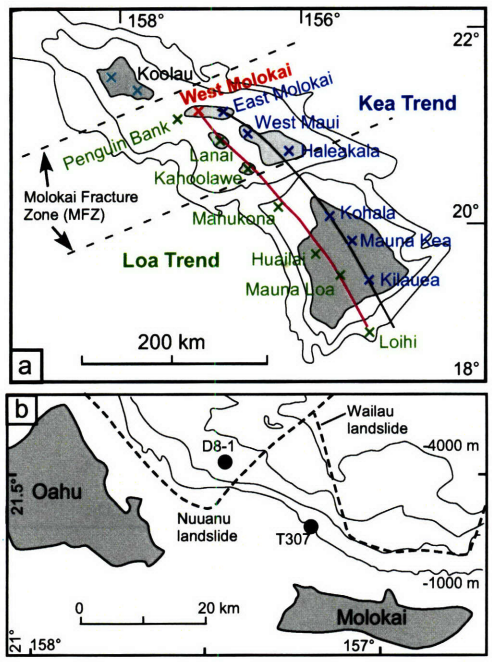
158°
156°
22°
Koolau
West Molokai
East Molokai
Kea Trend
West Maui
Penguin Bank
Haleakala
Lanai
Kahoolawe
Molokai Fracture
Zone (MFZ)
Kohala
20°
Mauna Kea
Loa Trend
Hualalai
Mauna Loa
Kilauea
Loihi
200 km
a
18°
b
Wailau
landslide
-4000 m
D8-1
21.5°
Oahu
Nuuanu
landslide
T307
-1000 m
0
20 km
Molokai
21°
158°
157°

Fig. 2

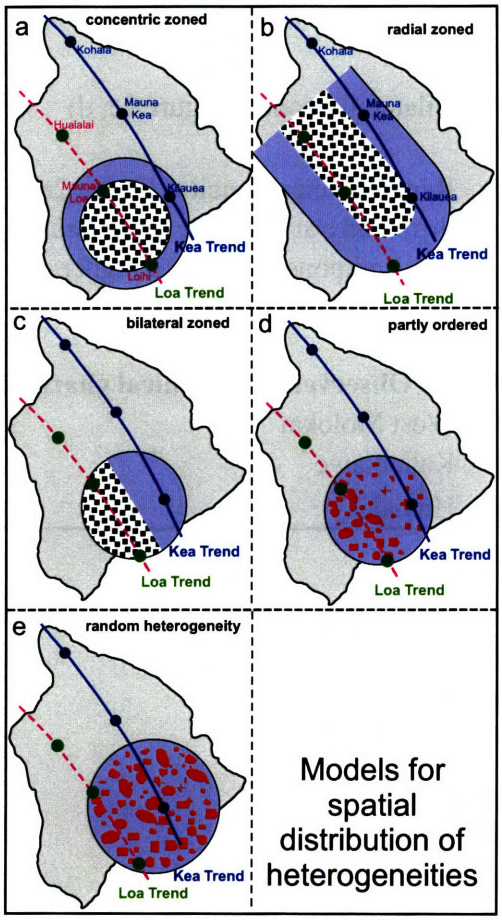
a
concentric zoned
Kohala
Mauna
Kea
Hualalai
Mauna
Loa
Kilauea
Kea Trend
Loihi
Loa Trend
b
radial zoned
Kohala
Mauna
Kea
Kilauea
Kea Trend
Loa Trend
c
bilateral zoned
Kea Trend
Loa Trend
d
partly ordered
Kea Trend
Loa Trend
e
random heterogeneity
Kea Trend
Loa Trend
Models for
spatial
distribution of
heterogeneities

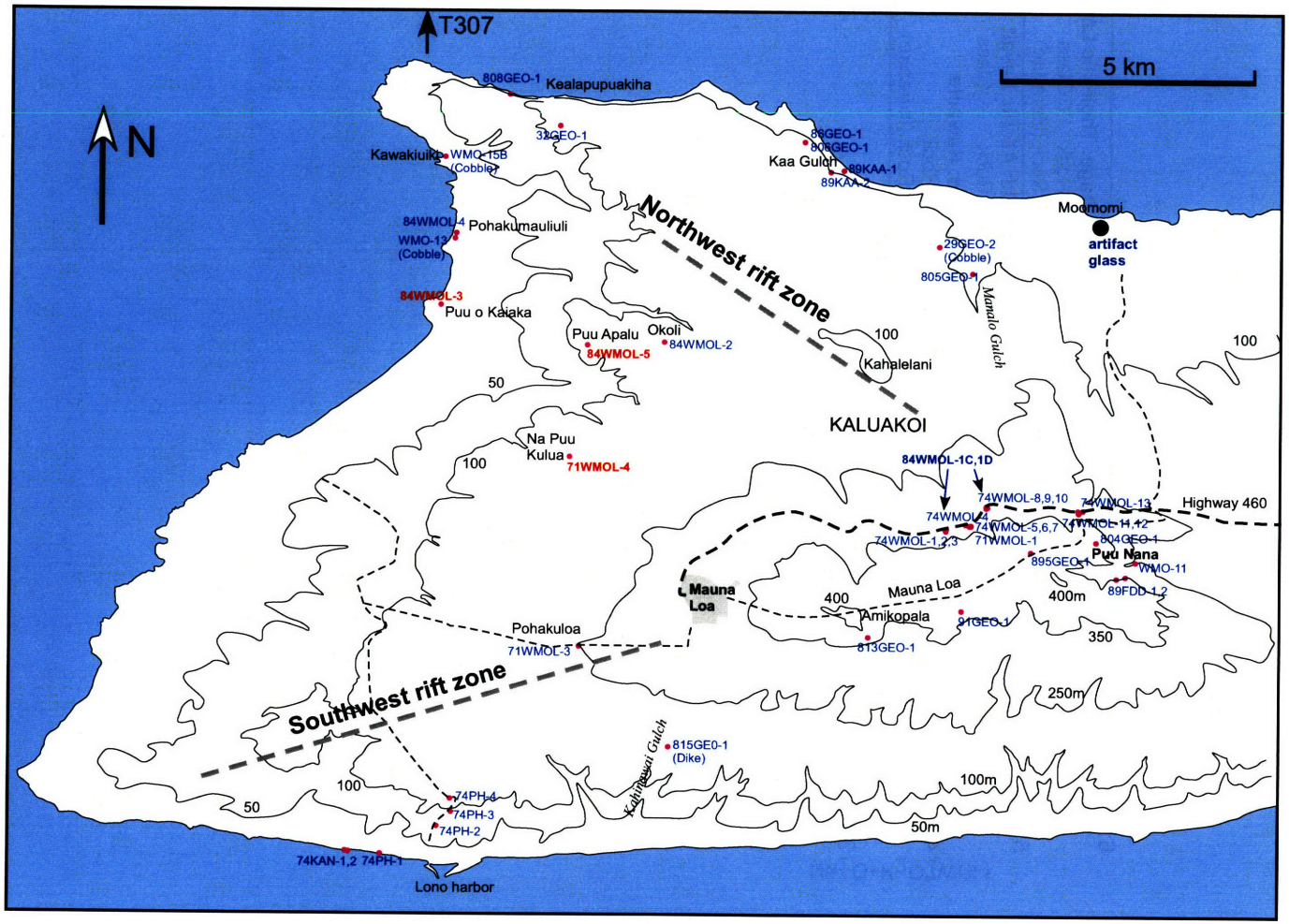
T307
N
5 km
808GEO-1
Kealapupuakiha
32GEO-1
88GEO-1
805GEO-1
Kaa Gulch
89KAA-1
89KAA-2
Kawakiuki
WMO-15B
(Cobble)
Moomomi
artifact
glass
84WMOL-4
Pohakumauliuli
WMO-13
(Cobble)
Northwest rift zone
29GEO-2
(Cobble)
805GEO-1
Manalo Gulch
84WMOL-3
Puu o Kaiaka
Puu Apalu
Okoli
84WMOL-2
84WMOL-5
100
Kahalelani
50
KALUAKOI
100
Na Puu
Kulua
71WMOL-4
84WMOL-1C,1D
74WMOL-8,9,10
74WMOL-13
Highway 460
74WMOL-4
74WMOL-5,6,7
74WMOL-11,12
74WMOL-1,2,3
71WMOL-1
804GEO-1
Puu Nana
895GEO-1
WMO-11
Mauna
Loa
400
Mauna Loa
400m
89FDD-1,2
Amikopala
91GEO-1
Pohakuloa
71WMOL-3
813GEO-1
350
Southwest rift zone
250m
Kahinawai Gulch
815GE0-1
(Dike)
100
100m
50
74PH-4
74PH-3
74PH-2
50m
74KAN-1,2
74PH-1
Lono harbor

Fig. 3

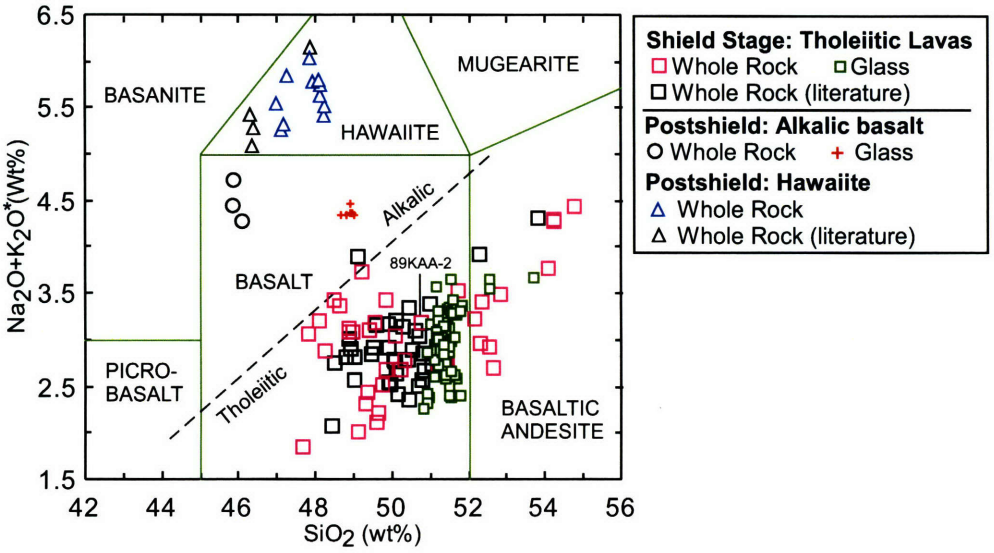
6.5
5.5
4.5
3.5
2.5
1.5
42
44
46
48
50
52
54
56
$Na_2O+K_2O^*(Wt\%)$
SiO_2 (wt%)
BASANITE
MUGEARITE
HAWAIITE
Alkalic
BASALT
89KAA-2
PICRO-
BASALT
Tholeiitic
BASALTIC
ANDESITE
Shield Stage: Tholeiitic Lavas
Whole Rock
Glass
Whole Rock (literature)
Postshield: Alkalic basalt
Whole Rock
Glass
Postshield: Hawaiite
Whole Rock
Whole Rock (literature)

Fig. 4

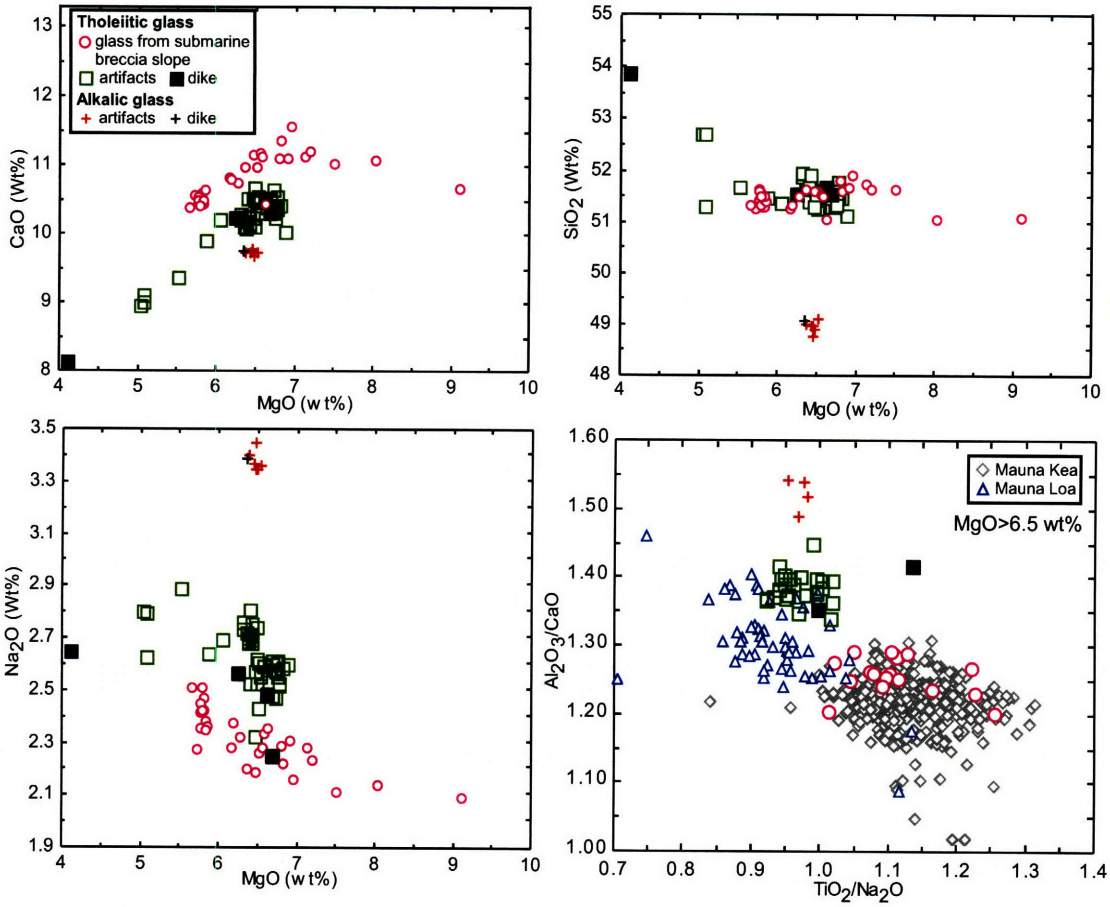
Tholeiitic glass
glass from submarine breccia slope
artifacts
dike
Alkalic glass
artifacts
dike
CaO (Wt%)
MgO (wt%)
SiO2 (Wt%)
MgO (wt%)
Na2O (Wt%)
MgO (wt%)
Mauna Kea
Mauna Loa
MgO>6.5 wt%
Al2O3/CaO
TiO2/Na2O

Fig. 5

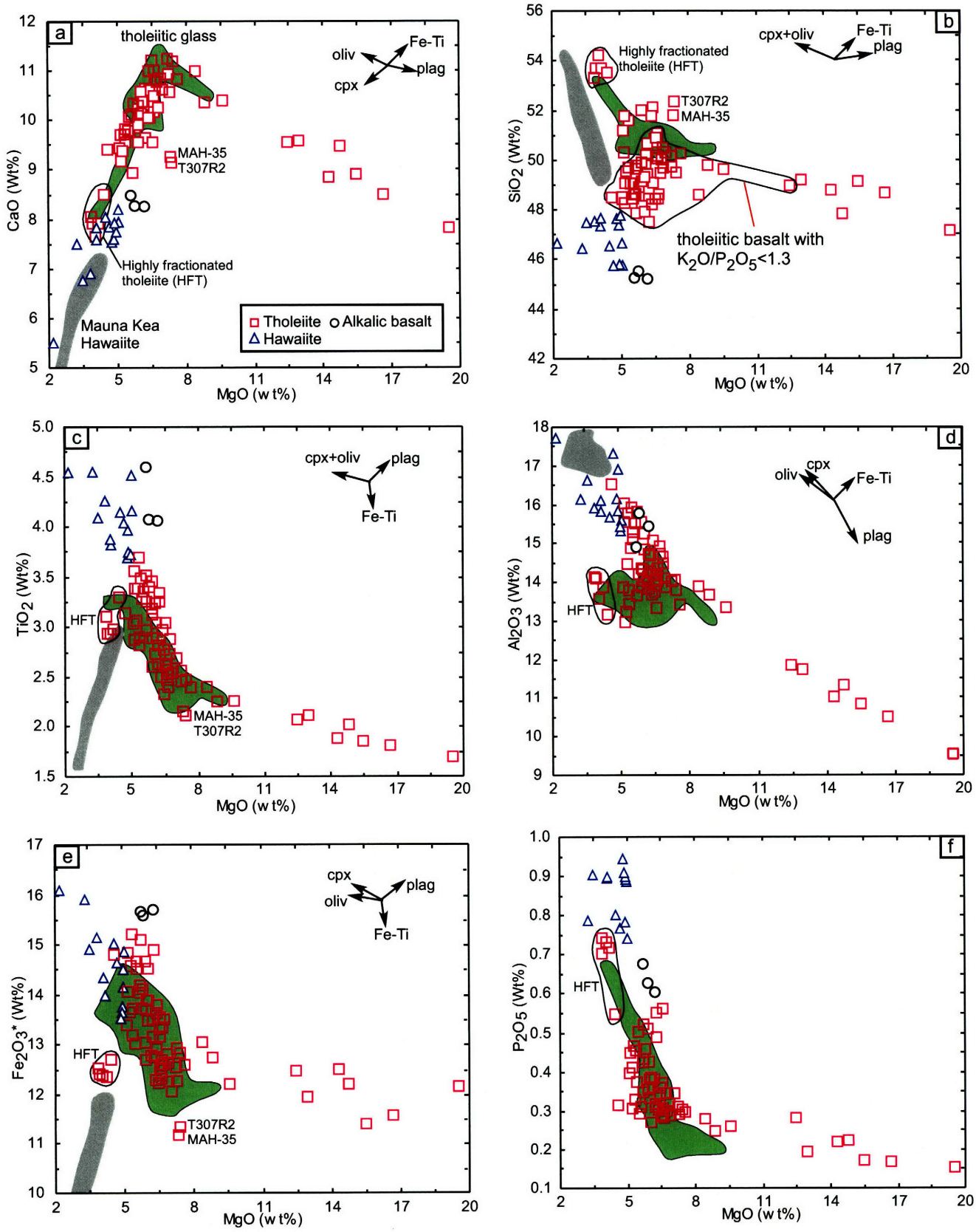
a
tholeiitic glass
oliv
Fe-Ti
plag
cpx
MAH-35
T307R2
Highly fractionated
tholeiite (HFT)
Mauna Kea
Hawaiite
Tholeiite
Alkalic basalt
Hawaiite
CaO (Wt%)
MgO (w t%)
b
cpx+oliv
Fe-Ti
plag
Highly fractionated
tholeiite (HFT)
T307R2
MAH-35
tholeiitic basalt with
K_2O/P_2O_5<1.3
SiO_2 (Wt%)
MgO (w t%)
c
cpx+oliv
plag
Fe-Ti
HFT
MAH-35
T307R2
TiO_2 (Wt%)
MgO (w t%)
d
oliv
cpx
Fe-Ti
plag
HFT
Al_2O_3 (Wt%)
MgO (w t%)
e
cpx
oliv
plag
Fe-Ti
HFT
T307R2
MAH-35
Fe_2O_3* (Wt%)
MgO (w t%)
f
HFT
P_2O_5 (Wt%)
MgO (w t%)

Fig. 6

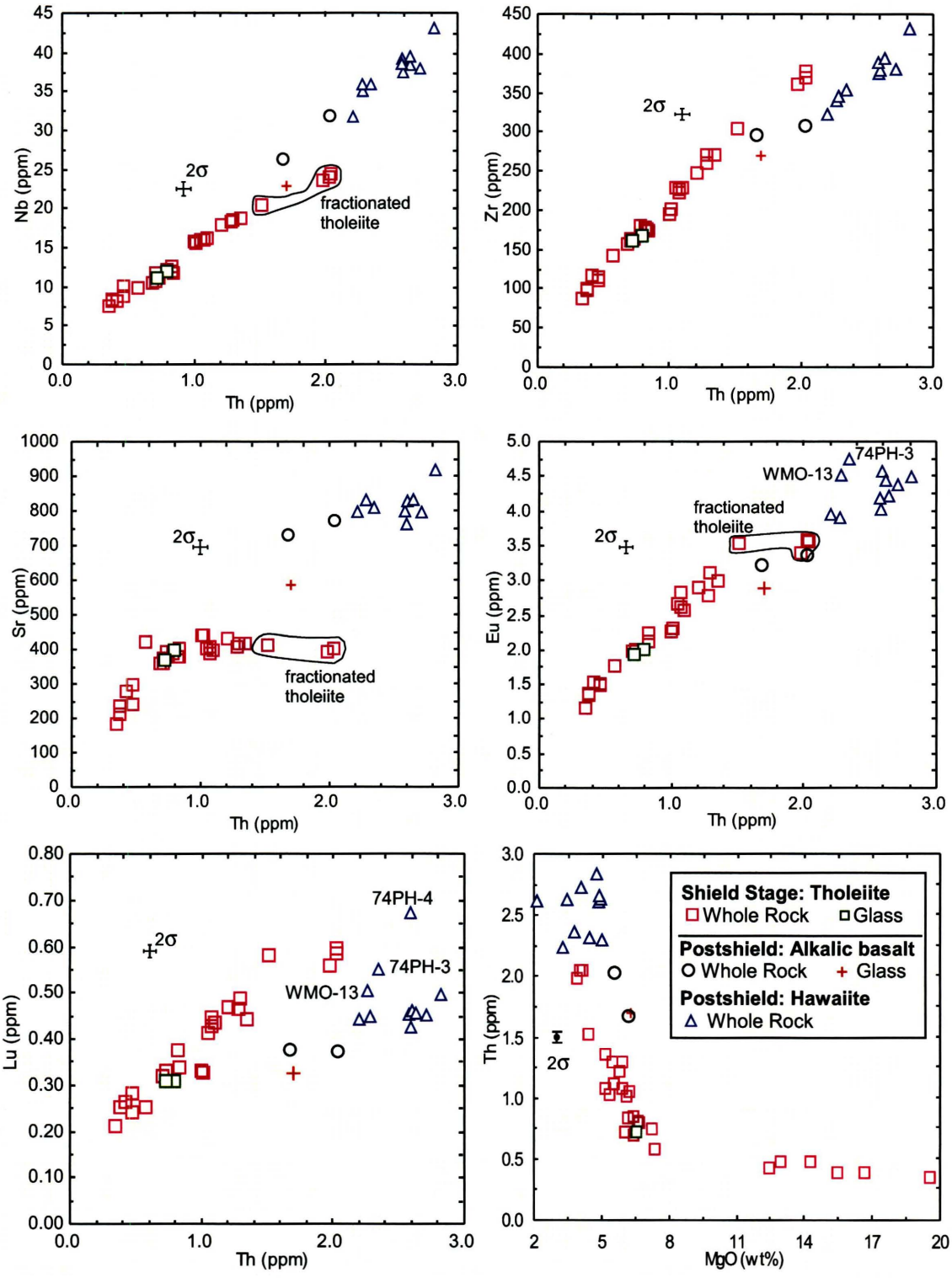
Nb (ppm)
Th (ppm)
2σ
fractionated tholeiite
Zr (ppm)
Sr (ppm)
Eu (ppm)
74PH-3
WMO-13
Lu (ppm)
74PH-4
Shield Stage: Tholeiite
Whole Rock
Glass
Postshield: Alkalic basalt
Whole Rock
Glass
Postshield: Hawaiite
Whole Rock
MgO (wt%)

Fig. 7

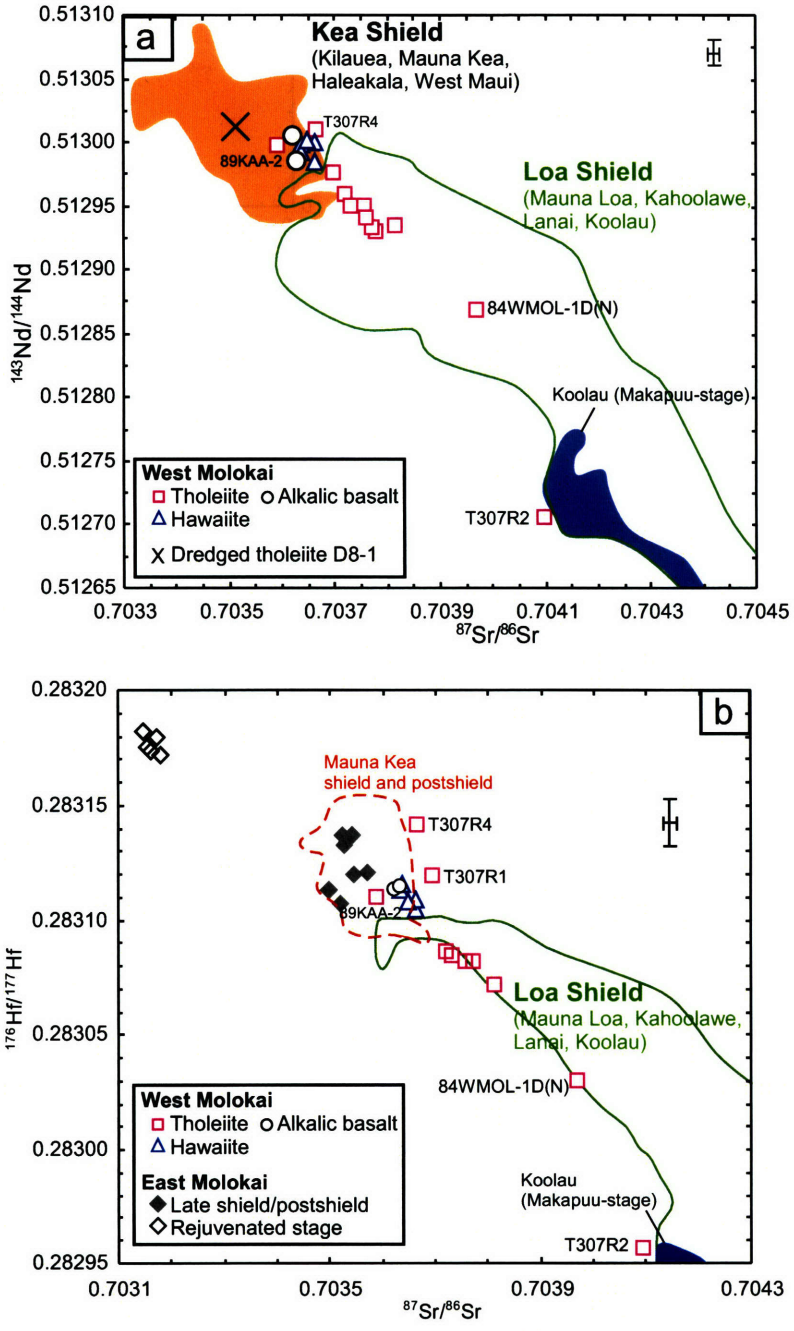
a
Kea Shield
(Kilauea, Mauna Kea,
Haleakala, West Maui)
T307R4
89KAA-2
Loa Shield
(Mauna Loa, Kahoolawe,
Lanai, Koolau)
84WMOL-1D(N)
Koolau (Makapuu-stage)
T307R2
West Molokai
Tholeiite Alkalic basalt
Hawaiite
X Dredged tholeiite D8-1
143Nd/144Nd
87Sr/86Sr
0.51310
0.51305
0.51300
0.51295
0.51290
0.51285
0.51280
0.51275
0.51270
0.51265
0.7033
0.7035
0.7037
0.7039
0.7041
0.7043
0.7045
b
Mauna Kea
shield and postshield
T307R4
T307R1
89KAA-2
Loa Shield
(Mauna Loa, Kahoolawe,
Lanai, Koolau)
84WMOL-1D(N)
Koolau
(Makapuu-stage)
T307R2
West Molokai
Tholeiite Alkalic basalt
Hawaiite
East Molokai
Late shield/postshield
Rejuvenated stage
176Hf/177Hf
87Sr/86Sr
0.28320
0.28315
0.28310
0.28305
0.28300
0.28295
0.7031
0.7035
0.7039
0.7043

Fig. 8

Fig. 9

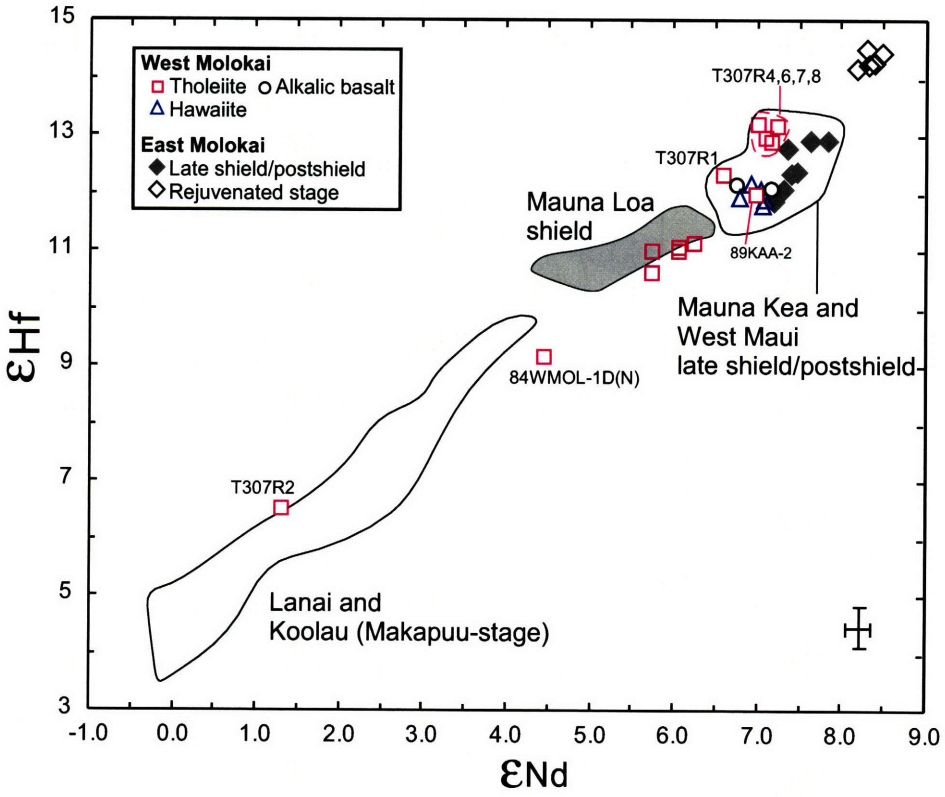
West Molokai
Tholeiite
Alkalic basalt
Hawaiite
East Molokai
Late shield/postshield
Rejuvenated stage
T307R4,6,7,8
T307R1
89KAA-2
Mauna Loa
shield
Mauna Kea and
West Maui
late shield/postshield
84WMOL-1D(N)
T307R2
Lanai and
Koolau (Makapuu-stage)
εHf
εNd
15
13
11
9
7
5
3
-1.0
0.0
1.0
2.0
3.0
4.0
5.0
6.0
7.0
8.0
9.0

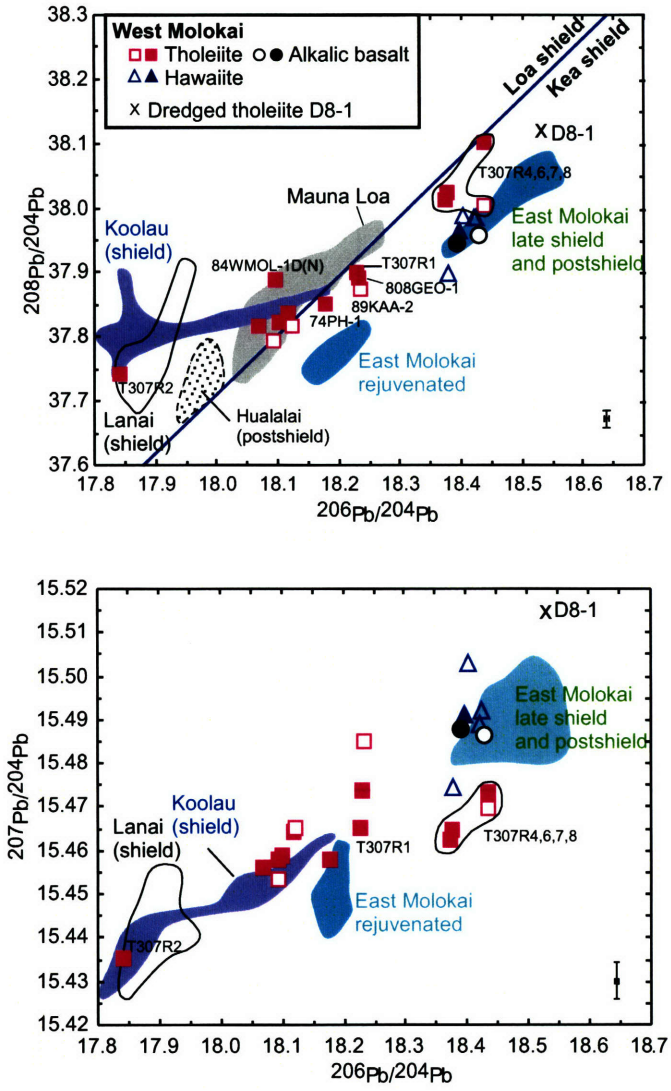
West Molokai
Tholeiite
Alkalic basalt
Hawaiite
Dredged tholeiite D8-1
Loa shield
Kea shield
D8-1
T307R4,6,7,8
Mauna Loa
Koolau
(shield)
East Molokai
late shield
and postshield
84WMOL-1D(N)
T307R1
808GEO-1
89KAA-2
74PH-1
East Molokai
rejuvenated
T307R2
Lanai
(shield)
Hualalai
(postshield)
208Pb/204Pb
206Pb/204Pb
38.3
38.2
38.1
38.0
37.9
37.8
37.7
37.6
17.8
17.9
18.0
18.1
18.2
18.3
18.4
18.5
18.6
18.7
D8-1
East Molokai
late shield
and postshield
Koolau
Lanai (shield)
(shield)
T307R1
T307R4,6,7,8
East Molokai
rejuvenated
T307R2
207Pb/204Pb
206Pb/204Pb
15.52
15.51
15.50
15.49
15.48
15.47
15.46
15.45
15.44
15.43
15.42
17.8
17.9
18.0
18.1
18.2
18.3
18.4
18.5
18.6
18.7

Fig. 10

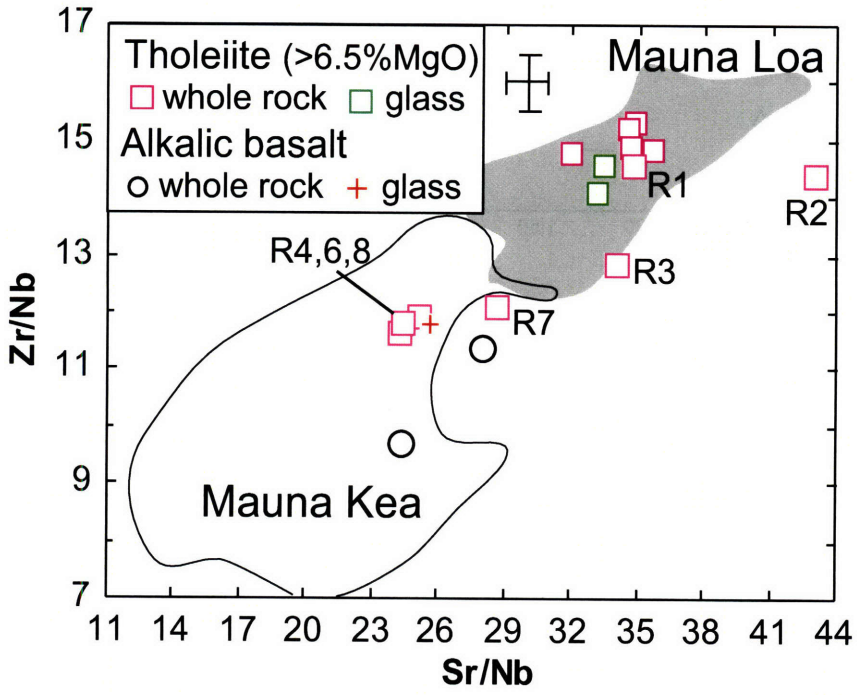
Tholeiite (>6.5%MgO)
whole rock
glass
Alkalic basalt
whole rock
glass
Mauna Loa
R1
R2
R3
R4,6,8
R7
Mauna Kea
Zr/Nb
Sr/Nb
17
15
13
11
9
7
11
14
17
20
23
26
29
32
35
38
41
44

Fig. 11

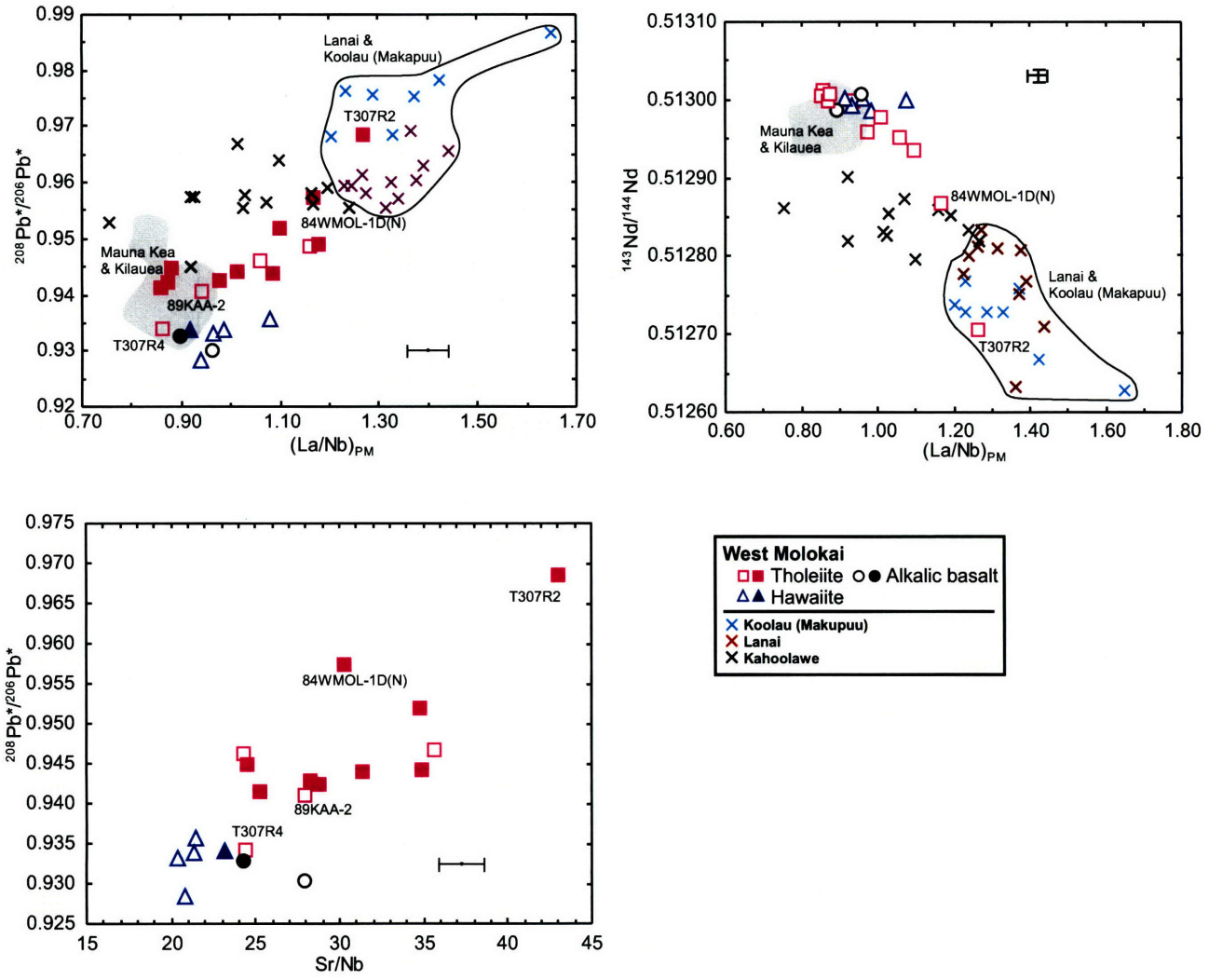
Lanai &
Koolau (Makapuu)
T307R2
84WMOL-1D(N)
Mauna Kea
& Kilauea
89KAA-2
T307R4
$^{208}Pb^*/^{206}Pb^*$
$(La/Nb)_{PM}$
$^{143}Nd/^{144}Nd$
Sr/Nb
West Molokai
Tholeiite
Alkalic basalt
Hawaiite
Koolau (Makupuu)
Lanai
Kahoolawe

Fig. 12

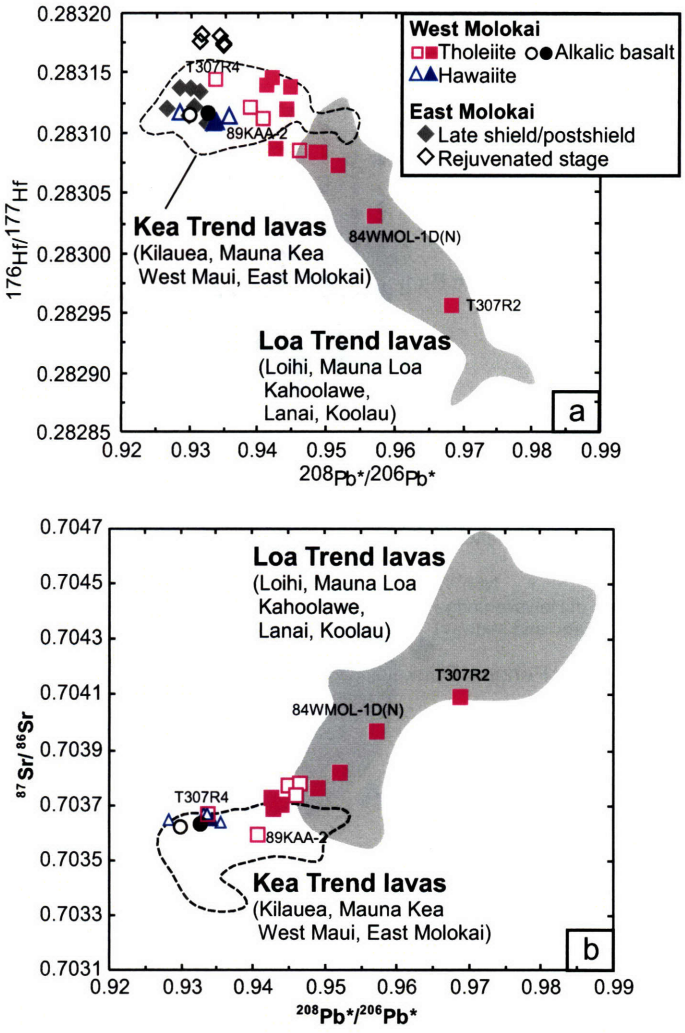
West Molokai
Tholeiite Alkalic basalt
Hawaiite
East Molokai
Late shield/postshield
Rejuvenated stage
T307R4
89KAA-2
Kea Trend lavas
(Kilauea, Mauna Kea
West Maui, East Molokai)
84WMOL-1D(N)
T307R2
Loa Trend lavas
(Loihi, Mauna Loa
Kahoolawe,
Lanai, Koolau)
a
$^{176}Hf/^{177}Hf$
$^{208}Pb^*/^{206}Pb^*$
b
$^{87}Sr/^{86}Sr$

Fig. 13

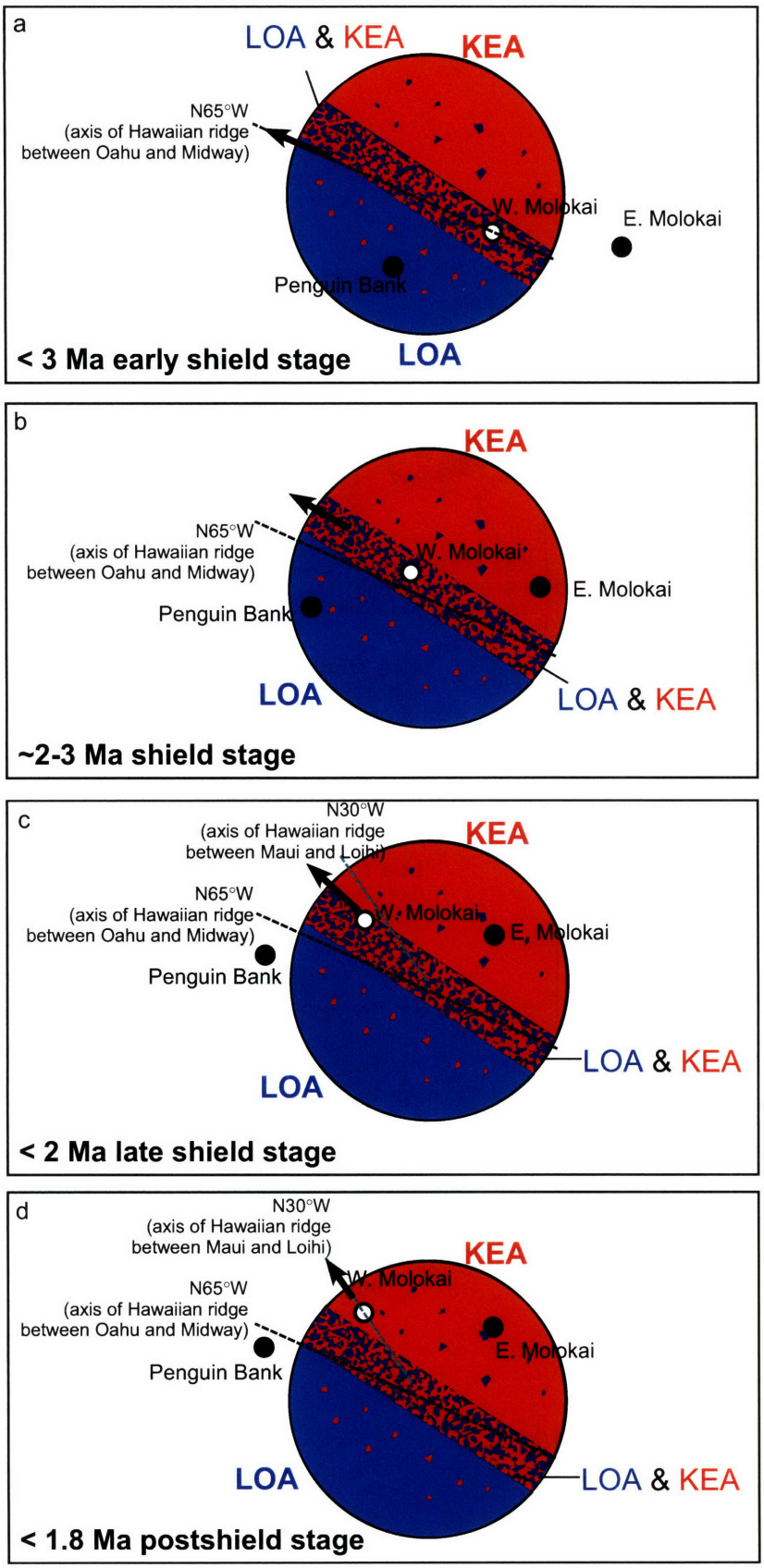
a
LOA & KEA
KEA
N65°W
(axis of Hawaiian ridge
between Oahu and Midway)
W. Molokai
E. Molokai
Penguin Bank
< 3 Ma early shield stage
LOA
b
KEA
N65°W
(axis of Hawaiian ridge
between Oahu and Midway)
W. Molokai
E. Molokai
Penguin Bank
LOA
LOA & KEA
~2-3 Ma shield stage
c
N30°W
(axis of Hawaiian ridge
between Maui and Loihi)
KEA
N65°W
(axis of Hawaiian ridge
between Oahu and Midway)
W. Molokai
E. Molokai
Penguin Bank
LOA & KEA
LOA
< 2 Ma late shield stage
d
N30°W
(axis of Hawaiian ridge
between Maui and Loihi)
KEA
W. Molokai
N65°W
(axis of Hawaiian ridge
between Oahu and Midway)
E. Molokai
Penguin Bank
LOA
LOA & KEA
< 1.8 Ma postshield stage

Fig. 14

Appendix

1. Analytical Methods

Glass major element compositions were analyzed by electron microprobe at the U.S. Geological Survey in Menlo Park (Table 2 and Appendix Table 1) using natural and synthetic standards as described in *Clague and Frey* [1982]. Major element contents for whole-rock samples, except 10 samples, were analyzed by X-ray fluorescence (XRF) with FeO, H_2O^+, H_2O^-, and CO_2 analyzed by classical wet chemical techniques at the U.S. Geological Survey (USGS) laboratories in Denver, Colorado, and Menlo Park, California, respectively (Table 3). Ten additional samples were analyzed by XRF at University of Massachusetts, Amherst (Table 3). Data for one sample, 71WMOL-4, analyzed by both laboratories (Univ. Mass and USGS) agree within 3% except for MnO (Table 3).

Trace elements for the seven dive samples (T307Rx) were analyzed at the Geoanalytical Laboratory at Washington State University. Information on methods, precision, and accuracy for samples analyzed at this facility are available at http://www.wsu.edu/~geolab/. Trace element abundances for all the other samples were determined at MIT by ICP-MS (Table 4) using a Fisons VG Plasmaquad 2+S with both internal and external drift monitors. Trace element results are reported as the mean of duplicate analyses obtained on different days. The chemical procedures and estimates of accuracy and precision were discussed by *Huang and Frey* [2003]. The 2 sigma uncertainty for BHVO-2, which is analyzed as an unknown sample, is better than ±3%. Ten of the fourteen samples with REE-Y enrichment were not analyzed by ICP-MS but their trace element abundances were determined by XRF and Instrumental Neutron Activation Analysis (INAA) at USGS, Denver.

Samples for Sr, Nd, Hf and Pb isotopic analyses were chosen so as to encompass

the full range of compositions (Table 5). Two dive samples (T307R1 and R4) were analyzed at Carleton University on a Finnigan MAT261 multi-collector mass spectrometer running in static mode. For these two samples, analyses were done on two powder splits. The Sr splits were washed for eight days in hot 6M HCl whereas the splits for Nd and Pb were washed in hot 1.5M HCl overnight. Subsequently they were rinsed twice with ultra-pure H_2O before dissolution in HF-HNO_3. Information on methods, precision and accuracy for these two samples (T307R1 and R4), and values for standards analyzed at this facility is in *Cousens et al.* [2003].

Hafnium isotopic analyses (and Nd isotopic ratios for acid-leached (in hot 6M HCl) submarine samples T307R1, R2, R4, R6, R7 and R8) were determined at the Ecole Normale Supérieure in Lyon (ENSL) following the procedure described in *Blichert-Toft et al.* [1997]. Hafnium isotopic compositions were measured by MC-ICP-MS at ENSL using a Nu Plasma 500 HR coupled with a desolvating nebulizer Nu DSN-100. The analytical procedure was similar to that of *Blichert-Toft et al.* [1997] with the exception that potential W isobaric interferences on mass 180 were monitored on mass 183 instead of mass 182. The Faraday cups were positioned to collect masses 173 (Yb monitor; L3), 175 (Lu monitor; L2), 176 (Hf, Lu, Yb; L1), 177 (Hf; Ax), 178 (Hf; H1), 179 (Hf; H2), 180 (Hf, Ta, W; H3), 181 (Ta monitor; H4) and 183 (W Monitor; H5). On-line mass fractionation-corrected corrections for Yb, Lu, Ta and W isobaric interferences were either zero (Lu and Yb) or zero to negligible (Ta and W). Sixty ratios, in 3 blocks of 20 ratios each, were measured for each sample with an integration time of 10 seconds per scan. In order to monitor machine performance, the JMC-475 Hf standard was analyzed systematically in alternation with samples and gave 0.282162 ± 0.000012 (2 sigma; n = 28) for $^{176}Hf/^{177}Hf$ during the three run session of the present samples, corresponding to an external

reproducibility of 0.35ε (Tables 5 and 6). $^{176}Hf/^{177}Hf$ was normalized for mass fractionation relative to $^{176}Hf/^{177}Hf$=0.7325 using an exponential law. Hafnium total procedural blanks were less then 20 pg for all sample batches. Uncertainties reported on Hf measured isotope ratios are in-run $2\sigma/\sqrt{n}$ analytical errors in last decimal place, where n is the number of measured isotope ratios.

The Nd for the six samples analyzed at ENSL for their Nd isotope compositions was recovered from the CaMg-fluoride precipitates left over from the Hf separation chemistry and purified by a two-step procedure using first a cation-exchange column to separate the REE fraction and then an HDEHP column to isolate Nd. Neodymium isotopic compositions likewise were measured by MC-ICP-MS at ENSL using the Nu Plasma HR coupled with a desolvating nebulizer Nu DSN-100 and the same approach as for the Hf isotopic measurements. The Faraday cups were positioned to collect masses 140 (Ce monitor; L3), 142 (Nd, Ce; L2), 143 (Nd; L1), 144 (Nd, Sm; Ax), 145 (Nd; H1), 146 (Nd; H2), 147 (Sm monitor; H3), 148 (Nd, Sm; H4) and 150 (Nd, Sm; H5). Samarium isobaric interference corrections on Nd were zero. Our in-house JMC Nd standard (batch #801149A) was run in alternation with the samples and gave 0.512126 ± 0.000012 (2 sigma; n = 3) for $^{143}Nd/^{144}Nd$ during the single short run session of the present samples (Table 5), and corresponds within error to the accepted value of the La Jolla Nd standard of 0.511846 as determined by cross calibration measurements. $^{143}Nd/^{144}Nd$ was normalized for mass fractionation relative to $^{146}Nd/^{144}Nd = 0.7219$ using an exponential law. The Nd total procedural blank was less then 20 pg for the single sample batch analyzed in this study. Uncertainties reported on Nd measured isotope ratios are in-run 2σ analytical errors in last decimal place.

Twelve samples were analyzed for Pb isotopic ratios by the triple-spike technique

at the Max-Planck-Institut fur Chemie (MPI) following the procedure of *Abouchami et al.* [2000]. The average ratios measured for NBS-981 by the triple spike method are $^{206}Pb/^{204}Pb$ = 16.9447 ± 0.0015, $^{207}Pb/^{204}Pb$ = 15.5024 ± 0.0015 and $^{208}Pb/^{204}Pb$ = 36.7350 ± 0.0034 (2 sigma) on the basis of 12 runs during the course of this study. The data reported in Table 5 were normalized to the values of *Galer and Abouchami* [1998]. Data obtained by the triple-spike method and conventional TIMS at MIT (see following text) have comparable machine in-run uncertainties. They agree within 0.1% for $^{206}Pb/^{204}Pb$ and the data sets are highly correlated (Table 5; Appendix Figure 1a). For $^{207}Pb/^{204}Pb$ and $^{208}Pb/^{204}Pb$ both data sets agree within 0.2%, although they are more scattered which is likely due to the larger uncertainties in mass fractionation correction for conventional TIMS data (Appendix Figure 1).

All other isotopic data were obtained at MIT using the following procedures. In order to avoid the effects of post-magmatic alteration on isotopic ratios, a 6.0 M HCl multi-step acid leaching procedure was used prior to dissolving in HF-HNO_3 [*Xu et al.*, 2005]. After verification of complete dissolution, samples were evaporated and the residual cake was dissolved overnight in 1 mL 6.0 M HCl, and aliquots were taken for Sr (0.25 mL), Pb (0.25 mL) and Nd (0.5 mL) isotope analysis. The aliquots were dried on a hot plate. The Sr aliquot was dissolved using 0.5 mL concentrated 14 M HNO_3 and then fluxed on a hot plate for at least one hour before drying. Then 0.5 mL 3.5 M HNO_3 was added and digested for 24 hours. The Nd and Pb aliquots were dissolved using 3 mL 1 M HCl and 0.5 mL 1.1 M HBr, respectively, and digested for 24 hours.

Sr was separated from other elements using 50 μL columns filled with Eichrome Sr-Spec resin. The Sr aliquot was loaded onto the column followed by rinsing with 1.2 mL 3.5 M HNO_3. Sr was then eluted with 800 μL MQ H_2O. A drop of 0.1 M

H_3PO_4 was added to the eluate before drying.

Pb was separated by anion exchange using HBr. The Pb aliquot was loaded onto 120 μL columns containing Eichrom AG1-X8 anion exchange resin. The columns were then washed with 0.5 mL 1.1 M HBr and 0.5 mL 2 M HCl, and Pb was eluted with 1 mL 6 M HCl. A drop of 0.1 M H_3PO_4 was added to the eluate before drying. For Ca- and Mg-rich samples, this procedure was repeated to improve separation of Pb from Ca.

Separation of Nd and Sm for isotopic analysis requires two ion exchange procedures. The first column separates out the rare earth elements from the bulk rock solution, whereas the second column separates Nd from the other rare earth elements. Rare earth element separation from bulk rock solution utilizes an 8 cm^3 column containing Bio-Rad AG® 50W-X8 resin. The Nd aliquot was loaded onto the column and washed by 12 mL 1 M HCl followed by 60 mL 3 M HCl, which removes the bulk of the Fe and Al in the solution, and then washed by 5 mL 3 M HNO_3, which removes the bulk of the Ba. The change from HCl to HNO_3 also allows some separation of Nd and Sm from Ce and La on the first column. The rare earth element concentrate was eluted with 30 mL 3M HNO_3 and dried down. The concentrate was dissolved in 100 μL 0.3 M HCl for the second column, on which Nd was separated from the other rare earth elements using 0.3 and 0.5 M HCl on a 5 cm^3 column filled with Eichrome LN-Spec resin.

Sr, Nd and Pb were run on a thermal ionization multi-collector mass spectrometer (GV Isoprobe-T) at MIT. Sr was loaded in phosphoric acid on Re filaments with $TaCl_5$ activator, and run in dynamic mode with an average ^{88}Sr signal of 3V. Pb was loaded on Re filaments with phosphoric acid and silica gel, and run in static mode with an average ^{208}Pb signal of 1 - 1.5V. Nd was loaded with phosphoric acid on the

Re side filaments of a triple filament assembly, and run in dynamic mode as Nd metal with an average ^{142}Nd signal of 1 - 1.5V. The blanks for Sr, Nd and Pb were 300 pg, 100 pg and 10 pg, respectively. See Table 5 footnotes for normalization procedures, precision estimates and data for Sr and Nd standards.

The Pb analyses are corrected for fractionation using the NBS-981 standard. The average ratios measured for NBS-981 are $^{206}Pb/^{204}Pb = 16.896 \pm 0.016$, $^{207}Pb/^{204}Pb = 15.437 \pm 0.022$ and $^{208}Pb/^{204}Pb = 36.527 \pm 0.070$ (2 sigma) on the basis of 61 runs during the course of this study. The MIT isotope lab routinely uses a fractionation correction of 0.12 ± 0.03 %/amu, based on the values of *Todt et al.* [1996]. Considering the uncertainties of in-run and mass fractionation correction, the 2 sigma reproducibility is better than 0.1% for $^{206}Pb/^{204}Pb$. One of the two full procedure duplicates agrees within 0.1% and the other agrees within 0.2% (Table 5); triple spike data suggest that there is measurable sampling heterogeneity [*Abouchami et al.*, 2000]. The reported data in Table 5 are normalized to the values of *Galer and Abouchami* [1998] for NBS-981, which require a fractionation correction of 0.135%/amu, and are within the uncertainty of the routinely used fractionation corrections.

2. Post-magmatic alteration

Except for historic eruptions Hawaiian subaerial lavas have been affected to variable extents by post-magmatic alteration; the effects of such alteration must be evaluated before using geochemical data to constrain magmatic processes and magma sources. The most common observation is that low-temperature, subaerial alteration in the Hawaiian environment results in loss of K, Rb, Ba and U [e.g., *Feigenson et al.*, 1983; *Frey et al.*, 1994]. We estimated K_2O loss by identifying samples with anomalously low K_2O/P_2O_5 (<1.29) (Appendix Figure 2); such samples range widely

to anomalously high K/Rb (260 to 2669), Ba/Rb (15 to 436 relative to the 11.3 value of most fresh oceanic basalts [*Hofmann and White*, 1983]), Nb/U (49 to 102) and low Ba/Th (57 to 140) (Appendix Figure 3). In our isotopic analyses some samples with anomalous abundance ratios were included, but we used a multi-step acid-leaching procedure in an effort to recover the isotopic characteristics of the magmas. The well-defined $^{87}Sr/^{86}Sr$ vs. $^{143}Nd/^{144}Nd$ correlation (Figure 8a) suggests that the leaching was successful in removing the relatively high $^{87}Sr/^{86}Sr$ material caused by alteration [e.g., *Huang et al.*, 2005].

There are, however, other post-magmatic processes; in particular, some Hawaiian lavas have been enriched in REE and Y but typically not in other incompatible elements [e.g., *Clague*, 1987; *Fodor et al.*, 1989; *Fodor et al.*, 1992; *Frey et al.*, 1994]. Although the process is not well-understood, the REE and Y enrichment is apparently caused by formation of a groundmass rhabdophane-type phosphate [*Fodor et al.*, 1989; *Cotten et al.*, 1995]. This process can be recognized by anomalously high La/Nb and low Zr/Y, commonly accompanied by a relative depletion in Ce, which is inferred to reflect an oxidizing environment. Fourteen of 40 West Molokai tholeiitic whole-rocks have La/Nb >1.25 and Zr/Y < 3.5 (Appendix Figure 4). The dramatic effect of such alteration is evident on a mantle-normalized plot for incompatible element abundances (Appendix Figure 5). Although there is no strong evidence that this REE-Y enrichment affects isotopic ratios [*Clague*, 1987; *Cotten et al.*, 1995], i.e., the REE-Y mobilization and deposition is highly localized, we did not analyze these West Molokai lavas for isotopic ratios.

Appendix references

Abouchami, W., S. J. G. Galer, and A. W. Hofmann (2000), High precision lead isotope systematics of lavas from the Hawaiian Scientific Drilling Project, *Chem. Geol.*, *169*, 187-209.

Blichert-Toft, J., C. Chauvel, and F. Albarède (1997), Separation of Hf and Lu for high-precision isotope analysis of rock samples by magnetic sector multiple collector ICP-MS, *Contrib. Mineral. Petrol.*, *127*, 248-260.

Clague, D. A. (1987), Petrology of West Molokai Volcano, *Geol. Soc. Am. Abs.*, *19*, 366.

Clague, D. A., and F. A. Frey (1982), Petrology and Trace-Element Geochemistry of the Honolulu Volcanics, Oahu - Implications for the Oceanic Mantle Below Hawaii, *J. Petrol.*, *23*, 447-504.

Cotten, J., A. Ledez, M. Bau, M. Caroff, R. C. Maury, P. Dulski, S. Fourcade, M. Bohn, and R. Brousse (1995), Origin of Anomalous Rare-Earth Element and Yttrium Enrichments in Subaerially Exposed Basalts - Evidence from French-Polynesia, *Chem. Geol.*, *119*, 115-138.

Cousens, B. L., D. A. Clague, and W. D. Sharp (2003), Chronology, chemistry, and origin of trachytes from Hualalai Volcano, Hawaii, *Geochem. Geophy. Geosyst.*, *4*, doi:10.1029/2003GC000560.

Feigenson, M. D., A. W. Hofmann, and F. J. Spera (1983), Case studies on the origin of basalt II, The transition from tholeiitic to alkalic volcanism on Kohala Volcano, Hawaii, *Contrib. Mineral. Petrol.*, *V84*, 390-405.

Fodor, R. V., G. Dobosi, and G. R. Bauer (1992), Anomalously High Rare-Earth Element Abundances in Hawaiian Lavas, *Anal Chem*, *64*, A639-A643.

Fodor, R. V., D. P. Malta, G. R. Bauer, and R. S. Jacobs (1989), Microbeam analyses of rare-earth element phosphate in basalt from Kahoolawe Island, Hawaii, paper presented at the 24th Annual Conference of the Microbeam analytical society, San Francisco, CA.

Frey, F. A., M. O. Garcia, and M. F. Roden (1994), Geochemical Characteristics of Koolau Volcano - Implications of Intershield Geochemical Differences among Hawaiian Volcanos, *Geochim. Cosmochim. Acta*, *58*, 1441-1462.

Galer, S. J. G., and W. Abouchami (1998), Practical application of lead triple spiking for correction of instrumental mass discrimination, *Mineral. Mag.*, *62A*, 491-492.

Hofmann, A. W., and W. M. White (1983), Ba, Rb and Cs in the Earths Mantle, *Zeitschrift Fur Naturforschung Section a-a Journal of Physical Sciences*, *38*, 256-266.

Huang, S., and F. A. Frey (2003), Trace element abundances of Mauna Kea basalt from phase 2 of the Hawaii Scientific Drilling Project: Petrogenetic implications of correlations with major element content and isotopic ratios, *Geochem. Geophy. Geosyst.*, *4*, doi:10.1029/2002GC000322.

Huang, S., M. Regelous, T. Thordarson, and F. A. Frey (2005), Petrogenesis of lavas from Detroit Seamount: Geochemical differences between Emperor Chain and Hawaiian volcanoes, *Geochem. Geophy. Geosyst.*, *6*, doi:10.1029/2004GC000756.

Macdonald, G. A., and T. Katsura (1964), Chemical compositional of Hawaiian lavas, *J. Petrol.*, *5*, 82-133.

Shinozaki, K., Z.-Y. Ren, and E. Takahashi (2002), Geochemical and Petrological characteristics of Nuuanu and Wailau landslides blocks, in *Hawaiian Volcanoes: Deep Underwater Perspectives*, edited by E. Takahashi, et al., pp. 297-310, Geophysical Monograph, AGU, Washington, D.C.

Sun, S.-S., and W. F. McDonough (1989), Chemical and isotopic systematics of oceanic basalts: implications for mantle composition and processes. In: Saunders, A.D., Norry, M.J. (eds.). Magmatism

in the Ocean Basins, *Geological Society Special Publication*, *42*, 313-345.

Todt, W., R. A. Cliff, A. Hanser, and A. W. Hofmann (1996), Evaluation of a $^{202}Pb/^{205}Pb$ double spike for high-precision lead isotope analysis, *Geophys. Monogr., Am. Geophys. Union*, *95*, 429-437.

Weisler, M. I., and D. A. Clague (1998), Characterization of archaeological volcanic glass from Oceania: The utility of three techniques, in *Archaeological Obsidian Studies: Methods and theory*, edited by M. S. Shackley, pp. 103-128, Plenum Press, New York and London.

Xu, G., F. A. Frey, D. A. Clague, D. Weis, and M. H. Beeson (2005), East Molokai and other Kea-trend volcanoes: Magmatic processes and sources as they migrate away from the Hawaiian hot spot, *Geochem. Geophy. Geosyst.*, *6*, doi:10.1029/2004GC000830.

Appendix figure caption:

Appendix Figure 1. Comparison of Pb isotopic ratios analyzed by conventional TIMS and the triple-spike method. The 2 sigma errors shown are the maximum in-run uncertainties which are similar for conventional TIMS and triple-spike data. Both data sets are highly correlated for $^{206}Pb/^{204}Pb$, but they are more scattered for $^{207}Pb/^{204}Pb$ and $^{208}Pb/^{204}Pb$. Two samples which were analyzed in duplicate by conventional TIMS (filled symbols) are shown in the figures. The dashed lines connect the duplicates in panels a, b, c and d. The lines in panels "e" and "f" link the different data for the same sample. Filled pink squares are TIMS duplicates.

Appendix Figure 2. K_2O vs P_2O_5 for West Molokai whole-rocks and glasses. All the glasses (green squares) and whole-rocks with $K_2O/P_2O_5>1.29$ (filled pink squares and circles) define a strong positive trend whereas whole-rocks with $K_2O/P_2O_5<1.21$ (open squares and circles) are offset to lower K_2O at a given P_2O_5. We inferred that samples with $K_2O/P_2O_5<1.21$ have lost K; these samples were corrected for K loss by adding K_2O so that they plot on the regression line derived from the "normal" samples. Data sources: this study, *Macdonald and Katsura* [1964] and *Shinozaki et al.* [2002].

Appendix Figure 3. K_2O/P_2O_5 vs K/Rb, Ba/Rb, Ba/Th and Nb/U for West Molokai lavas. Tholeiitic lavas with $K_2O/P_2O_5<1.3$ have experienced loss of K, Rb, U and Ba (for some lavas) during postmagmatic alteration.

Appendix Figure 4. Zr/Y vs (a) $(La/Nb)_{PM}$ and (b) Ce/Ce* for West Molokai lavas. Subscript PM designates normalized to primitive mantle value of *Sun and McDonough* [1989]. Ce* is Ce abundance interpolated from primitive mantle normalized abundances of La and Nd. Some West Molokai lavas range to very low

Zr/Y (<3.5) and $(La/Nb)_{PM}$ (>1.2) ratios, and these lavas are inferred to reflect a REE-Y enrichment process. Eight out of ten lavas with REE-Y enrichment also have a negative Ce anomaly (see Appendix Figure 5). Error bars shown are 2 sigma uncertainties. Data for Hawaiian shield stage lavas from GEOROC (http://georoc.mpch-mainz.gwdg.de/georoc/).

Appendix Figure 5. Incompatible trace element abundances in West Molokai tholeiitic shield lavas normalized to the primitive mantle [*Sun and McDonough*, 1989]. The gray field shows the range for 17 tholeiitic basalts; only lavas with >4.5% MgO analyzed by ICP-MS are shown. Data points are shown for samples with anomalous ratios involving rare earth elements (REE) and Y that are interpreted as an alteration feature [*Clague*, 1987]. Sample 74WMOL-6 is the most extreme example but three additional samples have anomalously high La/Nb, Nd/Sr, Sm/Zr, Eu/Ti and Y/Zr.

Appendix Table 1. Glass compositions (wt%) for dikes and artifacts

	SiO_2	TiO_2	Al_2O_3	FeO*	MnO	MgO	CaO	Na_2O	K_2O	P_2O_5	S	Total
Postshield stage lavas												
Alkalic basalt												
89KAA-1 (dike)	49.5	3.32	15.0	11.72	0.16	6.41	9.83	3.42	0.98	0.56	0.01	100.9
WM21R-5	49.0	3.27	14.9	11.62	0.17	6.49	9.68	3.35	1.01	0.72	0.00	100.2
WM24-2	48.8	3.23	14.4	11.76	0.17	6.49	9.67	3.34	0.97	0.58	0.01	99.4
WM24-14	49.4	3.24	15.0	11.84	0.15	6.42	9.79	3.43	0.98	0.58	0.02	100.8
WM28-7	48.5	3.22	14.6	11.45	0.16	6.41	9.64	3.41	1.01	0.63	0.01	99.0
WM28-17	49.7	3.26	15.2	11.75	0.17	6.53	9.86	3.42	1.01	0.63	0.01	101.5
WM890-1	49.0	3.30	14.9	11.80	0.17	6.50	9.82	3.36	1.00	0.64	0.01	100.5
Shield stage lavas												
Tholeiite												
WM-11 (dike)	53.6	3.27	13.6	12.40	0.18	4.11	8.08	2.63	1.02	0.67	0.01	99.6
89FDD-1 (dike)	51.4	2.55	14.5	11.20	0.16	6.70	10.26	2.24	0.51	0.30	0.01	99.8
WFD (dike)	52.1	2.50	14.3	11.16	0.16	6.69	10.58	2.50	0.51	0.38	0.00	100.9
WFD-1 (dike)	52.0	2.66	14.6	11.41	0.17	6.33	10.31	2.58	0.55	0.33	0.02	101.0
WM820-1	52.0	2.87	14.1	11.66	0.18	4.99	8.81	2.76	0.84	0.49	0.02	98.7
WM820-2	52.5	3.00	14.1	11.79	0.17	5.08	8.95	2.61	0.92	0.55	0.01	99.7
WM28-12	51.5	3.32	13.7	13.36	0.19	5.13	9.12	2.80	0.78	0.52	0.02	100.4
WM24-1	52.0	3.04	14.1	12.19	0.20	5.59	9.40	2.90	0.77	0.53	0.01	100.7
WM40-2	51.2	2.86	13.9	12.13	0.18	5.87	9.83	2.62	0.55	0.40	0.02	99.6
WM28-20	51.2	2.77	13.9	11.77	0.16	6.06	10.15	2.68	0.62	0.45	0.01	99.8
WM21-66B	52.2	2.62	14.5	11.05	0.17	6.44	10.30	2.74	0.61	0.38	0.00	101.0
WM21-74	51.4	2.56	14.4	10.95	0.17	6.36	10.00	2.68	0.57	0.34	0.01	99.4
WM24-3	51.3	2.52	14.2	11.12	0.18	6.47	10.02	2.72	0.58	0.38	0.00	99.5
WM24-4	51.7	2.61	14.2	11.00	0.19	6.38	10.13	2.67	0.59	0.36	0.01	99.8
WM24-6	51.6	2.62	14.2	11.11	0.17	6.43	10.13	2.75	0.58	0.39	0.01	100.0
WM24-11	51.9	2.57	14.6	11.03	0.17	6.41	10.12	2.73	0.59	0.38	0.01	100.5
WM28-3	52.1	2.58	14.7	10.95	0.15	6.44	10.25	2.70	0.59	0.39	0.01	100.9
WM28-4	51.5	2.58	14.2	10.97	0.17	6.40	10.04	2.66	0.60	0.35	0.00	99.5
WM28-6	52.1	2.54	14.5	10.92	0.17	6.37	10.23	2.74	0.60	0.33	0.01	100.5
WM28-8	52.0	2.58	14.4	10.90	0.16	6.44	10.26	2.72	0.61	0.35	0.01	100.4
WM28-9	51.2	2.54	14.1	10.93	0.17	6.38	10.11	2.66	0.58	0.34	0.01	99.0
WM28-10	52.0	2.63	14.2	10.84	0.15	6.35	10.27	2.76	0.60	0.36	0.01	100.2
WM28-11	52.1	2.60	14.5	10.72	0.16	6.46	10.28	2.71	0.60	0.33	0.00	100.5
WM28-18	52.1	2.67	14.5	10.80	0.17	6.47	10.28	2.82	0.62	0.36	0.01	100.8
WM28-21	52.0	2.57	14.2	11.06	0.17	6.45	10.12	2.71	0.60	0.37	0.01	100.3
WM21-71	51.6	2.50	14.3	11.56	0.16	6.50	10.22	2.57	0.47	0.32	0.01	100.2
WM24-12	51.2	2.45	14.4	11.43	0.18	6.58	10.27	2.58	0.48	0.30	0.01	99.9
WM24-13	51.4	2.49	14.6	10.96	0.16	6.53	10.47	2.60	0.51	0.29	0.01	100.0
WM21-66A	50.9	2.51	14.1	10.84	0.18	6.70	10.25	2.52	0.56	0.36	0.00	98.9
WM21-69	51.0	2.44	14.1	10.86	0.19	6.69	10.16	2.57	0.53	0.36	0.01	98.9
WM21-72	50.9	2.50	14.1	10.86	0.17	6.77	10.27	2.55	0.52	0.34	0.01	99.0
WM21-73	51.5	2.53	14.1	11.07	0.17	6.71	10.48	2.61	0.58	0.35	0.01	100.1
WM21R-1	51.3	2.57	14.2	10.99	0.17	6.72	10.28	2.56	0.55	0.36	0.01	99.7
WM21R-3	51.2	2.38	14.1	11.03	0.17	6.60	10.29	2.55	0.54	0.39	0.01	99.3
WM21R-4	51.2	2.41	14.6	10.87	0.17	6.53	10.47	2.55	0.54	0.34	0.01	99.7
WM21R-6	51.7	2.48	14.3	10.99	0.16	6.72	10.42	2.60	0.55	0.35	0.01	100.3
WM24-5	51.2	2.50	14.2	11.19	0.16	6.74	10.61	2.46	0.46	0.33	0.01	99.9
WM24-7	51.6	2.36	14.4	11.23	0.18	6.73	10.53	2.48	0.49	0.31	0.01	100.3
WM24-8	51.4	2.50	14.4	11.04	0.18	6.79	10.32	2.51	0.54	0.28	0.00	100.0
WM24-10	52.0	2.34	14.4	10.90	0.16	6.82	10.56	2.53	0.50	0.31	0.01	100.5
WM26-1	51.1	2.40	14.2	10.83	0.18	6.67	10.29	2.55	0.53	0.34	0.00	99.1
WM26-2	51.6	2.51	14.3	11.08	0.16	6.79	10.31	2.61	0.53	0.34	0.01	100.2
WM28-13	50.9	2.56	14.4	11.22	0.18	6.88	9.96	2.58	0.57	0.37	0.01	99.6
WM28-14	51.3	2.62	14.2	11.22	0.15	6.78	10.20	2.61	0.58	0.36	0.01	100.0
WM28-15	51.6	2.54	14.7	11.15	0.17	6.44	10.53	2.53	0.51	0.31	0.00	100.5

WM21R-2	51.6	2.42	14.6	10.83	0.16	6.52	10.68	2.62	0.52	0.35	0.01	100.3
WM21R-7	50.9	2.38	14.7	10.86	0.18	6.50	10.40	2.53	0.52	0.37	0.01	99.4
WM28-1	51.1	2.47	14.5	11.31	0.17	6.51	10.41	2.42	0.50	0.36	0.01	99.8
WM28-2	51.6	2.58	14.3	11.37	0.15	6.53	10.51	2.53	0.49	0.34	0.01	100.4
WM28-16	51.7	2.58	14.7	11.44	0.17	6.54	10.58	2.34	0.50	0.30	0.01	100.9

Data from Weisler and Clague [1998]

Except for glass on dikes, all data are for artifacts collected from the north coast near Moomomi (See Figure 3)

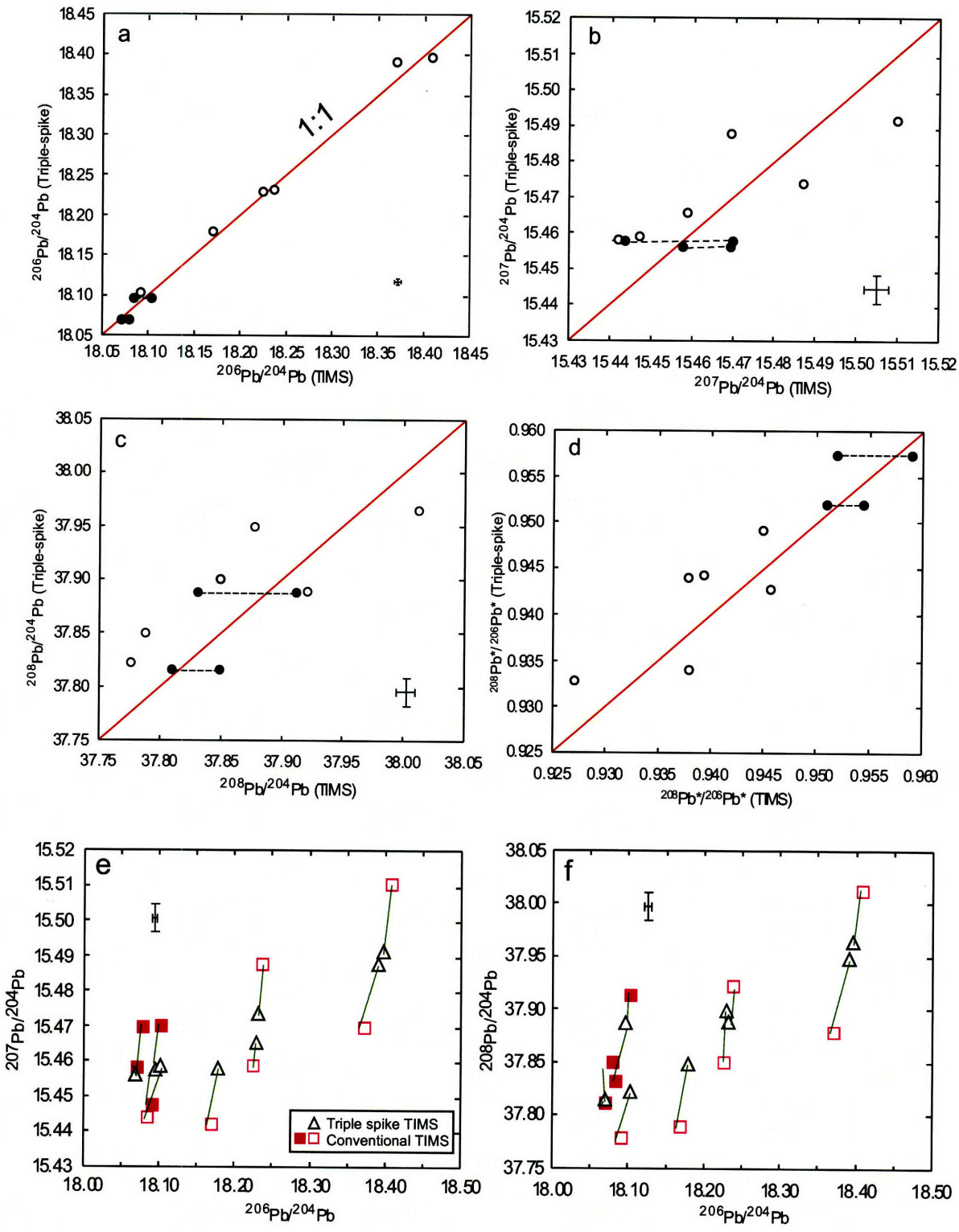

Appendix Figure 1

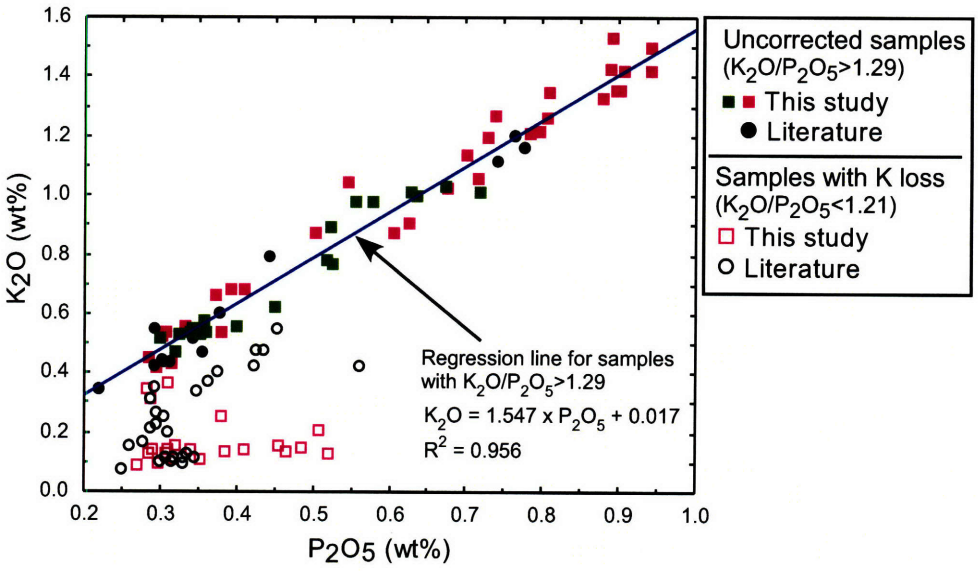

Appendix Figure 2

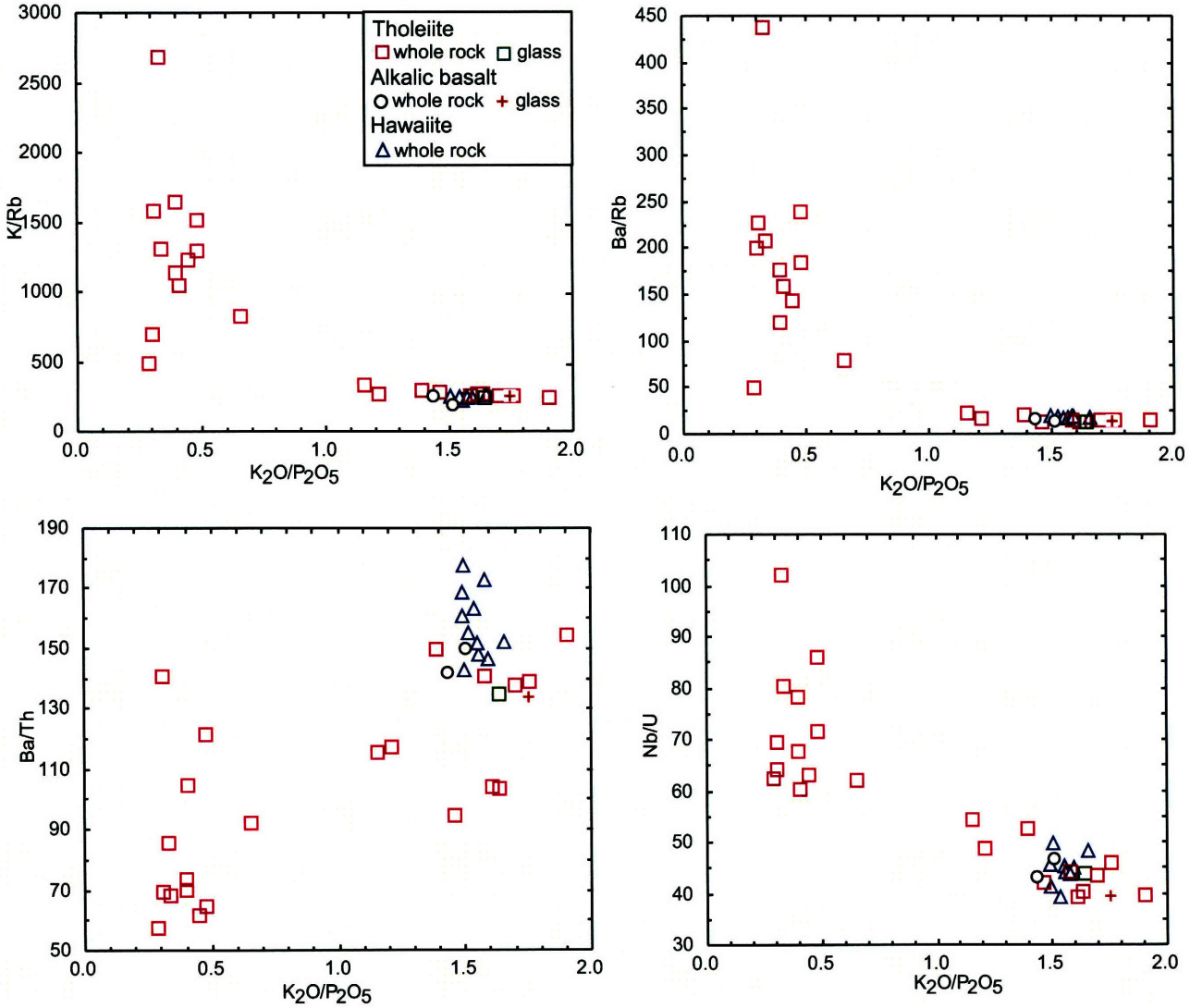

Appendix Figure 3

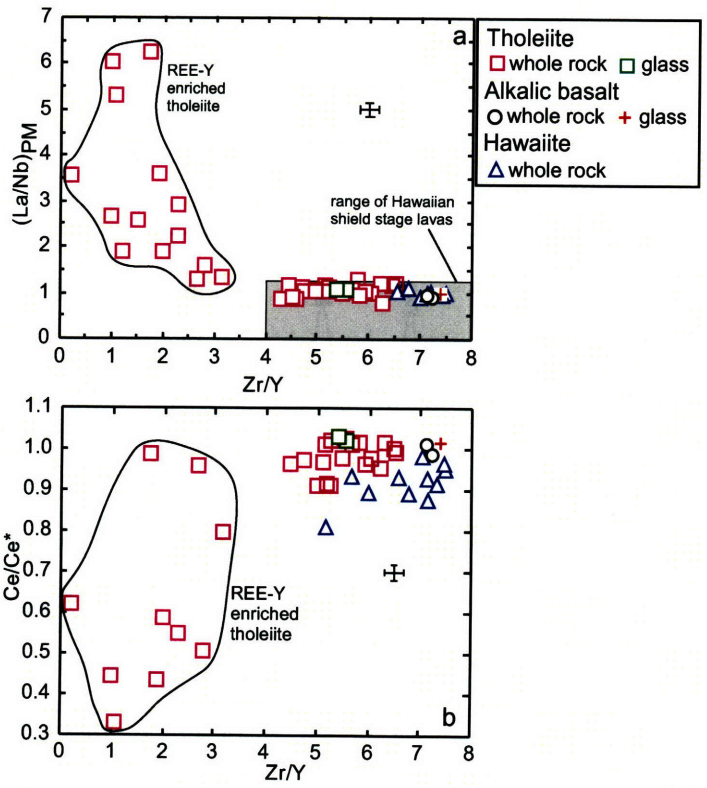

Appendix Figure 4

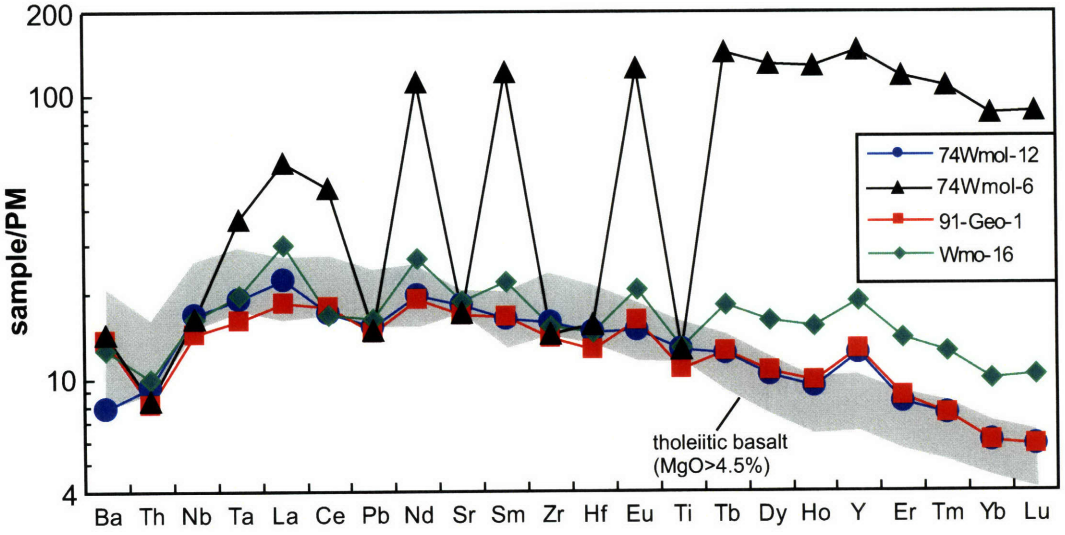

Appendix Figure 5

Chapter 4 Major and Trace Element Composition of Mauna Kea Basalt from Phase 2b of the Hawaii Scientific Drilling Project (3109-3335 Meters Below Sea Level)

Abstract

The Hawaii Scientific Drilling Project recovered ~3.3 km of basalt by coring into the flank of Mauna Kea volcano at Hilo, Hawaii. The first stage of HSDP Phase 2 drilling (Phase 2a) cored Mauna Kea lavas to a depth of 3109 meters below sea level (mbsl) and the second stage of drilling (Phase 2b) extended 225 m below the penetration of Phase 2a. In this study we report the trace element composition of 22 reference suite samples from the Phase 2b drill core. The major and trace element compositions of these 22 samples are similar to the shield lavas in the overlying Phase 2a lavas. One intrusive unit from the top of Phase 2b core belongs to the distinctive low SiO_2 group of shield tholeiitic basalt that is abundant at depths of 2233-2481 mbsl in the Phase 2a core; the other 21 samples are high SiO_2 group lavas.

Two alternative models have been proposed to explain the major element contents of the low and high SiO_2 groups: (1) melt-peridotite reaction whereby high SiO_2 lavas were derived from low SiO_2 magmas by reacting with overlying peridotite, specifically dissolving pyroxenes and precipitating olivine (*Stolper et al., Geochemistry, Geophysics and Geosystems, 2004*). We find that this model cannot explain the between group differences in trace element ratios, such as in Nb/Zr vs Ti/Zr. (2) A pyroxenite source model whereby both the low and high SiO_2 group magmas were derived from secondary pyroxenites (*Herzberg, Nature, 2006*) formed by reacting partial melt of eclogite with peridotite (*Sobolev et al., Nature, 2005*). The model for the low SiO_2 group has been recently modified (Herzberg, personal communication, 2007) to include mixing of melts derived from the secondary pyroxenite and peridotite to generate low SiO_2 magma. This melt mixing process can explain the mixing trends defined by the low SiO_2 lavas in Pb isotopic ratios and Nb/Zr vs Sm/Yb and Ti/Zr.

1. Introduction

As Hawaiian volcanoes grow, they typically progress through four volcanic stages as the lithosphere approaches, overrides and recedes from the hotspot [e.g., *Clague and Dalrymple*, 1987], i.e., an alkalic preshield stage (~ 3% of volcano volume); main tholeiitic basalt shield stage (~95-98% of the volume); alkalic postshield stage (~1% of the volume); alkalic rejuvenated stage (<1% of the volume) (Figure 1). Mauna Kea is the largest Hawaiian volcano that has evolved through the alkalic postshield stage, and it was chosen for the Hawaiian Scientific Drilling Project (HSDP). The objective of the HSDP is to sample both the early submarine growth and the subsequent subaerial growth of Mauna Kea. Studies of the cores are focussed on understanding the temporal variation in eruption style and the geochemical characteristics of lavas erupted throughout building of the Mauna Kea shield (see papers on Theme of Hawaii Scientific Drilling Project in Geochemistry, Geophysics, Geosystems). The location of the HSDP drill holes is on the southeast flank of Mauna Kea near the coastal city of Hilo. At this location Mauna Kea lavas are overlain by Mauna Loa shield lavas (Figures 2 and 3).

During HSDP Phase 1 drilling, 280 m of lavas from Mauna Loa and 776 m of underlying subaerially erupted Mauna Kea lavas were recovered, ranging in age from < 200 ka to ~400 ka [*Sharp et al.*, 1996; *Stolper et al.*, 1996]. The uppermost Mauna Kea lavas (58 m) are postshield lavas that include intercalated alkalic and tholeiitic basalt [*Yang et al.*, 1996]. Relative to shield tholeiitic basalt, the postshield lavas have lower SiO_2 at a given MgO and higher La/Yb and Nb/Zr. Such results indicate that during the transition from shield to postshield volcanism, there was a decrease on extent of melting and increasing pressure of melt segregation (e.g., [*Yang et al.*, 1996]).

Although isotopically similar (Sr, Nd, Hf and Pb) tholeiitic and alkalic basalt are intercalated within the postshield stage, on a longer time scale, the temporal evolution from shield to postshield stage volcanism is characterized by decreasing $^{87}Sr/^{86}Sr$ and $^{206}Pb/^{204}Pb$ and increasing $^{143}Nd/^{144}Nd$ and $^{176}Hf/^{177}Hf$ [e.g., *Chen and Frey*, 1985; *Lassiter et al.*, 1996; *Blichert-Toft and Albarède*, 1999; *Abouchami et al.*, 2000; *Bryce et al.*, 2005]. These isotopic trends indicate that the plume core, sampled during shield-stage volcanism, is isotopically different from the cooler plume margin, sampled by postshield stage volcanism. A concentric radially zoned plume has been inferred [e.g., *Lassiter et al.*, 1996].

The first stage of HSDP Phase 2 drilling (designated as Phase 2a) cored Mauna Kea lavas to a depth of 3109 meters below sea level (mbsl) with an age of 635 ka at the bottom of the core [*Sharp and Renne*, 2005]. The drill hole sampled 245 m of subaerial Mauna Loa lavas before penetrating into Mauna Kea lavas. Like lavas from the Phase 1 drilling hole, the uppermost Phase 2a Mauna Kea lavas are inter-layered tholeiitic and alkalic basalt which belong to the postshield stage (e.g., [*Rhodes and Vollinger*, 2004]) (Figure 3). Most importantly, the Phase 2a core sampled shield building tholeiitic basalt that includes the subaerial to submarine transition for Mauna Kea at ~1079 mbsl [*Stolper et al.*, 2004]. The submarine lavas include pillow lavas, hyaloclastites, massive flows and intrusive units [*Seaman et al.*, 2000]) (Figure 3).

An important result is that the HSDP Phase 2a core contains two intercalated compositionally distinct groups of shield tholeiitic basalt which are distinguished by different SiO_2 contents at a given MgO content [e.g., *Rhodes and Vollinger*, 2004; *Stolper et al.*, 2004]. The low SiO_2 group lavas have major, trace element and isotopic compositions that are similar to lavas from Loihi seamount; for example, the low SiO_2 lavas have relatively high Nb/Zr ratios, high $^{3}He/^{4}He$ ratios, and high $^{208}Pb/^{204}Pb$ at a

given $^{206}Pb/^{204}Pb$ [Fig.4 and *Eisele et al.*, 2003; *Huang and Frey*, 2003; *Kurz et al.*, 2004; *Rhodes and Vollinger*, 2004]. Stolper et al. [2004] argued that the low SiO_2 lavas were derived from partial melting of peridotite and that the high SiO_2 lavas were derived from the low SiO_2 magmas by reacting with overlying residual peridotite, i.e., dissolution of SiO_2-rich orthopyroxene and clinopyroxene and precipitation of SiO_2-poor olivine. In contrast, Herzberg [2006] argued that both the low and high SiO_2 groups of tholeiitic basalt were derived from pyroxenite sources. Regardless of derivation from peridotite or pyroxenite sources, the distinctive isotopic differences between the two SiO_2 groups, most obviously, relatively high $^{3}He/^{4}He$ and $^{208}Pb^*/^{206}Pb^*$ (defined as $(^{208}Pb/^{204}Pb - 29.475) / (^{206}Pb/^{204}Pb - 9.307)$) in the low SiO_2 group (Figure 4), require isotopically different sources within the plume core [e.g., *Blichert-Toft et al.*, 2003; *Eisele et al.*, 2003; *Kurz et al.*, 2004].

In this chapter I discuss the major and trace element composition of samples from additional drill core, designated as Phase 2b, extending ~225 m below the 3109 m penetration of the HSDP Phase 2a core. The studied reference suite comprises 22 samples from 17 different units (Table 1), including three intrusive samples (from Units 3a, 18 and 20b), three massive lavas from Unit 14, two pillow breccia samples (Units 4 and 10), and 14 pillow lavas (Figure 3; Table 1). Eighteen of the 22 samples are moderately olivine phyric (3-5 vol% olivine), one sample (from Unit 20b) is highly olivine – phyric (>15 vol% olvine), and the other three samples are aphyric or sparsely olivine-phyric (from Units 2d, 3a and 19b) (Table 1).

2. Analytical Procedures

We determined abundances of trace elements for the reference suite of samples from HSDP Phase 2b using inductively coupled plasma mass spectrometry

(ICP-MS) following the procedure described in Huang and Frey [2003] (Table 2). Trace element results are reported as the mean of duplicate analyses of the same solution obtained on different days; the duplicates generally agree within ±5%. The USGS standard BHVO-2 was dissolved and run as unknown with the reference suite samples; for BHVO-2 the relative standard deviation (RSD, defined as 1σ divided by the average) is less than 4% (Table 2). The average values agree within 2% of those reported by Huang and Frey [2003] except for Sr, Zr and U which are within 3% (Table 2). Some trace elements (Nb, Zr, Y, Rb, Sr, Ba, Cr) were analyzed by both XRF and ICP-MS, and the results generally agree within 5% except for Y (7%) and Ba (10%) [*Rhodes and Vollinger, 2006 unpublished data*] (Appendix Figure 1).

3. Results

3.1 Major elements *(unpublished XRF data from Rhodes and Vollinger, 2006)*:

Except for two samples from Units 3a and 20b that have MgO 12.7% and 11.7%, respectively, the other samples (20) have limited variations in major element contents (SiO_2: 50.1 - 50.8%; Fe_2O_3*: 12.3 - 12.7%; CaO: 10.5 – 11%; Al_2O_3: 12.8 – 13.7%; MgO: 6.6 – 8.2%) (Table 3, Figure 5). The Phase 2b samples generally overlap with Phase 2a high SiO_2 group lavas in MgO vs major element correlation plots except one sample from Unit 3a (Figure 5). Relative to the other Phase 2b samples, intrusive lava from Unit 3a has distinctively lower SiO_2, higher Al_2O_3 and Fe_2O_3* at a given MgO, and it plots in the field of low SiO_2 group lavas from HSDP Phase 2a (Figure 5). This sample also has anomalously high K_2O content (Figure 5).

3.2 Trace elements

In plots of Th abundance vs abundance of other incompatible trace elements, the Phase 2b samples generally overlap with Phase 2a samples (Figure 6). Trends for

relatively mobile elements, such as Rb, Ba, Pb and U show more scatter than trends for immobile elements, such as Nb, Zr and Hf (Figure 6).

Units 3a and 20b with the highest MgO contents have the lowest abundances of immobile incompatible element (e.g., Nb and Th) among Phase 2b samples (Figure 6). However, the sample from Unit 3a with anomalously high K_2O content also has very high Rb (20.1 ppm) (Figures 5 and 6). This sample has lower Sr abundance at a given Th relative to the other Phase 2a and 2b samples (Figure 6). The lower Zr and Hf abundances for the low SiO_2 group lava (Unit 3a) at a given Th are consistent with the generally lower Zr and Hf for low SiO_2 group lavas from HSDP Phase 2a core (Figure 6).

On a primitive mantle normalized diagram, the 22 Phase 2b samples have a relative Th depletion which is characteristic of Hawaiian lavas [*Hofmann and Jochum*, 1996; *Yang et al.*, 2003; *Huang et al.*, 2005a] (Figure 7). There is a negative slope from Ta to heavy rare earth elements (Figure 7), but in detail, like the Phase 2a core lavas, the Phase 2b lavas have a slight Sm depletion relative to Zr and Hf which contrasts with the Hawaiian rejuvenated stage lavas which generally have depletions of Zr and Hf relative to Sm (Figure 7) [*Yang et al.*, 2003]. There is a significant peak at Ta (Figure 7). The average Nb/Ta ratio for all Phase 2b shield lavas, 14.3±0.9, is similar to that of Phase 2a shield avas, 13±2 [*Huang and Frey*, 2003]. These values are lower than that of the primitive mantle value of 17.4 [*Sun and McDonough*, 1989]. However, the HSDP samples may have low ratios because of Ta contamination arising from use of a WC shatterbox to prepare the powders (see [*Huang and Frey*, 2003; *Huang et al.*, 2005b]). Indeed, Hawaiian tholeiitic basalts crushed in agate have higher Nb/Ta ratios than HSDP lavas (e.g., Kahoolawe tholeiitie = 14.9±0.6, Huang et al. [2005b]; West Molokai tholeiite = 15.6±0.6, Xu et al. [2007]).

Like lavas from the HSDP Phase 2a core, Ba/La, Ba/Nb and Ba/Th are variable (factor of 8.6 to 9.5) in Phase 2b samples and these ratios are strongly correlated with each other (Figure 8). In contrast to ratios involving Ba, other incompatible trace element ratios, such as Nb/Zr, Nb/Sr, La/Nb and La/Yb, are much less variable; they typically vary by < 5%, the analytical uncertainty (Figure 9). Exceptions are intrusive Units 3a and 20b which define the extremes of Phase 2b samples, but these extremes are within the range defined by Phase 2a samples (Figure 9).

Incompatible element ratios do not vary systematically with depth in the Phase 2a core [*Huang and Frey*, 2003] or Phase 2b core (Figure 9). However, a systematic periodicity of ~18 Ka for isotopic ratios, La/Yb and Nb/Zr was identified in the Phase 2a core by Blichert-Toft et al. [2003].

4. Discussion

4.1 Post-magmatic alteration

It is well known that Cs, Rb, K, U, to lesser extent Pb, Sr and Ba, are mobile during post-magmatic alteration of Hawaiian lavas (e.g., [*Feigenson et al.*, 1983; *Frey et al.*, 1994; *Huang and Frey*, 2003]). As shown in Figure 10, abundances of Cs, Rb, K, U and Pb are more variable than abundances of relatively immobile incompatible trace elements.

Sample R6 from Unit 3a with the highest MgO content (12.7 wt%) has very high LOI (5.56%, Table 3), anomalously high K_2O and Rb contents (K_2O, 0.95% vs <0.50% for the other 21 samples; Rb, 21 ppm vs <9 ppm for the other samples; Table 2; Figures 5 and 6); also this sample has anomalously high K_2O/P_2O_5 (4.7), low Ba/Rb and the highest Ce/Pb and Nb/U ratios (Figure 11). At a given Th content Unit

3a has lower Pb and Sr contents than the other 21 samples (Figure 6). Clearly this sample has experienced K and Rb addition and loss of U, Pb and Sr, but it does not show Ba loss or addition (Figure 11). Although they do not have relatively high LOI (loss on ignition, 0.65% and 0.36%, respectively), at a given K_2O/P_2O_5 two other samples, R60 (Unit 13) and R129 (Unit 20b), have high K/Rb and low Ce/Pb indicating the loss of Rb and Pb addition (Figure 11).

In this study, multiple samples were analyzed from pillow Unit 7 (R16 and R30) and Unit 13 (R60, R80 and R93) and the massive Unit 14 (R101, R108 and R112). These samples can be used to evaluate the variability within the thick flows (up to 50 m). Except for ratios involving U, Ba and Pb, within unit variations of incompatible element ratios vary by < 3%, even for ratios involving elements with quite different incompatibilities, such as La/Yb and Nb/Zr (Figure 12). In contrast within Unit 14, Nb/U varies by 20.5%, in Unit 7 Ba/X (X is Rb, Th, Nb or La) ratios vary by 3.4% to 4.7%, and in Unit 13, Ba/X vary by 7% to 21% and Ce/Pb varies by 7% (Figure 12). Such within flow variability of Nb/U, Ba/X and Ce/Pb preclude use of these ratios in constraining magmatic processes. Similarly, Huang et al. (unpublished) found that within four thick (9.3 to 98 m) Phase 2a units, within unit abundance ratios of Nb/U, Ba/X and Ce/Pb vary by 5 to 21% whereas La/Yb and Nb/Zr varied by < 2%.

4.2 Occurrence of low SiO_2 lavas in the Phase 2b core

Low SiO_2 lavas with distinct geochemical compositions, similar to Loihi lavas, are present in the deeper part of the HSDP Phase 2a core [*Eisele et al.*, 2003; *Huang and Frey*, 2003; *Kurz et al.*, 2004; *Rhodes and Vollinger*, 2004; *Stolper et al.*, 2004]. The proportion of low SiO_2 glasses is up to 50% for submarine glasses; however, low SiO_2 glasses are relatively rare in the shallower part of the section [*Stolper et al.*,

2004]. The paucity of the low SiO_2 lavas type in the shallower part of the core may indicate a change in source compositions, melting conditions, or magma plumbing system. It is, therefore, important to determine if the proportion of low SiO_2 lavas increases with depth. Incompatible element ratios can be used to identify low SiO_2 group lavas [*Huang and Frey*, 2003]. For instance, low SiO_2 group lavas define distinctive trends in Nb/Zr vs La/Yb, Sm/Yb and Ti/Zr (Figure 13; see also Figure 10 of Huang and Frey [2003]). Although these ratios are affected by degree of melting and crystal fractionation, Nb/Zr ratios in Hawaiian lavas are correlated with isotopic ratios, and they reflect source characteristics (e.g., Figure 14 of Huang and Frey [2003]). As discussed by Huang and Frey [2003] the horizontal and negative trends of La/Yb and Sm/Yb vs Nb/Zr, respectively (Figure 13), are inconsistent with trends predicted by variable extents of melting. Mixing of distinct components, one being Loihi-like, is inferred.

Among the Phase 2b lavas the sample from Unit 3a is offset to higher Nb/Zr at a given La/Yb or Sm/Yb, plotting within the field defined by low SiO_2 group lavas from HSDP Phase 2a (Figure 13). It also has relatively high Ti/Zr which is a diagnostic signature of the low SiO_2 lavas (Figure 13). Clearly the lava from Unit 3a is a low SiO_2 group lava (see also Figure 5). All the other Phase 2b lavas have lower Nb/Zr and Ti/Zr and are close to or overlap with the ratios of high SiO_2 group Phase 2a lavas (Figure 13); these Phase 2b lavas belong to high SiO_2 group.

It is important to note that Unit 3a is an intrusive unit only about 18 meters below the deepest low SiO_2 group glass (intrusive) in the Phase 2a core. In fact, below 2500 mbsl in the Phase 2a core 26 of 28 intrusive glasses and 2 of the 3 whole-rock intrusives belong to the low SiO_2 group (Figures 4 and 8 of Stolper et al. [2004] and [*Rhodes and Vollinger*, 2004]). These low SiO_2 intrusive lavas were proposed to

represent flank eruptions where magma bypassed the main magma chambers [*Stolper et al.*, 2004]. Seaman et al. [2004] estimated that these intrusive units were emplaced <30 ka after the pillows and hyaloclastites they intruded. We infer that the only low SiO_2 sample (Unit 3a) in the reference suite of Phase 2b samples is a continuation of the low SiO_2 group intrusives that are abundant at ~ 3000 mbsl [*Rhodes and Vollinger*, 2004; *Stolper et al.*, 2004]. It is noteworthy that the low SiO_2 group lavas (whole rock and glass) are not continuously present in the drill core. For example, there is 184 m gap with no low SiO_2 group lavas from 2654 to 2838 mbsl (Figure 8 of Stolper et al. [2004]).

4.3 Origin of low SiO_2 and high SiO_2 group lavas: Evaluation of *Stolper et al.* [2004] hypothesis

Based on major element data, Stolper et al. [2004] proposed that low SiO_2 magma ascended from the plume source and interacted with overlying residual, plume-related peridotite thereby generating high SiO_2 magmas. In contrast, eruption of low SiO_2 magma occurred when low SiO_2 magma escaped such melt-peridotite interaction by ascending through olivine-rich conduits developed by previous melt-peridotite interaction. In this context, the proportion of low SiO_2 lavas should increase with decreasing eruption age. Although this inference is inconsistent with the paucity of low SiO_2 lavas in the upper part of the Phase 2b core, it is consistent with most of the low SiO_2 lavas below 2500 m occurring as intrusives (see Figure 4 of Stolper et al. [2004]).

4.3.1 Constraints from incompatible element ratios: Low and high SiO_2 group lavas define distinctive trends in plots of Nb/Zr vs La/Yb and Sm/Yb and Ti/Zr vs La/Yb (Figure 13); these different trends cannot be explained by differences in degree of melting or crystal fractionation [*Huang and Frey*, 2003]. Can these trends be

explained by low SiO_2 magmas reacting with residual peridotite to form high SiO_2 magmas? According to melt-peridotite reaction equation of Stolper et al. [2004],

$$C^i_{high-SiO_2-magma} = 0.918 \times C^i_{low-SiO_2-magma} + 0.119 \times C^i_{opx} + 0.079 \times C^i_{cpx} - 0.116 \times C^i_{oliv} \quad (1)$$

where C is the concentration of a trace element *i* (such as Nb) in high and low SiO_2 magmas and minerals (cpx, opx and oliv). If minerals in the residual spinel peridotite that reacts with the low SiO_2 magma are in equilibrium with high SiO_2 magma during the melt-peridotite reaction, then the concentrations of trace element *i* in clinopyroxene (cpx), orthopyroxene (opx) and olivine are:

$$C^i_{opx} = D^i_{opx} \times C^i_{high-SiO_2-magma}; \quad (2)$$

$$C^i_{cpx} = D^i_{cpx} \times C^i_{high-SiO_2-magma}; \quad (3)$$

$$C^i_{oliv} = D^i_{oliv} \times C^i_{high-SiO_2-magma}; \quad (4)$$

where D is the partition coefficient between minerals (opx, cpx, and olivine) and melt (high SiO_2 magma).

Substituting equations (2), (3) and (4) into the melt-peridotite reaction equation (1),

$$C^i_{high-SiO_2-magma} = 0.918 \times C^i_{low-SiO_2-magma} + 0.119 \times D^i_{opx} \times C^i_{high-SiO_2-magma} +$$

$$0.079 \times D^i_{cpx} \times C^i_{high-SiO_2-magma} - 0.116 \times D^i_{oliv} \times C^i_{high-SiO_2-magma}$$

leads to,

$$C^i_{high-SiO_2-magma} = 0.918 \times C^i_{low-SiO_2-magma} / (1 - 0.119 \times D^i_{opx} - 0.079 \times D^i_{cpx} + 0.116 \times D^i_{oliv}) \quad (5)$$

Therefore, the trace element concentrations for high SiO_2 magma can be calculated with equation (5) by using the observed low SiO_2 magma compositions and estimates for the partition coefficients. Based on results in Table 4, we conclude that the melt-peridotite reaction model cannot explain the differences in abundance of incompatible elements between the low and high SiO_2 groups. Firstly, the reaction results in an increase of magma mass; therefore abundances of incompatible elements should be

lower in the high SiO_2 magma, but they are observed to be higher (Table 4). Secondly, the ~15% decrease in Nb/Zr and Ti/Zr from the low to high SiO_2 magma cannot be explained by a reaction involving pyroxenes and olivine (Table 4).

4.3.2 Constraint from Pb isotopic ratios: Phase 2a high and low SiO_2 lavas form distinct but intersecting trends in $^{208}Pb/^{204}Pb$-$^{206}Pb/^{204}Pb$ (Figure 14); consequently three isotopically distinct components are required. Clearly Pb isotopic data are inconsistent with mixing of only two components, such as a low SiO_2 magma reacting with residual peridotite.

4.4 Origin of low SiO_2 and high SiO_2 group lavas: Evaluation of *Herzberg* [2006] model

Herzberg [2006] argued that both low and high SiO_2 magmas are too deficient in CaO and enriched in Ni to have formed from a peridotite source and that only a small population of CaO-Al_2O_3 rich glasses [*Stolper et al.*, 2004] were formed by melting of peridotite. Herzberg [2006] proposed that both low and high SiO_2 magmas are melts derived from different pyroxenite. According to this model [*Herzberg*, 2006 and personal communication, 2007], the plume has two major lithologies, peridotite and eclogite which originated as recycled oceanic crust and sediment. Silicic melt generated by low extent of melting of this eclogite at high pressure reacted with peridotite to form the olivine-free secondary pyroxenite [*Sobolev et al.*, 2005]; this secondary pyroxenite melts to produce high SiO_2 magma, whereas low SiO_2 magma are mixing of melts derived from peridotite and an olivine-bearing reaction zone formed at the eclogite-peridotite interface at shallow pressure (Figure 15).

The positive Sm/Yb vs Nb/Zr trend defined by high SiO_2 lavas is consistent with residual garnet in the source (Figure 13). The negative trend of Sm/Yb vs Nb/Zr for low SiO_2 lavas (Figure 13) and strong correlations of Sm/Yb and Nb/Zr vs Pb

isotopic ratios (Figure 11 of Huang and Frey [*Huang and Frey*, 2003]) are consistent with low SiO_2 lavas formed by mixing of melts derived from two end-members (such as peridotite and pyroxenite).

In the Herzberg model ([2006] and personal communication, 2007) high SiO_2 magma is formed from secondary pyroxenite with no residual olivine, but in contrast residual olivine is present during the formation of low SiO_2 magma. Since Ni is highly compatible in olivine, this model predicts lower Ni content in low SiO_2 magma. In contrast, the Stolper et al. [2004] model predicts lower Ni content in high SiO_2 lavas. At a given MgO content both low and high SiO_2 whole-rocks have similar Ni contents (Figure 16), but the MgO content (17.42%, Stolper et al. [2004]) calculated for the primary magma of low SiO_2 lavas is higher than that calculated for the high SiO_2 magma (15.95%, Stolper et al. [2004]). That is, the low SiO_2 primary magma has higher Ni contents than that of high SiO_2 primary, which is consistent with the model of Stolper et al. [2004].

5. Conclusions

The chemical compositions (major and trace element abundances) of the 22 reference suite samples for the Phase 2b HSDP drill core are similar to the shield lavas in the overlying Phase 2a lavas. Most notable is that an intrusive unit in the Phase 2b core belongs to the distinctive low SiO_2 group of shield tholeiitic basalt that is abundant at depths of 2233-2481 m in the Phase 2a core.

A hypothesis for the occurrence of the low and high SiO_2 groups is that the high SiO_2 magmas formed by reaction of ascending, plume-derived, low SiO_2 magma with an overlying plume-related, peridotite residual from earlier partial melting [*Stolper et al.*, 2004]. While a melt (low SiO_2 magma)-peridotite reaction can explain

the major element differences between the low- and high-SiO_2 groups, we find that this model cannot explain the between group differences in Nb/Zr and Ti/Zr. In addition in a $^{208}Pb/^{204}Pb$ vs. $^{206}Pb/^{204}Pb$ plot, different trends are defined by the two magma groups; therefore at least three isotopically distinct components are required. Low and high SiO_2 whole rocks overlap in Ni-MgO plot, but calculated low SiO_2 primary magma has higher MgO content (17.42 wt%) than that of the high SiO_2 primary magma (15.95 wt%) [*Stolper et al.*, 2004]. Therefore high SiO_2 primary magma has lower Ni contents than that of low SiO_2 primary magma, consistent with Stolper et al. [2004] model.

Herzberg ([2006] and personal communication, 2007) proposed an alternative hypothesis for the low and high SiO_2 groups. According to this model, high SiO_2 magma was derived from the secondary pyroxenite as proposed by Sobolev et al. [2005] whereas the low SiO_2 magma are mixture of melts derived from peridotite and pyroxenite endmembers. This model predicts that higher Ni contents in high SiO_2 primary magma, which is inconsistent with whole rock Ni data (Figure 16). However, the Herzberg model does explain the mixing trend by the low SiO_2 lavas, i.e., mixing between a peridotite-derived, Loihi-like, partial melt with a high SiO_2 magma derived from secondary pyroxenite (Figures 13 and 14).

Acknowledgement

I thank R. Kayser and F. Dudas for their assistance in ICP-MS analysis and clean lab, respectively. J.M Rhodes and M. Vollinger are thanked for sharing their unpublished major and trace elements XRF data and the discussions. C. Herzberg is thanked for numerous discussions of his model.

References

Abouchami, W., S. J. G. Galer, and A. W. Hofmann (2000), High precision lead isotope systematics of lavas from the Hawaiian Scientific Drilling Project, *Chem. Geol.*, *169*, 187-209.

Abouchami, W., A. W. Hofmann, S. J. G. Galer, F. A. Frey, J. Eisele, and M. Feigenson (2005), Lead isotopes reveal bilateral asymmetry and vertical continuity in the Hawaiian mantle plume, *Nature*, *434*, 851-856.

Blichert-Toft, J., and F. Albarède (1999), Hf isotopic compositions of the Hawaii Scientific Drilling Project core and the source mineralogy of Hawaiian basalts, *Geophy. Res. Lett.*, *26*, 935-938.

Blichert-Toft, J., D. Weis, C. Maerschalk, A. Agranier, and F. Albarède (2003), Hawaiian hot spot dynamics as inferred from the Hf and Pb isotope evolution of Mauna Kea volcano, *Geochem. Geophy. Geosyst.*, *4*, doi:10.1029/2002GC000340.

Bryce, J. G., D. J. DePaolo, and J. C. Lassiter (2005), Geochemical structure of the Hawaiian plume: Sr, Nd, and Os isotopes in the 2.8 km HSDP-2 section of Mauna Kea volcano, *Geochem. Geophy. Geosyst.*, *6*, doi:10.1029/2004GC000809.

Chen, C. Y., and F. A. Frey (1985), Trace-Element and Isotopic Geochemistry of Lavas from Haleakala Volcano, East Maui, Hawaii - Implications for the Origin of Hawaiian Basalts, *Journal of Geophysical Research-Solid Earth and Planets*, *90*, 8743-8768.

Clague, D. A., and G. B. Dalrymple (1987), The Hawaiian-Emperor volcanic chain: Part I: Geologic evolution, *U.S. Geol. Sury. Prof. Pap.*, *1350*, 5-54.

Eisele, J., W. Abouchami, S. J. G. Galer, and A. W. Hofmann (2003), The 320 kyr Pb isotope evolution of Mauna Kea lavas recorded in the HSDP-2 drill core, *Geochem. Geophy. Geosyst.*, *4*, doi:10.1029/2002GC000339.

Feigenson, M. D., A. W. Hofmann, and F. J. Spera (1983), Case studies on the origin of basalt II, The transition from tholeiitic to alkalic volcanism on Kohala Volcano, Hawaii, *Contrib. Mineral. Petrol.*, *V84*, 390-405.

Frey, F. A., M. O. Garcia, and M. F. Roden (1994), Geochemical Characteristics of Koolau Volcano - Implications of Intershield Geochemical Differences among Hawaiian Volcanos, *Geochim. Cosmochim. Acta*, *58*, 1441-1462.

Garcia, M. O., K. H. Rubin, M. D. Norman, J. M. Rhodes, D. W. Graham, D. W. Muenow, and K. Spencer (1998), Petrology and geochronology of basalt breccia from the 1996 earthquake swarm of Loihi seamount, Hawaii: magmatic history of its 1996 eruption, *Bull. Volcano.*, *59*, 577-592.

Herzberg, C. (2006), Petrology and thermal structure of the Hawaiian plume from Mauna Kea volcano, *Nature*, *444*, 605-609.

Hofmann, A. W., and K. P. Jochum (1996), Source characteristics derived from very incompatible trace elements in Mauna Loa and Mauna Kea basalts, Hawaii Scientific Drilling Project, *J. Geophy. Res.*, *101*, 11831-11839.

Huang, S., and F. A. Frey (2003), Trace element abundances of Mauna Kea basalt from phase 2 of the Hawaii Scientific Drilling Project: Petrogenetic implications of correlations with major element content and isotopic ratios, *Geochem. Geophy. Geosyst.*, *4*, doi:10.1029/2002GC000322.

Huang, S., M. Regelous, T. Thordarson, and F. A. Frey (2005a), Petrogenesis of lavas from Detroit Seamount: Geochemical differences between Emperor Chain and Hawaiian volcanoes, *Geochem. Geophy. Geosyst.*, *6*, doi:10.1029/2004GC000756.

Huang, S. C., F. A. Frey, J. Blichert-Toft, R. V. Fodor, G. R. Bauer, and G. P. Xu (2005b), Enriched components in the Hawaiian plume: Evidence from Kahoolawe Volcano, Hawaii, *Geochem. Geophy. Geosyst.*, *6*, doi:10.1029/2005GC001012.

Kent, A. J. R., D. A. Clague, M. Honda, E. M. Stolper, I. D. Hutcheon, and M. D. Norman (1999), Widespread assimilation of a seawater-derived component at Loihi Seamount, Hawaii, *Geochim. Cosmochim. Acta*, *63*, 2749-2761.

Kurz, M. D., J. Curtice, D. E. Lott, and A. Solow (2004), Rapid helium isotopic variability in Mauna Kea shield lavas from the Hawaiian Scientific Drilling Project, *Geochem. Geophy. Geosyst.*, *5*, doi:10.1029/2002GC000439.

Lassiter, J. C., D. J. DePaolo, and M. Tatsumoto (1996), Isotopic evolution of Mauna Kea volcano: Results from the initial phase of the Hawaii Scientific Drilling Project, *J. Geophy. Res.*, *101*, 11769-11780.

Norman, M. D., and M. O. Garcia (1999), Primitive magmas and source characteristics of the Hawaiian plume: petrology and geochemistry of shield picrites, *Earth Planet. Sci. Lett.*, *168*, 27-44.

Rhodes, J. M., and M. J. Vollinger (2004), Composition of basaltic lavas sampled by phase-2 of the Hawaii Scientific Drilling Project: Geochemical stratigraphy and magma types, *Geochem. Geophy. Geosyst.*, *5*, doi:10.1029/2002GC000434.

Seaman, C., M. Garcia, and E. Stolper (2000), Core logs and summarizing data, California Institute of Technology, Pasadena.

Seaman, C., S. B. Sherman, M. O. Garcia, M. B. Baker, B. Balta, and E. Stolper (2004), Volatiles in glasses from the HSDP2 drill core, *Geochem. Geophy. Geosyst.*, *5*, doi:10.1029/2003GC000596.

Sharp, W. D., and P. R. Renne (2005), The Ar-40/Ar-39 dating of core recovered by the Hawaii Scientific Drilling Project (phase 2), Hilo, Hawaii, *Geochem. Geophy. Geosyst.*, *6*, doi:10.1029/2004GC000846.

Sharp, W. D., B. D. Turrin, P. R. Renne, and M. A. Lanphere (1996), The Ar-40/Ar-39 and K/Ar dating of lavas from the Hilo 1-km core hole, Hawaii scientific drilling project, *J. Geophy. Res.*, *101*, 11607-11616.

Sobolev, A. V., A. W. Hofmann, S. V. Sobolev, and I. K. Nikogosian (2005), An olivine-free mantle source of Hawaiian shield basalts, *Nature*, *434*, 590-597.

Stolper, E., S. Sherman, M. Garcia, M. Baker, and C. Seaman (2004), Glass in the submarine section of the HSDP2 drill core, Hilo, Hawaii, *Geochem. Geophy. Geosyst.*, *5*, doi:10.1029/2003GC000553.

Stolper, E. M., D. J. DePaolo, and D. M. Thomas (1996), Introduction to special section: Hawaii scientific drilling project, *J. Geophy. Res.*, *101*, 11593-11598.

Sun, S.-S., and W. F. McDonough (1989), Chemical and isotopic systematics of oceanic basalts: implications for mantle composition and processes. In: Saunders, A.D., Norry, M.J. (eds.). Magmatism in the Ocean Basins, *Geological Society Special Publication*, *42*, 313-345.

Valbracht, P. J., H. Staudigel, M. Honda, I. McDougall, and G. R. Davies (1996), Isotopic tracing of volcanic source regions from Hawaii: Decoupling of gaseous from lithophile magma components, *Earth Planet. Sci. Lett.*, *144*, 185-198.

Yang, H. J., F. A. Frey, and D. A. Clague (2003), Constraints on the Source Components of Lavas Forming the Hawaiian North Arch and Honolulu Volcanics, *J. Petrol.*, *44*, 603-627.

Yang, H. J., F. A. Frey, J. M. Rhodes, and M. O. Garcia (1996), Evolution of Mauna Kea volcano: Inferences from lava compositions recovered in the Hawaii Scientific Drilling Project, *J. Geophy. Res.*, *101*, 11747-11767.

Figure caption

Figure 1 Cross section of a Hawaiian volcano showing four growth stages (Modified from Clague [1987]).

Figure 2 Map of Hawaii showing the location of the HSDP2 drill core on the southeast flank of Mauna Kea which is covered by a thin veneer (245 m) of Mauna Loa lavas. Also shown are the principal rift zones of each volcano (black lines) and Loihi seamount. The two colored lines extending southeast from the summits of Mauna Loa and Mauna Kea show the approximate plate motion trajectory of the summits for the last few hundred thousand years, assuming a plate velocity of 10 cm/yr. Mauna Kea was close to the present coastline just southeast of Kilauea at 620 Ka before present (the age of the base of the HSDP Phase 2a core). The inset shows the location of Mauna Kea and the two parallel chains of volcanoes, referred to as Loa and Kea trends that make up the Hawaiian Islands, dashed lines are fracture zones in the oceanic lithosphere. Figure is from Kurz et al. [2004].

Figure 3 Lithologic column of the HSDP Phase 2a and 2b core holes showing different lithology units (from **http://www.icdp-online.de**). No core was recovered from rotary drilled intervals.

Figure 4 Covariations of $^{3}He/^{4}He$ ratios with radiogenic $^{208}Pb^{*}/^{206}Pb^{*}$ (defined as $(^{208}Pb/^{204}Pb - 29.475) / (^{206}Pb/^{204}Pb - 9.307)$) ratios in lavas from the HSDP Phase 2a core. Loihi field is shown for comparison. Data sources: Eisele et al. [2003] and Kurz et al. [2004] for HSDP Phase 2a lavas; Bennett et al. (1996), Valbracht et al. [1996], Kent et al. [1999] and Norman and Garcia [1999] for Loihi field.

Figure 5 Contents of MgO vs SiO_2, CaO, Al_2O_3, $Fe_2O_3^{*}$, TiO_2, Na_2O, K_2O and P_2O_5 for HSDP Phase 2a and 2b lavas. The postshield lavas from Phase 2a are not plotted in this figure and subsequent figures since these lavas represent the transition from shield to postshield as Mauna Kea moved away from the hotspot. We use Huang and Frey [2003] grouping for postshield, high and low SiO_2 lavas. Note that among Phase 2b samples only Unit 3a overlaps with the low SiO_2 group in Phase 2a. Data from Rhodes and Vollinger ([2004], and 2006 unpublished).

Figure 6 Abundance of Th versus Rb, Pb, Ba, U, Sr, Nb, Zr and Hf (all in ppm). The error bars shown are ±3%.

Figure 7 Primitive mantle normalized incompatible element abundances for samples from Phase 2b core. PM stands for primitive mantle [*Sun and McDonough*, 1989].

Figure 8 Ba/Nb vs Ba/La and Ba/Th for HSDP Phase 2b lavas. Multiple samples were analyzed from Unit 7, 13 and 14. The error bars shown are ±3%.

Figure 9 Variation of Nb/Zr, La/Yb, La/Nb, Sr/Nb, Ba/Th with depth for HSDP Phase 2a and 2b lavas. The error bars are ±3%.

Figure 10 Trace element abundance variations for Phase 2b lavas. Unit 3a which is a low SiO_2 lava and Unit 20b with the highest MgO content are not included. Abundance range is the maximum abundance divided by minimum abundance.

Figure 11 K_2O/P_2O_5 vs K/Rb, Ce/Pb, Ba/Th, Ba/Rb and Nb/U. Sample R6 from Unit 3a has very high K_2O/P_2O_5, Ce/Pb and Nb/U ratios. The error bars are ±3%.

Figure 12 Variability of trace element ratios for high SiO_2 lavas from the Phase 2b and comparisons of variability of multiple samples from Units 7, 13, and 14 relative to variability for all samples. Variability is calculated using the mean and 1 sigma standard deviation, specifically, one sigma standard deviation/mean.

Figure 13 Nb/Zr vs Sm/Yb and La/Yb and Ti/Zr vs La/Yb for HSDP Phase 2b lavas. For comparison low SiO_2 (triangle) and high SiO_2 (field) lavas from Phase 2a and Loihi glass (field) are also shown. Since La/Yb and Sm/Yb are sensitive to degree of melting, only tholeiitic glass data are included in the Loihi glass field. The large squares are estimated primary magma compositions for low SiO_2 (blue) and high SiO_2 (pink) lavas (See Table 4 for details). The error bars shown are ±3%. Data sources: Loihi glass – Garcia et al. [1998]; Mauna Kea HSDP Phase 2a – Huang and Frey [2003] and Phase 2b – this study and Rhodes and Vollinger [*2006, unpublished data*].

Figure 14 $^{208}Pb/^{204}Pb$-$^{206}Pb/^{204}Pb$ for HSDP Phase 2a lavas. The dashed line is the regression line for high SiO_2 lavas. Low SiO_2 lavas are offset from the trend defined by high SiO_2 lavas and they trend toward the field for Loihi lavas; overall 3 components with distinct Pb isotopic ratios are required to explain Mauna Kea shield lavas. The 2σ uncertainty is less than the size of the symbols. Data from Eisele et al. [2003] and Abouchami et al. [2005].

Figure 15 Processes proposed to explain three magma groups in the Mauna Shield ([*Herzberg*, 2006] and personal communication, 2007). High Ca-K_2O group is derived by partial melting of peridotite; high SiO2 group is derived by partial melting of secondary pyroxenite and low SiO2 group is derived by partial melt of a different secondary pyroxenite and mixed with partial melt derived from peridotite.

Figure 16 MgO vs Ni for HSDP Phase 2a lavas. Ni contents for low and high SiO_2 primary magmas are calculated using the regression equations and MgO contents for primary magmas from Stolper et al. [2004]. Data from Rhodes and Vollinger [2004].

Table 1 HSDP Phase 2b reference suite: sample list

Unit	Sample	rock type	
2a	R6 0.85-1.2*	pillow	moderately olivine phyric
3a	R6 2.15-3.0	intrusive	aphyric
2b	R8 0.5-0.7	pillow	moderately olivine phyric
2d	R10 4.35-4.7	pillow	aphyric
4	R11 5.3-5.7	pillow breccia	moderately olivine phyric
5	R13 0.1-0.5	pillow	moderately olivine phyric
7	R16 5.2-6.0	pillow	moderately olivine phyric
7	R30 4.24-5.2	pillow	moderately olivine phyric
9	R51 2.4-3.6	pillow	moderately olivine phyric
10	R56 1.0-1.5	pillow breccia	moderately olivine phyric
11	R57 5.0-5.9	pillow	moderately olivine phyric
13	R60 7.6-8.4	pillow	moderately olivine phyric
13	R80 2.8-3.5	pillow	moderately olivine phyric
13	R93 1.4-2.0	pillow	moderately olivine phyric
14	R101 4.4-4.9	massive	moderately olivine phyric
14	R108 0.0-0.7	massive	moderately olivine phyric
14	R112 7.1-7.7	massive	moderately olivine phyric
15	R116 6.25-7.2	pillow	moderately olivine phyric
17	R122 1.85-2.65	pillow	moderately olivine phyric
18a	R125 4.9-5.3	intrusive	moderately olivine phyric
19b	R127 1.4-2.2	pillow	aphyric to sparsely phyric
20b	R129 5.8-6.5	intrusive	highly olivine phyric

Moderately olivine phyric: 3-5% olivine; highly olivine phyric: >15% olivine

* indicates the depth interval (ft) in an unit where sample was collected, for example, the Unit 2a sample was taken from the 0.85 to 1.2 (feet) interval, meausred from the top of the unit, in this unit.

Table 2 Trace element abundance in reference suite of HSDP Phase 2b samples (ppm)

Sample	mbsl	unit	Rb	Cs	Ba	Th	U	Nb	Ta	Be	La	Ce	Pb	Pr	Nd	Sr	Sm	Zr	Hf
R6 (0.85-1.2)	3111	2a	7.91	0.054	116	0.978	0.334	14.7	1.09	0.70	12.4	31.7	0.945	4.63	21.9	308	5.82	158	4.14
R6 (2.15-3.0)	3113	3a	20.1	0.053	84	0.685	0.219	11.5	0.79	0.60	9.1	23.2	0.536	3.42	16.2	201	4.34	115	3.05
R8 (0.5-0.7)	3115	2b	6.26	0.091	117	0.963	0.367	14.0	0.97	0.73	11.7	29.8	0.914	4.38	20.8	305	5.59	154	4.05
R10 (4.35-4.7)	3122	2d	6.93	0.075	101	0.994	0.329	14.9	1.08	0.89	12.3	31.2	0.923	4.59	21.5	313	5.75	164	4.20
R11 (5.3-5.7)	3125	4	6.94	0.072	99	0.987	0.333	15.2	1.12	0.88	12.3	31.3	0.890	4.56	21.5	321	5.79	167	4.19
R13 (0.1-0.5)	3128	5	6.54	0.080	107	0.962	0.324	14.6	1.02	0.82	12.1	30.5	0.872	4.52	21.3	310	5.63	160	4.06
R16 (5.2-6.0)	3134	7	6.54	0.084	115	0.963	0.322	14.6	1.02	0.82	12.0	30.6	0.914	4.49	21.1	313	5.69	160	4.10
R30 (4.25-5.2)	3152	7	6.48	0.090	107	0.948	0.319	14.3	0.97	0.84	11.9	29.9	0.860	4.43	20.9	307	5.57	158	4.03
R51 (2.4-3.6)	3172	9	8.07	0.109	117	0.969	0.357	14.7	1.04	0.84	12.1	30.8	0.864	4.54	21.3	314	5.64	161	4.10
R56 (1.0-1.5)	3183	10	6.33	0.080	96	0.966	0.324	14.4	1.04	0.86	11.8	30.0	0.905	4.40	21.0	307	5.59	158	4.10
R57 (5-5.9)	3185	11	6.06	0.084	99	0.930	0.307	13.8	1.01	0.70	11.5	29.2	0.864	4.33	20.4	294	5.54	152	3.95
R60 (7.6-8.4)	3191	13	5.16	0.072	133	0.946	0.314	13.7	0.99	0.69	11.8	29.6	1.034	4.37	20.8	299	5.57	151	4.01
R80 (2.8-3.5)	3226	13	6.31	0.095	110	0.906	0.299	13.6	0.93	0.77	11.4	28.8	0.888	4.28	20.1	305	5.41	151	3.89
R93 (1.4-2.0)	3245	13	6.41	0.090	122	0.915	0.309	13.7	0.94	0.78	11.3	28.7	0.891	4.27	20.1	303	5.39	151	3.96
R101 (4.4-4.9)	3255	14	6.63	0.046	112	0.896	0.318	13.8	0.95	0.80	11.2	28.5	0.877	4.26	20.0	307	5.37	152	3.87
R108 (0-0.7)	3275	14	8.12	0.071	125	1.013	0.334	15.3	1.02	0.94	12.4	31.6	0.971	4.70	22.1	321	5.83	169	4.25
R112 (7.7-7.7)	3282	14	6.42	0.054	106	0.882	0.432	13.2	0.93	0.76	11.0	28.2	0.822	4.19	19.7	299	5.33	147	3.80
R116 (6.25-7.2)	3296	15	6.53	0.086	102	0.880	0.297	13.6	0.92	0.80	11.2	28.4	0.857	4.19	19.7	312	5.36	151	3.83
R122 (1.85-2.65)	3312	17	8.54	0.118	123	1.035	0.376	15.8	1.07	0.83	13.1	33.2	0.911	4.94	22.9	324	6.09	173	4.40
R125 (4.9-5.3)	3316	18a	8.59	0.118	103	0.945	0.315	14.5	1.03	0.83	11.8	30.1	0.877	4.46	21.0	309	5.57	159	4.06
R127 (1.4-2.2)	3321	19b	8.36	0.114	105	0.949	0.329	15.0	1.01	0.82	12.1	30.9	0.854	4.53	21.2	332	5.59	157	3.95
R129 (5.8-6.5)	3324	20b	4.12	0.039	83	0.652	0.218	10.4	0.74	0.68	8.8	23.1	0.784	3.51	16.7	267	4.69	131	3.28
BHVO-2			9.50	0.099	134	1.276	0.435	18.6	1.20	1.06	15.2	37.9	1.530	5.45	24.9	389	6.19	173	4.47
RSD (%, n=3)			3.47	1.95	1.45	1.02	1.50	2.05	1.09	13.19	0.82	1.06	0.89	1.46	1.00	2.42	0.96	2.04	1.59

mbsl indicates meter below sea level.

RSD is defined as 1σ divided by the mean

Data were analyzed by ICP-MS at MIT

Element order is determined by incompatibility during melting of a peridotite source with compatibility increases from Rb to Cr.

Eu	Tb	Gd	Dy	Ho	Y	Er	Tm	Li	Yb	Lu	Sc	Cr
1.94	1.00	6.25	5.66	1.10	29.7	2.78	0.40	3.94	2.24	0.32	29.5	319
1.46	0.76	4.64	4.30	0.84	22.4	2.13	0.30	3.90	1.73	0.24	26.6	543
1.87	0.96	5.98	5.42	1.06	28.8	2.69	0.38	4.55	2.17	0.31	30.1	353
1.94	1.00	6.16	5.60	1.11	30.6	2.77	0.39	5.19	2.26	0.32	32.9	348
1.96	0.99	6.24	5.65	1.11	31.3	2.79	0.39	5.04	2.24	0.32	33.2	367
1.92	0.99	6.02	5.59	1.06	30.2	2.71	0.39	4.49	2.20	0.32	31.4	351
1.95	0.97	5.97	5.58	1.08	30.0	2.69	0.39	4.59	2.20	0.31	31.4	363
1.92	0.96	5.92	5.51	1.06	29.6	2.68	0.39	4.57	2.17	0.31	31.7	349
1.94	0.99	6.07	5.64	1.08	30.1	2.74	0.40	3.95	2.24	0.32	31.9	365
1.90	0.97	5.94	5.50	1.06	29.5	2.67	0.40	4.84	2.20	0.32	31.7	358
1.84	0.94	5.80	5.35	1.02	28.2	2.58	0.38	4.01	2.13	0.30	28.2	319
1.88	0.95	5.89	5.41	1.04	28.1	2.67	0.40	3.72	2.18	0.31	27.9	320
1.84	0.94	5.78	5.32	1.03	28.5	2.61	0.38	4.25	2.16	0.31	30.8	352
1.83	0.94	5.79	5.34	1.02	28.6	2.64	0.38	4.31	2.10	0.31	31.0	346
1.84	0.93	5.69	5.30	1.03	28.8	2.63	0.38	4.69	2.09	0.31	32.4	353
1.97	1.01	6.33	5.79	1.11	31.4	2.81	0.40	5.73	2.30	0.34	33.3	334
1.81	0.92	5.60	5.25	1.03	28.2	2.60	0.37	5.03	2.09	0.30	31.9	356
1.83	0.93	5.72	5.27	1.02	28.9	2.60	0.37	4.42	2.10	0.29	32.8	382
2.07	1.04	6.45	5.91	1.16	31.9	2.93	0.41	3.63	2.33	0.33	30.4	275
1.90	0.96	5.95	5.54	1.08	29.9	2.69	0.39	4.30	2.18	0.31	31.7	355
1.87	0.93	5.82	5.28	1.03	28.8	2.63	0.37	4.09	2.06	0.30	31.8	218
1.59	0.82	4.99	4.63	0.91	25.7	2.34	0.34	4.36	1.86	0.26	30.5	699
2.04	0.96	6.22	5.34	1.02	27.8	2.55	0.35	4.36	2.03	0.28	31.9	282
0.50	0.77	1.60	1.06	0.33	2.81	0.77	4.48	8.90	1.45	0.76	3.70	1.74

Table 3 Major element contents in reference suite of HSDP Phase 2b samples (wt%)

Sample	Unit	SiO_2	TiO_2	Al_2O_3	Fe_2O_3*	MnO	MgO	CaO	Na_2O	K_2O	P_2O_5	TOTAL	LOI
R6 (0.85-1.2)	2a	50.31	2.58	13.15	12.37	0.17	7.75	10.62	2.39	0.48	0.25	100.07	0.75
R6 (2.15-3.0)	3a	47.31	2.32	11.98	13.02	0.17	12.67	9.59	1.91	0.95	0.20	100.12	5.65
R8 (0.5-0.7)	2b	50.35	2.50	13.17	12.34	0.17	7.96	10.67	2.33	0.31	0.24	100.04	0.91
R10 (4.35-4.7)	2d	50.37	2.60	13.15	12.45	0.18	7.71	10.76	2.37	0.39	0.25	100.23	0.72
R11 (5.3-5.7)	4	50.37	2.59	13.15	12.46	0.18	7.72	10.76	2.35	0.37	0.25	100.20	0.86
R13 (0.1-0.5)	5	50.24	2.55	13.13	12.42	0.17	7.77	10.63	2.49	0.33	0.25	99.99	0.70
R16 (5.2-6.0)	7	50.27	2.54	13.12	12.52	0.17	8.01	10.60	2.35	0.31	0.25	100.14	0.92
R30 (4.25-5.2)	7	50.26	2.52	12.92	12.48	0.18	8.16	10.58	2.40	0.30	0.24	100.04	1.10
R51 (2.4-3.6)	9	50.39	2.53	12.90	12.60	0.18	8.03	10.60	2.46	0.36	0.25	100.30	0.80
R56 (1.0-1.5)	10	50.24	2.56	13.04	12.54	0.18	7.86	10.71	2.27	0.34	0.25	99.99	0.86
R57 (5-5.9)	11	50.20	2.54	13.13	12.53	0.17	7.91	10.65	2.28	0.33	0.25	99.99	1.04
R60 (7.6-8.4)	13	50.42	2.55	12.77	12.70	0.18	8.14	10.65	2.28	0.37	0.24	100.30	0.65
R80 (2.8-3.5)	13	50.32	2.48	13.04	12.51	0.17	8.00	10.74	2.35	0.32	0.23	100.16	0.70
R93 (1.4-2.0)	13	50.06	2.48	12.96	12.48	0.17	7.97	10.70	2.35	0.33	0.24	99.73	0.75
R101 (4.4-4.9)	14	50.27	2.42	13.07	12.34	0.16	8.10	10.63	2.28	0.40	0.23	99.90	0.60
R108 (0-0.7)	14	50.65	2.63	13.07	12.64	0.18	7.42	10.54	2.41	0.46	0.26	100.25	0.34
R112 (7.7-7.7)	14	50.23	2.41	12.90	12.50	0.18	7.91	10.81	2.35	0.41	0.23	99.93	0.45
R116 (6.25-7.2)	15	50.40	2.42	13.06	12.37	0.18	8.11	10.87	2.40	0.28	0.23	100.31	0.79
R122 (1.85-2.65)	17	50.76	2.74	13.67	12.38	0.17	6.60	10.68	2.65	0.34	0.27	100.24	0.61
R125 (4.9-5.3)	18a	50.39	2.54	12.99	12.56	0.18	7.90	10.63	2.49	0.33	0.24	100.25	0.90
R127 (1.4-2.2)	19b	50.41	2.59	13.74	12.25	0.17	6.94	10.99	2.42	0.31	0.24	100.07	1.14
R129 (5.8-6.5)	20b	49.75	2.13	11.93	11.81	0.17	11.74	9.91	2.19	0.30	0.20	100.13	0.36

Data from Rhodes and Vollinger [2006, unpublished]

Table 4 Comparsion of observed incompatible elements abudnace in high SiO_2 magma with those predicted by melt-peridotite reaction (equation 1 in text)

	Low SiO_2 magma (ppm)	High SiO_2 magma (ppm)		measured high SiO_2 / measured low SiO_2	calculated high SiO_2 / measured low SiO_2
	measured[a]	measured[a]	calculated[b]		
La	8.0	8.5	7.37	1.06	0.92
Nb	10.0	10.4	9.21	1.04	0.92
Zr	100	125	93	1.25	0.93
Sm	3.7	4.2	3.49	1.14	0.94
Yb	1.55	1.70	1.49	1.10	0.96
Ti	11088	11987	10637	1.08	0.96
Nb/Zr	0.10	0.083	0.10	0.83	0.99
Sm/Yb	2.39	2.47	2.34	1.03	0.98
La/Yb	5.16	5.00	4.94	0.97	0.96
Ti/Zr	111	96	115	0.86	1.03

[a] The observed low and high SiO_2 magma compositions were estimated using MgO-X correlations and extrapolating to MgO=17.4% and 16%, respectively; these MgO contents are from Table 3 of Stolper et al. [2004] and were calculated by adjusting via olivine addition the mean glass compositions for low- and high SiO_2 magmas to be in equilibrium with olivine of $Fo_{90.5}$.

[b] The high SiO_2 magma compositions were calculated using equation (5); partition coefficents between clinopyroxene, orthopyroxene and olivine and high SiO_2 magma are the spinel peridotite data set in Table A4 of Huang and Frey [2003]

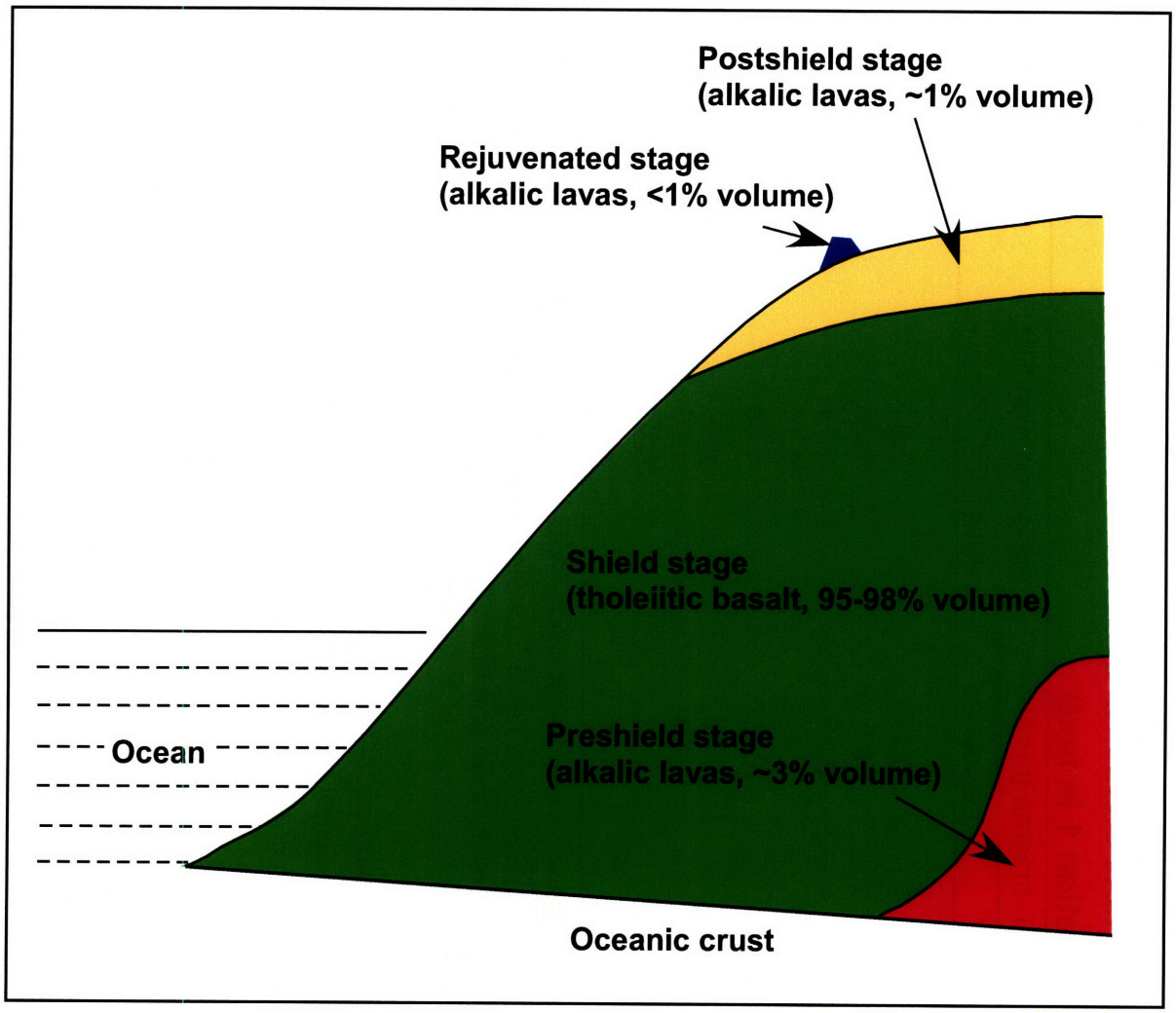
Postshield stage
(alkalic lavas, ~1% volume)
Rejuvenated stage
(alkalic lavas, <1% volume)
Shield stage
(tholeiitic basalt, 95-98% volume)
Ocean
Preshield stage
(alkalic lavas, ~3% volume)
Oceanic crust

Fig. 1

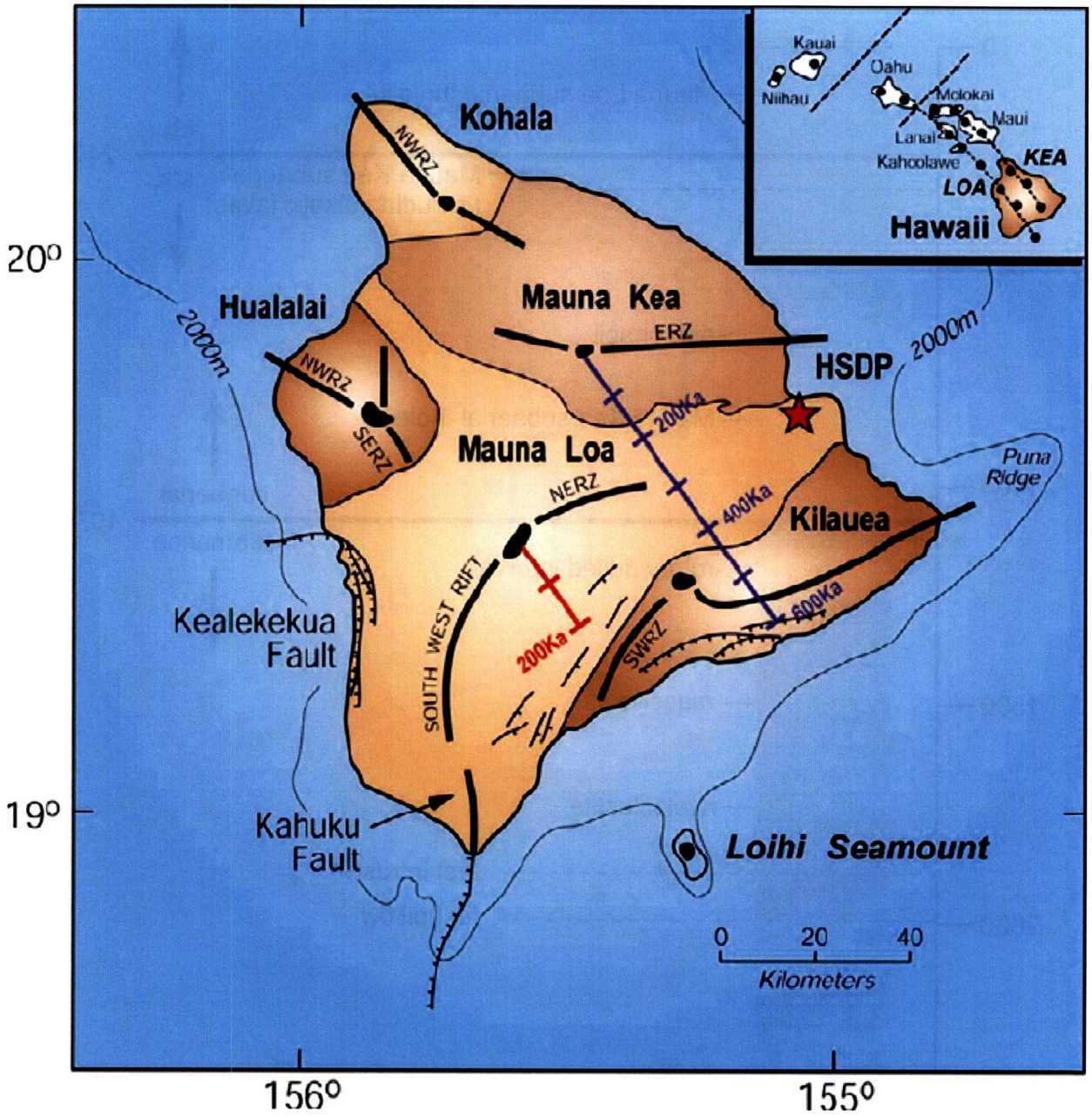
Kauai
Oahu
Niihau
Molokai
Maui
Lanai
Kahoolawe
KEA
LOA
Hawaii
Kohala
NWRZ
Hualalai
NWRZ
SERZ
Mauna Kea
ERZ
HSDP
2000m
2000m
200Ka
Mauna Loa
NERZ
400Ka
Kilauea
Puna Ridge
SOUTH WEST RIFT
200Ka
600Ka
SWRZ
Kealekekua Fault
Kahuku Fault
Loihi Seamount
0 20 40
Kilometers
20°
19°
156°
155°

Fig. 2

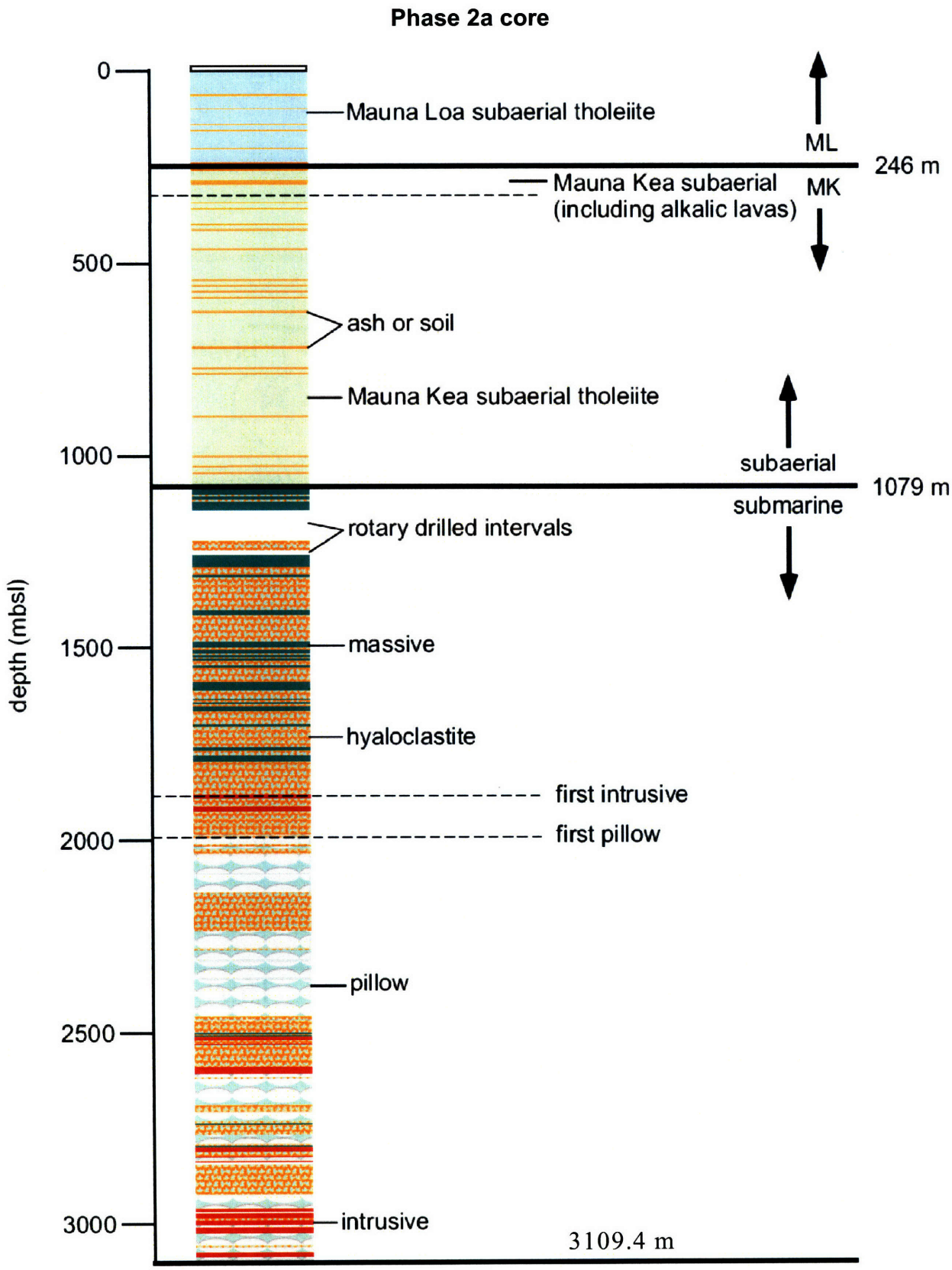
Phase 2a core
0
500
1000
1500
2000
2500
3000
depth (mbsl)
Mauna Loa subaerial tholeiite
ML
246 m
Mauna Kea subaerial
(including alkalic lavas)
MK
ash or soil
Mauna Kea subaerial tholeiite
subaerial
1079 m
submarine
rotary drilled intervals
massive
hyaloclastite
first intrusive
first pillow
pillow
intrusive
3109.4 m

Fig. 3a

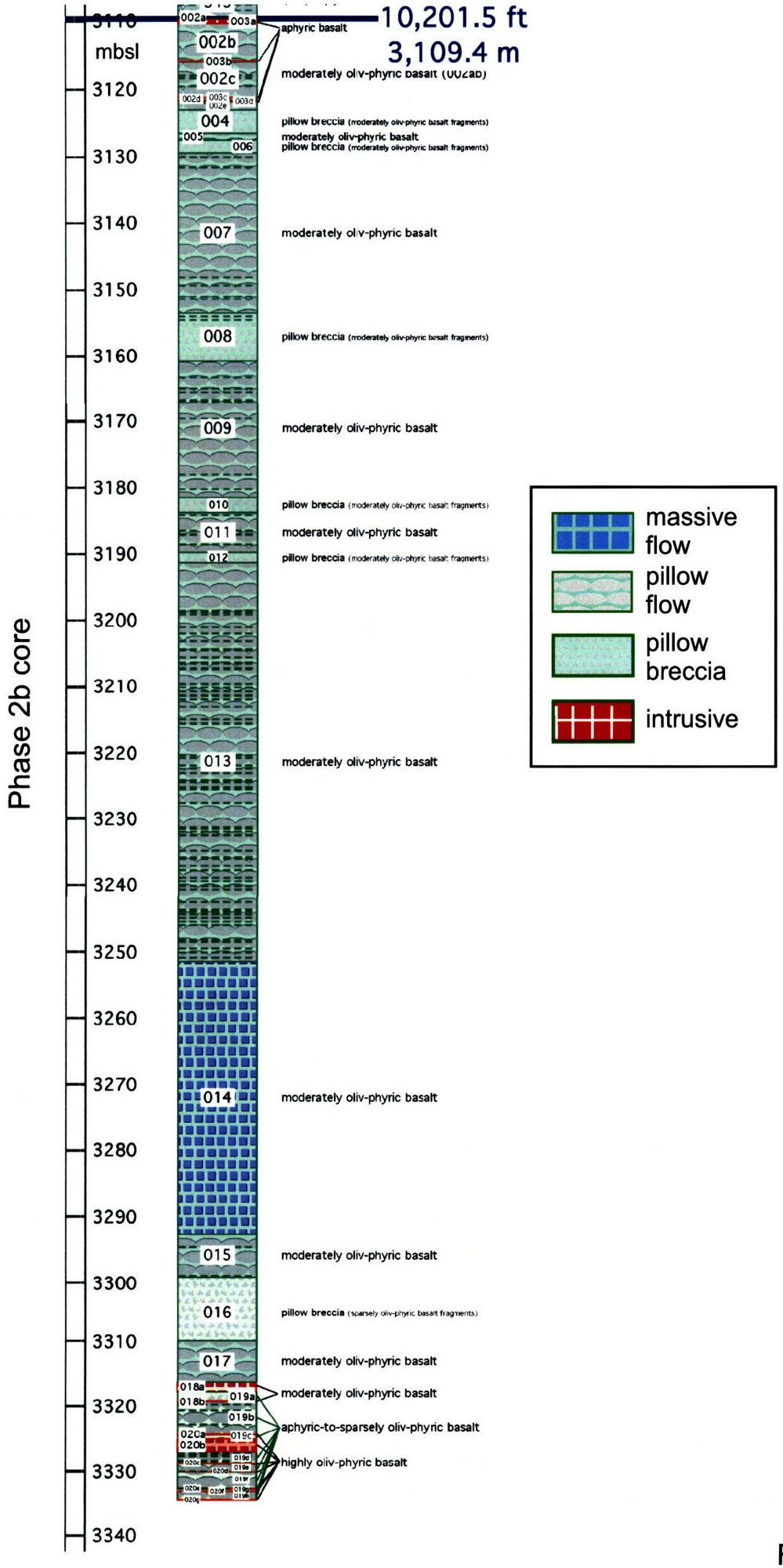
Phase 2b core
mbsl
3110
3120
3130
3140
3150
3160
3170
3180
3190
3200
3210
3220
3230
3240
3250
3260
3270
3280
3290
3300
3310
3320
3330
3340
10,201.5 ft
3,109.4 m
002a
003a
002b
003b
002c
002d
003c
002e
003d
004
005
006
007
008
009
010
011
012
013
014
015
016
017
018a
018b
019a
019b
020a
020b
019c
020c
019d
020d
019e
020e
020f
019f
019g
020g
019h
aphyric basalt
moderately oliv-phyric basalt (002ab)
pillow breccia (moderately oliv-phyric basalt fragments)
moderately oliv-phyric basalt
pillow breccia (moderately oliv-phyric basalt fragments)
moderately oliv-phyric basalt
pillow breccia (moderately oliv-phyric basalt fragments)
moderately oliv-phyric basalt
pillow breccia (moderately oliv-phyric basalt fragments)
moderately oliv-phyric basalt
pillow breccia (moderately oliv-phyric basalt fragments)
moderately oliv-phyric basalt
moderately oliv-phyric basalt
pillow breccia (sparsely oliv-phyric basalt fragments)
moderately oliv-phyric basalt
moderately oliv-phyric basalt
aphyric-to-sparsely oliv-phyric basalt
highly oliv-phyric basalt
massive flow
pillow flow
pillow breccia
intrusive

Fig. 3b

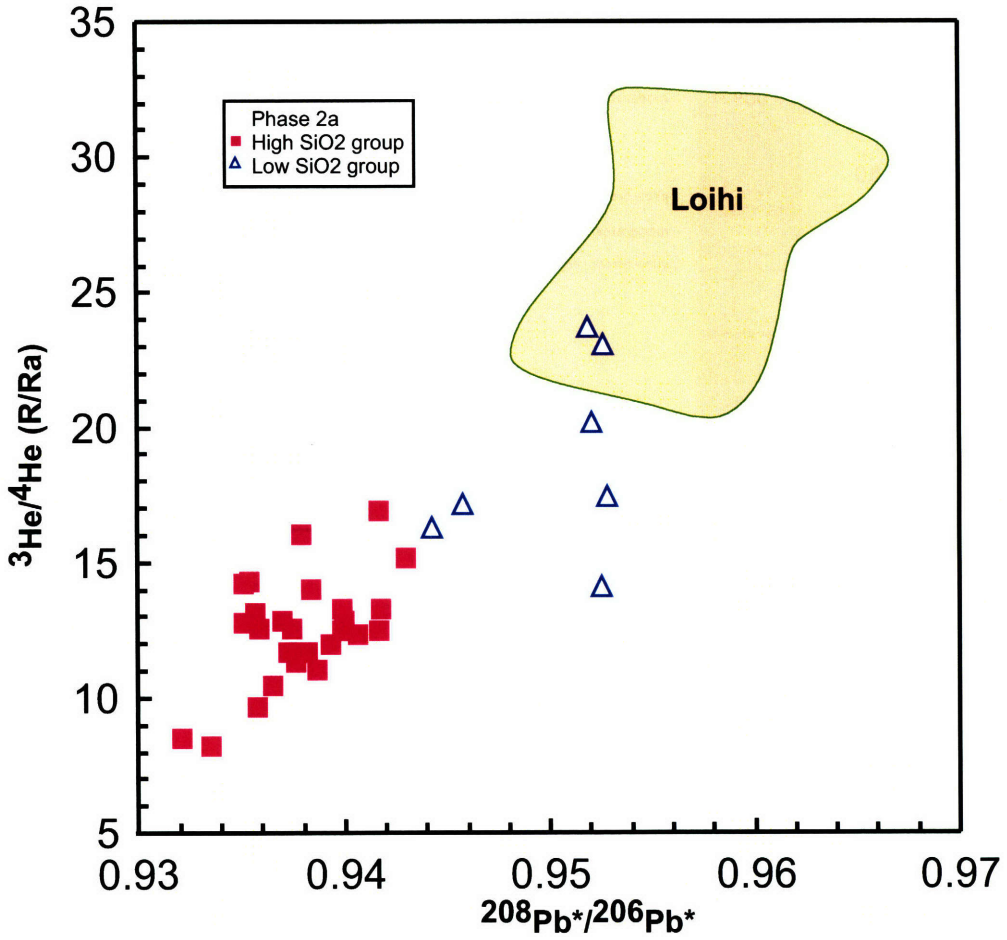
Phase 2a
High SiO2 group
Low SiO2 group
Loihi
35
30
25
20
15
10
5
0.93
0.94
0.95
0.96
0.97
$^{3}He/^{4}He$ (R/Ra)
$^{208}Pb^{*}/^{206}Pb^{*}$

Fig. 4

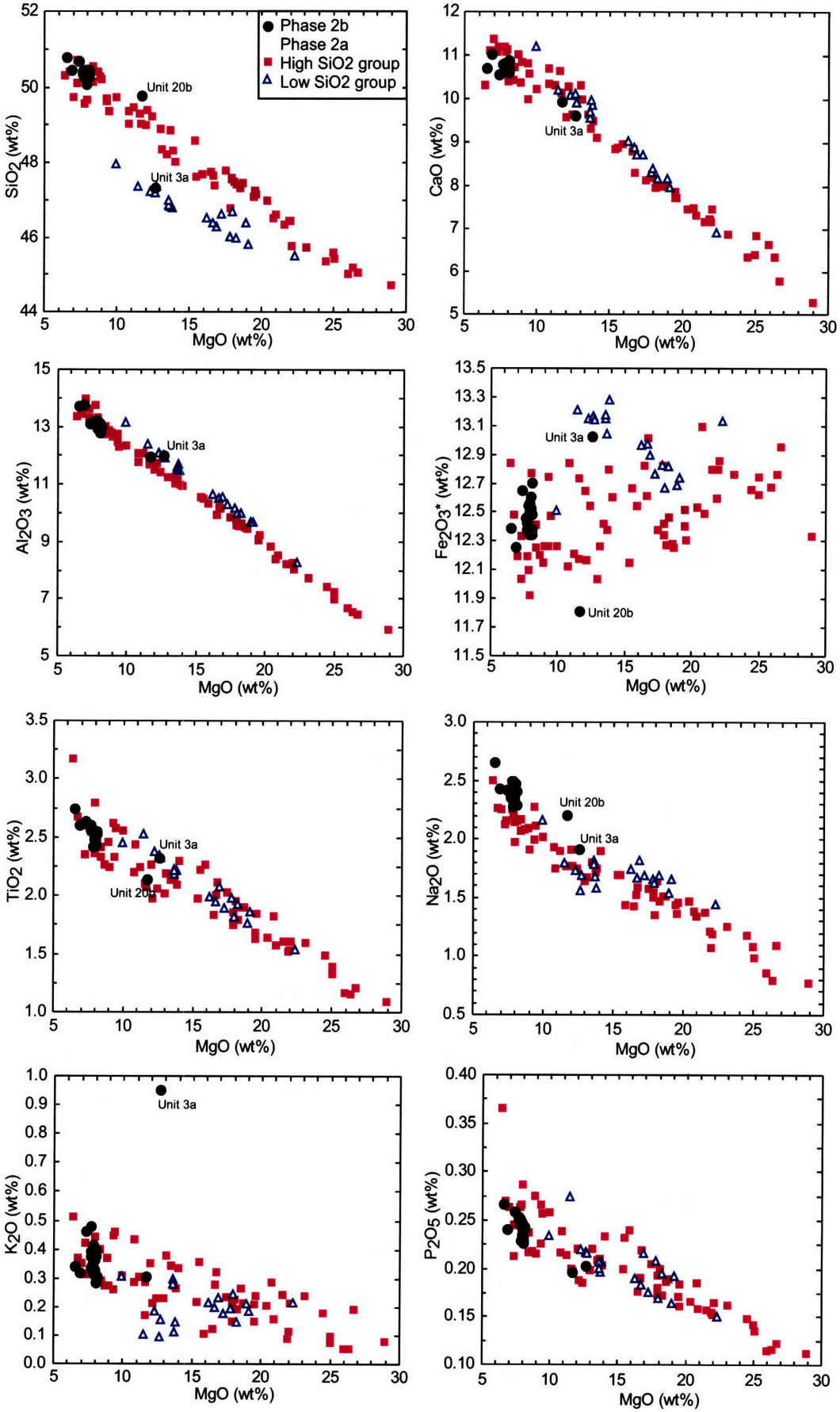
Phase 2b
Phase 2a
High SiO2 group
Low SiO2 group
Unit 20b
Unit 3a
SiO2 (wt%)
CaO (wt%)
Al2O3 (wt%)
Fe2O3* (wt%)
TiO2 (wt%)
Na2O (wt%)
K2O (wt%)
P2O5 (wt%)
MgO (wt%)

Fig. 5

Fig. 6

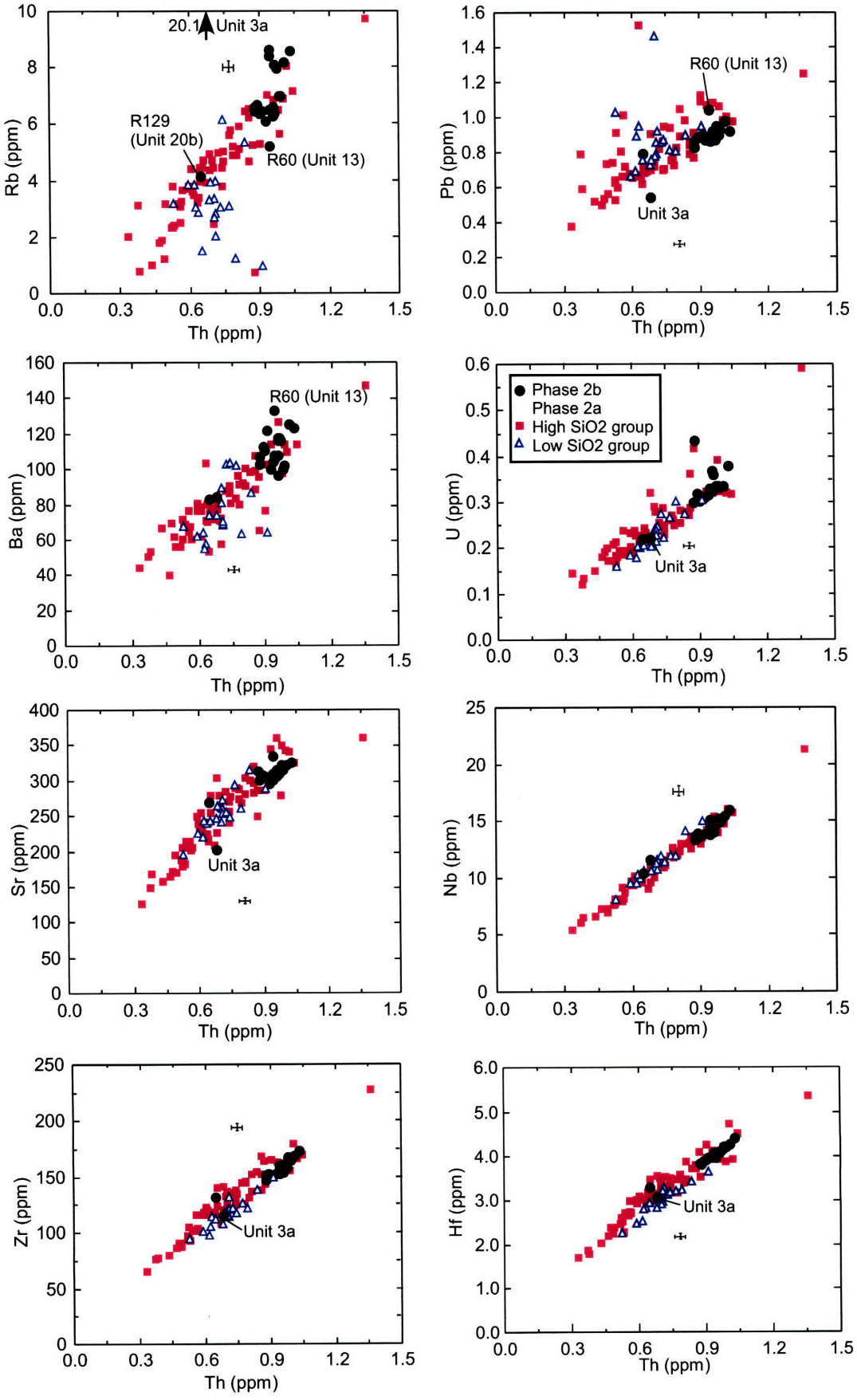
Rb (ppm)
Th (ppm)
20.1
Unit 3a
R129
(Unit 20b)
R60 (Unit 13)
Pb (ppm)
Unit 3a
Ba (ppm)
Phase 2b
Phase 2a
High SiO2 group
Low SiO2 group
U (ppm)
Sr (ppm)
Nb (ppm)
Zr (ppm)
Hf (ppm)

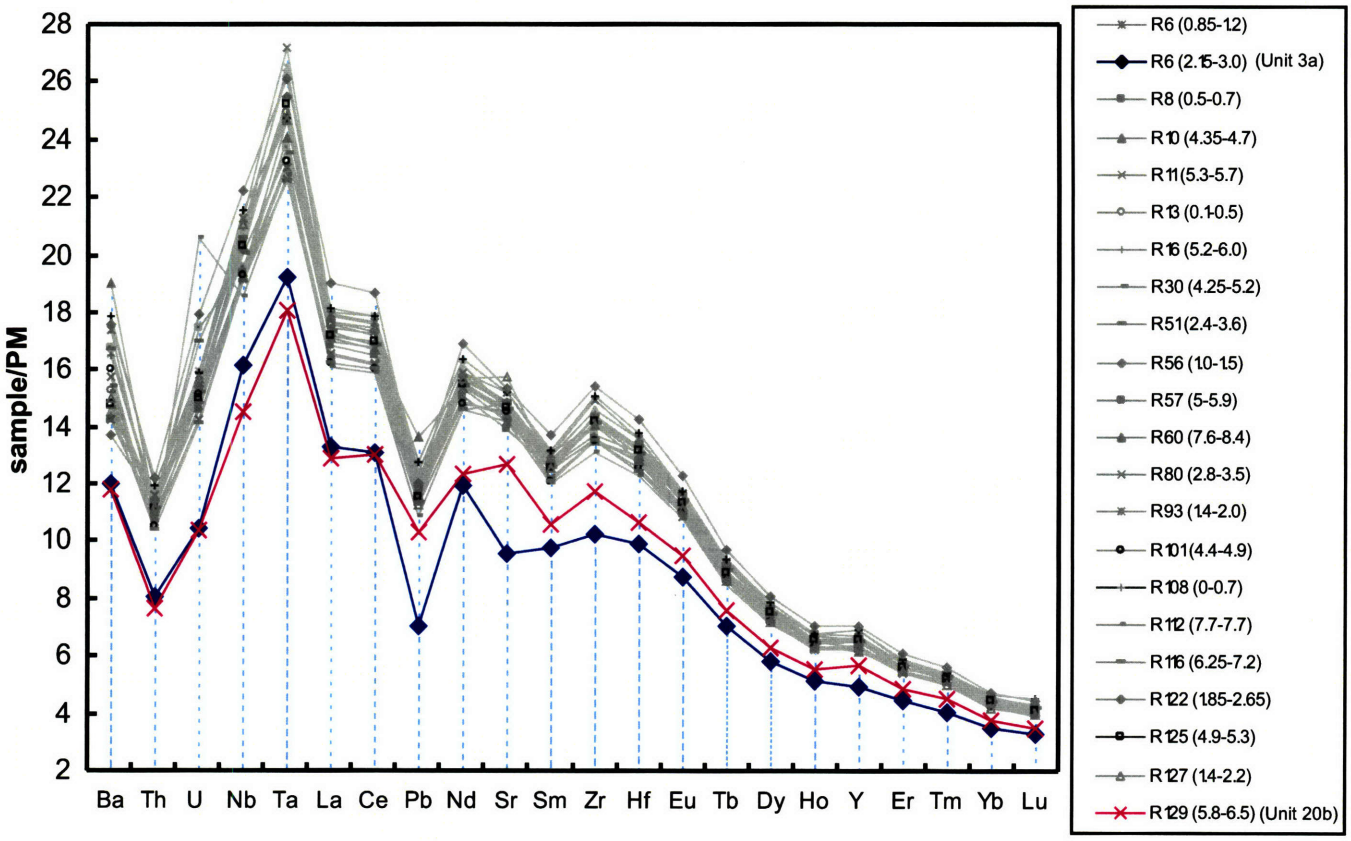
sample/PM
28
26
24
22
20
18
16
14
12
10
8
6
4
2
Ba Th U Nb Ta La Ce Pb Nd Sr Sm Zr Hf Eu Tb Dy Ho Y Er Tm Yb Lu
R6 (0.85-12)
R6 (2.15-3.0) (Unit 3a)
R8 (0.5-0.7)
R10 (4.35-4.7)
R11(5.3-5.7)
R13 (0.1-0.5)
R16 (5.2-6.0)
R30 (4.25-5.2)
R51(2.4-3.6)
R56 (10-15)
R57 (5-5.9)
R60 (7.6-8.4)
R80 (2.8-3.5)
R93 (14-2.0)
R101(4.4-4.9)
R108 (0-0.7)
R112 (7.7-7.7)
R116 (6.25-7.2)
R122 (1.85-2.65)
R125 (4.9-5.3)
R127 (14-2.2)
R129 (5.8-6.5) (Unit 20b)

Fig. 7

Fig. 8

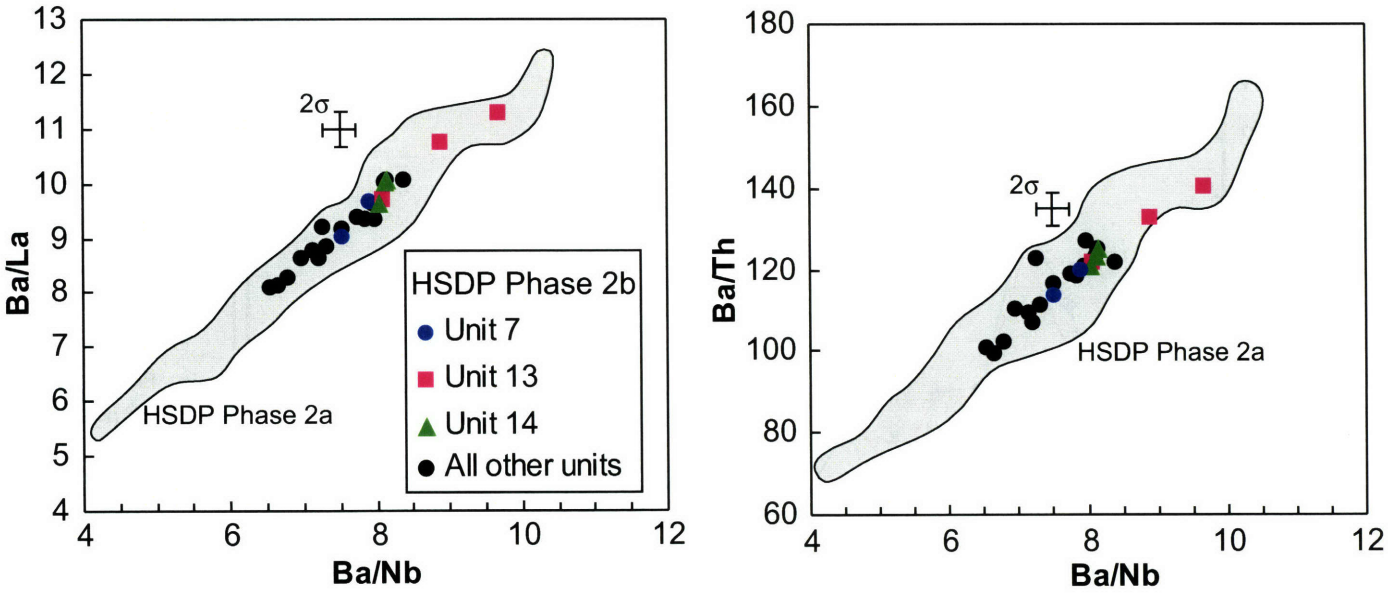
Ba/La
Ba/Nb
2σ
HSDP Phase 2a
HSDP Phase 2b
Unit 7
Unit 13
Unit 14
All other units
Ba/Th
Ba/Nb
2σ
HSDP Phase 2a

Fig. 9

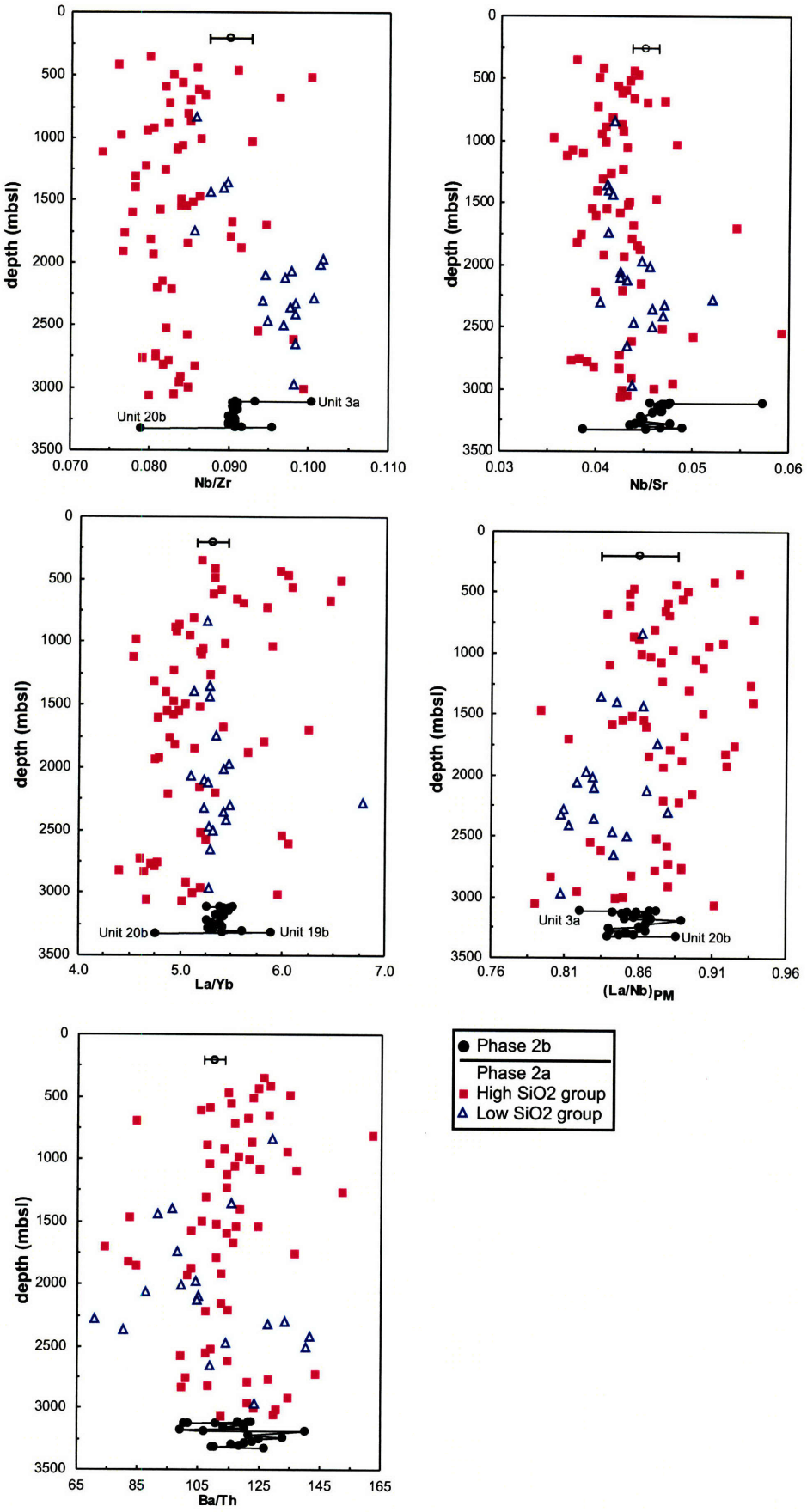
depth (mbsl)
Nb/Zr
Unit 20b
Unit 3a
Nb/Sr
La/Yb
Unit 20b
Unit 19b
(La/Nb)PM
Unit 3a
Unit 20b
Ba/Th
Phase 2b
Phase 2a
High SiO2 group
Low SiO2 group

Fig. 10

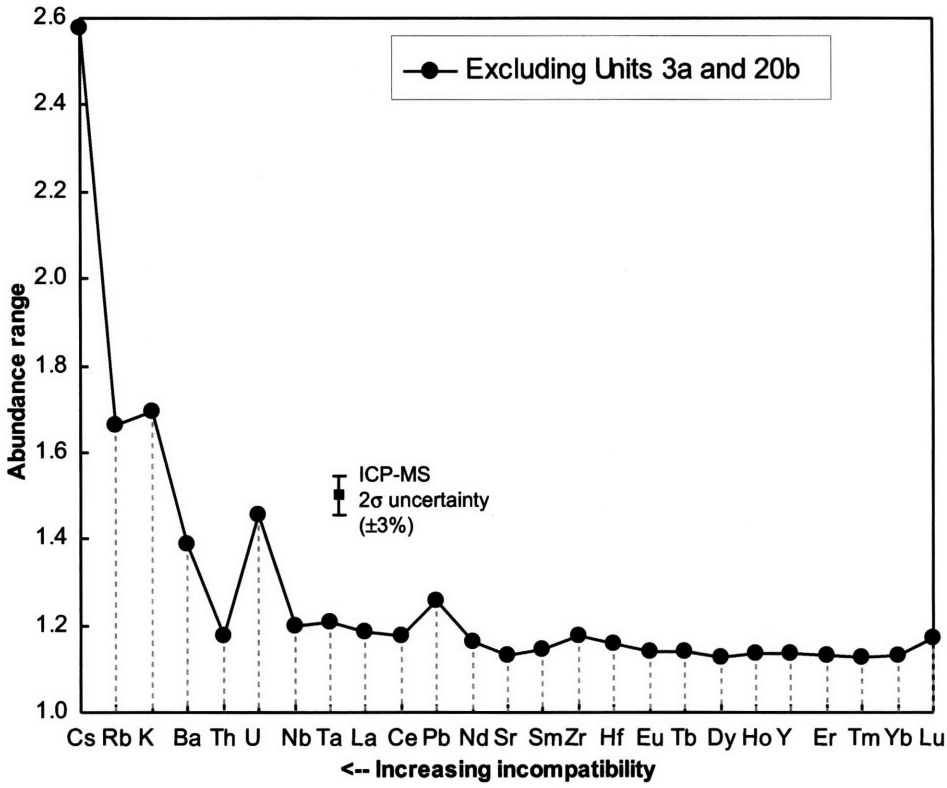
Excluding Units 3a and 20b
ICP-MS
2σ uncertainty
(±3%)
Abundance range
2.6
2.4
2.2
2.0
1.8
1.6
1.4
1.2
1.0
Cs Rb K Ba Th U Nb Ta La Ce Pb Nd Sr Sm Zr Hf Eu Tb Dy Ho Y Er Tm Yb Lu
<-- Increasing incompatibility

Fig. 11

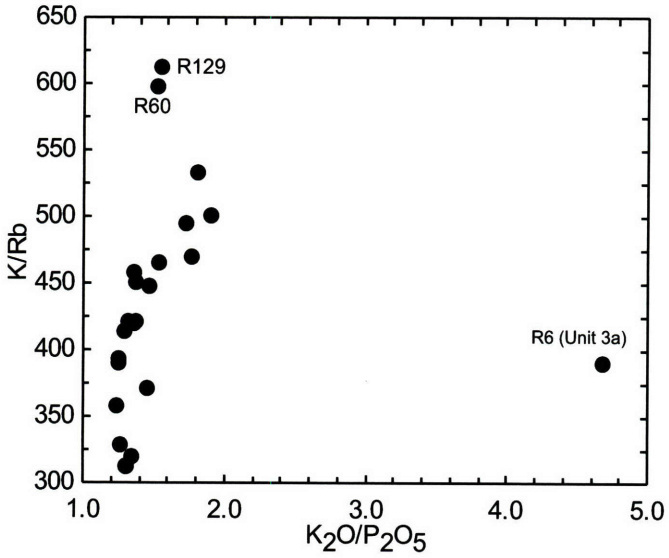
650
600
550
500
450
400
350
300
K/Rb
R129
R60
R6 (Unit 3a)
1.0
2.0
3.0
4.0
5.0
K_2O/P_2O_5

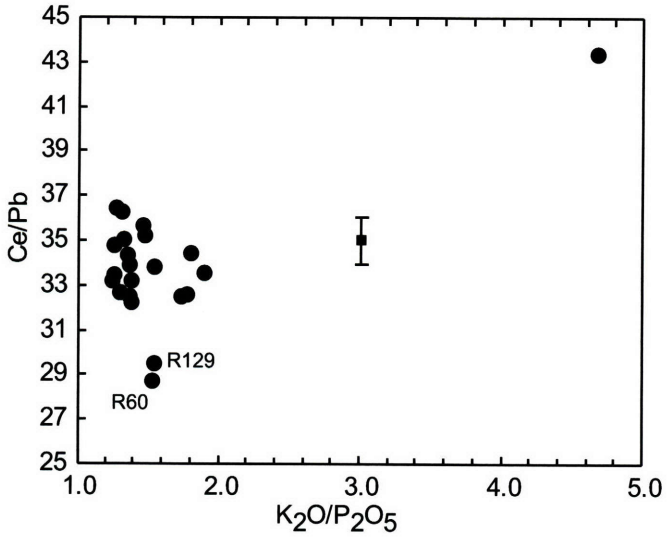
45
43
41
39
37
35
33
31
29
27
25
Ce/Pb
R129
R60
1.0
2.0
3.0
4.0
5.0
K_2O/P_2O_5

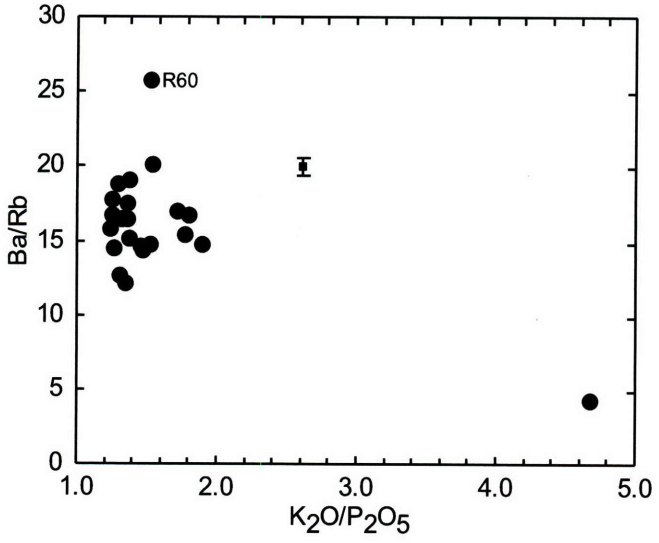
30
25
20
15
10
5
0
Ba/Rb
R60
1.0
2.0
3.0
4.0
5.0
K_2O/P_2O_5

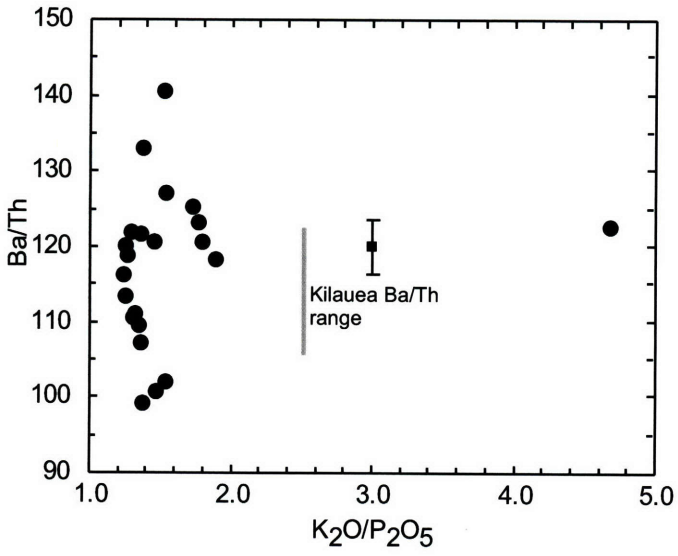
150
140
130
120
110
100
90
Ba/Th
Kilauea Ba/Th
range
1.0
2.0
3.0
4.0
5.0
K_2O/P_2O_5

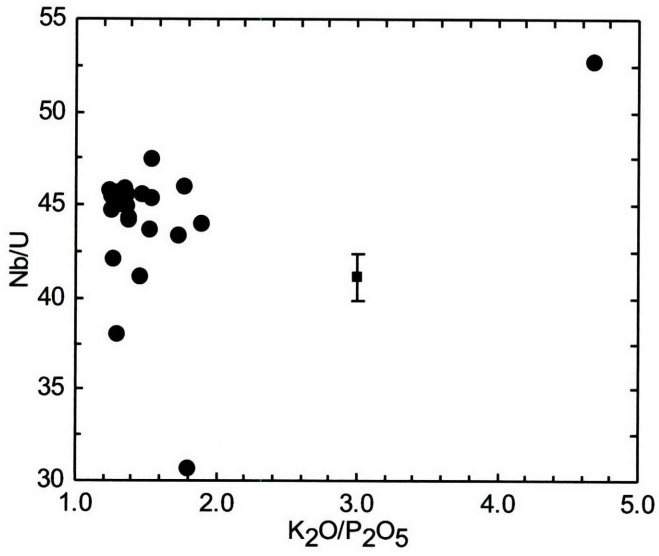
55
50
45
40
35
30
Nb/U
1.0
2.0
3.0
4.0
5.0
K_2O/P_2O_5

Fig. 12

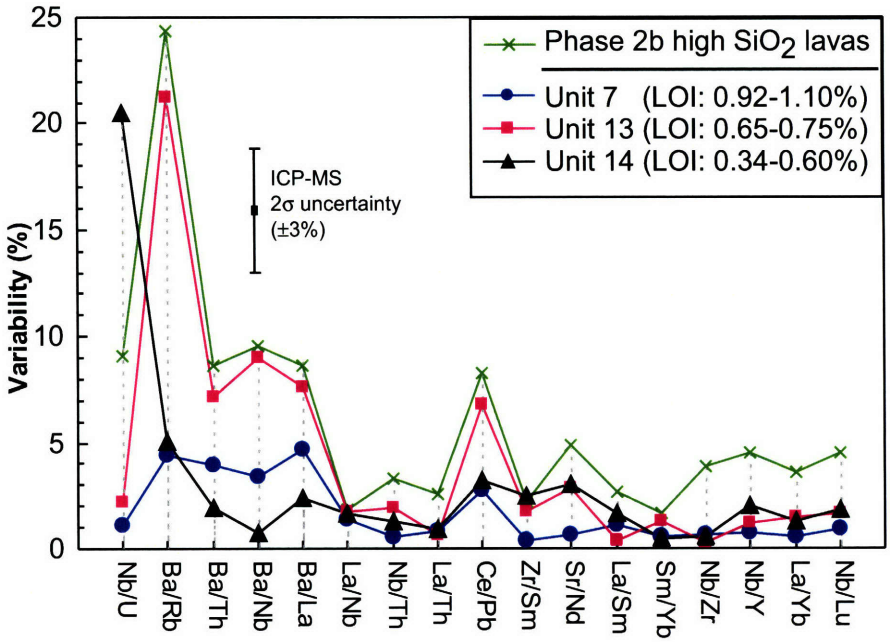
Phase 2b high SiO2 lavas
Unit 7 (LOI: 0.92-1.10%)
Unit 13 (LOI: 0.65-0.75%)
Unit 14 (LOI: 0.34-0.60%)
ICP-MS
2σ uncertainty
(±3%)
Variability (%)
25
20
15
10
5
0
Nb/U
Ba/Rb
Ba/Th
Ba/Nb
Ba/La
La/Nb
Nb/Th
La/Th
Ce/Pb
Zr/Sm
Sr/Nd
La/Sm
Sm/Yb
Nb/Zr
Nb/Y
La/Yb
Nb/Lu

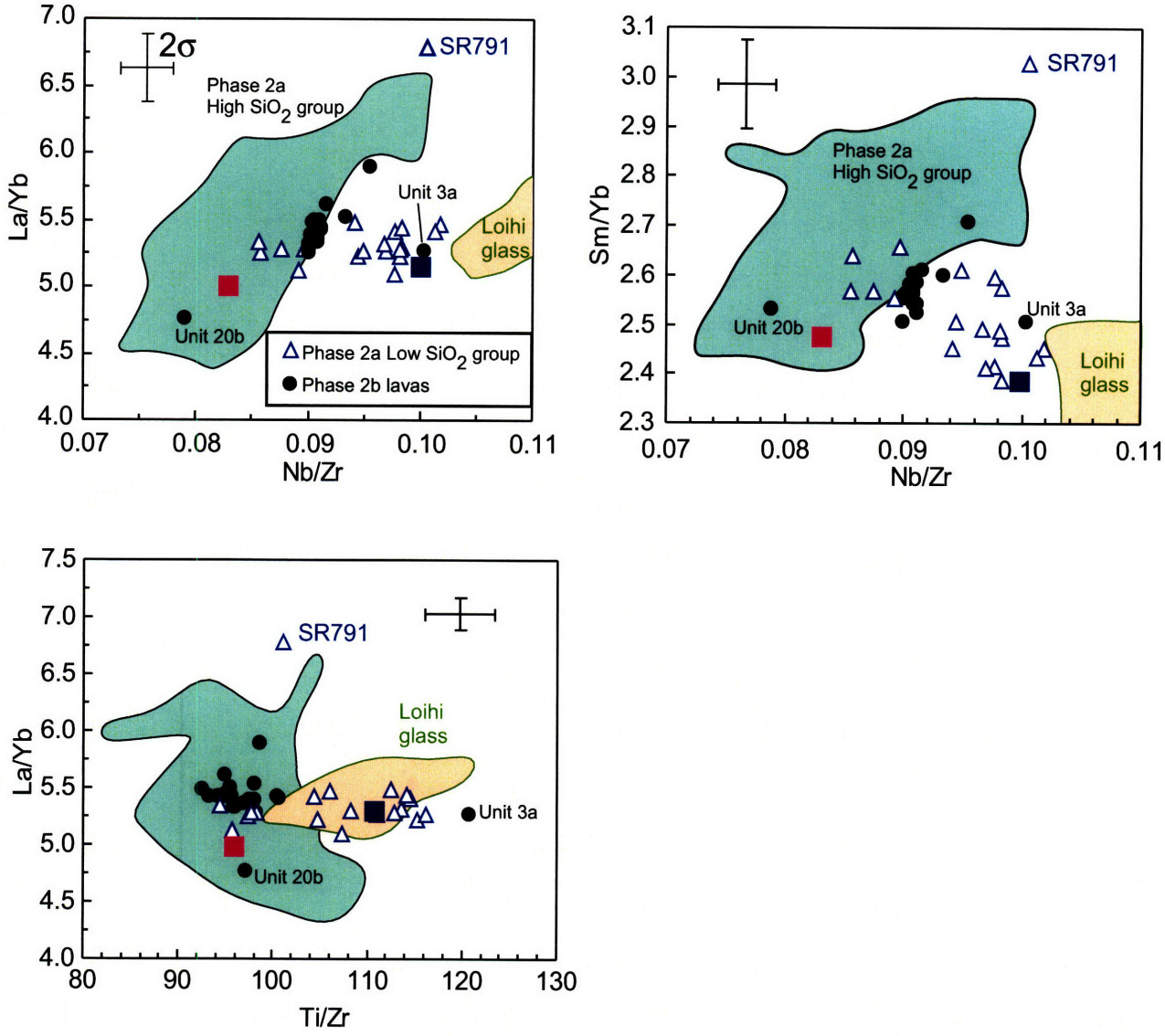
2σ
SR791
Phase 2a
High SiO2 group
Unit 3a
Loihi
glass
Unit 20b
Phase 2a Low SiO2 group
Phase 2b lavas
La/Yb
Nb/Zr
Sm/Yb
Ti/Zr

Fig. 13

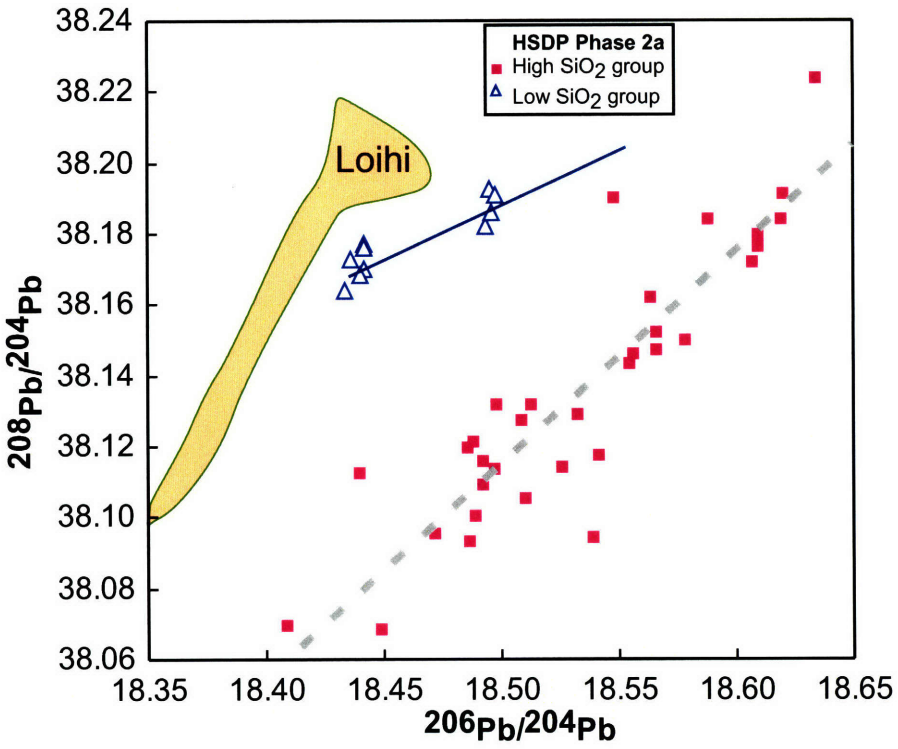
HSDP Phase 2a
High SiO2 group
Low SiO2 group
Loihi
38.24
38.22
38.20
38.18
38.16
38.14
38.12
38.10
38.08
38.06
208Pb/204Pb
18.35
18.40
18.45
18.50
18.55
18.60
18.65
206Pb/204Pb

Fig. 14

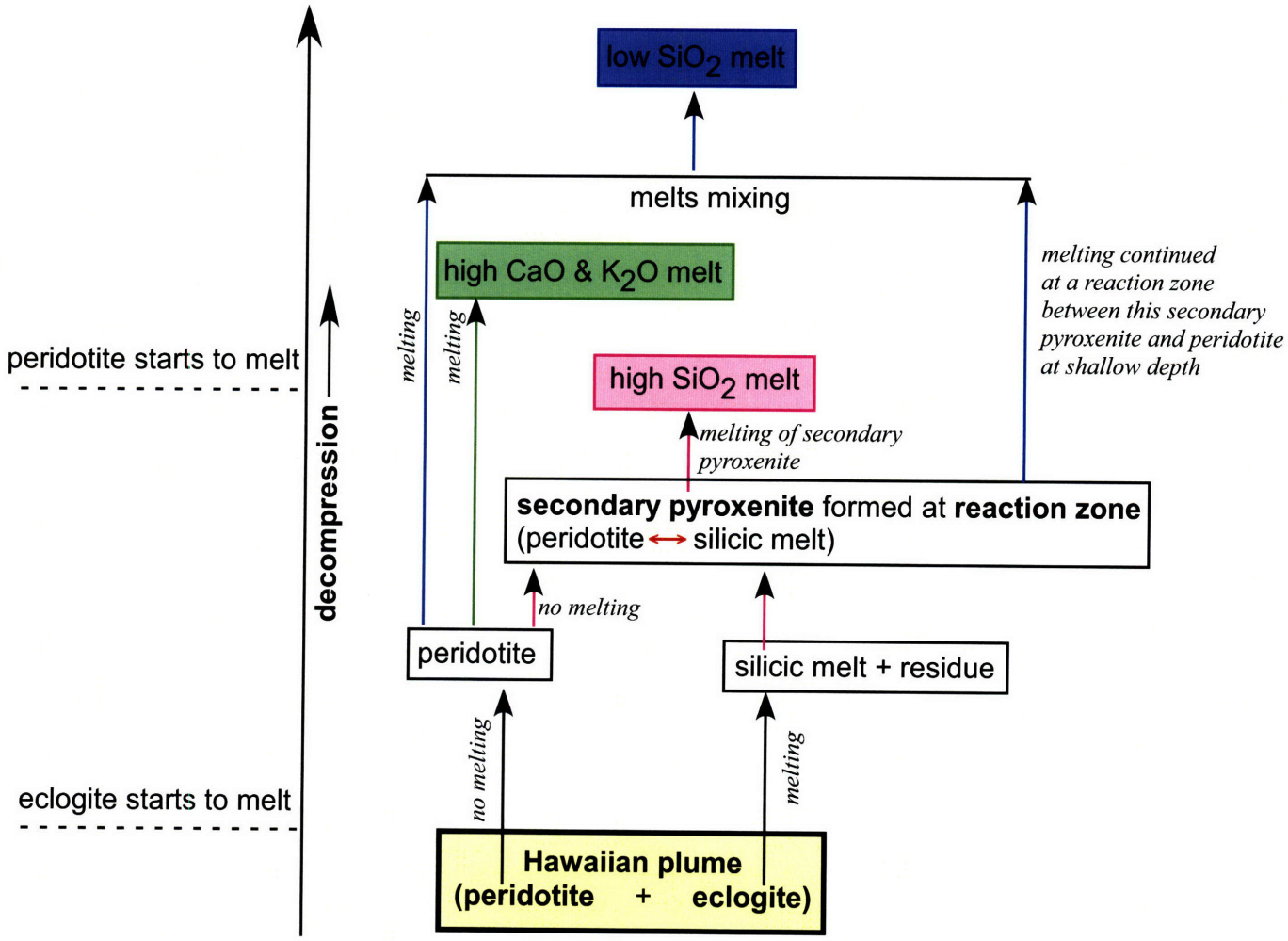
low SiO_2 melt
melts mixing
high CaO & K_2O melt
high SiO_2 melt
melting
melting
melting continued at a reaction zone between this secondary pyroxenite and peridotite at shallow depth
melting of secondary pyroxenite
secondary pyroxenite formed at reaction zone
(peridotite ↔ silicic melt)
no melting
peridotite
silicic melt + residue
peridotite starts to melt
decompression
eclogite starts to melt
no melting
melting
Hawaiian plume
(peridotite + eclogite)

Fig. 15

Fig. 16

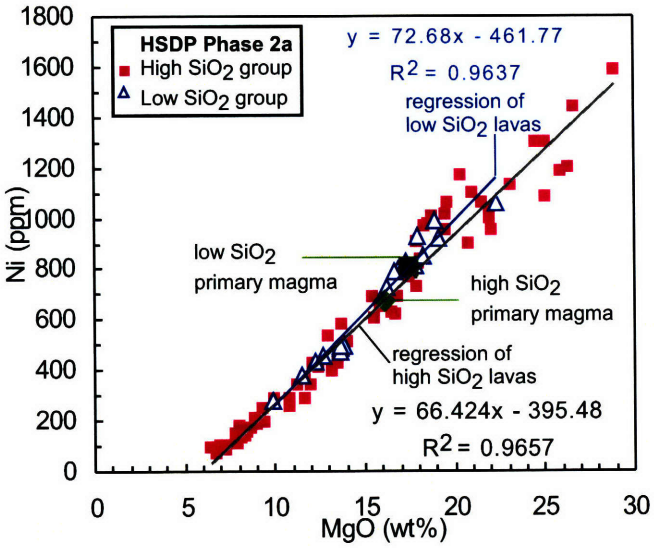
HSDP Phase 2a
High SiO2 group
Low SiO2 group
y = 72.68x - 461.77
R2 = 0.9637
regression of
low SiO2 lavas
low SiO2
primary magma
high SiO2
primary magma
regression of
high SiO2 lavas
y = 66.424x - 395.48
R2 = 0.9657
Ni (ppm)
MgO (wt%)
0
200
400
600
800
1000
1200
1400
1600
1800
0
5
10
15
20
25
30

Appendix figure caption

Appendix Figure 1 Comparison between trace element abundances in HSDP Phase 2b lavas obtained by ICP-MS at MIT and XRF at UMASS [Rhodes and Vollinger unpublished data, 2006].

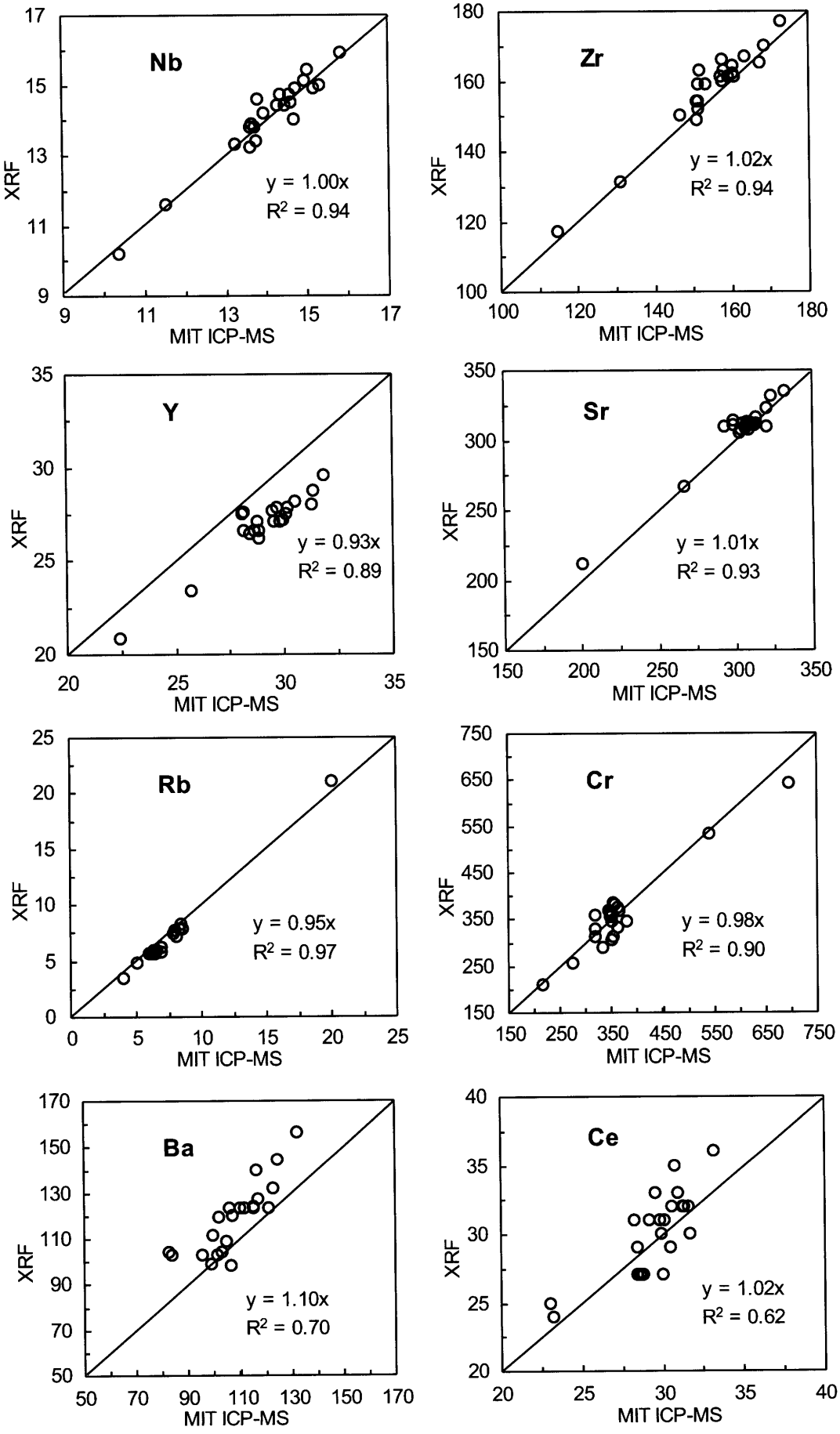

Appendix Fig. 1

Chapter 5 Evidence for mantle plumes at Kerguelen and Hawaii

1 Mantle plume hypothesis

1.1 Mantle plume hypothesis: definition and its significance

Plate tectonic theory successfully explains the geological processes occurring along plate boundaries. The mantle plume hypothesis [*Morgan*, 1971] addresses another set of global geological process such as within-plate volcanism. *Wilson* [1963] suggested that the age progression in the Hawaiian Islands was produced by the oceanic lithosphere moving over a stationary "hotspot" in the mantle. Later *Morgan* [1971] proposed that Wilson's hotspots were plumes of hot mantle that originated from a boundary layer at the core/mantle interface. The outer core may be 1500 °C hotter than the overlying mantle [*Braginsky and Roberts*, 1995]. A temperature difference of this magnitude will produce an unstable boundary layer above the core which can give rise to mantle plumes due to the density gradient. Plumes are an efficient mechanism for dispersing the heat flux. That is, mantle plumes are the inevitable consequence of a hot core [*Davies*, 2005]. Geodynamic modeling of mantle plumes, which takes into account the temperature dependence of the mantle's viscosity and compositional variation, confirm that the essential physics of the laboratory plumes are applicable to the mantle [e.g., *van Keken*, 1997; *Samuel et al.*, 2005].

Although there is debate about the role of mantle plumes throughout earth's history, there is a consensus that volcanoes forming long-lived, age progressive volcanic chains, such as the Hawaiian Ridge – Emperor Seamount chain and Ninetyeast Ridge, meet the criteria expected of mantle plume sources [*Courtillot et al.*, 2003; *Montelli et al.*, 2004]. Volcanism from long-lived mantle plumes is a consequence of important processes occurring within the earth, such as mantle convection [e.g., *Davies*, 1999] and recycling of oceanic plates at subduction zones into the deep mantle where they may then serve as source materials for mantle plumes [e.g., *Hofmann*, 1997].

1.2 Mantle plume hypothesis: predictions and observations

The mantle plume hypothesis meets the minimum requirement for a scientific hypothesis in that it was proposed to explain observations of hotspot volcanism and leads to testable predictions [*Campbell*, 2007]. In the following I apply the testable predictions in the context of Hawaiian and Kerguelen plumes.

1.2.1 Plume consists of a large head followed by a narrow tail

Plume head and tail are the classic features of a purely thermal plume [*Condie*, 2001]. The head-tail structure serves as a useful criterion in identifying a mantle plume. Continental flood basalts and submarine oceanic plateaus (Large Igneous Province, LIP) are the first eruptive products arising from the mantle plume head, and they share the following characteristics:

(a) They are the first eruptive product of a new mantle plume;

(b) They are enormous volumes, 2000 – 2500 km across [*White and Mckenzie*, 1989];

(c) They are preceded by uplift of ~500 – 1500 km [*Campbell*, 2007 and references therein];

(d) Eruption intervals are short compared to whole life of the mantle plume;

(e) Eruption rates are one to two orders of magnitude higher than that of the hotspot track that connects the LIP to current position of the plume;

Recently numerical modeling of thermo-chemical plumes revealed diverse characteristics that are different from classic thermal plumes due to the interaction between thermal and compositional buoyancy forces [*Farnetani and Samuel*, 2005; *Lin and van Keken*, 2005; *Lin and van Keken*, 2006]. For example, *Farnetani and Samuel* [2005] showed that if the head of a plume contains a high proportion of a dense component from the lowermost mantle, the ascent of the head can stall at the 670 km

discontinuity and develop secondary instabilities; in the end only a part of the head penetrates the discontinuity and gives rise to secondary plume that appears to originate from that discontinuity. Therefore, a plume head may be absent [*Farnetani and Samuel*, 2005] or multiple episodes of volcanism may be associated with a plume head [*Lin and van Keken*, 2005]. These results bring plume hypothesis into a new realm with potentially a much larger range of physical features that may account for a greater proportion of intraplate volcanism.

The Kerguelen plume has produced 15.2 to 24.1×10^6 km^3 of basaltic magma [*Coffin and Eldholm*, 1994] for at least 120 Ma [*Weis et al.*, 1989]. The long volcanic record of the Kerguelen plume includes a large igneous province (i.e., the Kerguelen Plateau-Broken Ridge), which may be associated with plume initiation, the >5000 km long 82–38 Ma Ninetyeast Ridge hotspot track, which formed as the Indian Plate migrated rapidly northwards over the plume, and recently active oceanic islands such as Kerguelen Archipelago, McDonald and Heard Islands (Figure 1). Formation of the Kerguelen LIP postdated continental breakup between India and Antarctica, with eruption ages ranging from ~119 Ma in the southern Kerguelen Plateau (SKP) to ~34 Ma in the northern Kerguelen Plateau. Peaks in magmatic output (~0.9 km^3/yr) occurred in the intervals of 119–110 and 105–95 Ma which are presumably associated with plume head(s) (Figure 2). The magmatic output for Ninetyeast Ridge is an order of magnitude lower (~0.1 km^3/yr) than for the plateau [*Coffin et al.*, 2002] at <82 Ma which is presumably the product of plume tail (Figure 2).

All these observations fit well with the plume initiation hypothesis, which attributes the high eruption rate and large area covered by flood basalts (i.e., the Kerguelen Plateau and Broken Ridge) to melting of a plume head, and the lower eruption rate of more focused Ninetyeast Ridge to melting of narrower plume tail.

At Hawaii, there is no known volcanism associated with plume head, however, it may either be subducted at the Kuril and Aleutian trenchs, or it stalled at the 670 km discontinuity without forming a observable plume head [*Farnetani and Samuel*, 2005]. The long-term average magmatic output for Hawaiian Ridge - Emperor Seamounts chain is 0.01-0.017 km^3/yr [*Robinson and Eakins*, 2006], but the average magma supply rate for the past 6 My is substantially higher (0.095 km^3/yr), which is similar to that of Ninetyeast Ridge (~0.1 km^3/yr).

1.2.2 Magmatism from plume tails should have a steady age progression of volcanoes

Both the Kerguelen and Hawaiian plumes have long-lived hotspot tracks (> 80 My). For the Kerguelen plume, the Ninetyeast Ridge is the hotspot track and has age progression of 38 My (south) to 82 My (north) (Figure 1). At Hawaii, the age of Hawaii Ridge -Emperor Seamount chain steadily increases from the Big Island (zero) to Detroit seamount of ~81 Ma [*Duncan and Keller*, 2004].

1.2.3 Both plume heads and tails should erupt high-temperature magmas

If mantle plumes originate from a thermal boundary layer they must be hotter than the mantle they ascend through. For example, the inferred temperature of primary magma have the potential to determine if the mantle beneath hotspots, such as Hawaii and Kerguelen, is in fact hotter than the mantle that which supplies most mid-oceanic ridge magma and whether the source regions are chemically different. *Putirka et al.* [2005; 2007] found that mantle potential temperature at Hawaii is ~270°C higher than that of mid-ocean ridge basalt (MORB) using a olivine-melt equilibrium approach. This result is confirmed by *Herzberg et al.* [2007]. However, this is a controversial result. *Green and Falloon* [2005] and *Falloon et al.* [2007] found that there are large variations (~115 °C) in both MORB parental liquids and Hawaiian lavas, and stated

that there is no systematic difference in source temperature between MORB and Hawaiian lavas. Both groups use similar approach, i.e., olivine-melt equilibrium, but *Falloon et al.* [2007] used constant values of Kd for Hawaii (0.29) and MORB (0.32) and maximum Fo at Hawaii is 90.7 whereas observed is 91.3. The constant Kd values used by Falloon et al. [2007] are not justified since *Putirka et al.* [2005] showed that they depend on pressure and compositions. Nevertheless, seismic evidence suggests that Hawaiian plume is ~100 °C hotter than Iceland [*Li et al.*, 2000].

Moreover, the buoyancy of mantle plumes can be caused by either temperature or composition or both. As mantle plumes are associated with distinctive geochemical compositions, it is likely that, instead of being pure thermal, mantle plume buoyancy is thermo-chemical or purely compositional; in this case significant excess temperatures are not required. Both Hawaii and Kerguelen plumes are likely thermo-chemical plumes. The Kerguelen plume is associated with a DUPAL isotopic anomaly and a very low velocity province at the core-mantle boundary [*Wen*, 2006]. The Hawaiian plume is associated with a localized zone of anomalously strong anisotropy caused by ancient subducted slab material spreading along the core-mantle boundary [*Fouch et al.*, 2001].

1.2.4 Plumes must originate from a hot boundary layer and can be detected by their seismic signature

The obvious way of showing that mantle plumes originate from a hot boundary layer (probably the core-mantle boundary) is to use seismic methods to trace ascending plumes from the upper mantle to their source. Seismic data do provide evidence that such conduits exist in the lower mantle at Kerguelen and Hawaii [*Montelli et al.*, 2004; *Lei and Zhao*, 2006; *Montelli et al.*, 2006; *Nolet et al.*, 2007] (Figures 3, 4 and 5). A note of caution is that the width of the proposed plume tail (~100 km) is near the limit of seismic resolution, and these seismic data cannot determine whether the plumes are

thermal or chemical features. However, one cannot argue against the existence of mantle plumes simply because seismic tomography cannot find such anomaly, which is the way as some plume skeptics do [*Foulger*, 2002].

1.2.5 Geochemical observations of plume-derived magma

Mantle plumes are physical features, but they are likely to be geochemically distinct from ambient mantle. Fluid dynamic models for the development of plumes indicate that they originate from boundary layers [*Griffiths and Campbell*, 1990], and when a plume is initiated, the plume head entrains surrounding mantle during upwelling whereas plume tail follows the previously formed conduit and entrainment of surrounding mantle is not necessary. Therefore, the plume head may have a different composition than a plume tail. The Kerguelen plume is a good test because lavas related to both the plume head and plume tail have been studied. Lavas recovered at central Kerguelen Plateau (Site 1138) were interpreted to represent the pure plume head composition [*Neal et al.*, 2002] whereas Mt. Crozier at Kerguelen Archipelago represents the pure plume tail composition [*Weis and Frey*, 2002], these lavas indeed have very different compositions (Figure 6) and these composition differences are not the result of the age differences [*Ingle et al.*, 2002].

Plume tails originate at the boundary layer with distinctly geochemical compositions. For the Kerguelen and Hawaii plumes, the boundary layer is the core-mantle boundary [*Montelli et al.*, 2004; *Montelli et al.*, 2006]. The Kerguelen plume locate has been shown to be within a very low velocity province at the base of the Earth's mantle, which attributed to the DUPAL anomaly in the South Atlantic and Indian Oceans [*Wen*, 2006].

The relationship between lava geochemistry and plumes can be inverted to interpret the chemical structure of the mantle. Since the lavas from Hawaiian Islands and

Kerguelen Archipelago are well known to be associated with melting of a plume tail, the geochemistry of these lavas can be used to decipher the chemical structure of the deep mantle. In this thesis I study the geochemical compositions of the rocks from Kerguelen Archipelago (Mt. Capitole) and Hawaiian Islands (Mauna Kea, East Molokai and West Molokai) which have very different isotopic compositions (Figure 7).

2. Mantle plume hypothesis: Alternative models

Plume advocates have focused on adapting the plume hypothesis to account for new and unpredicted observations. In the meantime, plume skeptics propose alternative models, for example:

2.1 Edge convection [*King and Anderson*, 1998]

When continents split, linear volcanic margins generally form, followed by anomalous magmatism in some parts of the new ocean, such as the North Atlantic Ocean. The edge convection model is based on the observation that where thick, cold continental lithosphere is juxtaposed against hot, oceanic asthenosphere, small-scale convection, caused by a horizontal temperature gradient, may develop at the continental margin and cause vigorous, time-dependent magmatism, i.e., the hotspot track of plume advocates.

2.2 Plate-tectonic processes [*Foulger*, 2004]

The mantle plume hypothesis commonly invokes recycling of oceanic crust, sediment and continental material to the core-mantle boundary where it is sampled by a mantle plume and brought up to the surface again. The plate-tectonic processes model suggests that recycled material is instead recirculated at much shallower depths. This model suggests that "anomalous" volcanism occurs where plates are in extension, either

in their interiors or near their boundaries and that the volume of magma produced is a function of the fertility and fusibility of the source material being tapped. For example, volcanism will be more voluminous if recycled material is tapped in addition to mantle peridotite.

2.3 Continental lithospheric delamination [*Anderson*, 2005]

Delamination of continental lithosphere can occur if it becomes thickened, transforms to dense phases such as eclogite, and catastrophically detaches and sinks. Numerical modeling predicts that surface subsidence is followed by extensive magmatism [e.g., *Elkins-Tanton*, 2005; *Lustrino*, 2005].

2.4 Meteorite impacts [e.g., *Jones et al.*, 2005]

It is possible that impacts could generate the large volumes of magma in a short time. Such a mechanism could explain the very short timescale of LIP formation. Numerical modeling [*Jones et al.*, 2005] suggests that the pressure-release (decompression) melting can trigger the volumes and magma fluxes observed in LIP, such as the Ontong Java Plateau [*Ingle and Coffin*, 2004].

In summary, these alternatives can explain some observations that the classical purely thermal plume model cannot explain, but the thermo-chemical plumes may be capable of explaining more features. In particular, decompression melting of a plume head offers a straightforward explanation for flood basalt eruptions, especially large volumes of basaltic magma erupted over a short time interval of a few million years. Also plume tails remain the most straightforward explanation for age-progressive volcanic chains. However, this does not mean that all intra-plate volcanism should be attributed to mantle plumes. For example, isolated seamounts and islands may be not related to mantle plumes; their origins must be considered case by case.

3. Origin of isotopic variability in Kerguelen Archipelago and Hawaiian lavas

The mantle is very heterogeneous and its isotopic composition can be divided into different endmembers such as enriched mantle I (EM-I), enriched mantle II (EM-II), depleted mantle (DM), HIMU and FOZO (or C) [e.g., *Hart et al.*, 1992; *Hanan and Graham*, 1996; *Hofmann*, 1997]. What causes these geochemical heterogeneities in the mantle? Three processes have been postulated that lead to the mantle heterogeneity. (1) Metasomatism in the mantle caused by fluids and melts reacting with peridotite [e.g., *Frey and Green*, 1974; *Workman et al.*, 2004]. For example, Samoan lavas are characterized by one of the endmember compositions (EM-II), i.e., high $^{87}Sr/^{86}Sr$ and low $^{143}Nd/^{144}Nd$. *Workman et al.* [2004] proposed that the enriched trace element and isotopic compositions in Samoan lavas were caused by sampling of recycled ancient metasomatised oceanic lithosphere; (2) Subduction of oceanic lithosphere and incorporation of recycled basalt into the source of HIMU lavas, such as at St. Helena and Cook-Austral [e.g., *Stracke et al.*, 2005], and recycled basalt and sediment into the source of EM-I lavas such as at Pitcairn Island [e.g., *Eisele et al.*, 2002]; (3) Incorporation of delaminated continental lithosphere into the source of EM-I lavas [e.g., *McKenzie and O'Nions*, 1983; *Escrig et al.*, 2004]. In the following section I discuss how these processes contributed to the geochemical variations observed in Kerguelen and Hawaiian lavas (Figure 7).

3.1 Role of continental material in Kerguelen-plume related lavas

The Indian Ocean formed as a result of continental rifting accompanying Gondwanaland breakup. There is compelling evidence for continental material in lavas forming the Kerguelen Plateau and Kerguelen Archipelago: (1) Continental crust (garnet-biotite gneiss clasts) occurs in a conglomerate intercalated with basalt flows at

Elan Bank (Figure 1); (2) Geophysical evidence for continental crust has been found in the Kerguelen Plateau, especially at Elan Bank and southern Kerguelen Plateau [*Borissova et al.*, 2003]; (3) Continental lithosphere derived xenoliths were found in lavas forming the Kerguelen Archipelago [*Hassler and Shimizu*, 1998; *Mattielli et al.*, 1999]; (4) Isotopic and incompatible element ratios indicate a component derived from continental crust (i.e., lower continental crust, LCC) in some Kerguelen Plateau lavas [*Mahoney et al.*, 1995; *Frey et al.*, 2002b]. In Chapter 1 I propose that two stage of mixing between Kerguelen plume, depleted mantle component and lower continental crust can explain the trace element and isotopic ratios of Kerguelen Archipelago lavas (Figure 16 of Chapter 1).

In detail, Kerguelen Archipelago lavas define isotopic trends (such as $^{87}Sr/^{86}Sr$ vs $^{206}Pb/^{204}Pb$) trending towards the field for lower continental crust (Figure 16 of Chapter one), therefore, we proposed that the mixing of Kerguelen plume and depleted components predated the involvement of lower continental crust. This makes sense especially if the depleted component is intrinsic to the Kerguelen plume whereas lower continental crust was dispersed into the Indian Ocean asthenosphere during breakup of Gondwanaland. In other words, two components within the Kerguelen plume mix with each other before mixing with LCC at shallower depth. These mixing sequences are different than that proposed for Indian MORB. *Escrig et al.* [2004] and *Meyzen et al.* [2005] proposed that depleted component was mixed with LCC and then mixed with a "C" component (i.e., common component in MORB).

3.2 Role of recycled oceanic crust and sediment in Hawaiian lavas

Unlike the Indian Ocean which formed concomitantly with continental rifting and opening of the ocean basin, the Pacific Ocean basin is not associated with continental rifting, but it is associated with many subduction zones, i.e., the Ring of

Fire. Indeed, fecycled oceanic crust and sediment has been proposed to be important in Hawaiian lavas [e.g., *Huang and Frey*, 2005; *Sobolev et al.*, 2005; *Herzberg*, 2006; *Sobolev et al.*, 2007]. Specifically, major and trace element contents and isotopic characteristics of Hawaiian lavas are consistent with recycled oceanic crust and sediment in their source: (1) at a given MgO content, most Hawaiian lavas are too depleted in CaO to be in equilibrium with mantle peridotite [*Herzberg*, 2006 and chapter 4]; (2) Hawaiian lavas have higher Ni content and Fe/Mn than expected for melts derived from peridotite [*Humayun et al.*, 2004; *Sobolev et al.*, 2005; *Sobolev et al.*, 2007]; (3) the high Sr/Nb and low Th/La of some Koolau lavas (Makapuu-stage) requires involvement of recycled sediment [*Huang and Frey*, 2005]; (4) the Os and oxygen isotopic ratios of Hawaiian lavas are consistent with recycled oceanic crust and sediment [*Lassiter and Hauri*, 1998; *Lassiter et al.*, 2000; *Yang et al.*, 2003].

3.3 Comparison of lavas derived from the Hawaiian and Kerguelen plumes

Compared to Kerguelen Archipelago lavas, Hawaiian lavas have lower $^{208}Pb^*/^{206}Pb^*$ (i.e., long-term Th/U difference) and $^{87}Sr/^{86}Sr$ ratios (long-term Rb/Sr difference) (Figure 7). These isotopic differences are consistent with a recycled oceanic crust component in the Hawaiian lavas and a recycled continental component in the Kerguelen lavas. Specifically lower continental crust has high Th/U (6.0, [*Rudnick and Gao*, 2004]) than MORB (2.5, [*Sun and McDonough*, 1989]) and sediment (4.1, [*Plank and Langmuir*, 1998]). Also at a given $^{208}Pb^*/^{206}Pb^*$, Hawaiian lavas have higher $^{87}Sr/^{86}Sr$ than those of Kerguelen Archipelago lavas (Figure 8), which is consistent with much lower Rb/Sr in LCC (0.03, [*Rudnick and Gao*, 2004]) than that of recycled sediment (0.18, [*Plank and Langmuir*, 1998]).

3.4 Role of depleted mantle component in Kerguelen Archipelago and Hawaiian lavas

Depleted components with relatively low $^{87}Sr/^{86}Sr$, high $^{143}Nd/^{144}Nd$ and $^{176}Hf/^{177}Hf$, compared to primitive mantle, are dominant components for MORB, and also play an important role for ocean island basalt (OIB). There has been controversy about the origin of depleted components in OIB; are they MORB-related or intrinsic-plume sources? Whether or not depleted material occurs deep within the mantle (i.e., below the MORB asthenospheric reservoir) is clearly of importance for geodynamic models of the Earth, and also bears on understanding regions of plume-ridge interactions.

3.4.1 Depleted mantle component in Kerguelen Archipelago lavas

Depleted components are important in Northern Kerguelen Plateau and older Kerguelen Archipelago lavas [e.g., *Yang et al.*, 1998; *Doucet et al.*, 2002; *Weis and Frey*, 2002]. As to the origin of these depleted components, there is debate whether it is Southeast Indian Ridge (SEIR) MORB-related [e.g., *Weis and Frey*, 2002] or intrinsic to the Kerguelen plume [*Frey et al.*, 2002a]. Arguments that support the SEIR-MORB origin are: (1) plate reconstruction indicates that the Kerguelen plume coincided with the SEIR axis at ~ 40 Ma [*Frey et al.*, 2000]; hence plume-ridge interaction was inevitable since lavas from Northern Kerguelen Plateau (such as Site 1140) were erupted when SEIR was <50 km away from the Kerguelen plume; (2) Site 1140 lavas define trends on isotopic plots pointing to SEIR N-MORB fields from the postulated Kerguelen plume field (Figures 11 and 16 from Chapter one); these trends can be explained by binary mixing of plume-MORB endmembers [*Weis and Frey*, 2002]; (3) There is a temporal variation of depleted component in Kerguelen Archipelago lavas, i.e., a depleted component is less important in younger lavas erupted further away from the ridge and more important in older lavas (Figure 8).

However, the plume-MORB binary mixing model proposed by *Weis and Frey* [2002] to explain the isotopic trends of Site 1140 lavas cannot explain the Th/Nb-La/Nb correlation shown in Figure 9. That is, Site 1140 lavas have higher Th/Nb at a given La/Nb than the postulated Kerguelen plume and SEIR MORB and lavas with higher La/Nb have lower $^{87}Sr/^{86}Sr$ (Figure 9). Therefore, a depleted component with high Th/Nb and La/Nb ratios quite different than in the SEIR-MORB source is inferred. What is the origin of this depleted component? Recycled sediment and continental material are known to be depleted in Nb, but recycled sediment and continental material have enriched, instead of depleted, isotopic composition (Figure 9). Pilet et al. [2004] proposed an alternative model to explain the Nb depletion in OIB. They argued that the high Nb/Th ratios might be the result of a metasomatic process, called percolative fractional crystallization, that produced veins containing pyroxene and Nb-rich oxide within the upper mantle. Most importantly, Site 1140 and other Kerguelen Archipelago lavas define a linear trend which does not extrapolate to the SEIR N-MORB field and Nb depletion will not change the slope of Th/Nb-La/Nb trend, a source component different from SEIR N-MORB is required to explain the linear mixing trend. An intrisic depleted component in the plume that is different from MORB source [*Frey et al.*, 2005] is proposed.

3.4.2 Depleted mantle component in Hawaiian lavas

The depleted mantle component dominates Hawaiian rejuvenated stage lavas [*Frey et al.*, 2005]. It also contributes to Hawaiian shield and postshield lavas [*Mukhopadhyay et al.*, 2003; *Xu et al.*, 2005]. In Chapter 2, I have shown that when the volcano moves away from the hotspot, the rejuvenated stage depleted component becomes more important (Figures 9 and 16 from Chapter 2). There is also controversy

whether this depleted component is intrinsic to the Hawaiian plume [*Frey et al.*, 2005] or MORB-source related [i.e., *Chen and Frey*, 1985]. Several geochemical arguments suggest that this depleted component is different from the Pacific MORB source: (1) Isotopic trends (such as $^{87}Sr/^{86}Sr$ vs $^{143}Nd/^{144}Nd$; $^{87}Sr/^{86}Sr$ vs $^{206}Pb/^{204}Pb$) defined by Hawaiian lavas, including rejuvenated stage lavas, do not trend towards the Pacific MORB field (Figures 9 from Chapter 2; [*Frey et al.*, 2005]); (2) Hawaiian lavas, including the ~ 80 Ma Detroit Seamount, have characteristic Ba/Th ratios that are higher than MORB [*Yang et al.*, 2003; *Huang et al.*, 2005], which requires a long-lived distinct source; (3) Hawaiian rejuvenated stage lavas define a linear trend on Th/Nb vs La/Nb that does not trend towards the EPR (Eastern Pacific Rise) N-MORB (Figure 10) which excludes the involvement of EPR N-MORB in Hawaiian rejuvenated stage lavas.

In summary, the depleted components sampled by Kerguelen Archipelago and Hawaiian lavas are different from MORB-related sources. Instead they are intrinsic to the Kerguelen and Hawaiian plumes.

4. Summary

The agreement between the predictions made from plume hypothesis and the observations from Kerguelen and Hawaii supports the existence of mantle plumes. For the cases of Kerguelen and Hawaii, the mantle plume hypothesis correctly predicts (1) rapid initial volcanism (for Kerguelen plume) followed by long time reduced volcanism from the plume tail (i.e Ninetyeast Ridge and Emperor Seamount-Hawaii Ridge); (2) plume head (if sampled) and tail should lead to compositionally different lavas as observed for the Kerguelen plume; (3) plume tails extend to a thermal boundary layer, at the core-mantle boundary, and have seismically detectable thermal and/or compositional anomalies.

Although there is little doubt that mantle plumes exist at Kerguelen and Hawaii, this does not mean that all intra-plate volcanism results from mantle plumes. Alternative models are needed to explain observations such as isolated seamounts and LIPs with no age progressive volcanic chains (i.e., the Ontong Java Plateau).

Both Kerguelen Archipelago and Hawaiian lavas are very heterogeneous in geochemical compositions, but the origin of isotopic variability for Kerguelen and Hawaii are different. At Kerguelen, this heterogeneity is attributed to contamination of Kerguelen plume by continental material that was incorporated into the upper mantle during the Gondwanaland break up. In contrast at Hawaii, ancient recycled oceanic crust and sediment was brought up by Hawaiian plume from the deep mantle, possible from the D'' region at the core-mantle boundary. The depleted components sampled by Kerguelen Archipelago and Hawaiian lavas are different from MORB-sources, and are probably intrinsic to the Kerguelen and Hawaiian plumes.

References

Anderson, D. L. (2005), Large Igneous Provinces, Delamination, and Fertile mantle, *Elements*, *1*, 271-275.

Borissova, I., M. F. Coffin, P. Charvis, and S. Operto (2003), Structure and development of a microcontinent: Elan Bank in the southern Indian Ocean, *Geochem. Geophy. Geosyst.*, *4*, doi:10.1029/2003GC000535.

Braginsky, S. I., and P. H. Roberts (1995), Equations Governing Convection in Earths Core and the Geodynamo, *Geophysical and Astrophysical Fluid Dynamics*, *79*, 1-97.

Campbell, I. H. (2007), Testing the plume theory, *Chem. Geol.*, *doi:10.1016/j.chemgeo.2007.01.024.*

Chen, C. Y., and F. A. Frey (1985), Trace-Element and Isotopic Geochemistry of Lavas from Haleakala Volcano, East Maui, Hawaii - Implications for the Origin of Hawaiian Basalts, *Journal of Geophysical Research-Solid Earth and Planets*, *90*, 8743-8768.

Coffin, M. F., and O. Eldholm (1994), Large Igneous Provinces - Crustal Structure, Dimensions, and External Consequences, *Reviews of Geophysics*, *32*, 1-36.

Coffin, M. F., M. S. Pringle, R. A. Duncan, T. P. Gladczenko, M. Storey, R. D. Muller, and L. A. Gahagan (2002), Kerguelen Hotspot Magma Output since 130 Ma, *J. Petrol.*, *43*, 1121-1137.

Condie, K. C. (2001), *Mantle plumes and their record in Earth history*, 302 pp., Cambridge University Press, Cambridge, UK.

Courtillot, V., A. Davaille, J. Besse, and J. Stock (2003), Three distinct types of hotspots in the Earth's mantle, *Earth Planet. Sci. Lett.*, *205*, 295-308.

Davies, G. F. (1999), *Dynamic Earth: Plate, plumes and mantle convection*, Cambridge University Press, Cambridge, UK.

Davies, G. F. (2005), A case for mantle plumes, *Chinese Science Bulletin*, *50*, 1541-1554.

Doucet, S., J. S. Scoates, D. Weis, and A. Giret (2005), Constraining the components of the Kerguelen mantle plume: A Hf-Pb-Sr-Nd isotopic study of picrites and high-MgO basalts from the Kerguelen Archipelago, *Geochem. Geophy. Geosyst.*, *6*, doi:10.1029/2004GC000806.

Doucet, S., D. Weis, J. S. Scoates, K. Nicolaysen, F. A. Frey, and A. Giret (2002), The Depleted Mantle Component in Kerguelen Archipelago Basalts: Petrogenesis of

Tholeiitic-Transitional Basalts From the Loranchet Peninsula, *J. Petrol.*, *43*, 1341-1366.

Duncan, R. A., and R. A. Keller (2004), Radiometric ages for basement rocks from the Emperor Seamounts, ODP Leg 197, *Geochem. Geophy. Geosyst.*, *5*.

Eisele, J., M. Sharma, S. J. G. Galer, J. Blichert-Toft, C. W. Devey, and A. W. Hofmann (2002), The role of sediment recycling in EM-1 inferred from Os, Pb, Hf, Nd, Sr isotope and trace element systematics of the Pitcairn hotspot, *Earth Planet. Sci. Lett.*, *196*, 197-212.

Elkins-Tanton, L. T. (2005), Continental magmatism caused by lithosphereic delamination, in *Plates, Plumes and Paradigms*, edited by G. R. Foulger, et al., Geological Society of America Special Paper.

Escrig, S., F. Capmas, B. Dupre, and C. J. Allegre (2004), Osmium isotopic constraints on the nature of the DUPAL anomaly from Indian mid-ocean-ridge basalts, *Nature*, *431*, 59-63.

Falloon, T. J., L. V. Danyushevsky, A. Ariskin, D. H. Green, and C. E. Ford (2007), The application of olivine geothermometry to infer crystallization temperatures of parental liquids: Implications for the temperature of MORB magmas, *Chem. Geol.*, *doi:10.1016/j.chemgeo.2007.01.015*.

Farnetani, C. G., and H. Samuel (2005), Beyond the thermal plume paradigm, *Geophy. Res. Lett.*, *32*, -.

Fouch, M. J., K. M. Fischer, and M. E. Wysession (2001), Lowermost mantle anisotropy beneath the Pacific: Imaging the source of the Hawaiian plume, *Earth Planet. Sci. Lett.*, *190*, 167-180.

Foulger, G. R. (2002), Plume, or plate tectonic processes?, *Astronomy & Geophysics*, *43*, 6.19-16.23.

Foulger, G. R. (2004), The "Plate" model for the genesis of melting anomalies, in *Plates, Plumes, and Planetary Processes*, edited by G. R. Foulger and D. M. Jurdy, Geological Society of America Special Paper.

Frey, F. A., M. F. Coffin, P. J. Wallace, D. Weis, X. Zhao, S. W. Wise, V. Wahnert, D. A. H. Teagle, P. J. Saccocia, D. N. Reusch, M. S. Pringle, K. E. Nicolaysen, C. R. Neal, R. D. Muller, C. L. Moore, J. J. Mahoney, L. Keszthelyi, H. Inokuchi, R. A. Duncan, H. Delius, J. E. Damuth, D. Damasceno, H. K. Coxall, M. K. Borre, F. Boehm, J. Barling, N. T. Arndt, and M. Antretter (2000), Origin and evolution of a submarine large igneous province: the Kerguelen Plateau and Broken Ridge, southern Indian Ocean, *Earth Planet. Sci. Lett.*, *176*, 73-89.

Frey, F. A., and D. H. Green (1974), Mineralogy, Geochemistry and Origin of Ilherzolite Inclusions in Victorian Basanites, *Geochim. Cosmochim. Acta*, *38*, 1023-1059.

Frey, F. A., S. Huang, J. Blichert-Toft, M. Regelous, and M. Boyet (2005), Origin of depleted components in basalt related to the Hawaiian hot spot: Evidence from isotopic and incompatible element ratios, *Geochem. Geophy. Geosyst.*, *6*, doi:10.1029/2004GC000757.

Frey, F. A., K. Nicolaysen, B. K. Kubit, D. Weis, and A. Giret (2002a), Flood Basalt from Mont Tourmente in the Central Kerguelen Archipelago: the Change from Transitional to Alkalic Basalt at ~25 Ma, *J. Petrol.*, *43*, 1367-1387.

Frey, F. A., D. Weis, A. Y. Borisova, and G. Xu (2002b), Involvement of Continental Crust in the Formation of the Cretaceous Kerguelen Plateau: New Perspectives from ODP Leg 120 Sites, *J. Petrol.*, *43*, 1207-1239.

Green, D. H., and T. J. Falloon (2005), Primary magmas at mid-ocean ridges, "hot spots" and other intraplate settings: constraints on mantle potential temperature, in *Plates, Plumes and Paradigms*, edited by G. R. Foulger, et al., pp. 217-247, Geological Society of America Special Paper.

Griffiths, R. W., and I. H. Campbell (1990), Stirring and structure in mantle starting plumes, *Earth Planet. Sci. Lett.*, *99*, 66-78.

Hanan, B. B., and D. W. Graham (1996), Lead and helium isotope evidence from oceanic basalts for a common deep source of mantle plumes, *Science*, *272*, 991-995.

Hart, S. R., E. H. Hauri, L. A. Oschmann, and J. A. Whitehead (1992), Mantle Plumes and Entrainment - Isotopic Evidence, *Science*, *256*, 517-520.

Hassler, D. R., and N. Shimizu (1998), Osmium isotopic evidence for ancient subcontinental lithospheric mantle beneath the Kerguelen Islands, southern Indian Ocean, *Science*, *280*, 418-421.

Herzberg, C. (2006), Petrology and thermal structure of the Hawaiian plume from Mauna Kea volcano, *Nature*, *444*, 605-609.

Herzberg, C., P. D. Asimow, N. T. Arndt, Y. Niu, C. M. Lesher, J. G. Fitton, M. J. Cheadle, and A. Saunders (2007), Temperatures in ambient mantle and plumes: Constraints from basalts, picrites, and komatiites, *Q02006, doi:10.1029/2006GC001390.*

Hofmann, A. W. (1997), Mantle geochemistry: The message from oceanic volcanism, *Nature*, *385*, 219-229.

Huang, S., M. Regelous, T. Thordarson, and F. A. Frey (2005), Petrogenesis of lavas from Detroit Seamount: Geochemical differences between Emperor Chain and Hawaiian volcanoes, *Geochem. Geophy. Geosyst.*, *6*, doi:10.1029/2004GC000756.

Huang, S. C., and F. A. Frey (2005), Recycled oceanic crust in the Hawaiian Plume: evidence from temporal geochemical variations within the Koolau Shield, *Contrib. Mineral. Petrol.*, *149*, 556-575.

Humayun, M., L. P. Qin, and M. D. Norman (2004), Geochemical evidence for excess iron in the mantle beneath Hawaii, *Science*, *306*, 91-94.

Ingle, S., and M. F. Coffin (2004), Impact origin for the greater Ontong Java Plateau?, *Earth Planet. Sci. Lett.*, *218*, 123-134.

Ingle, S., D. Weis, J. S. Scoates, and F. A. Frey (2002), Relationship between the early Kerguelen plume and continental flood basalts of the paleo-Eastern Gondwanan margins, *Earth Planet. Sci. Lett.*, *197*, 35-50.

Jones, A. P., K. Wunemann, and D. Price (2005), Impact volcanism as a possible origin for the Ontong Java Plateau (OJP), in *Plates, Plumes and Paradigms*, edited by G. R. Foulger, et al., Geological Society of America Special Paper.

Kempton, P. D., J. A. Pearce, T. L. Barry, J. G. Fitton, C. Langmuir, and D. M. Christie (2002), Sr-Nd-Pb-Hf isotope results from ODP Leg 187: Evidence for mantle dynamics of the Australian-Antarctic Discordance and origin of the Indian MORB source, *Geochem. Geophy. Geosyst.*, *3*, doi:10.1029/2002GC000320.

King, S. D., and D. L. Anderson (1998), Edge-driven convection, *Earth Planet. Sci. Lett.*, *160*, 289-296.

Lassiter, J. C., and E. H. Hauri (1998), Osmium-isotope variations in Hawaiian lavas: evidence for recycled oceanic lithosphere in the Hawaiian plume, *Earth Planet. Sci. Lett.*, *164*, 483-496.

Lassiter, J. C., E. H. Hauri, P. W. Reiners, and M. O. Garcia (2000), Generation of Hawaiian post-erosional lavas by melting of a mixed lherzolite/pyroxenite source, *Earth Planet. Sci. Lett.*, *178*, 269-284.

Lei, J. S., and D. P. Zhao (2006), A new insight into the Hawaiian plume, *Earth Planet. Sci. Lett.*, *241*, 438-453.

Li, X., R. Kind, K. Priestley, S. V. Sobolev, F. Tilmann, X. Yuan, and M. Weber (2000), Mapping the Hawaiian plume conduit with converted seismic waves, *Nature*, *405*, 938-941.

Lin, S.-C., and P. E. van Keken (2005), Multiple volcanic episodes of flood basalts caused by thermochemical mantle plumes, *Nature*, *436*, 250-252.

Lin, S. C., and P. E. van Keken (2006), Dynamics of thermochemical plumes: 2. Complexity of plume structures and its implications for mapping mantle plumes, *Geochem. Geophy. Geosyst.*, *7*, -.

Lustrino, M. (2005), How the delamination and detachment of lower crust can influence basaltic magmatism, *Earth Sci. Rev.*, *72*, 21-38.

Mahoney, J. J., D. W. Graham, D. M. Christie, K. T. M. Johnson, L. S. Hall, and D. L. Vonderhaar (2002), Between a Hotspot and a Cold Spot: Isotopic Variation in the Southeast Indian Ridge Asthenosphere, 86°E-118°E, *J. Petrol.*, *43*, 1155-1176.

Mahoney, J. J., W. B. Jones, F. A. Frey, V. J. M. Salters, D. G. Pyle, and H. L. Davies (1995), Geochemical Characteristics of Lavas from Broken Ridge, the Naturaliste Plateau and Southernmost Kerguelen Plateau - Cretaceous Plateau Volcanism in the Southeast Indian-Ocean, *Chem. Geol.*, *120*, 315-345.

Mattielli, N., D. Weis, J. S. Scoates, N. Shimizu, J. P. Mennessier, M. Grégoire, J. Y. Cottin, and A. Giret (1999), Evolution of heterogeneous lithospheric mantle in a plume environment beneath the Kerguelen Archipelago, *J. Petrol.*, *40*, 1721-1744.

McKenzie, D., and R. K. O'Nions (1983), Mantle Reservoirs and Ocean Island Basalts, *Nature*, *301*, 229-231.

Meyzen, C. M., J. N. Ludden, E. Humler, B. Luais, M. J. Toplis, C. Mevel, and M. Storey (2005), New insights into the origin and distribution of the DUPAL isotope anomaly in the Indian Ocean mantle from MORB of the Southwest Indian Ridge, *Geochem. Geophy. Geosyst.*, *6*, doi:10.1029/2005GC000979.

Montelli, R., G. Nolet, F. A. Dahlen, and G. Masters (2006), A catalogue of deep mantle plumes: New results from finite-frequency tomography, *Geochem. Geophy. Geosyst.*, *7*, -.

Montelli, R., G. Nolet, F. A. Dahlen, G. Masters, E. R. Engdahl, and S. H. Hung (2004), Finite-frequency tomography reveals a variety of plumes in the mantle, *Science*, *303*, 338-343.

Morgan, W. J. (1971), Convection plumes in the lower mantle, *Nature*, *230*, 42-43.

Mukhopadhyay, S., J. C. Lassiter, K. A. Farley, and S. W. Bogue (2003), Geochemistry of Kauai shield-stage lavas: Implications for the chemical evolution of the Hawaiian plume, *Geochem. Geophy. Geosyst.*, *4*, doi:10.1029/2002GC000342.

Neal, C. R., J. J. Mahoney, and W. J. Chazey, III (2002), Mantle Sources and the Highly Variable Role of Continental Lithosphere in Basalt Petrogenesis of the Kerguelen Plateau and Broken Ridge LIP: Results from ODP Leg 183, *J. Petrol.*, *43*, 1177-1205.

Niu, Y. L., and R. Batiza (1997), Trace element evidence from seamounts for recycled oceanic crust in the eastern Pacific mantle, *Earth Planet. Sci. Lett.*, *148*, 471-483.

Niu, Y. L., M. Regelous, I. J. Wendt, R. Batiza, and M. J. O'Hara (2002), Geochemistry of near-EPR seamounts: importance of source vs. process and the origin of enriched mantle component, *Earth Planet. Sci. Lett.*, *199*, 327-345.

Nolet, G., R. Allen, and D. Zhao (2007), Mantle plume tomography, *Chem. Geol.*, *doi:10.1016/j.chemgeo.2007.01.022*

Nolet, G., S.-I. Karato, and R. Montelli (2006), Plume fluxes from seismic tomography, *Earth Planet. Sci. Lett.*, *248*, 685-699.

Pilet, S., J. Hernandez, F. Bussy, and P. J. Sylvester (2004), Short-term metasomatic control of Nb/Th ratios in the mantle sources of intraplate basalts, *Geology*, *32*, 113-116.

Plank, T., and C. H. Langmuir (1998), The chemical composition of subducting sediment and its consequences for the crust and mantle, *Chem. Geol.*, *145*, 325-394.

Putirka, K. D. (2005), Mantle potential temperatures at Hawaii, Iceland, and the mid-ocean ridge system, as inferred from olivine phenocrysts: Evidence for thermally driven mantle plumes, *Geochem. Geophy. Geosyst.*, *6*, doi:10.1029/2005GC000915.

Putirka, K. D., M. Perfit, F. J. Ryerson, and M. G. Jackson (2007), Ambient and excess mantle temperatures, olivine thermometry, and active vs. passive upwelling, *Chem. Geol.*, *doi:10.1016/j.chemgeo.2007.01.014*.

Rehkämper, M., and A. W. Hofmann (1997), Recycled ocean crust and sediment in Indian Ocean MORB, *Earth Planet. Sci. Lett.*, *147*, 93-106.

Robinson, J. E., and B. W. Eakins (2006), Calculated volumes of individual shield volcanoes at the young end of the Hawaiian Ridge, *J. Volcano. Geoth. Res.*, *151*, 309-317.

Rudnick, R. L., and S. Gao (2004), Composition of the continental crust, in *Treatise on Geochemistry*, edited by H. D. Holland and K. K. Turekian, pp. 1-64, Elsevier-Pergamon, Oxford.

Samuel, H., C. G. Farnetani, and D. Andrault (2005), Heterogeneous lowermost mantle: compositonal constraints and seismological observables, *AGU Geophysical Monograph, 160*.

Sobolev, A. V., A. W. Hofmann, D. V. Kuzmin, G. M. Yaxley, N. T. Arndt, S. L. Chung, L. V. Danyushevsky, T. Elliott, F. A. Frey, M. O. Garcia, A. A. Gurenko, V. S. Kamenetsky, A. C. Kerr, N. A. Krivolutskaya, V. V. Matvienkov, I. K. Nikogosian, A. Rocholl, I. A. Sigurdsson, N. M. Sushchevskaya, and M. Teklay (2007), The amount of recycled crust in sources of mantle-derived melts, *Science, 316*, 412-417.

Sobolev, A. V., A. W. Hofmann, S. V. Sobolev, and I. K. Nikogosian (2005), An olivine-free mantle source of Hawaiian shield basalts, *Nature, 434*, 590-597.

Stracke, A., A. W. Hofmann, and S. R. Hart (2005), FOZO, HIMU, and the rest of the mantle zoo, *Geochem. Geophy. Geosyst., 6*, -.

Sun, S.-S., and W. F. McDonough (1989), Chemical and isotopic systematics of oceanic basalts: implications for mantle composition and processes. In: Saunders, A.D., Norry, M.J. (eds.). Magmatism in the Ocean Basins, *Geological Society Special Publication, 42*, 313-345.

van Keken, P. (1997), Evolution of starting mantle plumes: a comparison between numerical and laboratory models, *Earth Planet. Sci. Lett., 148*, 1-11.

Weis, D., Y. Bassias, I. Gautier, and J. P. Mennessier (1989), Dupal Anomaly in Existence 115 Ma Ago - Evidence from Isotopic Study of the Kerguelen Plateau (South Indian-Ocean), *Geochim. Cosmochim. Acta, 53*, 2125-2131.

Weis, D., and F. A. Frey (2002), Submarine Basalts of the Northern Kerguelen Plateau: Interaction Between the Kerguelen Plume and the Southeast Indian Ridge Revealed at ODP Site 1140, *J. Petrol., 43*, 1287-1309.

Wen, L. (2006), A compositional anomaly at the Earth's core-mantle boundary as an anchor to the relatively slowly moving surface hotspots and as source to the DUPAL anomaly, *Earth Planet. Sci. Lett., 246*, 138-148.

White, R., and D. Mckenzie (1989), Magmatism at Rift Zones - the Generation of Volcanic Continental Margins and Flood Basalts, *Journal of Geophysical Research-Solid Earth and Planets, 94*, 7685-7729.

Wilson, J. T. (1963), A possible origin of the Hawaiian Islands, *Canadian Journal of Physics, 41*, 863-870.

Workman, R. K., S. R. Hart, M. Jackson, M. Regelous, K. A. Farley, J. Blusztajn, M. Kurz, and H. Staudigel (2004), Recycled metasomatized lithosphere as the origin of the enriched mantle II (EM2) end-member: Evidence from the Samoan volcanic chain, *Geochem. Geophy. Geosyst., 5*, doi:10.1029/2003GC000623.

Xu, G., F. A. Frey, D. A. Clague, D. Weis, and M. H. Beeson (2005), East Molokai and other Kea-trend volcanoes: Magmatic processes and sources as they migrate away from the Hawaiian hot spot, *Geochem. Geophy. Geosyst.*, *6*, doi:10.1029/2004GC000830.

Yang, H.-J., F. A. Frey, D. Weis, A. Giret, D. Pyle, and G. Michon (1998), Petrogenesis of the flood basalts forming the northern Kerguelen Archipelago: Implications for the Kerguelen Plume, *J. Petrol.*, *39*, 711-748.

Yang, H. J., F. A. Frey, and D. A. Clague (2003), Constraints on the Source Components of Lavas Forming the Hawaiian North Arch and Honolulu Volcanics, *J. Petrol.*, *44*, 603-627.

Figure Captions:

Figure 1 Map showing the volcanic features attributed to the Kerguelen plume, i.e., the Kerguelen Plateau, Broken Ridge, Ninetyeast Ridge, Kerguelen Archipelago, and Heard Islands and possibly the Naturaliste Plateau, Bunbury and Rajmahal traps. Figure is from *Doucet et al.* [2005].

Figure 2 Estimated Kerguelen hotspot magma output since ~130 Ma. Figure is from *Coffin et al.* [2002].

Figure 3 Three-dimensional view of the plumes beneath Hawaii and Kerguelen in both P-wave and S-wave models. Figure is from *Montelli et al.* [2006].

Figure 4 Tomographic images with and without PKiKP rays. PKiKP is the P wave that propagates through the inner core. Figure is from *Lei and Zhao* [2006].

Figure 5 P-wave tomographic images from the surface down to the core-mantle boundary under (a) Hawaii and (b) Kerguelen. Solid triangles denote the locations of the surface hotspots. Modified from *Nolet et al.* [2007].

Figure 6 $^{206}Pb/^{204}Pb$ vs $^{87}Sr/^{86}Sr$ showing that Kerguelen plume head (Kerguelen Plateau Site 1138) and plume tail (Mt. Crozier from Kerguelen Archipelago) have very different compositions. Data from Neal et al. [*Neal et al.*, 2002] and D. Weis (unpublished data).

Figure 7 $^{87}Sr/^{86}Sr$ vs. $^{208}Pb^*/^{206}Pb^*$ (defined as ($^{208}Pb/^{204}Pb$-29.475) / ($^{206}Pb/^{204}Pb$-9.307)) for young Hawaiian lavas (< 3Ma) and Kerguelen Archipelago lavas which were age corrected to 25 Ma.

Figure 8 $^{143}Nd/^{144}Nd$ vs age for Kerguelen Archipelago lavas showing that a depleted component is less important in younger lavas which erupted further away from the ridge. Data from relevant references in Chapter 1.

Figure 9 Th/Nb vs La/Nb for Kerguelen Site 1140 lavas. Site 1140 lavas which were close to SEIR at eruption were interpreted as binary mixture of Kerguelen plume and SEIR N-MORB [*Weis and Frey*, 2002]. However, the most depleted Site 1140 lavas (i.e., with low $^{87}Sr/^{86}Sr$) have the highest Th/Nb and La/Nb ratios. Therefore, a depleted component (indicated by '?') with high Th/Nb ratios different than MORB is required. MORB field is defined by data from [*Rehkämper and Hofmann*, 1997; *Kempton et al.*, 2002; *Mahoney et al.*, 2002].

Figure 10 Th/Nb vs La/Nb for Hawaiian rejuvenated stage lavas [Yang et al., 2003; Xu et al., 2005] and EPR MORB [Niu and Batiza, 1997; Niu et al., 2002]. The linear trend defined by Hawaiian rejuvenated stage lavas barely extrapolates to EPR MORB field.

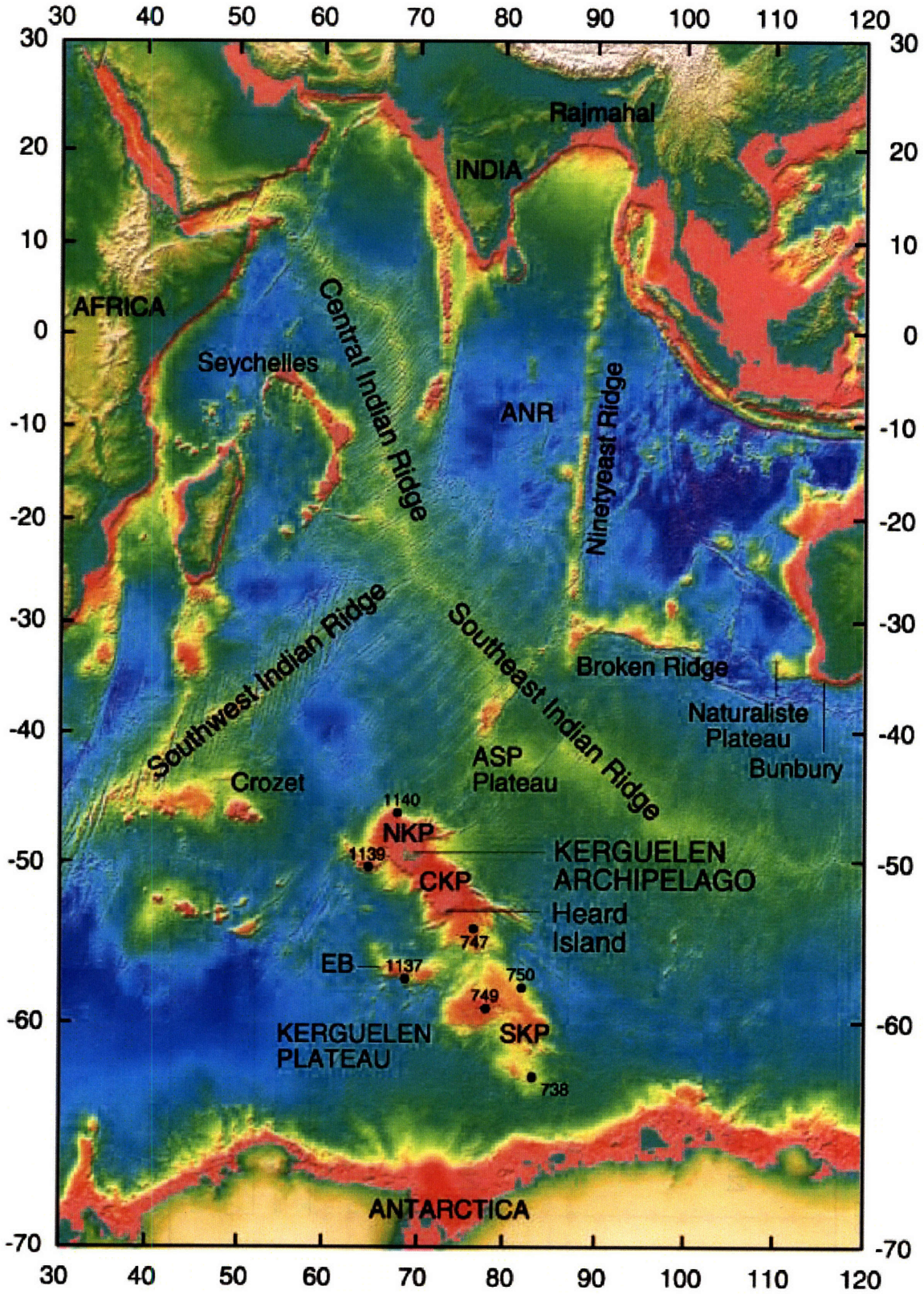
30
40
50
60
70
80
90
100
110
120
30
20
10
0
-10
-20
-30
-40
-50
-60
-70
Rajmahal
INDIA
AFRICA
Central Indian Ridge
Seychelles
ANR
Ninetyeast Ridge
Southwest Indian Ridge
Southeast Indian Ridge
Broken Ridge
Naturaliste Plateau
Bunbury
ASP Plateau
Crozet
1140
NKP
1139
KERGUELEN ARCHIPELAGO
CKP
Heard Island
747
EB
1137
750
749
KERGUELEN PLATEAU
SKP
738
ANTARCTICA

Figure 1

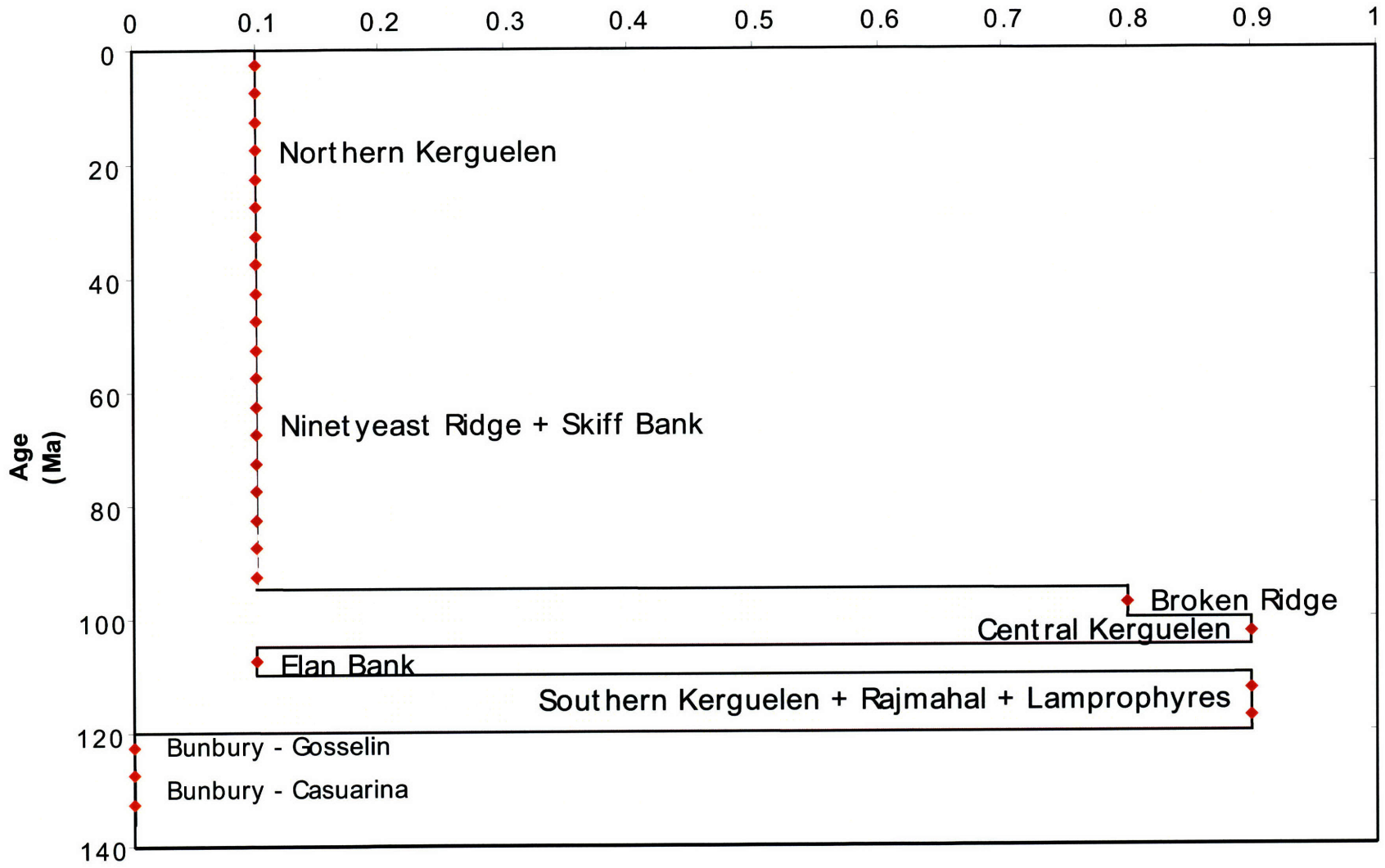
Kerguelen Hotspot Output
Magma Flux (km3/ yr)
0
0.1
0.2
0.3
0.4
0.5
0.6
0.7
0.8
0.9
1
Age (Ma)
0
20
40
60
80
100
120
140
Northern Kerguelen
Ninetyeast Ridge + Skiff Bank
Broken Ridge
Central Kerguelen
Elan Bank
Southern Kerguelen + Rajmahal + Lamprophyres
Bunbury - Gosselin
Bunbury - Casuarina

Figure 2

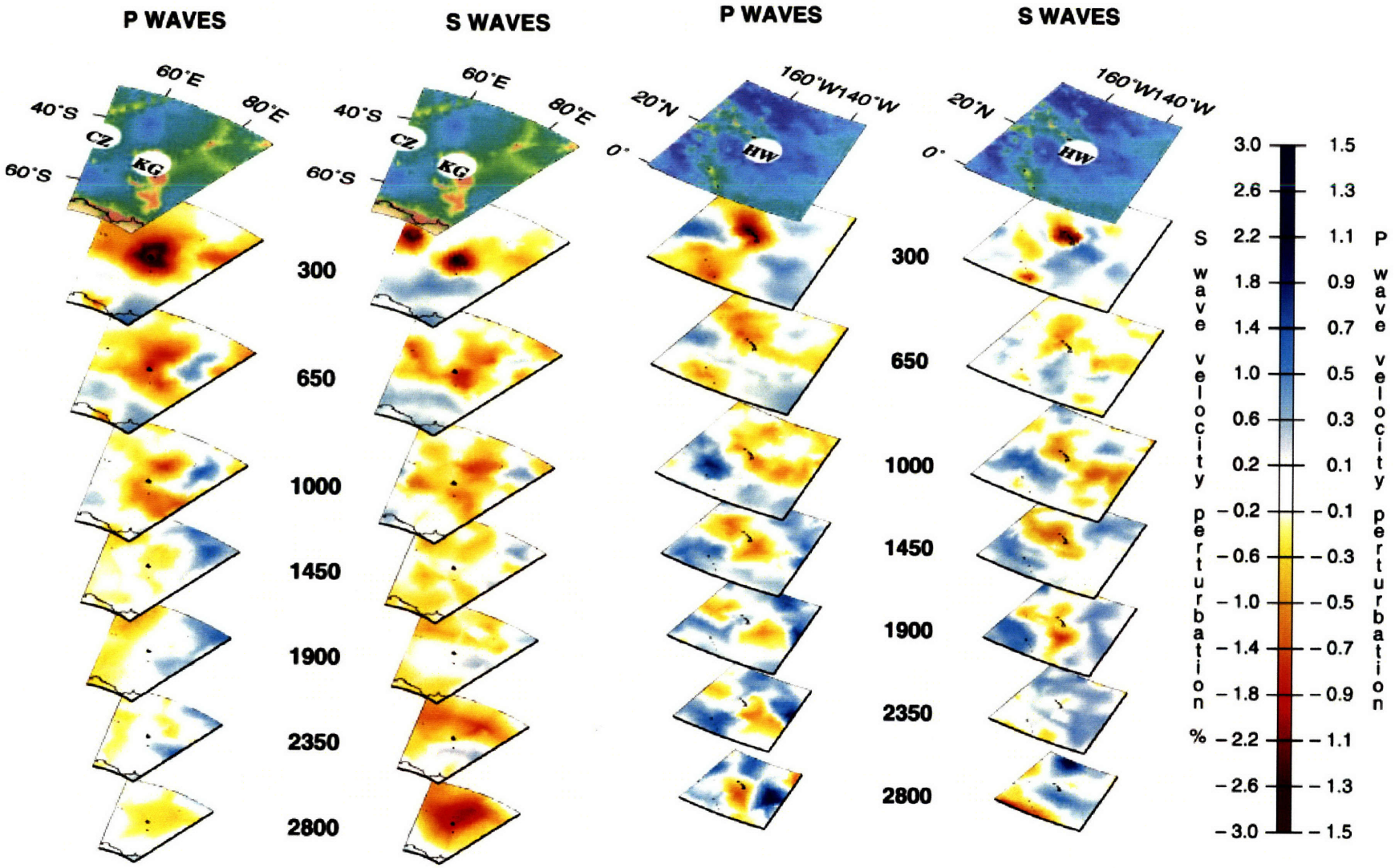
P WAVES
S WAVES
P WAVES
S WAVES
60°E
80°E
40°S
60°S
CZ
KG
20°N
0°
160°W
140°W
HW
300
650
1000
1450
1900
2350
2800
S wave velocity perturbation %
P wave velocity perturbation
3.0
2.6
2.2
1.8
1.4
1.0
0.6
0.2
−0.2
−0.6
−1.0
−1.4
−1.8
−2.2
−2.6
−3.0
1.5
1.3
1.1
0.9
0.7
0.5
0.3
0.1
−0.1
−0.3
−0.5
−0.7
−0.9
−1.1
−1.3
−1.5

Figure 3

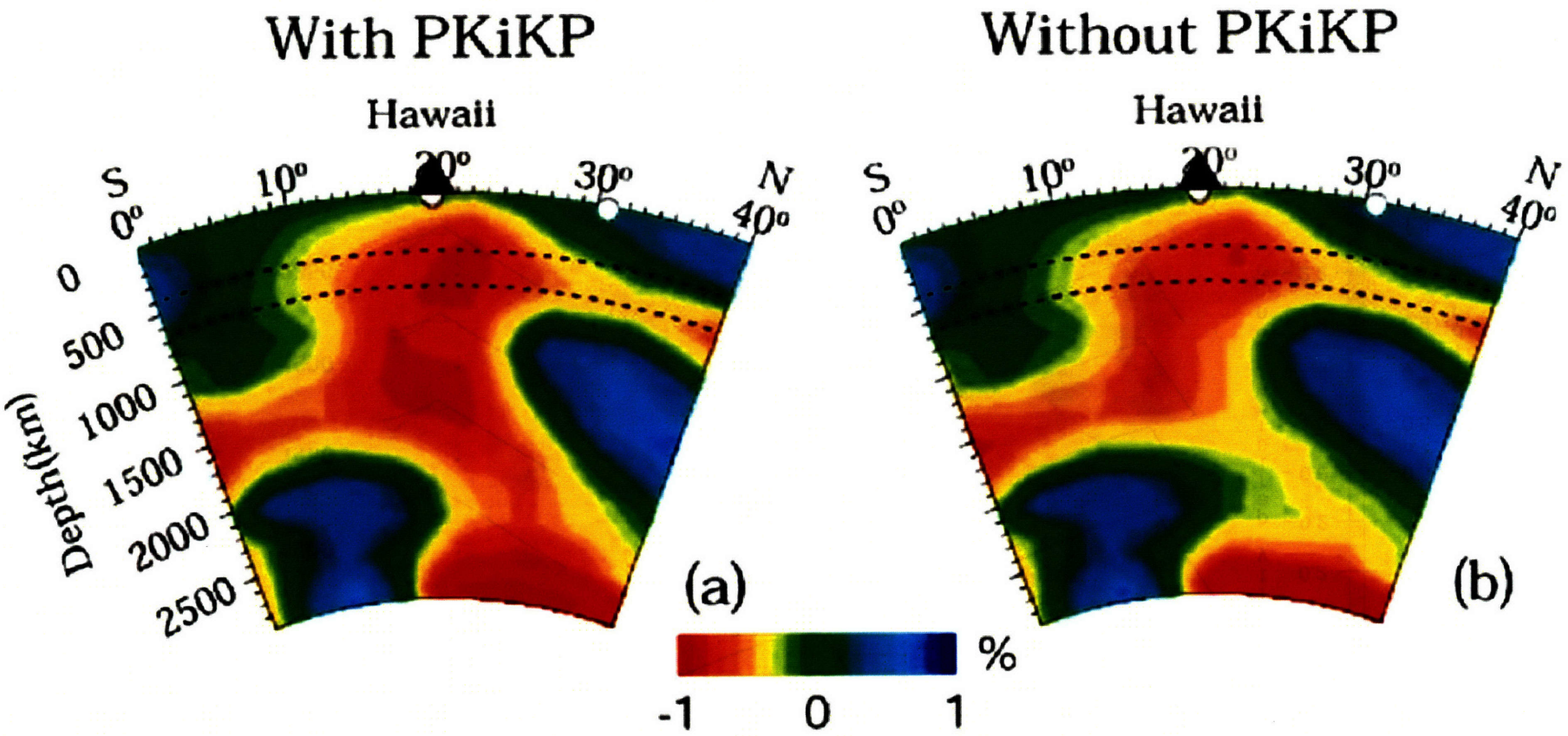
With PKiKP
Hawaii
S
0°
10°
20°
30°
N
40°
0
500
1000
1500
2000
2500
Depth(km)
(a)
%
-1
0
1
Without PKiKP
Hawaii
S
0°
10°
20°
30°
N
40°
(b)

Figure 4

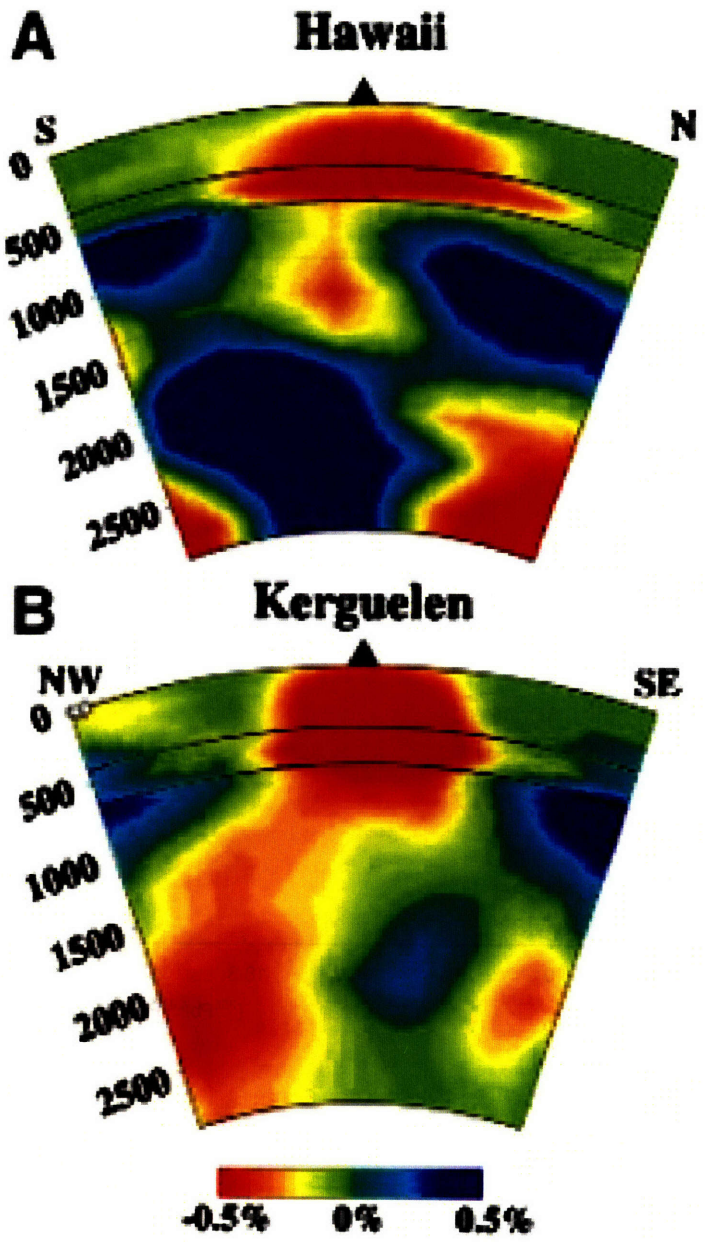
A
Hawaii
S
N
0
500
1000
1500
2000
2500
B
Kerguelen
NW
SE
0
500
1000
1500
2000
2500
-0.5%
0%
0.5%

Figure 5

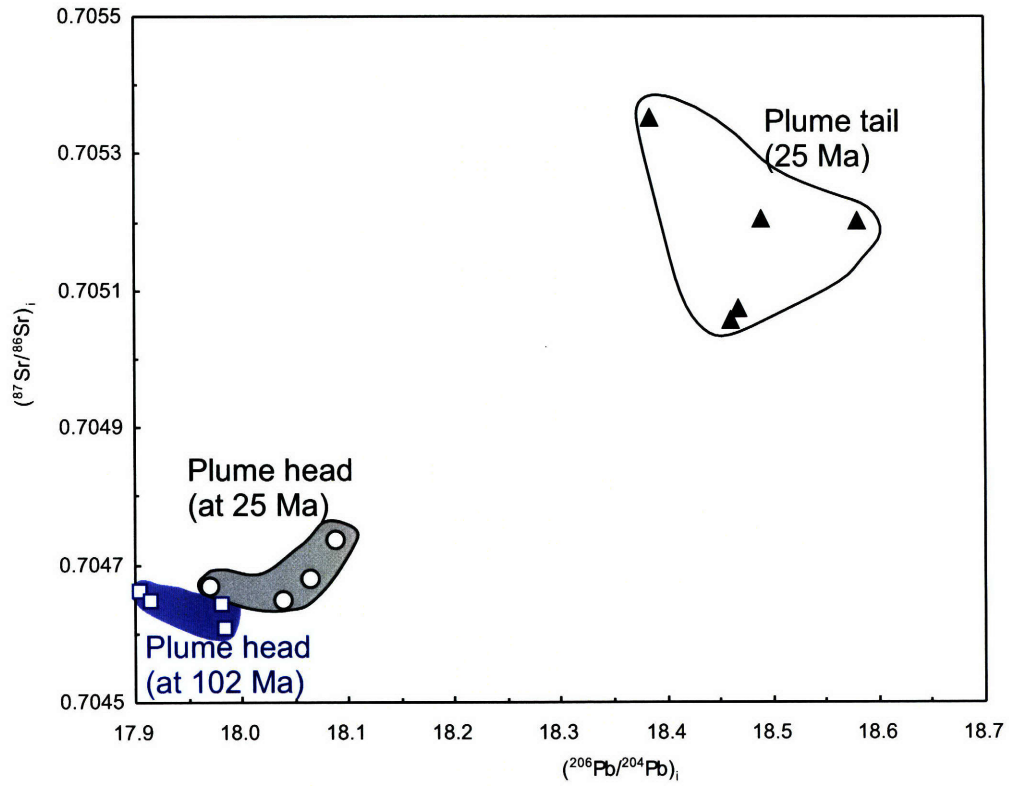
0.7055
0.7053
0.7051
0.7049
0.7047
0.7045
$(^{87}Sr/^{86}Sr)_i$
17.9
18.0
18.1
18.2
18.3
18.4
18.5
18.6
18.7
$(^{206}Pb/^{204}Pb)_i$
Plume tail
(25 Ma)
Plume head
(at 25 Ma)
Plume head
(at 102 Ma)

Figure 6

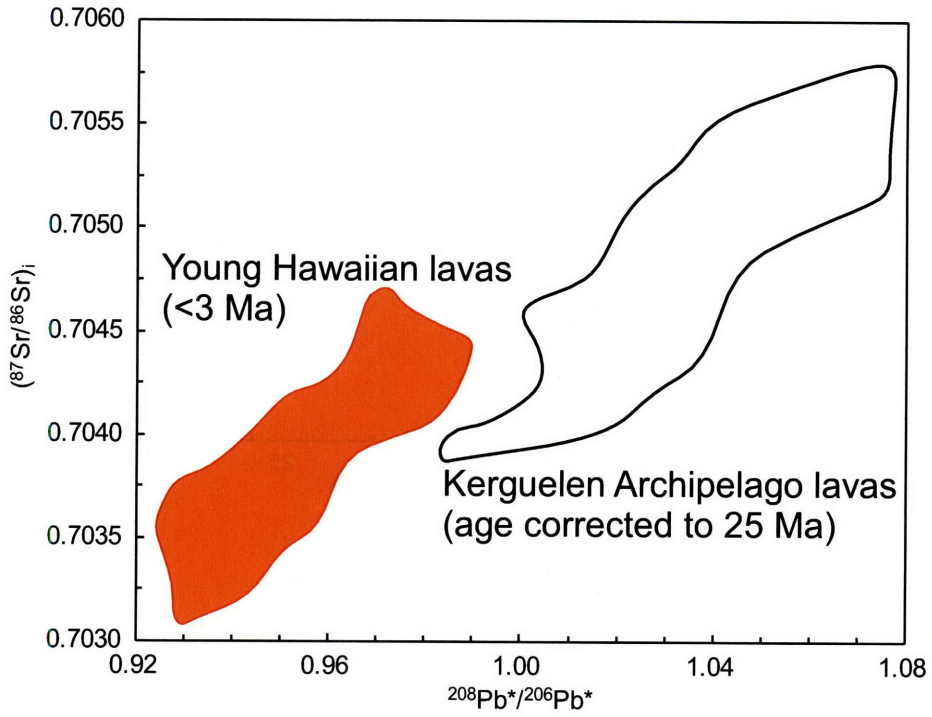
0.7060
0.7055
0.7050
0.7045
0.7040
0.7035
0.7030
$(^{87}Sr/^{86}Sr)_i$
Young Hawaiian lavas
(<3 Ma)
Kerguelen Archipelago lavas
(age corrected to 25 Ma)
0.92
0.96
1.00
1.04
1.08
$^{208}Pb^*/^{206}Pb^*$

Figure 7

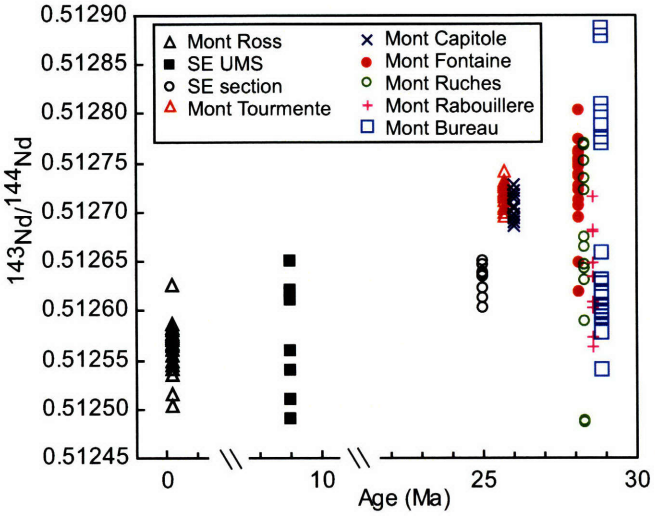
0.51290
0.51285
0.51280
0.51275
0.51270
0.51265
0.51260
0.51255
0.51250
0.51245
$^{143}Nd/^{144}Nd$
Mont Ross
SE UMS
SE section
Mont Tourmente
Mont Capitole
Mont Fontaine
Mont Ruches
Mont Rabouillere
Mont Bureau
0
10
25
30
Age (Ma)

Figure 8

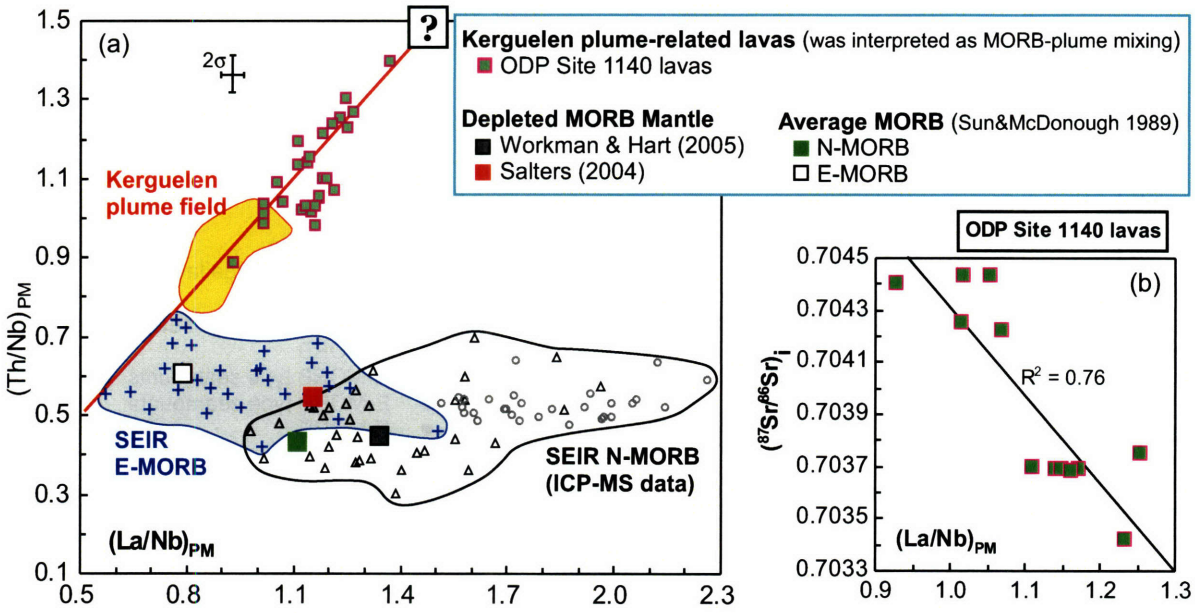
(a)
2σ
?
Kerguelen plume-related lavas (was interpreted as MORB-plume mixing)
ODP Site 1140 lavas
Depleted MORB Mantle
Workman & Hart (2005)
Salters (2004)
Average MORB (Sun&McDonough 1989)
N-MORB
E-MORB
Kerguelen plume field
SEIR E-MORB
SEIR N-MORB (ICP-MS data)
(Th/Nb)PM
(La/Nb)PM
1.5
1.3
1.1
0.9
0.7
0.5
0.3
0.1
0.5
0.8
1.1
1.4
1.7
2.0
2.3
ODP Site 1140 lavas
(b)
R2 = 0.76
(87Sr/86Sr)i
(La/Nb)PM
0.7045
0.7043
0.7041
0.7039
0.7037
0.7035
0.7033
0.9
1.0
1.1
1.2
1.3

Figure 9

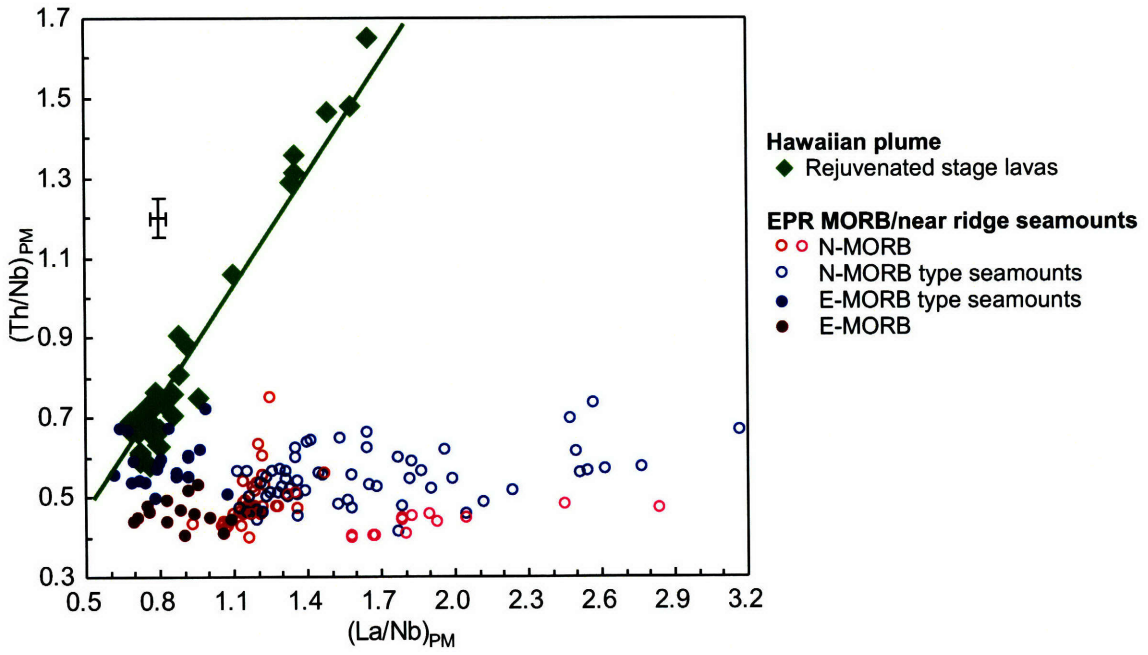
1.7
1.5
1.3
1.1
0.9
0.7
0.5
0.3
(Th/Nb)PM
0.5
0.8
1.1
1.4
1.7
2.0
2.3
2.6
2.9
3.2
(La/Nb)PM
Hawaiian plume
Rejuvenated stage lavas
EPR MORB/near ridge seamounts
N-MORB
N-MORB type seamounts
E-MORB type seamounts
E-MORB

Figure 10